

INAUGURAL – DISSERTATION

zur
Erlangung der Doktorwürde
der
Gesamtfakultät für Mathematik, Ingenieur- und Naturwissenschaften
der
Ruprecht-Karls-Universität
Heidelberg

vorgelegt von
M.Sc. Hermann Rivas Muñoz
aus Providencia, Chile

Tag der mündlichen Prüfung:

07.05.2025

Thema

**PALAEOENVIRONMENTAL CHANGES
IN THE LOWER CRETACEOUS COYHAIQUE GROUP,
SOUTHERN CHILE (AYSÉN-RÍO MAYO BASIN):
A MULTI-STRATIGRAPHICAL APPROACH**

MSc. Hermann Rivas Muñoz

Gutachter:

Prof. Dr. Wolfgang Stinnesbeck

Prof. Dr. Christian Salazar Soto

*“Patagonia es cordillera, campo abierto y ventarrón,
y es la más fiel tradición de un pasado que heredamos,
y al conocerla queramos en toda su dimensión,
llevarla en el corazón y mostrarle al extranjero
este paisaje pionero y el porqué del patagón...”*

Carlos Bello Durán “El Malebo”

*“Hay hombres que de su cencia
tienen la cabeza llena;
hay sabios de todas menas,
más digo, sin ser muy ducho,
es mejor que aprender mucho
el aprender cosas buenas.”*

El Gaucho Martín Fierro

To my family

Acknowledgements

I would like to express my deepest gratitude to my supervisors, Dr. Christian Salazar and Prof. Dr. Wolfgang Stinnesbeck, for believe in this project and for granting me the opportunity to conduct this research, which allowed me to study the rocks of my beloved Coyhaique. Their unwavering guidance, invaluable advice, and constant support have been instrumental throughout this academic journey.

I am also grateful to Prof. Dr. Oliver Friedrich, and Prof. Dr. Frank Keppler for their willingness to participate in the examination committee of this work.

I appreciate the feedback and contribution of Leonardo Pérez, Kevin Álvarez, and Javier Encina for their notable work as co-authors. I am also thankful to Dr. Elisabeth Eiche for her assistance with the geochemical analyses at the KIT. My thanks extend to my friends Dr. (c) Enrique Bostelmann and Dr. Manfred Vogt, and to the reviewers of the manuscripts presented here, for their insightful comments, which have greatly improved the quality of these scientific publications.

My sincere thanks to Valentina Maldonado, Benjamin Aldridge, Rayen Álvarez, Benjamín Gómez, María José Maiza, Juan Arbea, Melany Muñoz, César Pailacheo, Pascale Ergas, Héctor Ortiz, and Grisel Rivera for their eagerness and support during the fieldwork campaigns in Patagonia.

I am grateful to Olga Veloso, Roberto Pincheira, and José Barría for granting access to and providing guidance at the El Toqui Mine; and to José Antonio Bernabé, Mirta Ramírez, and José Bernabé Ramírez from the Fundo San Carlos for granting access to the outcrops at the Simpson River.

I would like to express my deepest appreciation to Francisco Cueto Berciano for his invaluable support and friendship. I also wish to acknowledge the following current and former members of Universität Heidelberg for their support at various stages of the development of this dissertation: Torsten Hoffmann, Ayten Eicher, Dr. Gregor Austermann, Dr. Anne Hildebrand, Dr. Alejandro Cisneros, Prof. Dr. Axel Schmitt, Dr. Sonja Storm, Dr. Till Drews, Dr. Georg Miernik, Oliver Wienand, Ilona Fin, Joachim Fillauer, Dr. Alexander Varychev, Seija Beckmann, Dr. Hartmut Jäger, Dr. Sven Brysch, Tanja Unger, Melanie Kling, Dr. Werner Fielitz, Raphaela Antimisaris, Susanne Sandbrink, and Elfriede Grohmann.

Words cannot fully express my gratitude to my family in Chile, for their endless love and companionship, and for their constant encouragement and unconditional support during these years. I am especially grateful to my parents, Isabel and Herman, to my brothers Harlan and Harry, to my granny Micha, and to my aunts and uncles Mabel, Chuncho, Kanda, Eli, Tencha, Arturo, Oscar, Papitín, Gabriel and Nena. I also thank José Francisco, Lastenia, Roli, Paulina, and to the “tía Patricia” (Beauchef). This thesis is dedicated to the memory of Silvia Cerda, Mario Bustos, and Arturo Hernández.

This endeavour would not have been possible without the love, companionship, and, above all, the infinite patience of Marlene Ruschel and our little Emilia. Thank you for everything. I am also immensely thankful to Gerold, Elisabeth and Simone for welcoming me as part of their own and being my adoptive family in Germany.

I can't finish this section without expressing my appreciation to my friends for their emotional support and companionship throughout the ups and downs of this journey. Special thanks to Ricardo and Julia Yau, Javier Durán, Karina Leiva, Nicolás Manríquez, Carlos Prieto, John Aspinwall, Javier Gallego, Alberto Rey, Birgit Glesius, Jordi Pujol, Dimitri Kostopoulus, Baruc Rodríguez, Aleko Kjaev, Miquel Barceló, Judith Görlich, Carlos Lasch, Matías Mosqueira, Felipe Miranda, Enrique Romero, Virginia Fischer, Omar Ramírez, Alejandro Pereyra, Sebastián Marty, Alejandra Vallejo, Polona Kramberger, Edith and Bruno Verhoeven, Marcela Vollmer, Jokín Arrieta, Antonio Cardin, Jazmín Reyes, Ever Rodríguez, Arkaitz Garay, Miguel López, Piero Arguello, Aarón Paguaga, Daniel Calvo, Nelson Butschbacher, JP Arenas, Philipp Iwan, Marcela García, Manolo Acevedo, Ivette Araya, Pier Barattini, Raúl Ugalde, Ignacio Vera, Felipe and Roberto Poblete, Rodrigo Mena, Nicole Poblete, Andrés Rezuc, Daniela Godoy, Hernán Leal, Camila Pineda, Edwin González, Francesca Casanueva, Exequiel Varela, Luis González, Cristian Vásquez, Héctor Salas, Sergio Ortega, Paulo Quezada, Nicolás López, Roxana Alonso, Jorge Mera, Vivian Schmidt, Pablo Lucero, Claudio Reyes, Luis Naves, and to my friends from Coyhaique, ex-Perdición, and the “Hiperáridos”. Sorry if I missed anyone!

I would like to extend a heartfelt thank you to Dr. Sara Figueroa, whose valuable advice and motivation played a crucial role in the completion of this project.

Finally, my sincere thanks go to Melanie Werner (former ERM GmbH), Georg Stiebeling (ERM GmbH), and to Till Wirth and Frank Stephan (WST GmbH), for their understanding and for allowing me to balance my work with my doctoral studies.

A todos y todas: “Gracias... totales”!!!

Funding

Financial support to this project was provided by the Chilean National Fund for Scientific and Technological Development (FONDECYT de Iniciación 11140176 of Prof. Dr. Christian Salazar), by the Chilean National Agency for Research and Development (ANID/DOCTORADO BECAS CHILE/2016–72170384), by the German Academic Exchange Service (DAAD, STIBET/“Studienabschlussbeihilfe Stipendium 2021”), and by the International Association of Sedimentologists (IAS/Postgraduate Research Grant 2020). Open access publication of Rivas *et al.* (2023; doi: 10.1007/s10347-023-00669-4; appended in section 9.2 of this document;) was enabled and financed by the project DEAL of the Alliance of German Science Organisations.

Abstract

This thesis presents the most detailed historical, stratigraphical, and paleoenvironmental analysis of the Aysén-Río Mayo Basin, and its sedimentary fill, i.e., the Coyhaique Group. The Aysén-Río Mayo Basin was a marginal basin developed in southern South America (currently Chile and Argentina) between the Late Jurassic-Early Cretaceous (Tithonian-Aptian). The study is based on the analysis of lithofacies, microfacies and fossil associations from thirty-six stratigraphic logs described in the Aysén Region of southern Chile (45°S). In the study area, the Coyhaique Group consists of a transgressive-regressive succession settled between the Valanginian-Aptian. Facies models of these rocks reveal mixed calcareous-volcaniclastic deposits, settled in volcanic apron- and carbonate ramp settings during the early marine transgression (Toqui Formation; Valanginian). These mixed deposits were covered by carbonaceous mudstone ("black shales") during the enhanced marine transgression (Katterfeld Formation; Valanginian-Hauterivian). Mudstone represents oxygen-poor shelf to slope marine settings; the onset of these lithologies may have been coeval to a humid global interval in the Valanginian, i.e., principally during the Weissert Event. A mid-Hauterivian high-productivity event in the basin is likely associated with coastal upwelling; it is here reported for the first time. Fine-grained deposits were gradually covered by heterolithic and sand-dominated sediments, which represent the progradation of prodelta and tidal-influenced delta systems during the regression (Apeleg Formation; Hauterivian-Aptian).

The geotectonic evolution of the Aysén-Río Mayo Basin was influenced by the break-up of the Gondwana supercontinent, and here to the onset of subduction of the western proto-South American margin and the formation of back-arc and intraplate extensional basins. Rifting-linked rhyolitic volcanism was widespread, partly superimposed to arc activity. For the period of basin development (Tithonian-Aptian) cool time-spans alternated with warm intervals, thus representing arid-humid cycles. The Aysén-Río Mayo Basin shares a similar depositional evolution with the Rocas Verdes Basin to the south. The basin was separated from the continental Cañadón Asfalto and Golfo San Jorge basins by tectonic highs.

Kurzfassung

Diese Dissertation stellt die bislang detaillierteste historische, stratigraphische und Paläoumwelt-Analyse des Aysén-Río Mayo Beckens und seiner sedimentären Füllung, der Coyhaique-Gruppe, dar. Das Aysén-Río Mayo Becken war ein Marginalbecken, das sich im südlichen Südamerika (heute Chile und Argentinien) zwischen dem spätesten Jura und der frühen Kreide (Tithonium-Aptium) entwickelte. Die vorliegende Studie basiert auf der Analyse von Lithofazies, Mikrofazies und fossilen Assoziationen aus sechsunddreißig sedimentären Bohr- und Oberflächenprofilen aus der Region Aysén im Süden Chiles (45°S). Im Studiengebiet besteht die Coyhaique-Gruppe aus einer transgressiv-regressiven Abfolge, die im Zeitraum vom Valanginium bis Aptium (Unterkreide) abgelagert wurde. Faziesmodelle dieser Gesteine belegen gemischte kalkhaltige-vulkanoklastische Abfolgen, die während der frühen marinen Transgression (Toqui-Formation; Valanginium) in vulkanisch-dominierten Apron- und Karbonat-Rampenumgebungen abgelagert wurden. Diese gemischten Ablagerungen wurden während der fortschreitenden marinen Transgression (Katterfeld-Formation; Valanginium-Hauterivium) von kalkhaltigen-organischen Tonsedimente („Schwarzen Schiefer“) überlagert. Diese Mergel und Tonsteine repräsentieren sauerstoffarme offene marine Schelf und Slope-Umgebungen; ihr Auftreten könnte mit einem globalen feuchten Zeitraum im Valanginium, dem Weissert Event, zusammenfallen. Ein hochproduktives Ereignis im mittleren Hauterivium, das mit Upwelling-Bedingungen in Verbindung steht, wird hier erstmals beschrieben. Die feinkörnigen Ablagerungen der Katterfeld Formation wurden mit graduellem Kontakt von heterolithischen und sandigen Sedimenten der Apeleg-Formation (Hauterivium-Aptium) überlagert, welche die Progradation von Prodelta- und Gezeiten-Deltasystemen während der Regression repräsentieren.

Während der Entwicklung des Beckens war die geotektonische Situation durch das Auseinanderbrechen des Gondwana-Superkontinents geprägt, welches sich in der Region durch den Beginn der Subduktion des westlichen proto-südamerikanischen Randes und die Bildung von Back-Arc- und extensionalen Intraplatten-Becken äußert. Rift-bedingter rhyolithischer Vulkanismus war weit verbreitet. Im Zeitraum der Beckenentwicklung wechselten sich warme und kühle Perioden miteinander ab und belegen arid-humide Zyklen. Das Aysén-Río Mayo Becken ähnelt in seiner Ablagerungsentwicklung dem Rocas-Verdes-Becken im Süden; auch wird eine

XIV

Verbindung mit dem Neuquén-Becken entlang des pazifischen Randes vermutet. Demgegenüber war das Becken wahrscheinlich von den kontinentalen Cañadón-Asfalto- und Golfo-San-Jorge-Becken durch tektonische Hochgebirgssysteme getrennt.

Contents

Acknowledgements	IX
Funding.....	XI
Abstract	XIII
Kurzfassung	XIV
Contents	XVI
State of the art.....	1
1. Introduction.....	2
1.1. Research presentation and objectives	2
1.1.1. General Objective.....	3
1.1.2. Specific objectives	3
1.2. Study area and fieldwork	4
1.3. Previous studies.....	5
1.4. Stratigraphic evolution of the Coyhaique Group.....	6
2. Materials and Methods	10
2.1. Stratigraphic logs.....	10
2.2. Rocks and fossils sampling	10
2.3. Thin sections, petrography, microphotography.....	11
2.4. Maps, figures, and illustrations	11
2.5. Classifications and guidelines.....	12
3. The Jurassic-Cretaceous World	13
3.1. Overall view of the Jurassic-Cretaceous (J-K) transition	13
3.1.1. Global Geotectonic Setting	13
3.1.2. Regional setting: J-K Magmatism.....	16
3.1.3. Regional setting: Extensional basins.....	17
3.2. J-K Global Paleoclimatic Setting.....	20
3.2.1. Late Jurassic.....	21
3.2.2. Early Cretaceous	23
3.2.3. J-K Regional Paleoclimatic Setting	25
3.3. Sea level changes	27
4. The Aysén-Río Mayo Basin.....	30
4.1. Onset and structure	30
4.2. Paleogeography of the Aysén-Río Mayo Basin.....	32
4.3. Geological setting, stratigraphy, and facies	34

4.3.1. Basement	36
4.3.2. Lago La Plata Group	36
4.3.3. Coyhaique Group	37
4.3.4. Basin Closure and Volcanism	39
4.4. Source areas and sedimentary provenance	40
5. Relationship between the Aysén-Río Mayo Basin (ARB) and coeval basins	44
5.1. Neuquén Basin (32°-40°S; Late Triassic - early Cenozoic)	45
5.2. Cañadón Asfalto Basin (42°-44°S; 68°-70°W; Early Jurassic - Cenozoic)	47
5.3. Golfo San Jorge Basin (44°-48°S; 66°-71°W; Early Jurassic - Quaternary)	48
5.4. Rocas Verdes Basin & Austral-Magallanes Basin (49°-56°S)	49
5.4.1. The area between the General Carrera and Argentino Lakes (46°-50°S)....	51
5.4.2. The area south of Lago Argentino (> 50°S)	53
5.5. Stratigraphic correlations of the Coyhaique Group	55
5.6. Gondwana connections	57
6. Summary and conclusions	61
7. References	65
8. Appendixes.....	85
8.1. Scientific Publication Nr. 1:	85
Facies and sequence stratigraphy of a mixed carbonate-volcaniclastic ramp in intra-arc settings: An example from the Toqui Formation (Lower Cretaceous), southern Chile (45°S).....	85
A B S T R A C T.....	87
1. Introduction.....	88
1.1. Geological setting.....	89
1.2. Material and methods.....	93
2. Lithofacies from the El Toqui Mining District.....	95
2.1. Pebbly lithofacies	95
2.2. Sandy lithofacies.....	97
2.3. Muddy lithofacies.....	101
2.4. Calcareous and mixed lithofacies.....	102
2.5. Igneous lithofacies.....	106
3. Facies associations and palaeoenvironmental analysis.....	106
3.1. Pebbly Volcaniclastic Facies Association (PVF)	106
3.2. Mixed Calcareous-Volcaniclastic Facies Association (CVF).....	106
3.3. Muddy Volcaniclastic Facies Association (MVF).....	107

3.4.	Sandy Volcaniclastic Facies Association (SVF)	107
3.5.	Muddy Pelagic Facies Association (MPF)	108
4.	Discussion	108
4.1.	Stratigraphy of the El Toqui Mine area.....	108
4.2.	Palaeogeography and volcanic source.....	110
4.3.	Sequence stratigraphy	110
5.	Conclusions	111
6.	Author credit.....	112
7.	Declaration of competing interest.....	112
8.	Acknowledgments.....	112
9.	Appendix A. Supplementary data.....	112
10.	References.....	112
8.2	Scientific Publication Nr. 2:	120
A “cool-water”, non-tropical, mixed volcaniclastic–carbonate ramp from the Early Cretaceous of southern Chile (45°40’S)		120
	Abstract	122
	Introduction	122
	Geological setting	124
	Materials and methods	125
	Facies analysis.....	127
	Petrography.....	127
	Microfacies.....	127
	Lithofacies.....	131
	Sedimentary logs and facies associations	137
	La Rosita Section (LRO)—gravelly, mixed inner ramp.....	137
	Muralla China Section (MCH)—wave- and storm-dominated inner-ramp.....	137
	Salto Río Pollux Section (SRP2)—mixed, distal mid-ramp	138
	Systematic paleontology	140
	<i>Archamphiroa jurassica</i>	140
	<i>Aetostreon spp.</i>	142
	Discussion.....	144
	Paleogeography.....	144
	Paleoenvironmental interpretation	144
	Regional comparison	146
	Conclusions	147

Declarations	148
References	148
8.3. Scientific Publication Nr. 3:	179
Deciphering the Early Cretaceous Patagonian “black shales”: paleoenvironmental analysis of the Katterfeld Formation, southern Chile (45°S)	179
Abstract	181
1. Introduction.....	182
1.1. Geological Setting.....	182
1.2. Local Stratigraphy.....	183
1.3. The Katterfeld Formation: Age and correlations.....	184
2. Material and Methods.....	184
2.1. Definitions and Guidelines	184
3. Facies associations: litho- and microfacies	185
3.1. Facies Association 1 (FA1): Distal volcanic apron hemipelagites	185
3.2. Facies Association 2 (FA2): Fossiliferous, mixed prodelta.....	186
3.3. Facies Association FA3: “Black shales” (shelf to slope hemipelagites) ..	188
3.4. Facies Association 3-B (FA3-B): Shelf hemipelagites with volcanic supply .	190
3.5. Facies Association 3-C (FA3-C): Outer-shelf pelagites, algal bloom pelagites.....	192
3.6. Facies Association 3-D (FA3-D): Shelf hemipelagites to offshore-transition	195
3.7. Facies Association 4 (FA4) – Prodelta.....	202
3.8. Facies Association 5 (FA5): Tide-influenced delta front.....	202
4. Discussion.....	203
4.1. Local Paleoenvironmental Evolution	203
4.2. Global Paleoenvironmental inferences.....	205
4.3. Sequence Stratigraphy	208
5. Conclusions	208
6. Acknowledgments.....	209
7. Funding.....	209
8. References.....	209
9. Supplementary Material	214
9.1. Sedimentary logs	214
9.2. Description of outcrops.....	240

9.3. Thin sections descriptions.....	276
--------------------------------------	-----

Figures and Illustrations

Figure 1. Location map.....	4
Figure 2. Comparison of geological Patagonian expeditions in the Aysén Region	6
Figure 3. Paleogeographic reconstruction of the supercontinent Gondwana and its domains (at ca. 200 Ma).....	14
Figure 4. Break-up of Gondwana between the Early Jurassic-Early Cretaceous	15
Figure 5: Detailed view of the Gondwana break-up during the development of the Aysén-Río Mayo Basin	15
Figure 6. Westwards migration patterns and location of the volcanic arc between the Triassic-Early Cretaceous.....	17
Figure 7. Evolution of extensional sedimentary basins in southernmost South America during the J-K transition	18
Figure 8. Tectonic setting during the onset of the Aysén-Río Mayo Basin.....	19
Figure 9. Paleoclimatic model showing symmetric climate zones during the Late Jurassic.....	22
Figure 10. Paleoclimate reconstruction for the Early Cretaceous (Berriasian)	24
Figure 11. Paleoclimate reconstruction for the Early Cretaceous (Aptian).....	25
Figure 12. Paleogeographic reconstruction for the Early Cretaceous, displaying the main marine connections/seaways between the South American basins and the Tethyan Realm.....	27
Figure 13. A) Long-term and short-term sea level curves for the Jurassic-Cretaceous transition (Tithonian-Berriasian) and Early Cretaceous	28

Figure 14. Inferred location, extension, and structure of the Aysén-Río Mayo Basin (ARB)	30
Figure 15. Paleotectonic setting of the Southern Andes during the J-K transition.	
Tectonic setting during the onset and main evolution of the Aysén-Río Mayo Basin	31
Figure 16. Location of the Río Mayo Basin (<i>sensu</i> Folguera & Iannizzotto, 2004) or “Río Mayo Embayment” (<i>sensu</i> Aguirre-Urreta & Ramos, 1981), showing its boundaries and structure.....	33
Figure 17. Stratigraphy of the Coyhaique Group. Rivas <i>et al.</i> (2021).....	35
Figure 18. Tectonic setting during the closure of the ARB.....	40
Figure 19. Main sediment source areas (yellow) of the Aysén-Río Mayo Basin in the area to the north of the General Carrera – Buenos Aires Lake	41
Figure 20. Inferred source areas, based on populations of detrital zircons, for the Aptian regressive sedimentary units exposed south of the General Carrera/Buenos Aires Lake	42
Figure 21. Location of the Aysén-Río Mayo Basin and the partly coeval adjacent basins	45
Figure 22. Tectonostratigraphic cross-section displaying the correlation of units south of the General Carrera/Buenos Aires Lake (46°28’S).....	53
Figure 23. North-to-south stratigraphic correlation of the J-K formations from Patagonia (45°-49°S; simplified).....	57
Figure 24. Paleobiographic distribution of steinmanellid bivalves in the Hauterivian, including their main realms and inferred connections	59

**PALAEOENVIRONMENTAL CHANGES
ACROSS THE JURASSIC-CRETACEOUS BOUNDARY
IN SOUTHERN CHILE (AYSÉN-RÍO MAYO BASIN):
A MULTI-STRATIGRAPHICAL APPROACH**

State of the art

1. Introduction

1.1. Research presentation and objectives

This dissertation presents a detailed historical, stratigraphical, and paleoenvironmental revision of the Aysén-Río Mayo Basin and its sedimentary fill, i.e., the Coyhaique Group (Tithonian-Aptian), in the Aysén Region from southern Chile (45°S). The Aysén-Río Mayo Basin was an intra-arc to back-arc, ensialic marginal basin which developed in southern South America (currently between ca. 43°-47°/49°S?) during the latest Late Jurassic and Early Cretaceous.

The structure of this dissertation includes:

- I. A presentation of research, objectives, and the study area (Chapter 1; sections 1.1; 1.2)
- II. A historical summary previous geological research addressing the Aysén-Río Mayo Basin (Chapter 1, section 1.3), including its stratigraphic scheme (Chapter 1, section 1.4).
- III. A description of materials and methods (Chapter 2).
- IV. A general review of the global geotectonic, paleogeographic and climatic context prevailing in the Jurassic-Cretaceous transition (Chapter 3).
- V. A detailed revision of the regional context and geological evolution of the Aysén-Río Mayo Basin (Chapter 4).
- VI. An analysis of the relationship between the Aysén-Río Mayo Basin and other coeval basins (Chapter 5).
- VII. Main results and conclusion of this work (Chapter 6), and the references cited in this presentation (Chapter 7).
- VIII. The principal publications derived from this investigation, published as peer-reviewed scientific articles (Chapters 8, Appendices).

- IX. The supplementary material used for this work, including the sedimentary logs, outcrop descriptions, and petrographic samples (Chapter 9).

1.1.1. General Objective

The principal objective of the present research is a revision and refined analysis of the geology and paleoenvironments of the Valanginian-Aptian marine sedimentary rocks conforming the Coyhaique Group (Tithonian-Aptian), exposed near the city of Coyhaique (45°34'S; 72°04'W), in the Aysén Region of southern Chile (45°S).

1.1.2. Specific objectives

- I. Bibliographical revision and stratigraphical updating of the Coyhaique Group and its conforming units, based on sources published in Chile, Argentina, and elsewhere.
- II. Development of sedimentary logs comprising the stratigraphic units of the Coyhaique Group as well as their formational contacts. Sampling of the main lithologies and their fossils.
- III. Meso- (outcrop scale) and microscopic description and characterization of the main lithologies, regarding their composition, sedimentary structures, fossil content, and classification.
- IV. Development of facies models for the lithological units conforming the Coyhaique Group, based on the sedimentological analysis of lithofacies and interpretation of depositional environments.
- V. Stratigraphic dating of sediment units using index fossils, lithostratigraphic correlations, and other available referential sources.
- VI. Incorporation of the Coyhaique Group in the regional and global paleoenvironmental context, and the proposal of paleoclimatic inferences, based on the lithology, depositional environments, and inferred ages.
- VII. Revision of the current stratigraphic classification; correlation of units conforming the Coyhaique Group in Chile and Argentina; correlation between the Aysén-Río Mayo Basin and the adjacent, coeval sedimentary basins.

1.2. Study area and fieldwork

The study area is located in the Coyhaique Province of the Aysén Region, in southern Chile (about 45°S; Fig. 1). In this region, thirty-four sedimentary surface sections and four mining drill cores were investigated. Outcrops were described from the area between the El Toqui Mine in the north (45°02'S, 71°56'W) and the Cerro La Virgen in the south (45°45'S, 71°59'W; Fig. 1). All surface outcrops are accessible via Route 7 ("Carretera Austral"), or by smaller rural roads detaching from the latter (e.g., Route X-421 to the El Toqui Mine).

Due to weather conditions and difficult logistics, fieldwork was carried out during summer seasons, i.e. in 2016 (January), 2017 (January), and 2018 (December). Access to drill cores was provided by the mining company Laguna Gold Ltd., owner of the El Toqui Mine at the time of sampling, but currently operated by the Sociedad Minera Pacífico del Sur.

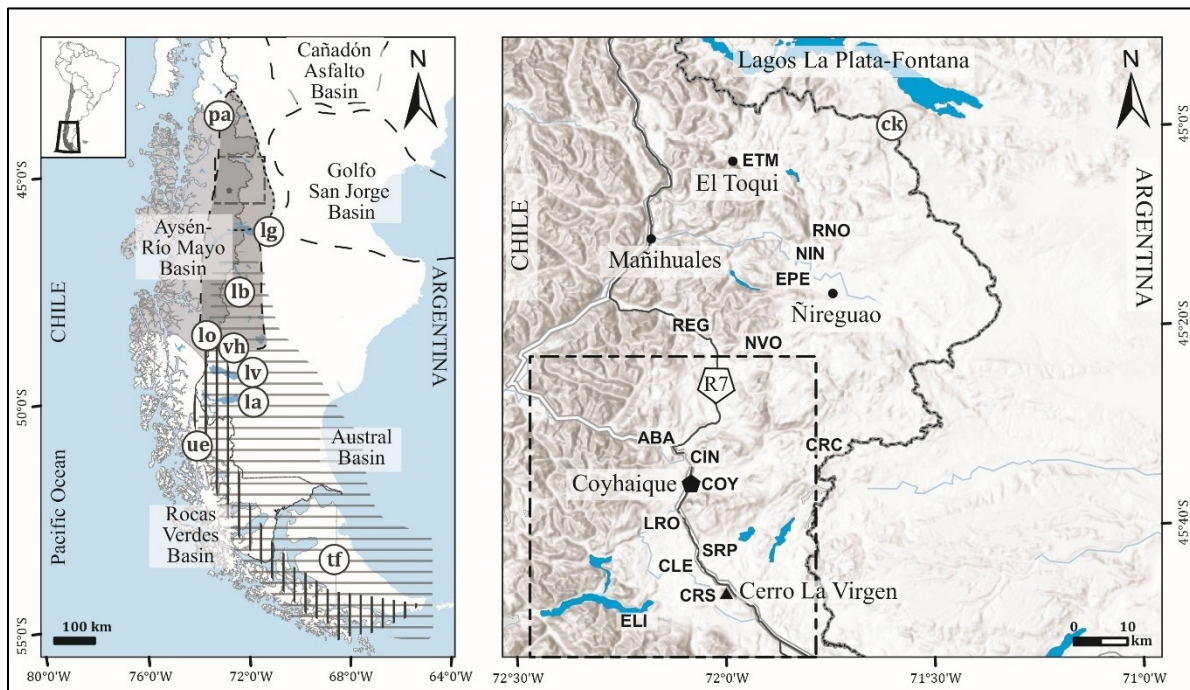


Figure 1. Location map. Left: Position of the Aysén-Río Mayo Basin in southern South America. Abbreviations: la = Lago Argentino; lb = Lago Belgrano; lg = Lago General Carrera / Buenos Aires; lo = Lago O'Higgins / San Martín; lv = Lago Viedma; pa = Palena; tf = Tierra del Fuego; ue = Última Esperanza; vh = Villa O'Higgins. Right: Regional map showing the localities studied in this work. A detailed description of this illustration can be found in Appendix 9.3. Abbreviations of localities might include several sedimentary logs; the exact position of sedimentary logs can be found as Supplementary Material (Chapter 10). Abbreviations: ABA = Alto Baguales (sections ABA, ABN, ABN2, ABN3, PRB); CIN = Cerro Cinchao (sections CCH1, CCH2,

Figure 1 (continuation). CDB; CLE = Cruce Lago Elizalde (section CLE); COY = Coyhaique (sections CMT, RCO); CRC = Cañadón Río Coyhaique (section CRC); CRS = Cañadón Río Simpson (sections CRS1, CRS2, CRS3, CRS4, CRS5, FSC); ELI = Lago Elizalde (section ELI2); EPE = Estero Pedregoso (section EPE); ETM = El Toqui Mine (sections ESA, ELC, ASN09, DCE19, PDT21, LCS453; see Rivas *et al.*, 2021); LRO = La Rosita (sections LRO, LRO2); MCH = Muralla China (section MCH); NIN = Ñireguao Norte (section NIN); NVO = Ñireguao-Villa Ortega (sections NVO1, NVO2); RNO = Río Norte (section RNO, RNO2); REG = Río Emperador Guillermo (section REG2); SPR = Salto Río Pólux (sections SRP1; SRP2). Figure modified from Rivas *et al.* (2025; submitted).

1.3. Previous studies

Outcrops of the Coyhaique Group are exposed in both Chile and Argentina (43°-47°S/49°S?; Fig. 1; see extended discussion in section 5.4), but their major surface extension is restricted to the Aysén Region and Chubut Province, respectively (Haller & Lapido, 1980; Haller *et al.*, 1981; Ramos, 1981). A brief historical summary regarding the study of the Coyhaique Group is presented here, with a focus on the published works addressing this unit in the Aysén Region of Southern Chile. In Argentina, the best exposures are located in the La Plata-Fontana Lakes area (Fig. 1). For an overview of the correlative Argentinian units, the reader is referred to Haller & Lapido (1980), Haller *et al.* (1981); Olivero (1982), and (Scasso, 1987; 1989).

In the Aysén Region, given its challenging geography and relatively late colonisation (Biblioteca Nacional de Chile, 2024; Fig. 2), the first formal geological descriptions of the Jurassic-Cretaceous sedimentary cover are from the first decades of the 20th century, followed by sporadic publications up to the early 1980s (see references below). These studies were carried out as part of geographical reconnaissance (Stephen, 1909; Quensel, 1911), during scientific expeditions (Fuenzalida & Latcham, 1935; Heim, 1940), or during exploration for oil and other natural resources (e.g., Ruiz, 1942; Duhart, 1960; Katz, 1961; IREN, 1967; Ortiz & Vergara, 1979; Wellmer *et al.*, 1983). A significant improvement in the geological knowledge of the region is seen during the “National Geological Mapping Program” carried out by the Chilean National Geological and Mining Service (“Servicio Nacional de Geología y Minería”; Espinosa & Fuenzalida, 1971; Niemeyer *et al.*, 1985; Suárez & De la Cruz, 1994a; De la Cruz *et al.*, 2003; Suárez *et al.*, 2007; Quiroz & Bruce, 2010).

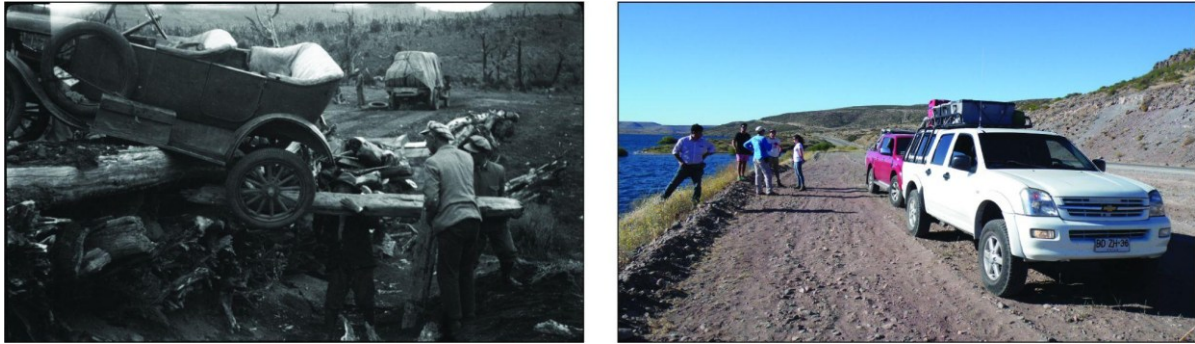


Figure 2. Comparison of geological Patagonian expeditions in the Aysén Region. Left: Macqueen expedition (1934) in the Aysén Region; note the challenging conditions and complex logistic to carry out former field investigations. In the background, burned logs as evidence of the forest fire intentionally spread during the colonization of the region (Bizama *et al.*, 2011). Right: Salazar expedition (2018) on the way to the Aysén Region, during the field work campaign carried out with a team of the Universidad del Desarrollo (Santiago, Chile), as part of the project FONDECYT de Iniciación 11140176.

In addition, other specific aspects of the Coyhaique Group have been investigated. These include its stratigraphy and sedimentology (e.g., Niemeyer *et al.*, 1985; Bell *et al.*, 1994; 1996; De la Cruz *et al.*, 1994; Suárez & De la Cruz, 1994; Gonzalez-Bonorino & Suárez, 1995; Suárez *et al.*, 1996; Suárez *et al.*, 2016; Késjar *et al.*, 2017; Rivas *et al.*, 2021), fossil content (e.g., Reyes, 1970; Covacevich *et al.*, 1994; Rubilar, 2000; Bell *et al.*, 2001; Bell, 2004; Aguirre-Urreta *et al.*, 2006; Pérez-Barría *et al.*, 2021; Poblete-Huanca *et al.*, 2021), the interaction of sedimentation and coeval volcanism (De la Cruz *et al.*, 1994; Demant *et al.*, 2010; Pankhurst *et al.*, 2003; Suárez *et al.*, 2005, 2009, 2023), mineralization (Wellmer *et al.*, 1983; Wellmer & Reeve, 1990; Bussey *et al.*, 2010a; 2010b), and basin evolution (Cecioni & Charrier, 1974; Skarmeta, 1976; Skarmeta & Charrier, 1976; Bell *et al.*, 1994; Suárez *et al.*, 2010a). The Coyhaique Group has also been addressed in some Chilean bachelor- and postgraduate theses (e.g., Skarmeta, 1974; Niemeyer, 1975; Townsend, 1998; Bruce, 2001; Ormazábal, 2018; Mimica, 2020; Aldridge, 2020; Riveros, 2020; Álvarez-Mena, 2024).

1.4. Stratigraphic evolution of the Coyhaique Group

In the Aysén Region, the first studies addressing the Upper Jurassic-Lower Cretaceous marine successions of the Aysén-Río Mayo Basin, depicted these sediments as a single stratigraphic unit (Table 1). Subsequently, in the 1960s, the sediment succession was formally defined as the Coyhaique Formation, with its type locality placed “between the homonymous city and the valley of the Baguales River” (IREN,

1967). There, some authors differentiated at least two facies (“lower muddy facies” vs “upper sandy facies”; Duhart, 1960; IREN, 1967; Espinosa & Fuenzalida, 1971), or a muddy-to-sandy coarsening-upwards trend (Skarmeta, 1974, 1976; Niemeyer *et al.*, 1985; Table 1). The formational name (Coyhaique Formation) was provisionally changed to Rincón del Zorro Formation (Espinosa & Fuenzalida, 1971), defined in the valley of the Coyhaique River, about 30 km to the east of Coyhaique (“Coyhaique Alto” area); however, given its widespread use, the original name was preferred by subsequent authors (e.g. Skarmeta, 1974, 1976). In the early 1980s, the Coyhaique Formation was promoted to group status in Argentina, comprising all Late Jurassic - Early Cretaceous marine sedimentary units of the Aysén-Río Mayo Basin (Haller & Lapido, 1980; Ramos, 1981).

In Chile, the current stratigraphic nomenclature was proposed by Suárez & De la Cruz (1994a; b; also 1992; 1993; *in* Gonzalez-Bonorino & Suárez, 1995). These authors established the correlation between the Chilean and Argentinian outcrops, adopting the formational nomenclature in use in Argentina, depicted as prioritarian (Ploszkiewicz & Ramos, 1977; Haller & Lapido, 1980; Ramos, 1981). Following the Argentinian scheme, the Coyhaique Formation was promoted to group, and its lower (muddy) and upper (sandy) informal members were assigned as Katterfeld- and Apeleg Formations, respectively. Additionally, Suárez & De la Cruz (1994a; b) defined a new unit (i.e., Toqui Formation) including mixed, calcareous- and volcanoclastic deposits, usually found either overlying the volcanic Ibáñez Formation, or underlying the Katterfeld Formation, as already reported in previous works (Katz, 1961; Reyes, 1970; see Table 1). These basal sedimentary deposits were considered by some authors to represent sedimentary intercalations within the uppermost volcanic strata of the underlying Lago La Plata Group (Charrier & Covacevich, 1978; Haller & Lapido, 1980; Olivero, 1987; Covacevich *et al.*, 1994); however, current studies depict the marine deposits in an upper stratigraphic position, but being locally interbedded with the volcanic succession (Scasso, 1989; Suárez & De la Cruz, 1994a; b; Suárez *et al.*, 2009; 2015). A historical summary and a new stratigraphical proposal for these basal mixed rocks, including its correlation with the Argentinian units, is now documented by Rivas *et al.* (2021; see Appendix 8.1).

Table 1. Evolution (summary) of the stratigraphic nomenclature for the Aysén-Río Mayo Basin (ARB) in the study area (Aysén Region). Based on Skarmeta (1974; 1976) and Niemeyer *et al.* (1985). Symbols: regular text = informal or generalised formational names (shallow-unspecific description, without a type section nor locality); **bold text** = formally defined units.

ARB STRATIGRAPHIC NOMENCLATURE (AYSÉN REGION)	AUTOR (YEAR)
"Schiefer Formation"	Quensel, 1911
"Arcillas negras de Coyhaique"	Fuenzalida & Latcham, 1935
Black unfossiliferous shale of Coyhaique	Heim, 1940
"Sedimentos marinos del Cretácico"	Ruiz, 1942
"Sedimentos Titonianos-Neocomianos"	Duhart, 1960
<ul style="list-style-type: none"> - "Serie de lutitas oscuras titonianas-neocomianas" - "Cuerpo de areniscas arcillosas gris-verdosas" 	
"Coyhaique-Schichten" (Coyhaique Schists)	Wetzel, 1960
"Formación Coyhaique" <ul style="list-style-type: none"> - "miembro inferior" (lutites) - "miembro superior" (sandstones) 	IREN, 1967 (Lahsen <i>et al.</i>)
"Pizarras negras de Coyhaique" <ul style="list-style-type: none"> - "miembro arenoso inferior" - "miembro superior de lutitas" 	Reyes, 1970
"Formación Rincón del Zorro" <ul style="list-style-type: none"> - "facies de lutitas" - "facies de areniscas" 	Espinosa & Fuenzalida, 1971
"Formación Coyhaique" <ul style="list-style-type: none"> - "miembro inferior de lutitas"¹ - "miembro superior arenoso"¹ 	Skarmeta (1974, 1976) Cecioni & Charrier (1974) ¹ Niemeyer (1975); Niemeyer <i>et al.</i> (1985)
Coyhaique Formation <ul style="list-style-type: none"> - "Lower Coyhaique Formation" (sedimentary) - "Upper Coyhaique Formation" (volcano-sedimentary) 	Wellmer <i>et al.</i> (1983); Wellmer & Reeve (1990)

Table 1. Stratigraphy of the Coyhaique Group (Continuation).

Coyhaique Group (Argentina)² <ul style="list-style-type: none"> - Cotidiano Formation + “Arroyo Pedregoso Beds” ³ - Tres Lagunas Formation + “Arroyo Blanco Beds” + “Arroyo de la Mina Beds” ^{3,4} - Katterfeld Formation - Apeleg Formation 	Haller & Lapido (1980) ² Ramos (1981) ³ Masiuk & Nakayama (1978) ⁴
Coyhaique Group (Chile, as referred to in Argentina) <ul style="list-style-type: none"> - Toqui Formation⁵ <ul style="list-style-type: none"> - “Miembro Calcáreo” (Calcareous Member) - “Miembro Arenoso” (Sandy Member) - “Miembro Piroclástico” (Pyroclastic Member) - Katterfeld Formation - Apeleg Formation 	Suárez & De la Cruz (1994a) ⁵ Suárez <i>et al.</i> (1996) and onwards
Coyhaique Group <ul style="list-style-type: none"> - Toqui Formation* <ul style="list-style-type: none"> - Manto Member (calcareous)* - San Antonio Member (volcaniclastic)* - Katterfeld Formation - Apeleg Formation 	* Rivas <i>et al.</i> (2021; after Suárez & De la Cruz, 1994a)

2. Materials and Methods

2.1. Stratigraphic logs

In the field, thirty-six sedimentary and volcano-sedimentary sections were measured, described and named after their closest geographical locality (e.g., section ELC: “Estero La Concordia”). Thickness of each section was measured using a Brunton compass mounted to a Jacob’s staff or, alternatively, with a measuring rod. The thickness of singular sections varies between 4.1 and 365.2 m (logs CRS2 and PDT21, respectively), with a total measured thickness of ca. 2.327 m. From the outcrops, 14 stratigraphic logs were directly used for the publications here annexed (see Chapter 8 – Appendixes). Other outcrops, which were not published yet, have served as context regarding sampled fossils, whereas even others were used as a reference or for comparison with better exposures, and some of them will be presented in future studies (section 9.1). The description of sedimentary logs already published is presented in section 9.2.

2.2. Rocks and fossils sampling

Rock samples were taken from every principal lithology. They are here specified with their respective log (abbreviation) and stratigraphic position above the base (e.g., ABA-1.0 = section “Alto Baguales”, sample taken at 1.0 m above the base). For fossils, the suffix (F) was added, sometimes together with the suffix (R) for specimens detached from the outcrop (*ex-situ* or “rodado”). In case of relatively thick, homogeneous successions (e.g., black mudstone), an equidistant sampling was preferred, taking samples each 3-5 m of section, avoiding highly weathered or brittle horizons, when it was possible. Index layers as well as strata with particular structures (e.g., concretions, fossils) were also sampled. A total of 284 rock samples and 141 fossils were collected, although these numbers may vary after preparation, as some specimens were badly preserved or several of them were occasionally included in a single fossiliferous sample.

Fossils were cleaned and prepared in the facilities of the Geology School (“Salazar’s Lab”), at the Faculty of Engineering of the Universidad del Desarrollo in Santiago, Chile.

Macrofossils include marine invertebrates, dominated by cephalopods (ammonites, belemnites, few nautilids) and bivalves (mostly oysters), and scarce gastropods, echinoderms, and corals. Plant remains (e.g. imprints, coal lenses) are rare and marine vertebrate only comprise a single ichthyosaurid? vertebra and two small fish teeth. Rocks and fossils sampled were initially hosted in the Faculty of Engineering of the Universidad del Desarrollo (2017-2020), but they are currently deposited at the School of Geology of the Universidad Mayor in Santiago, Chile. They will be housed in the collection of the Regional Museum of Aysén in Coyhaique, Chile.

2.3. Thin sections, petrography, microphotography

Petrological, microfacial and sedimentary provenance analysis comprised the analysis of 104 standard thin sections (26 mm × 46 mm, 30 µm thick); these were examined in a Leica DMLP petrographic microscope, with an Olympus camera mounted for microphotographs (model Pen Lite 7). Thin sections were prepared by Ilona Fin, Oliver Wienand, and Joachim Fillauer, in the laboratories of the Institute of Earth Sciences of the Universität Heidelberg. Modal composition of sandstones was analysed after point-counting, carried out with a mobile stage (Stepping Stage™) and the software PETROG Lite (Conwy Valley Systems Limited). SEM-imagery of microfossils was carried out in a ZEISS WITec RISE EVO MA15 electron microscope, in the laboratories of the Institute of Earth Sciences of the Universität Heidelberg. The preparation of samples for SEM-imagery followed the methodology of Munnecke *et al.* (2000). A brief description of the thin sections analysed here is presented in section 9.3.

2.4. Maps, figures, and illustrations

Digital and physical geological cartography as well as basin geological information was obtained from the official publications of the “Servicio Nacional de Geología y Minería” (SERNAGEOMIN, Chile) and from the “Servicio Geológico Minero

Argentino” (SEGEMAR, Argentina). Digital elevation models (“DEMs”) of the study area were downloaded from the USGS EarthExplorer website (<https://earthexplorer.usgs.gov>). Georeferencing of geological maps, visualisation of elevation models, and creation of maps were carried out in ArcMap (ESRI) and later improved in Adobe Illustrator CS6. The latter was also used for the digitalization of the sedimentary logs, and to produce vectorial illustrations. Minor corrections of pictures, including colour-enhancement and creation of panoramic images were done with Adobe Photoshop CS6.

2.5. Classifications and guidelines

Stratigraphic concepts used here follow the guidelines of The North American Commission on Stratigraphic Nomenclature (2005), while chronostratigraphic categories are based on the International Chronostratigraphic Chart v2019/05, v2022/10, and v2024/12 (emend. from Cohen *et al.*, 2013; for Appendixes 9.1, 9.2, and 9.3, respectively). Modal classification of sandstones is after Garzanti (2019), while, for calcareous rocks, “Folk’s Revised Classification of Limestones” was preferred (Wright, 1992; Flügel, 2004; Flügel & Munnecke, 2010). Mixed calcareous-volcaniclastic sediments were classified following Mount (1985), as well as a non-genetic classification for volcaniclastic rocks (Fisher, 1961, 1966; Cas & Wright, 1987; Fisher & Schmincke, 1994).

Description and characterization of sediments is based on the Udden-Wentworth scale for grain-size (Blair & McPherson, 1999); Folk *et al.* (1970) for textural classification, and Campbell (1967) for bedding properties.

3. The Jurassic-Cretaceous World

This chapter presents a summary of the global and regional geotectonic, magmatic, and paleoclimatic conditions prevailing during the Jurassic-Cretaceous boundary. These will serve as a frame of reference to understand the evolution of the Aysén-Río Mayo Basin.

3.1. Overall view of the Jurassic-Cretaceous (J-K) transition

The Jurassic - Cretaceous transition is at present the last Phanerozoic system boundary without an accepted global definition (e.g., Gradstein, 2012; Wimbledon, 2017; Granier, 2020). This is due to faunal and floral provincialism, i.e., the distribution of organisms confined to particular geographical areas or “provinces”, separated by physical barriers (British Geological Survey, 2022), as well as absence of significant global events, faunal turnovers, or interregional markers (e.g., Remane, 1991; Rogov *et al.*, 2010; Gale *et al.*, 2020; Hesselbo *et al.*, 2020).

Globally, the J-K transition is placed during an interval of substantial tectonic plate reorganisation following the break-up of the supercontinent Pangea, which initiated during the Early Jurassic (ca. 200 Ma; Seton *et al.*, 2012; Müller *et al.*, 2016). This rifting phase caused the division of Pangea into two smaller supercontinents: Laurasia, comprising North America, Europe and Asia, and located in the northern hemisphere; and Gondwana, conformed by South America, Africa, Madagascar, Antarctica, Arabia, and Australia, and situated in the south (Fig. 3).

3.1.1. Global Geotectonic Setting

In the southern hemisphere, the geotectonic setting during the Jurassic-Cretaceous transition is controlled by the break-up of the Gondwana supercontinent. This provoked a westward relative movement of the proto-South American plate, and

the onset of subduction at its western continental margin in the Early Jurassic (Mpodozis & Ramos, 2008).

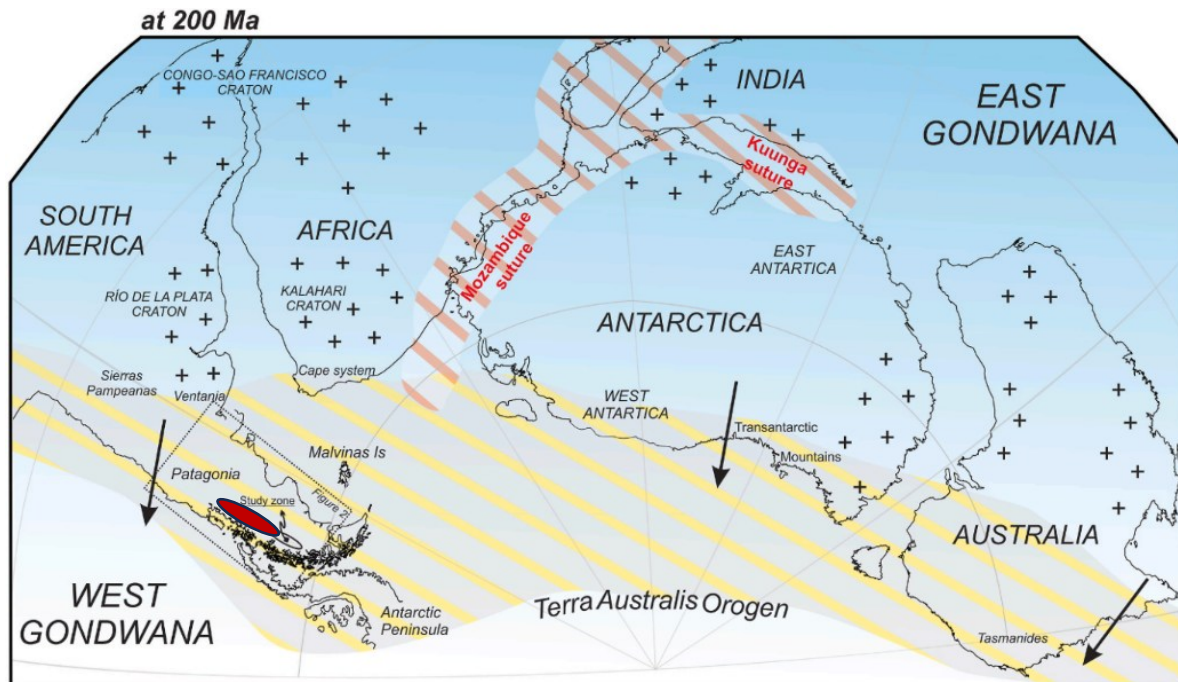


Figure 3. Paleogeographic reconstruction of the supercontinent Gondwana and its domains (at ca. 200 Ma). This figure highlights the formation of a Palaeozoic-Late Triassic orogen before the supercontinent break-up; black arrows indicate the younging direction of the trench-forearc system. Note the inferred position of the continents and the location of the Antarctic Peninsula at the western margin of West Gondwana, attached to Patagonia (left-lower corner). Modified from Suárez *et al.* (2021; adapted from Suárez *et al.*, 2019). The approximate location of the Aysén-Río Mayo Basin is indicated with a red ellipsoid.

The break-up of Gondwana has usually been regarded as triggered by the onset of the Karoo-Ferrar Large Igneous Province (LIP; main activity between ca. 184-179 Ma; Jourdan *et al.*, 2005; Fig. 4), provoking the separation of West- and East Gondwana and the opening of the West Indian Ocean (Segev, 2002; Frizon De Lamotte *et al.*, 2015). However, given the hiatus between the Karoo magmatism and the onset of seafloor-spreading in the Southern Ocean (at ca. 160 Ma between Africa and Antarctica; Jokat *et al.*, 2003), the break-up might have been triggered by divergent mantle flows, instead (Jokat *et al.*, 2003; König & Jokat, 2006). The fragmentation was completed with the separation of South America and Africa in the mid Early Cretaceous, which is linked to the emplacement of the Paraná-Etendeka LIP (main activity at 133 Ma; Segev, 2002; Frizon De Lamotte *et al.*, 2015; Figs. 4, 5).

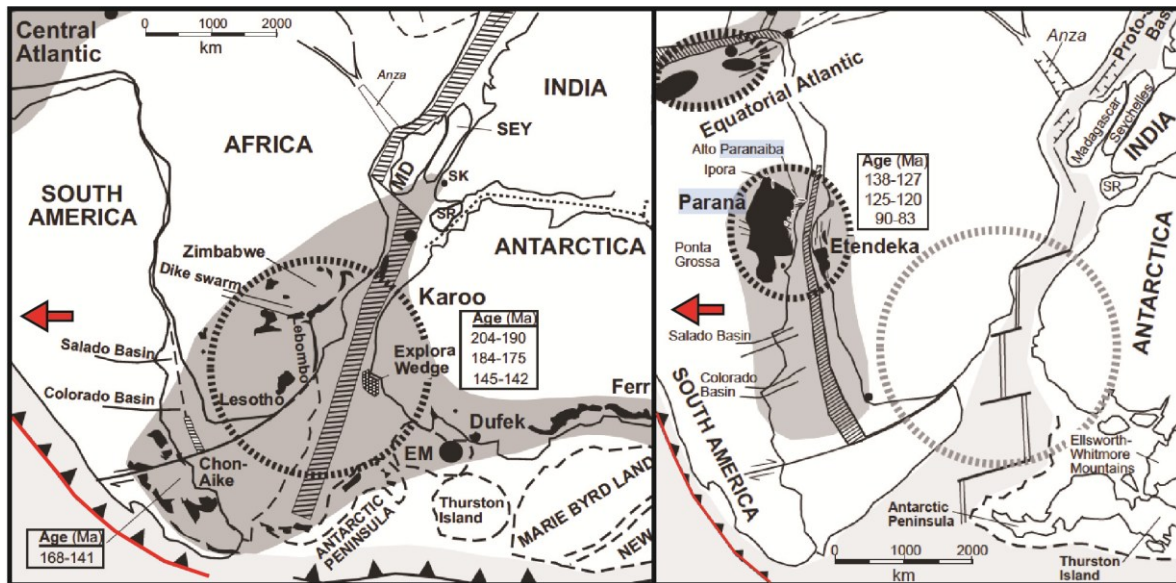


Figure 4. Break-up of Gondwana between the Early Jurassic-Early Cretaceous. Left (Early Jurassic): During the effusion of the Karoo-Ferrar Large Igneous Province (LIP); Right (Early Cretaceous): During the effusion of the Paraná-Etendeka LIP between proto-South America and Antarctica. Note the westward displacement of proto-South America (red arrow), and the onset of a subduction system at its western margin (red line). Modified from Segev (2002). Note: according to the current paleotectonic models, the position of the Antarctic Peninsula may not be correct in this figure (see Figs. 3 and 5).

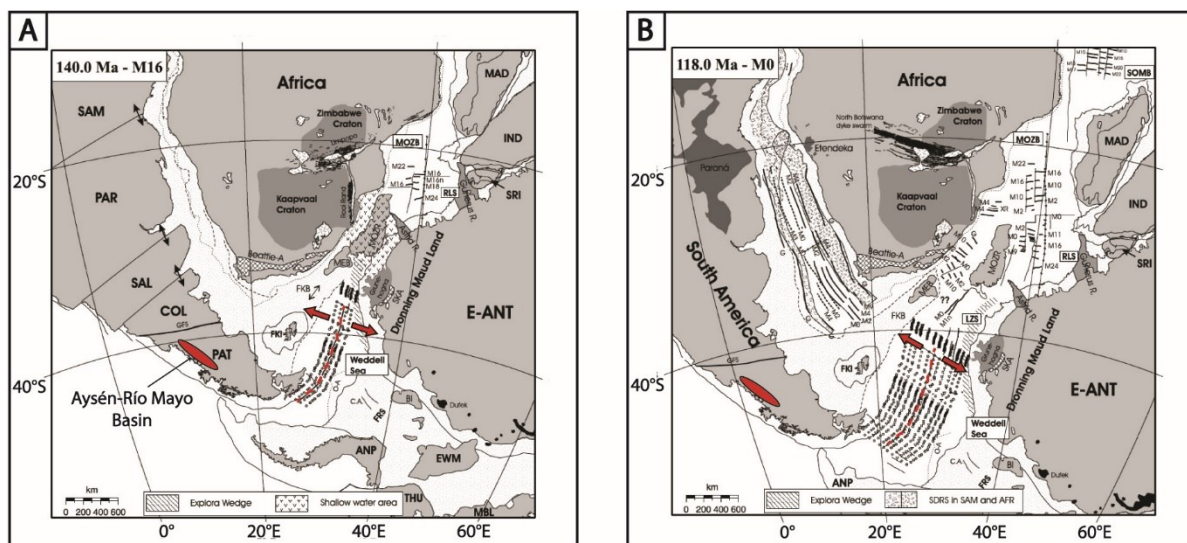


Figure 5: Detailed view of the Gondwana break-up during the development of the Aysén-Río Mayo Basin (red ellipsoid). Figure shows the location of main rifting zones, and it highlights the opening of the Weddell Sea between Antarctica and South America/Africa (red arrows). The possible influence of the Weddell Sea rifting in the intracontinental Patagonian extension is discussed in Section 5.4 (Rocas Verdes Basin). Terrains mentioned in text: ANT = Antarctica; ANP = Antarctic Peninsula; FKI = Falkland Islands; MOZB = Mozambique Basin; PAT = Patagonia. Modified from König & Jokat (2006).

3.1.2. Regional setting: J-K Magmatism

In the course of the break-up of Gondwana, Mesozoic subduction at the paleo-Pacific margin was initiated coeval to rifting in the southernmost continental area (e.g., Riccardi, 1988; Uliana *et al.*, 1989; Franzese *et al.*, 2003). Arc magmatism is reflected by the emplacement of the Subcordilleran Batholith, active during the Early Jurassic (187–178 Ma) along the mid-portion of Central Patagonia (ca. 41°–44°S; Rapela *et al.*, 2005; Mpodozis & Ramos, 2008; Fig. 6). At its eastern margin, this volcanic arc is associated with a retro-arc foreland- to intra-arc basin (“Chubut Basin” *sensu* Suarez & Marquez, 2007).

The emplacement of the Subcordilleran Batholith is concurrent with the effusion of large-scale intraplate silicic magmatism conforming the Chon Aike Large Igneous Province (LIP); this magmatism spread in Patagonia and in the eastern Antarctic Peninsula during the Jurassic (185–155 Ma; Pankhurst *et al.*, 1998; 2003; Rapela *et al.*, 2005; Jordan *et al.*, 2020; Fig. 6). Note that the paleogeographic position of the Antarctic Peninsula has been modelled as attached to the southwestern margin of Gondwana until the Early Cretaceous (Storey *et al.*, 1996; Hervé *et al.*, 2006; Figs., 3, 5). The Chon Aike rhyolitic volcanism is interpreted to reflect crustal anatexis after lithospheric thinning (Pankhurst & Rapela, 1995; Pankhurst *et al.*, 2000; 2003). Its first stages were likely influenced by heat anomalies following the Karoo-Ferrar LIP volcanism (Pankhurst *et al.*, 1998; Rapela *et al.*, 2005; Mpodozis & Ramos, 2008; Jordan *et al.*, 2020), though its main cause was inherited extension during “continental drift” of proto-South America, following the Pangea supercontinent break-up (Pankhurst *et al.*, 1998; 2000; Rapela *et al.*, 2005; Fig. 4).

During the Mid-Late Jurassic, the volcanic arc migrated westwards, as indicated by the emplacement of the Patagonian Batholith at the Pacific continental margin (e.g., Haller & Lapido, 1980; Pankhurst *et al.*, 1999; Suárez & De la Cruz, 2001; Hervé *et al.*, 2007; Fig. 6). This important intrusion currently displays an exposure in southern South America of more than 1500 km, between ca. 40°–56°S (Rolando *et al.*, 2002; Mpodozis & Ramos, 2008; Echaurren *et al.*, 2017). This westward migration has been interpreted as caused by a retreating trench/slab (i.e., moving away from the continental mass) with

an increasing dip angle (i.e., “slab rollback”; Rapela *et al.*, 2005; Echaurren *et al.*, 2016; 2017; Fig. 7).

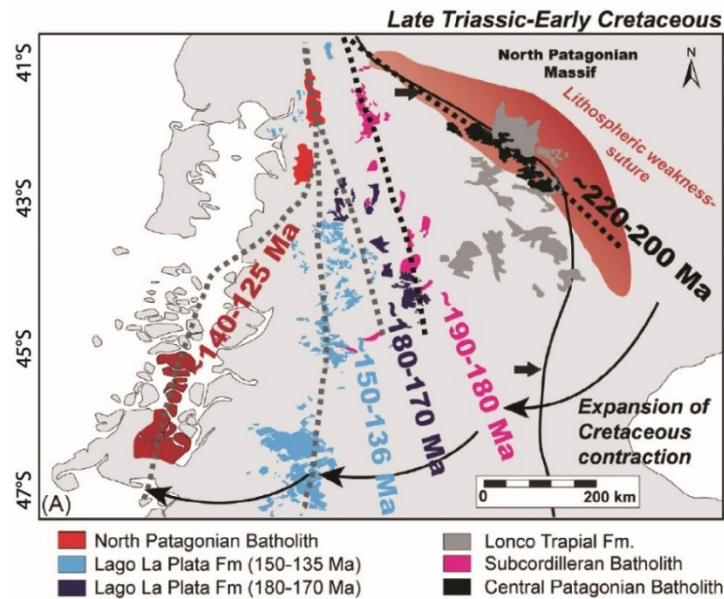


Figure 6. Westwards migration patterns and location of the volcanic arc between the Triassic-Early Cretaceous. The marine sedimentation in the Aysén-Río Mayo Basin was coeval to the deposition of the Lago La Plata Group (light grey; intra-arc/back-arc position), and corresponds to the intrusion of the Patagonian Batholith (red; back-arc position). Figure from Echaurren *et al.* (2019).

The Patagonian Batholith is mainly conformed by metaluminous and calc-alkaline plutonic rocks (Pankhurst *et al.*, 1999; 2003), dominated by type-I granitic suites (e.g., Suárez *et al.*, 2005, 2010a; Echaurren *et al.*, 2016), with subordinate gabbroic rocks (Bruce, 2001; Pankhurst *et al.*, 1999; Hervé *et al.*, 2007). This magmatism was bimodal and relatively continuous between the Late Jurassic and the Late Cretaceous (Suárez *et al.*, 2015, 2023; Fig. 6), showing a main magmatic pulse during the late Early Cretaceous (Echaurren *et al.*, 2016), followed by volcanic gap during the Paleocene, an Eocene-Miocene reactivation (Suárez *et al.*, 2015), and only sporadic activity in the Neogene (Pankhurst *et al.*, 1999; Hervé *et al.*, 2007).

3.1.3. Regional setting: Extensional basins

In central- and southern Patagonia (south of 40°S), extensional tectonics triggered the development of rift basins during the J-K transition, and intraplate rhyolitic volcanism of the Chon Aike LIP (see 3.1.2 above) (e.g., Cañadón Asfalto Basin, San Jorge Basin; Riccardi, 1988; Scasso, 1989; Uliana *et al.*, 1989; Franzese *et al.*, 2003; Fig. 7). Nevertheless, rifting at the western continental margin is regarded as caused by back-

extension focused on the eastern side of the coeval volcanic arc, i.e., the Patagonian Batholith (Bartholomew & Tarney, 1984; Depine & Ramos, 2004; Echaurren *et al.*, 2016, 2017). For example, in the Aysén-Río Mayo Basin (43°-49°S *sensu* Suárez *et al.*, 2010a), back-arc extension has been linked to a steep subducting slab (“Marianas type” *sensu* Depine & Ramos, 2004), caused by “slab rollback” (Echaurren *et al.*, 2016, 2017; see below). Alternatively, some authors have considered this episode of back-arc extension as rift-related (Suárez *et al.*, 2010a).

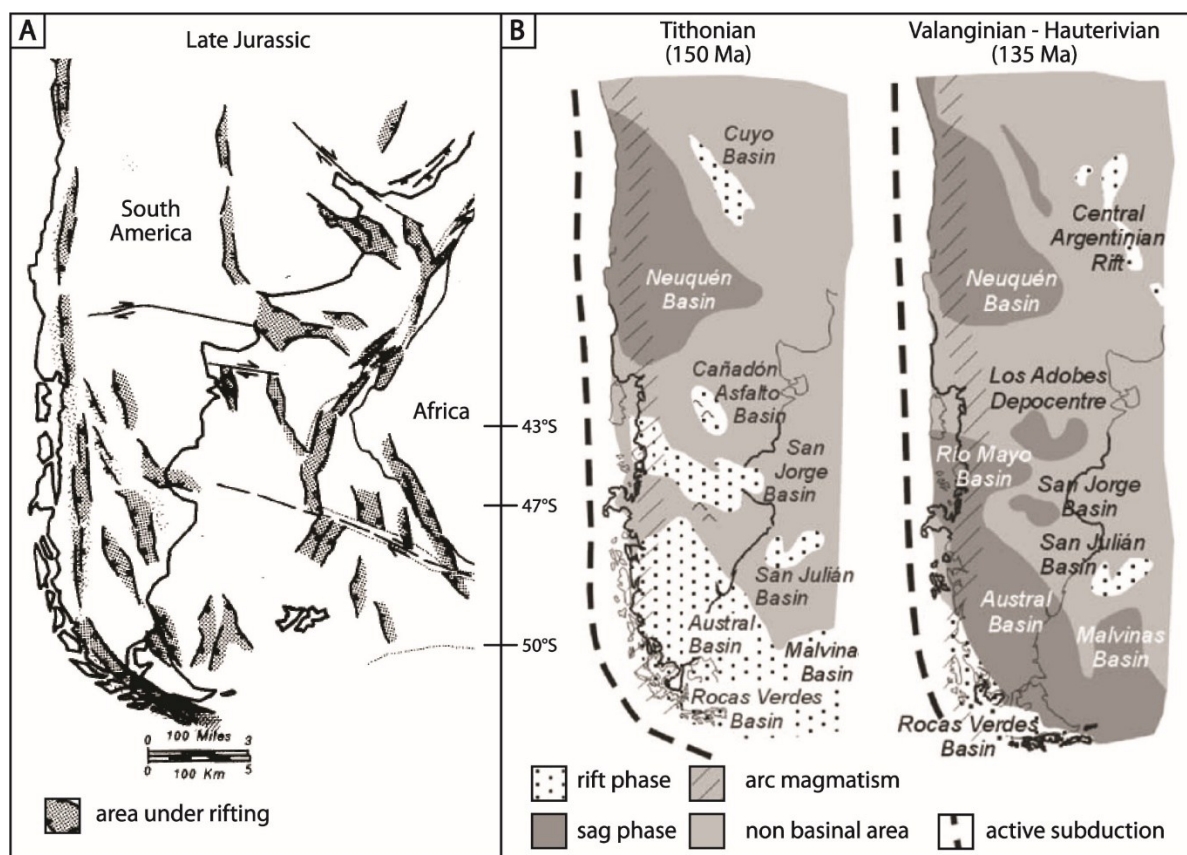


Figure 7. Evolution of extensional sedimentary basins in southernmost South America (continental outline) during the J-K transition. A) Areas of extension in the Late Jurassic (dark-grey coloured) of Uliana *et al.* (1989). B) Outlines of extensional basins for the latest Jurassic and Early Cretaceous *sensu* folguer. See discussion in Chapter 5 for more information regarding these basins and their relationship with the ARB. Note the inferred connection between the southernmost basins (ARB & AMB) during the Valanginian-Hauterivian. In B) the ARB is referred to as “Río Mayo Basin” (Argentinian nomenclature); in addition, the authors depict both the Rocas Verdes and the Austral/Magallanes basins as coeval. Latitude is approximate.

Slab rollback, i.e. the rotation and steepening of a subducting slab through time, and its subsequent “trench-pull force” over the overriding plate, is considered to be the main variable causing back-arc extension in subduction systems (Nakakuki & Mura, 2013; Niu, 2018; Fig. 8). Back-arc extension can be incomplete, with the formation of

ensialic marginal basins developed above rifted continental crust; or it is complete, causing the disruption and separation of the continental lithosphere, with the formation of an island arc separated from the continent by oceanic crust (Tarney *et al.*, 1981). In the Aysén-Río Mayo Basin, given its development directly above the metamorphic basement (see section 4.3), and the absence of evidence of oceanic crustal lithosphere, back-arc extension was most likely incomplete, thus depicting an ensialic marginal basin (*sensu* Tarney *et al.*, 1981; Fig. 8).

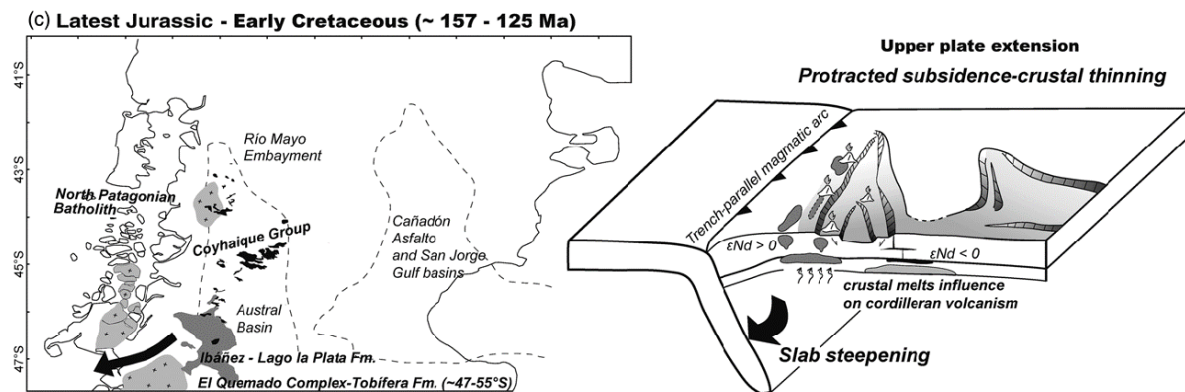


Figure 8. Tectonic setting during the onset of the Aysén-Río Mayo Basin. Left: Map displaying the outline of the main J-K extensional basins between 43°-47°S (see discussion in section 5.3); it also shows the westward migration of the volcanic arc and its emplacement in the western continental margin. Right: Cross section displaying the intra-arc/back-arc extension, interpreted as caused by a steepening subducting slab ("slab-rollback"). Figure from Echaurren *et al.* (2017).

South of ca. 50°S, the extensional regime was different, leading to seafloor-spreading in a deep marginal basin known as "Rocas Verdes Marginal Basin" (Dalziel *et al.*, 1974; Dalziel, 1981; see discussion in section 5.4). This led Suárez *et al.* (2010a) to propose the existence of a "trench-to-trench" transcurrent fault separating both segments north and south of ca. 49°-50°S. The Rocas Verdes Basin (RVB) has been interpreted to have a back-arc origin (Dalziel, 1981), though its genesis is still under debate, since some authors regard it as a "failed-arm" of the Weddell Sea (Stern & De Wit, 2003; Mpodozis, 2007). The onset of sea-floor spreading has been dated to about 160 Ma in the Weddell Sea, coeval to the development of the RVB (Ghidella *et al.*, 2002). Nevertheless, current models set this value to about 147 Ma (König & Jokat, 2006), i.e. after the emplacement of the oldest ophiolitic complexes in the RVB (see section 5.4).

3.2. J-K Global Paleoclimatic Setting

The Mesozoic has long been interpreted as a period of greenhouse climate, characterised by elevated atmospheric CO₂ and high, mean global surface temperatures (e.g., Berner & Kothavala, 2001; Kauffman & Johnson, 2009; Price, 2009). Overall, long-term greenhouse pulses are linked to sea-floor spreading, provoking high mean sea-water levels after ocean water displacement (Retallack, 2009; see Section 3.3); while transient greenhouse periods may be explained by several causes, e.g. extensive volcanic activity, impact events, or destabilisation of methane hydrates (Retallack, 2009; Dera *et al.*, 2011). Global evidence points to a Jurassic and Cretaceous climate substantially hotter than today (Price, 2009; Retallack, 2009). This has been inferred from the latitudinal distribution of plants and animals (Rees *et al.*, 2000, 2004; Sellwood & Valdes, 2008; Benson *et al.*, 2012), climate-sensitive sediments (e.g., paleosols; carbon vs evaporites in humid and arid settings, respectively; Rees *et al.*, 2004), high global values of atmospheric carbon dioxide (Berner & Kothavala, 2001), and lower oxygen isotopic values (Sellwood & Valdes, 2008).

An alternative hypothesis depicts a Jurassic-Cretaceous paleoclimate characterised by long-termed warm “greenhouse” events, alternating with short-termed “cold snaps” (Price, 1999; Donnadieu *et al.*, 2011). Globally, the most remarkable J-K cool-snaps are depicted as occurring during the late Tithonian, the mid-late Valanginian, and across the Aptian-Albian boundary (Price, 1999; Cavalheiro *et al.*, 2021), though these have been questioned by some authors (Föllmi, 2012; Jenkyns *et al.*, 2012). These Mid Jurassic-Early Cretaceous “cool-modes” are supported by tentative glacial deposits (Frakes *et al.*, 1992), by the presence of glendonite (Price, 1999; Rogov *et al.*, 2021), by elevated oxygen isotopic values of fossil shells (Veizer *et al.*, 2000; Dera *et al.*, 2011; Korte *et al.*, 2015), by carbon-isotopic excursions and TEX₈₆ palaeothermometry (Cavalheiro *et al.*, 2021), and by computer-generated General Circulation Models or “GCM” (Price, 1999; Sellwood & Valdes, 2008).

Criticism to J-K paleoclimate models addresses the equivocal evidence for some glacial deposits (Price, 1999; 2009; Sellwood & Valdes, 2008; Jenkyns *et al.*, 2012), and the fact that glendonites may not necessarily reflect low sea-surface temperatures or sub-freezing conditions (Föllmi, 2012; see below). In addition, some delta 18-oxygen

curves are decoupled from the pCO₂ trends (Korte *et al.*, 2015), resulting in contrasting interpretations (Veizer *et al.*, 2000); and several GCM do not correlate well with the fossil record (Price, 1999; Rees *et al.*, 2000, 2004), reflecting the use of inadequate boundary conditions.

From the latter, glendonite, a pseudomorph of the metastable carbonate mineral ikaite, has extensively been used as a proxy for cold water or near-freezing conditions, as this mineral has usually been reported from high-latitude deposits (Rogov *et al.*, 2021). In modern-day settings, ikaite typically forms at temperatures ranging between -2° to 7°C (Bischoff *et al.*, 1993; Föllmi, 2012; Rogov *et al.*, 2021). However, its utility as a paleotemperature indicator may be limited, since it could also reflect upwelling, highly productive organic-rich sediments, or alkaline environments (Föllmi, 2012; Jenkyns *et al.*, 2012; Rogov *et al.*, 2021). In a global perspective, this mineral is particularly abundant in Mid-Jurassic, Valanginian, Aptian, and Albian sediments; it is less common in the Late Jurassic, rare in the Berriasian and Barremian, and absent in the early Aptian and Late Cretaceous; the last two periods have been usually regarded as experiencing global warmth (Rogov *et al.*, 2021, and references therein).

3.2.1. Late Jurassic

The Jurassic Period is characterised by the appearance of symmetric global climate zones (biomes) north and south of the paleo-equator (Rees *et al.*, 2000, 2004; Sellwood & Valdes, 2008; Price, 2009; Fig. 9). Based on floral diversity, Late Jurassic biomes reflect a lower pole-to-equator temperature gradient (Rees *et al.*, 2000, 2004; Kauffman & Johnson, 2009); this has also been supported by faunal provincialism, identified in the Mid-Jurassic and subsequent periods (Frakes *et al.*, 1992, Price, 1999; Price, 2009 and references therein). However, provincialism might also reflect other physical controls (Price, 1999; Sellwood & Valdes, 2008), such as differences in sea-water densities (Bjerrum *et al.*, 2001).

Overall, Late Jurassic biome models comprise relatively arid or seasonally wet low-latitudes (within ca. 30-40° north and south of the equator), warm-temperate mid-latitudes (between ca. 30°-60° N/S), and cool-temperate high latitudes (about >60° N/S).

Polar ice caps were likely absent (Rees *et al.*, 2000, 2004; Sellwood & Valdes, 2008; Fig. 9).

General Circulation Models for the Late Jurassic indicate tentative CO₂ values at least four times the current ones, with about 5°-10°C whole Earth- and 8°C ocean depth-temperatures warmer than today (Sellwood & Valdes, 2008; Fig. 9B). Nevertheless, an alternation of short-termed (0.5-1.0 Ma) cold- and warm Jurassic climate modes has been inferred from oscillations in oxygen isotopic curves (Dera *et al.*, 2011; Korte *et al.*, 2015). In particular, brief Late Jurassic “cold modes” are proposed as occurring in the middle-late Oxfordian, and in the early - late Tithonian (Dera *et al.*, 2011).

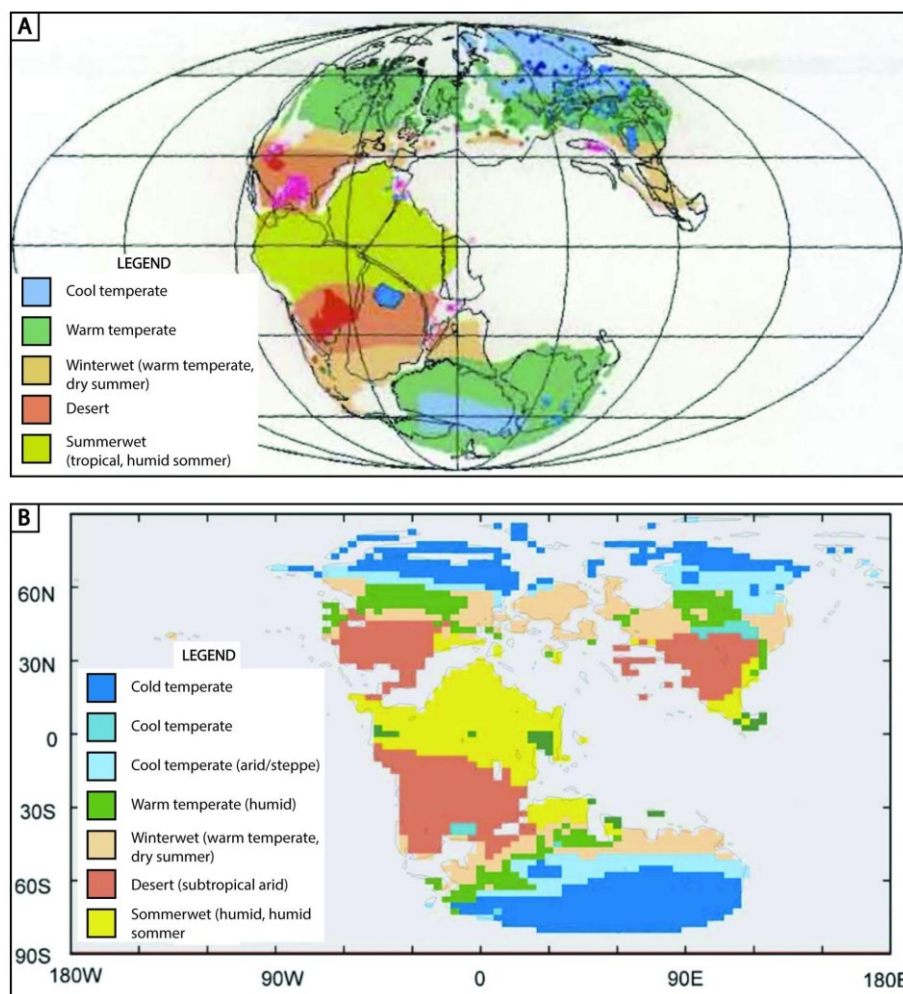


Figure 9. Paleoclimatic model showing symmetric climate zones during the Late Jurassic. A) Model of biomes/climate zones based on paleo- and lithological evidence (Modified from Rees *et al.* (2000)). B) Model of biomes for the Late Jurassic using a General Circulation Model (GCM) based on predicted atmospheric data (Modified from Sellwood & Valdes, 2006, 2008). Note the contrast between high-latitude temperatures/biomes inferred by both models, being colder in the one generated by GCM.

3.2.2. Early Cretaceous

Just like the Jurassic, the climate during the Cretaceous may have been characterised by symmetric biomes (Figs. 10, 11). Even though, paleoclimate may have changed from cool-temperate conditions in the Early Cretaceous, to (extremely) warm conditions during the mid- and Late Cretaceous (Kauffman & Johnson, 2009), reaching a thermal maximum at ca. 90 Ma (Price, 2009). Early Cretaceous biomes may have consisted of hot-arid belts surrounding the equator, followed by mid-latitude warm-humid belts, and high-latitude temperate-humid belts (Hay & Floegel, 2012, and references therein; Figs. 10, 11). The main contrast between the Early- and the Late Cretaceous is the presence of a wide, arid equatorial zone in the former, and the appearance of a humid belt in the latter (Hay & Floegel, 2012); although, this has been regarded as paradoxical by Hay (2017).

There are contrasting models for Cretaceous paleoclimate. While some authors infer an equable warm climate, with a low temperature gradient and the absence of polar ice caps (Hay, 2008; Föllmi, 2012), others depict episodic cooling (Kessels *et al.*, 2006), or even a seasonal growth of polar ice (e.g., Price, 1999; Price, 2009; Price *et al.*, 2000; McArthur *et al.*, 2007; Mutterlose *et al.*, 2009; Tennant *et al.*, 2017; Cavalheiro *et al.*, 2021). Warm Cretaceous models infer fluctuating CO₂ levels between twice- and four times the present values, with an estimated sea-surface paleotemperature greater than 30°C in the equatorial zone (Kauffman & Johnson, 2009, and references therein), i.e., about 6-12 °C warmer than today (Price, 2009). In contrast, Cretaceous “cool snaps” have been supported by the same hypotheses proposed for the Jurassic ones (glacial deposits, glendonite, faunal provincialism, oxygen and or carbon isotopes). However, this supporting evidence is considered to be debatable (Price, 2009; Föllmi, 2012).

An alternative model for the Early Cretaceous paleoclimate considers a fluctuation between arid/“normal” and humid/“reinforced” greenhouse conditions (Föllmi, 2012). Arid conditions are characterised by enhanced evaporation, low weathering rates and low nutrient influx (therefore, low productivity); and *vice versa* for humid periods (Föllmi, 2012). The former may have been longer-termed, occurring in the latest Jurassic-early Berriasian (Retallack, 2009), late Barremian, and late Aptian (Föllmi, 2012; Fig. 11). Humid periods may have been short-termed (< 1-3 Ma), but more

intense and widespread. The latter have been linked to “episodes of environmental change”, commonly marked by positive CO₂ excursions, demise of carbonate platforms, and sedimentation of organic-rich facies (“black shales”; Weissert *et al.*, 1998; Erba *et al.*, 2004; Cavalheiro *et al.*, 2021). These events include the Weissert (Valanginian); Faraoni (Hauterivian), Taxy (late Barremian-earliest Aptian), Selli (early Aptian), Fallot (early late Aptian), and Paquier (late Aptian-early Albian) Episodes (Föllmi, 2012).

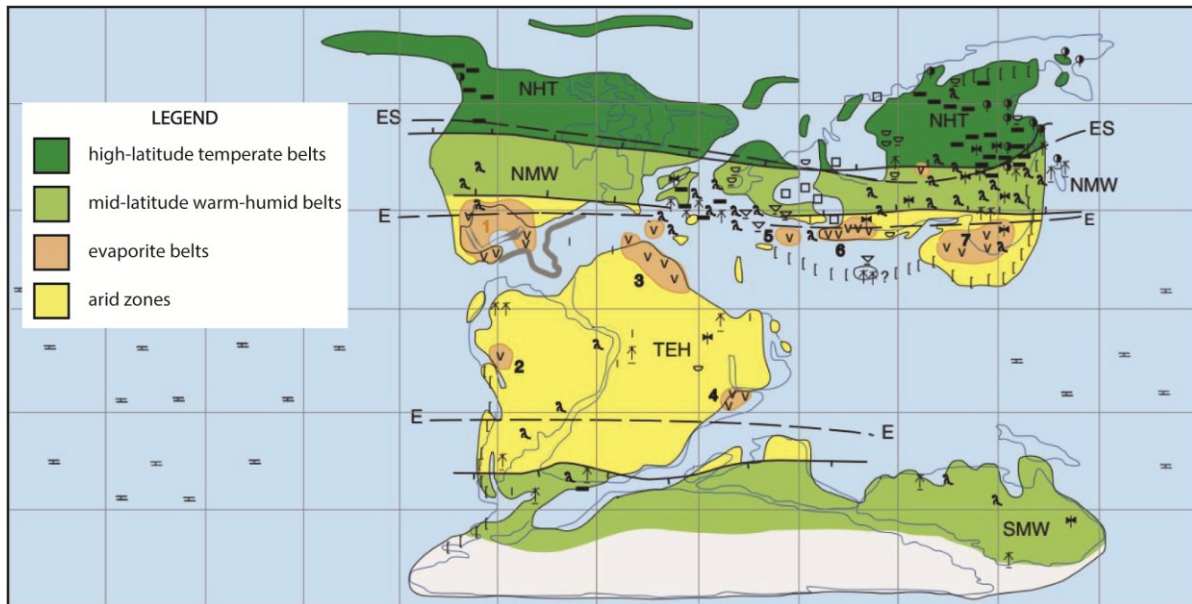


Figure 10. Paleoclimate reconstruction for the Early Cretaceous (Berriasian). Just like the Late Jurassic, the Early Cretaceous also displays a symmetric zonation of climate zones or biomes. Modified from Hay & Floegel (2012; after Chumakov *et al.*, 1995). The original maps of Chumakov *et al.* (1995) are based on the distribution of climate sensitive fossils and sediments (see discussion in text). Abbreviations (from north to south): Biomes: NHT = Northern high-latitude temperate humid belt; NMW = Northern mid-latitude warm humid belt; TEH = Tropical-equatorial hot arid belt; SMW = Southern mid-latitude warm humid belt; SHT = Southern high-latitude temperate humid belt. Boundaries (facing poleward): Discontinuous black lines (E; ES) = external boundaries of main Equatorial, and Euro-Sinian zones, respectively; Continuous black lines with short bar = Boundaries of climate zones. Legend is also valid for Fig. 11 (Aptian).

According to Hay (2017), several unsolved problems regarding the Cretaceous paleoclimate should be revisited. These comprise major uncertainties in the global land-vs-sea temperatures, the amount and type of greenhouse gases, the influence of the hydrological cycle, as well as sea-level changes, among others. The main issues to be addressed are:

- i) Modelled land-vs-sea temperatures are either too cold or warm, conflicting with the distribution of fossil plants in polar- and equatorial zones, respectively (Hay & Floegel, 2012).
- ii) Paleotemperature proxies are usually restricted to the atmospheric CO₂, which may have been overestimated, disregarding other greenhouse gases (CH₄, H₂O).

iii) Although humid biomes have been inferred during the Cretaceous, numerical simulations do not consider the influence of continental bodies of water (ponds and lakes), generating less plausible models.

iv) Short-termed eustatic variations, usually linked to polar ice formation (Price, 2009), may also be triggered by the infill and release of water in lakes and groundwater systems. The latter could also modify the oxygen isotopic records (Föllmi, 2012; Hay, 2017, and references therein).

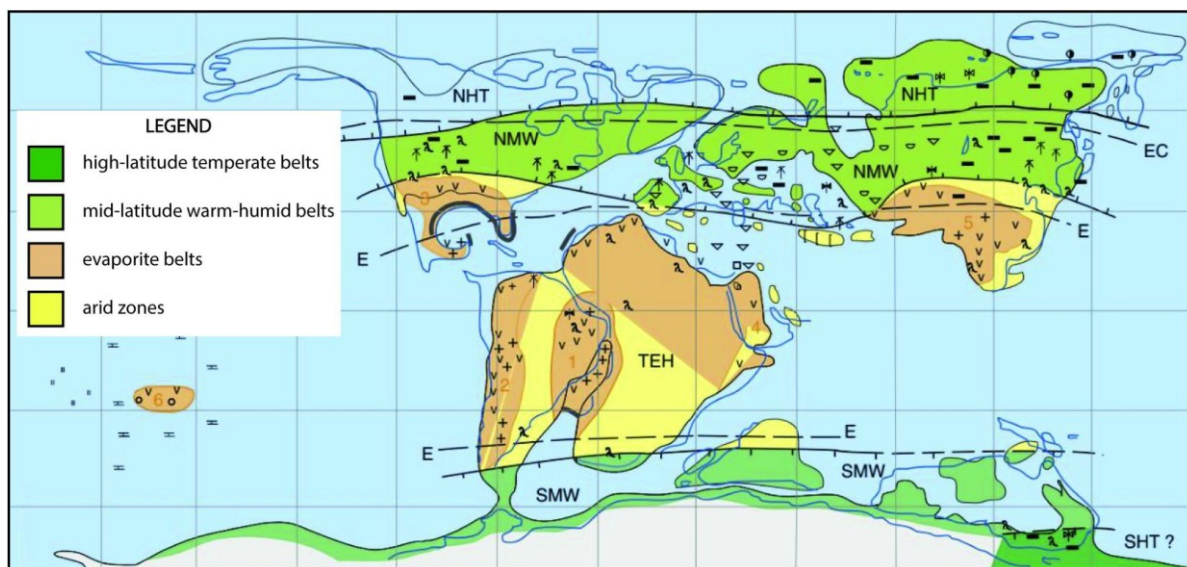


Figure 11. Paleoclimate reconstruction for the Early Cretaceous (Aptian). Modified from Hay & Floegel (2012; after Chumakov *et al.*, 1995). See legend in Fig. 10 (Berriasian).

3.2.3. J-K Regional Paleoclimatic Setting

In a wider context, high-latitude ($>50^{\circ}\text{S}$), warm sea-surface temperatures (around 25°C) have been suggested during the Jurassic-Cretaceous transition from the Antarctic/Southern Ocean in the Falkland-Malvinas Plateau ($51^{\circ}\text{S}/53^{\circ}\text{S}$ current- and paleo-latitude, respectively; Jenkyns *et al.*, 2012; Vickers *et al.*, 2019), and from the Weddell Sea Basin (Cavalheiro *et al.*, 2021). In these areas, paleotemperatures might have been highest during the Oxfordian-Kimmeridgian, and slightly cooler, but still temperate ($>25^{\circ}\text{C}$), in the Tithonian, and in the Early Cretaceous (Hauterivian-Barremian, or Barremian-Albian; see discussion in Price & Gröcke, 2002; Fig. 12). Data from the Weddell Sea Basin confirm a Valanginian warm interval, followed by a

remarkable drop in the sea surface temperature of about 3°-4°C during part of the Weissert Event (“cold end”) at ca. 133 Ma (Cavalheiro *et al.*, 2021).

In the Aysén-Río Mayo Basin (ARB), warm and humid conditions have been suggested for the period of deposition of the Coyhaique Group (Tithonian-Aptian), but these have only been based on the presence of calcareous rocks (Ramos, 1976; Charrier & Covacevich, 1978; Olivero, 1982; Scasso, 1989; Bell *et al.*, 1994, 1996; Townsend, 1998). In particular, warm conditions during the J-K transition are supported by the presence of late Tithonian high-latitude thermophilic organisms (*sensu* Sellwood & Valdes, 2006), including coral-stromatoporoid reefs in the Cotidiano Formation (Ramos, 1978; Leinfelder *et al.*, 2005; Bucur *et al.*, 2009), and crocodyliforms from the Toqui Formation (De la Cruz & Suárez, 2006; Novas *et al.*, 2015; Suárez *et al.*, 2016), while Berriasian-Valanginian coral reefs have been reported from the Tres Lagunas Formation (Scasso & Kiessling, 2002). Southwards of 46°S, an Early Cretaceous temperate-humid paleoclimate ($T > 23^{\circ}$) has also been suggested, based upon the modal composition of the Springhill Formation, and based on belemnite-isotopic oxygen data from the Río Mayer Formation (e.g., Riccardi, 1971; Charrier & Covacevich, 1978; Escosteguy *et al.*, 2003, and references therein). Both the Springhill- and Río Mayer Formations have been regarded as partly correlative with the Toqui- and Katterfeld Formations, respectively (see section 5.4).

On the other hand, evidence supporting cold snaps is inconclusive in the Aysén-Río Mayo Basin. For example, based on the high-latitude distribution of Andean steinmanellids, Cooper & Leanza (2017) inferred an adaptation of these bivalves to “cool temperate” or “subpolar” settings. In addition, relatively cooler conditions in the Valanginian? were proposed by Rivas *et al.* (2023), based on red algae-rich limestone (“maerl”-like) of the Toqui Formation. The authors depict a heterozoan faunal assemblage, usually associated with -but not limited to- non-tropical or “cool water” settings (*sensu* James, 1997; Kindler & Wilson, 2010).

Indirect evidence of “cool-snaps” in the Aysén Region during the J-K transition may be inferred from paleoclimatic data for Central Chile (33°S), southernmost

Patagonia (51°-52°S; Rocas Verdes Basin, see section 5.4), and for the Antarctic Peninsula (62°-71°S; Brysch, 2018). On the basis of depositional environments, sometimes coupled with the occurrence of microglendonite, Brysch (2018) proposed several “cool-snap intervals” for southern South America; these are usually associated with sea-level lowstands, interpreted by him as glacioeustatic. These cool intervals may have occurred in the late Tithonian-earliest Berriasian, latest Berriasian, Valanginian, earliest Hauterivian, late Barremian-early Aptian, and earliest Albian (Brysch, 2018). However, as shown in section 3.2, besides conflicting with other paleotemperature proxies mentioned above, the mere presence of this mineral may not necessarily reflect sea-water sub-freezing conditions.

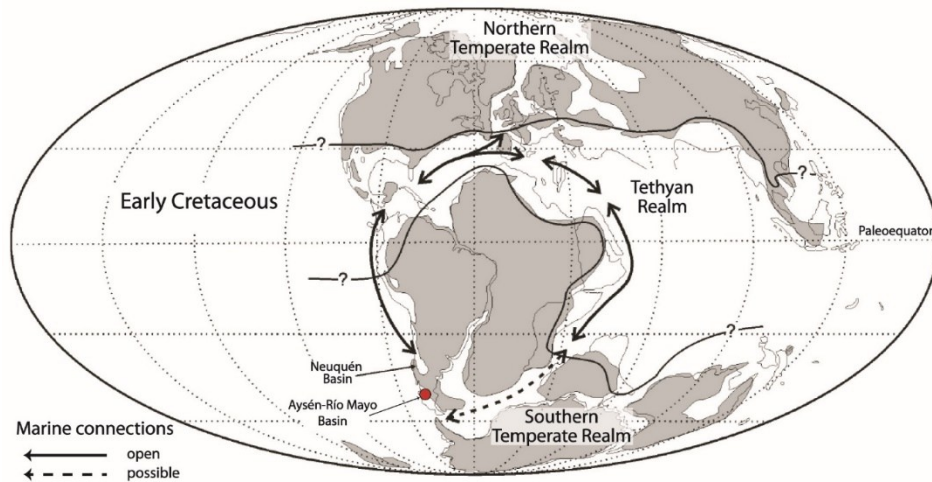


Figure 12. Paleogeographic reconstruction for the Early Cretaceous, displaying the main marine connections/seaways between the South American basins and the Tethyan Realm (black solid lines with arrows). Boundaries to high-latitude temperate zones are marked as black solid lines (without arrows) are also represented. Modified from Aguirre-Urreta et al. (2008).

3.3. Sea level changes

Mesozoic global eustatic curves show a 1st order long-term sea-level rise throughout the whole era, starting in the Early Jurassic. Early Jurassic values are similar to the present day mean sea-level (“pdmsl”; Haq, 2018), and show a major fall in the Late Cretaceous (e.g., Ruban, 2015). During the Jurassic, eustatic curves display a gradual long-term sea level rise, reaching a peak at the Kimmeridgian - Tithonian boundary (as high as ca. 140 m above pdmsl; Haq, 2018), with a medium fall of about 40 m at the J-K transition (Tithonian - Berriasian; Haq, 2014, 2018), before stabilising at about 110 m

above pdmsl during the Berriasian (Fig. 13). The latter was followed by a long-term sea-level fall starting in the latest Berriasian, reaching the lowest Cretaceous sea level in the mid-Valanginian (ca. 75 m above pdmsl; Haq, 2014, 2018), though this minimum has also been proposed for the early Hauterivian (Müller *et al.*, 2008; Fig. 13).

After the Valanginian, global eustasy models are contrasting and difficult to correlate (see Figure 4D in Müller *et al.*, 2008; Figure 5 in Ruban, 2015). On one hand, the model of Haq (2014) depicts a long-term sea-level rise following the mid-Valanginian trough, reaching a peak in the early Barremian (ca. 160-170 m above pdmsl); the latter was followed by a minor sea-level fall of about 20 m (at ca. 140 m above pdmsl), reaching a stagnant period in the early Albian (Fig. 13B). On the other hand, the model of Müller *et al.* (2008) infers a post-Valanginian sea-level rise, with a peak in the mid-Aptian (at ca. 150 m above pdmsl; Fig. 13B).

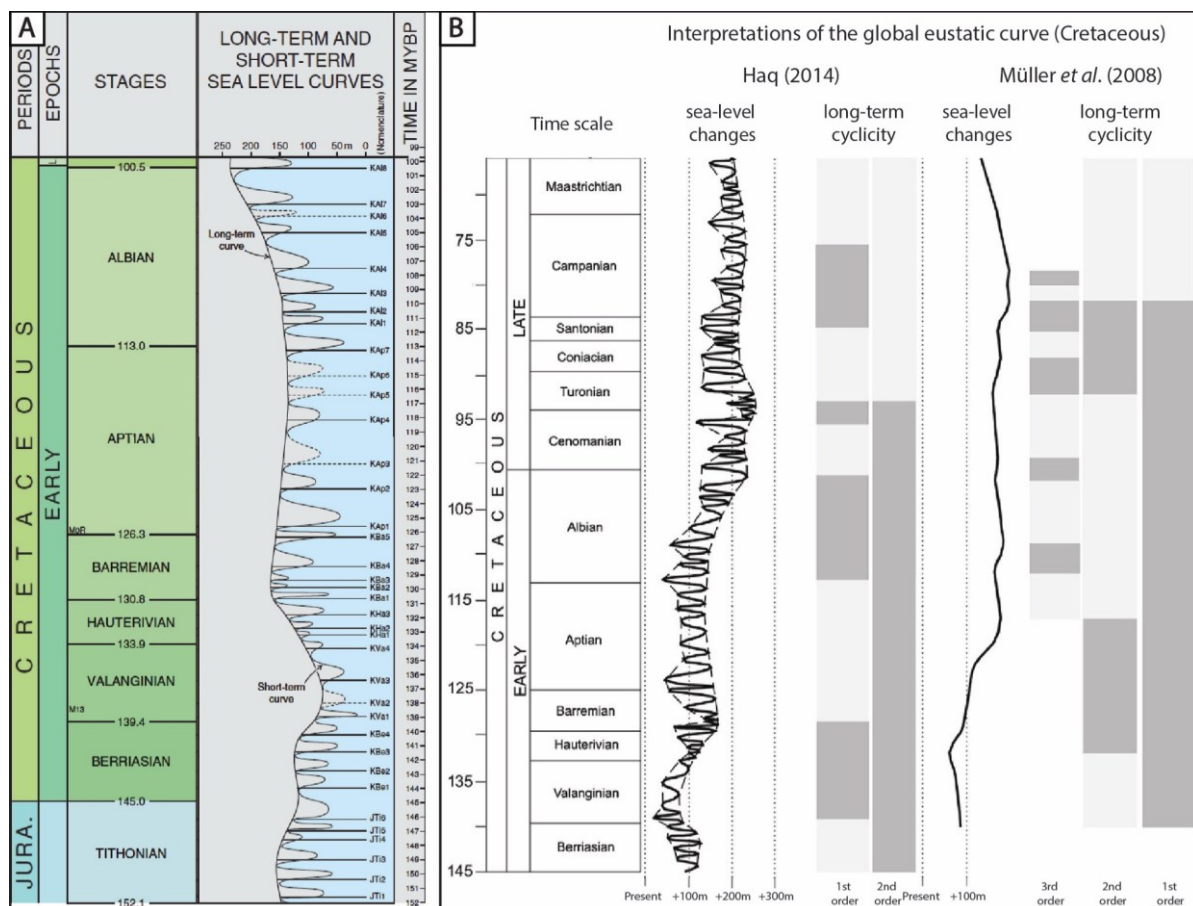


Figure 13. A) Long-term and short-term sea level curves for the Jurassic-Cretaceous transition (Tithonian-Berriasian) and Early Cretaceous. Modified from Haq (2014; 2017). B) Comparison of two long-term sea level curves inferred for the Early Cretaceous together with their hierarchical interpretations (1st, 2nd, 3rd order; sensu Haq, 2014; Müller *et al.*, 2008); modified from Ruban (2015).

A disadvantage of using long-term global eustatic curves is based on the interpretation with data obtained mostly from European and North American basins (Haq, 2014, 2018). This includes inferred short-termed sea-level falls/rises from sequence stratigraphic models as well as ammonite-based biochronostratigraphy. During the J-K transition, nevertheless, index fossils display a marked provinciality (Riccardi, 1991; Lehmann *et al.*, 2015), hindering global correlation (Haq, 2014, 2018). Therefore, these eustatic models should be interpreted with caution when working with meridional stratigraphic units, like the ones addressed here.

4. The Aysén-Río Mayo Basin

4.1. Onset and structure

The Aysén-Río Mayo Basin (ARB, *sensu* Gianni *et al.*, 2019) was a back-arc basin (Aguirre-Urreta & Ramos, 1981; Ramos & Aguirre-Urreta, 1994) with local intra-arc and retro-arc depocenters (Skarmeta, 1976; Aguirre-Urreta & Ramos, 1981; Suárez & De la Cruz, 1994a; Iannizzotto *et al.*, 2004; Suárez *et al.*, 2010a; Gianni *et al.*, 2019; Suárez *et al.*, 2023; Fig. 14). It developed in the southwestern margin of West Gondwana (proto-South America) during the Tithonian-Aptian (Scasso, 1989; Haller & Lapido, 1980; Bell *et al.*, 1996; Townsend, 1998; Suárez *et al.*, 2010a). Previously, the ARB has been referred to as the “Aysén Basin” in Chile (Suárez & De la Cruz, 1994a; Bell *et al.*, 1996; Bell & Suárez, 1997), and as the “Río Mayo Embayment” in Argentina (Aguirre-Urreta & Ramos, 1981; Ramos & Aguirre-Urreta, 1994; Olivero & Aguirre-Urreta, 2002; Fig. 14B).

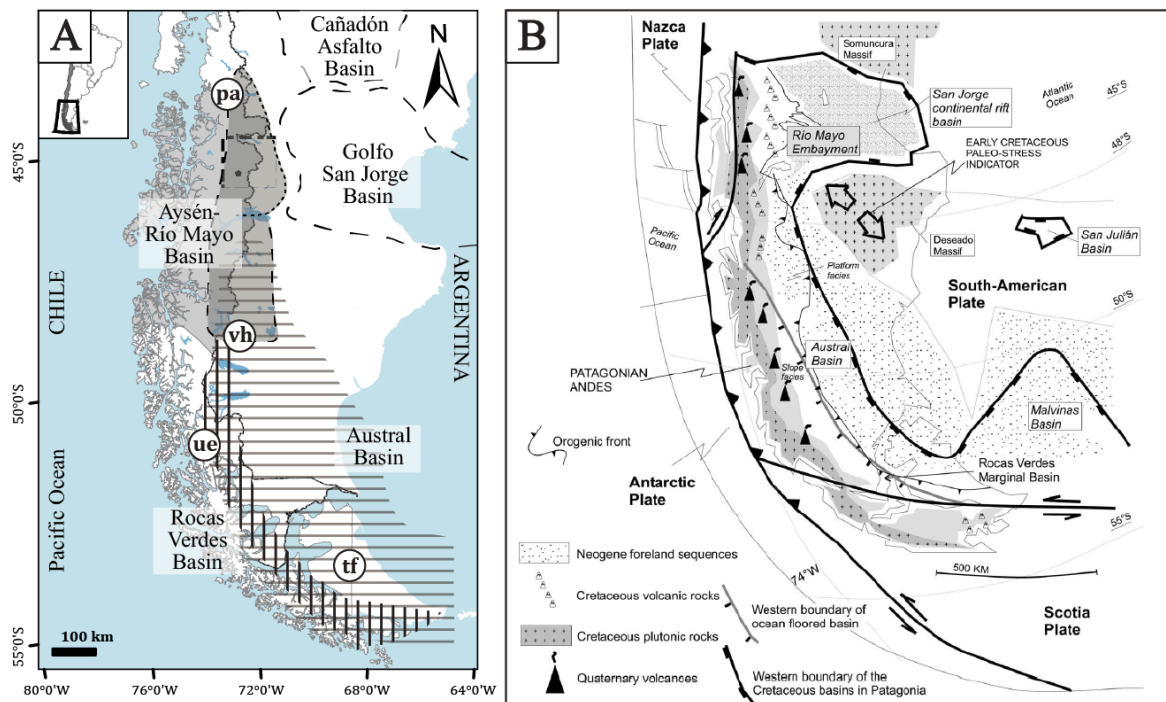


Figure 14. Inferred location, extension and structure of the Aysén-Río Mayo Basin (ARB). A: Short-dashed Line: Outline of the ARB *sensu* Suárez *et al.* (2010a); dotted line: “Río Mayo Embayment” *sensu* Aguirre-Urreta & Ramos (1981). In A), outlines of the adjacent basins *sensu*: Rocas Verdes Basin (Calderón *et al.*, 2013); Cañadón Asfalto Basin (Figari *et al.*, 2015); Austral Basin (Fosdick *et al.*, 2020); Golfo San Jorge Basin (Ramos, 2015). Study area is indicated in the black square. Abbreviations: pa = Palena; tf = Tierra del Fuego; ue = Última Esperanza Province; vh = Villa O’Higgins. Fig. 14A taken from Rivas *et al.* (2025; submitted). B) Location of the ARB (“Río Mayo Embayment”), adjacent basins, and the coeval magmatic arc. Note that in this model the Aysén-Río Mayo Basin is considered to be the northern part of the Austral Basin. Fig. 14B taken from Folguera & Iannizzotto (2004). The comparison and correlation of basins is addressed in Chapter 5.

The onset of the basin is regarded to occur during the Mid-Late Jurassic (Scasso, 1989), but most likely, it began to develop in the Late Jurassic, caused by back-arc extension to the east of the coeval volcanic arc (Patagonian Batholith; see section 3.1.3; Fig. 15). Extension in the ARB has been interpreted as caused by slab-rollback (Echaurren *et al.*, 2017), conforming an ensialic marginal basin (Haller & Lapido, 1980; Suárez *et al.*, 1996, 2009; Figs. 8, 15).

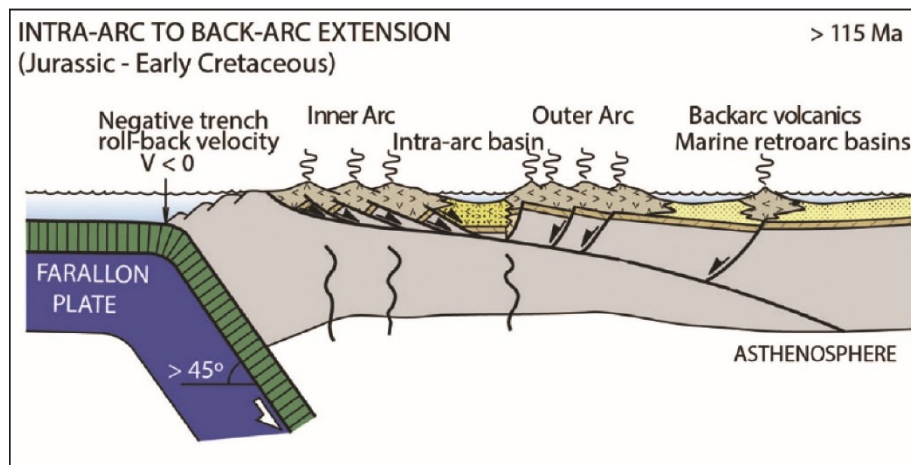


Figure 15. Paleotectonic setting of the Southern Andes during the J-K transition. Tectonic setting during the onset and main evolution of the Aysén-Río Mayo Basin. This stage is characterized by a high-angle subduction (“slab-rollback”, see Fig. 8), arc volcanism, and intra-arc/back-arc extension. Figure from Gianni *et al.* (2019; after Ramos, 2009).

Outcrops associated with the ARB have been identified at the eastern flank of the Northern- or Central Patagonian Cordillera (43°-49°S *sensu* Charrier & Covacevich, 1978; and Haller & Lapido, 1980, respectively; Fig. 16), between Futaleufú (Chile) - Carrenleufú (Argentina) to the north (“Continental Chiloé” or Palena Province; Fuenzalida, 1965; Thiele *et al.*, 1978; De la Cruz *et al.*, 1995; Fig. 14A), and the Cochrane-Pueyrredón Lake to the south (around 47°30’S; Scasso, 1989; Fig. 14). The southern margin of the basin is still discussed: While some authors infer meridional extension reaching only to the General Carrera/Buenos Aires Lake (around 46°30’S; Haller & Lapido, 1980; Haller *et al.*, 1981;), others believe it may reach down to 49°-50°S (Suárez *et al.*, 2010a; Fig. 14A).

At its western margin, the basin is flanked by the Patagonian Cordillera (Skarmeta, 1976; Scasso, 1989; Haller & Lapido, 1980; Aguirre-Urreta, 1990), whereas its easternmost outcrops are exposed around the Aldea Apeleg in Argentina (44°41’S;

70°51'W; Figs. 14B, 16). Correlative rocks might extend eastwards in the subsurface, as shown from oil-prospection drill cores drilled by YPF in Argentina (“Yacimientos Petrolíferos Fiscales”), around the eastern flank of the Sierra de San Bernardo, at the confluence of the Senguerr and Mayo Rivers (ca. 45°46'S; 69°40'W; Scasso, 1987, 1989; Fig. 16). To the northeast and southeast, the basin is flanked by the North Patagonian- and the Deseado Massifs, respectively (Figs. 14B, 16); these cratonic blocks comprise Proterozoic-Paleozoic metamorphic rocks, which remained stable and rigid during the Meso-Cenozoic geological evolution (Riccardi, 1988; Ramos, 1989; Aguirre-Urreta, 1990).

4.2. Paleogeography of the Aysén-Río Mayo Basin

The Aysén-Río Mayo Basin (ARB) was sub-triangular in outline, elongated in a NW-SE strike (Aguirre-Urreta & Ramos, 1981; Scasso, 1989). Its northern part, located between Futaleufú and the Coyhaique (43°-45°S), consisted of a narrow strip placed parallel to the Patagonian Cordillera (Figs. 8, 14, 16); there, the close relationship between marine- and volcanoclastic sediments indicates an intra-arc basin configuration (Skarmeta, 1976; Charrier & Covacevich, 1978; Aguirre-Urreta & Ramos, 1981; Ramos & Palma, 1983; Scasso, 1989; Suárez & De la Cruz, 1994a; Folguera & Iannizzotto, 2004; Suárez *et al.*, 2009, 2023; Figs. 14B, 15). Southwards of the Fontana Lake, the ARB widened towards the extra-Andean zone to the southeast, conforming a gulf that reached the Deseado River at ca. 46°S (“Río Mayo Embayment” *sensu* Aguirre-Urreta & Ramos, 1981). From this point, the paleogeographic models of the basin diverge: some authors restrict the ARB to this latitude, from where it pinches out towards the cordilleran area (Fig. 14B). Even though, a connection is likely kept with the meridional Rocas Verdes Basin (*sensu* VanderLeest *et al.*, 2022), and/or with the “Austral Basin” through a narrow seaway (e.g., Scasso, 1989; Aguirre-Urreta & Ramos, 1981; Aguirre-Urreta, 1990, 2002), while other authors infer a continuity of the basin reaching to the Viedma Lake at ca. 49°S (Suárez *et al.*, 2010a; see discussion in section 5.4).

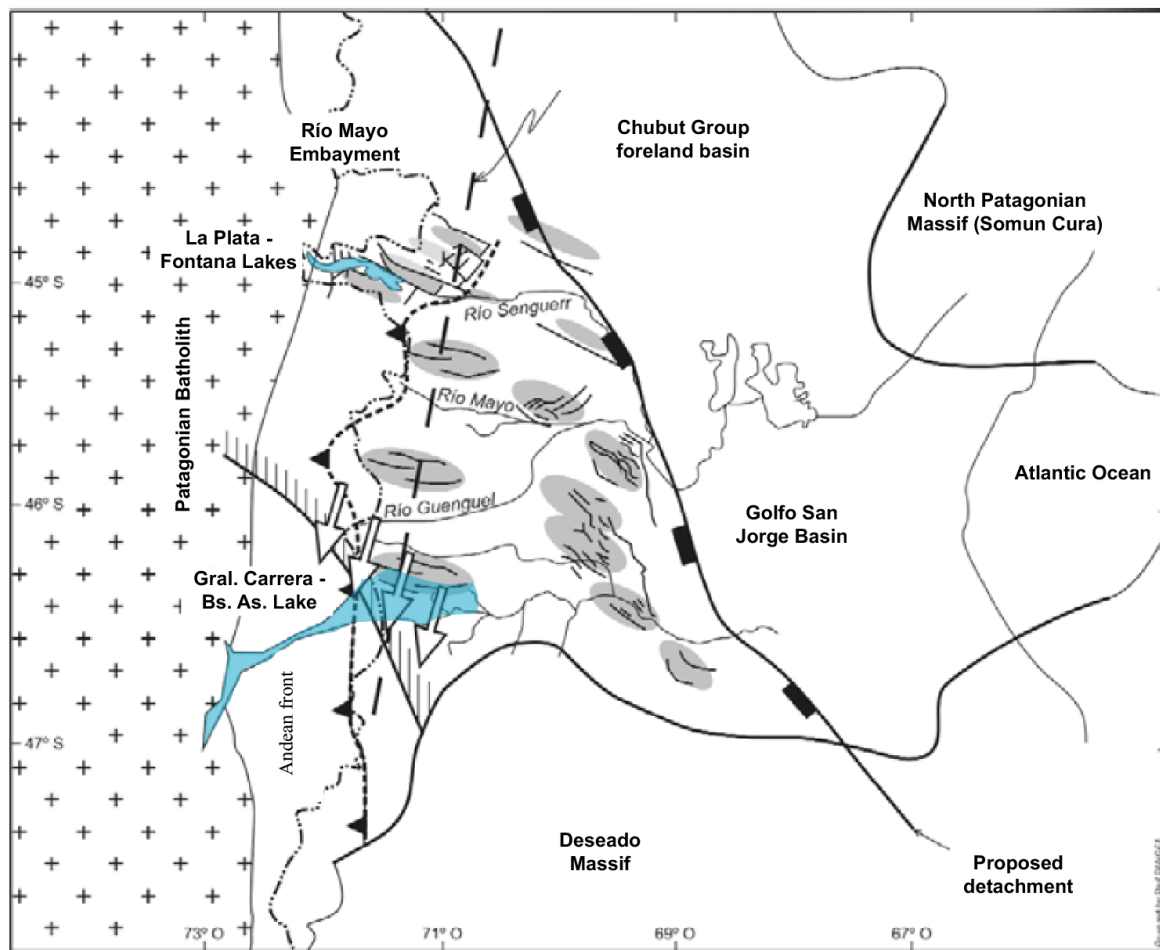


Figure 16. Location of the Río Mayo Basin (*sensu* Folguera & Iannizzotto, 2004) or “Río Mayo Embayment” (*sensu* Aguirre-Urreta & Ramos, 1981), showing its boundaries and structure. Note its western boundary marked by the Patagonian Batholith, and its north- and southeastern boundaries limited by two cratonic blocks (Somun Cura and Deseado Massifs). Modified from Mpodzis & Ramos (2008, after Folguera & Iannizzotto, 2004).

Internally, the basin topography was extensional (Skarmeta, 1976; Haller & Lapido, 1980; Scasso, 1989), comprising several grabens and hemigrabens, separated by NW-SE-oriented horsts bounded by high-angle faults (basin-and-range-like), which might represent the reactivation of basement sutures (Ploszkiewicz & Ramos, 1977; Folguera & Iannizzotto, 2004; Iannizzotto *et al.*, 2004; Suárez *et al.*, 2023; Fig. 14B, 15, 16). Major faults were interrupted by minor NE-SW and E-W-oriented structures or accommodation zones (Scasso, 1989; Folguera & Iannizzotto, 2004; Fig. 16). Thickest depocenters were placed in tectonic troughs (Fig. 16). From these, the most important grabens may have been located in the Fontana Lake area (Masiuk & Nakayama, 1978; Aguirre-Urreta & Ramos, 1981), and around the city of Coyhaique, both being separated by a volcano?-tectonic high (Skarmeta, 1976; Scasso, 1989) located near the Cerro Katterfeld (“Mañihuales-Toqui High” *sensu* Folguera & Iannizzotto, 2004; Fig. 14B). At

its eastern margin, the ARB was likely bounded by a NW-oriented horst (“Dorsal Río Mayo” *sensu* Suero, 1955 in Scasso, 1987), being separated from coeval continental basins developed to the east (Scasso, 1989; Figs. 14B, 16; see discussion in section 5.3).

At its western margin, the ARB was connected with the Pacific Ocean. This connection was established at least in the Tithonian, starting with the flooding of discrete and small shallow-marine basins; the latter were bounded and locally restricted by an island arc to the west (Skarmeta, 1976; Charrier & Covacevich, 1978; Aguirre-Urreta & Ramos, 1981; Mpodozis & Ramos, 1990; Scasso, 1989; Haller & Lapido, 1980; Townsend, 1998; Fig. 14B). Sea-gates along the basin, which allowed for connection with the Pacific, would have been located at the northwestern margin (Scasso, 1989), and a second at about the O’Higgins/San Martín Lake (Aguirre-Urreta & Ramos, 1981).

4.3. Geological setting, stratigraphy, and facies

The infill of the Aysén-Río Mayo Basin consists of subaerial volcanic sediments (Lago La Plata Group, Kimmeridgian? - Valanginian) underlying a transgressive-regressive succession known as the Coyhaique Group, deposited between the Tithonian - Aptian (Haller & Lapido, 1980; Haller *et al.*, 1981; Suárez & De la Cruz, 1994a; Suárez *et al.*, 2010a; Fig. 17). In Chile, this group comprises three formations, separated by transitional or sharp contacts (Ploszkiewicz & Ramos, 1977; Scasso, 1987, 1989; Suárez & De la Cruz, 1994a; Gonzalez-Bonorino & Suárez, 1995; Suárez *et al.*, 1996; Bell & Suárez, 1997; De la Cruz *et al.*, 2003; Suárez *et al.*, 2010a; 2010b, among many others; Fig. 17). The Coyhaique Group includes, from base to top:

I) The Toqui Formation (Tithonian-Valanginian): composed of mixed calcareous-volcaniclastic rocks, deposited in shallow marine settings.

II) The Katterfeld Formation (Valanginian-Hauterivian, Barremian?): conformed by black mudstone and minor sandstone, settled in shelf settings.

III) The Apeleg Formation (Hauterivian-Aptian): this unit consists of heterolithic to sandy-gravelly sediments with a shallowing-upwards trend; they were deposited in coastal settings.

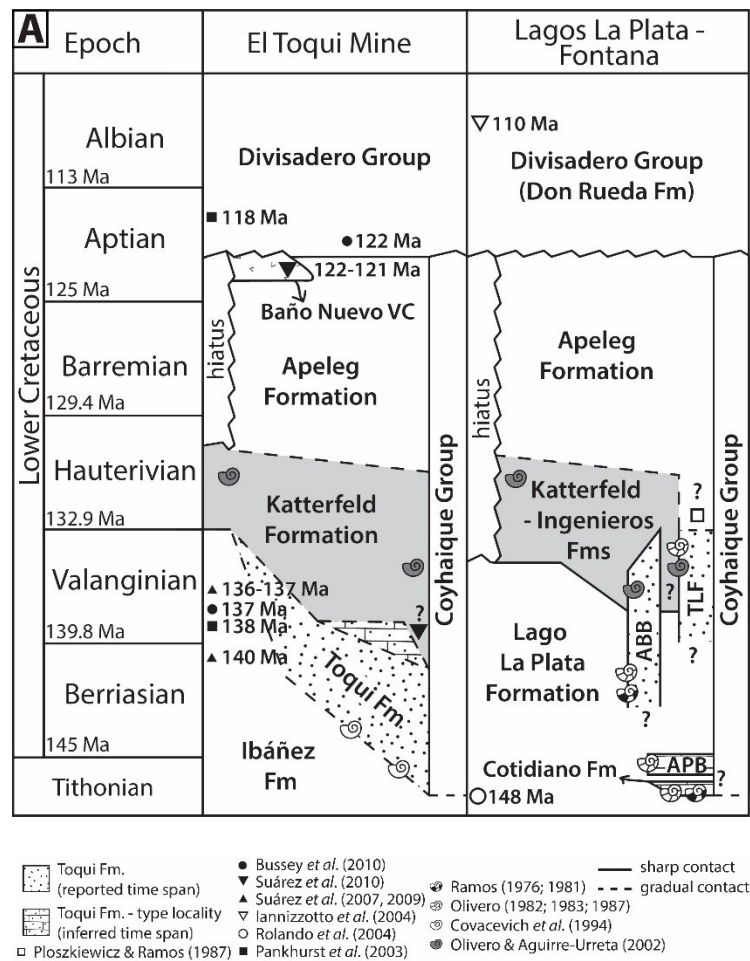


Figure 17. Stratigraphy of the Coyhaique Group. Rivas et al. (2021).

The marine sedimentation occurred between two volcanic pulses, being capped by the subaerial, volcanic strata of the Divisadero Group at the top (Aptian-Cenomanian; e.g., Skarmeta, 1976; Haller & Lapido, 1980; Haller *et al.*, 1981; Ramos, 1981; Niemeyer *et al.*, 1985; De la Cruz *et al.*, 1994; Gonzalez-Bonorino & Suárez, 1995; Suárez *et al.*, 2009, 2010a; Fig. 17).

The thickness of these marine units is highly variable, given their discrete and incomplete exposure as well as lateral changes in facies (Scasso, 1987, 1989). Overall, mixed calcareous-volcaniclastic rocks (Toqui Fm. and correlative units) display an average thickness lower than 100 m (maximum < 300m; Scasso, 1989); whereas maximum thickness of the Katterfeld Formation may fluctuate between 400 - 650 m

(Scasso, 1989; Bell *et al.*, 1994). The thickest deposits correspond to the Apeleg Formation, estimated to reach between approx. 350 m (Gonzalez-Bonorino & Suárez, 1995) and around 1000 - 1200 m (Ploszkiewicz & Ramos, 1977; Bell *et al.*, 1994), increasing in thickness in Argentina (Gonzalez-Bonorino & Suárez, 1995).

4.3.1. Basement

The basement of the ARB comprises upper Paleozoic metaturbidites, metabasites and marbles of the Eastern Andean Metamorphic Complex, originally representing sediments deposited in a passive margin (Bell & Suárez, 2000; Hervé *et al.*, 2008). Locally, these rocks also include marine and continental volcano-sedimentary units from the Lower Jurassic (Ploszkiewicz, 1987; Scasso, 1989; Ferrari & Bessone, 2015), deposited in an older foreland basin system (“Chubut Basin” *sensu* Suarez & Marquez, 2007). In the study area, the basement is not exposed (Suárez *et al.*, 1996, 2007; De la Cruz *et al.*, 2003), but it crops out discretely in the area around the Fontana - La Plata Lakes (Ploszkiewicz, 1987; Scasso, 1989; Olivero, 1982; Folguera & Iannizzotto, 2004; Ciccioli *et al.*, 2020); it is extensively exposed to the south, between the General Carrera/Buenos Aires and O’Higgins/San Martín Lakes (46°-49°S; Niemeyer, 1975; Suárez *et al.*, 1996; De la Cruz *et al.*, 2004; Quiroz & Bruce, 2010).

4.3.2. Lago La Plata Group

The ARB basin fill begins with volcanic- and volcano-sedimentary rocks of the Lago La Plata Group (including the Lago La Plata- and Ibáñez Formations, their correlative units, and informal members; De la Cruz *et al.*, 1994; 2003; Fig. 17). An angular unconformity separates these sediments from the underlying basement (Olivero, 1982). The Lago La Plata Group represents the extrusive counterpart of the Patagonian Batholith (e.g., Skarmeta, 1976; Skarmeta & Charrier, 1976; Charrier & Covacevich, 1978; Haller & Lapido, 1980, 1982; Pankhurst *et al.*, 1999; 2003; Suárez *et al.*, 2009, 2010a, 2023), though its older rocks are possible related to the youngest volcanism of the Chon Aike Large Igneous Province (V3-stage *sensu* Pankhurst *et al.*, 1998; 2003; see section 3.1.2). The Lago La Plata Group comprises rhyolitic and andesitic rocks, synextensionally settled in subaerial- and, locally, in submarine settings, during the Middle Jurassic - Early Cretaceous (De la Cruz *et al.*, 1994; Suárez *et al.*, 1996; Folguera & Iannizzotto, 2004; Suárez *et al.*, 2007, 2009; Echaurren *et al.*, 2016; Rivas *et*

al., 2021, 2023). In the study area, they range from the Kimmeridgian to Valanginian (Suárez *et al.*, 2005, 2015; Fig. 17).

The Lago La Plata Group underlies -and locally interfingers with- the mixed calcareous-volcaniclastic deposits of the basal Coyhaique Group (e.g., Ramos, 1981; Olivero, 1987; Scasso, 1989; Covacevich *et al.*, 1994; De la Cruz *et al.*, 1994; Suárez *et al.*, 1996; Fig. 17); this reflects marine sedimentation coeval to active volcanism (Skarmeta, 1976; Suárez *et al.*, 2015, 2023).

4.3.3. Coyhaique Group

The early marine transgression is represented by calcareous and mixed calcareous-volcaniclastic deposits settled in shallow marine settings (Scasso, 1987, 1989). Mixed facies include biohermal limestone, sandy-gravelly limestone, and bioclastic-volcanic sandstone and mudstone. These conform the Toqui Formation in Chile and its correlative units in Argentina (e.g., Suárez & De la Cruz, 1994a; Bell *et al.*, 1994; Suárez *et al.*, 2007; see review in Rivas *et al.*, 2021; Fig. 17, and section 5.5). Even though the age of these deposits is not clearly defined, sedimentation was diachronous between the (Kimmeridgian?) Tithonian-Valanginian and majorly occurred in small tectonic basins controlled by an irregular topography (Skarmeta, 1976; Skarmeta & Charrier, 1976; Haller & Lapido, 1980; Ramos, 1981; Scasso, 1989).

These coastal facies display variable thicknesses as well as rapid lateral and vertical facies changes, reflecting input of local sources and changing sediment dispersion patterns (Scasso, 1989). Overall, early transgressive facies depict the development of shallow carbonate platforms around volcanic islands (e.g., Haller & Lapido, 1980; Haller *et al.*, 1981; Ramos & Palma, 1983; Suárez *et al.*, 1996; Townsend, 1998; De la Cruz *et al.*, 2003; Suárez *et al.*, 2009, 2010a; Rivas *et al.*, 2021), with the local development of fan-deltas around tectonic highs (Scasso, 1989; Hechem *et al.*, 1993). South of Coyhaique, the development of a carbonate ramp controlled by a heterozoan faunal association (red-algae, echinoderms, bivalves), might indicate a cool-water setting in the basin during the Valanginian (Rivas *et al.*, 2023).

Shallow-marine facies are conformably covered by black mudstone of the Katterfeld Formation (Ramos, 1981; Suárez & De la Cruz, 1994a; Suárez *et al.*, 1996; 2007; Bussey *et al.*, 2010a; Rivas *et al.*, 2021), deposited between the Valanginian-Barremian (e.g., Olivero & Aguirre-Urreta, 2002; Késjar *et al.*, 2017). Locally, mudstone unconformably overlies the Lago La Plata Group, reflecting the burial of elevated areas during the enhanced transgression (Scasso, 1987, 1989; Suárez *et al.*, 2007). Mudstone is carbonaceous, laminated or brittle; it usually bears thin sandy layers and ovoidal carbonate concretions, which may contain invertebrate fossils (Ramos, 1981; Olivero & Aguirre-Urreta, 2002). These fine-grained facies are widely spread along and across the basin, representing distal shelf to slope settings (Ramos, 1976, 1981; Suárez & De la Cruz, 1994a; Suárez *et al.*, 2010a), and local prodeltaic deposits (Scasso, 1989; and the “Ingenieros Formation” *sensu* Folguera & Iannizzotto, 2004; Iannizzotto *et al.*, 2004) deposited during the post-rift or sag-phase (Scasso, 1989; Suárez & De la Cruz, 1994a; Bell *et al.*, 1994).

The dark coloured and organic-rich rocks of the Katterfeld Formation indicates deposition under oxygen-deficient conditions, likely occurring in restricted settings (Cecioni & Charrier, 1974; Skarmeta, 1974; Charrier & Covacevich, 1978; Aguirre-Urreta, 1990). The onset of black mudstone might have occurred under global humid conditions (Weisser Event; Valanginian). Locally, fossiliferous mudstone provides evidence for high productivity events possibly linked to coastal upwelling (Rivas *et al.*, 2025; submitted – in review).

Upsection, the marine succession displays a shallowing- and coarsening-upwards trend, changing from heterolithic facies towards glauconitic sandstone and conglomerate of the Apeleg Formation, deposited in coastal-paralic environments during the Hauterivian-Aptian (Ploszkiewicz & Ramos, 1977; Scasso, 1989; González-Bonorino & Suárez, 1995; Rivas *et al.*, 2025, submitted – in review). The Apeleg Formation has a transitional contact with the Katterfeld Formation, but in the Tres Lagunas area, it may overlie the Tres Lagunas Formation (Ploszkiewicz & Ramos, 1977; Masiuk & Nakayama, 1978; Scasso, 1989). The Apeleg Formation is characterised by a rich ichnofauna (Skolithos and Cruziana ichnofacies) indicative of shallow water

environments (Scasso, 1987, 1989), but it also contains bivalve coquinites and fossil wood (Ploszkiewicz & Ramos, 1977; Gonzalez-Bonorino & Suárez, 1995). The Apeleg Formation represents the transition from shallow-marine to coastal, and finally subaerial settings (deltaic, fluvial) during the regressive stage in the basin (Scasso, 1987, 1989; Ploszkiewicz & Ramos, 1977; Gonzalez-Bonorino & Suárez, 1995; Suárez & De la Cruz, 1994a; 2000; Suárez *et al.*, 2010a, 2010b). These deltaic systems may have advanced to the south and southwest, following the gradual retreat of the sea to the south (Scasso, 1989; Gonzalez-Bonorino & Suárez, 1995; Suárez *et al.*, 2015).

4.3.4. Basin Closure and Volcanism

The marine regression was coeval to tectonic contraction in the basin (Gianni *et al.*, 2019), as inferred from syn-compressional growth strata in the Apeleg Formation as well as its local angular unconformity with the overlying Divisadero Group (Suárez & De La Cruz, 2000). The final marine stages of the Apeleg Formation were also synchronous with the reactivation of arc volcanism, as reflected by the tuff cones of the Baño Nuevo Volcanic Complex, exposed near the Ñirehuao Village, about 50 km northeast of Coyhaique (Demant *et al.*, 2010; Suárez *et al.*, 2010b). Volcanic beds of this complex are interbedded with- and overlie the shallow marine sediments of the Apeleg Formation, representing a Surtseyan-like volcanism, with evidence of magma-water interaction (Demant *et al.*, 2010; Suárez *et al.*, 2010b).

During the late Early Cretaceous, a major pulse of arc-magmatism occurred along the Patagonian Batholith between 43°-47° (Pankhurst *et al.*, 2003), blanketing the marine deposits after basin closure (Aguirre-Urreta & Ramos, 1981; De la Cruz *et al.*, 1994; Fig. 18). Arc activity is associated with the creation of positive volcanic landforms at the western continental margin, provoking the inversion of the regional slope (changing to eastwards-dipping) and the displacement of the depocenters to the extra-Andean zone in the east (Aguirre-Urreta & Ramos, 1981; Scasso, 1989; Suárez *et al.*, 2010a; Echaurren *et al.*, 2016; Gianni *et al.*, 2019; Fig. 18). This volcanic pulse is represented by the subaerial, volcanic-volcaniclastic rocks of the Divisadero Group (Aptian-Cenomanian), lying conformably, but locally unconformably, above the Apeleg

Formation (Haller & Lapido, 1980; Suárez *et al.*, 2015, 2010a; Suárez *et al.*, 2023). They mark the end of marine basin evolution in this area (Suárez *et al.*, 2015, 2010a).

Both compression and arc-reactivation is regarded as caused by the westward migration of the South American plate, triggered by an accelerated sea floor-spreading rate along the Mid Atlantic Ridge during the final separation of South America and Africa (e.g., Haller & Lapido, 1980; Aguirre-Urreta & Ramos, 1981; Franzese *et al.*, 2003; Kraemer *et al.*, 2002; Fildani *et al.*, 2008; Mpodozis *et al.*, 2011; Suárez *et al.*, 2010a; Echaurren *et al.*, 2016; Cuitiño *et al.*, 2019; Ghiglione *et al.*, 2016; Gianni *et al.*, 2019; Ramos *et al.*, 2019).

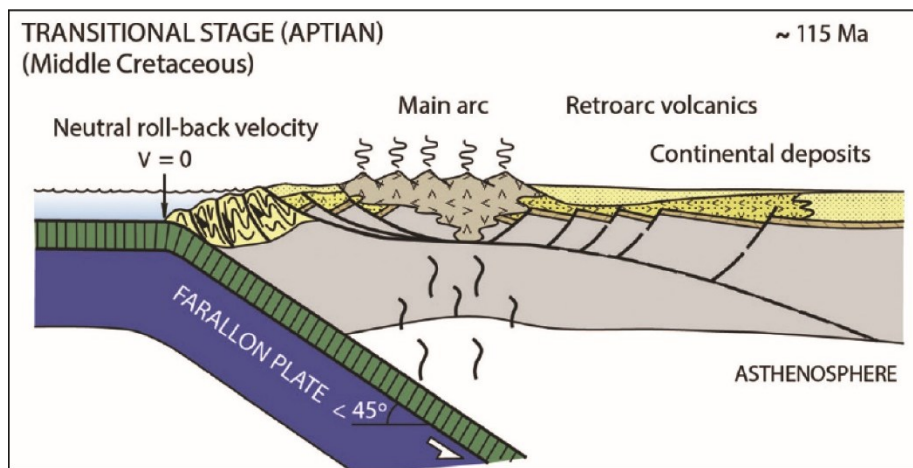


Figure 18. Tectonic setting during the closure of the ARB. This stage is marked by shallower subducting slab, triggering basin inversion, shortening-uplift, and the onset of a retroforeland volcanoclastic sedimentation. Taken from Gianni *et al.* (2019; after Ramos, 2009).

4.4. Source areas and sedimentary provenance

In the Aysén Region, radiometric dating of volcanic-volcaniclastic rocks indicate an active arc between the Late Jurassic - Late Cretaceous (Suárez *et al.*, 2015, 2023). This is reflected in the populations of detrital zircons from the Coyhaique Group and adjacent units (Suárez *et al.*, 2015, 2023). In the Coyhaique Group, the main age components comprise crystals with ages ranging between 160-136 Ma. They are linked to volcanism of the Ibáñez Formation or, alternatively, the V3-stage of the Chon Aike LIP (Suárez *et al.*, 2009, 2015, 2023; see section 3.1.2). A second component includes zircons with ages

between 136-125 Ma, which still lack a volcanic counterpart (Suárez *et al.*, 2015, 2023). However, the latter may have been linked to coeval plutons located along the western flank of the Patagonian Cordillera, which were referred to by Suárez *et al.* (2023) as the “Missing Volcanic Arc” or MIVA.

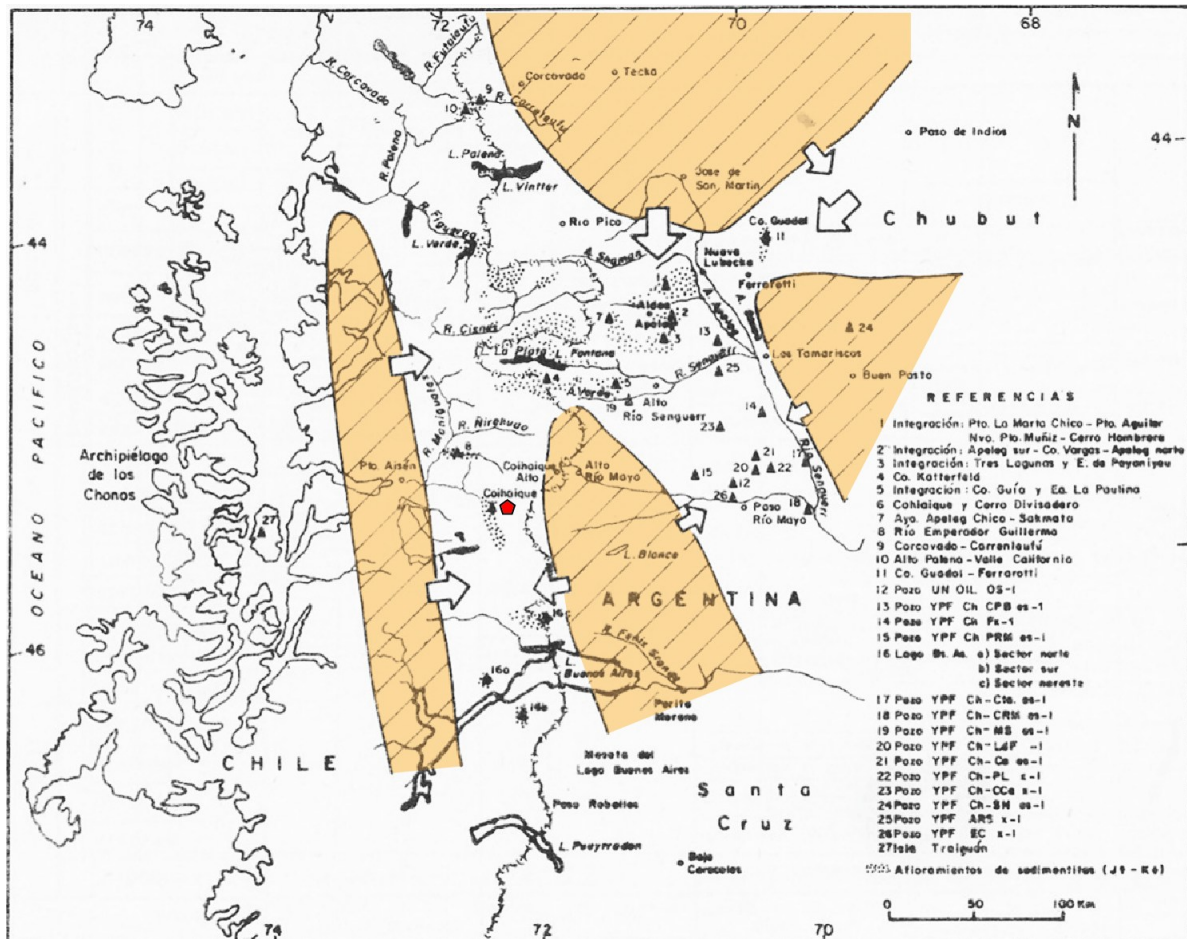


Figure 19. Main sediment source areas (yellow) of the Aysén-Río Mayo Basin in the area to the north of the General Carrera – Buenos Aires Lake. The city of Coyhaique is marked with a red polygon. Modified from Scasso (1989).

North of ca. 46°S, a major provenance shift is inferred to have occurred during the regressive marine phase (Apeleg Formation), with sediment sources located in the northern and northeastern part of the basin (Scasso, 1989; Fig. 19). In particular, besides the Patagonian Batholith sources, the Apeleg Formation also bears Late Triassic-Late Jurassic detrital zircons (U-Pb ages between 210-160 Ma; Suárez *et al.*, 2015). These sediments may have been derived from the Central Patagonian Batholith (approx. 220-200 Ma, Zaffarana *et al.*, 2014; see section 3.1.2), the Subcordilleran Batholith (187-178

Ma, Rapela *et al.*, 2005), the Chon Aike LIP (185-155 Ma; Pankhurst *et al.*, 1998), or from the “Liassic” sedimentary units exposed in the Chubut Province of Argentina (Ferrari & Bessone, 2015; Suárez *et al.*, 2015).

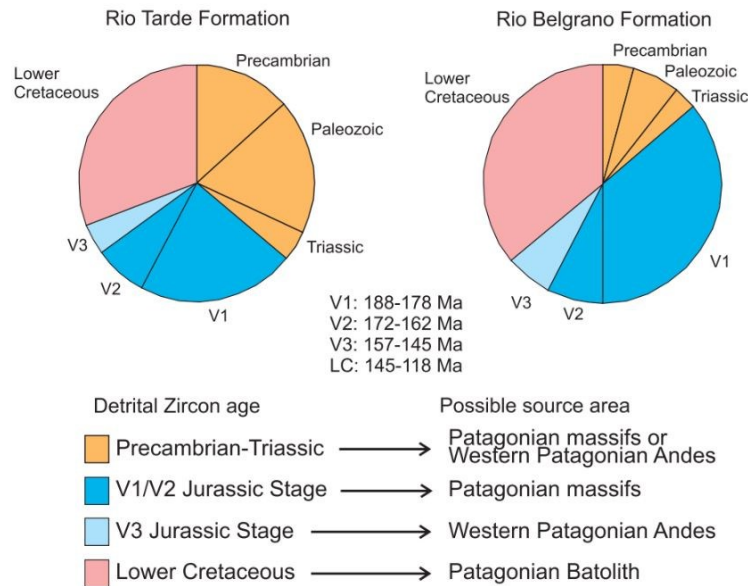


Figure 20. Inferred source areas, based on populations of detrital zircons, for the Aptian regressive sedimentary units exposed south of the General Carrera/Buenos Aires Lake (see discussion in text). Main source areas reflect exposure of the metamorphic basement (Precambrian-Palaeozoic), the Chon Aike Large Igneous Province (V1 to V3), and the igneous products of the Lower Cretaceous Patagonian Batholith. Taken from Ghiglione *et al.* (2015). For a model of the temporal evolution of the magmatic arc in southern South America, see Figure 5

South of the General Carrera/Buenos Aires Lake (ca. 46°S), sedimentary provenance shows a similar pattern. Early transgressive units display detrital zircons derived from the Ibáñez Formation or Chon Aike V3 (158-138 Ma; 150-146 Ma weighted means; Suárez *et al.*, 2016; Fig. 20). Upsection, zircon populations of the regressive Río Belgrano and Río Tarde Formations indicate a main source from the Chon Aike V1 and V2 stages (182-180 Ma, and 173-175 Ma, respectively; Ghiglione *et al.*, 2014, 2015), and scarce grains derived from the V3 stage (El Quemado Complex, 157-153 Ma). Both the Chon Aike V1 and V2 sediments reflect an input from the North Patagonian- and Deseado Massif, respectively, which are capped by these volcanic rocks (Ghiglione *et al.*, 2014, 2015; Figs. 16, 19, 20). In addition, a 122 Ma age component is remarkable, which is associated with volcanic activity of the Patagonian Batholith (Ghiglione *et al.*, 2014, 2015).

Although minor, the basement was also an area of sediment supply, as observed in metamorphic clasts within the regressive facies, as well as Triassic, Palaeozoic, and Proterozoic ages obtained by radiometric dating (Suárez *et al.*, 2023). This reflects a provenance from the North Patagonian- and Deseado Massifs (Ghiglione *et al.*, 2015), or from the Eastern Andean Metamorphic Complex to the west (Aramendía *et al.*, 2018). Basement-linked detrital zircons in both the Apeleg- and Río Belgrano Formations may have been derived from exhumed areas, after the tectonic inversion and uplift of the basin, occurring at ca. 122 Ma (Barberón *et al.*, 2015; Ghiglione *et al.*, 2015; Aramendía *et al.*, 2018; Barberón *et al.*, 2019).

5. Relationship between the Aysén-Río Mayo Basin (ARB) and coeval basins

During the Jurassic-Cretaceous transition, the western border of southernmost South America was characterised by the development of back-arc basins, while the central and eastern continental zones were characterized by the formation of passive extensional basins after rifting (Uliana *et al.*, 1989; Franzese *et al.*, 2003; see section 3.1.3; Figs. 7, 21). The evolution of the Aysén-Río Mayo Basin (ARB) and other coeval Patagonian marginal basins can be summarised in the following steps:

- 1) Back-arc extension (Mid-Late Jurassic-Early Cretaceous): development of marginal ensialic basins, reaching seafloor-spreading south of 50°S.
- 2) Syn-extensional and arc volcanism (Late Jurassic-Early Cretaceous): Chon Aike Large Igneous Province and Patagonian Batholith.
- 3) Early transgression (latest Jurassic-earliest Cretaceous: syn-rift to early post-rift phases; mixed coastal facies.
- 4) Sag-phase (Early Cretaceous): thermal subsidence; shelf-slope facies.
- 5) Marine regression (late Early Cretaceous - earliest Late Cretaceous): tectonic shortening, basin closure, regressive facies.
- 6) Arc reactivation (late Early Cretaceous - earliest Late Cretaceous): volcanic-volcaniclastic sedimentation.

The Aysén-Río Mayo Basin (**ARB**) was partly coeval to four adjacent basins: the Neuquén Basin to the north (**NQB**; sub-chapter 5.1), the Cañadón Asfalto Basin to the east-northeast (**CAB**; sub-chapter 5.2), the Golfo San Jorge Basin to the east (**SJB**; sub-chapter 5.3), and the Rocas Verdes Basin to the south (**RVB**; sub-chapter 5.4; Fig. 21). Its relationship with the Austral-Magallanes Basin to the south-southeast (**AMB**) will also be discussed (sub-chapter 5.4). Compared to these basins, the Aysén-Río Mayo Basin had a shorter lifespan (inverted in the Aptian), and a relatively thin sedimentary filling with a poor development of petroleum systems (Duhart, 1960).

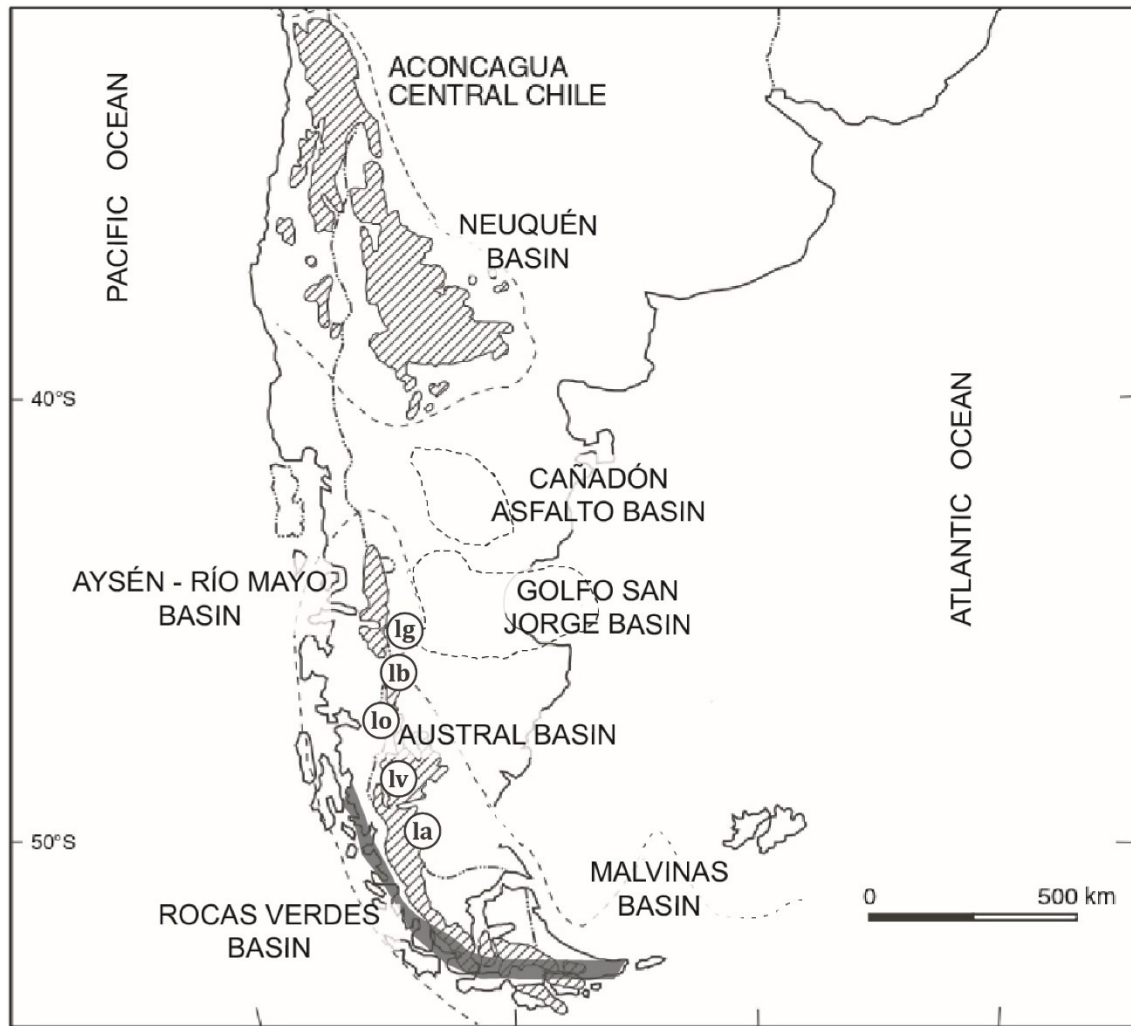


Figure 21. Location of the Aysén-Río Mayo Basin and the partly coeval adjacent basins. The Rocas Verdes Basin (RVB) is represented as a grey-coloured area at the western margin of the Austral-Magallanes Basin (outline of the RVB after Muller *et al.*, 2021). Modified from Aguirre-Urreta *et al.* (2007). Circles = Approximate location of places mentioned in text, from north to south: lg = General Carrera / Buenos Aires Lake; lb = Belgrano Lake; lo = O'Higgins / San Martín Lake; lv = Viedma Lake; la = Argentino Lake.

5.1. Neuquén Basin (32°-40°S; Late Triassic - early Cenozoic)

The Neuquén Basin was a polyphase basin developed at the central-southwestern margin of proto-South America during the Meso-Cenozoic (Howell *et al.*, 2005; Fig. 21). Its formation includes three phases: 1) a Late Triassic-Early Jurassic intraplate extensional stage (mainly continental), associated with large transcurrent faults systems, prior to the onset of the Mesozoic subduction; 2) a major Early Jurassic-Early Cretaceous back-arc stage, linked to a steep Pacific subduction, and characterised by post-rift sedimentation (mainly marine); and 3) a Late Cretaceous-Cenozoic retro-arc foreland stage (mainly continental), characterised by compression, inversion, and

flexural subsidence, after accelerated plate convergence and shallow subduction (e.g., Howell *et al.*, 2005).

The ARB was partly coeval to the second phase of the NQB, i.e. deposition of the Mendoza Group (Tithonian-Barremian). Both basins may have been separated by a tectonic high or ridge (“Dorsal de Concepción/Chubut” *sensu* Aubouin *et al.*, 1973 in Charrier & Covacevich, 1978; Riccardi, 1988), though the existence of this ridge has been questioned (Vicente, 2006). An absence of this ridge is supported by the continuity of the Jurassic volcanic arc along the southwestern margin of South America, and by the inferred connection between the Neuquén Basin and the Cañadón Asfalto (CAB) and Golfo San Jorge basins (SJB) during the Late Cretaceous (Vicente, 2006). The boundary between the NQB and the ARB has also been interpreted as a regional accommodation zone separating two morphostructural Andean segments, known as the “Bariloche Transversal” (Musacchio & Simeoni, 2008); however, this transfer zone is depicted as emplaced around ca. 47°S in its original conception (Corvalán, 1989 in Jacques, 2003; 2004), and thus further southwards from the Neuquén Basin.

A separation between both basins has also been inferred from their faunal associations, i.e., while the NQB fossils display a dominant Tethyan affinity with some influence of the Indo-Pacific Realm (Aguirre-Urreta *et al.*, 2008; Salazar & Stinnesbeck, 2016; Salazar *et al.*, 2020), the ARB fauna is regarded as endemic or more related to the Indo-African Realm (Fuenzalida, 1964; Reyes, 1970; Masiuk & Nakayama, 1978). Nevertheless, sparse fossils were shared, reflecting possible connections along the Pacific margin (Aguirre-Urreta *et al.*, 2008). The latter include cephalopods, determined only at genus-level (*Chacantuceras*, *Crioceratites*, and *Olcostephanus*; Aguirre-Urreta & Rawson, 1998; Aguirre-Urreta *et al.*, 2005; 2007; 2008; *Cymatoceras*; Cichowolski, 2003; Salazar *et al.*, 2014), trigoniids (Reyes, 1970; Lazo, 2007), red algae (*Archamphiroa jurassica*; Steinmann, 1930; Bucur *et al.*, 2009; Rivas *et al.*, 2023), and foraminifera (*Lenticulina nodosa*, *Astacolus gibber*; Masiuk & Nakayama, 1978; Rivas *et al.*, 2025, submitted – in review).

5.2. Cañadón Asfalto Basin (42°-44°S; 68°-70°W; Early Jurassic - Cenozoic)

The Cañadón Asfalto Basin (CAB) was an extensional basin located in Central Patagonia, between the North Patagonian Massif and the Golfo San Jorge Basin (SJB; Figari *et al.*, 2015; Allard *et al.*, 2022; Fig. 21). Both the Cañadón Asfalto (CAB) and the Golfo San Jorge basins (SJB) have been regarded as generated by intraplate extension after the supercontinent break-up, though other hypotheses include extension linked to the opening of the Weddell Sea, or back-arc extension after slab-rollback (Allard *et al.*, 2022). The structure of the CAB consists of hemigrabens limited by Paleozoic basement blocks (Figari *et al.*, 2015), and its evolution comprises three main extensional phases separated by periods of tectonic inversion.

The J-K basin fill of the CAB is predominantly subaerial, except for Upper Cretaceous marine rocks, linked to an Atlantic transgression. Three megasequences, separated by unconformities, have been defined in the CAB (Allard *et al.*, 2022):

- 1) Megasequence I (Hettangian-Upper Jurassic/Hauterivian?): lacustrine, volcanoclastic and fluvial deposits settled during rifting.
- 2) Megasequence II (Barremian-Turonian?): fluvial-alluvial deposits of the Chubutian Group (Barremian-Campanian; see “Chubutian Cycle” in 5.3 below).
- 3) Megasequence III (Campanian-Cenozoic): shallow marine units from an Atlantic transgression (Campanian-Danian), and continental sediments settled in intermontane basins during inversion-extension alternations.

Based on their contrasting facies, there was, apparently, no connection between the CAB and the ARB. In addition, there is a stratigraphic hiatus in the CAB (Tithonian-Hauterivian *sensu*; Valanginian-Barremian *sensu* Allard *et al.*, 2022), during marine sedimentation in the ARB.

5.3. Golfo San Jorge Basin (44°-48°S; 66°-71°W; Early Jurassic - Quaternary)

The Golfo San Jorge Basin (SJB) is a mainly extensional basin developed in Central-Eastern Patagonia, at the Atlantic margin of South America (Sylwan, 2001; Sylwan *et al.*, 2011; Fig. 21). Its onset is regarded as caused by intracratonic extension following the Mid-Late Jurassic rifting, as well as the subsequent back-arc extension (Figari *et al.*, 2002; Sylwan, 2001; Sylwan *et al.*, 2011 *et al.*, *op. cit.*, Ramos, 2015; see section 3.1.3). The SJB extends between the Patagonian Cordillera and the Atlantic Ocean, including an offshore extension; latitudinally, it is bounded by two cratonic blocks (structural highs), the North Patagonian- or Somun Cura Massif to the north, and the Deseado Massif to the South (Sylwan, 2001; Sylwan *et al.*, 2011; Ramos, 2015).

The basin fill of the SJB consists of five megasequences deposited above a Palaeozoic igneous-metamorphic basement rocks. Megasequences are separated by unconformities, reflecting an alternation of rifting and foreland phases (Figari *et al.*, 2002; Ramos, 2015). In the SJB, the J-K boundary comprises three megasequences (MS-0 to MS-II):

- 1) MS0 (Mid-Upper Jurassic): “Megasequence 0” or “Volcanic-Sedimentary Complex” (“economic basement”), synextensionally settled during the early rifting.
- 2) MS-I (Tithonian-Hauterivian): “Megasequence I” or “Neocomian Cycle”, deposited during the late rifting.
- 3) MS-II (Barremian-Aptian): “Megasequence II”, including the initial part of the “Chubutian Cycle”, associated with the early sag-phase (Sylwan, 2001; Sylwan *et al.*, 2011).
- 4) MS-III/IV: The Megasequence III was deposited in the Cenozoic under alternating extension and inversion phases, whereas Megasequence IV includes Quaternary deposits (Sylvan *et al.*, 2011).

The MS-0 includes subaerial volcanic rocks, depicted as part of the Chon-Aike LIP (Pankhurst *et al.*, 1998); they are partly coeval to the Lago La Plata Group (Sylwan, 2001;

Sylwan *et al.*, 2011; see sections 3.1.2 and 4.3.2). The unit underlies the MS-I, comprising lacustrine- (Pozo Anticlinal Aguada Bandera Formation; Tithonian-Valanginian) and lacustrine-deltaic-estuarine deposits (Pozo Cerro Guadal Formation; Valanginian-Hauterivian) of the Las Heras Group. The latter is covered by tuffaceous, fluvio-deltaic-lacustrine rocks of the Pozo D-129 and Matasiete Formations (Barremian-Aptian), which conform the lowermost units of the MS-II (see Figure 7 in Figari *et al.*, 2002; Figure 4 in Sylwan *et al.*, 2011).

Given the continental nature of the SJB filling, both the SJB and ARB are regarded as separated by a N-S-oriented tectonic high, also referred to as “Dorsal Río Mayo” (Suero, 1955 in Scasso, 1987). However, the report of marine microfossils from several drill cores of the Pozo Anticlinal Aguada Bandera Formation, at the western margin of the SJB, reflects brief marine incursions from the Pacific. These are linked to the maximum flooding stage in the ARB, depicted as occurring in the Aptian (Scasso, 1987, 1989), or in the Hauterivian (Aguirre-Urreta, 1990). Given the ambiguous age of the Pozo Anticlinal Aguada Bandera Formation (Kimmeridgian? Tithonian-Valanginian; Sylwan *et al.*, 2011), this event must be revised.

5.4. Rocas Verdes Basin & Austral-Magallanes Basin (49°-56°S)

Historically, the Aysén-Río Mayo Basin (43°-49°S *sensu* Suárez *et al.*, 2010a), has been depicted as the northern part of a unique, widespread trough known as Austral- or Magallanes Basin (43°-56°S), as named in Argentina and Chile, respectively (**AMB**; Figs. 7, 21; e.g., Fuenzalida, 1964; Leanza & Leanza, 1973; Riccardi, 1976; 1977; Masiuk & Nakayama, 1978; Riccardi & Roller, 1980; Aguirre-Urreta & Ramos, 1981; Ramos, 1989; Aguirre-Urreta, 2002; Suárez *et al.*, 2009, 2010a; Carrizo & Del Fueyo, 2015; Ramos *et al.*, 2019; Suárez *et al.*, 2023). The latter has also been referred to as the “Patagonian Basin” -or “geosyncline”- in earliest studies (Cecioni & Charrier, 1974; Charrier & Covacevich, 1978; Masiuk & Nakayama, 1978). The two basins display distinct lithological and structural features as well as different geological evolution to the north and south of the Viedma Lake, at about 49°S (Cecioni & Charrier, 1974; Charrier & Covacevich, 1978; Suárez & De la Cruz, 1994a; Bell *et al.*, 1996; Townsend, 1998; Suárez *et al.*, 2010a; Aramendía *et al.*, 2018). Suárez *et al.* (2010a) proposed a separation of the basins in two tectonic segments: the “Aysén Segment” to the north of parallels 49th-50th

south, comprising the Aysén-Río Mayo Basin, and the “Magallanes Segment” to the south. Both segments may have been separated by an E-W-trending transform fault (Suárez *et al.*, 2010a; see section 3.1.3).

In the literature, there is no *consensus* regarding the onset and nature of the Austral-Magallanes Basin (AMB). Some authors consider the Mid Jurassic - Early Cretaceous Rocas Verdes Marginal Basin (RVB) as the extensional part in the whole evolution of the AMB (Natland *et al.*, 1974; Biddle *et al.*, 1986; Arbe, 1989; Aguirre-Urreta, 1990; Suárez *et al.*, 2010a; Richiano *et al.*, 2015; 2019; Barberón *et al.*, 2019; Cuitiño *et al.*, 2019); others depict both troughs as two independent, partly coeval, parallel basins (Franzese *et al.*, 2003; Navarrete *et al.*, 2018); while still other authors even restrict the RVB only to the ophiolitic complexes conforming the paleo-seafloor (“rocas verdes” *sensu stricto*; Mpodozis & Ramos, 2008). The approach adopted here distinguishes both the extensional and the foreland stages (e.g., Fosdick *et al.*, 2011; Richiano *et al.*, 2019; VanderLeest *et al.*, 2022), i.e. it restricts the Rocas Verdes Basin to the back-arc extensional phase (Mid Jurassic - Early Cretaceous), including the syn-/post-rift stages and the seafloor-spreading event. In that interpretation, the Austral-Magallanes Basin is restricted to the foreland evolution, starting in the late Early- to early Late Cretaceous, after the inversion of the RVB (Wilson, 1991; Stern & De Wit, 2003; Fildani & Hessler, 2005; Mpodozis, 2007; Dávila *et al.*, 2019; Muller *et al.*, 2021).

An additional stratigraphical complication arises from the lateral variability of sedimentary systems along- and across the Patagonian basins (ARB, RVB, AMB), changing between- or within singular depocenters (Cuitiño *et al.*, 2019). This has resulted in multiple binational stratigraphic schemes proposed in Chile and Argentina, defining correlative formations from outcrops, subsurface, and offshore drill cores (e.g., see “Cuadro 3” in Charrier & Covacevich, 1978; Table 18 in Riccardi, 1988; Figure 7 in Arbe, 1989; Figure 1 in Arbe, 2002; Figure 2 in Mpodozis *et al.*, 2011; Figure 2 in Cuitiño *et al.*, 2019; Figure 2 in VanderLeest *et al.*, 2022). Based on the previous, a brief description of both segments, north and south of 49°-50°S (Suárez *et al.*, 2010a; Ghiglione *et al.*, 2015), will be separately presented here.

5.4.1. The area between the General Carrera and Argentino Lakes (46°-50°S)

Early Cretaceous rocks exposed south of the General Carrera/Buenos Aires Lake (46°30'S) are referred to as the northern part of the AMB (e.g., Aguirre-Urreta, 1990; Ramos, 1989; De la Cruz *et al.*, 2004, Ghiglione *et al.*, 2015; Richiano *et al.*, 2015; Aramendía *et al.*, 2018; Barberón *et al.*, 2019; Fig. 21), though some authors regard them as the septentrional part of the RVB (Richiano *et al.*, 2019; VanderLeest *et al.*, 2022; Fig. 21). Although facies and timing of marine sedimentation are slightly different in both segments, they might have been connected, undergoing a similar geological evolution during the J-K transition, at least southwards until 48°S (Aguirre-Urreta & Ramos, 1981; Riccardi, 1988; Scasso, 1989; De la Cruz *et al.*, 2003; Suárez *et al.*, 2010a; Barberón *et al.*, 2019; Fig. 21).

On the Chilean side (46°-48°S), the J-K stratigraphy follows the same scheme proposed for the Coyhaique area to the north (43°-46°S), i.e. extending the distribution of the Lago La Plata- (Ibáñez Formation), Coyhaique-, and Divisadero Groups (De la Cruz *et al.*, 2003; 2004; see section 4.3). In contrast, in the Santa Cruz Province of Argentina (46°-52°S), these units are known by different formational names (e.g., Giacosa *et al.*, 2001; Escosteguy *et al.*, 2003). There, the Upper Jurassic syn-extensional volcanic rocks comprise the El Quemado Complex (157-153 Ma; Pankhurst *et al.*, 2000), which is partly correlative to the Lago La Plata Group (Ramos, 1989; Pankhurst *et al.*, 2000; 2003).

In the Belgrano-Pueyrredón Lake area (46°-48°S), the marine stage is represented by the Pueyrredón Group, overlying the El Quemado Complex (Ramos, 1979; Giacosa *et al.*, 2001; Figs. 22, 23). There, the late rifting and early sag-phase corresponds to the sandy beds of the Springhill Formation (Berriasian-Valanginian in this area; Giacosa *et al.*, 2001 and references therein), defined in the Magallanes segment (54°S; see section 5.4.2), and deposited in continental to coastal settings during the early transgression (Ramos, 1979; Giacosa *et al.*, 2001; Escosteguy *et al.*, 2003). The Springhill Formation passes transitionally to black mudstone of the Río Mayer Formation (Valanginian? Hauterivian-Barremian in this area; Aguirre-Urreta & Ramos, 1981; Kraemer & Riccardi, 1997; Giacosa *et al.*, 2001; Ghiglione *et al.*, 2015; Aramendía *et al.*,

2018), settled in distal shelf settings during the maximum flooding stage (Ramos, 1979; Giacosa *et al.*, 2001). The latter is gradually covered by the regressive, coastal facies of the Río Belgrano Formation, the youngest member of the Pueyrredón Group (Barremian-Aptian; Riccardi, 1988; Aguirre-Urreta & Ramos, 1981; Giacosa *et al.*, 2001; Ghiglione *et al.*, 2015; Figs. 22, 23). In contrast to the Coyhaique Group, which underlies volcanic strata (Divisadero Group), the marine succession in this area is covered by fluvial and tuffaceous rocks assigned to the Río Tarde Formation (Aptian-lower Cenomanian; Aguirre-Urreta & Ramos, 1981; Giacosa *et al.*, 2001; Ghiglione *et al.*, 2015).

South of 48°S, regressive facies display a lithological change, reflecting a delayed onset of the coastal retreat. This is shown by the transitional contact between the Río Mayer Formation and the coastal-fluvial facies of the Kachaike Formation (= Piedra Clavada Formation; Aptian-lower Cenomanian; Fig. 22) at the O'Higgins/San Martín Lake (48°S; Riccardi, 1988; Ramos, 1979; Giacosa *et al.*, 2001; Richiano *et al.*, 2012; Ghiglione *et al.*, 2015; 2016), and by the estuarine-continental deposits of the Puesto El Moro Formation (Albian-Turonian?), exposed around the eponymous lake (49°S; Giacosa *et al.*, 2001; Richiano *et al.*, 2012; Varela *et al.*, 2019).

The fine-grained facies of the Río Mayer Formation, linked to the sag-phase, have been identified as far south as the Argentino Lake (50°S), where the stratigraphical classification between both the Aysén and Magallanes segments (*sensu* Suárez *et al.*, 2010a) is partly overlapped (see Fig. 2.2. in Richiano *et al.*, 2012). To the south, in the Magallanes segment, the Río Mayer Formation has been correlated with the Zapata Formation (Berriasian-Albian, see section 5.4.2), though the latter reflects a deeper depositional setting (shelf-slope; Fig. 22).

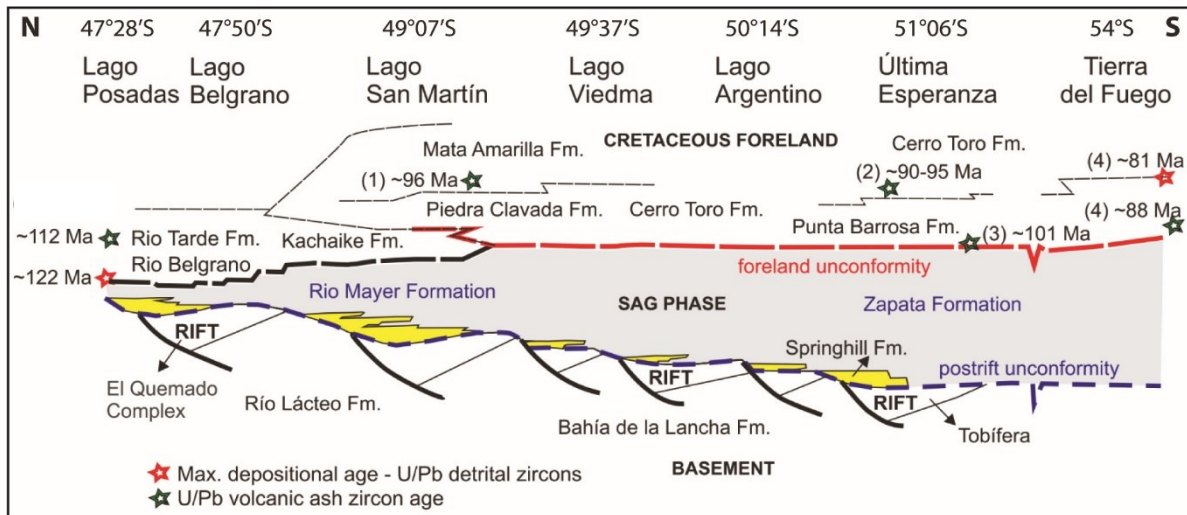


Figure 22. Tectonostratigraphic cross-section displaying the correlation of units south of the General Carrera/Buenos Aires Lake (46°28'S). Note: 1) the syn-rift sedimentation of the volcanoclastic deposits above the basement; 2) the discontinuous and diachronic (northwards-younging), retrogradational early transgressive facies (yellow); 3) The relatively thinner sag-phase successions north of 49°S and their diachronic top (southwards younging). Modified from Ghiglione *et al.* (2015; after Arbe, 2002; and references therein).

5.4.2. The area south of Lago Argentino (> 50°S)

In the Magallanes Segment (*sensu* Suárez *et al.*, 2010a), the Mid-Late Jurassic rifting resulted in the formation of a hemigraben-controlled extensional topography (Dalziel, 1981; Hanson & Wilson, 1991; Mpodozis *et al.*, 2011), considered here as the onset of the “Rocas Verdes Basin” (RVB; see next paragraph). Tectonic troughs were synextensionally filled by marine volcano-sedimentary deposits of the Tobífera Formation (Wilson, 1991; Pankhurst *et al.*, 1998; 2000; Fildani & Hessler, 2005), unconformably overlying the Paleozoic basement (Fig. 22). Volcanic rocks emplaced between ca. 170-140 Ma are regarded as part of the Chon Aike LIP (e.g., Pankhurst *et al.*, 1998; 2000; Fildani *et al.*, 2003; Muller *et al.*, 2021; VanderLeest *et al.*, 2022).

During the Late Jurassic - earliest Early Cretaceous, rifting progressed to seafloor spreading, triggering the northward-directed “unzipping” of a deep marginal basin (“Rocas Verdes Marginal Basin” *sensu stricto*; Dalziel, 1974; 1981; Stern & De Wit, 2003; VanderLeest *et al.*, 2022 and references therein; Figs. 21, 22). This paleo-seafloor comprises several obducted ophiolitic complexes with ages between 152 - 142 Ma (Calderón *et al.*, 2007). To the east, the proto-oceanic basin was bounded by a normal-faulted, passive or “cratonic” margin, with a west-facing slope (see Figure 2 in Hanson & Wilson, 1991; Figure 15 in Wilson, 1991). The genesis of the RVB is still discussed, with

either back-arc extension, or rifting after opening of the Weddell Sea, as possible causes (Mpodozis & Ramos, 2008).

During the latest Late Jurassic - Early Cretaceous, extension was followed by thermal subsidence, and the north- and eastwards expansion of the marine transgression (Fildani & Hessler, 2005; Mpodozis *et al.*, 2011; VanderLeest *et al.*, 2022). The early transgression comprises the continental- to shallow marine deposits of the Springhill Formation, settled here between the Tithonian-Valanginian (Thomas, 1949; Riccardi, 1976; Arbe, 2002; Mpodozis *et al.*, 2011; Schwarz *et al.*, 2011; Figs. 22, 23), though an older age for this unit has also been inferred (Oxfordian-Kimmeridgian? Arbe, 2002, and references therein). The retrograding facies of the Springhill Fm. eroded the Tobífera Formation, filling hemigrabens in the northern and eastern parts of the RVB (Biddle *et al.*, 1986; Arbe, 2002; Mpodozis *et al.*, 2011; Fig. 22). Its lower subaerial facies depict input of local sources, with exposure throughout the Berriasian (Arbe, 2002; Schwarz *et al.*, 2011).

In the western parts of the RVB, shelf- and slope settings were covered by dark-coloured mudstone and fine-grained sandy rhythmites of the Zapata Formation (and correlative fine-grained units), conformably overlying the Tobífera Formation (Biddle *et al.*, 1986; Wilson, 1991; Suárez *et al.*, 2010a; Fig. 22). These fine-grained facies comprise a Berriasian-Albian (Turonian?) time-span (Wilson, 1991; Fildani *et al.*, 2008; Cuitiño *et al.*, 2019; and references therein).

The onset of the compression, and beginning of a foreland stage, is marked by the thicker sandy rhythmites of the Punta Barrosa Formation (Biddle *et al.*, 1986; Wilson, 1991; Fildani *et al.*, 2003; Figs. 22, 23). The Punta Barrosa Formation overlies the Zapata Formation with a transitional contact; the succession displays a thickening-upwards trend, reflecting a reversal of the source area (Biddle *et al.*, 1986; Wilson, 1991; Fildani *et al.*, 2003). The extensional-to-foreland transition has been regarded as occurring across the Albian-Cenomanian boundary (Wilson, 1991; Cuitiño *et al.*, 2019), but the Punta Barrosa Formation may not be older than Turonian (92 Ma *sensu* Fildani *et al.*,

2003). As shown in 5.4.1, in the northern segment the marine stage ended in the Aptian (43°-48°S) or Albian (49°-50°S). In contrast, in the RVB there is a gap between the inferred beginning of the tectonic shortening (Punta Barrosa Formation; Figs. 22, 23) and the onset of the foreland Austral-Magallanes Basin (AMB). This gap has been interpreted as the lapse between the closure and inversion of the Rocas Verdes Basin and the obduction of the ophiolite complexes (RVB; Fildani *et al.*, 2003; Suárez *et al.*, 2010a; Mpodozis *et al.*, 2011; Ghiglione *et al.*, 2016; Cuitiño *et al.*, 2019).

5.5. Stratigraphic correlations of the Coyhaique Group

Precise correlation of the early transgressive rocks of the Coyhaique Group is difficult, due to their scattered and discontinuous exposures (covered and/or faulted), rapid lateral changes of facies (Haller & Lapido, 1980; Scasso, 1987; 1989; Suárez & De la Cruz, 1994a; De la Cruz *et al.*, 2003), and punctuated relative ages, usually inferred indirectly from fossils or contact relationships (e.g., Covacevich *et al.*, 1994; De la Cruz *et al.*, 1996; Suárez *et al.*, 1996; 2005; 2009). In Chile, these rocks have been included in a singular unit known as the Toqui Formation (Tithonian-Valanginian, Hauterivian? Suárez *et al.*, 2009; 2010a; 2015; Fig. 23). The unit comprises mixed calcareous-volcaniclastic sections with changing lithological compositions and scattered inferred ages (see Table 2 of Suárez *et al.*, 2009; and Figure 2A of Rivas *et al.*, 2021), including Tithonian (Fuenzalida, 1965; De la Cruz *et al.*, 1995; 1996; Suárez *et al.*, 2016), Berriasian (Covacevich *et al.*, 1994; De la Cruz *et al.*, 1996), and Valanginian exposures (Pankhurst *et al.*, 2003; De la Cruz *et al.*, 2003; Suárez *et al.*, 2005; 2015; Rivas *et al.*, 2023).

In Argentina, in the area adjacent to the La Plata-Fontana Lakes, these rocks have been categorised as several singular units, which have been historically correlated with the Toqui Formation (Suárez & De la Cruz, 1994a; De la Cruz *et al.*, 2003). These formations include: 1) the Upper Jurassic Cotidiano Formation (Oxfordian-Kimmeridgian *sensu* Ramos, 1976; 1981; upper Tithonian *sensu* Olivero, 1987; Bucur *et al.*, 2009), and the “Arroyo Pedregoso Beds” (upper Tithonian *sensu* Ramos, 1981; Olivero, 1982; 1987); and 2) the Early Cretaceous “Arroyo Blanco Beds” (Berriasian-Hauterivian *sensu* Olivero, 1982; 1987; upper Valanginian *sensu* Olivero & Aguirre-Urreta, 2002), and the Tres Lagunas Formation (Valanginian-lower Hauterivian *sensu*

Ploszkiewicz & Ramos, 1977; Berriasian *sensu* Olivero, 1983; Tithonian? – upper Valanginian *sensu* Scasso & Kiessling, 2002; Fig. 23).

As presented in section 5.4, southwards of 46°S, the Coyhaique Group is correlative to the Pueyrredón Group, and in particular the Springhill Formation which has been chronostratigraphically correlated with both the Toqui- and the Tres Lagunas Formations (Riccardi, 1976; Riccardi & Rolleri, 1980; De la Cruz *et al.*, 2003; Nullo *et al.*, 2006; Fig. 23). The Springhill Formation was defined in Tierra del Fuego (54°S; Thomas, 1949), but it has been identified as far north as Cochrane/Pueyrredón Lake (47°S; Ramos, 1979; Giacosa & Franchi, 2001).

Between 46°-50°S, the Katterfeld Formation may be litho- and partly chronostratigraphically correlative with the Río Mayer Formation (Godoy *et al.*, 1997; Giacosa & Franchi, 2001; Escosteguy *et al.*, 2003; De la Cruz *et al.*, 2003; and references therein; Fig. 23); given their depositional environments, both units may nevertheless represent different geotectonic settings (Godoy *et al.*, 1997). South of 50°S, a partial correlation is established with the Zapata Formation and its organic-rich equivalents in subsurface (e.g., Pampa Rincón Formation, Lower Palermo Aike Formation, Lower Inoceramus Formation, “Estratos con Favrella”; Biddle *et al.*, 1986; Mpodozis *et al.*, 2011; see section 5.4.2).

The regressive rocks of the Apeleg Formation might be litho- and chronostratigraphically correlative to the Río Belgrano Formation, exposed between 46°-48°S (De la Cruz *et al.*, 2003; Fig. 23).

The Coyhaique Group was covered by the volcanic Divisadero Group, identified as south as 47°S (Aguirre-Urreta & Ramos, 1981). To the south, this volcanic group is chronostratigraphically correlative with the siliciclastic Río Tarde-, Kachaike-, Piedra Clavada-, and Lago Viedma Formations (Fig. 23).

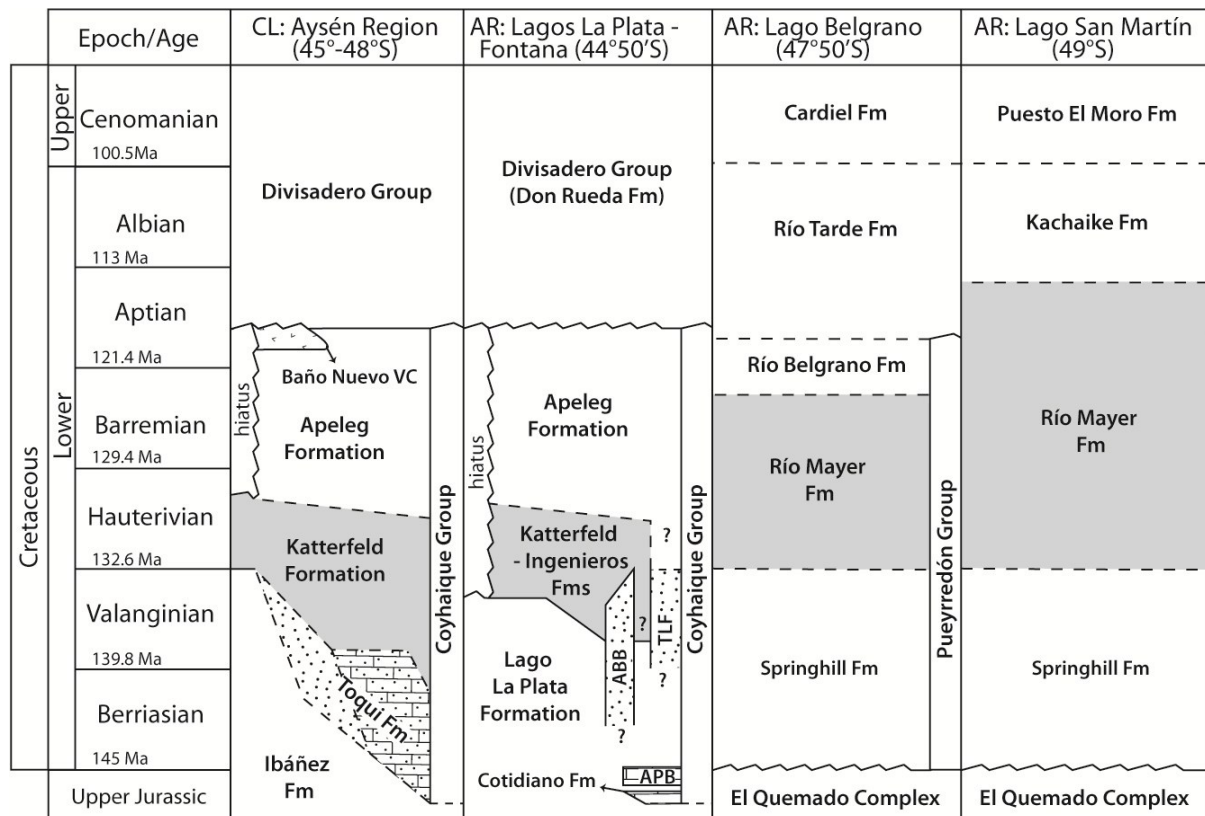


Figure 23. North-to-south stratigraphic correlation of the J-K formations from Patagonia (45°-49°S; simplified). Abbreviations: Outcrops are both exposed in Chile (CL) and Argentina (AR); ABB = "Arroyo Blanco Beds"; APB = "Arroyo Pedregoso Beds"; TLF = Tres Lagunas Formation; VC = Volcanic Complex. For an extended version addressing the units exposed south of 49°S, see Figure 22. References for the Aysén Region and the La Plata and Fontana Lakes, modified from Rivas *et al.* (2021; and references therein). For the Belgrano and San Martín Lakes, see Ghiglione *et al.* (2015), Richiano *et al.* (2015), Aramendía *et al.* (2018), and Varela *et al.* (2019).

5.6. Gondwana connections

Based on similar or shared fossil content, marine connections have been suggested between the Patagonian marine basins (ARB, RVB) and coeval basins from south of Gondwana. These reflect the opening of shallow seaways and the migration of fauna during Valanginian-Hauterivian times and onwards, after the break-up of the supercontinent during the Late Jurassic - Early Cretaceous (Cecioni & Charrier, 1974; Malumian & Masiuk, 1975; Aguirre-Urreta & Ramos, 1981; Aguirre-Urreta, 1990; Riccardi, 1991; Aguirre-Urreta *et al.*, 2008; Stinnesbeck *et al.*, 2014). The latter started at ca. 167 Ma, with the separation between South Africa and Antarctica, causing the opening of the Somali- and Mozambique Basins (Jokat *et al.*, 2003; König & Jokat, 2006). However, based on the presence of Tithonian ammonite taxa with Tethyan and Indo-Pacific affinities in Central Chile and Argentina (NQB), a connection to the Tethyan Realm through either the Hispanic Corridor or the Indo-Austral Seaway may have been

established as early as the latest Jurassic (Salazar, 2012; Stinnesbeck et al., 2014; Salazar & Stinnesbeck, 2016).

A relationship between Patagonian and South African basins has been inferred from the *Lenticulina nodosa*-*Astacolus gibber* foraminiferal assemblage, reported from both the Lower Cretaceous Katterfeld- (ARB) and Pampa Rincón Formations (RVB; Malumian & Masiuk, 1975; Masiuk & Nakayama, 1978). This assemblage is shared with the Majunga (Mahajanga) Basin in Madagascar; while the *Majungaella nematis* ostracod assemblage in the ARB is shared with the Algoa Basin in South Africa (Masiuk & Nakayama, 1978; Musacchio & Simeoni, 2008). An African affinity has also been proposed by Sigal *et al.*, (1970 in Natland *et al.*, 1974), based on foraminifera registered in the Springhill Formation.

A Patagonian and Indo-African connection is also supported by trigoniids recognized in the Coyhaique Group (Fuenzalida, 1964; Reyes, 1970; Cecioni & Charrier, 1974), in particular *Transitrighonia herzogi* (*ex Steinmanella herzogi* in Reyes, 1970; Cooper & Leanza, 2017), *Pterotrighonioides rogersi* (*ex Megatrighonia rogersi* in Reyes, 1970; Cooper, 2015a), and *Iotrighonia stowi* (*I. stowi* var. *aisenensis* Reyes, 1970; Cooper, 2015c). In addition, Lower Cretaceous (“Neocomian”) oysters of the genus *Aetostreon* recorded in southern Chile (Coyhaique) and Argentina display affinities with specimens from Pakistan and middle-eastern Africa (Cecioni & Charrier, 1974; Rubilar, 2000). Both steinmanellids and *Aetostreon* may have migrated from the Andean Subrealm to the other provinces (Cooper & Leanza, 2017; Toscano & Lazo, 2020, respectively; Fig. 24).

Ammonites in the Patagonian basins (ARB, RVB) display strong endemism, but sporadic immigration of genera also occurred (Riccardi, 1984; 1991; Aguirre-Urreta, 1990; 2000); this was usually associated with highstands (e.g.; Aguirre-Urreta *et al.*, 2002; 2007; Lehmann *et al.*, 2015). In contrast to central Chile and Argentina (NQB), where Tithonian taxa with a Tethyan affinity are abundant (Aguirre-Urreta *et al.*, 2008; Salazar & Stinnesbeck, 2016; Salazar *et al.*, 2020), Patagonian ammonites with a Tithonian-Berriasian age are not well represented, including only sparse genera (e.g.,

Aulacosphinctes, *Berriasella*, *Blanfordiceras*; Riccardi, 1988; 1984; 1991; Covacevich *et al.*, 1994).

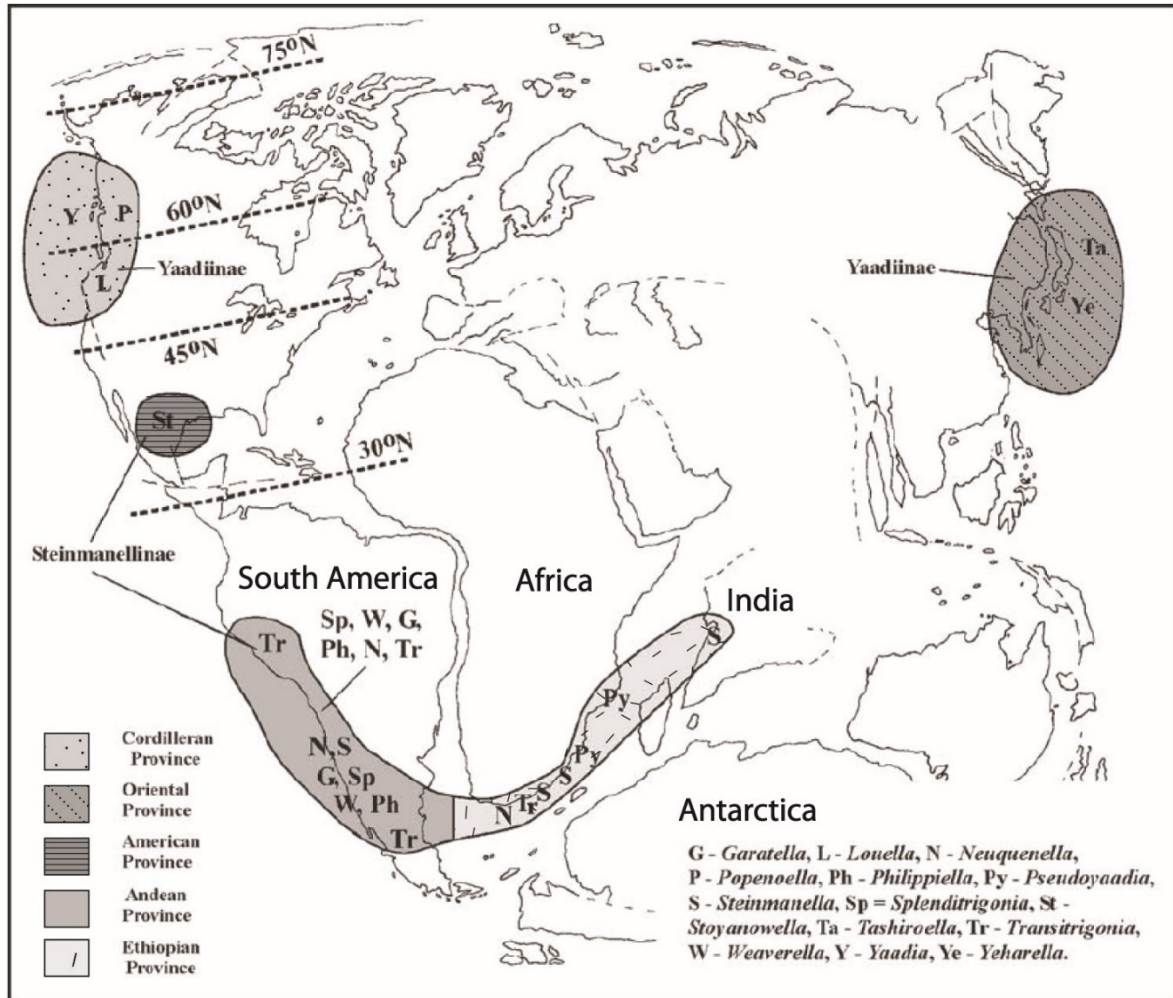


Figure 24. Paleobiogeographic distribution of steinmanellid bivalves in the Hauterivian, including their main realms and inferred connections (see discussion in text). Note the southern connection between southern South America and the Indo-African zones. Modified from Cooper & Leanza (2017).

In the ARB, endemism is more marked during the Valanginian-Hauterivian, an interval characterized by low faunal diversity (e.g., *Chacantuceras*, *Favrella*; Riccardi, 1991; Aguirre-Urreta *et al.*, 2007; Lehmann *et al.*, 2015); however, some connections are inferred from the sporadic immigration of genera with a Tethyan-Boreal affinity (e.g., crioceratitids, *Kilianella*, *Thurmanniceras*; Aguirre-Urreta, 1990; Riccardi, 1991; Aguirre-Urreta, 2002; Olivero & Aguirre-Urreta, 2002). The Barremian is regarded as the onset of the “Austral Realm” (including Patagonia, Australia, Africa, and Madagascar), providing evidence of a free marine circulation between the southern

parts of Patagonia and Africa (e.g., *Cryptocrioceras*, *Sanmartinoceras*; Aguirre-Urreta, 1990; Lehmann *et al.*, 2015). In southernmost South America, the faunal diversity of ammonites reaches a maximum in the Aptian, due to an open circulation in the South Atlantic Ocean, marked by the cosmopolitan distribution of ancyloceratids in the Tethyan-, Boreal-, and Austral Realms (Aguirre-Urreta, 1990; 2002; Lehmann *et al.*, 2015).

6. Summary and conclusions

This dissertation presents the most comprehensive historical, stratigraphical, and paleoenvironmental revision of the Aysén-Río Mayo Basin and its sedimentary fill, i.e., the Coyhaique Group, to date (Chapter 1). The Aysén-Río Mayo Basin was a marginal basin developed during the Jurassic-Cretaceous transition (Tithonian-Aptian) in southwestern Gondwana, currently southern Chile and Argentina (latitude 43°-47°/49°S?, also known as Central Patagonia). Thirty-eight sedimentary logs were described between the El Toqui Mine and Cerro La Virgen, in the Coyhaique Province, Aysén Region (45°S; see Chapter 2). Facies models of the Coyhaique Group in the study area depict a transgressive-regressive succession settled between the Valanginian-Aptian.

An overview of the global and regional geotectonic, magmatic, and paleoclimatic conditions prevailing during the Jurassic-Cretaceous transition is also discussed in Chapter 3. Overall, the geotectonic setting is marked by the break-up of the Gondwana supercontinent and the westwards relative displacement of the proto-South American plate (sub-chapter 3.1), reactivating the subduction at its western margin. Extensional tectonics after continental break-up, together with back-arc extension, triggered the generated rift-basins across the proto-South American continent. The J-K magmatism was marked by a widespread rhyolitic effusion linked to cortical anatexis (Chon Aike Large Igneous Province), and the emplacement of consecutive volcanic arcs, experiencing a westwards-migration caused by slab rollback. The Late Jurassic – Early Cretaceous paleoclimate is characterized by the appearance of symmetric climate zones south and north of the equator (see sub-chapter 3.2.). Models depict long-termed warm periods (greenhouse events) interrupted by short-termed cool-spans. Alternatively, these changes may represent an alternation of arid and humid periods. This warm-cool alternating trend has also been inferred for the southern hemisphere (e.g., Brysch, 2018, Cavalheiro et al., 2021) where the presence of cool-spans has been tentatively proposed for the Aysén-Río Mayo Basin (see Appendix 8.2; Rivas *et al.*, 2023). The J-K global eustasy shows a relative sea level fall starting in the Tithonian and reaching a minimum

in the Valanginian. The latter was followed by a gradual sea level rise reaching a maximum either in the Barremian or in the Aptian (see sub-chapter 3.3).

Paleoenvironmental analysis of the Coyhaique Group presented here is based on lithofacies, sedimentary petrography, and fossils associations. Facies models show that the early marine transgression is characterized by mixed calcareous-volcaniclastic deposits of the Toqui Formation, i.e. the lowermost member of this group. These mixed rocks represent the growth of subaqueous volcanic aprons, and the sporadic development of small carbonate platforms above an irregular, extensional topography (see Appendix 8.1, Rivas *et al.*, 2021). Faunal associations are controlled by heterozoan-type organisms, which comprise mainly oysters, red algae, and echinoderms. A carbonate ramp conformed by “maerl-like”-rich sediments from south of Coyhaique might depict a cool-water setting in the basin during the Valanginian (see Appendix 8.2; Rivas *et al.*, 2023).

The enhanced marine transgression is represented by “black shales” of the Katterfeld Formation, i.e., middle lithological unit of the Coyhaique Group. Facies analysis of this carbonaceous lithostratigraphic unit evidences the onset of oxygen-poor, shelf to slope settings. Hemipelagic sedimentation alternated with periodic explosive volcanism, and punctuated events of high-productivity, likely associated with coastal-upwelling. The onset of mudstone sedimentation might have been coeval to a period of high humidity linked to the globally known “Weissert Event” (see Appendix 8.2; Rivas *et al.*, 2025, submitted - in review). During the marine regression, deep-water sediments were gradually covered by tidal-influenced deltaic sediments of the Apeleg Formation, i.e., the uppermost member of the Coyhaique Group (see Appendix 8.3; Rivas *et al.*, 2025, submitted - in review).

The relationship between the Aysén-Río Mayo Basin and the adjacent coeval basins (see Chapter 5) shows a connection, and a partly similar depositional evolution with the Rocas Verdes Basin to the south in southernmost Chile and Argentina. The faunal correlation with the Neuquén Basin from central Chile and Argentina might depict

a connection along the Pacific margin. There is no inferred connection with the Cañadón Asfalto- and San Jorge basins, or only a short-termed marine incursion in the latter, since these basins are apparently exclusively continental; they were likely separated from the Aysén-Río Mayo Basin by tectonic highs. A correlation and connection with the South African basins has been proposed based on trigoniids and benthic foraminifers. As inferred from ammonites, an open circulation is better established starting in the Barremian, with the onset of the “Austral Realm”.

This work represents a contribution to the geological knowledge of southern Chile, in particular the Aysén Region, which, due to its isolation and challenging geography, has historically remained little studied. Results presented here provide a reference scheme of the Aysén-Río Mayo basin, although during the development of this work, several research questions have arisen, which remain to be investigated. Future studies should concentrate on the analytical study of these rocks, including their micropaleontology, geochemistry, isotopy and radiometric dating. This set of data would allow us to better comprehend the evolution of the Patagonian depositional systems and their relationship with coeval basins. It may also provide evidence for the extent of global events towards southern high latitudes.

7. References

- Aguirre-Urreta, M. B. (1990). Paleogeography and biostratigraphy of the Austral basin in Argentina and Chile: An appeal for sound systematics. *Episodes*, 13(4), 247–255. <https://doi.org/10.18814/epiiugs/1990/v13i4/004>
- Aguirre-Urreta, M. B. (2002). Invertebrados del Cretácico Inferior. In M. J. Haller (Ed.), *Geología y Recursos Naturales de Santa Cruz: Vol. II-6* (pp. 439–459).
- Aguirre-Urreta, M. B., Casadío, S., Cichowolski, M., Lazo, D. G., & Rodríguez, D. L. (2008). Afinidades paleobiogeográficas de los invertebrados cretácicos de la Cuenca Neuquina. *Ameghiniana*, 45(3), 591–611.
- Aguirre-Urreta, M. B., Mourgues, F. A., Rawson, P. F., Bulot, L. G., & Jaillard, E. (2007). The Lower Cretaceous Chañarcillo and Neuquén Andean basins: Ammonoid biostratigraphy and correlations. *Geological Journal*, 42(2), 143–173. <https://doi.org/10.1002/gj.1068>
- Aguirre-Urreta, M. B., & Ramos, V. A. (1981). Estratigrafía y Paleontología de la Alta Cuenca del río Roble, Cordillera Patagónica—Provincia de Santa Cruz. *VIII Congr. Geol. Argentino, Actas, III*, 101–133.
- Aguirre-Urreta, M. B., & Rawson, P. (1998). The Early Cretaceous (Valanginian) ammonite Chacantuceras gen. Nov. - A link between the Neuquén and Austral basins. *Revista de la Asociacion Geologica Argentina*, 53(3), 354–364.
- Aguirre-Urreta, M. B., Rawson, P. F., Concheyro, G. A., Bown, P. R., & Ottone, E. G. (2005). Lower Cretaceous (Berriasian-Aptian) biostratigraphy of the Neuquén Basin. *Geological Society, London, Special Publications*, 252(1), 57–81. <https://doi.org/10.1144/GSL.SP.2005.252.01.04>
- Aguirre-Urreta, M. B., Suárez, M., Bruce, Z., De la Cruz, R., & Ramos, V. A. (2000). Bioestratigrafía y amonoideos de la Formación Katterfeld, (Cretácico Inferior) en Puerto Ibáñez, XI región, Chile. *IX Congr. Geol. Chileno, Actas*, 2, 183–187.
- Aguirre-Urreta, M. B., Suárez, M., & De La Cruz, R. (2006). Amonoideos hauteriviano-barremianos en la Formación Apeleg, Patagonia Central. *XI Congr. Geol. Chileno, Actas*, 2, 17–20.
- Aguirre-Urreta, M. B., Suárez, M., De la Cruz, R., & Ramos, V. A. (2007). Ammonoids (Crioceratitinae, Hauterivian) from the Austral Basin, Chile. *Ameghiniana*, 44(2).
- Aldridge, B. (2020). *Estratigrafía y sedimentología de la Formación Toqui en las cercanías del Cerro Visera, Mallín Grande, Región de Aysén, Chile* [Memoria de Título]. Universidad Andrés Bello.
- Allard, J. O., Paredes, J. M., Foix, N., Giacosa, R. E., Buetti, S. A., & Sánchez, F. M. (2022). Estratigrafía de la Cuenca de Cañadón Asfalto. In *Geología y Recursos Naturales de la Provincia del Chubut* (pp. 465–488). Asociación Geológica Argentina.
- Álvarez-Mena, K. (2024). *Iconología de la Formación Apeleg en el área de Ñirehuao—Baño Nuevo (Región de Aysén del General Carlos Ibáñez Del Campo): Taxonomía, implicaciones estratigráficas y paleoambientales* [Memoria de Título]. Universidad de Concepción.
- Aramendía, I., Ramos, M. E., Geuna, S., Cuitiño, J. I., & Ghiglione, M. C. (2018). A multidisciplinary study of the Lower Cretaceous marine to continental transition in the northern Austral-

- Magallanes basin and its geodynamic significance. *Journal of South American Earth Sciences*, 86, 54–69. <https://doi.org/10.1016/j.jsames.2018.06.010>
- Arbe, H. A. (1989). Estratigrafía, discontinuidades y evolución sedimentaria del Cretácico en la Cuenca Austral, Provincia de Santa Cruz. In G. A. Chebli & L. A. Spalletti (Eds.), *Cuencas Sedimentarias Argentinas* (pp. 419–442).
- Arbe, H. A. (2002). Análisis Estratigráfico del Cretácico de la Cuenca Austral. In M. J. Haller (Ed.), *Geología y Recursos Naturales de Santa Cruz: Vol. II-6* (pp. 103–128).
- Barberón, V., Ronda, G., Aramendía, I., Suárez, R. J., Ramos, M. E., Naipauer, M., Sue, C., & Ghiglione, M. C. (2019). Tectonic evolution of the northern Austral-Magallanes basin in the Southern Patagonian Andes from provenance analysis. *Journal of South American Earth Sciences*, 95, 102234. <https://doi.org/10.1016/j.jsames.2019.102234>
- Barberón, V., Ronda, G., Leal, P. R., Sue, C., & Ghiglione, M. C. (2015). Lower Cretaceous provenance in the northern Austral basin of Patagonia from sedimentary petrography. *Journal of South American Earth Sciences*, 64, 498–510. <https://doi.org/10.1016/j.jsames.2015.08.014>
- Bartholomew, D. S., & Tarney, J. (1984). Crustal extension in the Southern Andes (45–46°S). *Geological Society, London, Special Publications*, 16(1), 195–205. <https://doi.org/10.1144/GSL.SP.1984.016.01.15>
- Bell, C. M. (2004). Asteroid and Ophiuroid Trace Fossils from the Lower Cretaceous of Chile. *Palaeontology*, 47(1), 51–66. <https://doi.org/10.1111/j.0031-0239.2004.00347.x>
- Bell, C. M., Angseesing, J. P. A., & Townsend, M. J. (2001). A Chondrophorine (Medusoid Hydrozoan) from the Lower Cretaceous of Chile. *Palaeontology*, 44(5), 1011–1023. <https://doi.org/10.1111/1475-4983.00212>
- Bell, C. M., De la Cruz, R., Suárez, M., & Townsend, M. J. (1996). The evolution of the Aysen Basin, an early Cretaceous epicontinental interior seaway in the southernmost South America. In *Géodynamique andine: Résumés étendus* (Centre IRD de Bondy; pp. 289–292). ORSTOM. <http://www.documentation.ird.fr/hor/fdi:010008580>
- Bell, C. M., & Suárez, M. (1997). The Lower Cretaceous Apeleg Formation of the Aisen basin, Southern Chile. Tidal sandbar deposits of an epicontinental sea. *Andean Geology*, 24(2), 203–225. <https://doi.org/10.5027/andgeoV24n2-a05>
- Bell, C. M., & Suárez, M. (2000). The Río Lácteo Formation of Southern Chile. Late Paleozoic orogeny in the Andes of southernmost South America. *Journal of South American Earth Sciences*, 13(1–2), 133–145. [https://doi.org/10.1016/S0895-9811\(00\)00005-5](https://doi.org/10.1016/S0895-9811(00)00005-5)
- Bell, C. M., Townsend, M. J., Suárez, M., & De la Cruz, R. (1994). The depositional environments of the Lower Cretaceous Coyhaique Group, Aysén Basin, southern Chile (45°–46°S). *VII Congr. Geol. Chileno, Actas, I*, 402–403.
- Benson, R. B. J., Rich, T. H., Vickers-Rich, P., & Hall, M. (2012). Theropod Fauna from Southern Australia Indicates High Polar Diversity and Climate-Driven Dinosaur Provinciality. *PLoS ONE*, 7(5), e37122. <https://doi.org/10.1371/journal.pone.0037122>
- Berner, R. A., & Kothavala, Z. (2001). GEOCARB III: A revised model of atmospheric CO₂ over Phanerozoic time. *American Journal of Science*, 301(2), 182–204. <https://doi.org/10.2475/ajs.301.2.182>
- Biblioteca Nacional de Chile. (2024, February 12). Exploradores y colonos en Aysén (1870–1927). *Memoria Chilena*. <https://www.memoriachilena.gob.cl/602/w3-article-620.html>

- Biddle, K. T., Uliana, M. A., Mitchum Jr., R. M., Fitzgerald, M. G., & Wright, R. C. (1986). The stratigraphic and structural evolution of the central and eastern Magallanes Basin, southern South America. *Special Publications of the International Association of Sedimentologists*, 8, 41–61.
- Bischoff, J. L., Fitzpatrick, J. A., & Rosenbauer, R. J. (1993). The Solubility and Stabilization of Ikaite ($\text{CaCO}_3 \cdot 6\text{H}_2\text{O}$) from 0° to 25°C: Environmental and Paleoclimatic Implications for Thiolite Tufa. *The Journal of Geology*, 101(1), 21–33. <https://doi.org/10.1086/648194>
- Bizama, G., Torrejón, F., Aguayo, M., Muñoz, M. D., Echeverría, C., & Urrutia, R. (2011). Pérdida y fragmentación del bosque nativo en la cuenca del río Aysén (Patagonia-Chile) durante el siglo XX. *Revista de Geografía Norte Grande*, 49, 125–138. <https://doi.org/10.4067/S0718-34022011000200008>
- Bjerrum, C. J., Surlyk, F., Callomon, J. H., & Slingerland, R. L. (2001). Numerical paleoceanographic study of the Early Jurassic Transcontinental Lurasian Seaway. *Paleoceanography*, 16(4), 390–404. <https://doi.org/10.1029/2000PA000512>
- Blair, T. C., & McPherson, J. G. (1999). Grain-size and textural classification of coarse sedimentary particles. *Journal of Sedimentary Research*, 69(1), 6–19. <https://doi.org/10.2110/jsr.69.6>
- British Geological Survey. (2022). Faunal Provincialism. In *Dictionary of Geological Terms*. <https://www.encyclo.co.uk/local/23001>
- Bruce, Z. (2001). *Mesozoic geology of the Puerto Ingeniero Ibáñez area, 46° south, Chilean Patagonia* [PhD Thesis]. University of Canterbury.
- Brysch, S. (2018). *Changes in climate and palaeoenvironment during the Late Jurassic–Early Cretaceous in southern South America and western Antarctica* [PhD Thesis, Ruprecht-Karls-Universität Heidelberg]. <http://www.ub.uni-heidelberg.de/archiv/25582>
- Bucur, I. I., Kiessling, W., & Scasso, R. A. (2009). Re-description and neotypification of *Archamphiroa jurassica* Steinmann 1930, a calcareous red alga from the Jurassic of Argentina. *Journal of Paleontology*, 83(6), 962–968. <https://doi.org/10.1666/09-052.1>
- Bussey, S. D., Kakariaka, A., & Meinert, L. D. (2010a). Geology of the El Toqui Zn-Au skarn district, Aysen Region, Chile. *Geol. Soc. Nevada 2010 Symposium: Great Basin Evolution and Metallogeny*, 1, 179–199.
- Bussey, S. D., Kakariaka, A., & Meinert, L. D. (2010b). Skarn, Porphyry, Vein, and Replacement Mineralization in the Toqui District, Southern Chile. In R. J. Goldfarb, E. E. Marsh, & T. Monecke (Eds.), *The Challenge of Finding New Mineral Resources: Global Metallogeny, Innovative Exploration, and New Discoveries* (pp. 399–420). Soc. Econ. Geol. Spec. Publ. <https://doi.org/10.5382/SP.15.2.04>
- Calderón, M., Fildani, A., Hervé, F., Fanning, C. M., Weislogel, A., & Cordani, U. (2007). Late Jurassic bimodal magmatism in the northern sea-floor remnant of the Rocas Verdes basin, southern Patagonian Andes. *Journal of the Geological Society*, 164(5), 1011–1022. <https://doi.org/10.1144/0016-76492006-102>
- Calderón, M., Prades, C. F., Hervé, F., Avendaño, V., Fanning, C. M., Massonne, H.-J., Theye, T., & Simonetti, A. (2013). Petrological vestiges of the Late Jurassic–Early Cretaceous transition from rift to back-arc basin in southernmost Chile: New age and geochemical data from the Capitán Aracena, Carlos III, and Tortuga ophiolitic complexes. *Geochemical Journal*, 47(2), 201–217. <https://doi.org/10.2343/geochemj.2.0235>

- Campbell, C. V. (1967). Lamina, Laminaset, Bed and Bedset. *Sedimentology*, 8(1), 7–26. <https://doi.org/10.1111/j.1365-3091.1967.tb01301.x>
- Carrizo, M. A., & Del Fueyo, G. M. (2015). The Early Cretaceous megaflora of the Springhill Formation, Patagonia. Paleofloristic and Paleoenvironmental inferences. *Cretaceous Research*, 56, 93–109. <https://doi.org/10.1016/j.cretres.2015.03.006>
- Cas, R. A. F., & Wright, J. V. (1987). *Volcanic successions: Modern and Ancient. A geological approach to processes, products and successions*. Chapman & Hall.
- Cavalheiro, L., Wagner, T., Steinig, S., Bottini, C., Dummann, W., Esegbue, O., Gambacorta, G., Giraldo-Gómez, V., Farnsworth, A., Flögel, S., Hofmann, P., Lunt, D. J., Rethemeyer, J., Torricelli, S., & Erba, E. (2021). Impact of global cooling on Early Cretaceous high pCO₂ world during the Weissert Event. *Nature Communications*, 12(1), 5411. <https://doi.org/10.1038/s41467-021-25706-0>
- Cecioni, G., & Charrier, R. (1974). Relaciones entre la Cuenca Patagónica, la Cuenca Andina y el Canal de Mozambique. *Ameghiniana*, XI(1), 1–38.
- Charrier, R., & Covacevich, V. (1978). Paleogeografía y bioestratigrafía del Jurásico Superior y Neocomiano en el sector austral de los Andes Meridionales Chilenos (42°–56° latitud sur). *II Congr. Argentino de Paleont. Estrat. y I Cong. Latinoam. Paleont., Actas*, V, 153–175.
- Chumakov, N. M., Zharkov, M. A., Herman, A. B., Doludenko, M. P., Kalandadze, N. N., Lebedev, E. L., Ponomarenko, A. G., & Rautian, A. S. (1995). Climatic Belts of the Mid-Cretaceous Time. *Stratigraphy and Geological Correlation*, 3, 42–63.
- Ciccioli, P. L., Limarino, C. O., Isbell, J. L., Taboada, A. C., Pagani, M. A., & Gulbranson, E. L. (2020). Interpreting detrital modes and geochemistry of sandstones from the late Paleozoic Tepuel-Genoa Basin: Paleogeographic implications (Patagonia, Argentina). *Journal of South American Earth Sciences*, 104, 102858. <https://doi.org/10.1016/j.jsames.2020.102858>
- Cichowolski, M. (2003). The nautiloid genus *Cymatoceras* from the Cretaceous of the Neuquén and Austral basins, Argentina. *Cretaceous Research*, 24(4), 375–390. [https://doi.org/10.1016/S0195-6671\(03\)00050-8](https://doi.org/10.1016/S0195-6671(03)00050-8)
- Cohen, K. M., Finney, S. C., Gibbard, P. L., & Fan, J.-X. (2013). The ICS International Chronostratigraphic Chart. *Episodes*, 36(3), 199–204. <https://doi.org/10.18814/epiiugs/2013/v36i3/002>
- Cooper, M. R. (2015c). On the Iotrigoniidae (Bivalvia: Trigoniida); their palaeobiogeography, evolution and classification. *Neues Jahrbuch Für Geologie Und Paläontologie - Abhandlungen*, 277(1), 49–62. <https://doi.org/10.1127/njgpa/2015/0495>
- Cooper, M. R. (2015a). On the Pterotrigoniidae (Bivalvia, Trigoniida): Their biogeography, evolution, classification and relationships. *Neues Jahrbuch Für Geologie Und Paläontologie - Abhandlungen*, 277(1), 11–42. <https://doi.org/10.1127/njgpa/2015/0488>
- Cooper, M. R., & Leanza, H. A. (2017). On the Steinmanellidae (Bivalvia: Myophorelloidea); their palaeo-biogeography, evolution and classification. *Neues Jahrbuch Für Geologie Und Paläontologie - Abhandlungen*, 285(3), 313–335. <https://doi.org/10.1127/njgpa/2017/0683>
- Covacevich, V., De la Cruz, R., & Suárez, M. (1994). Primer hallazgo de fauna del Berriasiano inferior (Neocomiano) en la Formación Ibáñez, región XI, Aisén. *VII Congr. Geol. Chileno, Actas*, I, 425–429.

- Cuitiño, J. I., Varela, A. N., Ghiglione, M. C., Richiano, S., & Poiré, D. G. (2019). The Austral-Magallanes Basin (southern Patagonia): A synthesis of its stratigraphy and evolution. *Latin American Journal of Sedimentology and Basin Analysis*, 26(2), 155–166.
- Dalziel, I. (1981). Back-arc extension in the southern Andes: A review and critical reappraisal. *Philosophical Transactions of the Royal Society of London. Series A, Mathematical and Physical Sciences*, 300(1454), 319–335. <https://doi.org/10.1098/rsta.1981.0067>
- Dalziel, I. W. D., de Wit, M. J., & Palmer, K. F. (1974). Fossil marginal basin in the southern Andes. *Nature*, 250(5464), 291–294. <https://doi.org/10.1038/250291a0>
- Dávila, F. M., Ávila, P., & Martina, F. (2019). Relative contributions of tectonics and dynamic topography to the Mesozoic-Cenozoic subsidence of southern Patagonia. *Journal of South American Earth Sciences*, 93, 412–423. <https://doi.org/10.1016/j.jsames.2019.05.010>
- De la Cruz, R., & Suárez, M. (2006). *Geología del área Puerto Guadal-Puerto Sánchez, Región Aisén del General Carlos Ibáñez del Campo*. SERNAGEOMIN.
- De la Cruz, R., Suárez, M., Belmar, M., Quiroz, D., & Bell, M. (2003). *Geología del área Coihaique-Balmaceda, Región Aisén del General Carlos Ibáñez del Campo*. SERNAGEOMIN.
- De la Cruz, R., Suárez, M., Covacevich, V., & Quiroz, D. (1996). Estratigrafía de la zona de Palena y Futaleufú (43°15'-43°45' latitud S), X Región, Chile. *XIII Congr. Geol. Argentino y III Congr. Explor. Hidroc., Actas, I*, 417–424.
- De la Cruz, R., Suárez, M., & Demant, A. (1994). Facies volcánicas del Mesozoico de Aisén (sector noreste), 44°-47° lat. S., Chile (Formaciones Ibáñez y Divisadero). *VII Congr. Geol. Chileno, Actas, I*, 27–31.
- De la Cruz, R., Suárez, M., Quiroz, D., Cortés, J., Belmar, M., & Covacevich, V. (1995). *Estratigrafía y ambientes depositacionales de las unidades del Mesozoico Superior—Cenozoico en la zona de Palena y Futaleufú, X Región*. SERNAGEOMIN.
- De la Cruz, R., Welkner, D., Suárez, M., & Quiroz, D. (2004). *Geología del Área Oriental de las Hojas Cochrane y Villa O'Higgins, Región Aisén del General Carlos Ibáñez del Campo*. SERNAGEOMIN.
- Demant, A., Suárez, M., De la Cruz, R., & Bruguier, O. (2010). Early Cretaceous Surtseyan volcanoes of the Baño Nuevo Volcanic Complex (Aysén Basin, Eastern Central Patagonian Cordillera, Chile). *Geologica Acta*, 8(2), 207–219. <https://doi.org/10.1344/105.000001530>
- Depine, G., & Ramos, V. (2004). Geología de la Quebrada Honda, cuenca del lago La Plata, Chubut. *Revista de la Asociación Geológica Argentina*, 59(4), 643–654.
- Dera, G., Brigaud, B., Monna, F., Laffont, R., Pucéat, E., Deconinck, J.-F., Pellenard, P., Joachimski, M. M., & Durllet, C. (2011). Climatic ups and downs in a disturbed Jurassic world. *Geology*, 39(3), 215–218. <https://doi.org/10.1130/G31579.1>
- Donnadieu, Y., Dromart, G., Goddérís, Y., Pucéat, E., Brigaud, B., Dera, G., Dumas, C., & Olivier, N. (2011). A mechanism for brief glacial episodes in the Mesozoic greenhouse. *Paleoceanography*, 26(3), 10 pp. <https://doi.org/10.1029/2010PA002100>
- Duhart, J. (1960). *Resultado de Estudios Geológicos en parte N.E de la Provincia de Aysen* (No. BSNGM 2623; p. 65 pp). Instituto de Investigaciones Geológicas.
- Echaurren, A., Folguera, A., Gianni, G., Orts, D., Tassara, A., Encinas, A., Giménez, M., & Valencia, V. (2016). Tectonic evolution of the North Patagonian Andes (41°–44° S) through recognition

of syntectonic strata. *Tectonophysics*, 677–678, 99–114.
<https://doi.org/10.1016/j.tecto.2016.04.009>

Echaurren, A., Oliveros, V., Folguera, A., Ibarra, F., Creixell, C., & Lucassen, F. (2017). Early Andean tectonomagmatic stages in north Patagonia: Insights from field and geochemical data. *Journal of the Geological Society*, 174(3), 405–421. <https://doi.org/10.1144/jgs2016-087>

Escosteguy, L., Dal Molín, C., Franchi, M., Geuna, S., & Lapido, O. (2003). *Hoja Geológica 4772-II Lago Buenos Aires. Provincia de Santa Cruz. Instituto de Geología y Recursos Minerales, Servicio Geológico Minero Argentino* (Vol. 339). SEGEMAR Boletín.

Espinosa, W., & Fuenzalida, R. (1971). *Geología de las Hojas Rivero, Puerto Aisén y Balmaceda entre los Paralelos 45° y 46° de Latitud Sur*. Instituto de Investigaciones Geológicas.

Ferrari, M., & Bessone, S. (2015). Una nueva localidad marina de edad jurásica temprana en la cuenca sudoccidental del Chubut, Argentina. *Andean Geology*, 42(3), 349–363.
<https://doi.org/10.5027/andgeoV42n3-a04>

Figari, E., Scasso, R. A., Cúneo, R., & Escapa, I. (2015). Estratigrafía y evolución geológica de la Cuenca de Cañadón Asfalto, provincia del Chubut, Argentina. *Latin American Journal of Sedimentology and Basin Analysis*, 22(2), 135–169.

Figari, E., Strelkov, E., Cid de la Paz, M. S., Celaya, J., Laffitte, G., & Villar, H. J. (2002). Cuenca del Golfo San Jorge: Síntesis estructural, estratigráfica y geoquímica. In M. J. Haller (Ed.), *Geología y Recursos Naturales de Santa Cruz* (Vol. 3, pp. 571–601).

Fildani, A., Cope, T. D., Graham, S. A., & Wooden, J. L. (2003). Initiation of the Magallanes foreland basin: Timing of the southernmost Patagonian Andes orogeny revised by detrital zircon provenance analysis. *Geology*, 31(12), 1081. <https://doi.org/10.1130/G20016.1>

Fildani, A., & Hessler, A. M. (2005). Stratigraphic record across a retroarc basin inversion: Rocas Verdes–Magallanes Basin, Patagonian Andes, Chile. *Geological Society of America Bulletin*, 117(11), 1596. <https://doi.org/10.1130/B25708.1>

Fildani, A., Romans, B. W., Fosdick, J. C., Crane, W. H., & Hubbard, S. M. (2008). Orogenesis of the Patagonian Andes as reflected by basin evolution in southernmost South America. In *Arizona Geological Society Digest* (Vol. 22, pp. 259–268).

Fisher, R. V. (1961). Proposed Classification of Volcaniclastic Sediments and Rocks. *Geological Society of America Bulletin*, 72(9), 1409. [https://doi.org/10.1130/0016-7606\(1961\)72\[1409:PCOVSA\]2.0.CO;2](https://doi.org/10.1130/0016-7606(1961)72[1409:PCOVSA]2.0.CO;2)

Fisher, R. V. (1966). Rocks composed of volcanic fragments and their classification. *Earth-Science Reviews*, 1(4), 287–298. [https://doi.org/10.1016/0012-8252\(66\)90010-9](https://doi.org/10.1016/0012-8252(66)90010-9)

Fisher, R. V., & Schmincke, H.-U. (1994). Volcaniclastic Sediment Transport and Deposition. In K. Pye (Ed.), *Sediment Transport and Depositional Processes* (pp. 351–388). Blackwell Scientific Publications.

Flügel, E. (2004). *Microfacies of Carbonate Rocks*. Springer. <https://doi.org/10.1007/978-3-642-03796-2>

Flügel, E., & Munnecke, A. (2010). *Microfacies of carbonate rocks: Analysis, interpretation and application* (2. ed. [erw.]). Springer.

- Folguera, A., & Iannizzotto, N. F. (2004). The lagos La Plata and Fontana fold-and-thrust belt: Long-lived orogenesis at the edge of western Patagonia. *Journal of South American Earth Sciences*, 16(7), 541–566. <https://doi.org/10.1016/j.jsames.2003.10.001>
- Folk, R. L., Andrews, P. B., & Lewis, D. W. (1970). Detrital sedimentary rock classification and nomenclature for use in New Zealand. *New Zealand Journal of Geology and Geophysics*, 13(4), 937–968. <https://doi.org/10.1080/00288306.1970.10418211>
- Föllmi, K. B. (2012). Early Cretaceous life, climate and anoxia. *Cretaceous Research*, 35, 230–257. <https://doi.org/10.1016/j.cretres.2011.12.005>
- Fosdick, J. C., Romans, B. W., Fildani, A., Bernhardt, A., Calderon, M., & Graham, S. A. (2011). Kinematic evolution of the Patagonian retroarc fold-and-thrust belt and Magallanes foreland basin, Chile and Argentina, 51°30'S. *Geological Society of America Bulletin*, 123(9–10), 1679–1698. <https://doi.org/10.1130/B30242.1>
- Fosdick, J. C., VanderLeest, R. A., Bostelmann, J. E., Leonard, J. S., Ugalde, R., Oyarzún, J. L., & Griffin, M. (2020). Revised Timing of Cenozoic Atlantic Incursions and Changing Hinterland Sediment Sources during Southern Patagonian Orogenesis. *Lithosphere*, 2020(1), 8883099. <https://doi.org/10.2113/2020/8883099>
- Frakes, L. A., Francis, J. E., & Syktus, J. I. (1992). *Climate Modes of the Phanerozoic* (1st ed.). Cambridge University Press. <https://doi.org/10.1017/CBO9780511628948>
- Franzese, J., Spalletti, L., Pérez, I. G., & Macdonald, D. (2003). Tectonic and paleoenvironmental evolution of Mesozoic sedimentary basins along the Andean foothills of Argentina (32°–54°S). *Journal of South American Earth Sciences*, 16(1), 81–90. [https://doi.org/10.1016/S0895-9811\(03\)00020-8](https://doi.org/10.1016/S0895-9811(03)00020-8)
- Frizon De Lamotte, D., Fourdan, B., Leleu, S., Leparmentier, F., & De Clarens, P. (2015). Style of rifting and the stages of Pangea breakup. *Tectonics*, 34(5), 1009–1029. <https://doi.org/10.1002/2014TC003760>
- Fuenzalida, H. (1964). *El geosinclinal Andino y el geosinclinal de Magallanes* (Vol. 5). Universidad de Chile.
- Fuenzalida, H., & Latcham, R. (1935). Observaciones geológicas del territorio del Aysén. *Boletín Del Museo Nacional de Historia Natural, Chile*, 14, 31–36.
- Fuenzalida, R. (1965). Reconocimiento geológico de Alto Palena (Chiloé continental). In *Anales de la Facultad de Ciencias Físicas y Matemáticas* (Vol. 22, pp. 91–158).
- Gale, A. S., Mutterlose, J., Batenburg, S., Gradstein, F. M., Agterberg, F. P., Ogg, J. G., & Petrizzo, M. R. (2020). The Cretaceous Period. In *Geologic Time Scale 2020* (pp. 1023–1086). Elsevier. <https://doi.org/10.1016/B978-0-12-824360-2.00027-9>
- Garzanti, E. (2019). Petrographic classification of sand and sandstone. *Earth-Science Reviews*, 192, 545–563. <https://doi.org/10.1016/j.earscirev.2018.12.014>
- Ghidella, M. E., Yáñez, G., & LaBrecque, J. L. (2002). Revised tectonic implications for the magnetic anomalies of the western Weddell Sea. *Tectonophysics*, 347(1–3), 65–86. [https://doi.org/10.1016/S0040-1951\(01\)00238-4](https://doi.org/10.1016/S0040-1951(01)00238-4)
- Ghiglione, M. C., Likerman, J., Barberón, V., Beatriz Giambiagi, L., Aguirre-Urreta, M. B., & Suarez, F. (2014). Geodynamic context for the deposition of coarse-grained deep-water axial channel systems in the Patagonian Andes. *Basin Research*, 26(6), 726–745. <https://doi.org/10.1111/bre.12061>

- Ghiglione, M. C., Naipauer, M., Sue, C., Barberón, V., Valencia, V., Aguirre-Urreta, M. B., & Ramos, V. A. (2015). U–Pb zircon ages from the northern Austral basin and their correlation with the Early Cretaceous exhumation and volcanism of Patagonia. *Cretaceous Research*, 55, 116–128. <https://doi.org/10.1016/j.cretres.2015.02.006>
- Ghiglione, M. C., Ramos, V. A., Cuitiño, J., & Barberón, V. (2016). Growth of the Southern Patagonian Andes (46–53°S) and Their Relation to Subduction Processes. In A. Folguera, M. Naipauer, L. Sagripanti, M. C. Ghiglione, D. L. Orts, & L. Giambiagi (Eds.), *Growth of the Southern Andes* (pp. 201–240). Springer International Publishing. https://doi.org/10.1007/978-3-319-23060-3_10
- Giacosa, R. E., & Franchi, M. (2001). *Hojas Geológicas 4772-III Lago Belgrano y 4772-IV Lago Posadas. Provincia de Santa Cruz. Instituto de Geología y Recursos Minerales, Servicio Geológico Minero Argentino* (Vol. 256). SEGEMAR Boletín.
- Gianni, G. M., Navarrete, C., Echaurren, A., Díaz, M., Butler, K. L., Horton, B. K., Encinas, A., & Folguera, A. (2019). Northward propagation of Andean genesis: Insights from Early Cretaceous synorogenic deposits in the Aysén-Río Mayo basin. *Gondwana Research*, 77, 238–259. <https://doi.org/10.1016/j.gr.2019.07.014>
- Godoy, E., Quiroz, D., & Sepúlveda, V. (1997). La Formación Río Mayer (Neocomiano) y el basamento reactivado en Sierra de la Concepción, Aysen. *VIII Congr. Geol. Chileno, Actas, I*, 75–79.
- Gonzalez-Bonorino, G., & Suárez, M. (1995). Paleoambientes sedimentarios de la Formación Apeleg, Cretácico Inferior de la Cuenca de Aisen, Region XI, Chile. *Andean Geology*, 22(1), 115–126. <https://doi.org/10.5027/andgeoV22n1-a07>
- Gradstein, F. M. (2012). *The geologic time scale 2012* (1st ed). Elsevier.
- Granier, B. R. C. (2020). Introduction to thematic issue, “The transition of the Jurassic to the Cretaceous: An early XXIth century holistic approach.” *Cretaceous Research*, 114, 104530. <https://doi.org/10.1016/j.cretres.2020.104530>
- Haller, M. J., & Lapido, O. R. (1980). El Mesozoico de la Cordillera Patagónica Central. *Revista de La Asociación Geológica Argentina*, XXXV(2), 230–247.
- Haller, M. J., & Lapido, O. R. (1982). The Jurassic-Cretaceous volcanism in the septentrional Patagonian Andes. *Earth-Science Reviews*, 18, 395–410.
- Haller, M. J., Lapido, O. R., Lizuaín, A., & Page, R. (1981). El mar tithono-neocomiano en la evolución de la Cordillera Norpatagónica. In *Cuencas Sedimentarias del Jurásico y Cretácico de América del Sur* (Vol. 1, pp. 221–237). Com. Sudam. Jura. Cretac.
- Hanson, R. E., & Wilson, T. J. (1991). Submarine rhyolitic volcanism in a Jurassic proto-marginal basin; southern Andes, Chile and Argentina. In *Geological Society of America Special Papers* (Vol. 265, pp. 13–28). Geological Society of America. <https://doi.org/10.1130/SPE265-p13>
- Haq, B. U. (2014). Cretaceous eustasy revisited. *Global and Planetary Change*, 113, 44–58. <https://doi.org/10.1016/j.gloplacha.2013.12.007>
- Haq, B. U. (2018). Jurassic Sea-Level Variations: A Reappraisal. *GSA Today*, 4–10. <https://doi.org/10.1130/GSATG359A.1>
- Hay, W. W. (2008). Evolving ideas about the Cretaceous climate and ocean circulation. *Cretaceous Research*, 29(5–6), 725–753. <https://doi.org/10.1016/j.cretres.2008.05.025>

- Hay, W. W. (2017). Toward understanding Cretaceous climate—An updated review. *Science China Earth Sciences*, 60(1), 5–19. <https://doi.org/10.1007/s11430-016-0095-9>
- Hay, W. W., & Floegel, S. (2012). New thoughts about the Cretaceous climate and oceans. *Earth-Science Reviews*, 115(4), 262–272. <https://doi.org/10.1016/j.earscirev.2012.09.008>
- Hechem, J., Figari, E., & Homovc, J. (1993). Secuencias deposicionales en el Neocomiano del lago Fontana, Chubut, Argentina. *XII Congr. Geol. Argentino y II Congr. Explor. Hidroc., Actas, II*, 119–123.
- Heim, A. (1940). Geological Observations in the Patagonian Cordillera (Preliminary Report). *Eclogae Geologicae Helveticae*, 33, 25–51.
- Hervé, F., Calderón, M., & Faúndez, V. (2008). The metamorphic complexes of the Patagonian and Fuegian Andes. *Geologica Acta*, 11.
- Hervé, F., Miller, H., & Pimpirev, C. (2006). Patagonia—Antarctica Connections before Gondwana Break-Up. In D. K. Fütterer, D. Damaske, G. Kleinschmidt, H. Miller, & F. Tessensohn (Eds.), *Antarctica* (pp. 217–227). Springer-Verlag. https://doi.org/10.1007/3-540-32934-X_26
- Hervé, F., Pankhurst, R. J., Fanning, C. M., Calderón, M., & Yaxley, G. M. (2007). The South Patagonian batholith: 150 my of granite magmatism on a plate margin. *Lithos*, 97(3–4), 373–394. <https://doi.org/10.1016/j.lithos.2007.01.007>
- Hesselbo, S. P., Ogg, J. G., Ruhl, M., Hinnov, L. A., & Huang, C. J. (2020). The Jurassic Period. In *Geologic Time Scale 2020* (pp. 955–1021). Elsevier. <https://doi.org/10.1016/B978-0-12-824360-2.00026-7>
- Howell, J. A., Schwarz, E., Spalletti, L. A., & Veiga, G. D. (2005). The Neuquén Basin: An overview. *Geological Society, London, Special Publications*, 252(1), 1–14. <https://doi.org/10.1144/GSL.SP.2005.252.01.01>
- Iannizzotto, N. F., Folguera, A., Leal, P. R., & Iaffa, D. (2004). Control tectónico de las secuencias volcánicas neocomianas y paleogeografía en la zona del Lago La Plata (45°S). Sector interno de la faja plegada y corrida de los lagos La Plata y Fontana. *Revista de La Asociación Geológica Argentina*, 59(4), 655–670.
- IREN. (1967). *Provincia de Aisen: Inventario Preliminar de los Recursos Naturales* (No. 20; p. 205). Instituto de Investigación de Recursos Naturales.
- Jacques, J. M. (2004). The influence of intraplate structural accommodation zones on delineating petroleum provinces of the Sub-Andean foreland basins. *Petroleum Geoscience*, 10(1), 1–19. <https://doi.org/10.1144/1354-079303-582>
- Jacques, JohnM. (2003). A tectonostratigraphic synthesis of the Sub-Andean basins: Implications for the geotectonic segmentation of the Andean Belt. *Journal of the Geological Society*, 160(5), 687–701. <https://doi.org/10.1144/0016-764902-088>
- James, N. P. (1997). The cool-water carbonate depositional realm. In N. P. James & J. Clarke (Eds.), *Cool-Water Carbonates* (pp. 1–20). SEPM.
- Jenkyns, H. C., Schouten-Huibers, L., Schouten, S., & Sinninghe Damsté, J. S. (2012). Warm Middle Jurassic–Early Cretaceous high-latitude sea-surface temperatures from the Southern Ocean. *Climate of the Past*, 8(1), 215–226. <https://doi.org/10.5194/cp-8-215-2012>

- Jokat, W., Boebel, T., König, M., & Meyer, U. (2003). Timing and geometry of early Gondwana breakup. *Journal of Geophysical Research: Solid Earth*, 108(B9), 2002JB001802. <https://doi.org/10.1029/2002JB001802>
- Jordan, T. A., Riley, T. R., & Siddoway, C. S. (2020). The geological history and evolution of West Antarctica. *Nature Reviews Earth & Environment*, 1(2), 117–133. <https://doi.org/10.1038/s43017-019-0013-6>
- Jourdan, F., Féraud, G., Bertrand, H., Kampunzu, A. B., Tshoso, G., Watkeys, M. K., & Le Gall, B. (2005). Karoo large igneous province: Brevity, origin, and relation to mass extinction questioned by new $^{40}\text{Ar}/^{39}\text{Ar}$ age data. *Geology*, 33(9), 745. <https://doi.org/10.1130/G21632.1>
- Katz, H. (1961). Sobre la ocurrencia de Cretáceo Superior marino en Coyhaique, Provincia de Aisén. In *Anales de la Facultad de Ciencias Físicas y Matemáticas* (Vol. 21, pp. 113–131). Universidad de Chile.
- Kauffman, E. G., & Johnson, C. C. (2009). Cretaceous Warm Climates. In V. Gornitz (Ed.), *Encyclopedia of Paleoclimatology and Ancient Environments* (pp. 213–217). Springer Netherlands. https://doi.org/10.1007/978-1-4020-4411-3_51
- Késjar, D., Fözy, I., Price, G., Condon, D., Salazar, C., & Pálffy, J. (2017). Integrated Lower Cretaceous stratigraphy from the Aisén Basin, Patagonia, Chile. In B. Sames (Ed.), *10th International Symposium on the Cretaceous—Abstracts* (Vol. 120, p. 142). Berichte der Geologischen Bundesanstalt. https://opac.geologie.ac.at/wwwopacx/wwwopac.ashx?command=getcontent&server=images&value=BR0120_142.pdf
- Kessels, K., Mutterlose, J., & Michalzik, D. (2006). Early Cretaceous (Valanginian - Hauterivian) calcareous nannofossils and isotopes of the northern hemisphere: Proxies for the understanding of Cretaceous climate. *Lethaia*, 39(2), 157–172. <https://doi.org/10.1080/00241160600763925>
- Kindler, P., & Wilson, M. E. J. (2010). Carbonate grain associations: Their use and environmental significance, a brief review. In M. Mutti, W. E. Piller, & C. Betzler (Eds.), *Carbonate systems during the Oligocene-Miocene climatic transition* (pp. 35–48). Blackwell Pub.
- König, M., & Jokat, W. (2006). The Mesozoic breakup of the Weddell Sea. *Journal of Geophysical Research: Solid Earth*, 111(B12), 2005JB004035. <https://doi.org/10.1029/2005JB004035>
- Korte, C., Hesselbo, S. P., Ullmann, C. V., Dietl, G., Ruhl, M., Schweigert, G., & Thibault, N. (2015). Jurassic climate mode governed by ocean gateway. *Nature Communications*, 6(1), 10015. <https://doi.org/10.1038/ncomms10015>
- Kraemer, P., Ploszkiewicz, J. V., & Ramos, V. A. (2002). Estructura de la Cordillera Patagónica Austral entre los 46° y 52° S. *XV Congr. Geol. Argentino, Actas, I-21*, 1–12.
- Kraemer, P., & Riccardi, A. C. (1997). Estratigrafía del Jurásico y Cretácico de la región comprendida entre los lagos Argentino y Viedma (49°40' - 50°10' lat. S), Provincia de Santa Cruz, Argentina. *Revista de La Asociación Geológica Argentina*, 52(3), 333–360.
- Lazo, D. G. (2007). Early Cretaceous bivalves of the Neuquén Basin, west-central Argentina: Notes on taxonomy, palaeobiogeography and palaeoecology. *Geological Journal*, 42(2), 127–142. <https://doi.org/10.1002/gj.1080>

- Leanza, A. F., & Leanza, H. A. (1973). Pseudofavrella gen. Nov. (Ammonitina) del Hauteriviano de Neuquén, sus diferencias con Favrella R. Douville, 1909, del Aptiano de Patagonia Austral y una comparación entre el geosinclinal Andino y el geosinclinal Magallánico. *Boletín de La Academia Nacional de Ciencias, Córdoba, Argentina*, 50(1–4).
- Lehmann, J., Ifrim, C., Bulot, L., & Frau, C. (2015). Paleobiogeography of Early Cretaceous Ammonoids. In C. Klug, D. Korn, K. De Baets, I. Kruta, & R. H. Mapes (Eds.), *Ammonoid Paleobiology: From macroevolution to paleogeography* (Vol. 44, pp. 229–257). Springer Netherlands. https://doi.org/10.1007/978-94-017-9633-0_9
- Leinfelder, R. R., Schlagintweit, F., Werner, W., Ebli, O., Nose, M., Schmid, D. U., & Hughes, G. W. (2005). Significance of stromatoporoids in Jurassic reefs and carbonate platforms—Concepts and implications. *Facies*, 51(1–4), 288–326. <https://doi.org/10.1007/s10347-005-0055-8>
- Malumian, N., & Masiuk, V. (1975). Foraminíferos de la Formación Pampa Rincón (Cretácico Inferior), Tierra del Fuego, Argentina. *Revista Española de Micropaleontología*, VII(3), 579–600.
- Masiuk, V., & Nakayama, C. (1978). Sedimentitas marinas mesozoicas del lago Fontana: Su importancia. *VII Congr. Geol. Argentino, Actas, II*, 361–378.
- McArthur, J. M., Janssen, N. M. M., Reboulet, S., Leng, M. J., Thirlwall, M. F., & van de Schootbrugge, B. (2007). Palaeotemperatures, polar ice-volume, and isotope stratigraphy (Mg/Ca, $\delta^{18}\text{O}$, $\delta^{13}\text{C}$, $87\text{Sr}/86\text{Sr}$): The Early Cretaceous (Berriasian, Valanginian, Hauterivian). *Palaeogeography, Palaeoclimatology, Palaeoecology*, 248(3–4), 391–430. <https://doi.org/10.1016/j.palaeo.2006.12.015>
- Mimica, V. (2020). *Paleontología sistemática y estratigrafía de la Facies (a) de Formación Toqui (Titoniano-Valanginiano) y sus implicancias paleoambientales en las cercanías de Puerto Guadal, región de Aysén* [Memoria de Título]. Universidad Andrés Bello.
- Mount, J. (1985). Mixed siliciclastic and carbonate sediments: A proposed first-order textural and compositional classification. *Sedimentology*, 32(3), 435–442. <https://doi.org/10.1111/j.1365-3091.1985.tb00522.x>
- Mpodozis, C. (2007). The Late Cretaceous Magallanes foreland basin in the Última Esperanza Region. *Field Trip Guide of the International Geological Congress on the Southern Hemisphere*, 9–27.
- Mpodozis, C., Mella, P., & Pavda, D. (2011). Estratigrafía y megasecuencias sedimentarias en la Cuenca Austral-Magallanes, Argentina y Chile. *VIII Congreso de Exploración y Desarrollo de Hidrocarburos, Actas*, 35, 97–137.
- Mpodozis, C., & Ramos, V. (1990). The Andes of Chile and Argentina. In G. E. Erickson, M. T. Cañas Pinochet, & J. A. Reinemund (Eds.), *Geology of the Andes and its Relation to Hydrocarbon and Mineral Resources. Circum-Pac. Counc. Energy Miner. Resour., Earth Sci. Ser.* (Vol. 11, pp. 59–90).
- Mpodozis, C., & Ramos, V. A. (2008). Tectónica jurásica en Argentina y Chile: Extensión, subducción oblicua, rifting, deriva y colisiones? *Revista de La Asociación Geológica Argentina*, 63(4), 481–497.
- Müller, R. D., Sdrolias, M., Gaina, C., Steinberger, B., & Heine, C. (2008). Long-Term Sea-Level Fluctuations Driven by Ocean Basin Dynamics. *Science*, 319(5868), 1357–1362. <https://doi.org/10.1126/science.1151540>

- Müller, R. D., Seton, M., Zahirovic, S., Williams, S. E., Matthews, K. J., Wright, N. M., Shephard, G. E., Maloney, K. T., Barnett-Moore, N., Hosseinpour, M., Bower, D. J., & Cannon, J. (2016). Ocean Basin Evolution and Global-Scale Plate Reorganization Events Since Pangea Breakup. *Annual Review of Earth and Planetary Sciences*, 44(1), 107–138. <https://doi.org/10.1146/annurev-earth-060115-012211>
- Muller, V. A. P., Calderón, M., Fosdick, J. C., Ghiglione, M. C., Cury, L. F., Massonne, H.-J., Fanning, C. M., Warren, C. J., Ramírez De Arellano, C., & Sternai, P. (2021a). The closure of the Rocas Verdes Basin and early tectono-metamorphic evolution of the Magallanes Fold-and-Thrust Belt, southern Patagonian Andes (52–54°S). *Tectonophysics*, 798, 228686. <https://doi.org/10.1016/j.tecto.2020.228686>
- Muller, V. A. P., Calderón, M., Fosdick, J. C., Ghiglione, M. C., Cury, L. F., Massonne, H.-J., Fanning, C. M., Warren, C. J., Ramírez De Arellano, C., & Sternai, P. (2021b). The closure of the Rocas Verdes Basin and early tectono-metamorphic evolution of the Magallanes Fold-and-Thrust Belt, southern Patagonian Andes (52–54°S). *Tectonophysics*, 798, 228686. <https://doi.org/10.1016/j.tecto.2020.228686>
- Musacchio, E. A., & Simeoni, M. (2008). Valanginian and Hauterivian marine ostracods from Patagonia (Argentina): Correlations and palaeogeography. *Revue de Micropaléontologie*, 51(3), 239–257. <https://doi.org/10.1016/j.revmic.2007.07.001>
- Mutterlose, J., Bornemann, A., & Herrle, J. (2009). The Aptian Albian cold snap: Evidence for “mid” Cretaceous icehouse interludes. *Neues Jahrbuch Für Geologie Und Paläontologie - Abhandlungen*, 252(2), 217–225. <https://doi.org/10.1127/0077-7749/2009/0252-0217>
- Nakakuki, T., & Mura, E. (2013). Dynamics of slab rollback and induced back-arc basin formation. *Earth and Planetary Science Letters*, 361, 287–297. <https://doi.org/10.1016/j.epsl.2012.10.031>
- Natland, M. L., Eduardo, G. P., Cañon, A., & Ernst, M. (1974). A System of Stages for Correlation of Magallanes Basin Sediments. In *Geological Society of America Memoirs* (Vol. 139, pp. 1–126). Geological Society of America. <https://doi.org/10.1130/MEM139-p1>
- Navarrete, C. R., Gianni, G. M., Echaurren, A., & Folguera, A. (2018). Lower Jurassic to Early Paleogene Intraplate Contraction in Central Patagonia. In A. Folguera, E. Contreras-Reyes, N. Heredia, A. Encinas, S. B. Iannelli, V. Oliveros, F. M. Dávila, G. Collo, L. Giambiagi, A. Maksymowicz, M. P. Iglesia Llanos, M. Turienzo, M. Naipauer, D. Orts, V. D. Litvak, O. Alvarez, & C. Arriagada (Eds.), *The Evolution of the Chilean-Argentinean Andes* (pp. 245–271). Springer International Publishing. https://doi.org/10.1007/978-3-319-67774-3_10
- Niemeyer, H. (1975). *Geología de la región comprendida entre el lago General Carrera y el río Chacabuco. Provincia de Aisén, Chile*. Universidad de Chile.
- Niemeyer, H., Skarmeta, J., Fuenzalida, R., & Espinosa, W. (1985). *Hojas Península Taitao y Puerto Aisén, Región Aisén del General Carlos Ibáñez del Campo*. SERNAGEOMIN.
- Niu, Y. (2018). Geological understanding of plate tectonics: Basic concepts, illustrations, examples and new perspectives. *Global Tectonics and Metallogeny*, 10(1), 23–46. <https://doi.org/10.1127/gtm/2014/0009>
- Novas, F. E., Salgado, L., Suárez, M., Agnolín, F. L., Ezcurra, M. D., Chimento, N. R., de la Cruz, R., Isasi, M. P., Vargas, A. O., & Rubilar-Rogers, D. (2015). An enigmatic plant-eating theropod from the Late Jurassic period of Chile. *Nature*, 522(7556), 331–334. <https://doi.org/10.1038/nature14307>

- Nulló, F., Blasco, G., Risso, C., Combina, A., & Otamendi, J. (2006). *Hoja Geológica 5172-I y 5175-II El Calafate Provincia de Santa Cruz. Instituto de Geología y Recursos Minerales, Servicio Geológico Minero Argentino* (Vol. 396). SEGEMAR Boletín.
- Olivero, E. (1982). *Estratigrafía de la cuenca sur del Lago Fontana, Provincia del Chubut* [PhD Thesis, Universidad de Buenos Aires].
http://hdl.handle.net/20.500.12110/tesis_n1722_Olivero
- Olivero, E. (1987). Cefalópodos y bivalvos titonianos y hauterivianos de la Formación Lago La Plata, Chubut. *Ameghiniana*, 24(3–4), Article 3–4.
- Olivero, E., & Aguirre-Urreta, M. B. (2002). Sucesión de amonoideos de la Formación Katterfeld (Valanginiano-Hauteriviano) en su área tipo, Lago Fontana, Chubut. *XV Congr. Geol. Argentino, Actas*, 6 pp.
- Olivero, E. B. (1983). Amonoideos y bivalvos berriasianos de la cantera Tres Lagunas, Chubut. *Ameghiniana*, 20(1–2), Article 1–2.
- Ormazábal, M. (2018). *Estratigrafía y sedimentología mesozoica en torno a Puerto Ingeniero Ibáñez (~46°17'S), Cordillera Patagónica, Región de Aysén, Chile* [Memoria de Título]. Universidad Andrés Bello.
- Ortiz, A., & Vergara, M. (1979). *Perspectivas de Desarrollo de los Recursos de la Región de Aisen del General Carlos Ibáñez del Campo* (No. 26). Instituto de Investigación de Recursos Naturales.
- Pankhurst, R., Hervé, F., Fanning, M., & Suárez, M. (2003). Coeval plutonic and volcanic activity in the Patagonian Andes: The Patagonian Batholith and the Ibáñez and Divisadero formations, Aysén, Southern Chile. *X Congr. Geol. Chileno, Actas*, 5 pp.
- Pankhurst, R. J., Leat, P. T., Sruoga, P., Rapela, C. W., Márquez, M., Storey, B. C., & Riley, T. R. (1998). The Chon Aike province of Patagonia and related rocks in West Antarctica: A silicic large igneous province. *Journal of Volcanology and Geothermal Research*, 81(1–2), 113–136.
[https://doi.org/10.1016/S0377-0273\(97\)00070-X](https://doi.org/10.1016/S0377-0273(97)00070-X)
- Pankhurst, R. J., & Rapela, C. R. (1995). Production of Jurassic rhyolite by anatexis of the lower crust of Patagonia. *Earth and Planetary Science Letters*, 134(1–2), 23–36.
[https://doi.org/10.1016/0012-821X\(95\)00103-J](https://doi.org/10.1016/0012-821X(95)00103-J)
- Pankhurst, R. J., Riley, T. R., Fanning, C. M., & Kelley, S. P. (2000). Episodic Silicic Volcanism in Patagonia and the Antarctic Peninsula: Chronology of Magmatism Associated with the Break-up of Gondwana. *Journal of Petrology*, 41(5), 605–625.
<https://doi.org/10.1093/petrology/41.5.605>
- Pankhurst, R. J., Weaver, S. D., Hervé, F., & Larrondo, P. (1999). Mesozoic-Cenozoic evolution of the North Patagonian Batholith in Aysen, southern Chile. *Journal of the Geological Society*, 156(4), 673–694. <https://doi.org/10.1144/gsjgs.156.4.0673>
- Pérez-Barría, L., Bostelmann, J. E., Varela, J. P., Aldunate, J., & Heinsen, M. (2021). Museo Regional de Aysén (45 S, Coyhaique): Un nuevo repositorio oficial de paleontología en la zona austral de Chile. *XII Congreso de La Asociación Paleontológica Argentina. Libro de Resúmenes*, 38.
- Płoszkiewicz, J. V. (1987). *Descripción Geológica de la Hoja 47 c—"Apeleg", Provincia del Chubut: Carta Geológico-económica de la República Argentina, Escala 1:200.000* (Vol. 204). SEGEMAR Boletín.

- Ploszkiewicz, J. V., & Ramos, V. A. (1977). Estratigrafía y tectónica de la Sierra de Payaniyeu (Provincia del Chubut). *Revista de La Asociación Geológica Argentina*, XXXII(3), 209–226.
- Poblete-Huanca, A., Suárez, M., Rubilar-Rogers, D., Gressier, J. B., Arraño, C., & Ormazábal, M. (2021). First record of a Lower Cretaceous (Hauterivian) plesiosaur from Chile. *Cretaceous Research*, 128, 104963. <https://doi.org/10.1016/j.cretres.2021.104963>
- Price, G. (1999). The evidence and implications of polar ice during the Mesozoic. *Earth-Science Reviews*, 48(3), 183–210. [https://doi.org/10.1016/S0012-8252\(99\)00048-3](https://doi.org/10.1016/S0012-8252(99)00048-3)
- Price, G. D. (2009). Mesozoic Climates. In V. Gornitz (Ed.), *Encyclopedia of Earth Sciences Series: Encyclopedia of Paleoclimatology and Ancient Environments* (pp. 554–558). Springer Science+Business Media.
- Price, G. D., & Gröcke, D. R. (2002). Strontium-isotope stratigraphy and oxygen- and carbon-isotope variation during the Middle Jurassic–Early Cretaceous of the Falkland Plateau, South Atlantic. *Palaeogeography, Palaeoclimatology, Palaeoecology*, 183(3–4), 209–222. [https://doi.org/10.1016/S0031-0182\(01\)00486-2](https://doi.org/10.1016/S0031-0182(01)00486-2)
- Price, G. D., Ruffell, A. H., Jones, C. E., Kalin, R. M., & Mutterlose, J. (2000). Isotopic evidence for temperature variation during the early Cretaceous (late Ryazanian–mid-Hauterivian). *Journal of the Geological Society*, 157(2), 335–343. <https://doi.org/10.1144/jgs.157.2.335>
- Quensel, P. (1911). Geologisch-petrographische Studien in der patagonischen Cordillera. *Bull. of the Geol. Inst. of Upsala*, XL.
- Quiroz, D., & Bruce, Z. (2010). *Geología del área Puerto Ingeniero Ibáñez—Villa Cerro Castillo*. SERNAGEOMIN.
- Ramos, M. E., Suárez, R., Boixart, G., Ghiglione, M., & Ramos, V. A. (2019). The structure of the northern Austral Basin: Tectonic inversion of mesozoic normal faults. *Journal of South American Earth Sciences*, 94, 102197. <https://doi.org/10.1016/j.jsames.2019.05.013>
- Ramos, V. (1989). Andean Foothills Structures in Northern Magallanes Basin, Argentina. *AAPG Bulletin*, 73. <https://doi.org/10.1306/44B4A28A-170A-11D7-8645000102C1865D>
- Ramos, V. A. (1976). Estratigrafía de los lagos La Plata y Fontana, Provincia del Chubut, República Argentina. *I Congr. Geol. Chileno, Actas*, 1, 43–64.
- Ramos, V. A. (1978). *Los arrecifes de la Formación Cotidiano (Jurásico Superior) en la Cordillera Patagónica y su significado paleoclimático*. 15(1–2), 97–111.
- Ramos, V. A. (1979). Tectónica de la región del río y lago Belgrano, Cordillera Patagónica—Argentina. *II Congr. Geol. Chileno, Actas*, B1-32.
- Ramos, V. A. (1981). *Descripción Geológica de la Hoja 47 ab—"Lago Fontana", Provincia del Chubut: Carta Geológico-económica de la República Argentina, Escala 1:200.000* (Vol. 183). SEGEMAR Boletín.
- Ramos, V. A. (2009). Anatomy and global context of the Andes: Main geologic features and the Andean orogenic cycle. In S. M. Kay, V. A. Ramos, & W. R. Dickinson, *Backbone of the Americas: Shallow Subduction, Plateau Uplift, and Ridge and Terrane Collision*. Geological Society of America. [https://doi.org/10.1130/2009.1204\(02\)](https://doi.org/10.1130/2009.1204(02))
- Ramos, V. A. (2015). Evolución de la Cuenca Golfo San Jorge: Su estructuración y régimen tectónico. *Revista de la Asociación Geológica Argentina*, 72(1), 12–20.

- Ramos, V. A., & Aguirre-Urreta, M. B. (1994). Cretaceous Evolution of the Magallanes Basin. In J. A. Salfity (Ed.), *Cretaceous Tectonics of the Andes* (pp. 316–345). Vieweg+Teubner Verlag. https://doi.org/10.1007/978-3-322-85472-8_7
- Ramos, V. A., & Palma, M. (1983). Las lutitas pizarreñas fosilíferas del Cerro Dedo y su evolución tectónica; Lago La Plata, Provincia del Chubut. *Revista de La Asociación Geológica Argentina*, XXXVIII(2), 148–160.
- Rapela, C. W., Pankhurst, R. J., Fanning, C. M., & Hervé, F. (2005). Pacific subduction coeval with the Karoo mantle plume: The Early Jurassic Subcordilleran belt of northwestern Patagonia. *Geological Society, London, Special Publications*, 246(1), 217–239. <https://doi.org/10.1144/GSL.SP.2005.246.01.07>
- Rees, P. M., Noto, C. R., Parrish, J. M., & Parrish, J. T. (2004). Late Jurassic Climates, Vegetation, and Dinosaur Distributions. *The Journal of Geology*, 112(6), 643–653. <https://doi.org/10.1086/424577>
- Rees, P. M., Ziegler, A. M., & Valdes, P. J. (2000). Jurassic phytogeography and climates: New data and model comparisons. In B. T. Huber, K. G. MacLeod, & S. L. Wing (Eds.), *Warm climates in earth history* (pp. 297–318). Cambridge university press.
- Remane, J. (1991). The Jurassic-Cretaceous boundary: Problems of definition and procedure. *Cretaceous Research*, 12(5), 447–453. [https://doi.org/10.1016/0195-6671\(91\)90001-S](https://doi.org/10.1016/0195-6671(91)90001-S)
- Retallack, G. J. (2009). Triassic-Jurassic Climates. In V. Gornitz (Ed.), *Encyclopedia of Paleoclimatology and Ancient Environments* (pp. 962–968). Springer Netherlands. https://doi.org/10.1007/978-1-4020-4411-3_224
- Reyes, R. (1970). *La Fauna de Trigonias de Aisén* (No. 26). Instituto de Investigaciones Geológicas.
- Riccardi, A. (1971). Estratigrafía en el oriente de la Bahía de la Lancha. Lago San Martín, Santa Cruz, Argentina. *Revista Del Museo de La Plata. Nueva Serie. Sección Geología*, 7(61), 245–318.
- Riccardi, A. (1977). Berriasian invertebrate fauna from the Springhill Formation of southern Patagonia. *Neues Jahrbuch Für Geologie Und Paläontologie*, 155(2), 216–252.
- Riccardi, A. (1988). *The Cretaceous System of Southern South America*. Geol. Soc. Am. Mem. <https://doi.org/10.1130/MEM168>
- Riccardi, A. C. (1976). Paleontología y edad de la Formación Springhill. *I Congr. Geol. Chileno, Actas*, 1, 41–56.
- Riccardi, A. C. (1984). Las asociaciones de amonitas del Jurásico y Cretácico de la Argentina. *Noveno Congr. Geol. Argentino, Actas*, IV, 559–595.
- Riccardi, A. C. (1991). Jurassic and cretaceous marine connections between the Southeast Pacific and Tethys. *Palaeogeography, Palaeoclimatology, Palaeoecology*, 87(1–4), 155–189. [https://doi.org/10.1016/0031-0182\(91\)90134-D](https://doi.org/10.1016/0031-0182(91)90134-D)
- Riccardi, A. C., & Rolleri, E. O. (1980). Cordillera Patagónica Austral. *Geología Regional Argentina*, 1173–1306.
- Richiano, S., Gómez-Peral, L. E., Varela, A. N., Gómez Dacal, A. R., Cavarozzi, C. E., & Poiré, D. G. (2019). Geochemical characterization of black shales from the Río Mayer Formation (Early Cretaceous), Austral-Magallanes Basin, Argentina: Provenance response during Gondwana

break-up. *Journal of South American Earth Sciences*, 93, 67–83.
<https://doi.org/10.1016/j.jsames.2019.04.009>

Richiano, S., Varela, A. N., Cereceda, A., & Poiré, D. G. (2012). Evolución paleoambiental de la Formación Río Mayer, Cretácico Inferior, Cuenca Austral, Provincia de Santa Cruz, Argentina. *Latin American Journal of Sedimentology and Basin Analysis*, 19(1), 3–26.

Richiano, S., Varela, A. N., Gómez-Peral, L. E., Cereceda, A., & Poiré, D. G. (2015). Composition of the Lower Cretaceous source rock from the Austral Basin (Río Mayer Formation, Patagonia, Argentina): Regional implication for unconventional reservoirs in the Southern Andes. *Marine and Petroleum Geology*, 66, 764–790. <https://doi.org/10.1016/j.marpetgeo.2015.07.018>

Rivas, H., Salazar, C., & Stinnesbeck, W. (2021). Facies and sequence stratigraphy of a mixed carbonate-volcaniclastic ramp in intra-arc settings: An example from the Toqui Formation (Lower Cretaceous), southern Chile (45°S). *Journal of South American Earth Sciences*, 109, 103292. <https://doi.org/10.1016/j.jsames.2021.103292>

Rivas, H., Salazar, C., & Stinnesbeck, W. (2023). A “cool-water”, non-tropical, mixed volcaniclastic–carbonate ramp from the Early Cretaceous of southern Chile (45°40'S). *Facies*, 69(3), 14. <https://doi.org/10.1007/s10347-023-00669-4>

Riveros, D. (2020). *Estratigrafía y sedimentología en torno a Mallín Grande, Cordillera Patagónica, Región de Aysén, Chile* [Memoria de Título]. Universidad Andrés Bello.

Rogov, M., Ershova, V., Vereshchagin, O., Vasileva, K., Mikhailova, K., & Krylov, A. (2021). Database of global glendonite and ikaite records throughout the Phanerozoic. *Earth System Science Data*, 13(2), 343–356. <https://doi.org/10.5194/essd-13-343-2021>

Rogov, M., Zakharov, V. A., & Nikitenko, B. L. (2010). The Jurassic-Cretaceous boundary problem and the myth on J/K boundary extinction. *Earth Science Frontiers*, 17, 13–14.

Rolando, A. P., Hartmann, L. A., Santos, J. O. S., Fernandez, R. R., Etcheverry, R. O., Schalamuk, I. A., & McNaughton, N. J. (2002). SHRIMP zircon U–Pb evidence for extended Mesozoic magmatism in the Patagonian Batholith and assimilation of Archean crustal components. *Journal of South American Earth Sciences*, 15(2), 267–283. [https://doi.org/10.1016/S0895-9811\(02\)00015-9](https://doi.org/10.1016/S0895-9811(02)00015-9)

Ruban, D. A. (2015). Mesozoic long-term eustatic cycles and their uncertain hierarchy. *Geoscience Frontiers*, 6(4), 503–511. <https://doi.org/10.1016/j.gsf.2014.06.001>

Rubilar, A. E. (2000). *Aetostreon* sp. Nov. Del Neocomiano, sur de Chile y Argentina, y su afinidad morfológica con *Gryphaea* Lamarck. *IX Congr. Geol. Chileno, Actas*, 2, 249–253.

Ruiz, C. (1942). *Geología de la Provincia de Aysén* (p. 87). Instituto de Investigaciones Geológicas.

Salazar, C., Martínez, A., Villanelo, L., & Stinnesbeck, W. (2014). *Cymatoceras perstriatum* (Steuer, 1897) (Cephalopoda, Nautiloidea) from the early Berriasian-early Valanginian (Lower Cretaceous) of Central Chile. *Boletín Del Museo Nacional de Historia Natural*, 63, 179–186.

Salazar, C., & Stinnesbeck, W. (2016). Tithonian–Berriasian ammonites from the Baños del Flaco Formation, central Chile. *Journal of Systematic Palaeontology*, 14(2), 149–182. <https://doi.org/10.1080/14772019.2015.1027310>

Salazar, C., Stinnesbeck, W., & Álvarez, M. (2020). Ammonite biostratigraphy and bioevents in the Jurassic – Cretaceous boundary of central Chile. *Cretaceous Research*, 107, 104282. <https://doi.org/10.1016/j.cretres.2019.104282>

- Scasso, R. A. (1987). *Estratigrafía y ambientes de sedimentación del ciclo sedimentario del Jurásico Superior y Cretácico Inferior de la región sudoccidental del Chubut, con referencias a la columna estratigráfica general del área* [PhD Thesis, Universidad de Buenos Aires].
http://hdl.handle.net/20.500.12110/tesis_n2054_Scasso
- Scasso, R. A. (1989). La Cuenca Sedimentaria del Jurásico Superior y Cretácico Inferior de la Región Sudoccidental del Chubut. In G. A. Chebli & L. A. Spalletti (Eds.), *Cuencas Sedimentarias Argentinas* (pp. 395–417).
- Scasso, R. A., & Kiessling, W. (2002). Earliest Cretaceous high latitude reefs in Tres Lagunas (Chubut Province, Argentina). *XV Congr. Geol. Argentino, Actas*, 6 pp.
- Schwarz, E., Veiga, G. D., Spalletti, L. A., & Massaferro, J. L. (2011). The transgressive infill of an inherited-valley system: The Springhill Formation (lower Cretaceous) in southern Austral Basin, Argentina. *Marine and Petroleum Geology*, 28(6), 1218–1241.
<https://doi.org/10.1016/j.marpetgeo.2010.11.003>
- Segev, A. (2002). Flood basalts, continental breakup and the dispersal of Gondwana: Evidence for periodic migration of upwelling mantle flows (plumes). *Stephan Mueller Special Publication Series*, 2, 171–191. <https://doi.org/10.5194/smsps-2-171-2002>
- Sellwood, B. W., & Valdes, P. J. (2006). Mesozoic climates: General circulation models and the rock record. *Sedimentary Geology*, 190(1–4), 269–287.
<https://doi.org/10.1016/j.sedgeo.2006.05.013>
- Sellwood, B. W., & Valdes, P. J. (2008). Jurassic climates. *Proceedings of the Geologists' Association*, 119(1), 5–17. [https://doi.org/10.1016/S0016-7878\(59\)80068-7](https://doi.org/10.1016/S0016-7878(59)80068-7)
- Seton, M., Müller, R. D., Zahirovic, S., Gaina, C., Torsvik, T., Shephard, G., Talsma, A., Gurnis, M., Turner, M., Maus, S., & Chandler, M. (2012). Global continental and ocean basin reconstructions since 200Ma. *Earth-Science Reviews*, 113(3–4), 212–270.
<https://doi.org/10.1016/j.earscirev.2012.03.002>
- Skarmeta, J. (1974). *Geología de la región continental de Aisén entre los 45 y 46 lat. Sur*. Universidad de Chile.
- Skarmeta, J. (1976). Evolución tectónica y paleogeográfica de los Andes Patagónicos de Aisén (Chile), durante el Neocomiano. *I Congr. Geol. Chileno, Actas*, B, 1–15.
- Skarmeta, J., & Charrier, R. (1976). Geología del sector fronterizo de Aysén entre los 45° y 46° de latitud sur, Chile. *VI Congr. Geol. Argentino, Actas*, I, 267–286.
- Steinmann, G. (1930). Sobre *Archamphiroa jurassica*. *Revista Del Museo de La Plata*, 32, 1–8.
- Stephen, H. (1909). *Viajes de Exploracion i Estudio en la Patagonia Occidental 1892-1902* (Santiago, Chile). Imprenta Cervantes.
- Stern, C. R., & De Wit, M. J. (2003). Rocas Verdes ophiolites, southernmost South America: Remnants of progressive stages of development of oceanic-type crust in a continental margin back-arc basin. *Geological Society, London, Special Publications*, 218(1), 665–683.
<https://doi.org/10.1144/GSL.SP.2003.218.01.32>
- Stinnesbeck, W., Frey, E., Rivas, L., Perez, J. P., Cartes, M. L., Soto, C. S., & Lobos, P. Z. (2014). A Lower Cretaceous ichthyosaur graveyard in deep marine slope channel deposits at Torres del Paine National Park, southern Chile. *Geological Society of America Bulletin*, 126(9–10), 1317–1339. <https://doi.org/10.1130/B30964.1>

- Storey, B. C., Vaughan, A. P. M., & Millar, I. L. (1996). Geodynamic evolution of the Antarctic Peninsula during Mesozoic times and its bearing on Weddell Sea history. *Geological Society, London, Special Publications*, 108(1), 87–103. <https://doi.org/10.1144/GSL.SP.1996.108.01.07>
- Suárez, M., & De la Cruz, R. (1994a). *Estratigrafía del Jurásico Superior—Cretácico Inferior de la Cordillera Patagónica Oriental (45°-46° latitud sur), Chile: Facies, Paleogeografía*. SERNAGEOMIN.
- Suárez, M., & De la Cruz, R. (1994b). Estratigrafía y paleogeografía mesozoica de Aisén Nororiental. *VII Congr. Geol. Chileno, Actas, I*, 538–542.
- Suárez, M., & De la Cruz, R. (2000). Tectonics in the eastern central Patagonian Cordillera (45°30'–47°30'S). *Journal of the Geological Society*, 157(5), 995–1001. <https://doi.org/10.1144/jgs.157.5.995>
- Suárez, M., & De la Cruz, R. (2001). Jurassic to Miocene K–Ar dates from eastern central Patagonian Cordillera plutons, Chile (45°–48° S). *Geological Magazine*, 138(1), 53–66. <https://doi.org/10.1017/S0016756801004903>
- Suárez, M., De la Cruz, R., Aguirre-Urreta, M. B., & Fanning, M. (2005). Diachronic Tithonian-Valanginian marine transgression of the Coyhaique Group, Aysén Basin (43°-47°S), Chile. *XVI Congr. Geol. Argentino, Actas, I*, 305–308.
- Suárez, M., De La Cruz, R., Aguirre-Urreta, M. B., & Fanning, M. (2009). Relationship between volcanism and marine sedimentation in northern Austral (Aisén) Basin, central Patagonia: Stratigraphic, U–Pb SHRIMP and paleontologic evidence. *Journal of South American Earth Sciences*, 27(4), 309–325. <https://doi.org/10.1016/j.jsames.2008.11.009>
- Suárez, M., De la Cruz, R., & Bell, C. M. (1996). Estratigrafía de la región de Coyhaique (latitud 45°-46° S), Cordillera Patagónica, Chile. *XIII Congr. Geol. Argentino y III Congr. Explor. Hidroc., Actas, I*, 575–590.
- Suárez, M., De la Cruz, R., & Bell, C. M. (2007). *Geología del área Ñireguao-Baño Nuevo, Región Aisén del General Carlos Ibáñez del Campo*. SERNAGEOMIN.
- Suárez, M., De la Cruz, R., Bell, M., & Demant, A. (2010). Cretaceous slab segmentation in southwestern Gondwana. *Geological Magazine*, 147(2), 193–205. <https://doi.org/10.1017/S0016756809990355>
- Suárez, M., De la Cruz, R., Etchart, H., Marcelo, M., & Mark, F. (2015). Síntesis de la cronología magmática Meso-Cenozoica de Patagonia Central, Aysén, Chile: Edades U–Pb SHRIMP. *XIV Congr. Geol. Chileno, Actas*, 789–792.
- Suárez, M., De la Cruz, R., Fanning, M., Novas, F., & Salgado, L. (2016). Tithonian age of dinosaur fossils in central Patagonian, Chile: U–Pb SHRIMP geochronology. *International Journal of Earth Sciences*, 105(8), 2273–2284. <https://doi.org/10.1007/s00531-015-1287-7>
- Suárez, M., Demant, A., Cruz, R. D. L., & Fanning, C. M. (2010). ⁴⁰Ar/³⁹Ar and U–Pb SHRIMP dating of Aptian tuff cones in the Aisén Basin, Central Patagonian Cordillera. *Journal of South American Earth Sciences*, 29(3), 731–737. <https://doi.org/10.1016/j.jsames.2009.11.003>
- Suárez, M., Gressier, J. B., Rossel, P., & De la Cruz, R. (2023). Lower cretaceous missing volcanic arc. A migrating arc, central Patagonian cordillera, Chile: Detrital zircon U–Pb geochronology. *International Journal of Earth Sciences*, 112(3), 907–923. <https://doi.org/10.1007/s00531-022-02272-4>

- Suarez, M., & Marquez, M. (2007). Cuenca de retroarco toarciana en Patagonia central (Chubut), Argentina: Cierre, migración del arco y ambiente tectónico durante el Jurásico Medio. *Andean Geology*, 34(1), 63–80. <https://doi.org/10.5027/andgeoV34n1-a04>
- Suárez, R., Ghiglione, M. C., Sue, C., Quezada, P., Roy, S., Rojo, D., & Calderón, M. (2021). Paleozoic-early Mesozoic structural evolution of the West Gondwana accretionary margin in southern Patagonia, Argentina. *Journal of South American Earth Sciences*, 106, 103062. <https://doi.org/10.1016/j.jsames.2020.103062>
- Suárez, R., González, P. D., & Ghiglione, M. C. (2019). A review on the tectonic evolution of the Paleozoic-Triassic basins from Patagonia: Record of protracted westward migration of the pre-Jurassic subduction zone. *Journal of South American Earth Sciences*, 95, 102256. <https://doi.org/10.1016/j.jsames.2019.102256>
- Sylwan, C. A. (2001). Geology of the Golfo San Jorge Basin, Argentina. *Journal of Iberian Geology*, 27, 123–157.
- Sylwan, C. A., Droeven, C., Iñigo, J., Mussel, F., & Padva, D. (2011). Cuenca del Golfo San Jorge. *VIII Congreso de Exploración y Desarrollo de Hidrocarburos, Actas. VIII Congreso de Exploración y Desarrollo de Hidrocarburos*, Mar del Plata, Argentina.
- Tarney, J., Windley, B. F., & Kröner, A. (1981). Marginal basins through geological time. *Philosophical Transactions of the Royal Society of London. Series A, Mathematical and Physical Sciences*, 301(1461), 217–232. <https://doi.org/10.1098/rsta.1981.0107>
- Tennant, J. P., Mannion, P. D., Upchurch, P., Sutton, M. D., & Price, G. D. (2017). Biotic and environmental dynamics through the Late Jurassic-Early Cretaceous transition: Evidence for protracted faunal and ecological turnover: Jurassic-Cretaceous biotic and abiotic dynamics. *Biological Reviews*, 92(2), 776–814. <https://doi.org/10.1111/brv.12255>
- The North American Commission on Stratigraphic Nomenclature. (2005). North American Stratigraphic Code. *The American Association of Petroleum Geologists Bulletin*, 89(11), 1547–1591.
- Thiele, R., Castillo, J. C., Hein, R., Romero, G., & Ulloa, M. (1978). Geología del sector fronterizo de Chiloé Continental entre los 43°00'—43°45' latitud sur, Chile (Columnas de Futaleufú y Palena). *VII Congr. Geol. Argentino, Actas, I*, 577–591.
- Thomas, C. R. (1949). Geology and Petroleum Exploration in Magallanes Province, Chile. *AAPG Bulletin*, 33(9), 1553–1578. <https://doi.org/10.1306/3D933DEE-16B1-11D7-8645000102C1865D>
- Toscano, A. G., & Lazo, D. G. (2020). Taxonomic revision and palaeobiogeographic affinities of Berriasian–Valanginian oysters from the Vaca Muerta and Mulichinco formations, southern Mendoza, Neuquén Basin, Argentina. *Cretaceous Research*, 109, 104358. <https://doi.org/10.1016/j.cretres.2019.104358>
- Townsend, M. J. (1998). *The palaeogeography of the Lower Cretaceous Aysén Basin of southern Chile* [PhD Thesis, University of Bristol]. <https://ethos.bl.uk/OrderDetails.do?uin=uk.bl.ethos.246282>
- Uliana, M. A., Biddle, K. T., & Cerdan, J. (1989). Mesozoic Extension and the Formation of Argentine Sedimentary Basins. In A. J. Tankard & H. R. Balkwill (Eds.), *Extensional tectonics and stratigraphy of the North Atlantic margins* (pp. 599–614). AAPG. <https://ezproxy.aub.edu.lb/login?url=http://ebooks.geoscienceworld.org/content/extensional-tectonics-and-stratigraphy-of-the-north-atlantic-margins>

- VanderLeest, R. A., Fosdick, J. C., Malkowski, M. A., Romans, B. W., Ghiglione, M. C., Schwartz, T. M., & Sickmann, Z. T. (2022). Tectonic Subsidence Modeling of Diachronous Transition From Backarc to Retroarc Basin Development and Uplift During Cordilleran Orogenesis, Patagonian-Fuegian Andes. *Tectonics*, 41(10), e2021TC006891. <https://doi.org/10.1029/2021TC006891>
- Varela, A. N., Richiano, S., D'Elia, L., Moyano Paz, D., Tettamanti, C., & Poiré, D. G. (2019). Sedimentology and stratigraphy of the Puesto El Moro Formation, Patagonia, Argentina: Implications for upper cretaceous paleogeographic reconstruction and compartmentalization of the Austral-Magallanes Basin. *Journal of South American Earth Sciences*, 92, 466–480. <https://doi.org/10.1016/j.jsames.2019.03.030>
- Veizer, J., Godderis, Y., & François, L. M. (2000). Evidence for decoupling of atmospheric CO₂ and global climate during the Phanerozoic eon. *Nature*, 408(6813), 698–701. <https://doi.org/10.1038/35047044>
- Vicente, J. C. (2006). Dynamic Paleogeography of the Jurassic Andean Basin. *Revista de La Asociación Geológica Argentina*, 61(3), 408–437.
- Vickers, M. L., Bajnai, D., Price, G. D., Linckens, J., & Fiebig, J. (2019). Southern high-latitude warmth during the Jurassic–Cretaceous: New evidence from clumped isotope thermometry. *Geology*, 47(8), 724–728. <https://doi.org/10.1130/G46263.1>
- Wellmer, F. W., & Reeve, E. J. (1990). The Toqui Zinc-Lead-Copper-Silver Deposits, Aysén Province, Chile. In L. Fontboté, G. C. Amstutz, M. Cardozo, E. Cedillo, & J. Frutos (Eds.), *Stratabound Ore Deposits in the Andes* (pp. 473–484). Springer. https://doi.org/10.1007/978-3-642-88282-1_36
- Wellmer, F. W., Reeve, E. J., Wentzlau, E., & Westenberger, H. (1983). Geology and ore deposits of the Toqui District, Aysen, Chile. *Economic Geology*, 78(6), 1119–1143. <https://doi.org/10.2113/gsecongeo.78.6.1119>
- Wetzel, W. (1960). Die Coyhaique-Schichten des patagonischen Neocoms, und ihre Ammoniten. *Neues Jahrbuch Für Geologie Und Paläontologie*, 6, 246–254.
- Wilson, T. J. (1991). Transition from back-arc to foreland basin development in the southernmost Andes: Stratigraphic record from the Ultima Esperanza District, Chile. *Geological Society of America Bulletin*, 103(1), 98–111. [https://doi.org/10.1130/0016-7606\(1991\)103<0098:TFBATF>2.3.CO;2](https://doi.org/10.1130/0016-7606(1991)103<0098:TFBATF>2.3.CO;2)
- Wimbledon, W. A. P. (2017). Developments with fixing a Tithonian/Berriasian (J/K) boundary. *Volumina Jurassica*, 1, 0–0. <https://doi.org/10.5604/01.3001.0010.7467>
- Wright, V. P. (1992). A revised classification of limestones. *Sedimentary Geology*, 76(3–4), 177–185. [https://doi.org/10.1016/0037-0738\(92\)90082-3](https://doi.org/10.1016/0037-0738(92)90082-3)
- Zaffarana, C. B., Somoza, R., & López De Luchi, M. (2014). The Late Triassic Central Patagonian Batholith: Magma hybridization, 40Ar/39Ar ages and thermobarometry. *Journal of South American Earth Sciences*, 55, 94–122. <https://doi.org/10.1016/j.jsames.2014.06.006>

8. Appendixes

8.1. Scientific Publication Nr. 1:

Facies and sequence stratigraphy of a mixed carbonate-volcaniclastic ramp in intra-arc settings: An example from the Toqui Formation (Lower Cretaceous), southern Chile (45°S)

Authors: Rivas, H.; Salazar, C.; Stinnesbeck, W.

Published in: Journal of South American Earth Sciences (Elsevier)

Year: 2021

Author contribution (CRediT)

Hermann Rivas: Software, Formal analysis, Investigation, Data curation, Writing – original draft, Writing – review & editing, Visualization.

Christian Salazar: Conceptualization, Methodology, Resources, Writing—review and editing, Supervision, Project administration, Funding acquisition.

Wolfgang Stinnesbeck: Resources, Writing – review & editing, Supervision, Project administration.

Citation: Rivas, H., Salazar, C., & Stinnesbeck, W. (2021). Facies and sequence stratigraphy of a mixed carbonate-volcaniclastic ramp in intra-arc settings: An example from the Toqui Formation (Lower Cretaceous), southern Chile (45° S). *Journal of South American Earth Sciences*, 109, 103292. <https://doi.org/10.1016/j.jsames.2021.103292>

1. Publikation/Publication:

Vollständige bibliographische Referenz/Complete bibliographic reference:

Rivas, H., Salazar, C., & Stinnesbeck, W. (2021). Facies and sequence stratigraphy of a mixed carbonate-volcaniclastic ramp in intra-arc settings: An example from the Toqui Formation (Lower Cretaceous), southern Chile (45 S). Journal of South American Earth Sciences, 109, 103292.

2. Erst- oder gleichberechtigte Autorenschaft/First or equal authorship:**Ja/Yes**

Nein/No

3. Veröffentlicht/Published

Zur Veröffentlichung akzeptiert/Accepted

Q1/Q2* 0.708

*SCImago Journal Rank (SJR) indicator

Ja/Yes ☒ Nein/No

Im Erscheinungsjahr oder im letzten verfügbaren Vorjahr/In the year of publication or the last prior year available: 2021

Eingereicht/Submitted

Noch nicht eingereicht/Not yet submitted

4. Beteiligungen/Contributions**

Contributor Role	Doktorand/in/ Doctoral student	Co-Autor/in 1/ Co-author 1	Co-Autor/in 2/ Co-author 2
Name, first name	Rivas, Hermann	Salazar, Christian	Stinnesbeck, Wolfgang
Methodology	<input type="checkbox"/>	<input checked="" type="checkbox"/>	<input type="checkbox"/>
Software	<input checked="" type="checkbox"/>	<input type="checkbox"/>	<input type="checkbox"/>
Validation	<input type="checkbox"/>	<input checked="" type="checkbox"/>	<input type="checkbox"/>
Formal analysis	<input checked="" type="checkbox"/>	<input type="checkbox"/>	<input type="checkbox"/>
Investigation	<input checked="" type="checkbox"/>	<input type="checkbox"/>	<input type="checkbox"/>
Resources	<input type="checkbox"/>	<input checked="" type="checkbox"/>	<input checked="" type="checkbox"/>
Data Curation	<input checked="" type="checkbox"/>	<input type="checkbox"/>	<input type="checkbox"/>
Writing-Original Draft	<input checked="" type="checkbox"/>	<input type="checkbox"/>	<input type="checkbox"/>
Writing-Review&Editing	<input checked="" type="checkbox"/>	<input checked="" type="checkbox"/>	<input checked="" type="checkbox"/>
Visualization	<input checked="" type="checkbox"/>	<input type="checkbox"/>	<input type="checkbox"/>
Supervision	<input type="checkbox"/>	<input checked="" type="checkbox"/>	<input checked="" type="checkbox"/>
Project administration	<input type="checkbox"/>	<input checked="" type="checkbox"/>	<input checked="" type="checkbox"/>
Funding acquisition	<input type="checkbox"/>	<input checked="" type="checkbox"/>	<input type="checkbox"/>

**Kategorien des CRediT (Contributor Roles Taxonomy, <https://credit.niso.org/>)

Hiermit bestätige ich, dass alle obigen Angaben korrekt sind/I confirm that all declarations made above are correct.

Unterschrift/Signature

Doktorand/in/Doctoral student

Co-Autor/in 1/Co-author 1

Co-Autor/in 2/Co-author 2

Betreuungsperson/Supervisor:

Hiermit bestätige ich, dass alle obigen Angaben korrekt sind und dass die selbstständigen Arbeitsanteile des/der Doktoranden/in an der aufgeführten Publikation hinreichend und signifikant sind/I confirm that all declarations made above are correct and that the doctoral student's independent contribution to this publication is significant and sufficient to be considered for the cumulative dissertation.

Wolfgang Stinnesbeck

Name/Name



Unterschrift/Signature

20.03.2025

Datum/Date



Contents lists available at ScienceDirect

Journal of South American Earth Sciences

journal homepage: www.elsevier.com/locate/jsames

Facies and sequence stratigraphy of a mixed carbonate-volcaniclastic ramp in intra-arc settings: An example from the Toqui Formation (Lower Cretaceous), southern Chile (45°S)

Hermann Rivas^a, Christian Salazar^{b,*}, Wolfgang Stinnesbeck^a^a Institut für Geowissenschaften, Universität Heidelberg, Im Neuenheimer Feld 234, 69120, Heidelberg, Germany^b Escuela de Geología, Facultad de Ciencias, Universidad Mayor, San Pío X 2422, 7510041, Providencia, Chile

ARTICLE INFO

Keywords:

Petrography
Oyster
biostrome
Gravity flow
Coyhaique
Group Austral
Basin
Patagonia

ABSTRACT

The Toqui Formation in the Northern Austral Basin, or Aysén - Río Mayo Basin in Central Patagonia (43°–49°S), is the basal member of the transgressive-regressive Coyhaique Group of Tithonian-Aptian age. A revision of the basin fill, focusing on the early transgressive units exposed in Chile and Argentina at 45°–46°S, is presented. In order to explain the lithological variability of the mixed calcareous-volcaniclastic Toqui Formation and the evolution of its depositional environments, a detailed sedimentological-petrographic analysis of two outcrops and four drill cores was executed at the type locality, El Toqui Mine (45°S). Twenty-three lithofacies were recognized, arranged in five facies associations. The Toqui Formation comprises three facies associations (Calcareous-, Muddy-, and Sandy Volcaniclastic), and is here redefined as conformed by two members: Manto- and Mina San Antonio Members. Its Manto Member conformably overlies volcanic rocks of the Ibáñez Fm., settled as subtidal Gilbert-type delta foresets, conforming a proximal-medial volcanic apron (Kimmeridgian- Valanginian). The Manto Member includes mixed calcareous-volcaniclastic sandstone, bioclastic wacke- floatstone, and oyster boundstone, depicted as patch-reefs developed in a carbonate mid- and outer-ramp. The Manto Member is covered by tuffaceous mudstone and volcanic sandstone of the Mina San Antonio Member, representing a prograding, eruption-fed shelf delta, conforming a medial-distal volcanic apron. Upsection, the volcaniclastic succession retrogrades into outer-shelf hemipelagic mudstone of the Katterfeld Formation. Overall, the Aysén Basin depicts a not fully developed marginal basin, i.e. formed by extension but without onset of seafloor spreading. The early marine transgression is linked to a relative sea-level rise caused by tectonic sub-sidence (back-arc extension), and the subsequent flooding of continental, intra-arc volcanic terrains comprising a transgressive system tract. Carbonate platforms aggraded as highstand system tracts over the subtidal volcanic topography, suggesting periods of tectono-volcanic quiescence. Ramps were covered by prograding deltaic deposits, reflecting a normal regression caused by high volcaniclastic input and local, shallow intrusion-related volcanic uplift (inflation). Upwards, the volcaniclastic succession grades to prodelta and hemipelagic deposits of a major transgressive system tract. The onset of pelagic conditions depicts an important relative sea-level rise, regarded as caused by “post-rift” thermal subsidence, possibly enhanced by the Valanginian high global eustasy. Lithological differences between the Toqui Formation in Chile and the partly coeval transgressive units exposed in Argentina (44°50'–47°S), i.e. Cotidiano, Tres Lagunas, and Springhill Formations, is considered as caused by diachronic development of ramps, lateral facies changes, and differential volcaniclastic input. Deposition of the Toqui Formation thus reflects a complex interaction between tectonic subsidence, coastal volcanism, and patch-reef growth.

* Corresponding author.

E-mail addresses: hermann.rivas@geow.uni-heidelberg.de (H. Rivas), christian.salazar@umayor.cl (C. Salazar), wolfgang.stinnesbeck@geow.uni-heidelberg.de (W. Stinnesbeck).

<https://doi.org/10.1016/j.jsames.2021.103292>

Received 18 August 2020; Received in revised form 18 March 2021; Accepted 22 March 2021

Available online 31 March 2021

0895-9811/© 2021 Elsevier Ltd. All rights reserved.

1. Introduction

During the Tithonian-Aptian, a marine incursion spread over a back-arc to intra-arc basin in central Patagonia (43°-49°S), known as the northern Austral Basin (e.g. Riccardi, 1988; Suárez et al., 1996; 2010a), but also referred as Aysén Basin (Bell et al., 1996; Suárez et al., 1996) or Río Mayo Embayment (Aguirre-Urreta and Ramos, 1981; Folguera and Iannizzotto, 2004, Fig. 1-A). The volcano-sedimentary basin fill comprises the volcanic rocks of the Ibáñez- and Lago La Plata Fms., overlain by a transgressive-regressive marine sequence conformed by the Coyhaique Group (Haller and Lapido, 1980, Fig. 1-B; 2-A). The Coyhaique Group comprehends, from base to top, the mixed calcareous-volcaniclastic Toqui Fm. (Tithonian-Valanginian, Hauterivian?), covered by- and grading to the pelitic-siliciclastic Katterfeld Fm. (Valanginian-Hauterivian, Barremian?), which grades to the sandy-siliciclastic Apeleg Fm. (Hauterivian-Aptian) (Suárez & De La Cruz, 1994; Suárez et al., 2009; 2010a, Fig. 2-A). The Toqui Fm. represents the early transgressive, shallow-marine deposits from the Aysén Basin (e.g. Suárez et al., 2005; 2007).

In the El Toqui Mining District (Fig. 1-B, C), one of the largest Zn-Pb deposits in Chile (Kojima and Campos, 2011), stratabound skarn mineralization is emplaced in the Lower Cretaceous marine succession (Wellmer et al., 1983; Bussey et al., 2010a, b). This mining district was defined as the type locality of the Toqui Formation (Suárez & De La Cruz, 1994). The Toqui Fm. comprises mixed calcareous-volcaniclastic

rocks including bioclastic limestone and subaqueous, volcanic sandstone-mudstone (Wellmer et al., 1983; Bussey et al., 2010a, b). These rocks were grouped in three informal members: a basal “calcareous association”, underlying interbedded “pyroclastic-calcareous” and “sandy-calcareous associations” (Suárez & De La Cruz, 1994; Suárez et al., 2007; Fig. 2-B). However, this subdivision is debatable since the three members partially interfinger and the sandstone units are mainly volcanoclastic. In addition, the current scheme does not clearly state the relationship between the contrasting lithological members of the formation (calcareous vs volcanoclastic), neither their correlation or lateral variations with other similar outcrops; also, no detailed depositional model for its settling has been provided.

In order to contextualize the onset of the Tithonian-Early Cretaceous marine transgression in the 45°-46° S segment of central Patagonia, the Aysén Basin fill and its evolution are here revised (Fig. 2-A; Section 1.1).

In particular, the marine transgression is linked to the development of carbonate platforms in volcanic settings (Section 3.2); this topic has not been thoroughly documented from ancient deposits (Dorobek, 2008b), nor has the sequence stratigraphy of these deposits been analyzed in detail (e.g. Emery and Myers, 1996; Catuneanu, 2017; Section 4.3).

Based on the analysis of six sedimentary logs from the El Toqui Mine (four drill cores and two outcrops), and 56 thin sections (Figs. 3-8), a detailed facies model for the Toqui Fm. and its adjacent stratigraphic

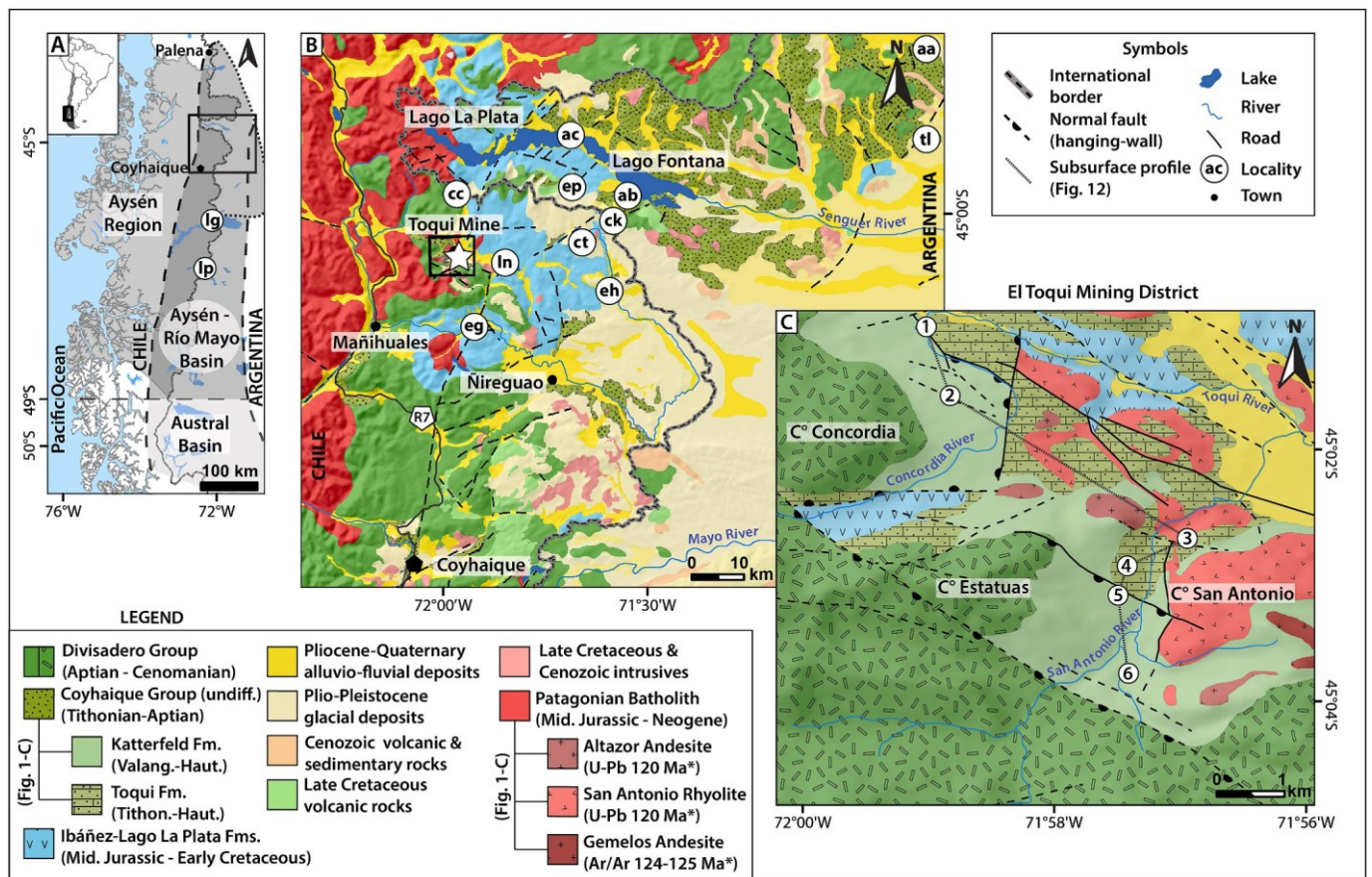


Fig. 1. A) Location map. Dashed Line: Outline of the Northern Austral Basin or Aysén (*sensu* Suárez et al., 2010a); dotted line: Río Mayo Embayment (*sensu* Aguirre-Urreta and Ramos, 1981). Abbreviations: lg: Lago General Carrera; lp: Lago Pueyrredón. See discussion in text. B) Regional geological map between Coyhaique and Fontana-La Plata Lakes (Modified from Lizuáin et al., 1995; De La Cruz et al., 2003; SERNAGEOMIN, 2003; Suárez et al., 2007). White star marks the location of the El Toqui Mine (type locality of the Toqui Formation, *sensu* Suárez & De La Cruz, 1994), for location see black square in Fig. 1-A. C) El Toqui Mining District geological map, modified from Bussey et al. (2010a, b), for location see black square in Fig. 1-B. Sedimentary logs analyzed here include two outcrops and four drill cores (numbers 1-6): 1) ELC (outcrop); 2) DCE19; 3) ESA (outcrop); 4) LCS453; 5) ASN09; 6) PDT21 (Figs. 3-10). Localities and abbreviations mentioned in text: aa: Aldea Apeleg; ac: Arroyo/Mallín Cotidiano (Cotidiano Fm. type locality *sensu* Ramos, 1976); C° = Cerro (hill); cc: Cerro Catedral; ck: Cerro Trincheras; eg: Estero El Gato; eh: Estero La Horqueta; ln: Lago Norte; ep: Estero Pedregoso & Arroyo Flores; tl: Tres Lagunas Quarry - Laguna Salada (Tres Lagunas Fm. type locality *sensu* Płoszkiewicz and Ramos, 1977); R7: Carretera Austral (Route 7). * Names and ages of local intrusive from Bussey et al. (2010a, b).

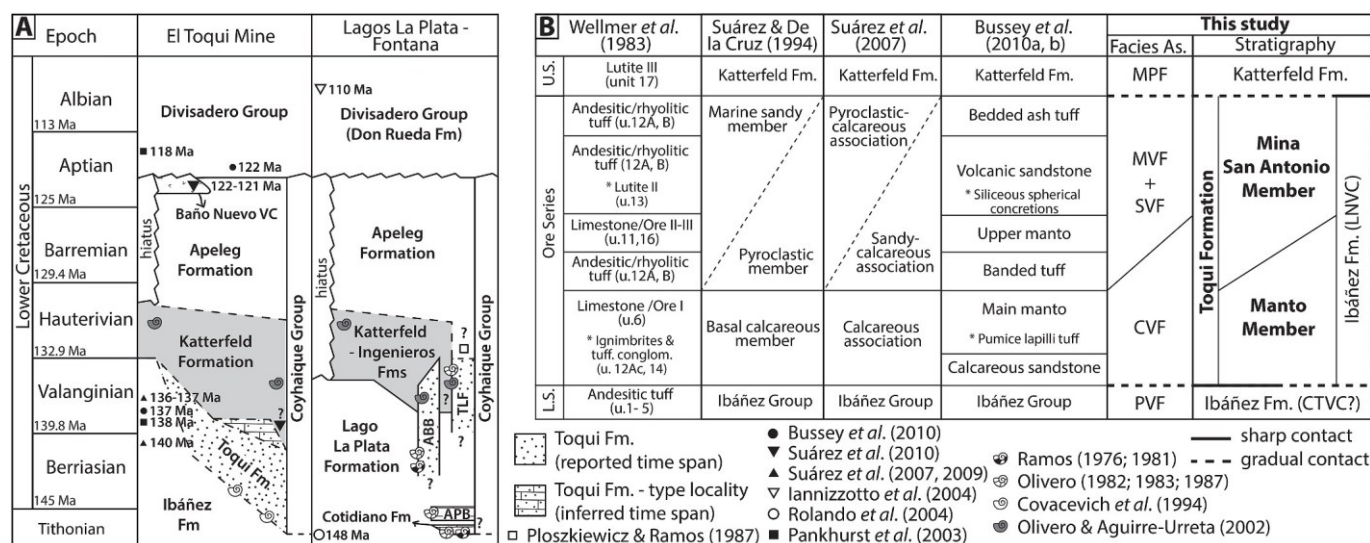


Fig. 2. (2-columns, black & white) Stratigraphy. A) Chronostratigraphic scheme for the Coyhaique Group and surrounding units at the El Toqui Mine in Chile and the Lagos La Plata-Fontana area in Argentina (based on Ramos, 1976; 1981; Masiuk and Nakayama, 1978; Olivero, 1982; 1983; 1987; Ploszkiewicz and Ramos, 1977; 1987; Covacevich et al., 1994; Olivero and Aguirre-Urreta, 2002; Pankhurst et al., 2003; Folguera and Iannizzotto, 2004; Rolando et al., 2004; Suárez et al., 2007; 2009; 2015; Bussey et al., 2010a, b). Symbols represent remarkable ages, fossils, and stratigraphic contacts mentioned in previous studies. Abbreviations: ABB = Arroyo Blanco Beds (*sensu* Olivero, 1982; Olivero and Aguirre-Urreta, 2002); APB = Arroyo Pedregoso Beds (*sensu* Ramos, 1976; 1981); TLF = Tres Lagunas Formation (Tres Lagunas Quarry); Fm = Formation; VC = Volcanic Complex. B) New stratigraphic scheme proposed for the Toqui Formation, and correlation of its facies associations with the previous models (based on Wellmer et al., 1983; Suárez et al., 2007; 2009, and Bussey et al., 2010a, b). Abbreviations: L.S. = Lower Series; U.S. = Upper Series; u. = unit (Wellmer et al., 1983); Facies As. = Facies Associations from El Toqui Mine (FA): Pebbly Volcaniclastic FA (PVF; Section 3.1); Mixed Calcareous-Volcaniclastic FA (CVF; Section 3.2); Muddy Volcaniclastic FA (MVF; Section 3.3); Sandy Volcaniclastic FA (SVF; Section 3.4); Muddy Pelagic FA (MPF; Section 3.5). Ibáñez Fm. members: Cerro Trinchera Volcanic Complex (CTVC); Lago Norte Volcanic Complex (LNVC).

units (i.e. Ibáñez Fm. (base); Katterfeld Fm. (top)) as well as their depositional environment is presented (Figs. 10 and 11). The model depicts the development and evolution of carbonate ramps in subtidal volcanic settings, affected by tectonic subsidence, differential volcanic input, inflation/deflation of volcanic edifices, and proliferation of shallow-marine epifaunal communities. The role of long-term variables, including thermal subsidence and changes in global eustasy, are also discussed. The evolutionary model proposed here for the Toqui Formation, may be helpful to better comprehend the dynamics of other ancient calcareous-volcaniclastic complexes.

1.1. Geological setting

The Toqui Fm. is known from southern Chile, between 43° and 47° South (De La Cruz et al., 1996; Welkner et al., 2004), and defined by Suárez & De La Cruz (1994) at the eponymous mining district located on the upper course of the Toqui River in the Aysén Region of Southern Chile, at about 60 km north of the regional capital of Coyhaique (45°34'S; 72°03'W; Fig. 1-B, C). There, outcrops of the formation are rare in the area and complete sections are only known from the sub-surface, i.e. bore holes and underground mining descriptions (Wellmer et al., 1983; Bussey et al., 2010b).

The Toqui Fm. is depicted as deposited during a marine transgression (e.g. Bell et al., 1996; Suárez et al., 2005; 2010a). The subsidence and following transgression were likely caused by back-arc extension, triggered by high-angle subduction along the southwestern margin of Gondwana (Suárez et al., 2010a; Nakakuki and Mura, 2013; Echaurren et al., 2017), coinciding with the Late Jurassic–Early Cretaceous break-up of this supercontinent (e.g. Riccardi, 1988; Uliana et al., 1989; Mpodozis and Ramos, 2008). Back-arc extension occurred to the east of the arc conformed by the Patagonian Batholith, which began its emplacement during the Late Jurassic (Pankhurst et al., 1999; Suárez & De La Cruz, 2001; Hervé et al., 2007; Fig. 1-B).

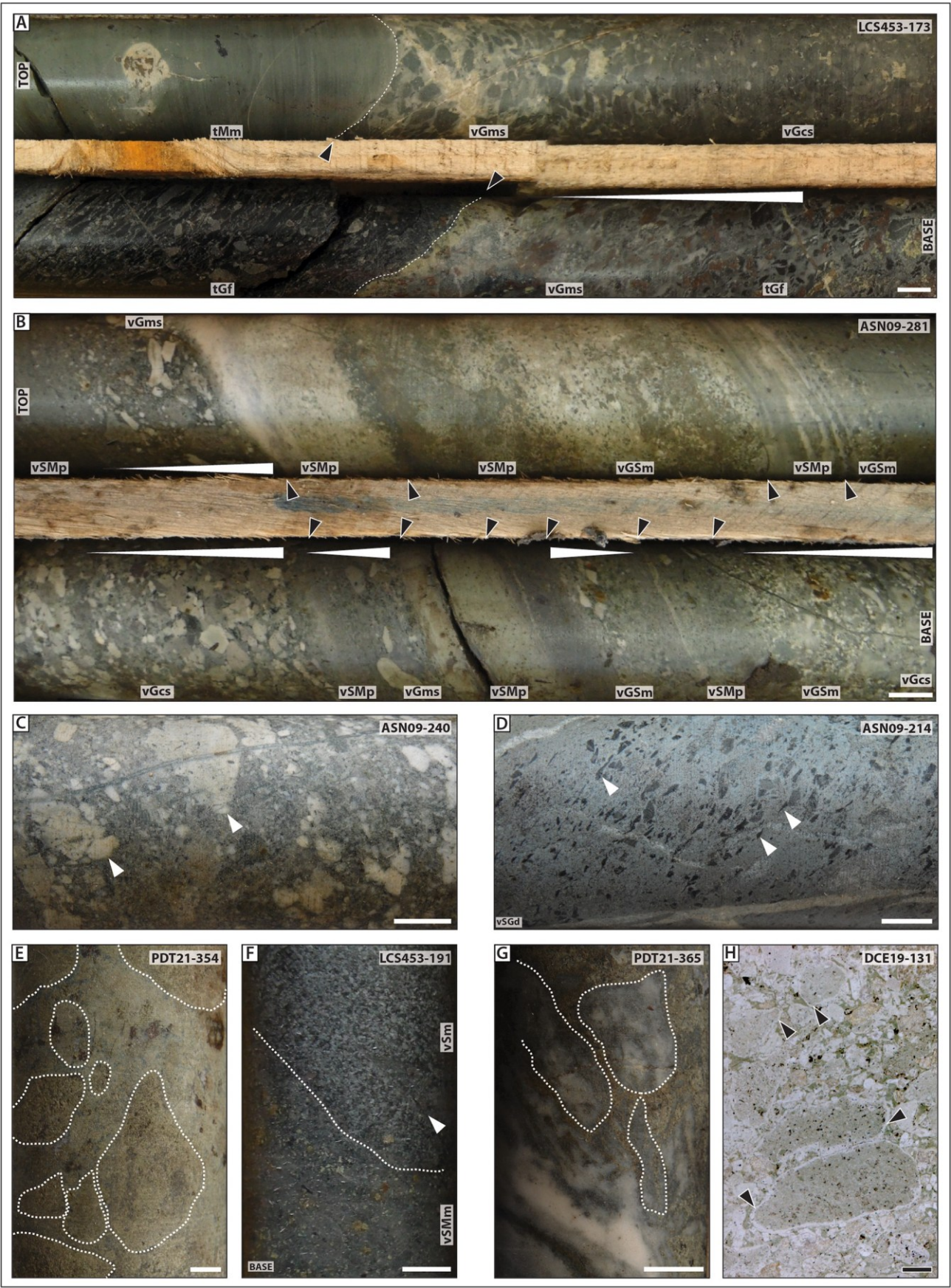
In Central Patagonia (43°–49°S), extensional tectonics resulted in a back-arc basin formed by a series of local intra-arc and retro-arc

depocenters (Folguera and Iannizzotto, 2004; Suárez et al., 2010a), known either as the Aysén Basin or the Río Mayo Embayment (Aguirre-Urreta and Ramos, 1981; Bell et al., 1996; Fig. 1-A). Its constituent sub-basins were arranged in NW- and minor NE-oriented half grabens (Fig. 1-C), considered to result from fault-reactivation of basement sutures (Ploszkiewicz and Ramos, 1977; Folguera and Iannizzotto, 2004; Iannizzotto et al., 2004). The basement is exposed as small, isolated outcrops between Lago Fontana and the areas adjacent to Aldea Apeleg (Fig. 1-B). It comprehends Paleozoic metamorphic and metasedimentary units of the Arroyo Flores Schists (Olivero, 1982; Folguera and Iannizzotto, 2004; Fig. 1-B), and the Tepuel Group (Ploszkiewicz, 1987; Ciccioli et al., 2020), as well as Early Jurassic sedimentary rocks included in the Osta Arena and Mulanguineu Formations (Ploszkiewicz, 1987; Ferrari and Bessone, 2015).

Initially, these depocenters were syn-tectonically filled by the volcanic products of the Upper Jurassic–Lower Cretaceous Ibáñez- and Lago La Plata Formations (Folguera and Iannizzotto, 2004; Suárez et al., 2009; Echaurren et al., 2016). These volcanic deposits overlie the basement with an erosional or angular unconformity (Olivero, 1982; Niemeyer et al., 1985; Ploszkiewicz, 1987; Fig. 2-A; Fig. 10). Due to an increase in subsidence causing a marine incursion, the basin was filled by a transgressive-regressive sequence of Tithonian–Aptian age (Suárez et al., 2005, 2010a), known as the Coyhaique Group (Haller and Lapido, 1980; Haller et al., 1981). Between the Tithonian–early Hauterivian, onset of the marine sedimentation of the Coyhaique Group was partly coeval to the youngest volcanism of the Ibáñez Formation (e.g. Olivero, 1987; Covacevich et al., 1994; Suárez et al., 2009; Fig. 2-A).

1.1.1. Volcanism linked to the Ibáñez Formation

The volcanic rocks of the Ibáñez Formation are identified between 43° and 49°S (Welkner et al., 2004; Fig. 1-A), though correlative units are also exposed throughout southern South America (i.e. >41°S, Pankhurst et al., 2000; Echaurren et al., 2016). Deposits include caldera-related volcanism, mostly emplaced in subaerial environments (De la Cruz et al., 1994; Folguera and Iannizzotto, 2004; Suárez et al.,



(caption on next page)

Fig. 3. (Whole page, coloured). Example of lithofacies from the Pebbly Volcaniclastic Facies Association (PVF, i.e. Ibáñez Fm.). A) Part of the LCS453 drill core at depth ca. 173 m. White dotted lines and black arrows mark the sharp bedding; white arrows indicate grading. Upper part: sharp boundary between clast-to matrix-supported, monomictic volcanic conglomerate (lithofacies vGcs-ms) and massive tuffaceous mudstone (tMm); lower part: sharp boundary between compacted volcanic breccia (tGf) and matrix-supported volcanic breccia (vGms), both with fiamme texture. B) Part of the ASN09 drill core at depth ca. 281 m. Upper part: alternation of parallel and diffuse laminated, volcanic sandstone-mudstone (vSMp), also massive sandstone-mudstone (vMSm), pebbly sandstone (vGSm), and coarse- to fine-grained conglomerate (vGms); lower part: several graded beds (normal, inverse) of volcanic conglomerate-breccia (vGms-cs), pebbly sandstone (vGSm), and minor massive or diffuse laminated sandstone-mudstone (vSMp); C) Close-up of diffuse-bedded pebbly sandstone and volcanic breccia. White arrow points to monomictic, altered volcanic clasts (vGSp); D) Monomictic, pebbly volcanic sandstone to matrix-supported breccia (lithofacies vGSm-p), some clasts display a fiamme texture. White arrows mark clasts with a shard-like shape; E) Altered, matrix-supported volcanic breccia, lithic clasts display a diffuse margin (dotted lines), similar to the matrix (vGms); F) Dotted line marks the sharp contact between massive volcanic sandstone-mudstone (vSm), sometimes pebbly, and diffuse laminated volcanic sandstone (vSMp). White arrow indicates the diffuse bedding plane; G) Parallel-bedded volcanic mudstone (vMp), its upper part has been perturbed to an “autobreccia-like” texture (clasts surrounded by dotted lines), possibly caused by diagenetical compaction (vBm); H) Thin section of volcanic pebbly litharenite (vGSm; parallel light). Its rounded volcanic clasts display an isopachous and isotropic margin (black arrows), interpreted as overcooled or “chilled”, original vitreous matrix replaced to chlorite. Possibly resedimented hyaloclastites. Scale in pictures (white) = 1 cm; black = 1 mm.

2007). They represent the Late Jurassic (Oxfordian?-Kimmeridgian) to Early Cretaceous (early Hauterivian) extrusive counterpart of the Patagonian Batholith (Pankhurst et al., 2003; Suárez et al., 2010a; 2016; Gianni et al., 2018; Fig. 1-B).

In the study area, in a 30 km radius around El Toqui Mine, the Ibáñez Formation comprises three informal members, from base to top formed by: (1) lava, pyroclastic and volcaniclastic rocks of the Cerro Trinchera Volcanic Complex (Upper Jurassic – lower Berriasian); (2) silicic domes, ignimbrite and volcanic breccia of the Lago Diunco Domes (Upper Jurassic – lower Berriasian); and (3) lava and related volcanic necks, hypabyssal bodies, pyroclastic, volcaniclastic, and minor mixed, fossiliferous calcareous-siliciclastic rocks of the Lago Norte Volcanic Complex (Upper Jurassic? – upper Valanginian-lower Hauterivian; e.g. Covacevich et al., 1994; De La Cruz et al., 1994; Suárez et al., 2007; 2009). These volcanic complexes are interpreted as produced by subaerial, coastal and local subaqueous explosions with eruption styles ranging from vulcanian to surtseyan (Suárez et al., 2007, 2009).

To the northeast, in adjacent Argentina, correlative volcanic rocks are grouped in the Lago La Plata Formation, though Suárez et al. (2009) interpreted the Catedral Formation, exposed south of the Lago La Plata (Folguera and Iannizzotto, 2004), as equivalent to the Lago Norte Volcanic Complex (Fig. 1-B). The volcanic deposits underlie and partly interlayer the marine rocks of the Coyhaique Group (e.g. Ramos, 1981; Olivero, 1987; Rolando et al., 2004; Suárez et al., 2009).

1.1.2. Marine incursion: the Coyhaique Group

The transgressive-regressive sequence conforming the Coyhaique Group comprehends three formations: the Toqui-, Katterfeld- and Apeleg Fms. (Fig. 2-A). The Toqui Formation represents the basal or transgressive unit and consists of discrete and discontinuous, calcareous, volcaniclastic and siliciclastic deposits (Suárez and De la Cruz, 1994; Suárez et al., 2007). It was deposited, during the Tithonian-Valanginian (Hauterivian? Suárez et al., 2009; 2010a), in shallow marine environments adjacent to an island arc (Skarmeta, 1976; Haller et al., 1981; Suárez et al., 2007). The Toqui Formation has been correlated with the calcareous Cotidiano Formation, and with the pebbly-sandy calcareous Tres Lagunas Formation (Ramos, 1981; De la Cruz et al., 2003; Iannizzotto et al., 2004); the latter two are exposed in areas adjacent to the La Plata-Fontana lakes in Argentina (Płoszkiewicz and Ramos, 1977; Ramos, 1981; Fig. 1-B; 2-A; Sections 1.1.4; 4.1.2).

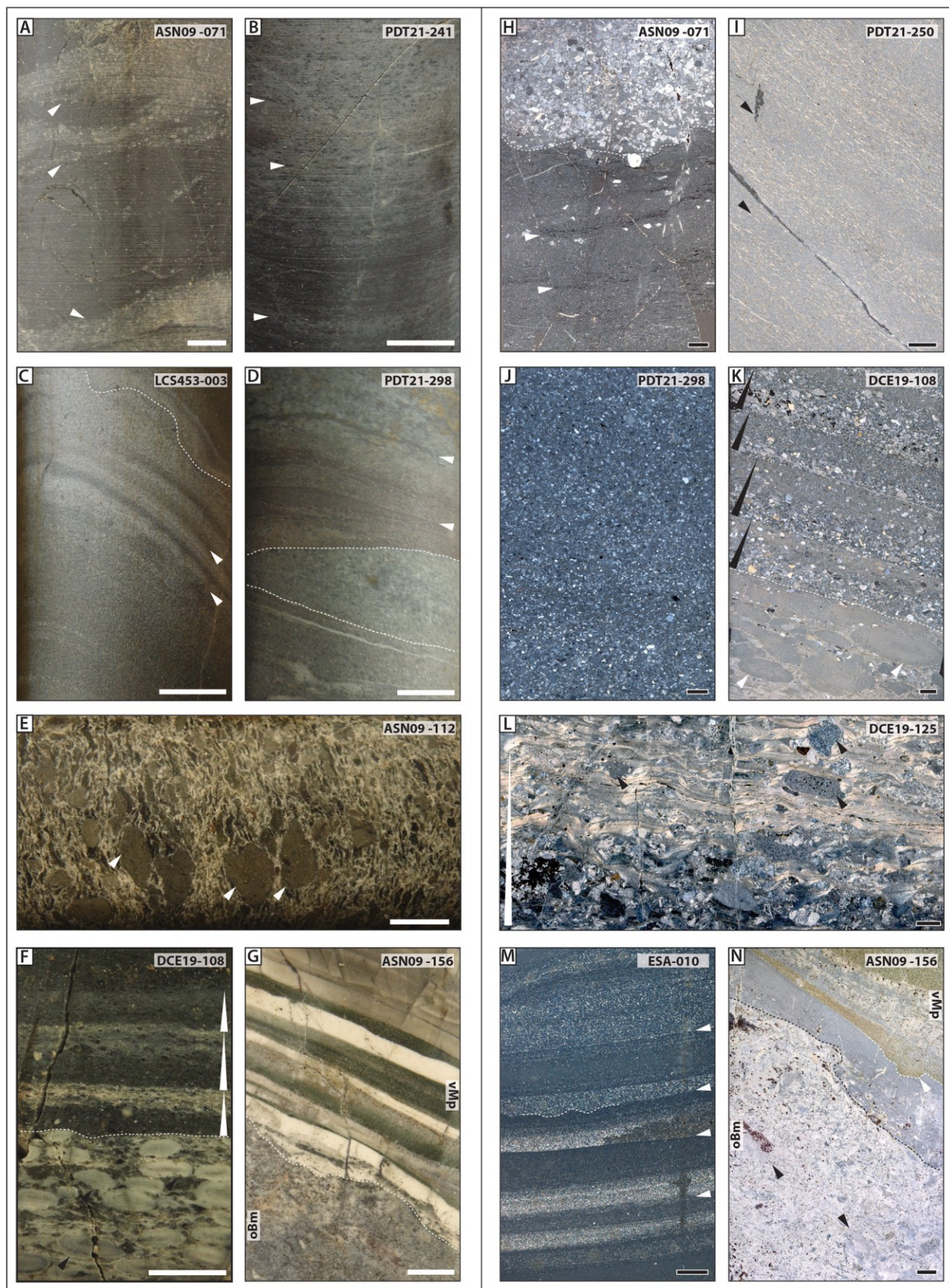
Outcrops assigned to the Toqui Formation along the Toqui River and adjacent areas are scattered and their lithology is extremely variable (e.g. Ramos, 1981; Covacevich et al., 1994; Suárez et al., 2007; 2009). Its lithology reaches up to 130 m (Table 1; Figs. 9 and 10), and includes isolated exposures of oyster-rich coquinites, mixed calcareous-volcanic sandstone, pebbly sandstone, volcanic conglomerate with calcareous matrix, fossiliferous mudstone, pyroclastic rocks and volcaniclastic sediments, some of them bearing bioclasts (Suárez et al., 1996, 2007). Other calcareous outcrops associated with volcaniclastic rocks, or underlying coherent volcanic facies, have been assigned to the Lago Norte Volcanic Complex by Suárez et al. (2007).

At the study area, near the Concordia-Toqui Rivers confluence (Fig. 1-C; 8-A, D), the Toqui Fm. conformably underlies the Katterfeld Formation (Valanginian-Hauterivian), i.e. the middle member of the Coyhaique Group (Ramos, 1981; Suárez et al., 2007). Although, the two formations may show a gradational or interlayering contact in subsurface (Bussey et al., 2010a). However, ca. 10–15 km southeast of the Toqui Mine, the Katterfeld Fm. conformably overlies volcanic rocks of the Lago Norte Volcanic Complex instead (Suárez et al., 2007). The Katterfeld Fm. consists of between 300 and 500 m of homogeneous and fissile mudstone rich in fossil bivalves and cephalopods (Ramos, 1981; Olivero and Aguirre-Urreta, 2002; Quiroz and Bruce, 2010; Fig. 8-E, F). It also displays several layers with calcareous concretions, and interbedded thin sandstone beds interpreted as turbidites (Suárez et al., 1996). The depositional environment of these sediments has been depicted as prodeltaic or corresponding to distal shelves (Ramos, 1976; Hechem et al., 1993; Suárez and De la Cruz, 1994; Bell et al., 1996).

1.1.3. Basin inversion and settling of the Apeleg Fm

The regressive stage is marked by the Apeleg Formation (Hauterivian-Aptian), the youngest unit of the Coyhaique Group, which overlies the Katterfeld Formation with a gradual contact (e.g. Skarmeta, 1976; Ramos, 1981; Bell and Suarez, 1997; Scasso, 1987; 1989; Fig. 2-A). The Apeleg Fm. has not been reported in the El Toqui Mining District; however, some ex-situ greenish, fine sandstone blocks with ichnofossils, typical of this formation, were here observed in poor exposures beside local roads at the northeastern flank of Cerro Estatuas (Fig. 1-C). In the areas adjacent to the mine, the Apeleg Fm. varies between 350 m and more than 700 m of sandy, pebbly, and heterolithic facies deposited in deltaic, intertidal and paralic environments (Ramos, 1981; Scasso, 1987, 1989; González-Bonorino and Suárez, 1995). Overall, these sedimentary systems are interpreted as prograding in a southwest direction during a regressive stage (Hechem et al., 1993; Gonzalez-Bonorino and Suárez, 1995); however, local paleocurrent dispersal reflect an irregular topography (Scasso, 1987).

The marine regression has been interpreted as caused by the onset of regional compression (Echaurren et al., 2016; Gianni et al., 2019). Compression was likely triggered by the westward displacement of the proto South American plate, caused by increased sea floor-spreading along the Mid Atlantic Ridge (Suárez et al., 2010a; Gianni et al., 2019; Ramos et al., 2019). Coeval to basin inversion, a new pulse of early Cretaceous arc-magmatism occurred along the Patagonian Batholith (Pankhurst et al., 2003). Ca. 40 km southeast of the Toqui Mine, the onset of arc reactivation is represented by a small volcanic field, formed by scattered volcanic outcrops of the lower Aptian Baño Nuevo Volcanic Complex (Ar/Ar & U–Pb 122–121 Ma, Suárez et al., 2010b). These volcanic deposits are interbedded with- and overlie shallow marine sandstone of the Apeleg Formation, and have been interpreted as ejected during a Surtseyan volcanic eruption, penecontemporaneous to the final stages of the marine sedimentation (Demant et al., 2010; Suárez et al., 2010b). Subsequently, between 43° and 47°S, the inverted marine Coyhaique Group was covered, disconformably and locally



(caption on next page)

Fig. 4. (Whole page, coloured) Lithofacies of the Muddy- and Sandy Volcaniclastic Facies Association (MVD; SVF, i.e. Mina San Antonio Member of the Toqui Fm.), and of the Muddy Pelagic FA (MPF, i.e. Katterfeld Fm.). Left side (A–G: Drill core): A) White arrows: volcanic sandstone (turbidites; lithofacies vSm; vSMg) perturbing the homogeneous dark mudstone of the Katterfeld Fm. (lithofacies Mp); B) Volcanic mudstone with diffuse and spotted lamination (lithofacies tMm; vMp). Arrows indicate bedding plane; C) Parallel laminated volcanic sandstone-mudstone with small-scale load- and scourmarks (lithofacies vSMp). Dotted line marks an erosive contact; arrows indicated bedding; D) Parallel laminated volcanic sandstone with irregular horizons interpreted as “glide planes” (sandy debrites; lithofacies vSMp); E) Oligomictic volcanic conglomerate with flammé texture (lithofacies tGf). Secondary white matrix formed by clay-minerals replacement of pumice. White arrows mark subrounded volcanic lithics; F) Contact between accretionary lapilli (black arrows) and normal-graded volcanic sandstone (lithofacies tGg-vSMg). White arrows indicate normal grading; G) Dotted line: erosive contact between oyster boundstone and fine-laminated volcanic mudstone (lithofacies oBm-vMp). Right side (H–N: Petrography): H) Dotted line: erosive basal contact of a crystal-rich turbidite (lithofacies vSm; vSMg) within the compacted hemipelagic mudstone (Mp) of the Katterfeld Fm. (Fig. 4-A); I) Compacted volcanic mudstone with diffuse parallel lamination (black arrows), original glassy composition replaced by phyllosilicates (Figs. 4-B); J) Massive to diffuse-laminated volcanic sandstone (lithofacies vSm); K) Sharp contact between accretionary lapillistone and normal-graded volcanic sandstone (lithofacies tGg-vSp; Fig. 4-F). White arrows point to accretionary lapilli; black arrows indicate normal grading; L) Foliated texture of a compacted volcanic conglomerate-breccia (tGf). Black arrows: volcanic lithics embedded in a secondary clay-rich matrix (originally pumiceous); M) Very fine laminated volcanic mudstone (“water-lain tuff”, lithofacies vMp). White arrows indicate sharp basal contacts; dotted line marks small-scale scouring; N) Black dotted line: contact between CVF (biostromes, lithofacies oBm) and MVF (volcanic mudstone, lithofacies vMp). White dotted line indicates a small-scale scourmark; black arrows point to recrystallized oyster fragments. Scale (white) = 1 cm; scale (black) = 2 mm.

conformably, by subaerial, rhyolitic to andesitic rocks of the Divisadero Group dated to the Aptian-early Cenomanian (Aguirre-Urreta and Ramos, 1981; Iannizzotto et al., 2004; Suárez et al., 2010a; Suárez et al., 2015; Fig. 2-A).

1.1.4. Age constrains of the marine transgression

Based on radiometric dating of volcanic and plutonic rocks from the El Toqui Mining District and nearby areas, the marine Coyhaique Group was deposited between the late Berriasian – early Aptian (Rolando et al., 2004; Suárez et al., 2007, 2009; Bussey et al., 2010a), although its base may reach to the Tithonian (Olivero, 1982; 1983; Covacevich et al., 1994; Fig. 2-A). At the El Toqui Mine, the Coyhaique Group disconformably underlies Aptian-Cenomanian volcanic rocks of the Divisadero Group (Suárez et al., 2007, 2015), of which the andesitic lower part was Ar/Ar-dated to 122.6 ± 0.8 Ma (Bussey et al., 2010a).

In the study area, the base of the Toqui Formation is delimited by U–Pb ages of the volcanic basement in the Lago Norte Volcanic Complex. These date to between 140.3 ± 2 and 136.1 ± 3.2 Ma (Suárez et al., 2007, 2009, 2015) and thus to the late Berriasian – early Valanginian. This scenario is supported by a U–Pb age of 137.8 ± 0.4 Ma obtained for the volcanic rocks of the Ibáñez Fm., from a drill core at the Toqui Mine (Bussey et al., 2010a). The top of the Toqui Formation is characterized by a gradual increase in mudstone, grading to the overlying Katterfeld Formation. The latter lithostratigraphic unit is Valanginian-Hauterivian in age as indicated by the presence of ammonites including *Kilianella* sp. aff. *K. superba*, *Thurmanniceras* sp., and *Favrella americana* at Cerro Katterfeld, located 30 km ENE from the mine (Olivero and Aguirre-Urreta, 2002; Fig. 1-B); though, given its gradual contact with the Toqui Fm., it may be as old as Berriasian (Suárez et al., 2010a). Therefore, the Toqui Formation, at its type locality, ranges between the uppermost late Berriasian – early Valanginian (Fig. 2-A).

Transgressive-cycle sediments bearing marine faunal elements (e.g. ammonites) of Tithonian-Berriasian age are reported from a 30 km radius in the wider vicinity of the mine (Covacevich et al., 1994; Suárez et al., 2009; Fig. 1-B; 2-A). They were originally assigned to the Ibáñez- and Lago La Plata Formations (Olivero, 1983; Covacevich et al., 1994; Suárez et al., 1996), but were re-assigned to the Toqui Formation by Suárez et al. (2007). For example, mixed sediments at the Lago Norte (Fig. 1-B), contain *Blandfordiceras* sp. (Covacevich et al., 1994; Suárez et al., 1996, 2009), thus indicating a late Tithonian age. This ammonite is also present at Estero El Gato (Fig. 1-B). The presence of *Groebiceras* sp. aff. *G. bifrons* in this locality (Covacevich et al., 1994) suggests that the section extends to the Berriasian. At Estero La Horqueta, limestone bearing *Neocosmoceras* sp. aff. *N. sayni* and *N. wichmanni* underlies mudstone of the Katterfeld Formation (Charrier and Covacevich, 1978; Covacevich et al., 1994). These ammonites represent Berriasian ages. In the Lagos La Plata-Fontana area of Argentina, the age of shallow-marine, sedimentary outcrops varies between the Tithonian-Hauterivian. For example, a late Tithonian age is inferred for the Arroyo Pedregoso Beds based on *Micracanthoceras*

ruedai, *Berriasella* sp., *Aulacosphinctes* sp., and *Subdichotomoceras* sp. (Olivero, 1987; Leanza, 1981). At the Tres Lagunas Quarry (Fig. 1-B; 2-A), calcareous rocks have a late Valanginian age based on *Chacantuceras ornatum* (Olivero, 1983; Aguirre-Urreta and Rawson, 1998); whereas the Arroyo Blanco Beds have an inferred late Valanginian- Hauterivian age based on *Paracrioceras* sp. (Olivero, 1987), and based on a Sr/Sr value of 0.707352 ± 0.000008 measured in shells of *Gryphaea* sp. (Olivero and Aguirre-Urreta, 2002).

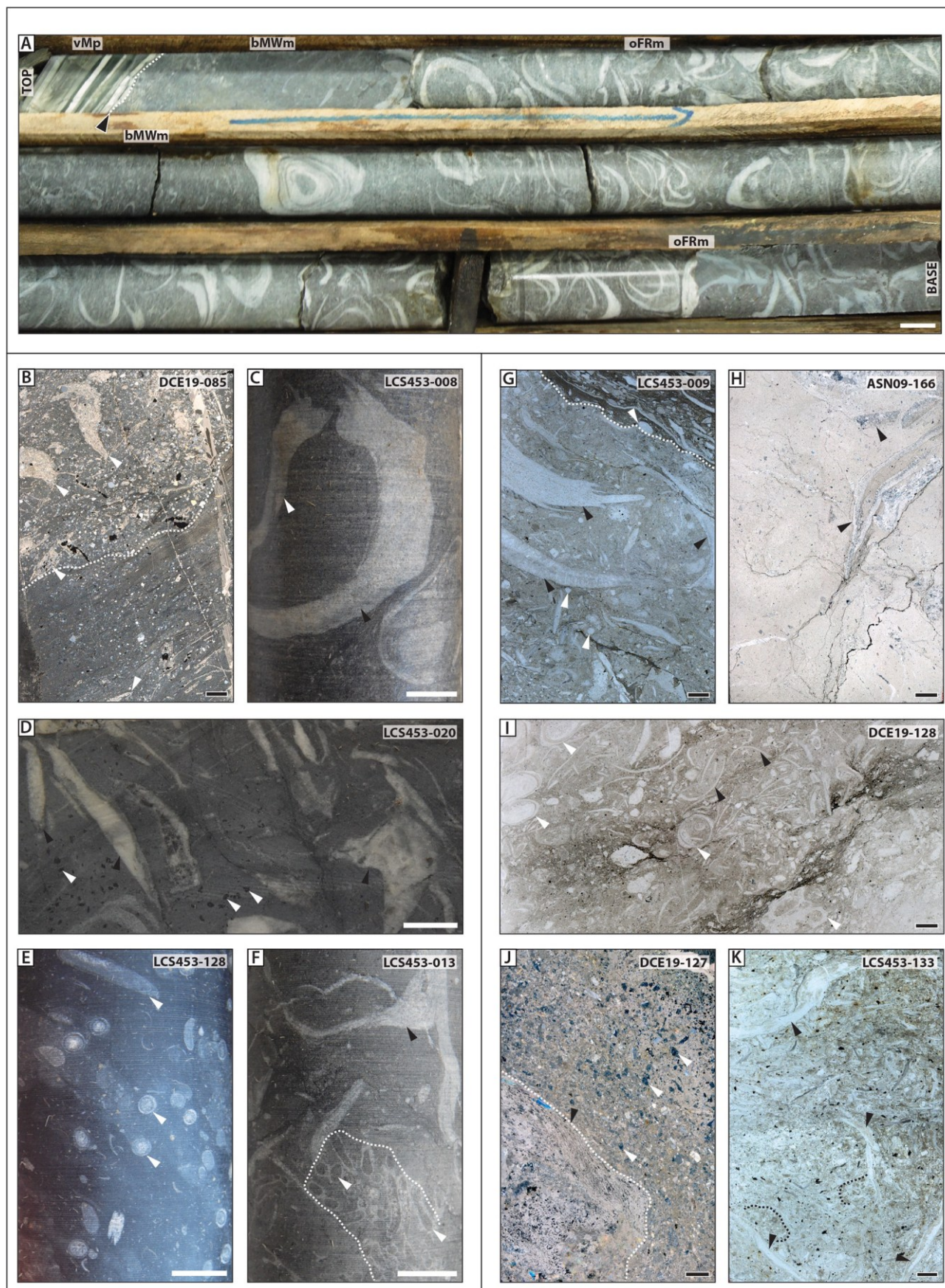
1.2. Material and methods

Description of the Toqui Fm. includes material from four drill cores (ASN09, DCE19, LCS453, PDT21; Figs. 3–6) and two outcrops (ELC, ESA; Figs. 7–8) from the El Toqui Mining District ($45^{\circ}02'S$, $71^{\circ}56'W$), between the Concordia River and Cerro San Antonio, on the southern bank of the E-W trending Toqui River (Fig. 1-C; 10). Except for core LCS453 drilled from subsurface, all cores come from a surface level; their vertical angle varies between oblique for LCS453 (-50°), and DCE19 (-70°), to almost vertical for PDT21 (-80°) and ASN09 (-90°). Their length was corrected using a vertical projection for the subsurface models (law of sines) as well as for real thickness of beds oblique to drill cores margins (Fig. 9-B). In the examples here presented, drill core photographs indicate their name and the depth in meters at which the picture was taken (e.g. PDT21-241; Figs. 3–6).

Thickness of the sections was established using a measuring tape for cores plus a Jacob's staff and Brunton compass for outcrops, with a total of 1085 m measured. Approximately 22 m of the ASN09 core have been lost (between 214.30 and 235.85 m); for this interval, the original core description was used, which is maintained by the mining company. At the time of sampling, the El Toqui Mine was owned by the Australian Laguna Gold mining company but it is now operated by the Chilean Minera Pacifico del Sur SpA (since 2019).

Field description was complemented with the petrographic analysis of 56 standard thin sections (26×46 mm, 30 μ m thick). From these, point-counting was carried out in six medium-coarse-grained sandstone samples, recording 400 grains per sample following the Gazzi-Dickinson method (Dickinson, 1970; Ingersoll et al., 1984), and using a Stepping- StageTM mounted on a Leica DMLP petrographic microscope and the software PETROG (see Supplementary Material S-1).

Stratigraphical redefinition is based on the guidelines of The North American Stratigraphic Code (2005), and chronostratigraphic categories follow the International Chronostratigraphic Chart, v2019/05 (emend. from Cohen et al., 2013). Descriptions of calcareous rocks follow the “Folk's Revised Classification of Limestones” (Wright, 1992; Flügel, 2004), and Klement (1967) and Kershaw (1994) for biostromes. Volcanic and volcaniclastic rocks were classified according to the non-genetic nomenclature of Fisher (1961; 1966), and the recommendations of Cas and Wright (1987). Grain-size classification is based on the Udden-Wentworth scale (sensu Blair and McPherson, 1999),



(caption on next page)

Fig. 5. (Whole page, coloured) Lithofacies of the Mixed Calcareous-Volcaniclastic Facies Association (CVF, i.e. Manto Member of the Toqui Fm). A: Panoramic view of a drill core, displaying the top of the CVF. Dotted line and black arrow mark the boundary between the Mixed Calcareous- and Muddy Volcaniclastic Facies Associations (CVF-MVF). Note alternation of oyster-rich- and oyster-poor beds. Left side (B: Thin section; C–F: Drill core): B) Bioclasts-bearing volcanic sandstone-mudstone (lithofacies bSWm; vSMp). Arrows indicate recrystallized oyster fragments; C) Cross-section of a two-valved, “gryph-shaped” oyster. Black arrow: thicker and concave-up left-valve; white arrow: relatively flat right valve (lithofacies bFRm, oBm); D) compacted oyster wacke-floatstone, formed by oyster-shell fragments (lithofacies bMWm, bFRm). Darker clasts are volcanic lithics (white arrows); E–F) serpulid-rich lithofacies in cross- and longitudinal-oblique section (sWFm). White arrows and dotted line: serpulid tubes; black arrow: oyster fragment. Right side (G–K: Petrography): G) Bioclastic floatstone with pack-wackestone matrix (bFRm). Dotted line marks zone with compaction diagenesis or “fitted packstone”; black arrows: oyster shells; white arrows: echinoid plates; H) Compaction diagenesis (stylolites) in an oyster-bearing wackestone (lithofacies bMWm). Black arrows: recrystallized oyster shells; I) Compacted, serpulid-rich pack-wackestone (lithofacies sWFm). White arrows mark serpulid tubes, some of them filled with cement; Black arrows: pelagic bivalves; J) oyster-bearing mixed-calcareous sandstone (bSWm). White arrows show volcanic lithics; dotted line and black arrow: partly recrystallized oyster; K) oyster boundstone with a bioclastic packstone matrix. Black arrows point to oysters; dotted lines: zones with concentration of peloids. Scale (white) = 1 cm; scale (black) = 2 mm.

sediment textural classification is from Folk et al. (1970), and bedding patterns are from Campbell (1967).

2. Lithofacies from the El Toqui Mining District

Twenty-three lithofacies have been recognized from outcrop and drill cores at the El Toqui Mining District (Table 1; Fig. 9). Based on their grain-size and composition, they were grouped in five major categories: pebbly- (Section 2.1), sandy- (Section 2.2), muddy- (Section 2.3), calcareous- (Section 2.4), and igneous lithofacies (Section 2.5). The main characteristics of these lithofacies are summarized in Table 1; a scheme of their distribution per section is shown in Fig. 9-A. These lithofacies were grouped in five facies association (Section 3).

In the following descriptions, the term “volcaniclastic” is used as a non-genetic term that comprehends “clastic volcanic material independent of their process of fragmentation, transporting agent, depositional environment, and grade of mixing with non-volcanic sediments” (Fisher, 1961; Fisher and Schmincke, 1984). If the clasts show evidence of a pyroclastic fragmentation mode, the adjective “tuffaceous” is used instead (Cas and Wright, 1987). These volcaniclastic sediments are interpreted as resedimented when there is no evidence of primary pyroclastic transport (McPhie et al., 1993; Fisher and Schmincke, 1994).

2.1. Pebbly lithofacies

These lithofacies are matrix-to clast-supported, mono-to oligomictic (2–3 dominant lithologies), and formed mostly by pebble-to cobble-sized clasts. Clasts are composed of porphyritic and minor aphanitic, coherent volcanic lithics, and altered juvenile pyroclasts interpreted as accessory. When altered, volcanic lithics are green-grey dark-coloured (chlorite, epidote, actinolite), or white-violet-pink pale tones when altered to silica, feldspar, sericite or calcite. Their matrix includes sand-sized volcanic lithics, plagioclase crystals, and volcanic mudstone usually devitrified or altered to sericite and chlorite.

Pebbly volcanic rocks were grouped in seven lithofacies (Table 1):

2.1.1. Matrix-supported volcanic breccia-conglomerate (vGms)

This lithofacies comprise mostly matrix-supported breccia and minor clast-supported conglomerate, arranged in decimeter-to meter-thick beds (Table 1). Its framework is formed by pebble-sized (diameter up to 35 mm), sub-angular to sub-rounded clasts (Fig. 3-A, B, E; 6-J). Exceptionally, one boulder-sized clast, 1.5 m in diameter, was observed at the LCS453 core. The matrix is formed by medium-to very coarse-grained volcanic sandstone and mudstone. Bed boundaries are usually sharp, or gradual to finer-grained lithofacies (vSMg, vSMp, vSm; Fig. 3-A, B, F). Internally, the lithofacies vGm is massive or it displays inverse-, normal-, and coarse-tail grading.

Interpretation: These structureless, coarse-grained lithologies are linked to dense, laminar flows and “in masse” settling (Lowe, 1982; Shanmugam, 2016). These matrix-supported deposits are interpreted as subaqueous, moderate-strength cohesive debris flow deposits or “debrites” (e.g. DM-2 debrites *sensu* Talling et al., 2012). Exceptionally, some layers displaying a clast-to matrix-supported arrangement of

volcanic lithics might represent subaqueous-settled, fallout deposits (McPhie et al., 1993).

2.1.2. Clast-supported volcanic conglomerate (vGcs)

This lithofacies is formed by clast-supported volcanic conglomerate and minor breccia, arranged in centimeter-to decimeter-thick beds (Table 1). It is internally massive, normal- or inverse-normal graded (Fig. 3-A, B; 6-R; 7-H). Except for its packed fabric and its sub-angular to rounded volcanic clasts, this lithofacies displays a composition analog to the matrix-supported vGms lithofacies.

Interpretation: These clast-supported beds are interpreted as density-modified grain-flow deposits (Lowe, 1982; Cas and Wright, 1987; McPhie et al., 1993).

2.1.3. Tuffaceous conglomerate-breccia with fiamme texture (tGf)

The lithofacies tGf is formed by clast- and minor matrix-supported volcanic breccia with fiamme texture, arranged in decimeter-thick beds (Table 1). Its framework includes pebble-cobble-sized, regular-to well-sorted, angular to sub-rounded volcanic clasts. Volcanic lithics are embedded in a secondary tuffaceous matrix, formed by diagenetically flattened pumice and minor volcanic sandstone (Fig. 3-A; 6-F, N). In most samples, pumice has been totally altered to phyllosilicates (Fig. 4-E, L). Internally, these rocks display a relict sub-parallel layering (pressure-solution seams); their beds are sharp-bounded, or grade to matrix-supported, massive breccia (vGm; Fig. 3-A).

Interpretation: This lithofacies has been interpreted as subaqueous-settled, fallout deposits with lapilli-sized clasts, affected by diagenetical compaction (Bull and McPhie, 2007; Bussey et al., 2010b). However, matrix-supported beds may reflect diagenetically compacted, eruption-fed debrites (vGm).

2.1.4. Graded, monomictic tuffaceous conglomerate (tGg)

This lithofacies is composed of a centimeter-thick bed normal-graded, tuffaceous conglomerate with monomictic pebble-sized clasts, embedded in a tuffaceous sandy mudstone matrix (Table 1). Clasts are oblate-spheroid in shape, well rounded and compacted, and internally massive or concentric, some nucleated over isolated plagioclase crystals (Fig. 4-F, K; 6-P). Bed boundaries are sharp. This lithofacies was only observed as a singular layer in subsurface (DCE19, PDT21 cores; Fig. 9-A), but it has also been reported from the ESA outcrop (Suárez & De La Cruz, 1994). This bed is recognized as a guide-horizon in the El Toqui Mining District, and referred to as “siliceous spherical concretions layer” (Bussey et al., 2010a).

Interpretation: Lithofacies tGg is interpreted as a subaqueous-settled, accretionary lapilli bed. It depicts the products of subaerial or shallow-water phreatomagmatic volcanism (Fisher and Schmincke, 1984; Boulter, 1987). Though rare, its formation has also been reported for subaqueous explosive volcanism (White, 2000).

2.1.5. Parallel-bedded, volcanic sandy breccia to pebbly sandstone (vGSp)

This lithofacies comprise an alternation of matrix-supported, pebbly volcanic sandstone to sandy breccia, arranged in decimeter-thick beds with crude parallel-bedding (Table 1). Gravel clasts are pale-coloured,

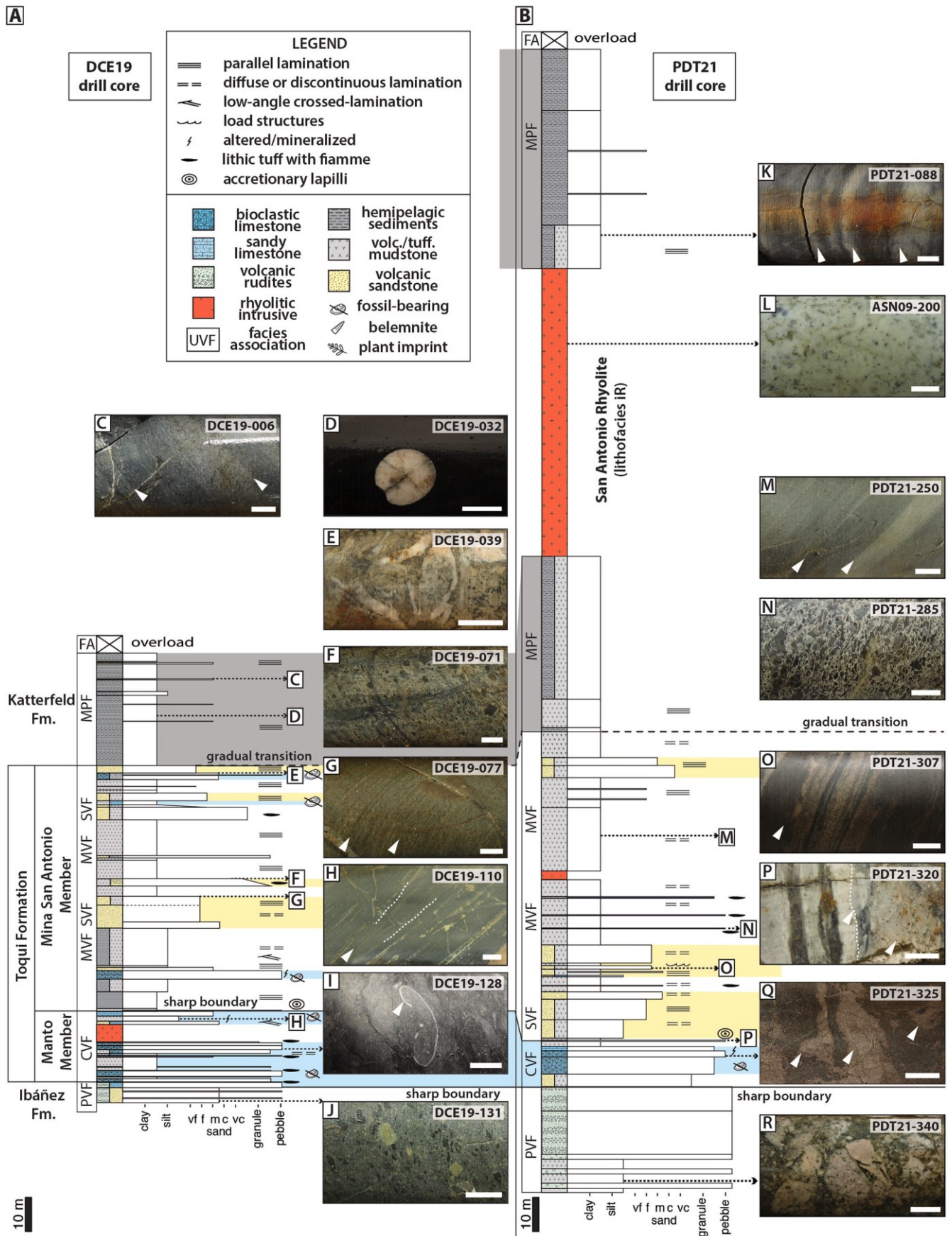


Fig. 6. (Whole page, coloured) Stratigraphic log of the longest and most complete drill cores studied here, DCE19 (Fig. 6-A) and PDT21 (Fig. 6-B; for location, see Fig. 1-C; 10). Pictures and lithofacies: C) Diffuse-bedded volcanic mudstone-sandstone of the Muddy Volcaniclastic Facies Association (MVF: lithofacies vMp; Table 1). White arrows mark bedding planes; D) Belemnite rostrum (cross-section) in black mudstone of the Muddy Pelagic Facies Association (MPF: lithofacies Mp); E) Altered biostromal limestone of the Mixed Calcareous-Volcaniclastic Facies Association (CVF: lithofacies bFRm; bSWm); F) Coarse-tail graded, tuffaceous conglomerate-breccia with fiamme texture (MVF: lithofacies tGf); G) Very-fine parallel laminated volcanic sandstone-mudstone (SVF: lithofacies vSMp). White arrows mark bedding planes; H) Low-angle cross-laminated sandstone, interpreted as “swaley” type (SVF: lithofacies vSMx). Arrow indicates intersection; dotted lines mark bedding planes; I) Compacted bioclastic wacke-floatstone with nodular fabric. Arrow point to a bivalve? cross section (CVF: lithofacies bMWm); J) Matrix-supported, oligomictic, altered volcanic conglomerate of the Pebbly Volcaniclastic Facies Association (PVF: lithofacies vGSm); K) Alternation of parallel-laminated (white arrows), volcanic (grey) and hemipelagic (black) mudstone (MVF-MPF boundary: lithofacies vMp-Mp); L) Lithofacies iR: rhyolitic intrusive (“San Antonio Rhyolite” *sensu* Bussey et al., 2010a); M) Alternation of parallel-laminated volcanic sandstone-mudstone (SVF: lithofacies vSMp). Arrows mark sharp bedding planes; N) Tuffaceous conglomerate-breccia with fiamme texture, secondary matrix of pumice altered to clay-minerals (MVF: lithofacies tGf); O) White arrow: alternation of parallel-laminated volcanic sandstone-mudstone with flame structures (SVF: lithofacies vSMp); P) Sharp contact between accretionary lapilli (right) and parallel-bedded volcanic sandstone-mudstone (SVF: lithofacies tGg, vSMg; dotted line). Arrows: compacted accretionary lapilli; Q) Bioclastic float-rudstone with oyster shells replaced by pyrrhotite (CVF: lithofacies bFRm; white arrows); R: Clast-supported, oligomictic volcanic breccia, matrix altered to chlorite-epidote (PVF: lithofacies vGcs). White scale in pictures = 1 cm. Legend also applies for the following figures (Figs. 7–8).

bad-sorted and sub-rounded. In volcanic breccia, clasts are pebble-sized (diameter up to 20 mm), whereas granule-to pebble-sized in sandstone. Sandstone is medium to very coarse-grained and poor-to regular-sorted. The framework arrangement is massive or normal-graded (Fig. 3-C).

Interpretation: Gravel-rich beds of lithofacies vGSm are interpreted as minor, moderate -strength cohesive debrites (DM-2 debrite *sensu* Talling et al., 2012). On the other hand, pebbly sandstone of this lithofacies is similar to the “Facies C” of Kataoka and Nakajo (2004), interpreted as “hyperconcentrated flow deposits”, and reclassified as sandy debrites by Shanmugam (1996, 2016). Therefore, lithofacies vGSp represents an alternation of sandy- and moderate-strength cohesive debrites.

2.1.6. Massive, volcanic sandy breccia to pebbly sandstone (vGSm)

The lithofacies vGSm is analog to the previous vGSp (parallel-bedded), but it lacks bedding. Volcanic clasts are angular-to rounded, and dark green-to dark-grey-coloured (Fig. 6-J). The petrographic analysis of a granule-sized pebbly sandstone assigned to this lithofacies, has shown abundant non-vesicular, ragged to sub-rounded clasts displaying isotropic and devitrified thin margins, interpreted as “chilled” (Fig. 3-H).

Interpretation: This matrix-supported lithofacies is interpreted as density flow deposits, varying from moderate-strength cohesive debrites (DM-2 debrites *sensu* Talling et al., 2012) to low-strength cohesive debrites (DM-1 debrites, *op. cit.*). In particular, some of these monomictic, lithic-rich debrites suggest deposition as resedimented hyaloclastites (McPhie et al., 1993; Schmidt and Schmincke, 2002).

2.1.7. Massive, monomictic volcanic pseudobreccia (vBm)

This lithofacies comprises discrete and local areas with clast-supported, monomictic volcanic breccia. Breccia clasts are pebble-sized and display sharp or diffuse margins (Table 1). When sharp, clasts are angular and preserve the internal bedding of the original rock (bedded volcanic mudstone, lithofacies vSMp) resembling an “auto-breccia” texture (Fig. 3-G). On the other hand, clasts with diffuse margins mix up with the original volcanic matrix.

Interpretation: These local pseudobreccia zones are interpreted as post-sedimentary and formed during compaction-diagenesis (McPhie et al., 1993). Alternatively, horizons with sharp clasts may reflect “brecciated horizons” from small-scale slump deposits (Shanmugam, 2016).

2.2. Sandy lithofacies

Volcanic sandstone is regular-to well-sorted, clast-to matrix-supported (“greywacke”), and very fine to medium-grained, minor pebbly. Its composition varies between lithic arkose and feldspathic litharenite (Fig. 3-F, H; 4). The original isotropic matrix has been devitrified, or altered to sericite or chlorite (Fig. 3-H). In some samples, matrix composition is similar to that of clasts, making distinction difficult.

The sandstone framework is dominated by non-vesicular volcanic

lithic clasts, euhedral to subhedral plagioclase crystals, and rare reworked pumice shards. Volcanic lithics are mono-oligomictic, poorly sorted, and sub-rounded to sub-angular. They are composed of SiO₂- poor, brown clasts with porphyritic, trachytic, vitrophyric or pilotaxitic texture, commonly devitrified, or altered to chlorite or iron oxides (Fig. 3-H, 4-H, J, K). SiO₂-rich glassy clasts are scarce and devitrified with a felsitic texture. Feldspars are dominated by plagioclase phenocrysts, with minor alkali feldspar (orthoclase, sanidine). Feldspar crystals appear fresh and twinned, within vitrophyric/porphyritic lithics or as singular fragments in the framework (Fig. 4-H, J). When altered, they are commonly replaced by actinolite-epidote, sericite, or calcite. Volcanic quartz is a minor component, observed as angular to rounded, fractured or margin-resorbed crystals (7–19%; see Supplementary Material). Six sandy lithofacies have been defined at the El Toqui Mine (Table 1):

2.2.1. Massive volcanic sandstone (vSm)

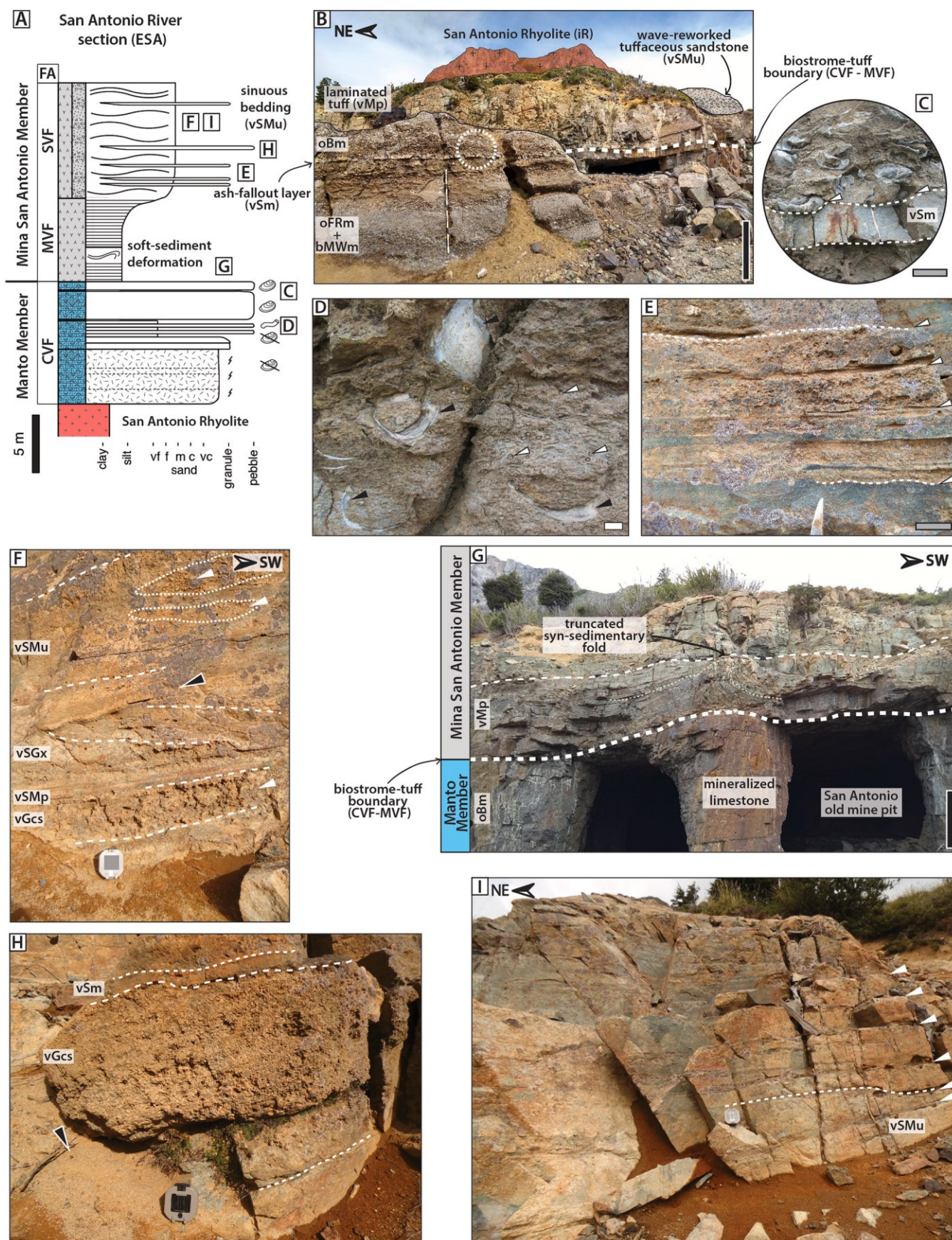
This lithofacies is composed of massive volcanic sandstone, sometimes muddy, arranged in decimeter-to meter-thick beds. Sandstone is well-sorted, fine-to medium-grained, exceptionally very coarse-grained. In thin section, it appears massive or displays a slight diffuse parallel lamination (Fig. 3-F; 4-J). Bed boundaries are sharp or it grades normally to massive, muddy-rich lithofacies (lithofacies tMm).

Interpretation: Massive sandstone has been typically classified as the Ta interval of the Bouma sequence for “high-density turbidites” (Lowe, 1982; Talling et al., 2012). However, the “Bouma sequence” model has been called into question by Shanmugam (1996, 2012, 2016), who considers this lithofacies as sandy debrites.

2.2.2. Cross-bedded, volcanic pebbly sandstone to conglomerate (vSGx)

Lithofacies formed by sigmoidal- and trough-cross-bedded, medium to very coarse-grained volcanic sandstone and sandy conglomerate (Fig. 8-C). Gravel clasts are granule-to pebble-sized. These lithologies are regular to well-sorted, arranged in thin-medium thick layers (<30 cm). Bedsets have sharp margins, with an inclined to slightly concave-up lower contact. At the ESA outcrop, bedding is truncated by a sharp boundary interpreted as a reactivation surface (Fig. 7-F).

Interpretation: This cross-bedded lithofacies depicts a bed load tractional transport through the movement of megaripples (Cas and Wright, 1987; Collinson et al., 2006). Given their sharp and erosive basal surfaces (scour-and-fill structures), these deposits are interpreted as the fill of shallow, deltaic distributary channels. At the ESA outcrop, these lithofacies are laterally correlative with undulated sandstone-mudstone (vSMu; Fig. 7-I), and with isolated lenses of clast-supported volcanic conglomerate (vGm; Fig. 7-H). Its reactivation surfaces reflect erosion and migration of megaripples in a lower shoreface sub-environment (Collinson et al., 2006).



(caption on next page)

Fig. 7. (Whole page, coloured). A) Stratigraphic log from the San Antonio (ex-mine pit) outcrop (ESA), displaying the sharp contact between both members of the Toqui Fm. (Fig. 2-B; 6-A, B, 9). B) General view of the outcrop showing calcareous tempestites and biostromal limestone (CVF: lithofacies bFRm + bMWm; oBm, respectively) in the foreground, underlying bedded tuffaceous rocks in the background (MVF); C) Close-up of the circle in B), displaying “gryph-shaped” oysters in life position over a grey-coloured dense tuff (lithofacies vSm). D) Detailed view of oyster autoparabiostrome. Black arrows: remobilized oyster shells; white arrows: isolated and colonial serpulid tubes (CVF: lithofacies bFRm; sWFm); E) parallel and wavy laminated, alternation of volcanic sandstone-mudstone and conglomerates (SVF: lithofacies vSMu; vGcs). White arrows: bedding planes; dotted lines: rippled surfaces. F) Cross- and parallel-bedded, pebbly and sandy volcanic lithofacies interpreted as the fill of shallow channels (SVF). Dashed lines: bedding planes; dotted lines & white arrows: pebbly lenses; black arrow: reactivation surface; G) Synsedimentary fold deforming the volcanic sandstone-mudstone succession of the Muddy Volcaniclastic Facies Association (MVF), directly over the contact between biostromal limestone of the CVF (Manto Member) and tuffaceous mudstone of the MVF (San Antonio Member); H) Volcanic conglomerate interpreted as a subaqueous debris flow (SVF: vGcs); black arrow shows basal inverse-grading; white arrow marks sharp boundary with the late and diluted sand sedimentation (lithofacies vSm); I) Undulating bedding of the SVF, interpreted as wave- and storm-reworked volcaniclastic deposits. Arrows indicate bed contacts. Scale in photos = 1 m (black); 1 cm (white); 5 cm (grey); hammer length = 33 cm; Brunton compass diameter ca. 10 cm.

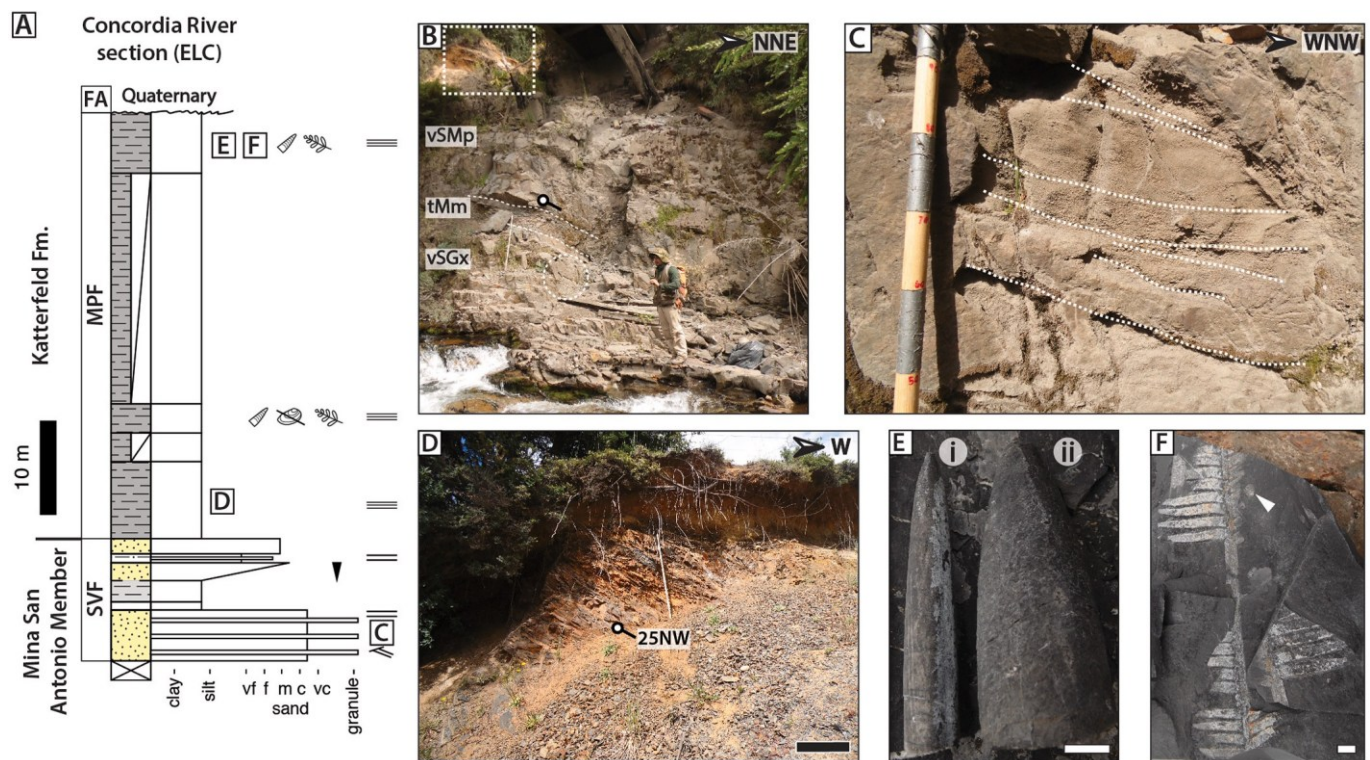


Fig. 8. (2-columns, coloured) A) Stratigraphic log from the Concordia River outcrop (ELC), displaying the contact between the San Antonio Member of the Toqui Fm. and the Katterfeld Fm. B) General view of the outcrop showing the inclined beds of sandy and muddy volcanic lithofacies (UVF); C) Close-up of the white circle in B), showing the low-angle tabular and trough cross-bedding (UVF: lithofacies vSGx). Divisions in Jacob's Staff = 10 cm; D) Close-up of the white square in B), displaying the dipped beds of the black mudstone of the Katterfeld Fm., conformable with the underlying volcaniclastic rocks. Reddish colour is caused by weathering and soil formation; E-F) Fossils from the lithofacies Mp-Mm (Katterfeld Fm.): E) Fragmented belemnite rostra, i) *Belemnopsis* sp.; ii) *Acroteuthis*? sp.; F) Fossil imprint of *Ptilophyllum* sp.

2.2.3. Undulated or rippled-bedded, volcanic sandstone-mudstone (vSMu)

The lithofacies vSMu comprise the alternation of volcanic sandy mudstone-muddy sandstone and clast-supported volcanic conglomerate (lithofacies vGc), with an undulated or rippled upper-surface (Fig. 7-E, I). Muddy-rich beds are centimeter to decimeter-thick, whereas pebbly beds are centimeter thick. Conglomerate is formed by granule to pebble-sized lithic and pumice clasts, arranged in massive or normally-graded beds (Fig. 7-E); sandstone is very fine-grained, well sorted, and mudstone is massive.

Interpretation: These deposits are interpreted as subtidal, re-sedimented volcaniclastic deposits (McPhie et al., 1993). Its undulated bedding is linked to wave- and storm-reworking, settled over the storm wave base, in a lower shoreface sub-environment (Reading, 1996; Collinson et al., 1996). In addition, the intercalation of pebbly lithofacies is depicted as deposits from sporadic grain flows.

2.2.4. Parallel bedded, volcanic sandstone to mudstone (vSMp)

This lithofacies comprehends bedded volcanic sandstone and

mudstone as well as their alternation, arranged in centimeter-to decimeter-thick bedsets. Sandstone is very fine-to medium-grained and well-sorted (Fig. 6-C, G, M, O). Both lithologies are internally massive or diffuse-finely laminated. Layers are arranged in parallel laminae and beds (thicker than 1 cm) with sharp or diffuse contacts, some of them displaying basal scourmarks (Fig. 4-C, D). Parallel lamination is sometimes perturbed by load, evident from flame-marks and convolute bedding (Fig. 6-O).

Interpretation: From its loadmarks and convolute lamination, this lithofacies depict a fast settling in a subaqueous environment. These beds are similar to the “LSS subfacies” of Bull and Cas (1991), and are here interpreted as amalgamated eruption-fed turbidites (Bouma T_{B-1} and T_{B-2} intervals *sensu* Talling et al., 2012). Some laminae sets display a wedge-shaped, irregular basal surface interpreted as a “glide plane” that may reflect minor slumping (Shanmugam, 1996, 2012, Fig. 4-D).

2.2.5. Cross-laminated, volcanic sandstone - mudstone (vSMx)

The lithofacies vSMx comprise an alternation of very fine-grained

Table 1

(Whole page, black & white) Summary of Facies Associations and their corresponding lithofacies, based on the previous descriptions. Abbreviations: 1) Code-prefix: b: bioclastic, i: intrusive; o: oyster-bearing; t: tuffaceous; v: volcanoclastic. 2) Code-lithology: (Calcareous) B: biostrome; cM: calcimudstone; F: floatstone; P: packstone; R: rudstone; W: wackestone. (Siliciclastic) G: pebbly (breccia-conglomerate); M: fine-grained (clay-silt, ash); S: sandstone. (Igneous) R: rhyolite 3) Code-suffix: cs: clast-supported; g: graded; m: massive; ms: matrix-supported; p: parallel laminated/bedded; u: undulated/rippled laminated; x: cross-laminated/bedded. 4) Grain Size (sand): VF: very fine; F: fine; M: medium; C: coarse; VC: very coarse. 5) Matrix: Calc: calcareous; Silic: siliciclastic; Tuff: tuffaceous; Volc: volcanic. 6) Fossil content: Amm: ammonite; Bel: belemnite; Bvv: bivalve; Micr: microfossils; Oys: oyster; Pla: plant imprint; Srp: serpulid. vi) Abundance: x >> y (high abundance of x, scarce y); x, y (same relative abundance of x and y); > y (y in traces). 7) Bedding (thickness): cm: centimeter; dm: decimeter; m: meter; dam: decameter.

Category	Lithofacies	Lithology	Type	Grain-size	Matrix size	Structures/ Observations	Fossils	Bedding	Interpretation
Igneous	iR	Rhyolitic intrusive	Hypabyssal	Medium-grained	Aphanitic	Porphyritic texture; quartz phenocrysts	–	m - dam	Subvolcanic intrusive (sill)
Calcareous Lithofacies	bGSg	Bioclasts-bearing, matrix supported, volcanic breccia	Mixed	Granule -pebble	Volc. Mud	Massive, coarse-tail normal grading	Oyst?	cm - dm	Wellmer et al. (1983) Bioclastic-bearing, cohesive debrites (Carbonate platform edge; slope?)
	bSWm	Calcareous volcanic sandstone - sandy wackestone	Mixed	M-C sand - pebble	W-P; cM; volcanic mud	Massive, solution seams (nodular)	Oys > Ech	cm - dm	Storm-reworked mixed shoals; mixed sandy debrites
	bMWm	Bioclastic calcimudstone to wackestone	Calcareous	Granule - pebble	cM	Massive, solution seams	Bvv; Ser; Ech	cm - dm	Pelagic carbonate mud (outer ramp - platform edge)
	sWFm	Serpulid-rich wackestone - floatstone		Granule	W - cM	Massive, tubes are bed-conformable	Ser >> Oys > Bvv; Ech	cm - dm	Bioturbated, pelagic carbonate mud (outer-ramp - platform edge)
	bFRm	Bioclastic floatstone-rudstone		Granule - cobble	W-P; cM	Massive, solution seams	Oys > Bvv; Ech; Ser	dm - m	Carbonate shoals (bioclastic tempestites) (carbonate mid-ramp)
	oBm	Oyster boundstone		Cobble	W-F; cM	Massive; concave-up & two-valved shells (life position)	Oys > Bvv, Ech >> Ser	dm - m	"Gryphaeid" oysters autobiostrume (carbonate mid-ramp/platform edge reef)
Muddy Lithofacies	Mp	Fossil-bearing, black, carbonaceous silty claystone	Siliciclastic	Silt - F sand	Silic. Mud	Parallel- and wavy lamination	Amm; Bel; Bvv; Micr; Pla	mm	(Hemi) pelagites (outer-shelf; offshore environment)
	vMp	Sharp-laminated, tuffaceous mudstone	Volcaniclastic	Silt - VF sand	Volc. Mud	Parallel lamination (sharp)	–	mm	Eruption-fed, ash turbidites, hemipelagites
	tMm	Massive to diffuse-laminated, tuffaceous mudstone		Silt - F sand	Tuff. Mud	Massive, parallel lamination (diffuse)	–	mm	Densite mud (<i>sensu</i> Talling et al., 2012), tuffaceous hemipelagites
Category	Lithofacies	Lithology	Type	Grain-size	Matrix size	Structures/ Observations	Fossils	Bedding	Interpretation
Sandy Lithofacies	vSMg	Graded volcanic sandstone - mudstone	Volcaniclastic	Pebble - F sand	Volc. Mud	Normal grading	–	mm - cm	Subaqueous-settled fallout deposits
	vSMx	Cross-laminated, volcanic sandstone - mudstone		VF sand	Volc. Mud	Low-angle cross-lamination (hummocky-swaley)	–	mm - cm	Storm-reworked, volcanoclastic deposits (lower shoreface subenvironment)
	vSMp	Parallel-bedded, volcanic sandstone to mudstone		VF-M sand	Volc. Mud	Parallel bedding/lamination (sharp, diffuse, contorted)	–	mm - cm	Amalgamated, eruption-fed turbidites (T _B interval <i>sensu</i> Talling et al., 2012); sandy debrites (<i>sensu</i> Shanmugam, 1996)
	vSMu	Undulated or rippled-bedded, volcanic sandstone-mudstone		VF-F sand	Volc. Mud	Undulated bedding, rippled upper surfaces	–	cm - dm	Storm-reworked, volcanoclastic deposits (lower shoreface subenvironment)
	vSGx	Cross-bedded, volcanic pebbly sandstone to conglomerate		Granule-pebble	Volc. M-VC sand, mud	Sigmoidal-, trough cross-bedding	–	cm - dm	Storm-reworked, distributary channel-fill (lower shoreface subenvironment)
	vSm	Massive volcanic (muddy) sandstone		F-M sand	Volc. Mud	Massive	–	cm - m	Sandy debrites (<i>sensu</i> Shanmugam, 1996)
	vGSm						–	cm - dm	

(continued on next page)

Category	Lithofacies	Lithology	Type	Grain-size	Matrix size	Structures/ Observations	Fossils	Bedding	Interpretation
Pebbly Lithofacies		Massive volcanic sandy breccia to pebbly sandstone		Granule - pebble	Volc. M-VC sand, mud	Massive, grading, clasts with "chilled margins"			Subaqueous, moderate-strength cohesive debrites; resedimented hyaloclastites
	vGSp	Parallel-bedded, volcanic sandy breccia to pebbly sandstone	Volcaniclastic	Granule-pebble	Volc. M-VC sand	Parallel bedding (sharp, diffuse), grading	-	cm - dm	Subaqueous, moderate-strength cohesive debrites; sandy debrites
	tGg	Graded, monomictic tuffaceous conglomerate		Pebble	Tuff. Mud	Normal grading, massive or concentric-layered clasts	-	cm	Subaqueous-settled fallout deposits; submarine eruption? (accretionary lapilli bed)
	tGf	Tuffaceous conglomerate-breccia with fiamme texture		Pebble	Pumice altered to phyllosilicates	Massive, normal-graded, sub-parallel bedding, pressure solution seams	-	cm - dm	Subaqueous-settled fallout deposits, minor debrites (diagenetically compacted)
	vGcs	Clast-supported volcanic conglomerate		Pebble	Volc. M-VC sand, mud	Massive, grading (normal, inverse-normal)	-	cm - m	Subaqueous, density-modified grain-flow deposits
	vGms	Matrix-supported volcanic breccia-conglomerate		Pebble - cobble	Volc. M-VC sand, mud	Massive, grading (inverse, normal, coarse-tail)	-	cm - m	Subaqueous, moderate-strength cohesive debrites
	vBm	Massive, monomictic volcanic pseudobreccia		Pebble - cobble	Volc. Mud? (altered)	Massive	-	cm - dm	Pseudobreccia (diagenetically compacted); slump deposits?

volcanic sandstone and tuffaceous silty mudstone with low-angle tabular cross-lamination ($<10^\circ$). Laminae pinch-out or display a differential thickness (thicker to the flatter area), and are interpreted as hummocky-swaley cross-lamination (Fig. 6-H).

Interpretation: This lithofacies is depicted as settled in a subtidal environment, over the storm wave base, in a lower shoreface sub-environment (Collinson et al., 2006; Dumas and Arnott, 2006).

2.2.6. Graded volcanic sandstone - mudstone (vSMg)

Lithofacies vSMg is formed by pebbly to medium-grained volcanic sandstone, grading to sandy volcanic mudstone, arranged in millimeter-to centimeter-thick, parallel-laminated laminae/beds (Fig. 4-F, K). Bed boundaries are sharp, or load-perturbed by the coarser clasts of the overlying bed. The gravel component in pebbly sandstones is monomictic.

Interpretation: This lithofacies is interpreted as formed by subaqueous-settled, ash-to lapilli-sized, fallout deposits (Fisher & Schmincke, 1984, 1994).

2.3. Muddy lithofacies

Mudstone includes tuffaceous claystone and silty/sandy claystone. It is massive, sharp-, or diffuse laminated. Sharp lamination is planar or basal-scoured, as evident from differences in colour, alteration or composition (Fig. 4-G, M); when diffuse, laminae are marked by subtle changes in colour, or by a secondary spotted/mottled fabric from parallel-aligned darker spots or opaques (Fig. 3-A; 5-B; 6-C, K). In thin sections, mudstone appears isotropic and devitrified, or replaced by sericite (Fig. 4-I, N). Some muddy lithofacies, located in the areas adjacent to rhyolite intrusive (lithofacies iR), are hardened and silicified reflecting incipient hornfels.

2.3.1. Massive to diffuse laminated, tuffaceous mudstone (tMm)

This lithofacies is formed by tuffaceous mudstone and minor fine-grained volcanic sandstone (Fig. 3-A). When diffuse bedded, layers are millimeter to centimeter-thick (Fig. 4-B, I). Its bed/laminae boundaries are gradual, usually grading from sharper-laminated lithofacies vSMp,

or interbedding with siliciclastic mudstone (Mp).

Interpretation: These rocks are interpreted as formed by clay- and silt-rich density flow deposits ("dense mud" *sensu* Talling et al., 2012). In particular, this lithofacies is depicted as a mixture between "Massive ungraded mud" ("T_{E-3} interval" *sensu* Talling et al., 2012), and "Laminated mud" ("T_{E-1} interval", *op. cit.*). Alternatively, massive mud might also be explained as formed by the settling of very fine ash as tuffaceous hemipelagites (Shanmugam, 2016).

2.3.2. Sharp parallel-laminated, tuffaceous mudstone (vMp)

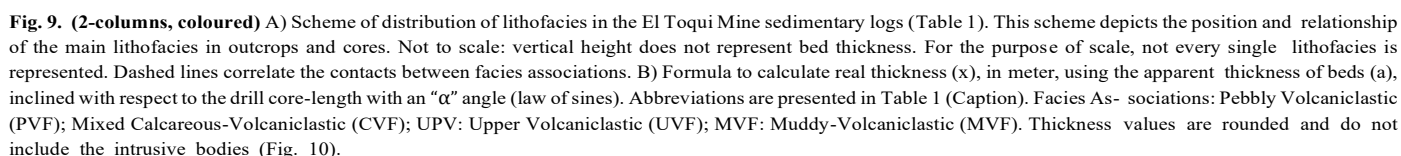
Lithofacies vMp is conformed by parallel-laminated, tuffaceous mudstone, sometimes silty. Mudstone is pale-coloured, with grey to greenish tones (Fig. 4-G, M, N; 6-M). Lamination is sharp to diffuse, alternating or grading to other muddy lithofacies (tMm; Mp, vSMp). Bed boundaries are sharp or grade from sand richer lithofacies, some of them display small-scale scourmarks (Fig. 4-N).

Interpretation: This lithofacies is interpreted as formed by the alternation of subaqueous-settled, ash-fallout deposits ("water-lain tuff" *sensu* Collinson et al., 2006), and eruption-fed ash-turbidites (Cas and Wright, 1987; Cantelli et al., 2008).

2.3.3. Fossil-bearing, black carbonaceous silty claystone (Mp)

This lithofacies is composed of a relatively homogenous, black to dark grey-coloured mudstone. Mudstone is apparently massive or finely laminated, sometimes fissile (Fig. 4-A, H; 8-D). Its fossil content includes: belemnite rostra (*Belemnopsis* sp.; *Acrotheutis*? sp.; Fig. 8-E), undetermined ammonite imprints, small bivalves (<2 cm), fern imprints (*Ptilophyllum* sp.; Fig. 8-F) and microfossils. Additionally, pyrite was found as small cumulus (<2 mm), as fromboids, as scattered cubes (<1 mm), and as patinae.

In thin section, it displays parallel-to wavy-lamination formed by small lenses of organic matter (Fig. 4-H). Additionally, they may include scattered radiolarians tests (1–3%), scarce pelagic foraminifers ($<1\%$), quartz and sericitized plagioclase ($<5\%$). Some samples display irregular pressure solution seams formed during compaction diagenesis. Alteration is represented by quartz and sericite veins, as well as by silt-to very-fine-sized scattered white mica (Fig. 4-H).



Calcareous lithofacies are compositionally impure, i.e. mixed with volcanoclastic sediment (Fig. 5). The terrigenous fraction is analog to the sandy and muddy lithofacies (Sections 2.2-2.3), and conformed mostly by fine-medium-grained volcanic clasts and isolated plagioclase (5–30%; Fig. 5-J). Their calcareous framework is dominated by coarse sand- to cobble-sized bioclasts. The matrix is carbonate mud, occasionally replaced by neomorphic microspar formed during compaction diagenesis (Fig. 5-G, H). In coarser bioclastic lithofacies (e.g. oBm, bFRm), the matrix consists of bioclastic wacke-packstone. Cement is rare. When present, it is blocky lime spar, or blocky-drusy mosaic fill of shell-voids; these features are interpreted as diagenetic and burial-formed. Primary isopachous columnar spar cement identified on the

At the El Toqui Mine, six calcareous-mixed lithofacies were

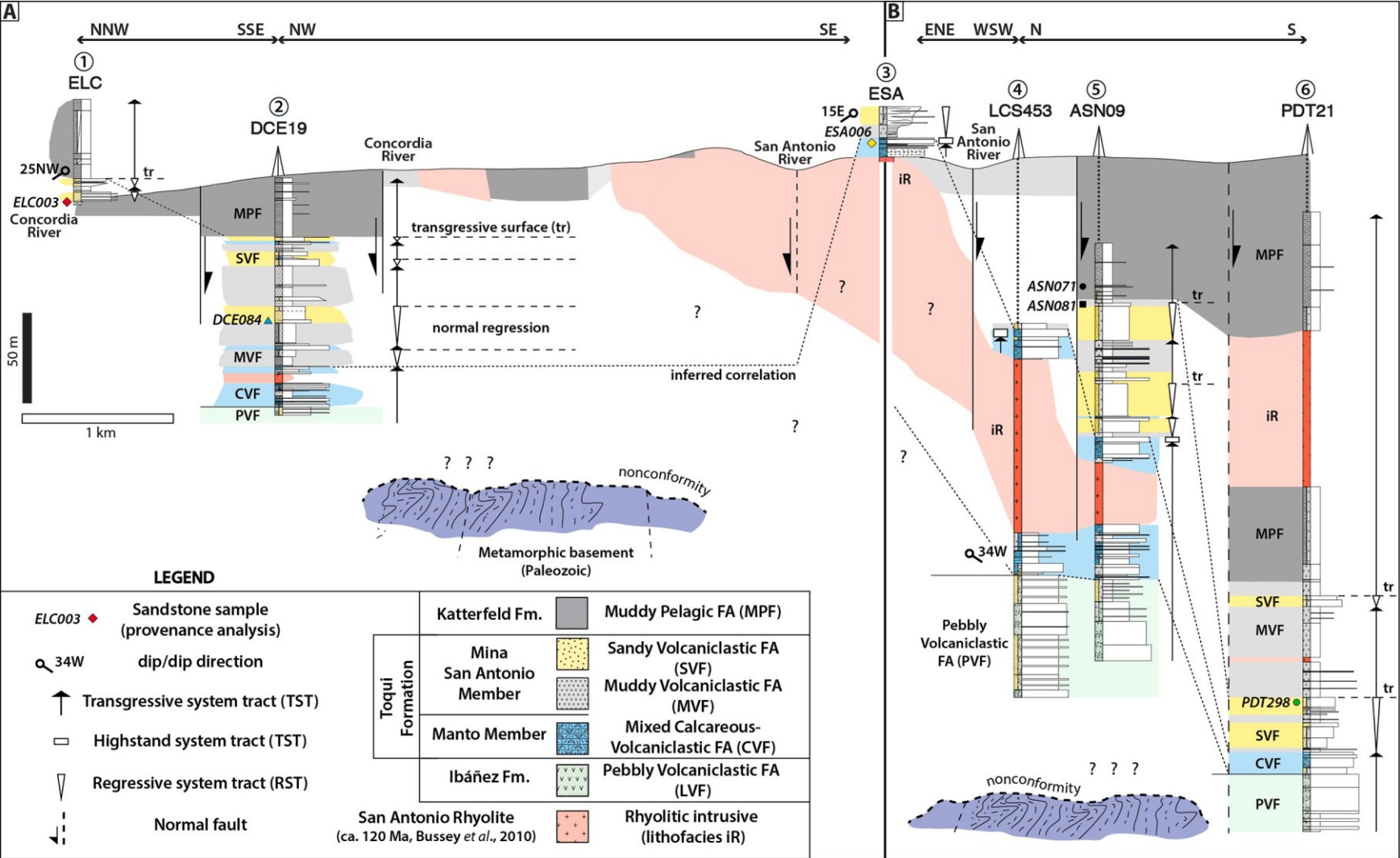
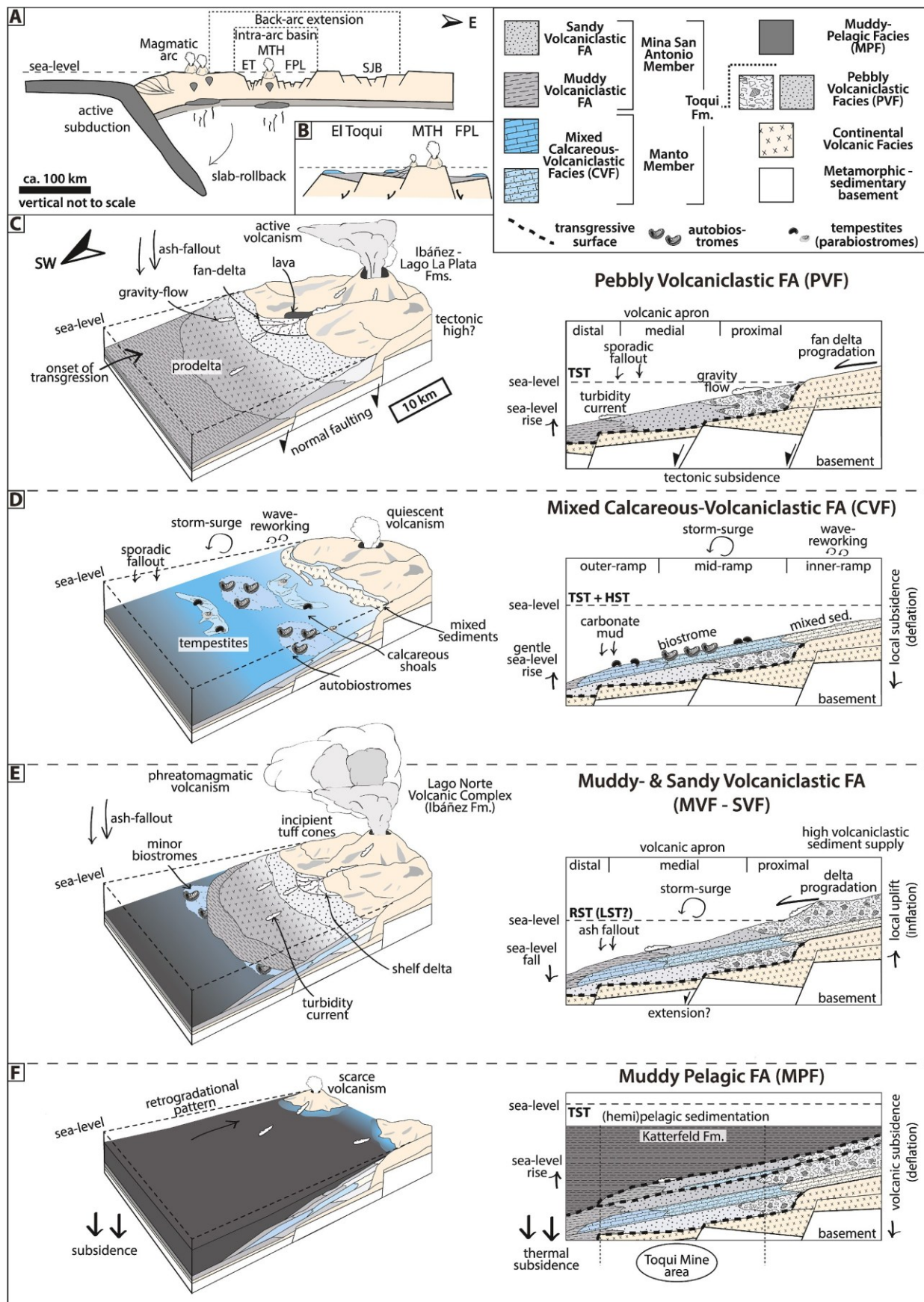


Fig. 10. (Whole page, coloured) Correlation of sedimentary logs, showing the location of drill cores, samples, facies associations and members here proposed. A sequence-stratigraphical scheme is presented to the right of the logs. Geographical position of the cores is shown in Fig. 1-C. Normal-faulting is based on the subsurface profiles of Bussey et al. (2010a, b). A (left side) and B (right side) represent a change in the strike of the subsurface profile (Fig. 1-C).



(caption on next page)

Fig. 11. (Whole page, coloured) A) Tectonic setting of the Northern Austral Basin at 45°S, during the Tithonian – Valanginian (Modified from Folguera and Iannizzotto, 2004; Iannizzotto et al., 2004; Echaurren et al., 2016). B) Close-up of the El Toqui-Lago La Plata area. ET: El Toqui depocenter; MTH: Mañihuales-El Toqui tectonic high; FPL: Fontana-La Plata Lakes (area) depocenter; SJB: San Jorge Basin, continental extensional basin, partly coeval to the Aysén-Río Mayo Basin (Based on Iannizzotto et al., 2004; Dorobek, 2008a). C–F) Geological model, vertical evolution, and sequence stratigraphy of facies associations from the El Toqui Mine area. C) Relative sea-level rise caused by tectonic subsidence; onset of a transgressive system tract (TST) and flooding of continental volcanoes (intra-arc position); developing of shallow-water volcanic aprons, fed by coarse-grain deltas (“Gilbert” type). D) Quiescent tectono-volcanic phase; developing of ramp depositional surfaces and colonization by epifaunal organisms; slight subsidence caused by volcanic deflation or lobe migration; sedimentation changes from a TST to a highstand system tract (HST) during aggrading autobiostromes. E) Relative sealevel fall, caused by local volcanic uplift (inflation); reactivation of phreatomagmatic volcanism and decrease in accommodation (sediment supply > accommodation), filled by eruption-fed shelf deltas; smothering of the biostromes. F) Waning volcanism and volcanic subsidence (deflation), followed by enhanced regional thermal subsidence (post-rift); coastal retreat and retrogradational stacking patterns; emplacement of pelagic, outer-shelf depositional environments (TST).

recognized (Table 1):

2.4.1. Oyster boundstone (oBm)

Oyster boundstone of the oBm lithofacies is almost exclusively formed by cup-shaped shells (ca. 110 mm length). Oyster are placed in a dominant concave-upwards position, and many of them have both valves (Fig. 5-A, C; 7-B, C). When complete, cup-shaped oysters are inequivalved, with a major and thicker left valve and displaying an exogyroid twist similar to *Gryphaea* sp., i.e. “gryph-like” (*sensu* Stenzel, 1971, Fig. 7-B, D). Oyster of lithofacies oBm are embedded in a bioclastic sandy wackestone-packestone matrix with abundant bivalve shell debris (30–40%), peloids (5%), and variable proportions of volcanic sand (<15%; Fig. 5-K).

Interpretation: Oyster boundstone is interpreted as autobiostromes (in-situ) settled on a sandy-muddy, subtidal marine environment. As inferred from its wacke-packestone matrix and the concave-up life-position of oysters observed at the ESA outcrop (Fig. 7-C), these animals had an epifaunal, reclining lifestyle, settled in a calcareous soft-bottom, or “ooze” (Stenzel, 1971; LaBarbera, 1981; Bayne, 2017). They required a relatively low-energy neritic environment, below the perturbation from the fair-weather base, i.e. on the distal carbonate mid-ramp to outer-ramp (Burchette and Wright, 1992; Flügel, 2004), or as platform edge “reefs” in a distally-steepened ramp (Scheibner and Reijmer, 1999). This lithofacies is similar to the SMF-7 and RMF-12 microfacies of Flügel (2004).

2.4.2. Bioclastic floatstone to rudstone (bFRm)

This lithofacies comprehend single beds or an alternation formed by loose- and dense-packed, fragmental bioclasts or “coquinites”. Bioclasts comprise mostly elongated oyster and bivalve-shell fragments (length up to 80 mm, average 10–20 mm), which are placed in a sub-horizontal, bed-conformable position (Fig. 5-A, D, F; 6-E; 7-A, D). Oyster shell fragments comprise up to 60% of the rock (average 15% in floatstone, and 30% in rudstone). Minor bioclasts include serpulids tubes and echinoid plates (<5%; Fig. 5-F; 7-D). Bioclasts are embedded in a bioclastic wackestone to “fitted” packstone matrix (Fig. 5-G). This lithofacies is common at the lower part of the ESA outcrop, and has also been observed in cores (Fig. 5-A; 7-A); these bioclasts-rich beds are usually interbedded with bioclasts-poor layers of the sFm and bMWm lithofacies, with a sharp basal and top contacts, or also passing gradually at top (Fig. 5-A).

Interpretation: Lithofacies bFRm depicts accumulation of shelly lags interpreted as bioclastic proximal tempestites (Aigner, 1985; Flügel, 2004), produced after wave- and storm-surge reworking of nearby autobiostromes (i.e. autoparabiostromes and parabiostromes *sensu* Kershaw, 1994). These processes typically occur over the storm-wave base, on a carbonate inner- and mid-ramp environment, but its deposits might be transported offshore by bottom currents (Burchette and Wright, 1992; Flügel, 2004). This lithofacies is analog to the RMF-28 and SMF-12 microfacies of Flügel (2004).

2.4.3. Serpulid-rich wackestone - floatstone (sWFm)

This lithofacies is formed by massive serpulid-rich wacke-floatstone. Serpulid tubes have a diameter of 3–4 mm, and are placed usually in a

sub-horizontal, bed-conformable position. They are single and elongated or planispiral, and minor colonial, and comprise about 5–15% of this lithofacies (Fig. 5-E, F; 7-C). Minor bioclasts include scattered bivalve fragments smaller than 2 cm (5–10%), interpreted as pelagic (Fig. 5-I). In thin section, some serpulid-rich beds are conformed by complete and fragmented tubes, some of them attached to oyster fragments. The carbonate matrix is formed by bioclastic calcimudstone to wackestone. This lithofacies is analog to the SMF-8 microfacies of Flügel (2004).

Interpretation: This lithofacies represents a quieter and relatively distal environment, interpreted as a bioturbated mud from a carbonate outer-ramp environment. Its position, usually between proximal tempestites of the bFRm lithofacies, reflects a dominant muddy sedimentation perturbed by sporadic storm-surges. Serpulids likely attached to reworked oyster-shell fragments, or their tubes were detached from the oyster autobiostromes during storm surges.

2.4.4. Bioclastic calcimudstone to wackestone (bMWm)

This lithofacies comprehends massive limestone with a nodular fabric, analog to the matrix of the previous lithofacies, but displaying scarce fossil content (around 10%; Fig. 5-A, D; 6-I). Bioclasts are granule-to pebble-sized, and comprise small pelagic bivalve shells (SMF-3 facies *sensu* Flügel, 2004), minor serpulid tubes and reworked oyster shells and echinoderm plates (Fig. 5-H). Its fabric resembles the “*Lithiotis* limestone” of Scheibner and Reijmer (1999).

Interpretation: This lithofacies reflects settling in a quiet environment, below the storm wave base, and with scarce or infrequent input of bioclastic debris. It depicts sedimentation on the carbonate outer ramp (e.g. microfacies RMF-3 and SMF-8 *sensu* Flügel, 2004), but it can also be found at the “reef or platform edge” from a distally steepened ramp (Scheibner and Reijmer, 1999; microfacies SMF-5 *sensu* Flügel, 2004).

2.4.5. Calcareous volcanic sandstone - sandy wackestone (vSWm)

This mixed lithofacies comprehend volcanic sandstone with a tuffaceous-calcareous matrix, and sandy bioclastic wackestone (Fig. 5-B). Sandstone is medium-coarse grained, minor pebbly or bearing scattered bioclasts (Fig. 5-J). Wackestone displays scattered plagioclase crystals and minor sand-sized volcanic lithics, but they are also concentrated around bioclasts, or packed as the insoluble component in “fitted” compacted packstone (Fig. 5-G). This lithofacies has diffuse decimeter-thick beds, usually interbedded with bioclast-poor calcareous lithofacies (bMWm, sWFm).

Interpretation: Lithofacies vSWm is interpreted as the shallow-marine reworking of minor and sporadic, fallout volcanoclastic deposits settled over the carbonate ramp. Alternatively, its interbedding between lithofacies bMWm and sWFm, might represent minor sandy debrites, after the remobilization of paralic volcanoclastic deposits towards the outer ramp during storm surges.

2.4.6. Bioclasts-bearing, pebbly sandstone to volcanic breccia (bGSg)

This lithofacies is similar to the pebbly vGSm lithofacies, but is coarse-tail normal graded, and its framework includes exclusively granule-pebble-sized bioclasts. Bioclasts are reworked and recrystallized, sub-rounded to sub-angular, and interpreted as oyster fragments. They are embedded in a black, devitrified volcanic matrix. Its bedding is

sharp, arranged in centimeter to decimeter-thick layers.

Interpretation: This lithofacies corresponds to subaqueous, moderate-strength cohesive debrites. As shown from the incorporated bioclasts, these eruption-fed debris flows crossed the incipient carbonate ramp and settled in a distal and steep position, interpreted as the platform edge from a distally steepened ramp (Scheibner and Reijmer, 1999; Flügel, 2004).

2.5. Igneous lithofacies

Igneous lithofacies comprehend rhyolitic rocks (lithofacies iR). Its thickness reaches up to ca. 100 m (drill core LCS453; Fig. 10), though previous studies report a thickness >600 m (Bussey et al., 2010a). Rhyolite is porphyritic, with 2–3 mm quartz phenocrysts embedded in a structureless, pale aphanitic groundmass (Fig. 6-L).

It intrudes the Mixed Calcareous-Volcaniclastic Facies Association at different depths (DCE19, LCS453, ASN09 drill cores; Figs. 6 and 10), or is also exposed at the base of the calcareous succession (ESA outcrop; Fig. 7A). In contrast, in the PDT21 drill core, intrusive rocks are observed twice within the Upper Volcaniclastic Facies Association (Fig. 6-B). Some rocks display contact metamorphism beside the intrusive, evident as silicification in volcaniclastic and muddy rocks (“baked”), whereas limestone appears silicified, marmorized, or replaced by galena-sphalerite skarn mineralization (Fig. 6-Q).

Interpretation: At the El Toqui Mine, the rhyolitic intrusive has been interpreted as a sill, up to 600 m-thick (Wellmer et al., 1983; Bussey et al., 2010a, b). This sill has been locally defined as the “San Antonio Rhyolite”, after its exposure at the homonymous hill (Bussey et al., 2010a).

3. Facies associations and palaeoenvironmental analysis

Based on marked lithological variations observed along the sedimentary logs from outcrop and subsurface at the El Toqui Mining District, the previous lithofacies were arranged in five facies associations (FA). These associations are linked to different depositional processes and environments, and are presented in their stratigraphical order. They comprise, from base to top: i) a Pebbly Volcaniclastic FA (PVF), depicting an eruption-fed, coarse-grained delta (proximal-medial volcanic apron); ii) a Mixed Calcareous-Volcaniclastic FA (CVF), linked to the development of carbonate ramps; iii) the Muddy- and Sandy Volcaniclastic FA (MVF; SMF), both marking a renewed volcanism and the progradation of an eruption-fed, shelf-delta (medium-distal volcanic apron); and iv) a Muddy Pelagic FA at top (MPF), reflecting flooding and pelagic sedimentation. These association and their component lithofacies are presented in Table 2.

3.1. Pebbly Volcaniclastic Facies Association (PVF)

The Pebbly Volcaniclastic Facies Association comprehends the lowermost lithosomes observed from subsurface cores at the El Toqui Mine. Its base was neither reached by drillings nor exposed in outcrops and, at the top, it underlies- and interbeds with the Mixed Calcareous-Volcaniclastic Facies Association (CVF; Section 3.2; Fig. 6-A, B).

The PVF comprehends at least 66 m of crude-to sharp-bedded volcanic rocks, mostly formed by coarse-grained lithofacies linked to debris- and grain flows deposits (Section 2.1: lithofacies vGms, vGcs, vGSsm, vGSp; Fig. 3; 6-J, R; Tables 1 and 2). The latter grade to- or are interbedded with sandy- and muddy volcanic lithofacies interpreted as eruption-fed turbidites (lithofacies vSMg, vSMp; Fig. 3-A, B, F), sandy debrites (vSm), and with minor subaqueous-settled fallout deposits (lithofacies tGf; Fig. 3-A). Coarser-grained lithofacies (pebble-cobble-sized clasts) are more common in the lower parts of this FA, whereas, to the top, sandy- and minor mixed calcareous-volcaniclastic lithofacies are dominant and resemble the SVF FA (Section 2.2; lithofacies vSMg,

vSMp, bGSp; Fig. 3-B, 9). The evidence of sporadic subaqueous-settled,

Table 2

(Two columns; black & white) Summary of facies association defined at the El Toqui Mining District. Font styles represent the abundance/importance of lithofacies in each FA: capital = dominant lithofacies (**vGms**); regular = minor lithofacies (tGf); italic = rare lithofacies (vBm). Lithofacies were presented in Section 2 and are summarized in Table 1. * Maximum thickness reported for the lithofacies iR (Bussey et al., 2010a, b).

Facies association (FA)	Lithofacies	Thickness	Depositional environment
Pebbly Volcaniclastic FA (PVF)	vGms, vGcs, vGSsm, vGSp tGf, vSMg, vSMp, vSm <i>vBm, bGSg, tMm</i>	> 66 m (LCS453)	Delta front (foresets), shallow-water & eruption-fed, Gilbert-type delta (proximal-medial volcanic apron)
Mixed Calcareous – Volcaniclastic FA (CVF)	vGms, vGcs, vGSsm, vGSp tGf, vSMg, vSMp, vSm <i>vBm, bGSg, tMm</i>	1.8 m (DCE19) - 39 m (ASN09)	Carbonate mid- and outer-ramp
Muddy Volcaniclastic FA (MVF)	vMp, tMm vSMp, vSMg, Mp <i>tGf, tGg</i>	1 m (ASN09) -47 m (PDT21)	Prodelta to distal delta slope, eruption-fed shelf/shoal delta (distal volcanic apron)
Sandy Volcaniclastic FA (SVF)	vSm, vSMg, vSMp vMp, tMm vSGx, vSMu, vSMx, <i>tGf, vBm</i>	2.2 m (DCE19) - 10 m (ASN09)	Wave- and storm-influenced, eruption-fed, delta front to delta slope (medial volcanic apron)
Muddy Pelagic FA (MPF)	Mp tMm, vMp, vSm, vSMg	> 90 m (PDT21)	(Hemi) pelagic, outer shelf
Rhyolitic intrusive	iR	2.3 m (PDT21) - 95 m (LCS453); 600 m	Subvolcanic intrusion, sill

fallout deposits (lithofacies tGf), resedimented hyaloclastites (lithofacies vGSsm), and its stratigraphic position underlying carbonate rocks, depict a subtidal depositional environment for the PVF.

Interpretation: These lithofacies reflect a subaqueous fast-settling over a steepened surface, from cohesive and turbulent density-flows (Postma, 1986; Middleton, 1993; Shanmugam, 1997). In particular, presence of grain-flow deposits indicates steep slopes up to 30°–35° (Cas and Wright, 1987; Collinson et al., 2006). These are interpreted as resedimented volcaniclastic deposits, which were either transported syneruptively or penecontemporaneously to littoral or shallow-water explosive volcanism. In addition, hyaloclastites might reflect minor lava-water interaction (McPhie et al., 1993; Fisher and Schmincke, 1994; Schmid and Schmincke, 2002; Batiza and White, 2015).

These deposits are interpreted as deposited in the steep foresets of a delta front subenvironment, conforming a shallow-water, coarse-grained- or fan-delta (“Gilbert-type delta” *sensu* Postma, 1990; Reading, 1996, Fig. 11-C). Sediments were likely carried by subaerial debris flows or lahars reaching the coast (Carey and Sigurdsson, 1984; Fisher, 1984; McPhie et al., 1993), by density flows triggered by gravitational collapse, or by coastal reworking of semi-consolidated debris (Cas and Wright, 1987; McPhie et al., 1993). Overall, the Pebbly Volcaniclastic Facies Association represents the development and growth of a proximal volcanic apron, deepening-upwards to a medial apron at top (Allen et al., 2007). Volcanic aprons are regarded as common structures around seamounts and volcanic islands, formed by wedge-shaped accumulation of littoral, eruption-fed or reworked volcaniclastic material (Fisher and Schmincke, 1984; Carey in Sigurdsson, 1999).

3.2. Mixed Calcareous-Volcaniclastic Facies Association (CVF)

The Mixed Calcareous-Volcaniclastic Facies Association overlies and partly interfingers with the upper beds of the PVF, and it is sharply

covered by the Muddy- and Sandy Volcaniclastic Facies Associations (MVF; SVF; Fig. 6; 7). It comprises between 2 and 39 m of mixed rocks and bioclastic limestone (lithofacies oBm, bFRm, sWFm, bMWm; Tables 1 and 2), and sporadic volcaniclastic beds interpreted as subaqueous-settled fallout deposits and sandy debrites (lithofacies tGf, vSm). At the ESA outcrop, the calcareous succession displays a shallowing-upwards trend between fragmental, loose- and dense-packed bioclastic limestone (bFRm, sFr, bMSm), interpreted as tempestites, and the dense-packed oyster autobiotomes (oBm; Fig. 7-A). There, oyster parabiotomes and autobiotomes are separated by an 8 cm-thick volcaniclastic layer. The latter is covered by oysters in life-position (Fig. 7-B, C).

In subsurface, this association is dominated by loose-packed, bioclastic lithofacies (bMWm; bSWm, sWFm; e.g. DCE19, PDT21), interbedded with minor oyster-rich calcareous tempestites (bFRm). At the top, it is capped by oyster autoparabiotomes of the oBm and bFRm lithofacies, interpreted as a shallowing-upwards trend (Fig. 5-A). Calcareous sedimentation was interrupted by sporadic volcaniclastic beds including sharp-bounded subaqueous-settled fallout deposits (lithofacies tGf; Fig. 6-A, B), volcaniclastic tempestites (vSMx; Fig. 6-H), and diffuse areas with mixed lithofacies (bSWm).

The CVF has its better development at the lower part of the El Toqui Mine sedimentary succession, directly over the subaqueous-settled, volcanic rocks of the Pebbly Volcaniclastic FA (Fig. 6-A, B; 9). However, it was also observed as minor calcareous intercalations along the succession, between the Sandy Volcaniclastic Facies Associations (SVF; Fig. 6-A, B, E; 9-A). At the El Toqui Mine, the lowermost and thickest mixed-calcareous rocks have been locally referred as Limestone I (Wellmer et al., 1983), and “Main Manto” (Bussey et al., 2010a, b; Kakarieka, 2003, Fig. 2); on the other hand, minor calcareous beds within the SVF have been referred as Limestone II/III (Wellmer et al., 1983, Fig. 2), “Upper Manto” (Bussey et al., 2010a, b; Fig. 2), and “Manto Alto” (Kakarieka, 2003).

Interpretation: Limestone and mixed rocks of the Mixed Calcareous-Volcaniclastic Facies Association depicts the sedimentation over an open marine, relatively quiet environment, interpreted as carbonate ramps. Ramps are gently steepened depositional surfaces without a break in slope (Burchette and Wright, 1992; Tucker et al., 1993), however, based on bioclastic-rich debrites and inferred platform-edge lithofacies; these ramps were locally distally steepened.

In the El Toqui Mine, the most remarkable lithofacies corresponds to the mid-ramp autobiotomes (oBm); muddier sedimentation was focused offshore over the outer ramp, i.e. before the storm wave base (Burchette and Wright, 1992; Flügel, 2004, Fig. 11-D). The presence of proximal, bioclastic tempestites between outer-ramp carbonate, indicates periodic storm perturbation of the biotomes, and remobilization by storm surges.

The presence of “gryph-shaped” oysters at the El Toqui Mine, i.e. *Gryphaea* spp. and their homeomorphs, reflects that the environment was strictly euhaline (Stenzel, 1971). This is also supported by the association of oysters with serpulids and echinoderms, which are also euhaline organisms (Scholle and Ullmer-Scholle, 2003; Flügel, 2004; Ippolitov et al., 2014). In the El Toqui Mine, these oysters were originally assigned to *Exogyra* cf. *E. coultoni* (Tapia et al., 1984 in Kakarieka, 2003), although, following the revision of Rubilar (2003), they probably correspond to the genus *Aetostreon* Bayle.

As shown from mixed lithofacies and minor volcaniclastic input (Fig. 11-D), ramps were located close to an active volcanic arc. The volcanic sediments had their source in sporadic eruptions (syn-eruptive), or sediments were remobilized offshore from paralic or continental, older unconsolidated deposits. Even though they partially disrupted the calcareous sedimentation (Fig. 7-A, B), the volcanism was relatively moderate, intermittent, or their products migrated laterally during this period (e.g. delta lobe migration; Reading, 1996), allowing for the proliferation of the benthic communities (e.g. Burchette and Wright, 1992; Schmidt and Schmincke, 2002; Ramalho et al., 2013;

Housego and Rosman, 2016).

Additionally, minor mixed or bioclastic limestone within the overlying volcaniclastic facies associations (MVF, SVF; Fig. 6-A, B, E; 9) is interpreted as small organic build-ups developed during short intervals of volcanic quiescence (Schmidt and Schmincke, 2002). Alternatively, they might represent an offshore-directed transport of bioclastic material, carried by eruption-fed gravity flows through passages across mid-ramp environments (Fig. 11-E).

3.3. Muddy Volcaniclastic Facies Association (MVF)

This association is formed mostly by sharp- and diffuse-laminated, volcanic and tuffaceous mudstone (lithofacies vMp, tMm; Fig. 4; Table 1), and minor volcanic sandstone (lithofacies vSMp; Figs. 4 and 6). Its thickness varies between 1 and 47 m (Table 2). The Muddy Volcaniclastic Facies Association was recognized directly overlying the oyster biotomes of the Mixed Calcareous-Volcaniclastic FA (e.g. ESA outcrop, DCE19 drill core; Fig. 4-G, N; 5-A; 6-A, B; 9), and interbedded with the Sandy Volcaniclastic Facies Association (e.g. ASN09, DCE19, PDT21 cores; Fig. 6-A, B; 9; 10). To the top of the succession, the Muddy Volcaniclastic FA overlies the Sandy Volcaniclastic FA and passes gradually to the Muddy Pelagic Facies Association (e.g. ELC outcrop; ASN09, PDT21 cores; Fig. 6; 8; 10).

At the ESA outcrop, this mud-rich alternation (vMp, vSMp) displays convolute lamination and a ca. 1 m-high, southwest-vergent, overturned synsedimentary fold (Fig. 7-G). In the DCE19 and PDT21 drill cores, the top of this basal laminated volcanic mudstone (vMp) is marked by a centimeter-thick accretionary lapilli bed, interpreted as subaqueous-settled (lithofacies tGg, Fig. 4-F, K; 6-A, B, P).

Interpretation: Fine-grained lithofacies of the Muddy Upper Volcaniclastic Association correspond mostly to eruption-fed ash-turbidites (Cas and Wright, 1987; Cantelli et al., 2008), subaqueous-settled fallout deposits (“water-lain tuffs” *sensu* Collinson et al., 2006), and tuffaceous hemipelagic sediments. Its fine-grained ash source is linked to the reactivation of a stable and explosive volcanism of likely phreatomagmatic style (Walker, 1981; Fisher and Schmincke, 1984; McPhie et al., 1993). These fine sediments were rapidly settled over an inclined subtidal surface, subsequently affected by soft-sediment deformation (Fig. 7-G). The latter is regarded as typical for water-saturated fine sediments (Heiken, 1971; Collinson et al., 2006; Alsop et al., 2019), and likely triggered by overstepping and loading of the sedimentary pile or by volcanic-triggered earthquake shocks (Allen, 1982; Fisher and Schmincke, 1984; Schneider, 2000).

Overall, this facies association is interpreted as settled in a prodelta environment, possibly reaching up to the distal delta slope (Reading, 1996; Bhattacharya, 2006, Fig. 11-E). Its formation is linked to the progradation of an eruption-fed, shoal-water- or shelf delta (Postma, 1990; Emery and Myers, 1996), as part of the growth of a distal volcanic apron (Allen et al., 2007).

3.4. Sandy Volcaniclastic Facies Association (SVF)

This association is rich in sandy volcanic lithofacies (vSm, vSMp, vSMg, vSMx; Figs. 4 and 6-G, H, M, O; Tables 1 and 2), with a variable contribution of volcanic mudstone (lithofacies vMp, tMm), and scarce breccia (vGSm, vSGx, vGc, vBm; Fig. 3; Table 1). Its thickness varies between 2.2 and 10 m (Table 2). It grades from- and interbeds with the Muddy Volcaniclastic Facies Association (MVF), displaying retrogradational parasequences set (Fig. 6-A, B; 10); it also overlies the Mixed Calcareous-Volcaniclastic FA with a sharp contact (LCS453 core, Fig. 9-A).

Its better exposure is located at the ESA outcrop (Fig. 1), where it grades from the MVF with a coarsening- and shallowing upwards succession (Fig. 7-A, B, G; 9). There, the succession passes from fine-laminated volcanic mudstone to undulated beds of volcanic sandstone and conglomerate, linked to a shallow-marine and storm-reworked

environment (lithofacies vSGx, vSMu; Fig. 7-E-F, I). Minor pebbly-rich lenses, laterally correlative with the tempestites, are interpreted as minor debrites and reworked grain-flow deposits (Fig. 7-E, H).

This facies association has also been recognized 4 km to the north-west of the ESA section, at the Concordia River outcrop (ELC), where volcanoclastic rocks include a ca. 10 m-thick succession of volcanic sandstone and mudstone (Fig. 8-A). Its base is not exposed, and it is conformably covered by black fissile mudstone (lithofacies Mp) of the Muddy Pelagic Facies Association (MPF; Fig. 8-D). The succession is formed by coarse-grained to pebbly-, cross-bedded volcanic sandstone (lithofacies vGSx; Fig. 8-A, C). Sandstone is covered by fissile grey volcanic mudstone (lithofacies tMm) which inversely grades to parallel-bedded, fine-medium sandstone (lithofacies vSMp). Sandy cross-bedded sets dip towards the NNE ($n=2$; Fig. 8-C).

In subsurface, this shallowing-upwards succession is less marked, lacking gravel-rich lithofacies, except for sporadic, sharp beds of volcanic conglomerate breccia, interpreted as subaqueous-settled fallout deposits (lithofacies vSMg and tGf, respectively; Fig. 3-E, K, L; 6-F, N, P). Upsection, the volcanoclastic succession is dominated by an alternation of massive and parallel-laminated sandy lithofacies (lithofacies vSMg, vSMp), and minor muddy laminates (lithofacies tMm, vMp; Fig. 6-A, B, 9).

Interpretation: Just as the Muddy Volcanoclastic FA (MVf), the deposits of the Sandy Volcanoclastic Facies Association covered the mid-outer ramp limestone and settled in a subtidal environment (Fig. 11-E). Its clastic nature, dominated by coarse ash and lapilli-sized fragments, comprising reworked pumice and oligomictic volcanic lithics, indicate re-sedimentation of syn-eruptive deposits (e.g. McPhie et al., 1993; Fisher and Schmincke, 1994; Allen et al., 2007). The volcanoclastic sediments were either remobilized from the paralic zone or transported offshore by sediment gravity flows and by tractive currents (Fisher, 1984; McPhie et al., 1993). However, at the ESA and ELC outcrops, cross-bedded pebbly sandstone is interpreted as the fill of shallow distributary channels, with a likely western-directed transport (lithofacies vSGx; Fig. 7-F, H).

Overall, the SVF grades from the MVF with a shallowing-upward trend, interpreted as the transition from a prodelta to a wave-storm influenced, shelf-delta environments (Potter et al., 2005; Fig. 11-E). In particular, its coarser grained lithofacies reflect a delta front-to delta slope sub-environment (Bhattacharya, 2006; Reading, 1996). These prograding units might reflect the development of a local, storm-influenced, “pyroclastic fan delta” (*sensu* Nemec, 1990), formed by the periodic supply of volcanoclastic material to the shoreline (e.g. continental debris flows, lahars), and conforming the medial and distal facies of a prograding volcanic apron (Allen et al., 2007, Fig. 11-E).

3.5. Muddy Pelagic Facies Association (MPF)

This association is dominated by fossil-bearing, black-dark grey pelagic mudstone (Mp; Fig. 6-D; 8-E, F), and sporadic thin layers of volcanic sandstone with elongated rip-up clasts, interpreted as ash turbidites (vSm, vSMg; Fig. 4-A, H). At its lower part, it also alternates with volcanic-tuffaceous mudstone (tMm, vMp), marking a gradual contact with the underlying Muddy Volcanoclastic Lithofacies (MVf; Fig. 6-C, K). However, at the ELC outcrop, this stratigraphic contact is sharp (Fig. 8-A, D). At the El Toqui Mine, the Muddy Pelagic FA has a minimum thickness of 90 m, and its top is not exposed (Fig. 6-A, B; 8; 10; Table 2), though, at the Cerro Estatuas, the MPF is covered by bioturbated muddy sandstone of the Apeleg Fm. (Section 1.1.3).

Interpretation: The Muddy Pelagic Facies Association represents a relatively deeper and calm-water, and potentially dysoxic environments (O'Brien and Slatt, 1990). Its composition is dominated by pelagic sediments, with a minor fine-grained tuffaceous component (hemipelagic) and scarce biogenic pelagic ooze with radiolarians. Carbonaceous (silty) claystone (Mp), the principal component of the MPF, is interpreted as slowly settled, even though its internal wavy lamination

may alternatively suggest the presence of faint bottom currents (O'Brien and Slatt, 1990; Pickering & Hiscott, 2016, Fig. 4-H).

These fine sediments likely settled in areas with restricted circulation (Fig. 11-E, F), focused in the deeper part of the basin, i.e. between tectonic highs (Dorobek, 2008a; Jones, 2010), or offshore-directed occupying the outer ramp zones, below the storm wave base (Burchette and Wright, 1992; Flügel, 2004). However, their dominance to the top of the sequence reflects a sea-level rise and generalized deeper, pelagic conditions (Fig. 11-F). Overall, the MPF is interpreted as deposited on an outer-shelf- or basinal environment, i.e. at the area located below the storm wave base and lacking coarse “tempestites” *sensu* Burchette and Wright (1992).

4. Discussion

4.1. Stratigraphy of the El Toqui Mine area

At the El Toqui Mining District, the Toqui Formation is here depicted as a mixed unit, composed by three facies associations. This formation is here redefined as formed by two formal members: 1) the calcareous-mixed and volcanoclastic rocks of the Mixed Calcareous-Volcanoclastic Facies Association (CVF), included here in the Manto Member; and 2) by the overlying Muddy- and Sandy Volcanoclastic Facies Associations (MVf; SVF), grouped in the Mina San Antonio Member.

The underlying Pebbly Volcanoclastic Facies Association is thus correlative to the Ibáñez Formation (*sensu* Suárez et al., 2007; 2009); whereas, at the top, the Toqui Formation is capped by the Muddy Pelagic Facies Association, which has been assigned to the Katterfeld Formation (*sensu* Suárez et al., 2007; Bussey et al., 2010a, b). The following section presents a detailed discussion regarding the local and regional stratigraphy. The previous and current schemes as well as the stratigraphy here proposed has been summarized in Fig. 2-B.

4.1.1. Redefinition of the Toqui Formation

The current stratigraphic scheme for the Toqui Formation, at its type locality (i.e. Toqui Mine, 45°S; Fig. 1-B, C), considers this unit as formed by three informal members or “facies associations”, named “calcareous”, “sandy-calcareous” and “pyroclastic-calcareous” associations (*sensu* Suárez & De La Cruz, 1994; Suárez et al., 2007). However, lithologies are highly variable outside the type area, i.e. in a ca. 50 km radius (e.g. De La Cruz et al., 1996; De La Cruz et al., 2003; De La Cruz and Suárez, 2006). It is also important to note that the above facies associations are usually exposed separately (Fig. 1-B), making their correlation difficult, and they have been mapped as discrete units to a regional scale (e.g. De La Cruz et al., 2003; De La Cruz and Suárez, 2006; Suárez et al., 2007).

In a regional approach in southern Chile (43°–47°S), all current stratigraphic models agree on the presence of calcareous-mixed rocks forming the early transgressive rocks of the Aysén Basin, included in the Toqui Fm. (e.g. “calcareous association” *sensu* Suárez et al., 2007; “sandy-calcareous association” *sensu* De La Cruz and Suárez, 2006, Fig. 2-B). Calcareous rocks are laterally linked to-, or covered by, volcanoclastic and epiclastic rocks (e.g. “sandy-calcareous”, “pyroclastic-calcareous” associations *sensu* Suárez et al., 2007; “association of sandstone, breccia and tuff”; “volcanoclastic association” *sensu* De La Cruz and Suárez, 2006).

While we agree with these previous views, the sedimentary rocks described here for the El Toqui Fm. type locality display a vertical succession with marked different lithofacies, linked to various sedimentary processes and depositional environments (Figs. 6–9; Table 1). This supports a formal lithostratigraphic subdivision of units previously considered as informal (NACSN, 2005). Thus, the following redefinition of the Toqui Formation is here proposed: The Manto Member is the lower unit and comprises the Mixed Calcareous-Volcanoclastic Facies Association (CVF; Fig. 2-B; 5; 7; 9; 10); it partly interfingers with- and underlies the Mina San Antonio Member formed by subaqueous-settled, fine-grained volcanoclastic rocks corresponding to the Muddy- and

Sandy Volcaniclastic Facies Associations (MVF, SVF: Fig. 2-B; 4; 6-10). The two members combined reach a maximum thickness of 133 m (drill core ASN09; Fig. 9).

The Manto Member thickness varies between 11 and 57 m and consists of oyster boundstone, bioclastic rud-floatstone, wackestone, calcimudstone, calcareous sandstone, sandy limestone and minor volcanic sandstone-mudstone (Fig. 5; 7; 9; 10; Tables 1 and 2). This member includes the “calcareous” and mixed “sandy-calcareous” associations of Suárez et al. (2007), which are considered redundant, given their mixed composition. It is named “manto”, as this term is widely used for exploration of mineralized limestone in the El Toqui Mine (Fig. 2-B; Bussey et al., 2010a, b).

Thickness of the Mina San Antonio Member varies between 13 and 91 m (Fig. 9); the unit is composed of volcanic and tuffaceous mudstone, volcanic sandstone and pebbly sandstone, minor volcanic breccia and lithic-vitreous lapillistone (Fig. 4; 6-10; Tables 1 and 2). The Mina San Antonio Member, as proposed here, includes the “pyroclastic-calcareous” association of Suárez et al. (2007) and the volcaniclastic lithofacies here described (Table 1); it is named after the San Antonio mine pit (45°02'43"S; 71°56'43"W), where both members as well as their stratigraphic contact are well exposed (Fig. 7-B, G).

The two members of the Toqui Fm. are interbedded, e.g. presence of minor limestone beds in the volcaniclastic member and viceversa (Fig. 6-A, B; 10-11), as also observed in the stratigraphy of ancient and recent volcanic deposits (Fischer and Schmincke, 1984). This alternation is linked to autocyclic sedimentary processes (Section 4.2).

The base of the Toqui Formation is marked by the appearance of limestone of the Manto Member (Wellmer et al., 1983; Suárez & De La Cruz, 1994; Suárez et al., 2007). The Manto Member overlies conformably, and partly interfingers with, the upper rocks of the Pebble Volcaniclastic Facies Association, here included in the Ibáñez Fm. (PVF-CVF contact: Fig. 2-B; 6-A, B; 9; 10). To the top, the Mina San Antonio Member of the Toqui Fm. grades into hemipelagic deposits of the Katterfeld Formation (MVF/SVF-MPF contact: Fig. 2-B; 6-A, B; 8-10). The Mina San Antonio Member might be laterally correlative to the volcanic sub-units of the Ibáñez Formation in the area, whether the Cerro Trinchera or the Lago Norte Volcanic Complexes (Suárez et al., 2007). Additionally, since “a member may extend laterally from one formation to another” (NACSN, 2005), the Mina San Antonio Member likely represents the resedimented, subtidal, lateral and partly coeval correlative of the continental pyroclastic and volcaniclastic rocks of the Ibáñez Fm. (Suárez et al., 2007, 2009).

4.1.2. Regional correlations

The shallow-marine, calcareous and volcaniclastic rocks of the Toqui Formation have been correlated with the Cotidiano Fm. (Tithonian) and the Tres Lagunas Formation (Tithonian-Hauterivian), respectively (Fig. 2-A); the latter are exposed in the Lagos La Plata-Fontana district in Argentina (e.g. Haller and Lapido, 1980; Ramos, 1981; De la Cruz et al., 2003; Suárez et al., 2010a, Fig. 1-B). However, direct correlation is hampered due to the restricted exposure of these units (e.g. Olivero, 1982; Scasso, 1987) and differences regarding their lithology, precise age, stratigraphic position and contact relationships (Masiuk and Nakayama, 1978). They are here tentatively interpreted as units diachronic with the Toqui Formation, which agrees with previous interpretations (Suárez et al., 2005, 2009).

The Toqui Formation has also been correlated with the Springhill Formation (De La Cruz et al., 2003), defined by Thomas (1949) in the Tierra del Fuego region of southern Patagonia (54°S) and identified as far north as Pueyrredón Lake (47°15'S; e.g. Ramos, 1979; Giacosa and Franchi, 2001), about 250 km south of the study area (Fig. 1-A). Even though both the Toqui and Springhill Fms. display shallow-marine transgressive facies, and are about coeval Berriasian-Valanginian deposits (e.g. Ramos, 1979; Aguirre-Urreta and Ramos, 1981; Barberón et al., 2019), their lithology contrasts significantly. The Toqui Fm. displays a dominance of marine calcareous and volcaniclastic

environments *versus* marine, epiclastic conglomerate and sandstone, minor tuff, coal beds and a transition to shale in the Springhill Fm. (Ramos, 1979).

“Gryph-shaped” oyster banks and oyster-rich coquinites are common taphofacies in the transgressive deposits in the Aysén Basin-Río Mayo Embayment (43°-47°S; e.g. Płoszkiewicz and Ramos, 1977; Masiuk and Nakayama, 1978; Ramos, 1981; Olivero, 1982; Bell et al., 1994; De La Cruz et al., 1996; Alfaro et al., 1997; Townsend, 1998; Suárez et al., 2007). Oyster-rich beds of the Manto Member (Toqui Fm.) are similar to oyster coquinites documented from the Arroyo Pedregoso Beds, although associated facies and stratigraphic ages differ (Ramos, 1976, 1981; Olivero, 1982). Similar “biostromal” rocks are identified in the Arroyo Blanco Beds (Olivero, 1982), and from the northern margin of Laguna Salada (Scasso, 1982). Despite differences in lithofacies and facies associations of these formations compare to the Toqui Fm., these deposits were dated to the Valanginian (Aguirre-Urreta and Rawson, 1998; Olivero and Aguirre-Urreta, 2002) and are therefore partially coeval to the Toqui Formation (Fig. 2-A).

On the other hand, the volcaniclastic San Antonio Member might be laterally equivalent to the coherent volcanic rocks of the Lago Norte Volcanic Complex (Fig. 1-B; 2-A), which are interbedded with- or overlies calcareous lithofacies at the Norte Lake and at the confluence of the Ñegua-El Gato Rivers (Covacevich et al., 1994; Suárez et al., 2007, 2009). In Argentina, in the Arroyo Pedregoso (Ramos, 1981; Olivero, 1987), volcaniclastic and coherent volcanic rocks associated with the marine deposits are probably older than the Mina San Antonio Member (Toqui Fm.); whereas, at the Arroyo Blanco, possibly coeval volcanic conglomerates represent facies more proximal than the fine debrites from the El Toqui area. Apparently, the fine pyroclastic supply was concentrated at, or preferentially transported to-, the area located southwest of the Lagos La Plata-Fontana area (Fig. 1-B).

The problematic correlation of the transgressive deposits is regarded as a consequence of the diachronic marine transgression over an irregular topography (Ramos, 1981; Folguera and Iannizzotto, 2004; Suárez et al., 2005), dominated by changing, active volcanic environments (Suárez et al., 2007; and here: Fig. 11). The latter provoked the development of several marine environments, which evolved separately as small carbonate ramps over the shallower parts of flooded hanging-wall blocks, in an evolving extensional basin (Scasso, 1989; Hechem et al., 1993; Dorobek, 2008a).

4.1.3. Intrusive units

The oldest intrusive rocks at El Toqui Mine correspond to the Gemelos Andesite ($^{40}\text{Ar}/^{39}\text{Ar}$ ca. 124–125 Ma, Bussey et al., 2010b), which was not investigated here. According to Bussey et al. (2010a, b), based on a peperite breccia surrounding a dike assigned to the Gemelos Andesite, this dike would have intruded the upper part of the Katterfeld Fm. when still un lithified. However, regarding the age of the Gemelos Andesite, coeval to the inferred age of the Apeleg Fm. (Section 1.1.3), two hypothesis emerge: i) the dike really intruded the Katterfeld Fm. and this would be its youngest relative age reported (Sections 1.1.2; 1.1.4); or ii) the dike is cutting the heterolithic lower facies of the Apeleg Fm., analog to the magma-sediment interaction with the Baño Nuevo Volcanic Complex, exposed to the southeast of the El Toqui Mine (Suárez et al., 2010b, Section 1.1.3). More evidence is needed to confirm one of these hypotheses.

Rhyolitic intrusive bodies, on the other hand, were detected in all sections, except for the ELC outcrop (Fig. 10). They sharply cut the Mixed Calcareous-Volcaniclastic FA, and the Muddy/Sandy Volcaniclastic Facies Associations (Fig. 6-A, B; 9; 10), causing some low-degree contact metamorphism (Section 2.3), which must therefore be younger. In addition, since the synsedimentary structures observed at the ESA outcrop are bedset-bounded and truncated, a gravity-driven origin is favoured instead of intrusion-induced (Alsop et al., 2019).

The rhyolite intrusive is part of the “San Antonio Rhyolite”, a 600 m-thick sill dated to U–Pb ca. 120 Ma (Bussey et al., 2010a, b). These

hypabyssal rocks were emplaced after the basin inversion and are coeval to the oldest deposits of the Divisadero Formation (Aptian-Cenomanian, Suárez et al., 2010a).

4.2. Palaeogeography and volcanic source

Marine rocks of the Toqui Fm. overlie volcanic rocks of the Ibáñez Fm. The latter has been regarded as formed by chiefly continental, and minor subaqueous deposits (Wellmer et al., 1983; Suárez et al., 2007). At the El Toqui Mine, the thickness of the underlying volcanic units, here represented in the Pebbly Volcaniclastic Facies Association (PVF; Section 3.1), reaches up to 150 m (Wellmer et al., 1983); whereas, in the area adjacent to the mine, correlative volcanic outcrops of the Ibáñez Fm. reach to 700 m-thickness (Suárez et al., 2007). Therefore, the extensional depocenters, developed over the metamorphic basement, were already partially filled by the volcanic rocks during the onset of the marine transgression (Fig. 11-B, C). There is no evidence of sea-floor spreading during the back-arc extensional phase in the Aysén-Río Mayo Basin (Suárez et al., 2010a), therefore, the marine incursion flooded continental volcanic terrains in the intra- and back-arc zone (Fig. 11-A, B). Overall, the Aysén Basin represents a not fully developed ensialic marginal basin (Tarney and Windley, 1981), occupied by an inland or epicontinental sea (Kusky, 2005; Suter, 2006).

4.2.1. Ramp development

In the El Toqui Mine area, the development of carbonate platforms of the Manto Member of the Toqui Fm. (CVF; Section 3.2), occurred over subaqueous-settled, volcanic rocks of the Ibáñez Fm. (PVF; Section 3.1), interpreted as part of a proximal-medial, subaqueous volcanic apron (Fig. 11-C). These coastal and subtidal deposits provided favourable conditions for a shallow marine, biogenic colonization during volcanic quiescence (Schmidt and Schmincke, 2002; Ramalho et al., 2013). Volcanism was intermittent or quiescent during the biostromal growth (Schmidt and Schmincke, 2002); or the onset of epifaunal communities was focused on gently-steepened surfaces after delta lobe migration (Emery and Myers, 1996).

Absence of slope deposits and high-reworking of bioclasts in autoparabiostromes support the shallow-marine, ramp-shape of the depositional surfaces, though distal carbonate platform-margin wedges, just above the slope-break, have also been interpreted in the mining district (Wellmer et al., 1983) and at Tres Lagunas (Hechem et al., 1993). At the El Toqui Mine, carbonate ramps were chiefly controlled by NW-SE normal faults (Fig. 1-C), regarded as vertical at the El Toqui Mining District (Ruz, 1993 in Suárez et al., 2007; Bussey et al., 2010a, Fig. 11). A deeper depositional environment is inferred at the southern part of the mining district, based on the minor thickness of limestones in the PDT21 core (Fig. 1-C; 11). In addition, an abrupt increase in depth is clear ca. 10 km to the south of the mine, at the southern flank of the Estatuas Hill (Fig. 1-B), where hemipelagic rocks of the Katterfeld Fm. conformably overlie the Ibáñez Fm. (Suárez et al., 2007, Fig. 2-A; 11-F).

4.2.2. Volcanic source

The carbonate ramp was abruptly covered by pyroclastic-volcaniclastic deposits from a prograding shoal-delta, fed by a reactivated littoral, explosive volcanism (MVF & SVF, i.e. Mina San Antonio Member of the Toqui Fm.; Fig. 2-B; 11). As inferred from synsedimentary structures (Fig. 7-G), volcaniclastic sediments prograded over a depositional surface dipping to the southwest (Fig. 11-E). Regarding the source of the volcaniclastic material, coarser grained lithofacies as well as thicker sandy units are more common in the eastern part of the district (ESA, ASN09 sections) and might indicate a more proximal position or a positive topography to the east (Fig. 1-C; 11). Also, unlike most drill cores, where the contact between the MVF and the MPF hemipelagites is gradual, at the ELC outcrop, this contact is sharp and conformable (Fig. 8-A, B, D); thus, a relatively more distal position is inferred when compared to the ESA outcrop (Fig. 11). In addition, paleocurrent

inferred from trough- and sigmoidal cross-bedding (ELC and ESA, respectively) indicate a westward-transport (Fig. 7-F; 8-C), however, since these structures may also reflect the flow-direction of shallow marine currents (e.g. shelf megaripples), or autocyclic deltaic processes (e.g. lobe migration), this interpretation is tentative.

Based on the descriptions of Suárez et al. (2007), volcanic domes and hypabyssal igneous bodies from the Cerro Trinchera and Lago Norte Volcanic Complexes emplaced in a ca. 30 km radius from the El Toqui Mine (Fig. 1-B), with an arc-shaped distribution within the E-S quadrant. These are regarded as the possible source of the pyroclastic material (Fig. 11-C, E). As shown by the mixed nature of the carbonate ramp lithofacies (CVF; Sections 2.3; 3.2), there is, apparently, no long volcanic hiatus between the Pebbly- and the Muddy/Sandy Volcaniclastic Facies Association (PVF-MVF/SMF). The contrast in grain-size, as well as in the type and intensity of alteration between these volcanic facies associations (Figs. 3–4; 6; 9), might be linked to differences in vent proximity, type of transport/settling, or diagenesis. Alternatively, the PVF could represent an older event during the volcanism of the Ibáñez Formation. This has already been proposed by Suárez et al. (2007), who recognized calcareous deposits overlying either the Cerro Trinchera Volcanic Complex (Upper Jurassic? – Berriasian) or the Lago Norte Volcanic Complex (Upper Jurassic? – Valanginian-Hauterivian), both local members of the Ibáñez Formation in the study area (Fig. 1-B; 2-A).

4.2.3. Long-term transgression

The whole succession was covered by hemipelagic deposits, indicating a retreating coast and onshore migration of outer shelf environments (Fig. 11-F). Scarce volcanic layers indicate the onset of a waning stage of volcanic island evolution (Carey and Sigurdsson, 1984), followed by subsidence (deflation) and erosion of the volcanic edifices (Ramalho et al., 2013). During this stage, the marine transgression was possibly accelerated by enhanced regional subsidence (Fig. 11-E), depicted as back-arc post-rift activity or sag-phase, leading to basin deepening and mudstone deposition of the Katterfeld Formation (Bell et al., 1996; Barberón et al., 2015).

4.3. Sequence stratigraphy

4.3.1. Background information

The evolution of shallow-marine environments is chiefly controlled by the interplay between relative sea-level changes and the amount of space available for sediment accumulation, or “accommodation” (e.g. Emery and Myers, 1996). These, in turn, depend on global variations in ocean volume (basin or water), known as eustasy, tectonics (subsidence/uplift), and the rate of sediment supply (Emery and Myers, 1996; Catuneanu, 2002; 2009, and references therein).

In brief, a relative sea-level rise, tectonic subsidence, or both, will “create” accommodation; a sea-level fall, uplift, and sediment supply will reduce the accommodation space. Therefore, a marine transgression, i.e. “the landward migration of a coastline” (Catuneanu, 2002) occurs when accommodation is created faster than its filling by sedimentation, and viceversa during a marine regression (Catuneanu, *op. cit.*).

In convergent margins, accommodation and coastal sedimentation are strongly influenced by tectonics. Deformation is expressed as a differential subsidence/uplift in a short-scale (e.g. faulting), or in a large-scale, e.g. flexural load, thermal subsidence (Dorobek, 1995, 2008b). In addition, the presence of an evolving volcanic arc can alter the local or regional subsidence/uplift trend, resulting in coastline displacement (Ramalho et al., 2013). For example, changes in subsidence and uplift in a volcanic area might be a consequence of the flexural load of the volcanic edifice, the inflation/deflation of the volcanic ground caused by pressure variations within the magma chamber (Blake and Cortés, 2018), or caused by isostatic rebound after mass-wasting events (Ramalho et al., 2013). Also, in subtidal systems, input of coherent volcanic rocks, or a high volcaniclastic sediment supply, will modify the

water-depth and accommodation space (Schmidt and Schmincke, 2002; Dorobek, 2008b; Ramalho et al., 2013).

Although diachronous, the marine transgression reflected by the Toqui Formation corresponds to a period of low global eustatic sea-level, prevailing during the late Tithonian – mid Valanginian (Haq, 2014; 2018, Section 1.1.4). This reinforces the hypothesis that accommodation in the area was tectonically controlled and likely triggered by normal faulting, a common feature in rift basins (e.g. “block-tilting”, *sensu* Dorobek, 2008a). In rift settings, syn-rift sequences are conformed by a basal brief transgressive system tract (TST), followed by a longer highstand system tract (HST) related to active and quiescent faulting, respectively (Martins-Neto and Catuneanu, 2010).

4.3.2. Sequence stratigraphy model for the El Toqui Mine area

At the El Toqui Mine, marine sedimentation starts with the gradual flooding of volcanic edifices and the subsequent development of a proximal-medial volcanic apron, conforming the local units of the Ibáñez Fm. (PVF; Section 3.1; Fig. 10; 11-C). The latter is followed by the conformable development of the shallow-marine, carbonate ramps, depicting the “start-up” phase of carbonate sedimentation during settling of the late TST (Emery and Myers, 1996). Upsection, proliferation of oyster autobiostrume (lithofacies oBm) over the mid-ramp depositional environment (Fig. 10; 11-D), reflects the “keep up” phase of these small reefs and the gently progradation of a HST (Catuneanu, 2002). Both the carbonate-dominated TST and HST depict a basal syn-rift sequence, and they conform the Manto Member of the Toqui Formation (CVF; Section 3.2; Fig. 2-B; 10; 11-D).

This syn-rift sequence associated with carbonate sedimentation (Fig. 5; 6-A, B; 9) ends with the abrupt volcanoclastic sedimentation of the Mina San Antonio Member of the Toqui Fm. (MVF, SVF; Sections 3.3–3.4; Fig. 4; 6-A, B; 9). These volcanoclastic facies associations depict an advancing coastline caused by the progradation of an eruption-fed, shelf/shoal delta (Emery and Myers, 1996; Reading, 1996), regarded as typical for normal regressions (Catuneanu et al., 2011). Since there is no evidence of exposure and subaerial erosion of the carbonate ramp, the shoreline would not have downstepped below the shelf-break during the regression (i.e. ex “Type 2 sequence boundary” *sensu* van Wagoner et al., 1988, term currently in disuse *sensu* Catuneanu et al., 2011).

Upsection, the alternation of facies associations of the Mina San Antonio Member (Toqui Fm.) display a retrogradational parasequences set (MVF & SVF; Fig. 6-A, B; 10). These relatively thinner, sandy parasequences depict minor progradational deltaic successions, linked to brief normal regressions during the settling of a longer-term TST (Emery and Myers, 1996; Catuneanu, 2002, 2017; Martins-Neto and Catuneanu, 2010). At the El Toqui Mine, there is not enough evidence to confirm if the normal regression occurred during a lowstand- or a highstand; therefore, these regressive deposits are here included in non-specific Regressive System Tracts (RST *sensu* Catuneanu et al., 2009; 2011, and references therein; Fig. 10; 11). However, a Lowstand System Tract (LST) might be favoured, considering a hypothetical sealevel fall triggered by the inflation of the volcanic edifice and adjacent areas (uplift), prior to the explosive volcanism (Fig. 11-E). As an example, volcanic inflation has been quantified to reach uplift values of several centimeter - decimeter per year in some volcanic islands (e.g. Santorini Volcano: 14 cm in one year, Newman et al., 2012; Semisopochnoi Volcano: ca. 25 cm in a two-year period, DeGrandpre et al., 2019).

Additionally, a prograding coast also obeys to a decrease in accommodation caused by a high sediment supply. In volcanic settings, a relatively high sediment-supply is typically linked to coasts of growing volcanic islands, in which craters successfully establish above sea-level (Holmes, 1965; Ramalho et al., 2013). At the El Toqui Mine, accommodation was filled and outpaced by eruption-fed, prograding deltas (Emery and Myers, 1996; Cattaneo and Steel, 2003; Catuneanu, 2009, Fig. 11-E). Minor carbonate deposition interbedded with the shelf-deltaic facies (MVF; SVF) reflects brief periods of volcanic quiescence (Fig. 6-A, B; 7-H; 9; 11-D, E”), or migration of the delta lobes,

followed by subsidence and flooding during the transgression (Emery and Myers, 1996, Fig. 11-F).

Towards the top, the cease, or reduction of explosive volcanism, marked by the dominance of hemipelagic sediments of the Katterfeld Fm. (MPF; Section 3.5), depicts an important sea-level rise or an enhanced transgression, of which the transgressive surface is likely represented by gradual boundary between the Muddy Volcanoclastic – and Muddy Pelagic Facies Associations (Fig. 6-K; 10; 11-F). Unlike the scattered and changing early transgressive outcrops of the Toqui Fm., i.e. Manto- and Mina San Antonio Members and their correlative units (Section 4.1.2), the Katterfeld Fm. has a regional expression, being identified between 43° and 48°S (De La Cruz et al., 1996; Welkner et al., 2004). Therefore, its settling may reflect either a regional, broad-wavelength thermal subsidence after the crustal stretching (“post-rift” phase, e.g. White and McKenzie, 1988; Dorobek, 2008a), with a sea-level rise enhanced by an increasing global eustasy starting in the Valanginian (Haq, 2014). Local variables to explain the subsidence include reactivation of normal-faulting, or the deflation and subsidence of the volcanic ground following the cease of littoral volcanism (Ramalho et al., 2013).

Given that rifting sequence stratigraphy models do not consider coeval active volcanism (Martins-Neto and Catuneanu, 2010), nor its consequences over shallow-marine volcanic settings (Ramalho et al., 2013), the scheme proposed here is tentative (Figs. 10 and 11). The basal syn-rift sequence proposed here correlates with the “Depositional Sequences I” of Hechem et al. (1993) for the Fontana Lake area (Fig. 1-B; 2-A). However, these authors considered limestone as part of a “Shelf-Margin System Tract” (“Depositional Sequence II” *sensu* Hechem et al., 1993, Fig. 2-A); currently considered to be part of the LST (Catunenu et al., 2011). Unlike the El Toqui Mining District, at the Fontana Lake area limestone is directly covered by shale of a TST, with minor prograding bedsets linked to a HST (Hechem et al., 1993). Upsection, the Katterfeld Fm. is regarded as deposited during a TST - HST (“Depositional Sequence III” *sensu* Hechem et al., 1993).

Even though the two depocenters experienced a similar initial evolutionary trend, i.e. at El Toqui Mine and Fontana Lake areas, they must have been separated by a topographic high (Iannizzotto et al., 2004, Fig. 11-A, B), likely affected by differential subsidence rates (Emery & Myers, 1996), and with a differential volcanic input (Suárez et al., 2009).

5. Conclusions

The Toqui Formation corresponds to the basal unit of the Lower Cretaceous Coyhaique Group (Tithonian-Aptian), a transgressive-regressive sequence of mixed volcanoclastic-calcareous, neritic sediments deposited in an epeiric sea. This inland sea covered the northern part of the back-arc Austral Basin (i.e. Aysén Basin or Rio Mayo Embayment; Section 1.1), developed in southwestern Gondwana. Based on field work, core description and petrography of the Toqui Formation at its type locality, the El Toqui Mine from the Coyhaique Province, Southern Chile (45°S), a new stratigraphic scheme and paleoenvironmental model is proposed.

The new stratigraphic scheme of the Toqui Formation considers a lower unit, named the Manto Member, formed by mixed calcareous-volcanoclastic and oyster-biostromal limestone; it underlies volcanoclastic mudstone and sandstone of the Mina San Antonio Member with a sharp but conformable contact (Fig. 2-B). Oyster-rich beds of the Manto Member are similar to the ones exposed at the Arroyo Pedregoso and Arroyo Blanco, south of Lago La Plata, Argentina; though, a marked difference in their ages and associated facies hampers their lithostratigraphical correlation. On the other hand, volcanoclastic rocks of the Mina San Antonio Member are likely the subaqueous, lateral equivalent of coherent volcanic rocks of the Cerro Trinchera- and Lago Norte Volcanic Complexes, both informal members of the Ibáñez Formation in the area.

The onset of the marine transgression was diachronous, ranging from Tithonian to Valanginian times (Section 1.1.4). The sea covered continental active volcanic terrains across an intra-arc extensional topography, on which mixed carbonate-volcaniclastic platforms developed in periods of volcanic quiescence. During the deposition of the early transgressive (TST)- and highstand system tracts (HST), carbonate ramps of the Manto Member capped the flooded topographic highs, conforming the subaqueous flanks of volcanic islands (Ibáñez Fm.). Ramps were covered by eruption-fed, prograding shelf-deltas of the Mina San Antonio Member, which marks the reactivation of explosive volcanism. These deposits are regarded as settled during brief normal regression events (RST), which alternated with the dominant transgression (TST, Fig. 10; 11). During the normal regressions, the settling of regressive system tracts reflects an exceptionally high sediment supply that overcame the accommodation space. The latter likely coexisted with a local volcanic uplift (inflation), provoking a relative sea-level fall.

As volcanism waned, deltaic deposits of the Mina San Antonio Member passed gradually to hemipelagic deposits of the Katterfeld Fm depicting a major transgressive surface. As the inland-sea level rose, the hemipelagic conditions spread from the restricted, deepest part of ramps or grabens, to an extended outer shelf environment (Fig. 10; 11). Sedimentation of the Katterfeld Fm. reflects a regional subsidence during the onset of a “post-rift” phase, possibly enhanced by a high global eustasy starting during the Valanginian (Haq, 2014). Overall, the type locality of the Toqui Formation reflects a complex pattern of relative sea-level changes, provoked by the interaction of volcanism, tectonic subsidence, and global eustasy, and their consequences on the development of carbonate platforms.

6. Author credit

Hermann Rivas: Software, Formal analysis, Investigation, Data curation, Writing – original draft, Writing – review & editing, Visualization. Christian Salazar: Conceptualization, Methodology, Writing – review & editing, Supervision, Funding acquisition. Wolfgang Stinnesbeck: Resources, Writing – review & editing, Supervision, Project administration

7. Declaration of competing interest

The authors declare that they have no known competing financial interests or personal relationships that could have appeared to influence the work reported in this paper.

8. Acknowledgments

We gratefully acknowledge geologists Olga Veloso, Roberto Pincheira and José Barriá, for arranging permits and their assistance during field work at the El Toqui Mine (Compañía Minera Pacífico del Sur SpA), and geologists Valentina Maldonado, Benjamin Aldridge and Rayen Álvarez for their field support in the Aysén Region. We are grateful to Dr. Sonja Storm and Dr. Axel Schmitt for their guidance during microphotography as well as Francisco Cueto for IT-support and Joachim Fillauer for thin section-preparation (Universität Heidelberg, Germany). We further acknowledge the careful and detailed reviews of Dr. Christoph Breitzkreuz (Technische Universität Bergakademie Freiberg, Germany), Dr. Eduardo Olivero (Centro Austral de Investigaciones Científicas, Argentina), and Dr. Andrés Folguera (Editor-in-Chief, JSAMES), which have significantly improved this manuscript. Financial support to this project was provided by the Chilean National Fund for Scientific and Technological Development (FONDECYT de Iniciación 11140176), and by the Chilean National Agency for Research and Development (ANID/DOCTORADO BECAS CHILE/2016–72170384).

9. Appendix A. Supplementary data

Supplementary data to this article can be found online at <https://doi.org/10.1016/j.jsames.2021.103292>.

10. References

- Aigner, T., 1985. Storm Depositional Systems: Dynamic Stratigraphy in Modern and Ancient Shallow-Marine Sequences. Springer-Verlag, Heidelberg.
- Aguirre-Urreta, M.B., Ramos, V.A., 1981. Estratigrafía y Paleontología de la Alta Cuenca del río Roble, Cordillera Patagónica - provincia de Santa Cruz, in VIII Congr. Geol. Argentino, Actas, Buenos Aires, Argentina III, 101–133.
- Aguirre-Urreta, B., Rawson, P., 1998. The Early Cretaceous (Valanginian) ammonite *Chacantuceras* gen. nov. - a link between the Neuquén and Austral basins. *Rev. Asoc. Geol. Argent.* 53 (3), 354–364.
- Alfaro, G., Helle, S., Kelm, U., Palma, S., 1997. Las ocurrencias de carbón en las nacientes del río Chacabuco, Aysén, Chile. In: VIII Congr. Geol. Chileno, Actas, Universidad Católica del Norte, Antofagasta, Chile, I, pp. 420–424.
- Allen, J.R.L., 1982. Structures and sequences related to gravity-current surges. In: *Sedimentary Structures Their Character and Physical Basis*, vol. II. Elsevier, Developments in Sedimentology 30B, Amsterdam, pp. 395–432.
- Allen, S.R., Hayward, B.W., Mathews, E., 2007. A facies model for a submarine volcanoclastic apron: the Miocene Manukau Subgroup, New Zealand. *Geol. Soc. Am. Bull.* 119, 725–742.
- Alsop, G.I., Weinberger, R., Marco, S., Levi, T., 2019. Identifying soft-sediment deformation in rocks. *J. Struct. Geol.* 125, 248–255. <https://doi.org/10.1016/j.jsg.2017.09.001>.
- Batiza, R., White, J.D.L., 1999. Submarine lavas and hyaloclastite. In: Sigurdsson, H. (Ed.), *The Encyclopedia of Volcanoes*. Elsevier, pp. 361–382.
- Barberón, V., Ronda, G., Leal, P.R., Sue, C., Ghiglione, M.C., 2015. Lower Cretaceous provenance in the northern Austral basin of Patagonia from sedimentary petrography. *J. S. Am. Earth Sci.* 64, 498–510. <https://doi.org/10.1016/j.jsames.2015.08.014>.
- Barberón, V., Ronda, G., Aramendia, I., Suárez, R.J., Ramos, M.E., Naipauer, M., Sue, C., Ghiglione, M.C., 2019. Tectonic evolution of the northern Austral-Magallanes basin in the Southern Patagonian Andes from provenance analysis. *J. S. Am. Earth Sci.* 95, 102234. <https://doi.org/10.1016/j.jsames.2019.102234>.
- Bayne, B.L., 2017. *Biology of Oysters*, vol. 41. Academic Press-Elsevier, Developments in aquaculture and fisheries science, London, p. 844.
- Bell, C.M., Townsend, M.J., Suárez, M., De la Cruz, R., 1994. The depositional environments of the lower Cretaceous Coyhaique Group, Aysén Basin, southern Chile (45°–46°S). In: VII Congr. Geol. Chileno, Actas, Concepción, Chile, vol. I, pp. 402–403.
- Bell, C.M., De la Cruz, R., Suárez, M., Townsend, M.J., 1996. The evolution of the Aysén Basin, an early Cretaceous epicontinental interior seaway in the southernmost South America. In: *Géodynamique Andine: Résumés Étendus*. ORSTOM, Colloques et Séminaires, Paris, pp. 289–292. <http://www.documentation.ird.fr/hor/fdi:010008580>. (Accessed October 2019).
- Bell, C.M., Suárez, M., 1997. The lower Cretaceous Apeleg Formation of the Aisen basin, southern Chile. Tidal sandbar deposits of an epicontinental sea: *Andean Geol.* 24, 203–225. <https://doi.org/10.5027/andgeoV24n2-a05>.
- Bhattacharya, J., 2006. Deltas. In: Posamentier, H.W., Walker, R.G. (Eds.), *Facies Models Revisited*. SEPM, Tulsa, OK, pp. 237–292. <https://doi.org/10.2110/pec.06.84>.
- Blair, T.C., McPherson, J.G., 1999. Grain-size and textural classification of coarse sedimentary particles. *J. Sediment. Res.* 69, 6–19. <https://doi.org/10.2110/jsr.69.6>.
- Blake, S., Cortés, J.A., 2018. Forecasting deflation, intrusion and eruption in inflating volcanoes. *Earth Planet Sci. Lett.* 481, 246–254.
- Boulter, C.A., 1987. Subaqueous deposition of accretionary lapilli: significance for palaeoenvironmental interpretations in Archaean greenstone belts. *Precambrian Res.* 34 (3–4), 231–246.
- Bull, S.W., Cas, R.A.F., 1991. Depositional controls and characteristics of subaqueous bedded volcanoclastics of the lower Devonian Snowy River volcanics. *Sediment. Geol.* 74, 189–215.
- Bull, K.F., McPhie, J., 2007. Fiamme textures in volcanic successions: flaming issues of definition and interpretation. *J. Volcanol. Geoth. Res.* 164, 205–216.
- Burchette, T.P., Wright, V.P., 1992. Carbonate ramp depositional systems. *Sediment. Geol.* 79, 3–57. [https://doi.org/10.1016/0037-0738\(92\)90003-A](https://doi.org/10.1016/0037-0738(92)90003-A).
- Bussey, S.D., Kakarieka, A., Meinert, L.D., 2010a. Geology of the El Toqui Zn-Au skarn district, Aysén region, Chile. In: *Geol. Soc. Nevada 2010 Symposium: Great Basin Evolution and Metallogeny*, Nevada, USA, vol. 1. Geol. Soc. Nevada, pp. 179–199.
- Bussey, S.D., Kakarieka, A., Meinert, L.D., 2010b. Skarn, porphyry, vein, and replacement mineralization in the Toqui district, southern Chile. In: Goldfarb, R.J., Marsh, E.E., Monecke, T. (Eds.), *The Challenge of Finding New Mineral Resources: Global Metallogeny, Innovative Exploration, and New Discoveries*, Soc. Econ. Geol. Spec. vol. 15. Publ., Soc. Econ. Geol. Spec. Publ., pp. 399–420. <https://doi.org/10.5382/SP.15.2.04>.
- Campbell, C.V., 1967. Lamina, laminaset, bed and bedset. *Sedimentology* 8, 7–26. <https://doi.org/10.1111/j.1365-3091.1967.tb01301.x>.
- Cantelli, A., Johnson, S., White, J.D.L., Parker, G., 2008. Sediment sorting in the deposits of turbidity currents created by experimental modeling of explosive subaqueous eruptions. *J. Geol.* 116, 76–93. <https://doi.org/10.1086/524676>.
- Carey, S., Sigurdsson, H., 1984. A Model of Volcanogenic Sedimentation in Marginal Basins, vol. 16. Geological Society, London, Special Publications, pp. 37–58. <https://doi.org/10.1144/GSL.SP.1984.016.01.04>.

- Carey, S., 1999. Volcaniclastic sedimentation around island arcs. In: Sigurdsson, H. (Ed.), *The Encyclopedia of Volcanoes*. Elsevier, pp. 627–642.
- Cas, R.A.F., Wright, J.V., 1996. Volcanic Successions: Modern and Ancient. A Geological Approach to Processes, Products and Successions. Chapman & Hall, London, p. 528.
- Cattaneo, A., Steel, R.J., 2003. Transgressive deposits: a review of their variability. *Earth Sci. Rev.* 62, 187–228. [https://doi.org/10.1016/S0012-8252\(02\)00134-4](https://doi.org/10.1016/S0012-8252(02)00134-4).
- Catuneanu, O., 2002. Sequence stratigraphy of clastic systems: concepts, merits, and pitfalls. *J. Afr. Earth Sci.* 35, 1–43.
- Catuneanu, O., Abreu, V., Bhattacharya, J.P., Blum, M.D., Dalrymple, R.W., Eriksson, P. G., Fielding, C.R., Fisher, W.L., Galloway, W.E., Gibling, M.R., Giles, K.A., Holbrook, J.M., Jordan, R., Kendall, C.G.StC., Macurda, B., Martinsen, O.J., Miall, A. D., Neal, J.E., Nummedal, D., Pomar, L., Posamentier, H.W., Pratt, B.R., Sarg, J.F., Shanley, K.W., Steel, R.J., Strasser, A., Tucker, M.E., Winker, C., 2009. Towards the standardization of sequence stratigraphy. *Earth Sci. Rev.* 92, 1–33.
- Catuneanu, O., Galloway, W.E., Kendall, C.G.S.C., Miall, A.D., Posamentier, H.W., Strasser, A., Tucker, M.E., 2011. Sequence stratigraphy: Methodology and nomenclature. *Newsl. Stratigr.* 44 (3), 173–245.
- Catuneanu, O., 2017. Sequence stratigraphy: guidelines for a standard methodology. In: *Stratigraphy & Timescales*, vol. 2. Elsevier, pp. 1–57.
- Charrier, R., Covacevich, V., 1978. Paleogeografía y bioestratigrafía del Jurásico Superior y Neocomiano en el sector austral de los Andes Meridionales Chilenos (42°–56° latitud sur). In: II Congr. Argentino de Paleont. Estrat. y I Cong. Latinoam. Paleont., Actas, Buenos Aires, Argentina, vol. V, pp. 153–175.
- Ciccioli, P.L., Limarino, C.O., Isbell, J.L., Taboada, A.C., Pagani, M.A., Gulbranson, E.L., 2020. Interpreting detrital modes and geochemistry of sandstones from the late Paleozoic Tepuel-Genoa Basin: paleogeographic implications (Patagonia, Argentina). *J. S. Am. Earth Sci.* 104, 102858.
- Cohen, K.M., Finney, S.C., Gibbard, P.L., Fan, J.-X., 2013. The ICS International Chronostratigraphic Chart: Episodes 36, 199–204. <https://doi.org/10.18814/epiugs/2013/v36i3/002>.
- Collinson, J.D., Mountney, N.P., Thompson, D.B., 2006. Structures created by deformation and disturbance. In: *Sedimentary Structures*, Harpenden, Terra, Classic Geology in Europe, vol. 13, pp. 182–242.
- Covacevich, V., De la Cruz, R., Suárez, M., 1994. Primer hallazgo de fauna del Berriasiano inferior (Neocomiano) en la Formación Ibáñez, región XI, Aisén, in VII Congr. Geol. Chileno, Actas, Concepción, Chile I, 425–429.
- DeGrandpre, K.G., Pesicek, J.D., Lu, Z., DeShon, H.R., Roman, D.C., 2019. High rates of inflation during a noneruptive episode of seismic unrest at Semisopochnoi Volcano, Alaska in 2014–2015. *G-cubed* 20 (12), 6163–6186.
- De la Cruz, R., Suárez, M., Demant, A., 1994. Facies volcánicas del Mesozoico de Aisén (sector noreste), 44°–47° lat. S., Chile (Formaciones Ibáñez y Divisadero). In: VII Congr. Geol. Chileno, Actas, Concepción, Chile, vol. I, pp. 27–31.
- De la Cruz, R., Suárez, M., Covacevich, V., Quiroz, D., 1996. Estratigrafía de la zona de Palena y Futaleufú (43°15'–43° 45' latitud S), X Región, Chile. In: XIII Congr. Geol. Argentino Y III Congr. Explor. Hidroc., Actas, Buenos Aires, Argentina, vol. I, pp. 417–424.
- De la Cruz, R., Suárez, M., Belmar, M., Quiroz, D., Bell, M., 2003. Geología del área Coihaique-Balmaceda, Región Aisén del General Carlos Ibáñez del Campo: SERNAGEOMIN, Carta Geológica de Chile. Serie Geología Básica 80, 40. Santiago, Chile.
- De la Cruz, R., Suárez, M., 2006. Geología del área Puerto Guadal-Puerto Sánchez, Región Aisén del General Carlos Ibáñez del Campo: SERNAGEOMIN, Carta Geológica de Chile. Serie Geología Básica 95, 58. Santiago, Chile.
- Demant, A., Suárez, M., Cruz, R. de la, Bruguié, O., 2010. Early cretaceous surtseyan volcanoes of the Baño Nuevo volcanic complex (Aysén Basin, eastern central Patagonian cordillera, Chile). *Geol. Acta* 8, 207–219. <https://doi.org/10.1344/105.000001530>.
- Dickinson, W.R., 1970. Interpreting detrital modes of graywacke and arkose. *J. Sediment. Res.* 40, 695–707. <https://doi.org/10.1306/74D72018-2B21-11D7-8648000102C1865D>.
- Dorobek, S., 1995. Synorogenic carbonate platforms and reefs in foreland basins: controls on stratigraphic evolution and platform/reef morphology. In: Dorobek, S.L., Ross, G.M. (Eds.), *Stratigraphic Evolution of Foreland Basins*. SEPM (Society for Sedimentary Geology).
- Dorobek, S., 2008a. Tectonic and depositional controls on syn-rift carbonate platform sedimentation. In: Lukaski, J., Simo, J.A., Toni (Eds.), *Controls on Carbonate Platform and Reef Development*, vol. 89. SEPM, SEPM Special Publication, Tulsa, OK, pp. 57–81. <https://doi.org/10.2110/pec.08.89>.
- Dorobek, S.L., 2008b. Carbonate-platform facies in volcanic-arc settings: characteristics and controls on deposition and stratigraphic development. In: *Special Paper 436: Formation and Applications of the Sedimentary Record in Arc Collision Zones*, vol. 436. Geological Society of America, pp. 55–90.
- Dumas, S., Arnott, R.W.C., 2006. Origin of hummocky and swaley cross-stratification—the controlling influence of unidirectional current strength and aggradation rate. *Geology* 34 (12), 1073–1076.
- Echaurren, A., Folguera, A., Gianni, G., Orts, D., Tassara, A., Encinas, A., Giménez, M., Valencia, V., 2016. Tectonic evolution of the North Patagonian Andes (41°–44° S) through recognition of syntectonic strata. *Tectonophysics* 677–678, 99–114. <https://doi.org/10.1016/j.tecto.2016.04.009>.
- Echaurren, A., Oliveros, V., Folguera, A., Ibarra, F., Creixell, C., Lucassen, F., 2017. Early Andean tectonomagmatic stages in north Patagonia: insights from field and geochemical data. *J. Geol. Soc.* 174, 405–421. <https://doi.org/10.1144/jgs2016-087>.
- Emery, D., Myers, K. (Eds.), 1996. *Sequence Stratigraphy*. Blackwell Science, Oxford, p. 297.
- Ferrari, M., Bessone, S., 2015. Una nueva localidad marina de edad jurásica temprana en la cuenca sudoccidental del Chubut, Argentina. *Andgeo* 42, 349–363.
- Fisher, R.V., 1961. Proposed classification of volcaniclastic sediments and rocks. *Geol. Soc. Am. Bull.* 72, 1409.
- Fisher, R.V., 1966. Rocks composed of volcanic fragments and their classification. *Earth Sci. Rev.* 1, 287–298.
- Fisher, R.V., 1984. *Submarine Volcaniclastic Rocks*, vol. 16. Geological Society, London, Special Publications, pp. 5–27. <https://doi.org/10.1144/GSL.SP.1984.016.01.02>.
- Fisher, R.V., Schmincke, H.-U., 1984. *Pyroclastic Rocks*. Springer, Berlin, p. 472. <https://doi.org/10.1007/978-3-642-74864-6>.
- Fisher, R.V., Schmincke, H.-U., 1994. Volcaniclastic sediment transport and deposition. In: Pye, K. (Ed.), *Sediment Transport and Depositional Processes*. Blackwell Scientific Publications, Oxford, pp. 351–388.
- Flügel, E., 2004. *Microfacies of Carbonate Rocks*. Springer, Berlin, p. 976. <https://doi.org/10.1007/978-3-642-03796-2>.
- Folguera, A., Iannizzotto, N.F., 2004. The lagos La Plata and Fontana fold-and-thrust belt: long-lived orogenesis at the edge of western Patagonia. *J. S. Am. Earth Sci.* 16, 541–566. <https://doi.org/10.1016/j.jsames.2003.10.001>.
- Folk, R.L., Andrews, P.B., Lewis, D.W., 1970. Detrital sedimentary rock classification and nomenclature for use in New Zealand. *N. Z. J. Geol. Geophys.* 13, 937–968.
- Giacosia, R.E., Franchi, M., Genini, A., Panza, J., 2001. Hojas geológicas 4772-III lago belgrano y 4772-IV lago posadas. Provincia de Santa Cruz. Instituto de Geología y Recursos Minerales, Servicio Geológico Minero Argentino: Buenos Aires, SEGEMAR Boletín 256, 68.
- Gianni, G.M., Dávila, F.M., Echaurren, A., Fennell, L., Tobal, J., Navarrete, C., Quezada, P., Folguera, A., Giménez, M., 2018. A geodynamic model linking Cretaceous orogeny, arc migration, foreland dynamic subsidence and marine incision in southern South America. *Earth Sci. Rev.* 185, 437–462. <https://doi.org/10.1016/j.earscirev.2018.06.016>.
- Gianni, G.M., Navarrete, C., Echaurren, A., Díaz, M., Butler, K.L., Horton, B.K., Encinas, A., Folguera, A., 2019. Northward propagation of andean genesis: insights from early cretaceous synorogenic deposits in the Aysén-rio Mayo Basin. *Gondwana Res.* 77, 238–259. <https://doi.org/10.1016/j.gr.2019.07.014>.
- Gonzalez-Bonorino, G., Suárez, M., 1995. Paleoaambientes sedimentarios de la Formación Apele, Cretácico Inferior de la Cuenca de Aisén, región XI, Chile. *Andean Geol.* 22, 115–126. <https://doi.org/10.5027/andgeoV22n1-a07>.
- Haller, M.J., Lapido, O.R., 1980. El mesozoico de la Cordillera patagónica central. *Rev. Asoc. Geol. Argent.* XXXV, 230–247.
- Haller, M.J., Lapido, O.R., Lizuain, A., Page, R., 1981. El mar tithono-neocomiano en la evolución de la Cordillera Norpatagónica. In: *Cuencas Sedimentarias del Jurásico y Cretácico de América del Sur*, Com. Sudam. Jura. Cretac., vol. 1, pp. 221–237.
- Haq, B.U., 2014. Cretaceous eustasy revisited. *Global Planet. Change* 113, 44–58. <https://doi.org/10.1016/j.gloplacha.2013.12.007>.
- Haq, B.U., 2018. Jurassic sea-level variations: a reappraisal. *GSA Today (Geol. Soc. Am.)* 4–10. <https://doi.org/10.1130/GSATG359A.1>.
- Hechem, J., Figari, E., Homoc, J., 1993. Secuencias deposicionales en el Neocomiano del lago Fontana, Chubut, Argentina, in XII Congr. Geol. Argentino y II Congr. Explor. Hidroc., Actas, Mendoza, Argentina II, 119–123.
- Heiken, G.H., 1971. Tuff rings: examples from the fort rock-christmas lake valley basin, south-central Oregon. *J. Geophys. Res.* 76, 5615–5626. <https://doi.org/10.1029/JB070i023p05615>.
- Hervé, F., Pankhurst, R.J., Fanning, C.M., Calderón, M., Yaxley, G.M., 2007. The South Patagonian batholith: 150 my of granite magmatism on a plate margin. *Lithos* 97, 373–394. <https://doi.org/10.1016/j.lithos.2007.01.007>.
- Holmes, A., 1965. *Principles of Physical Geology*. Nelson, London, p. 1288.
- Housego, R.M., Rosman, J.H., 2016. A model for understanding the effects of sediment dynamics on oyster reef development. *Estuar. Coast* 39, 495–509. <https://doi.org/10.1007/s12237-015-9998-3>.
- Iannizzotto, N.F., Folguera, A., Leal, P.R., Iaffa, D., 2004. Control tectónico de las secuencias volcánicas neocomianas y paleogeografía en la zona del Lago La Plata (45°S). Sector interno de la faja plegada y corrida de los lagos La Plata y Fontana: *Rev. Asoc. Geol. Argent.* 59, 655–670.
- Ingersoll, R., Bullard, T., Ford, R., Grimm, J., Pickle, J., Sares, S., 1984. The effect of grain size on detrital modes: a test of the gazzi-dickinson point-counting method. *SEPM Journal of Sedimentary Research* 54, 103–116.
- Ippolito, A.P., Vinn, O., Kupriyana, E.K., 2014. Written in stone: history of serpulid polychaetes through time. *Mem. Mus. Vic.* 71, 123–159. <https://doi.org/10.24199/jmmv.2014.71.12>.
- Jones, B., 2010. Warm-water neritic carbonates. In: James, N.P., Dalrymple, R.W. (Eds.), *Facies Models* 4, 4. Version. Geol. Assoc. of Canada, St. Johns, pp. 449–476.
- Kataoka, K., Nakajo, T., 2004. Flow transformation and depositional organization of debris flow-hyperconcentrated flow-streamflow spectrum in volcanic fan-delta setting the Pleistocene Lower and Middle Formations, Yachiho Group, central Japan. *Journal of the Sedimentological Society of Japan* 59 (59), 17–26.
- Kakariekia, A., 2003. Exploración y descubrimiento del depósito de Zinc Estatuas, Distrito Toqui, Aysén - Chile. In: X Congr. Geol. Chileno. Actas, Concepción, Chile, p. 10.
- Kershaw, S., 1994. Classification and geological significance of biostromes. *Facies* 31, 81–91. <https://doi.org/10.1007/BF02536934>.
- Klement, K.W., 1967. Practical classification of reefs and banks. *Bioherms and Biostromes: AAPG (Am. Assoc. Pet. Geol.) Bull.* 51, 167–168.
- Kojima, S., Campos, E., 2011. An overview of Chilean economic deposits. *SGA News* 10–17.
- Kusky, T.M., 2005. *Encyclopedia of Earth Science. Facts on File Inc*, New York, p. 529.
- LaBarbera, M., 1981. The ecology of mesozoic Gryphaea, Exogyra, and Ilymatogyra (Bivalvia: Mollusca) in a modern ocean. *Paleobiology* 7, 510–526.

- Leanza, H., 1981. Faunas de ammonites del Jurásico Superior y del Cretácico Inferior de América del Sur, con especial consideración de la Argentina, in *Cuencas sedimentarias del Jurásico y Cretácico de América del Sur*, Buenos Aires, Argentina, Com. Sudam. Jura. Cretac. 2, 559–597.
- Lizuaín, A., Ragona, D., Folguera, A., 1995. Mapa Geológico de la provincia del Chubut, República Argentina: secr. Min. Dir. Nac. Serv. Geol. Geological.
- Lowe, D.R., 1982. Sediment gravity flows; II. Depositional models with special reference to the deposits of high-density turbidity currents. *J. Sediment. Res.* 52 (1), 279–297.
- Martins-Neto, M.A., Catuneanu, O., 2010. Rift sequence stratigraphy. *Mar. Petrol. Geol.* 27, 247–253. <https://doi.org/10.1016/j.marpetgeo.2009.08.001>.
- Masiuk, Nakayama, C., 1978. Sedimentitas marinas mesozoicas del lago Fontana, provincia del Chubut. Su importancia. In: VII Congreso Geológico Argentino, Actas, Buenos Aires, Argentina, II, pp. 361–378.
- McPhie, J., Doyle, M., Allen, R.L., 1993. Volcanic textures: a guide to the interpretation of textures in volcanic rocks: Hobart. Centre Ore Depos. Explor. Stud. Univ. Tasmania 198.
- Middleton, G.V., 1993. Sediment deposition from turbidity currents. *Annu. Rev. Earth Planet Sci.* 21, 89–114. <https://doi.org/10.1146/annurev.ea.21.050193.000513>.
- Mpodozis, C., Ramos, V.A., 2008. Tectónica jurásica en Argentina y Chile: extensión, subducción oblicua, rifting, deriva y colisiones? *Rev. Asoc. Geol. Argent.* 63, 481–497.
- Nakakuki, T., Mura, E., 2013. Dynamics of slab rollback and induced back-arc basin formation. *Earth Planet Sci. Lett.* 361, 287–297.
- Nemec, W., 1990. Deltas—remarks on terminology and classification. In: Colella, A., Prior, D.B. (Eds.), *Coarse-Grained Deltas*. Wiley-Blackwell, Oxford, pp. 1–12. <https://doi.org/10.1002/9781444303858.ch1>.
- Newman, A.V., Stiros, S., Feng, L., Psimoulis, P., Moschas, F., Saltogianni, V., Jiang, Y., Papazachos, C., Panagiotopoulos, D., Karagianni, E., Vamvakaris, D., 2012. Recent geodetic unrest at Santorini caldera, Greece. *Geophys. Res. Lett.* 39 (6).
- Niemeyer, H., Skarmeta, J., Fuenzalida, R., Espinosa, W., 1985. Hojas Peninsula Taitao y Puerto Aisén, Región Aisén del General Carlos Ibáñez del Campo. SERNAGEOMIN, Santiago, Chile, p. 80.
- O'Brien, N.R., Slatt, R.M., 1990. *Argillaceous Rock Atlas*. Springer-Verlag, New York, p. 141.
- Olivero, E., 1982. Estratigrafía de la cuenca sur del Lago Fontana, Provincia del Chubut (PhD Thesis). Universidad de Buenos Aires, Buenos Aires, Argentina, p. 208. Retrieved from: http://hdl.handle.net/20.500.12110/tesis_n1722_Olivero.
- Olivero, E.B., 1983. Amonoideos y bivalvos berriasianos de la cantera Tres Lagunas. *Chubut: Ameghiniana* 20, 11–20.
- Olivero, E., 1987. Cefalópodos y bivalvos titonianos y hauerivianos de la Formación Lago La Plata. *Chubut: Ameghiniana* 24, 181–202.
- Olivero, E., Aguirre-Urreta, M.B., 2002. Sucesión de amonoideos de la Formación Katterfeld (Valanginiano-Hauteriviano) en su área tipo, Lago Fontana, Chubut. In: XV Congr. Geol. Argentino. Actas, El Calafate, Argentina, p. 6.
- Pankhurst, R.J., Weaver, S.D., Hervé, F., Larrondo, P., 1999. Mesozoico-cenozoico evolution of the North Patagonian Batholith in Aysén, southern Chile. *J. Geol. Soc.* 156, 673–694. <https://doi.org/10.1144/gsjgs.156.4.0673>.
- Pankhurst, R.J., Riley, T.R., Fanning, C.M., Kelley, S.P., 2000. Episodic silicic volcanism in Patagonia and the Antarctic Peninsula: chronology of magmatism associated with the break-up of Gondwana. *J. Petrol.* 41 (5), 605–625.
- Pankhurst, R., Hervé, F., Fanning, M., Suárez, M., 2003. Coeval plutonic and volcanic activity in the patagonian andes: the patagonian batholith and the Ibáñez and Divisadero formations, Aysén, southern Chile. In: X Congr. Geol. Chileno, Actas, Concepción, Chile, p. 5.
- Pickering, K.T., Hiscott, R.N., 2016. Deep-marine Systems: Processes, Deposits, Environments, Tectonics and Sedimentation. John Wiley & Sons Inc, Chichester, West Sussex ; Hoboken, NJ, p. 657.
- Ploszkiewicz, J.V., Ramos, V.A., 1977. Estratigrafía y tectónica de la Sierra de Payaniyeu (Provincia del Chubut). *Rev. Asoc. Geol. Argent.* XXXII, 209–226.
- Ploszkiewicz, J.V., 1987. Descripción Geológica de la Hoja 47 c - "Apeleg", Provincia del Chubut: Carta Geológico-económica de la República Argentina, Escala 1:200.000. SEGEMAR Boletín, p. 100.
- Postma, G., 1986. Classification for sediment gravity-flow deposits based on flow conditions during sedimentation. *Geology* 14, 291–294.
- Postma, G., 1990. Depositional architecture and facies of river and fan deltas: a synthesis. In: Colella, A., Prior, D.B. (Eds.), *Coarse-grained Deltas*, pp. 13–27. Blackwell Oxford.
- Potter, P.E., Maynard, J.B., Depetris, P.J., 2005. Mud and mudstones: Muddy depositional systems. Springer, Berlin, p. 297.
- Quiroz, D., Bruce, Z., 2010. Geología del Área Puerto Ingeniero Ibáñez-Villa Cerro Castillo, Región Aisén del General Carlos Ibáñez del Campo: Santiago, Chile, SERNAGEOMIN, Carta Geológica de Chile. Serie Geología Básica 124, 48.
- Ramallo, R.S., Quartau, R., Trenhaile, A.S., Mitchell, N.C., Woodroffe, C.D., Ávila, S.P., 2013. Coastal evolution on volcanic oceanic islands: a complex interplay between volcanism, erosion, sedimentation, sea-level change and biogenic production. *Earth Sci. Rev.* 127, 140–170. <https://doi.org/10.1016/j.earscirev.2013.10.007>.
- Ramos, M.E., Suárez, R., Boixart, G., Ghiglione, M., Ramos, V.A., 2019. The structure of the northern Austral Basin: tectonic inversion of mesozoic normal faults. *J. S. Am. Earth Sci.* 94, 102197. <https://doi.org/10.1016/j.jsames.2019.05.013>.
- Ramos, V.A., 1976. Estratigrafía de los lagos La Plata y Fontana, Provincia del Chubut, República Argentina, in I Congr. Geol. Chileno, Actas, Santiago, Chile 1, 43–64.
- Ramos, V.A., 1979. Tectónica de la región del río y lago belgrano, Cordillera Patagónica - Argentina, in II Congr. Geol. Chileno, Actas, Arica, Chile B1–B32.
- Ramos, V.A., 1981. Descripción Geológica de la Hoja 47 ab - "Lago Fontana", Provincia del Chubut: carta Geológico-económica de la República Argentina, Escala 1:200.000. SEGEMAR Boletín 183, 135.
- Reading, H.G., 1996. *Sedimentary Environments: Processes, Facies and Stratigraphy*, third ed. Blackwell, Oxford, p. 689.
- Riccardi, A., 1988. The cretaceous system of southern South America. *Geol. Soc. Am. Mem., Geological Society of America Memoirs* 168, 161. <https://doi.org/10.1130/MEM168>.
- Rolando, A., Hartmann, L., Santos, J., Fernández, R., Etcheverry, R., Schlamuk, I., McNaughton, N., 2004. SHRIMP U-Pb zircon dates from igneous rocks from the Fontana Lake region, Patagonia: implications for the age of magmatism, Mesozoic geological evolution and age of basement. *Rev. Asoc. Geol. Argent.* 59, 671–684.
- Rubilar, A.E., 2003. Nuevos estudios acerca de las ostras del Cretácico Inferior de Chile. In: X Congr. Geol. Chileno, Actas, Concepción, Chile, p. 10.
- Scasso, R.A., 1987. Estratigrafía y ambientes de sedimentación del ciclo sedimentario del Jurásico Superior y Cretácico Inferior de la región sudoccidental del Chubut, con referencias a la columna estratigráfica general del área (PhD Thesis). Universidad de Buenos Aires, Buenos Aires, Argentina, p. 345.
- Scasso, R.A., 1989. La Cuenca Sedimentaria del Jurásico Superior y Cretácico Inferior de la Región Sudoccidental del Chubut. In: Chebli, G.A., Spalletti, L.A. (Eds.), *Cuencas Sedimentarias Argentinas*, pp. 395–417.
- Scheibner, C., Reijmer, J.G., 1999. Facies patterns within a Lower Jurassic upper slope to inner platform transect (Jbel Bou Dahar, Morocco). *Facies* 41 (1), 55–80.
- Schmidt, R., Schmincke, H.-U., 2002. From seamount to oceanic island, Porto Santo, central East-Atlantic. *Int. J. Earth Sci.* 91, 594–614.
- Schneider, J.-L., 2000. Volcaniclastic sedimentation in submarine settings: products and processes. In: Leyrit, H., Bordet, P., Montenat, C. (Eds.), *Volcaniclastic Rocks, from Magmas to Sediments*. Gordon and Breach Science Publishers, Amsterdam, pp. 175–192.
- Scholle, P.A., Ulmer-Scholle, D.S., 2003. A Colour Guide to the Petrography of Carbonate Rocks: Grains, Textures, Porosity, Diagenesis. American Association of Petroleum Geologists, Tulsa, Oklahoma, U.S.A., p. 459.
- Servicio Nacional de Geología y Minería, 2003. Mapa Geológico de Chile: Versión digital. SERNAGEOMIN Publicación Geológica Digital Geological.
- Shanmugam, G., 1996. High-density turbidity currents: are they sandy debris flows? *J. Sediment. Res.* 66 (1), 2–10.
- Shanmugam, G., 1997. The Bouma Sequence and the turbidite mind set. *Earth Sci. Rev.* 42, 201–229. [https://doi.org/10.1016/S0012-8252\(97\)81858-2](https://doi.org/10.1016/S0012-8252(97)81858-2).
- Shanmugam, G., 2012. New Perspectives on Deep-Water Sandstones: Origin, Recognition, Initiation, and Reservoir Quality. Handbook of Petroleum Exploration and Production, vol. 9. Elsevier, Amsterdam, p. 488.
- Shanmugam, G., 2016. Slides, Slumps, Debris Flows, Turbidity Currents, and Bottom Currents. Reference Module in Earth Systems and Environmental Sciences. Elsevier, p. 87.
- Skarmeta, J., 1976. Evolución tectónica y paleogeográfica de los Andes Patagónicos de Aisén (Chile), durante el Neocomiano. In: I Congr. Geol. Chileno, Actas, Santiago, Chile, B, pp. 1–15.
- Stenzel, H.B., 1971. Oysters. In: Moore, R.C. (Ed.), *Treatise in Invertebrate Paleontology*, Part N, Volumen 3, Mollusca 6 (Bivalvia), vol. 3. Geological Society of America; University of Kansas, pp. N953–N1224.
- Suárez, M., De la Cruz, R., 1994. Estratigrafía y paleogeografía mesozoica de Aisén Nororiental. In: VII Congr. Geol. Chileno, Actas, Concepción, Chile, I, pp. 538–542.
- Suárez, M., De la Cruz, R., Bell, C.M., 1996. Estratigrafía de la región de Coyhaique (latitud 45°–46° S), Cordillera Patagónica, Chile. In: XIII Congr. Geol. Argentino Y III Congr. Explor. Hidroc., Actas, vol. I, pp. 575–590.
- Suárez, M., De la Cruz, R., 2001. Jurassic to Miocene K–Ar dates from eastern central Patagonian Cordillera plutons, Chile (45°–48° S). *Geol. Mag.* 138, 53–66. <https://doi.org/10.1017/S0016756801004903>.
- Suárez, M., De la Cruz, R., Aguirre-Urreta, M.B., Fanning, M., 2005. Diachronic titonian-valanginian marine transgression of the Coyhaique Group, Aysén Basin (43°–47°S), Chile. In: XVI Congr. Geol. Argentino, Actas, La Plata, Argentina, vol. I, pp. 305–308.
- Suárez, M., De la Cruz, R., Bell, C.M., 2007. Geología del área Ñireguao-Baño Nuevo, Región Aisén del General Carlos Ibáñez del Campo: Santiago, Chile, SERNAGEOMIN, Carta Geológica de Chile. Serie Geología Básica 108, 56.
- Suárez, M., De la Cruz, R., Aguirre-Urreta, B., Fanning, M., 2009. Relationship between volcanism and marine sedimentation in northern Austral (Aisén) Basin, central Patagonia: stratigraphic, U–Pb SHRIMP and paleontologic evidence. *J. S. Am. Earth Sci.* 27, 309–325. <https://doi.org/10.1016/j.jsames.2008.11.009>.
- Suárez, M., De la Cruz, R., Bell, M., Demant, A., 2010a. Cretaceous slab segmentation in southwestern Gondwana. *Geol. Mag.* 147, 193–205. <https://doi.org/10.1017/S0016756809990355>.
- Suárez, M., Demant, A., Cruz, R.D.L., Fanning, C.M., 2010b. 40Ar/39Ar and U–Pb SHRIMP dating of aptian tuff cones in the aysén basin, central patagonian cordillera. *J. S. Am. Earth Sci.* 29, 731–737. <https://doi.org/10.1016/j.jsames.2009.11.003>.
- Suárez, M., De la Cruz, R., Etchart, H., Marcelo, M., Mark, F., 2015. Síntesis de la cronología magnética Meso-Cenozoica de Patagonia Central, Aysén, Chile: edades U–Pb SHRIMP, in XIV Congr. Geol. Chileno, Actas, La Serena, Chile 789–792.
- Suárez, M., De la Cruz, R., Fanning, M., Novas, F., Salgado, L., 2016. Tithonian age of dinosaur fossils in central Patagonia, Chile: U–Pb SHRIMP geochronology. *Int. J. Earth Sci.* 105, 2273–2284. <https://doi.org/10.1007/s00531-015-1287-7>.
- Suter, J.R., 2006. Facies models revisited: elastic shelves. SEPM special publications. In: Posamentier, H.W., Walker, R.G. (Eds.), *SEPM, Tulsa, OK*, vol. 84, pp. 339–398.
- Talling, P.J., Masson, D.G., Sumner, E.J., Malgesini, G., 2012. Subaqueous sediment density flows: depositional processes and deposit types. *Sedimentology* 59, 1937–2003. <https://doi.org/10.1111/j.1365-3091.2012.01353.x>.
- Tarney, J., Windley, B.F., 1981. Marginal basins through geological time. *Philosophical Transactions of the Royal Society of London. Series A, Mathematical and Physical Sciences* 301 (1461), 217–232.

- The North American Commission on Stratigraphic Nomenclature, 2005. North American stratigraphic Code. *Am. Assoc. Petrol. Geol. Bull.* 89, 1547–1591.
- Thomas, C.R., 1949. Geology and Petroleum Exploration in Magallanes Province, Chile, vol. 33. *AAPG Bulletin*, pp. 1553–1578. <https://doi.org/10.1306/3D933DEE-16B1-11D7-8645000102C1865D>.
- Townsend, M.J., 1998. The Palaeogeography of the Lower Cretaceous Aysén Basin of Southern Chile (PhD Thesis). University of Bristol, Bristol, UK, p. 243.
- Tucker, M.E., Calvet, F., Hunt, D., 1993. Sequence stratigraphy of carbonate ramps: systems tracts, models and application to the muschelkalk carbonate platforms of eastern Spain. In: Posamentier, H.W., Summerhayes, C.P., Haq, B.U., Allen, G.P. (Eds.), *Sequence Stratigraphy and Facies Associations*. Blackwell Publishing Ltd., Oxford, UK, pp. 397–415.
- Uliana, M.A., Biddle, K.T., Cerdan, J., 1989. Mesozoic extension and the formation of Argentine sedimentary basins. In: Tankard, A.J., Balkwill, H.R. (Eds.), *Extensional Tectonics and Stratigraphy of the North Atlantic Margins*, vol. 46. AAPG, AAPG Mem, Tulsa, OK, pp. 599–614.
- Van Wagoner, J.C., Posamentier, H.W., Mitchum, R.M.J., Vail, P.R., Sarg, J.F., Loutit, T. S., Hardenbol, J., 1988. An overview of the fundamentals of sequence stratigraphy and key definitions. In: Wilgus, C.K., Hastings, B.S., Posamentier, H., van wagoner, J., Ross, C.A., Kendall, C.G. (Eds.), *Sea-Level Changes: an Integrated Approach*, SEPM Special Publications. SEPM, Tulsa, OK, p. 42.
- Walker, G.P.L., 1981. Generation and dispersal of fine ash and dust by volcanic eruptions. *J. Volcanol. Geoth. Res.* 11, 81–92. [https://doi.org/10.1016/0377-0273\(81\)90077-9](https://doi.org/10.1016/0377-0273(81)90077-9).
- Welkner, D., Suárez, M., Quiroz, D., 2004. Geología del Área Oriental de las Hojas Cochrane y Villa O'Higgins, Región Aisén del General Carlos Ibáñez del Campo: Santiago, Chile, SERNAGEOMIN, Carta Geológica de Chile. Serie Geología Básica 85, 57.
- Wellmer, F.W., Reeve, E.J., Wentzlau, E., Westenberger, H., 1983. Geology and ore deposits of the Toqui district, Aysén, Chile. *Econ. Geol.* 78, 1119–1143. <https://doi.org/10.2113/gsecongeo.78.6.1119>.
- White, N., McKenzie, D., 1988. Formation of the steer's head geometry of sedimentary basins by differential stretching of the crust and mantle. *Geology* 16, 250–253.
- White, J.D., 2000. Subaqueous eruption-fed density currents and their deposits. *Precambrian Res.* 101 (2–4), 87–109.
- Wright, V.P., 1992. A revised classification of limestones. *Sediment. Geol.* 76, 177–185. [https://doi.org/10.1016/0037-0738\(92\)90082-3](https://doi.org/10.1016/0037-0738(92)90082-3).

Facies and sequence stratigraphy of a mixed carbonate-volcaniclastic ramp in intra-arc settings: An example from the Toqui Formation (Lower Cretaceous), southern Chile (45°S)

Authors: Rivas, H.; Salazar, C.; Stinnesbeck, W.

Published in: Journal of South American Earth Sciences (Elsevier)

Year: 2021

Supplementary Material

S.1 Sedimentary Provenance

The microfacies analysis of six sandstones samples from the El Toqui Mine area (CVF x 1; UVF x 4; MVF x 1; Fig. 10 in manuscript) confirms the clear volcanic source of the clastic facies. Samples comprehend compositional immature sandstone, rich in volcanic lithics and feldspar minerals, with minor quartz, and some of them bear scarce remobilized bioclasts (Table S-1). Clasts are embedded in a fine-grained, devitrified or chloritized matrix, some rich in phyllosilicates interpreted as secondary matrix from pumice alteration. This secondary “illitic-smectitic matrix” is clearly formed after compacted pumice clasts (Fig. 4). Therefore, they are counted as “volcanic lithic” in the provenance representation (Table S-1; Fig. S-1).

According to the classic sandstone provenance models based on modal composition (e.g. Dickinson, 1970; Dickinson & Suczek, 1979; Dickinson *et al.*, 1983), most of the sample lie within the undissected to transitional magmatic arc source (Fig. S-1). However, an updated and more statistically reliable version of this diagram considers only three “fundamental” provenance areas, depicting a “magmatic arc” provenance for the samples of the Toqui Fm. (Weltje, 2006; Fig. S-1-B). Based on the high ash abundance (matrix), pumice-rich layers, and the presence of accretionary lapilli, a phreatomagmatic volcanism is inferred (Walker, 1981; Fisher & Schmincke, 1984; Fig. 8). Feldspar-enrichment was likely caused by the fragmentation of volcanic debris during transport or coastal reworking (Dickinson & Suczek, 1979).

Table S-1. (1.5-columns, black & white) Provenance Analysis. Normalized modal components point-counted for provenance analysis in sandstones from the Toqui Mine (sensu Ingersoll *et al.*, 1984). Q = quartz (m: mono-; p: polycrystalline); F = feldspars (P: plagioclase; K: alkali-feldspar); Lv=volcanic lithics; Lm = metamorphic lithics. Qt; F; Lt = total quartz, feldspar, lithics, respectively (Fig. 10). A graphic view and inferred provenance of these values is presented in Fig. 8. N = 400 grains per sample.

Modal Element	Grain	Sample					
		ELC_003	ESA_006	DCE_084	ASN_071	ASN_081	PDT_298
Lv	Andesitic volcanic lithic	63	32	79	42	90	77
	Felsic volcanic lithic	87	63	109	134	103	96
Lm	Metamorphic lithic	3	-	2	1	-	1
F	Plagioclase (P)	110	135	99	163	173	139
	Orthoclase (K)	14	-	15	3	-	8
	Sanidine (K)	5	1	3	-	-	1
Qt	Quartz - Monocrystalline (Qm)	78	14	61	49	34	63
	Quartz - Polycrystalline (Qp)	3	-	-	-	-	1
Matrix	Opaque mineral (Sulphides)	8	1	2	-	-	1
	Matrix, Illitic-Smectitic	24	146	21	1	-	3
	Matrix, Chlorite	-	1	7	7	-	10
Other	Carbonate grain; Bioclast	-	4	-	-	-	-
	White Mica	1	-	-	-	-	-
	Authigenic Mineral, Calcite	3	3	2	-	-	-
	Authigenic Mineral, Chalcedony	1	-	-	-	-	-

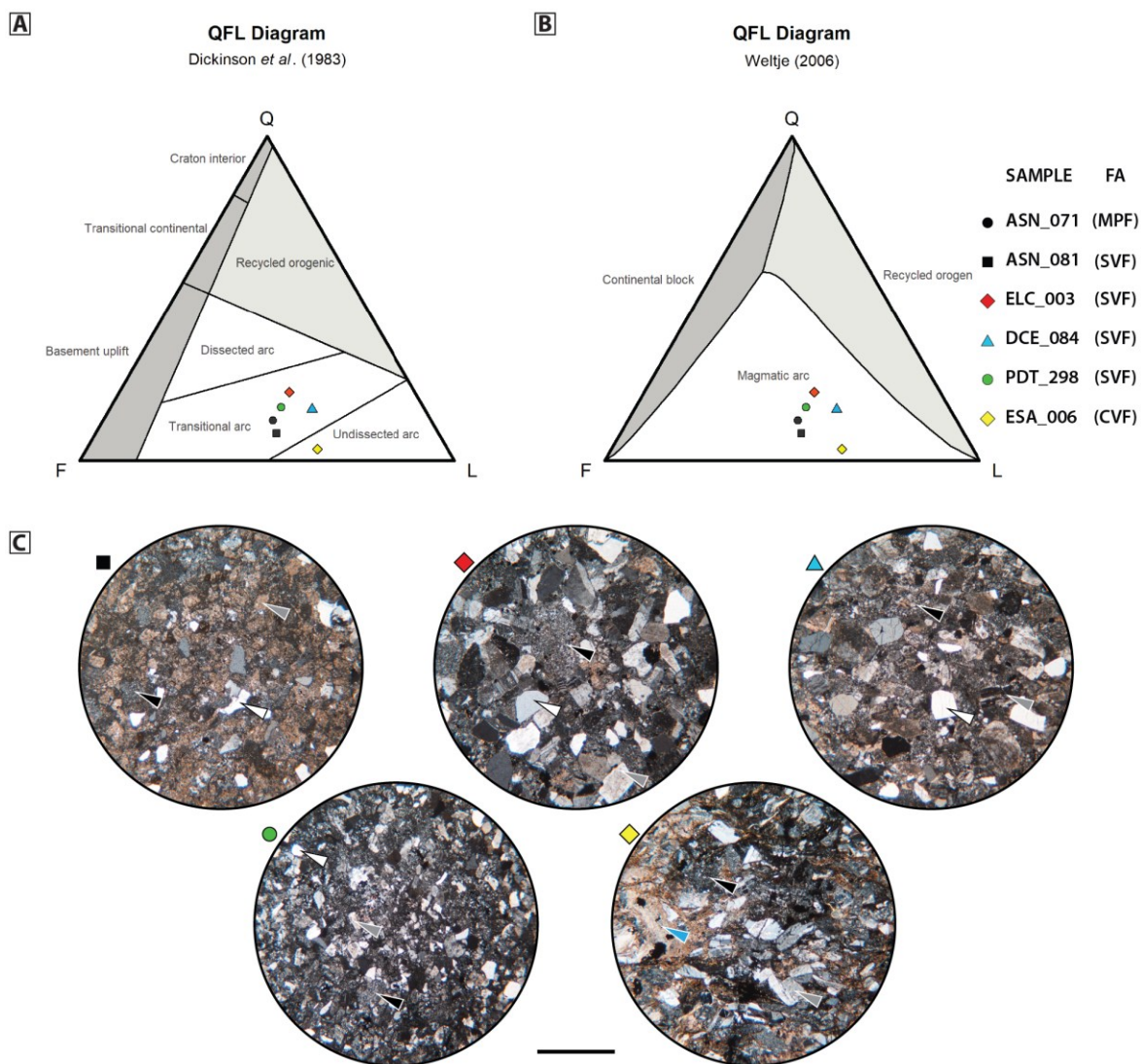


Figure S-1. (2-columns, colored) QFL provenance diagrams for the Toqui Formation arenites (Q = quartz, F = feldspar minerals, L = lithic fragments, total amounts (t), respectively). A) Model of Dickinson *et al.* (1983), displaying an undissected and transitional arc source. B) “Dickinson model” reviewed by Weltje (2006), supporting a magmatic arc source. Stratigraphic position of sandstone samples is presented in Fig. 10 (in manuscript). C) Crossed nicols microphotographs of volcaniclastic sandstone plotted in A, B). Arrows = white: quartz; grey: feldspar (sometimes sericitized); black: volcanic lithic; cyan: bioclast. Scale = 1.5 mm. Diagrams were plotted in R language, using the *ggtern* package (Hamilton & Ferry, 2018). Polygon vertices were obtained from Zahid & Barbeau (2011). FA: Facies Association (see Section 3 in main manuscript).

8.2 Scientific Publication Nr. 2:

A “cool-water”, non-tropical, mixed volcanoclastic–carbonate ramp from the Early Cretaceous of southern Chile (45°40’S)

Authors: Rivas, H.; Salazar, C.; Stinnesbeck, W.

Published in: *Facies* (Springer)

Year: 2023

Author contribution (CRediT)

Hermann Rivas: Software, Formal analysis, Investigation, Data curation, Writing—original draft, Writing—review and editing, Visualization.

Christian Salazar: Conceptualization, Methodology, Resources, Writing—review and editing, Supervision, Project administration, Funding acquisition.

Wolfgang Stinnesbeck: Resources, Writing—review and editing, Supervision, Project administration.

Citation: Rivas, H., Salazar, C. & Stinnesbeck, W. (2023). A “cool-water”, non-tropical, mixed volcanoclastic–carbonate ramp from the Early Cretaceous of southern Chile (45°40’S). *Facies* 69, 14. <https://doi.org/10.1007/s10347-023-00669-4>.

Formblatt Kumulative Dissertation

Stand 14.02.2023

1. Publikation/Publication:

Vollständige bibliographische Referenz/Complete bibliographic reference:

Rivas, H., Salazar, C., & Stinnesbeck, W. (2023). A "cool-water", non-tropical, mixed volcanoclastic-carbonate ramp from the Early Cretaceous of southern Chile (45° 40'S). *Facies*, 69(3), 14.**2. Erst- oder gleichberechtigte Autorenschaft/First or equal authorship:****Ja/Yes**

Nein/No

3. Veröffentlicht/Published

Zur Veröffentlichung akzeptiert/Accepted

Q1/Q2* 0.661

*SCImago Journal Rank (SJR) indicator

Ja/Yes ☒ Nein/No

Im Erscheinungsjahr oder im letzten verfügbaren Vorjahr/In the year of publication or the last prior year available: 2023

Eingereicht/Submitted

Noch nicht eingereicht/Not yet submitted

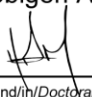
4. Beteiligungen/Contributions**

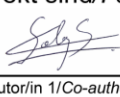
Contributor Role	Doktorand/in/ Doctoral student	Co-Autor/in 1/ Co-author 1	Co-Autor/in 2/ Co-author 2
Name, first name	Rivas, Hermann	Salazar, Christian	Stinnesbeck, Wolfgang
Methodology	<input type="checkbox"/>	<input checked="" type="checkbox"/>	<input type="checkbox"/>
Software	<input checked="" type="checkbox"/>	<input type="checkbox"/>	<input type="checkbox"/>
Validation	<input type="checkbox"/>	<input checked="" type="checkbox"/>	<input type="checkbox"/>
Formal analysis	<input checked="" type="checkbox"/>	<input type="checkbox"/>	<input type="checkbox"/>
Investigation	<input checked="" type="checkbox"/>	<input type="checkbox"/>	<input type="checkbox"/>
Resources	<input type="checkbox"/>	<input checked="" type="checkbox"/>	<input checked="" type="checkbox"/>
Data Curation	<input checked="" type="checkbox"/>	<input type="checkbox"/>	<input type="checkbox"/>
Writing-Original Draft	<input checked="" type="checkbox"/>	<input type="checkbox"/>	<input type="checkbox"/>
Writing-Review&Editing	<input checked="" type="checkbox"/>	<input checked="" type="checkbox"/>	<input checked="" type="checkbox"/>
Visualization	<input checked="" type="checkbox"/>	<input type="checkbox"/>	<input type="checkbox"/>
Supervision	<input type="checkbox"/>	<input checked="" type="checkbox"/>	<input checked="" type="checkbox"/>
Project administration	<input type="checkbox"/>	<input checked="" type="checkbox"/>	<input checked="" type="checkbox"/>
Funding acquisition	<input type="checkbox"/>	<input checked="" type="checkbox"/>	<input type="checkbox"/>

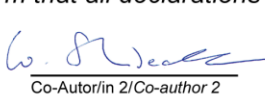
**Kategorien des CRediT (Contributor Roles Taxonomy, <https://credit.niso.org/>)

Hiermit bestätige ich, dass alle obigen Angaben korrekt sind/I confirm that all declarations made above are correct.

Unterschrift/Signature


 Doktorand/in/Doctoral student


 Co-Autor/in 1/Co-author 1


 Co-Autor/in 2/Co-author 2
Betreuungsperson/Supervisor:

Hiermit bestätige ich, dass alle obigen Angaben korrekt sind und dass die selbstständigen Arbeitsanteile des/der Doktoranden/in an der aufgeführten Publikation hinreichend und signifikant sind/I confirm that all declarations made above are correct and that the doctoral student's independent contribution to this publication is significant and sufficient to be considered for the cumulative dissertation.

 Wolfgang Stinnesbeck
 Name/Name


 Unterschrift/Signature

 20.03.2025
 Datum/Date



A “cool-water”, non-tropical, mixed volcanoclastic–carbonate ramp from the Early Cretaceous of southern Chile (45°40’S)

Hermann Rivas¹ · Christian Salazar² · Wolfgang Stinnesbeck¹

Received: 7 February 2022 / Accepted: 7 May 2023 / Published online: 16 June 2023

© The Author(s) 2023

Abstract

The Aysén-Río Mayo Basin was a back-arc/marginal basin developed in southwestern South America (43°–47°S) between the Tithonian–Aptian. Its sedimentary fill corresponds to the Coyhaique Group, which represents a transgressive–regressive succession. Six lithofacies and five microfacies were defined for three outcrops exposed south of Coyhaique (45°40’S). The outcrops have a mixed calcareous–volcanoclastic composition and were assigned to the early transgressive Toqui Formation, i.e., lowermost part of the Coyhaique Group. These mixed rocks comprise bioclastic–volcanoclastic conglomerate, gravelly allochemic sandstone, and gravelly–sandy allochem limestone. Bedding is sharp to amalgamated, sometimes rippled, depicting a wave- and storm-influenced, mixed inner- to mid-ramp. The ramp developed over a Valanginian, active volcanic terrain (Foitzick Volcanic Complex), source of the volcanoclastic sediments. Limestones are rich in reworked bioclasts, and controlled by calcitic organisms including gryphaeid oysters, non-geniculate red algae, and echinoid fragments, defining a heterozoan association (“maerl”-like sediments); less frequent are ahermatypic corals, serpulids, and carbonized wood. Based on their inferred paleolatitude (south of 45°–50°S), fossil assemblage (heterozoan), and kind of carbonate platform (ramp-type), these calcareous rocks of the Toqui Formation depict a “cool-water” (*sensu lato*), non-tropical setting. The fossil assemblage includes oysters (*Aetostreon* spp.), and abundant calcareous red algae attributed to *Archamphiroa jurassica* Steinmann (1930), a taxon previously known from the upper Tithonian Cotidiano Formation of Argentina. *A. jurassica* is here reported for the first time for the Lower Cretaceous of Chile, suggesting a broader upper Tithonian–Valanginian–Hauterivian? range for the species. The facies model presented here contrasts with the depositional environments depicted for correlative reefal rocks in Argentina (Tres Lagunas Formation), which reflect a “warm-water” setting. In the Aysén-Río Mayo Basin, the influence of sea-water key physical variables in the carbonate sedimentation, as well as the position and hydraulic regime of the carbonate platforms within the basin, and their interaction with the volcanism are still unclear.

Keywords Aysén-Río Mayo basin · Coyhaique Group · Toqui Formation · Marine transgression · *Archamphiroa jurassica* · *Aetostreon* sp

✉ Hermann Rivas
hermann.rivas@geow.uni-heidelberg.de

Christian Salazar
christian.salazar@umayor.cl

Wolfgang Stinnesbeck
wolfgang.stinnesbeck@geow.uni-heidelberg.de

¹ Institut für Geowissenschaften, Universität Heidelberg, Im Neuenheimer Feld 234, 69120 Heidelberg, Germany

² Escuela de Geología, Facultad de Ciencias, Universidad Mayor, Manuel Montt 367, 7500994 Providencia, Chile

Introduction

Mixed calcareous–volcanoclastic rocks are common constituents in the Late Jurassic–Early Cretaceous of southwestern South America (Central Patagonia, 43°–47°S); these deposits represent the early transgressive phase in the Aysén–Río Mayo Basin, whose marine stage developed during the Tithonian–Aptian (e.g., Aguirre-Urreta and Ramos 1981; Ramos 1981; Scasso 1987; 1989; Bell et al. 1996; Folguera and Iannizzotto 2004; Suárez et al. 2010a, b; Fig. 1A, B). In Chile, these mixed rocks are exposed as scattered outcrops in the Los Lagos and Aysén regions (De la Cruz et al. 1996; Welkner et al., 2004) and have been referred to as the Toqui Formation (Bell et al. 1994; Suárez and De la Cruz 1994a, b;

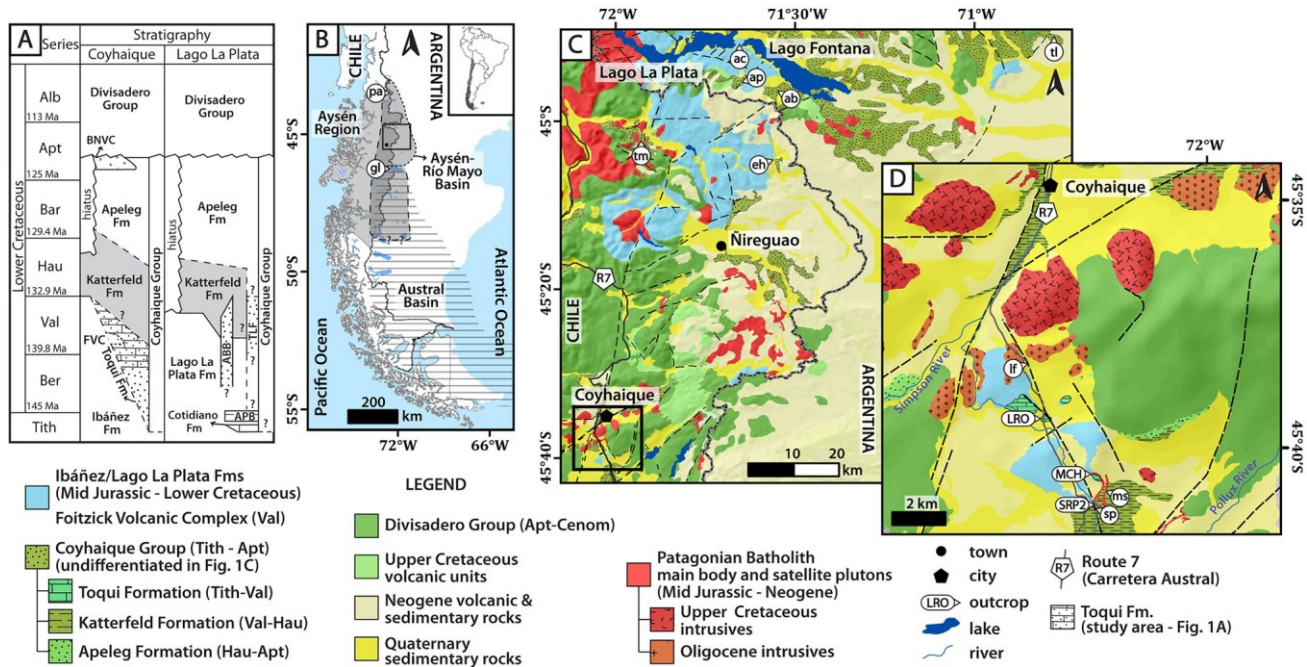


Fig. 1 Stratigraphy and location. **A** Regional chronostratigraphic chart (modified from Rivas et al. 2021). Some formational names have been abbreviated: *Fm* Formation, *APB* Arroyo Pedregoso Beds, *ABB* Arroyo Blanco Beds, *BNVC* Baño Nuevo Volcanic Complex, *FVC* Foitzick Volcanic Complex, *TLF* Tres Lagunas Formation (see “Stratigraphy and correlations”). **B** Regional map displaying the location of the Aysén-Río Mayo Basin, the Austral Basin, and localities mentioned in the text. Aysén-Río Mayo basin: dotted outline *sensu* Aguirre-Urreta and Ramos (1981); dashed outline *sensu* Suárez et al. (2010a); Austral Basin outline *sensu* Cuitiño et al. (2019). **C** Local geological map of the La Plata Lake and Coyhaique areas (simplified from Lizuáin et al. 1995; De la Cruz et al. 2003; Suárez et al. 2007).

Given the small areal exposures of the early transgressive, mixed- and calcareous rocks, all the formations are represented as part of the Coyhaique Group (undifferentiated). **D** Study area: Close-up of the area south of Coyhaique, displaying the outcrops studied here (modified from De la Cruz et al. 2003). *ab* Arroyo Blanco, *ac* Arroyo Cotidiano (type locality of the Cotidiano Fm.), *ap* Arroyo Pedregoso, *eh* Estero La Horqueta, *gl* General Carrera/Buenos Aires Lake, *pa* Palena (town), *R7* Route 7 (Carretera Austral), *tl* Tres Lagunas (Laguna Salada, type locality of the Tres Lagunas Fm.), *tm* El Toqui Mine (type locality of the Toqui Fm.). Outcrops here addressed: *MCH* Muralla China, *LRO* La Rosita, *SRP2* Salto Río Pollux

Fig. 1A, B). This unit comprises two members (*sensu* Rivas et al. 2021): the mixed, calcareous–volcaniclastic Manto Member conforming the basal portion of the Toqui Fm., and the volcaniclastic San Antonio Member which overlies and interfingers the Manto Member. Both members display marked lateral- and latitudinal facial changes, reflecting strong diachronism during the Tithonian–Valanginian interval (Suárez et al. 2005; 2010a, b), and the development of mixed, shallow-marine platforms over an irregular extensional topography (Scasso 1989; Hechem et al. 1993; Folguera and Iannizzotto 2004; Rivas et al. 2021).

In Argentina, the Toqui Formation has been correlated with coeval (Tithonian–Valanginian), calcareous and mixed units exposed in the area adjacent to the La Plata–Fontana lakes (e.g., Cotidiano and Tres Lagunas Formations; Sect. “Stratigraphy and correlations”; Fig. 1A). Overall, these mixed rocks represent transgressive deposits, depicted as settled in euhaline, shallow marine environments, and locally influenced by active volcanism (e.g., Ramos 1981; Płoszkiewicz and Ramos 1977; Olivero 1982; Scasso 1987;

1989; Bell et al. 1996; Suárez et al. 1996; De la Cruz et al. 2003; Scasso and Kiessling 2002; Iannizzotto et al. 2004).

Given the discrete, discontinuous, and diachronic exposure of these mixed calcareous–volcaniclastic units, they have been studied and interpreted separately (see review in Rivas et al. 2021; Fig. 1C), and several regional models for its sedimentation have been proposed (e.g., Skarmeta 1976; Aguirre-Urreta and Ramos 1981; Scasso 1989; Hechem et al. 1993; Bell et al. 1994; Townsend 1998; Folguera and Iannizzotto 2004; Suárez and De la Cruz 1994a, b). Here, a sedimentological and microfacial analysis is presented of three mixed volcaniclastic–calcareous sections, assigned to the Toqui Formation, and exposed south of Coyhaique in southern Chile (45°40'S; Fig. 1D). This study improves the understanding of the depositional environments of mixed rocks included in the Toqui Formation, and their relationship with the Argentinian exposures is also discussed. The outcrops presented here provide new insight into non-tropical or “cool-water” carbonate sedimentation as well as the development of carbonate ramps in volcanic arc settings.

Geological setting

The Aysén—Río Mayo Basin was a back-arc/marginal basin (see models without seafloor-spreading in Tarney et al. 1981; Artemieva 2023) formed at the southwestern margin of West Gondwana (proto-South America, ca. 43°–49°S) during the Late Jurassic and Early Cretaceous (Tithonian—Aptian, e.g., Aguirre-Urreta and Ramos 1981; Suárez et al. 2010a, b; Fig. 1B). Its onset is regarded as triggered by back-arc extension to the east of the coeval volcanic arc (Suárez et al. 2010a, b; Echaurren et al. 2016), which is represented by the Patagonian Batholith (Pankhurst et al. 1999; Suárez and De la Cruz 2001; Suárez et al. 2023; Fig. 1C). The basin developed unconformably over the basement, which consists of upper Paleozoic metamorphic and metasedimentary rocks as well as Lower Jurassic sedimentary units (e.g., Olivero 1982; Płoszkiewicz 1987; De la Cruz et al. 2003; Hervé et al. 2008; Fig. 1A).

The oldest units conforming the Aysén—Río Mayo basin fill, correspond to the Ibáñez Formation in Chile and the correlative Lago La Plata Formation in Argentina (e.g., Ramos 1976; Haller et al. 1981; Haller and Lapido 1982; De la Cruz et al. 1994; 2003; Fig. 1A). The Ibáñez Formation consists of calc-alkaline, subaerial- and minor submarine-settled, felsic volcanic- and volcanoclastic rocks, depicting the Late Jurassic–Early Cretaceous (Oxfordian?–early Hauterivian) extrusive counterpart of the Patagonian Batholith (Pankhurst et al. 2003; Suárez et al. 2005). These volcanic rocks syntectonically filled the extensional topography (Echaurren et al. 2016; Folguera and Iannizzotto 2004), whereas its uppermost strata underlie and interfinger with the shallow marine deposits of the Toqui Formation and correlative units (see Sect. “Stratigraphy and correlations” below), i.e., the lowermost part of the Coyhaique Group (e.g., Skarmeta 1976; Olivero 1982; Scasso 1989; Covacevich et al. 1994; Suárez et al. 2009; 2010a; Fig. 1A).

The Coyhaique Group is a transgressive–regressive succession of Tithonian–Aptian age (Ramos 1981; Scasso 1987; Covacevich et al. 1994; Bell et al. 1994; Suárez et al. 2010a; Suárez and De la Cruz 1994a, b), and linked to a back-arc “Pacific” marine incursion caused by tectonic-thermal subsidence (Skarmeta 1976; Haller and Lapido 1980; Aguirre-Urreta and Ramos 1981). In Chile, the Coyhaique Group includes three formations (Fig. 1A): (1) the Toqui Formation (Tithonian–Valanginian, Hauterivian?), corresponding to shallow-marine, mixed (calcareous–volcanoclastic) and tuffaceous rocks, deposited during the early transgression (De la Cruz et al. 1994; Suárez et al. 2009; Rivas et al. 2021); (2) the Katterfeld Formation (Valanginian–Barremian; Masiuk and Nakayama 1978; Aguirre-Urreta et al. 2000; Olivero and Aguirre-Urreta 2002; Kesjár et al. 2017) overlies the Toqui Fm. with a transitional or conformable contact and consists of tuffaceous and carbonaceous black mudstone,

settled in offshore environments during the post-rift stage (Scasso 1989; Suárez et al. 2007; 2010a); and 3) the Apeleg Formation (Hauterivian–Aptian) overlies the Katterfeld Formation with a gradational contact; it includes heterolithic, sandy, and gravelly facies, depicting tidal, and deltaic-paralic, regressive successions (e.g., Ramos 1981; Scasso 1989; Gonzalez-Bonorino and Suárez 1995; Bell and Suárez 1997; Fig. 1A).

The Aysén—Río Mayo Basin was inverted during the Aptian, linked to compression after a fast, westwards relative movement of the South American Plate (Suárez et al. 2010a, b; Gianni et al. 2019; Ramos et al. 2019). The latter reactivated the volcanic arc, resulting in local Surtseyan eruptions (Baño Nuevo Volcanic Complex; Demant et al. 2010; Suárez et al. 2010b; Fig. 1A), and the effusion of subaerial, intermediate, volcanic rocks of the Divisadero Group (Aptian–early Cenomanian). The Divisadero Group covers the underlying Coyhaique Group with a unconformable, but locally (para-)conformable contact (e.g., Aguirre-Urreta and Ramos 1981; Ramos 1981; De la Cruz et al. 1994; Suárez et al. 2010a; Fig. 1A).

Stratigraphy and correlations

In central Patagonia (43°–47°S), the early transgressive deposits of the Aysén—Río Mayo Basin (ARB) comprise a Tithonian – Hauterivian? range (e.g., Haller and Lapido 1980; Olivero 1983; 1987; Scasso 1989; Covacevich et al. 1994; Suárez et al. 2009), reflecting strong diachronism during the transgression (Suárez et al. 2005; Fig. 1A). The early transgressive rocks of the ARB have a mixed- and calcareous composition, and they depict shallow marine settings near volcanic centers (e.g., Ramos 1978; Suárez et al. 1996, 2009; Scasso and Kiessling 2002; Ramos and Lazo 2006; Rivas et al. 2021, and references therein).

In Argentina, these rocks have been treated as singular units (Fig. 1A), including: (i) the Cotidiano Formation (Oxfordian–Kimmeridgian *sensu* Ramos 1976; Ramos 1981; upper Tithonian *sensu* Olivero 1987; Bucur et al. 2009); (ii) the “Arroyo Pedregoso Beds” (upper Tithonian *sensu* Ramos 1981; Olivero 1982; 1987); (iii) the “Arroyo Blanco Beds” (Berriasian–Hauterivian *sensu* Olivero 1982; 1987; upper Valanginian *sensu* Olivero and Aguirre-Urreta 2002; Fig. 1A); and (iv) the Tres Lagunas Formation (at its type locality “Laguna Salada”, Valanginian–lower Hauterivian *sensu* Płoszkiewicz and Ramos 1977; Berriasian *sensu* Olivero 1983; Tithonian?–upper Valanginian *sensu* Scasso and Kiessling 2002; Fig. 1A).

The former three were regarded by Olivero (1987) as sedimentary alternations within the Lago la Plata Formation; this approach was followed by Covacevich et al. (1994) for some calcareous outcrops exposed north of the town of Ñireguao, including them within the Ibáñez Formation. In

the Chilean side, these mixed- and calcareous outcrops were later grouped together in the Toqui Formation (e.g., Bell et al. 1994; De la Cruz et al. 1996; 2003; Suárez and De la Cruz 1994a, b). The Toqui Formation was redefined by Rivas et al. (2021; after Bell et al. 1994; Suárez et al. 1996; Suárez and De la Cruz 1994a, b), as conformed by two members: the mixed calcareous–volcaniclastic Manto Member, interbedded and overlaid by the volcaniclastic San Antonio Member. In the area south of Coyhaique (45°35'S; Fig. 1D), these members appear discretely as mixed, either calcareous- or volcaniclastic-rich outcrops, depicting an upper Berriasian/lower Valanginian – Hauterivian? range (see “Age of the deposits”).

Age of the deposits

In the study area, the age of the Toqui Formation is interpreted to be late Berriasian/early Valanginian-Hauterivian? South of “Laguna Foitzick”, a late Berriasian age is based on a faunal association including Neocomitidae indet., and the similarity of this fauna with Berriasian outcrops exposed north of Ñireguao, at the “Estero La Horqueta” (Covacevich et al. 1994; Suárez et al. 1996; De la Cruz et al. 2003; Fig. 1C). In Laguna Foitzick, the Toqui Formation overlies the Foitzick Volcanic Complex, a local member of the Ibáñez Formation, with an erosion-angular unconformity, but locally displaying a peperitic contact (Bell et al. 1994; Suárez et al. 1996; Suárez and De la Cruz 1994a, b; Fig. 1A). There, rocks from the uppermost volcanic strata, below the unconformity, were dated to U–Pb 138.3 ± 1.3 Ma (Pankhurst et al. 2003), providing a “Valanginian or even younger” lower range limit for the sedimentary succession in the Coyhaique area (Suárez et al. 2005). A broader Berriasian-Hauterivian age (“Neocomian”) was inferred by Rubilar (2000) near the “Salto del Pollux”, based on a tentative new species of *Aetostreon* sp. In the same locality, Cecioni and Charrier (1974) reported findings of “*Belemnopsis patagoniensis*”, commonly found in the Lower Cretaceous of southernmost South America (Riccardi 1977; Aguirre-Urreta 2002; Ippolitov et al. 2015).

The top of the Toqui Formation is not exposed in the study area; however, in its type locality (El Toqui Mine), it pass transitionally to tuffaceous- and black mudstone of the Katterfeld Formation (Bussey et al., 2010; Rivas et al. 2021). At the Salto del Pollux locality (outcrop SRP2; Fig. 1D), the Toqui Formation is in tectonic contact with black mudstone of the Katterfeld Formation. There, the marine succession is confined by a post-depositional basaltic andesite sill dated to Ar–Ar 61 ± 0.4 Ma (“Muralla China Sill”; Petford and Turner 1996; De la Cruz et al. 2003), intruding both the Toqui- and Katterfeld Formations (Fig. 1D). Regionally, the Katterfeld

Formation provides a Valanginian–Barremian upper range limit for the Toqui Formation (Masiuk and Nakayama 1978; Aguirre-Urreta et al. 2000; Olivero and Aguirre-Urreta 2002; Kesjár et al. 2017).

Materials and methods

This study comprises three sedimentary sections exposed between south of the Laguna Foitzick and the waterfall of the Pollux River (known as “El Salto”, Fig. 1D), between 8 and 11 km south of Coyhaique, capital of the Aysén Region, Chile (45°34'S; Fig. 1B–C). They are accessed via Route 7. The three outcrops define a ca. 67 m-thick composite log (outcrops LRO, MCH, SRP2; Fig. 1D), and they have been assigned to the Toqui Formation (Suárez and De la Cruz 1994a, b; De la Cruz et al. 2003). Based on their lithology, these stratified rocks are here arranged in six lithofacies (Table 2); five microfacies were additionally defined based on the petrographic analysis of fourteen thin sections (Table 1). The outcrop LRO has been previously addressed (Bell et al. 1994; Townsend 1998; Suárez and De la Cruz 1994a, b) as well as outcrop SRP2 (Katz 1961).

Grain-size categories used here follow Blair and McPherson 1999, and modal compositions of sandstone are based on Garzanti 2019. Lithological description of limestone is after Wright (1992), whereas non-genetic schemes were preferred for mixed- (Mount 1985), and volcaniclastic sediments (Fisher 1961; 1966; Fisher and Schmincke 1984; Cas and Wright 1987). A brief glossary of the volcanic terms applied here can be found as supplementary material; the term “volcaniclastic” was preferred (instead of “volcanic”), to highlight the epiclastic nature of the volcanic material (e.g., volcaniclastic sandstone). Given the mixed nature of most of rocks analyzed here, depositional models for the interpretation of siliciclastic (e.g., Clifton 2006; Plint 2010), and for carbonate environments were required (e.g., Burchette and Wright 1992; Flügel 2010). Raw lithological data taken in the field are presented as supplementary material (Tables SM-1 to SM-3).

Measurements of microfossils were registered with the software ImageJ, using micro-photographs taken with an Olympus camera, model PEN Lite E-PL7. SEM images of thin sections were taken with a microscope ZEISS WITec RISE EVO MA15 at the Universität Heidelberg, following the procedure of Munnecke et al. (2000). Calculations were made in Microsoft Excel. Chronostratigraphic categories used here correspond with the ICS International Stratigraphic Chart v2022/02 (Cohen et al. 2013; updated). Illustrations were created with Adobe Illustrator CS6. Rocks and fossils samples are kept in the Geology Department of the Universidad Mayor in Santiago, Chile, as a temporary repository.

Table 1 Summary of the petrography and microfacies

Type	Micro-facies	Lithology	G-S	S	R	Allochems associations
Mixed Ca > Vc	Mf-1	Sandy-gravelly, volcanoclastic–bioclastic packstone to rudstone, with grainstone patches	M-G (P, Cb)	vp-p	sa-sr sa > sr	Bv , Al, Ec <u>Bv</u> , <u>Al</u> , <u>Ec</u> (Br, In, Se, Ca)
	Mf-2	Sandy-gravelly, volcanoclastic–bioclastic float–wackestone, with packstone patches	M-P (Cb)	vp	sa-sr	Bv , Al, Ec Br, In, Wo
Mixed Ca > > Vc	Mf-3 Mf-3a	Sandy, bioclastic grainstone to rudstone, with packstone patches. Sometimes red algae-rich (Mf-3a)	M-G (F, P)	vp r-w w	sa-sr sr-r	Al , Bv , <u>Ec</u> , (In) <u>Al</u> , <u>Bv</u> , <u>Ec</u> (Br, Wo, Fo, Os)
Mixed Vc > > Ca	Mf-4	Gravelly, bioclastic–volcanoclastic, quartzo-feldspathic-lithic to feldspathic-lithic sandstone [qFL, FL]. Sub-types: Organic matrix-rich (Mf-4om) With calcareous cement (Mf-4c)	M-C (F, G)	p-r r w	sa-sr sr	Bv , Al, Ec <u>Bv</u> , Al, Ec Bv, Al, Ec (Br)
Vc	Mf-5	Muddy, volcanoclastic, (litho-)quartzo-feldspathic sandstone [QF/lQF]	F-M	w-vw	a-sa	Bv, Al

Ca Calcareous, Vc Volcanoclastic, ‘>’ greater than, ‘>>’ much greater than. Lithology: Modal composition follows the scheme of Garzanti (2019; i.e., in an increasing order of abundance, e.g., [qLF] = quartzo-litho-feldspathic sandstone, where F>L>Q). G-S Grain-size (framework), Si silt; sand-grained, F fine, M medium, C coarse; gravel-sized, G granule, P pebble, Cb cobble. S Sorting, vp very poorly, p = poorly, r regularly, w well, vw very well. R Roundness, a angular, sa sub-angular, sr sub-rounded, r rounded. Allochem/Fossil type: Al calcareous red algae, Br bryozoans, Bv bivalves, Ca calcispheres, Ec echinoids, Fo foraminifers, In intraclasts, Os ostracods, Se serpulids, Wo carbonized fossil wood; Percentage (%; represented with different typographical emphasis): Al > 50%, Al > 20%, 10% < Al ≤ 20%, 1% < Al ≤ 5%, Al ≤ 1% (usually, n < 5), (Al) not present in all the thin sections associated with this microfacies

Table 2 Summary of facies associations, litho- and microfacies, and inferred depositional environments. Lithofacies occurrences (typography): bSGm = major, bSGm = secondary, bSGm = rare

Locality Facies Assoc	Litho- facies	Sedimentary structures	Micro-facies	Fossils (macro)	Remarkable fossils	Lithology	Interpretation	Depositional environment
La Rosita (LRO)	bSGm bGSm bSp	ms p-b (cr), s-bp	Mf-1 Mf-4	Oys; Alg; Ech; Cor; Bel; Woo	<i>Archamphiroa jurassica</i> <i>Belemnopsis</i> sp. <i>Aetostreon</i> sp.1	Mixed Cal > Sil	Wave-reworked gravel-sand bars, proximal tempestites	Mixed-carbonate inner ramp
Muralla China (MCH)	bLr bSGm bRp	m-r, r-b, p-b, a-b, s-bp	Mf-3 Mf-2	Alg; Oys; Ech; Bel; Woo; Ver	<i>Aetostreon</i> spp. <i>Archamphiroa jurassica</i> <i>Belemnopsis</i> sp. <i>Entolium?</i> sp. Pycnodontidae indet.	Mixed Cal > Sil	Carbonate sand bars; tempestites	Mixed-carbonate inner to mid-ramp
Salto Río Pollux (SRP2)	bSp bSp-c tSp-b	a-b, p-b, p-l s-bp	Mf-4	Alg; Oys; Bel	<i>Aetostreon</i> sp.2 <i>Archamphiroa jurassica</i> <i>Belemnopsis</i> sp.	Mixed Sil > Cal	Distal tempestites; turbidites?	Mixed, distal carbonate mid-ramp

Abbreviations of lithofacies and microfacies are explained below (Sects. “Petrography”, “Lithofacies”)

Sedimentary structures: a-b amalgamated bedding, cr crudely bedded, m-r megarippled, ms massive, p-b parallel bedding, p-l parallel lamination, r-b rippled-bedding, s-bp sinuous bed-planes. Fossils: Alg red algae, Bel belemnites, Ech echinoid, Oys oyster, Ver vertebrate remains (e.g., fish teeth), Woo carbonized wood. Composition: Cal calcareous, Sil Siliciclastic, “>” = richer than

Facies analysis

The litho- and microfacies of the Toqui Formation analysed here have a mixed volcanoclastic–bioclastic composition. Rocks were classified into six lithofacies (see “Lithofacies”; Table 2), supported by the characterization of five microfacies (Table 1), presented below.

Petrography

Microfacies comprise both ends of mixed rocks (calcareous- and terrigenous-rich), varying between gravelly–sandy allochem limestone and gravelly allochem sandstone (*sensu* Mount 1985). Calcareous-rich microfacies include volcanoclastic–bioclastic, pack–rudstone, float–wackestone, and grainstone (microfacies Mf-1 to Mf-3; Table 1, Figs. 2; 3). On the other hand, terrigenous-rich microfacies consist of bioclastic–volcanoclastic, quartzo-litho-feldspathic- to quartzo-feldspathic sandstone (microfacies Mf-4, Mf-5).

Calcareous-rich microfacies

Calcareous-rich microfacies comprise mostly skeletal allochems, and scarce intraclasts (Figs. 2; 3). Bioclasts are reworked and dominated by bivalves (mostly oysters), calcareous red algae, and echinoid fragments (Figs. 2A–F; 3A). Red algae is controlled by *Archamphiroa jurassica* Steinmann (1930), and scarce *Parachaetetes* sp. and “solenoporooids” (Bucur, pers. com., 2020; Fig. 2E, F). Less abundant bioclasts include reworked serpulids (Fig. 3A), bryozoans (Fig. 3G) and, rarely, benthic foraminifers (Fig. 3F) and ostracods. Non-skeletal allochem comprise intraclasts composed of bioclastic wackestone (intraclasts type 1, Fig. 3B), or formed of “cloudy” radiaxial fibrous calcite (intraclasts type 2; Fig. 3C). Bioclasts are sub-angular- to sub-rounded, usually affected by microboring, or sometimes conforming cortoids (Fig. 2B, F).

Matrix is neomorphic (microspar), but patches of mud-peloids and micritic envelopes were also observed (Fig. 3L). Intergranular porosity was filled by thin layers of isopachous and dog-toothed calcite, followed by granular, blocky, and syntaxial cements (Flügel 2010; Figs. 2C, E, F; 3K, L).

Terrigenous-rich microfacies

The terrigenous part is dominated by oligomictic, non-vesicular volcanic clasts and isolated crystals (Fig. 2C, I–K). Volcanic rock fragments are sub-angular to sub-rounded; they have an intermediate composition (quartz-trachyte) with a trachytic-porphyritic texture (potassium feldspar phenocrysts, minor plagioclase, scarce pyroxene and quartz; Fig. 3I, J). In contrast, felsic rock fragments are less frequent

(rhyolite, rhyodacite < 10%), displaying a felsitic or micropoikilitic texture (Fig. 3J). Volcanic groundmass is pale brown-coloured, partly devitrified or sericitized, or locally replaced to carbonates, Fe oxides-hydroxides, silica (chalcedony), or scattered opaques (Figs. 2A, D, K; 3I, J). Discrete crystals are dominated by euhedral–subhedral feldspars (mostly sanidine, minor orthoclase and plagioclase), slightly to moderately altered (Figs. 2K; 3I). Quartz is angular to sub-rounded, sometimes displaying resorption (Figs. 2J, K; 3I). Infrequent minerals include micas (mostly biotite; Figs. 2J, 3G), and rare rounded glauconite.

The terrigenous matrix is clay-silt-sized, brown- to gray-coloured (Figs. 2G, H; 3G–I), sometimes stained by Fe oxides-hydroxides (Figs. 2A, B). It bears silt-sized, angular crystals and opaque minerals, and it usually displays solution seams (Figs. 2G, H; 3H). In crossed nicols, it appears isotropic or partly sericitized, hindering its differentiation from discrete lithics and reflecting a similar composition with them (Fig. 3I, M–O). Locally, some altered-compacted lithics have been converted to pseudomatrix (Fig. 2A). Cementation is minor, including silica and clay cements (Figs. 2K; 3G), and wispy-shaped chert (Fig. 3I); but also, scattered calcite or dolomite (Figs. 2C, I–K, 3J).

Microfacies

Five microfacies were defined (microfacies Mf-1 to Mf-5); they are briefly described below and summarized in Table 1. These will be referred to in the following sections, linked to their associated lithofacies and outcrops. Detailed compositional information of each thin section can be found as supplementary material (Table SM-4).

Microfacies Mf-1: It comprises sandy–gravelly, volcanoclastic–bioclastic packstone to rudstone, with grainstone patches (Fig. 2A, B). Its fabric is poorly washed and massive, but locally imbricated (bivalves). Framework is rich in bioclasts and altered trachytic rock fragments embedded in argillaceous microspar, locally associated with mud-peloids (Fig. 3L), or clayey matrix (pseudomatrix, Fig. 2A, B). Bioclasts includes mostly oysters, followed by red algae and echinoids; serpulids (some of them attached to oysters; Fig. 3A) and intraclasts type 2 are sporadic; bryozoans and calcispheres are scarce (Fig. 3E).

Microfacies Mf-2: Formed of sandy–gravelly, volcanoclastic–bioclastic float–wackestone, with packstone patches (Fig. 2D). This microfacies is analog in fabric and allochems to Mf-1, though poorer sorted, richer in big-sized bioclasts, and poorer in volcanic lithics. Additionally, its neomorphism is stronger, with coarser microspar (pseudo-grainstone), calcite veins and solution seams (“fitted” packstone; Fig. 2D). Novel fossils include scarce inoceramid fragments.

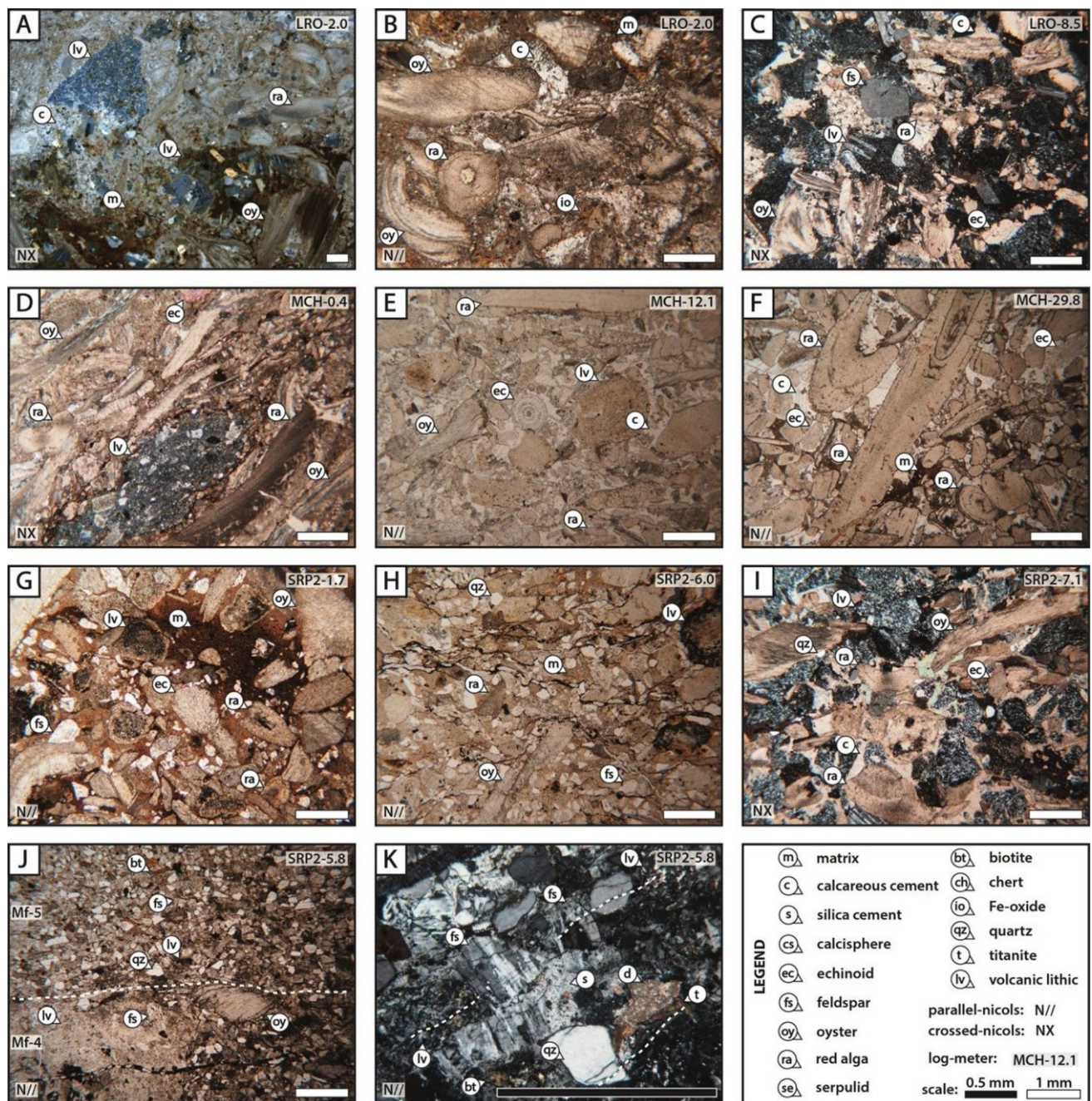
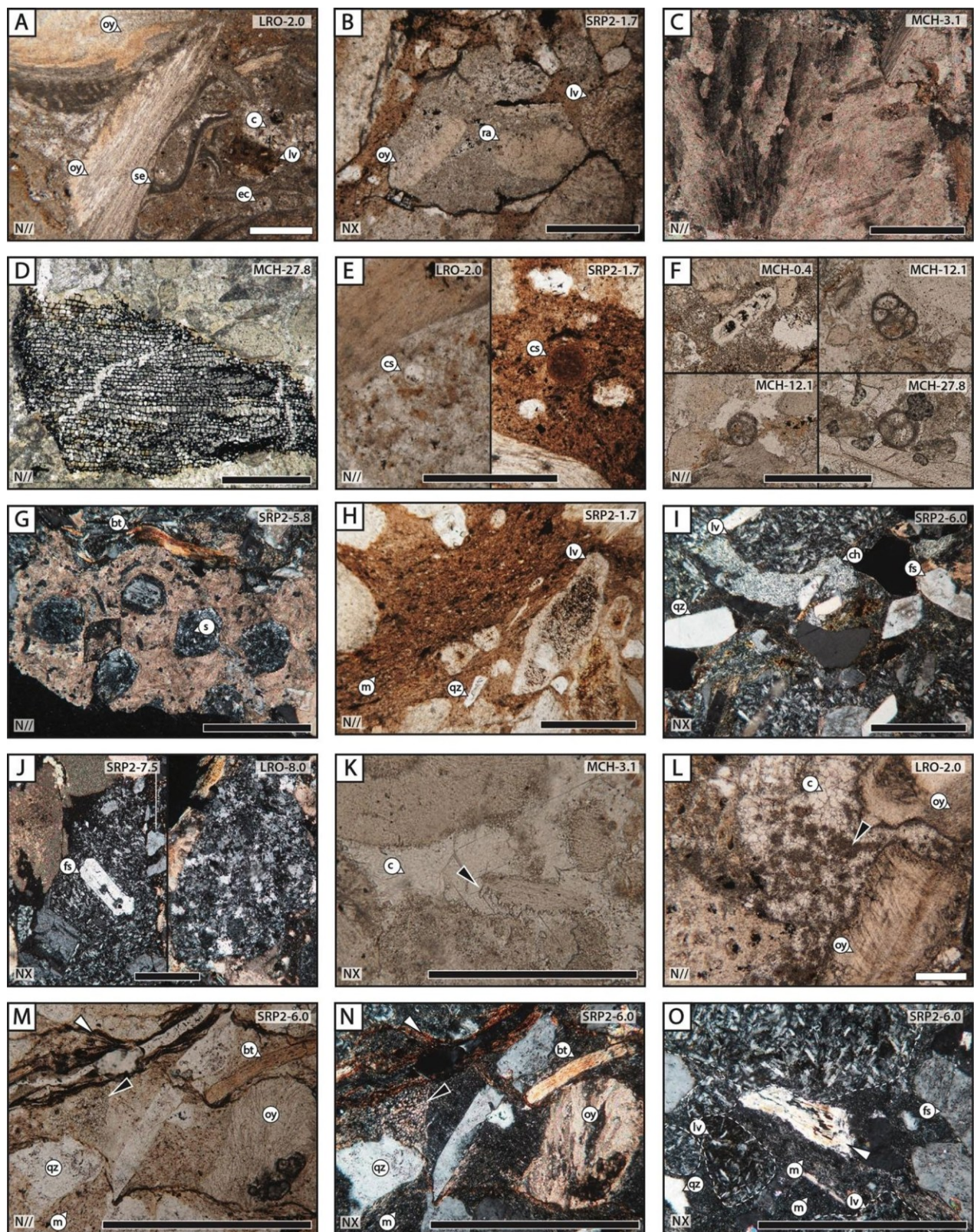


Fig. 2 Petrography and microfacies (Mf). A–C: LRO outcrop (Sect. “La Rosita Section (LRO) - gravelly, mixed inner ramp”). **A** Sandy–gravelly, volcanoclastic–bioclastic pack–rudstone with wackestone patches (Mf-1). **B** Another view of the previous sample (Fig. 2A) showing reworked fossils (some with an incipient micritic coating) and cementation (microfacies Mf-1). **C** Gravelly, bioclastic–volcanoclastic, quartzo-feldspatho-lithic sandstone with pseudo-grainstone patches (granular cements; sub-type Mf-4c). **D–F** MCH outcrop (Sect. “Muralla China Section (MCH) - wave- and storm-dominated inner-ramp”). **D** Sandy–gravelly, volcanoclastic–bioclastic float–wackestone with fitted packstone patches (Mf-2); **E** Sandy bioclastic grainstone; **F** red algae-rich grainstone (*A. jurassica*). **G–K** SRP2 outcrop (Sect. “Salto Río Pollux Section (SRP2)–mixed, distal mid-ramp”). **G** Gravelly, muddy, bioclastic–volcanoclastic (quartzo) feldspatho-lithic sandstone (rich in organic-matter; Mf-

4om); note pressure solution and differential alteration of volcanic lithics (rim-center). **H** Similar to previous, but finer-grained, poorer in organic matter and richer in argillaceous matrix. **I** Subtype of Mf-4 with poikilotopic calcareous cement (Mf-4c). **J** Alternation of (mixed) bioclastic–volcanoclastic, medium-coarse-grained, quartzo-feldspatho-lithic sandstone (Mf-4) and fine-medium-grained, litho-quartzo-feldspathic sandstone (Mf-5); dotted line marks the contact; note parallel lamination (micas). **K** Close-up of Mf-5 displaying its volcanoclastic-rich composition, and its strong silicification; dotted lines indicate aligned fractures. Localities and their respective layers are shown in the upper-right border of each picture (layout: LOG-METER; see position of samples in Fig. 4). Legend is the same for Fig. 3. Outcrops: LRO: La Rosita; MCH: Muralla China; SRP2 (Salto Río Pollux)



• **Fig. 3** Petrography and components. **A, C–D, F, K–L** Calcareous-rich microfacies; **B, G–J, M–O** volcanoclastic-rich microfacies. **A** Mixed, pack–rudstone with oysters and encrusted serpulids; note oxidation of the argillaceous-calcareous matrix (microfacies Mf-1). **B** Intraclasts type 1: bioclastic wackestone bearing the same fossils found discretely in the framework; note compaction, pressure solution and organic-rich matrix (microfacies Mf-4). **C** Intraclasts type 2: reworked clasts formed of radial calcite (microfacies Mf-2, 3). **D** Fragment of carbonized wood (microfacies Mf-3a). **E** Left: calcisphere from microfacies Mf-1; right: phosphatic algal cysts (acritarch?) from organic matter-rich microfacies Mf-4om. **F** Several benthic foraminifers from microfacies Mf-2, 3 and 4. **G** Reworked and strongly bioeroded bryozoan colony, from a devitrified volcanoclastic-rich sample (microfacies Mf-4); zoecia have been filled with clay- and silica cements. **H** Organic matter-rich matrix from microfacies Mf-4om; note pressure solution and concentric alteration of volcanic lithics. **I** Similar composition observed in volcanoclastic-rich microfacies Mf-4; note difficult differentiation of lithics and matrix as well as formation of clay and chert cements, likely after devitrification. **J** Compositional variability of volcanic lithics. Left: intermediate clast with trachytic texture (microfacies Mf-4); right: rhyolitic clasts with micropoikilitic texture (devitrified; microfacies Mf-4c). **K** Common marine calcareous cements found in the mixed rocks: isopachous dog-tooth around a bioclast (black arrow); porosity subsequently filled by blocky-type cement. **L** Pseudo-grainstone with a strong neomorphic texture; note the presence of mud peloids, not clear if primary of secondary (pseudomatrix; microfacies Mf-1). **M–O** Close-up of volcanoclastic-rich lithofacies Mf-4 (quartzo-feldspathic-lithic sandstone); note similar composition of volcanic lithics and matrix. **M–N** Compaction of matrix forming pressure solution seams (white arrow); note possible devitrified-replaced relict pumice clasts (vesicular? black arrow), and formation of argillaceous cements around clasts (sericite). **O** Picture displaying similar composition between volcanic lithics (dotted lines) and matrix, interpreted as originally vitreous (pyroclastic?); note white mica in the central part (white arrow)

Microfacies Mf-3: It comprises sandy volcanoclastic–bioclastic grainstone, and red algae-rich grainstone (sub-type Mf-3a; Fig., 2F), with rud-, wacke-, or packstone patches (Fig. 2E, F). Its fabric is massive or locally showing aligned bioclasts. In contrast to previous microfacies, this one is poorer in volcanic clasts, and allochems are better rounded and sorted. Bioclasts comprise mostly bivalves, red algae, and subordinate echinoids plates (Fig. 2E, F). Less frequent allochems include intraclasts type 2 (Fig. 3C), and scarce bryozoans, carbonized wood (Fig. 3D), benthic foraminifers (Fig. 3F), and ostracods. Matrix is patchy (microspar, mud-peloidal; Fig. 2F), or it occurs as micritic envelopes; cementation is analog to previous microfacies (see Sect. “Calcareous-rich microfacies”), though more abundant (Fig. 3K).

Microfacies Mf-4: This microfacies is composed of gravelly-muddy, mixed bioclastic–volcanoclastic, quartzo-feldspathic-lithic to feldspathic-lithic sandstone (Figs. 2C, I, J; 3I, M–O). Microfacies Mf-4 is poorly sorted, either rich in devitrified matrix, or bearing organic matter (Mf-4om; Figs. 2G, 3E, H). Some samples also show patches of calcitic cements (granular and poikilotopic, sub-type Mf-4c; Fig. 2C, I). Its framework is mostly composed of sub-angular to sub-rounded volcanic

lithics, and angular to sub-angular crystals. It displays a subtle parallel lamination (Fig., 2I, J), noticed by aligned elongated bioclasts or micas (mostly biotite, minor white mica).

Volcanic lithics are mostly intermediate, but some samples bear considerable felsic clasts (proportion intermediate:felsic = 9:1 to 6:4; Fig. 3I). Many rock fragments concentrate opaques in the core (Figs. 2G; 3H) or, when devitrified, they are replaced by chert (Fig. 3I), sericite, or calcite (pumice? Fig. 3M, N). Bioclasts comprise mostly reworked bivalves, and minor red algae and echinoids (Fig., 2C, G, I); bryozoans and intraclasts type 1 are scarce (Fig. 3B). Matrix is argillaceous-carbonaceous, and cements were already described (see “Terrigenous-rich microfacies”; Figs. 2I, K; 3G; M–O). Solution seams are common, concentrating insoluble residues and organic matter (Figs. 2G, 3H).

Microfacies Mf-5: Formed of (muddy) volcanoclastic quartzo-feldspathic sandstone with subtle parallel lamination (Fig. 2J, K). Its framework is fine- to medium-grained, dominated by angular to sub-angular crystals (mostly feldspars, followed by quartz, and minor lithics and micas). Volcanic lithics are subordinated, usually devitrified, or altered (Fig. 2K). Argillaceous matrix is scarce. Cements include calcite/dolomite, usually spotted or altering the framework (Fig., 2K); titanite was also observed. Bioclast and micas are elongated and imbricated; grains appear fractured in a preferential direction.

Interpretation of microfacies

Calcareous-rich microfacies reflect a major carbonate sedimentation incorporating reworked, older-altered volcanic rocks, or sporadic input of fresh volcanoclastics. Carbonate mud might have an allochthonous origin (mud-peloids, bioeroded clasts, absence of fecal pellets), and a minor bacterial origin (cortoids, microbial structures). Cementation depicts a phreatic marine environment and the subsequent porosity-filling during burial diagenesis (Flügel 2010). However, intraclasts type 2 may indicate erosion of aragonite-filled cavities in a coastal setting (later recrystallized to calcite; see Kendall and Tucker 1973). Coarse-grained, rud-floatstone microfacies (Mf-1, Mf-2) reflect a near-coast reworking influenced by currents (aligned bioclasts) and a rapid settling (poorly-sorted). Grainstones (Mf-3) depict a near-coast, good hydraulic sorting (Flügel 2010).

Terrigenous-rich microfacies indicate a submarine-settled, volcanoclastic sedimentation. For microfacies Mf-4, rounded lithics and abundant shell debris reflect epiclastic transport or coastal reworking. Non-vesicular volcanic rock fragments, and their core-margin differential alteration may be related to phreatomagmatism or quenching, respectively (Fisher and Schmincke 1984; Cas and Wright 1987). Allochems are analog to the ones found in the calcareous microfacies (Mf-1 to Mf-3),

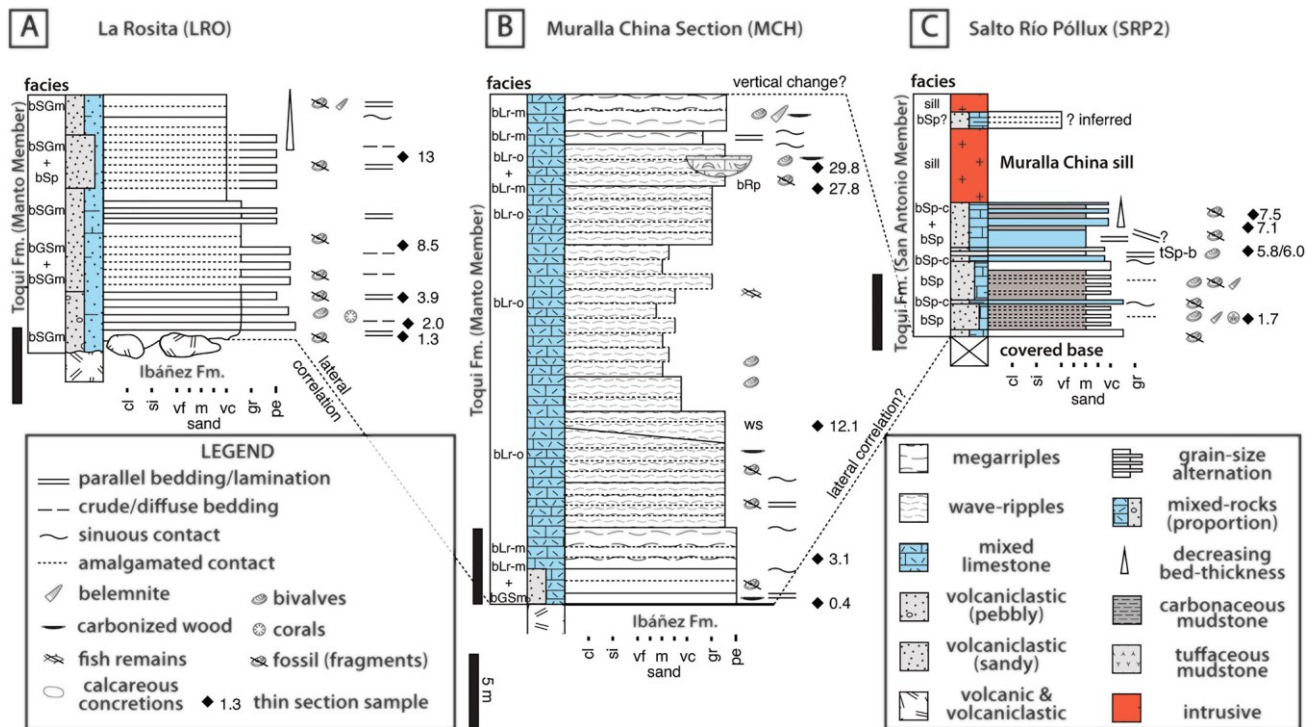


Fig. 4 Detailed view and correlation of sedimentary logs, including approximate stratigraphic position of the lithofacies (left size of the logs), and samples (small rhombs to the right). **A** La Rosita outcrop. **B** Muralla China outcrop. **C** Salto Río Póllux outcrop. See “Lithofa-

cies” and “Sedimentary logs and facies associations”. The legend is valid for the following illustrations (Figs. 5, 6, 7). Scale is the same for all outcrops

they were most likely swept off- (shell debris) or eroded from near-coast areas (cemented?). Given their poor textural maturity (matrix-rich) and devitrified matrix, these microfossils are interpreted as formed after remobilization of non-consolidated deposits. However, organic-rich samples (e.g., phosphatic algal cysts in Mf-40m; Fig. 3E) indicate sedimentation in a poorly oxygenated setting or during a period of high productivity (Capelli et al. 2021). Microfacies Mf-5 depicts remobilization of crystal-rich volcanoclastics, likely fractionated during the eruption or concentrated during the epiclastic transport (see Chapter 11 in Cas and Wright 1987). Its parallel lamination, and the incorporation of bioclasts is linked to current-transport. Calcareous cements are interpreted as diagenetical, while fractured crystals and titanite might reflect burial diagenesis and circulation of high-T pore fluids.

Lithofacies

Six lithofacies were defined in the study area; they are presented in decreasing grain-size order (Table 2). The main lithology is shown in upper case (e.g., R: rudstone; SG: sandstone > conglomerate, also sandy conglomerate), whereas lower case prefixes indicate composition (e.g., b: bioclastic; v: volcanoclastic). Suffixes refer to structures

(e.g., p: planar bedding; m: massive). Sedimentary logs and their associated lithofacies can be found in Fig. 4.

Mixed bioclastic–volcanoclastic, sandy conglomerate (bGSm)

This lithofacies is formed of bioclastic–volcanoclastic, sandy conglomerate, arranged in tabular beds (Fig. 5). Bedding is 0.3–0.4 m-thick, with sharp contacts, usually marked by changes in gravel content (Fig. 5I). The framework of lithofacies bGSm is matrix-supported (locally clast-supported), conformed by pebble-sized clasts (diameter: max = 2.5 cm, average = 1 cm), embedded in a coarse- to very coarse-grained, sandy–muddy calcareous matrix (Fig. 5E, I, J). Exceptionally, a singular bed of lithofacies bGSm bears cobble-sized lithics (sub-facies bGSm-g; clasts-size up to 15 cm, average 2–5 cm; Fig., 5G). Gravel is formed of massive to diffusely graded, volcanic rocks and frequent bioclasts (Fig. 5E, G, J). Lithics are poorly-sorted, rounded- to sub-angular, light-coloured and mono-oligomictic. Fossils are reworked, highly fragmented, and poorly packed; bioclasts are dominated by bedding-concordant, platy oyster shells (length up to 10 cm; Fig. 5E), though some beds also bear in situ and reworked colonial corals (Fig. 5J) as well as scarce carbonized wood remains.

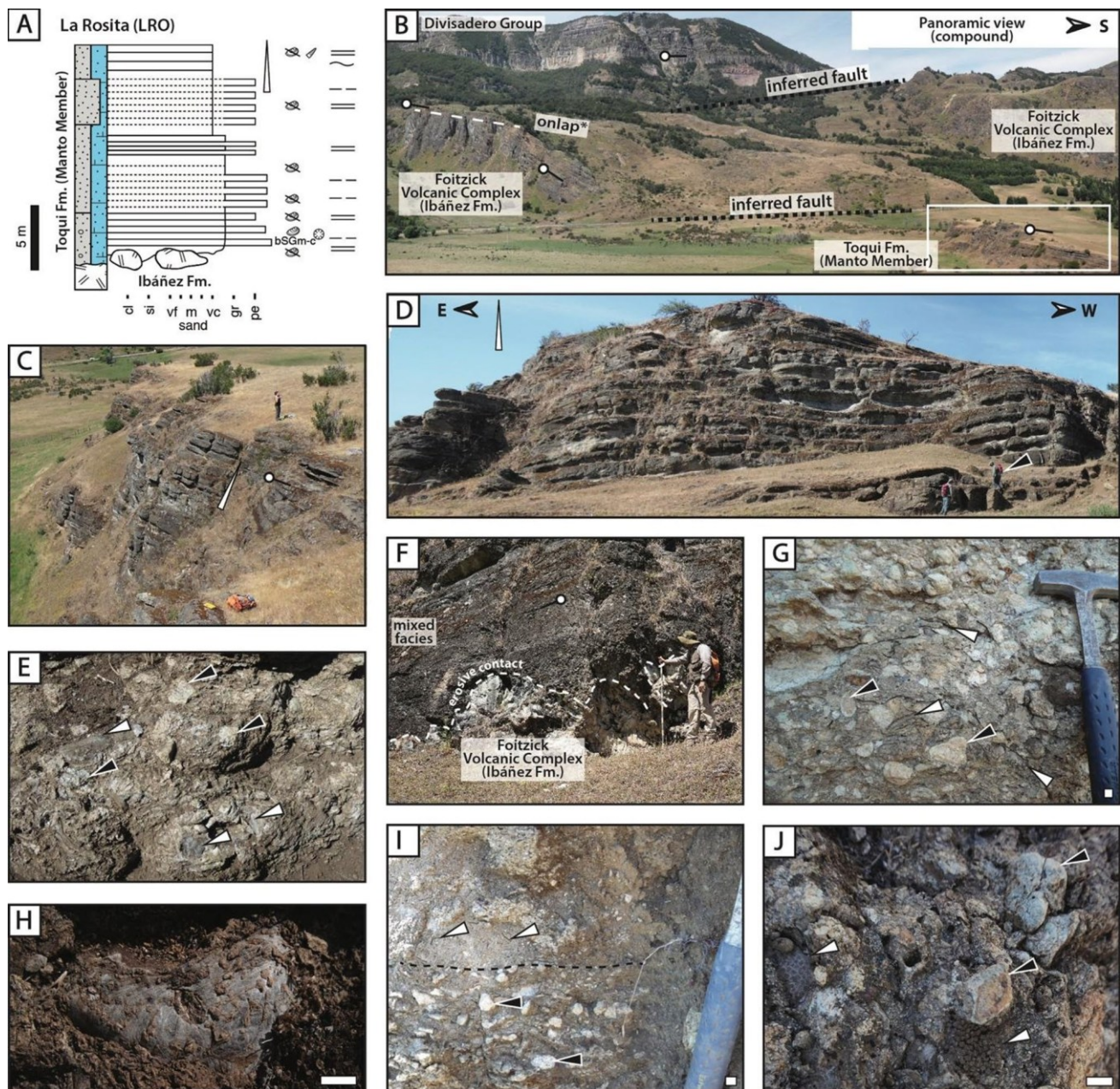
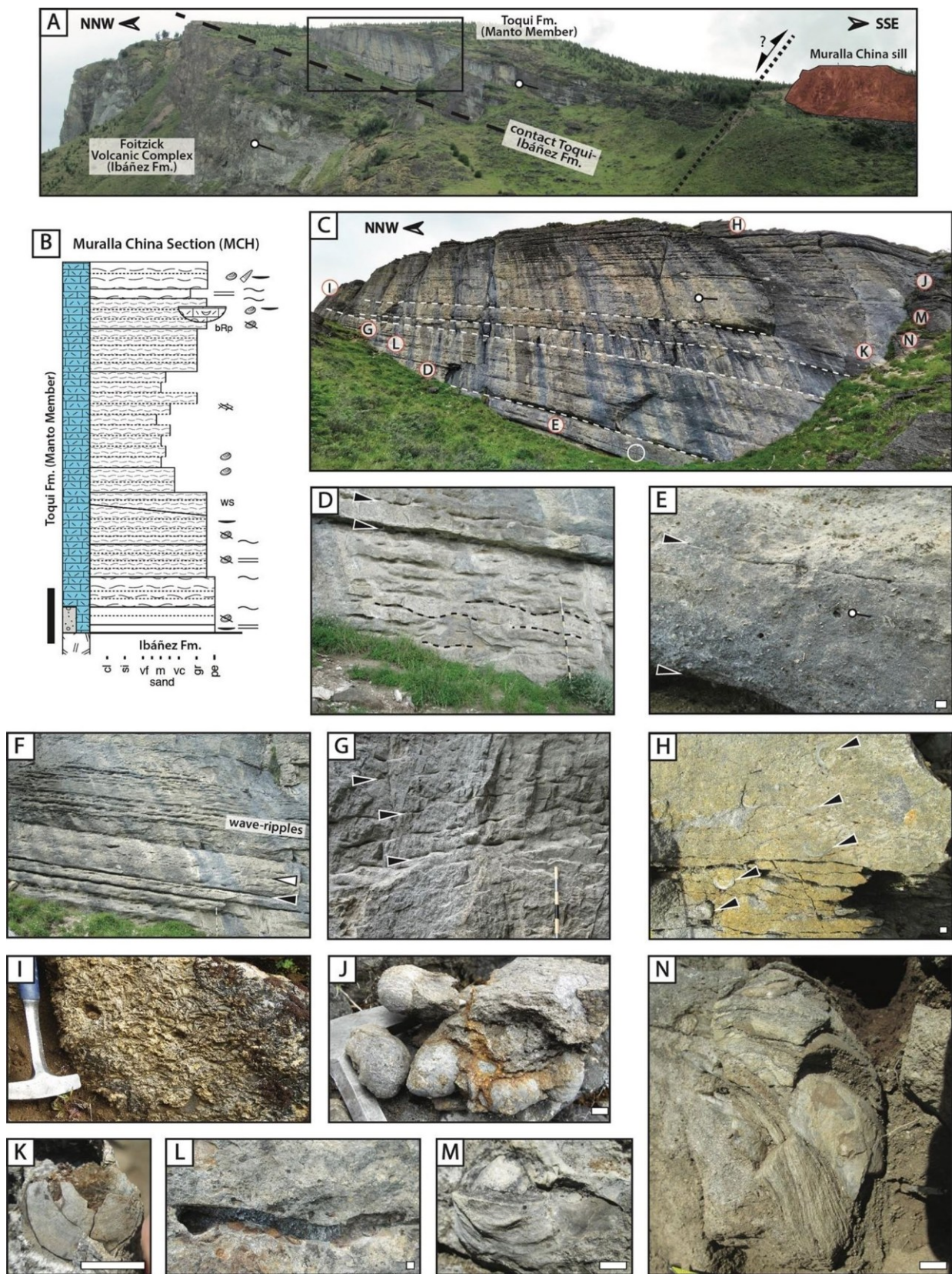


Fig. 5 La Rosita outcrop (LRO). **A** Simplified stratigraphic log; the complete one, including its lithofacies, is presented in Fig. 4A. **B** Panoramic view of the mixed calcareous outcrops, including the one here studied at the lower-right margin (white rectangle). **C** Close-up of the upper part of the outcrop, displaying a decreasing bed-thickness upwards (white arrow), and the alternation of sharp-sinuuous and amalgamated contacts. **D** Crudely/diffusely bedded strata of the LRO section, showing decreasing bed-thickness (white arrow) and differential weathering of beds forming overhangs (close-up of the white square from **B**); person as scale (black arrow). **E** Coarse-grained lithofacies composed of gravel-sized oyster fragments and volcanic lithics (lithofacies bGSm). **F** Erosive contact between the mixed lithofacies of the Toqui Formation (Manto Member) and the Foitz-

ick Volcanic Complex, a local member of the Ibáñez Formation. In **G**, **I**, **J**: Coarse-grained mixed lithofacies showing terrigenous material (black arrows: gravel-sized volcanic clasts) and bioclasts (white arrows). **G** Bioclastic-volcaniclastic, pebble-cobble-sized sandy conglomerate (lithofacies bGSm-g). **H** Reworked and bioeroded, big-sized gryphaeid oyster (*Aetostreon* sp.1). **I** Contact between lithofacies bGSm (mixed bioclastic-volcaniclastic, sandy conglomerate) and bSGm (mixed bioclastic-volcaniclastic, gravelly sandstone); white arrows point to reworked corals. **J** Close-up of lithofacies bGSm; note the preservation of colonial corals in life position (white arrows) between the gravel (black arrows). Scale bar = 1 cm. Legend for all pictures and sedimentary logs is presented in Fig. 4



• **Fig. 6** Muralla China outcrop (MCH). **A** Overview of the outcrop, displaying the contact relationship with the Ibáñez Fm. and the position of the “Muralla China sill”; black square: MCH outcrop. **B** Simplified stratigraphic log (complete profile in Fig. 4B). **C** Close-up of the MCH outcrop from A (Jacob’s staff as scale within white circle, 1.5 m-length); red circles with capital letters are linked to the pictures D–N. **D** megaripped bioclastic limestone (lithofacies bLr-m); note decimeter wave-length and amalgamated contacts. Black arrows: sharp erosive contacts (sinuous). **E** Gravelly–sandy bioclastic limestone (bSGm) with amalgamated contacts (dotted line) from the lowermost part of the outcrop; note sinuous contacts (black arrows) and scattered bioclasts. **F** Several parallel beds conformed of oscillation-rippled, sandy bioclastic limestone (lithofacies bLr-o); note some amalgamated contacts and parallel-arranged tafoni (white and black arrow, respectively). **G** Close-up of the previous, in a different part of the outcrop; rippled surfaces are marked with black arrows. **H** Reworked left valves of oysters (*Aetostreon* sp. and *A. sp.2*; black arrows), from a tempestite in the uppermost part of the outcrop. **I** Oyster coquinites from the northern part of the outcrop (lithofacies bRp). **J** An ex-situ cobble including a cluster of *Aetostreon* sp.2, likely fallen from the uppermost part of the outcrop (see **H**). **K** Reworked small pectinid (*Entolium?* sp.). **L** Carbonized fossil wood forming a thin-bedded coal bed. **M** Reworked, inequivalve, big-sized oyster. **N** Reworked, bioeroded, and articulated big-sized oyster (*Aetostreon* sp.1; also displayed in Fig. 9A–B). Scale bar (white) = 1 cm

The matrix of lithofacies bSGm consists of sandy–gravelly, volcanoclastic–bioclastic, packstone–rudstone, with grainstone patches (microfacies Mf-1; Fig. 2A, B).

Interpretation: Based on its mixed volcanoclastic–calcareous composition, coarse-grained and poorly sorted components, and reworked sessile and free-living epifauna, lithofacies bSGm represents deposition in a relatively high-energy coastal environment (Leithold and Bourgeois 1984; Plint 2010). Coarse-grained coastal sediments are usually linked to the reworking of fluvial mouth-bar deposits (Bourgeois and Leithold 1984; Hart and Plint 1995), though the monooligomictic composition of the volcanic clasts suggests erosion of a local source, as observed in some volcanic islands (Felton 2002; Felton et al. 2006). The tabular beds, poor sorting, and matrix-supported fabric, may indicate a rapid settling, likely occurring during storms (Leithold and Bourgeois 1984); the latter is also supported by the packstone and rudstone microfacies (Flügel 2010). Mixture of sub-rounded and sub-angular clasts might indicate abrasion in the beachface, during storm swells (“swash area”; Hart and Plint 1989; 1995).

Oyster-rich rudstone/coquinite (bRp)

The lithofacies bRp consists of an accumulation of cobble-sized, broken bivalve shells (40%), mostly oysters. Beds are sharp-bounded and decimeter-thick. Shells are fragmentary, platy- and wedge-shaped, arranged chaotically or concordant with bedding (Fig. 6I). They are clast-supported and

embedded in a light grey-coloured, fine-grained calcareous matrix.

Interpretation: This lithofacies corresponds to a basal lag formed by shell debris (Collinson et al. 2006). Based on its coarse grain-size, dense packing, and bedding-concordant bioclasts, it is interpreted as a “sedimentologic concentration” deposit, conforming proximal tempestites settled over the normal-weather wave base (Kidwell et al. 1986), and likely transported by storm-induced bottom flows (Flügel 2010).

Mixed bioclastic–volcanoclastic, gravelly sandstone (bSGm)

This lithofacies resembles the mixed conglomerate facies (bGSm), but it is finer grained. It consists of bioclastic–volcanoclastic, gravelly sandstone to granule-pebble-sized, sandy conglomerate (Fig. 5I). Strata of lithofacies bSGm are decimeter-thick, crudely bedded, amalgamated or grading from the gravel-rich ones (bGSm), though some sharp bed-boundaries are sinuous (Fig. 5C, D). Internal structures were not observed; they were likely effaced during weathering (Fig. 5D). Sandstone is medium- to very coarse-grained, whereas conglomerate is granule- to pebble-sized (clasts-size up to 1–2 cm, average < 1 cm), and usually sandy matrix-supported. Its framework is rich in volcanic lithics and fragmented oyster shells (length < 2 cm), and minor corals in some strata (Fig. 5I).

Under the microscope, the matrix of lithofacies bSGm varies between sandy, volcanoclastic–bioclastic limestone (microfacies Mf-1; Fig. 2B), and gravelly, bioclastic–volcanoclastic, quartzo-feldspatho-lithic sandstone (microfacies Mf-4c; Fig. 2C).

Interpretation: Analog to bGSm, lithofacies bSGm depicts a subtidal environment. Better sorting of clasts and oriented shell debris reflect current-influenced hydraulic sorting. Sinuous-topped, amalgamated beds depict periodic erosion–deposition pulses (Collinson et al. 2006), and subsequently wave- or current reworking (Walker and Plint 1992; Clifton 2006); whereas sharp contacts might represent reactivation surfaces. These tabular beds could represent the formation of gravelly–sandy low relief bedforms linked to alongshore currents (similar to Fig. 14 in Hart and Plint 1995; also “bed-load-sheets” *sensu* Carling 1999; or “carbonate sandbodies” *sensu* Wright and Burchette 1996). These bedforms are typically developed on the shoreface (Hart and Plint 1995).

Rippled, bioclastic (volcanoclastic) limestone (bLr)

The lithofacies bLr is composed of gravelly–sandy, bioclastic limestone, with a minor volcanoclastic content. It is arranged in tabular layers with sinuous bed boundaries,

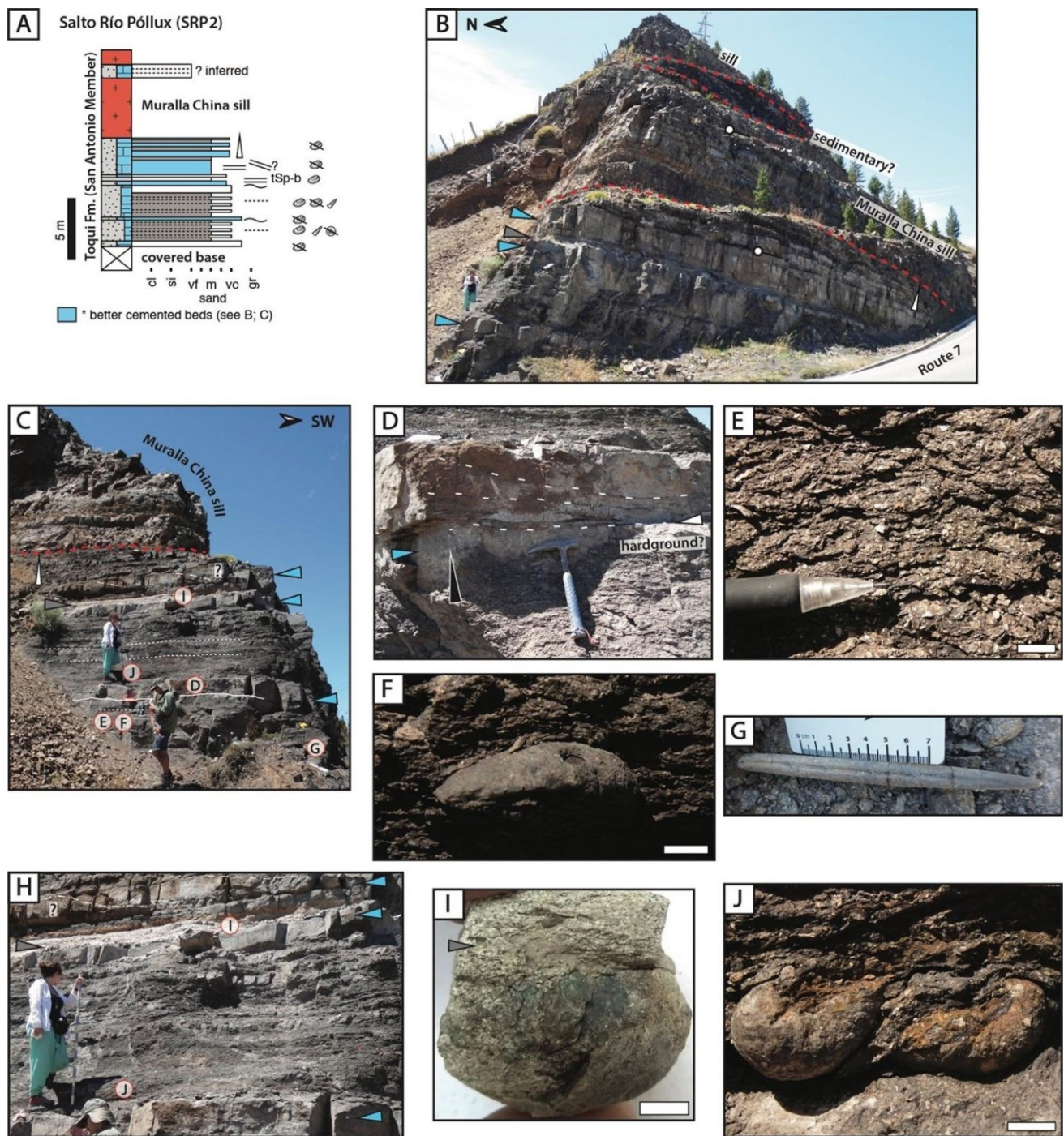


Fig. 7 Salto Río Pollux outcrop (SRP2). **A** Simplified sedimentary log. **B–C** Overall view of the outcrop displaying the inclined bedding, amalgamated beds, and intrusive contacts with the Muralla China sill (red dashed line). Light-blue arrows: calcareous beds; grey arrow: tuffaceous sandstone (lithofacies tSp-b); white arrow: decreasing bed-thickness upsection. **D** Overhang of carbonate-cemented bed of lithofacies bSp-c, exposed between brittle bedsets of lithofacies bSp; note the sinuous internal, amalgamated surfaces (hammer as scale). This layer corresponds to the lowermost light-blue arrow in **B–C**. **E** Close-up of lithofacies bSp (bioclastic, muddy sandstone);

note its dark-colour and matrix-rich composition as well as abundant comminuted shell debris (pencil as scale). **F** Reworked (convex-up) and bioeroded specimen of *Aetostreon* sp.2 within lithofacies bSp. **G** Complete, well-preserved specimen of *Belemnopsis* sp. **H** Close-up of **C**, displaying the middle position of the tuffaceous strata (lithofacies tSp-b); note diffuse cross-bedded? beds of calcareous sandstone (bSp-c) above. **I** *Aetostreon* sp.2 sampled from lithofacies tSp-b; the fossil stills bear sediments. **J** Gryphaeid oysters (*Aetostreon* sp.2) in life position conforming a small cluster. Scale bar (white) = 1 cm

usually amalgamated (Fig. 6C–E). Based on the grain-size and scale of ripples, two subtypes were defined: (i) bLr-m: “mega-rippled” (*sensu* Swift et al. 1983), or coarse-grained-rippled (*sensu* Leckie 1988), gravelly, bioclastic limestone (Fig. 6D, E); and (ii) bLr-o: oscillation-rippled, sandy, bioclastic limestone (Fig. 6F, G).

The mega-rippled subtype (bLr-m) consists of sandy–gravelly float–rudstone, bearing pebble- to cobble-sized bioclasts and volcanic lithics (1–2 cm-length, max = 9 cm-length in broken-disarticulated oyster shells). The framework is massively arranged, but, locally, it displays a sub-parallel arrangement of shells (Fig. 6E). Limestone is sharply bedded, arranged in decimeter to meter-thick bedsets with sinuous contacts (Fig. 6D). Internally, the subtype bLr-m displays symmetric large-sized ripples (wavelength \approx 50–90 cm; height \approx 15–20 cm; Fig. 6D). On the other hand, the oscillation-rippled subtype (bLr-o) is formed by mixed, gravelly–sandy calcarenites (grain size 1–5 mm, max: 1.7 cm), displaying smaller and regular symmetric ripples, and subordinate asymmetric ripples (wavelength \approx 20–30 cm; height \approx 10 cm; Fig. 6F, G).

The matrix of lithofacies bLr-m consists of sandy–gravelly, volcanoclastic–bioclastic float–wackestone with packstone patches (microfacies Mf-2; Fig. 2D), whereas subtype bLr-o is composed of sandy, bioclastic rudstone–grainstone, and red algae-rich grainstone (microfacies Mf-3, Mf-3a; Fig. 2E, F).

Interpretation: This lithofacies depicts a shallow marine environment emplaced above the fair-weather-wave base (Burchette and Wright 1992; Flügel 2010). Mega-ripples (bLr-m) have been regarded as the equivalent of hummocky cross-stratification for coarse-grained sediments, which are typically linked to storm-surge deposits (Leckie 1988; Cummings et al. 2009). Based on the previous, and on their poorly sorted microfacies (Mf-2), they are interpreted here as calcareous proximal tempestites (analog to “Facies A” of Pérez-López and Pérez-Valera 2012). On the other hand, given its grain size, better sorted microfacies (Mf-3), and symmetrical rippled-beds, lithofacies bLr-o reflects an oscillatory flow typical of fair-weather wave action, and minor influence of near-coast unidirectional currents (Collinson et al. 2006; Plint 2010).

Parallel-bedded, bioclastic–volcanoclastic, muddy sandstone (bSp)

Lithofacies bSp crops out as sandy, bioclastic mudstone to calcareous muddy sandstone; it is dark grey-coloured, and it expels a fetid odor when crushed (Fig. 7C, E).

Its bedding is arranged in decimeter-thick layers with diffuse, flat-amalgamated contacts (10–40 cm-thick; Fig. 7A–C, E, H). Beds are commonly friable; however, some better cemented strata serve as guide-beds, these have sharp margins with a rippled top or base (sub-facies bSp-c; Fig. 7B–D, H). Bedding is internally massive, but some beds display a coarse-tail grading of bioclasts (i.e., muddier tops, or diffuse amalgamated ripples (Fig. 7D). Shell debris are abundant, regularly to well-sorted, and highly fragmented (ca. 20–30% bioclasts, 2–3 mm-length; Fig. 7E); they comprise mostly bed-concordant bivalves, and some echinoids fragments. Other complete macrofossils are scattered, including reworked oysters and belemnites (Fig. 7F, G, I, J).

Microscopically, lithofacies bSp consists of gravelly–muddy, mixed bioclastic–volcanoclastic sandstone (microfacies Mf-4, Mf-5 subordinate).

Interpretation: Based on its amalgamated tabular beds, parallel lamination (microfacies Mf-4, Mf-5), sandy framework, bimodal bioclasts (fragmented–complete), and grading, this lithofacies reflects waning flows with an intermediate character between proximal (i.e., coarse-grained, bioclast-dominated; similar to “Facies B” of Pérez-López and Pérez-Valera 2012) and distal tempestites (i.e., interbedded with mud; Flügel 2010). The latter are usually difficult to differentiate from turbidites (e.g., “turbidite-like tempestites” *sensu* Myrow 1992; 2005), however, turbidites are finer grained (mud to fine-sand *sensu* Shanmugam 1997, 2002, 2016). Its volcanoclastic composition reflects remobilization of non-consolidated deposits to relatively quiet, soft-bottom subtidal settings.

Laminated, tuffaceous muddy sandstone (tSp-b)

This lithofacies is formed of bioclasts-bearing, medium-to-coarse-grained, muddy sandstone (Fig. 7C, H, I). Sandstone is friable, light grey-coloured, slightly calcareous, and partly altered to phyllosilicates. Bedding is arranged in centimeter-thick layers with parallel bedding (Fig. 7C, H), and its framework is rich in white-coloured, sand-sized rounded clasts, interpreted as altered pumice (Fig. 7I). Subordinately, it bears sand-sized micas and glauconite. Its fossil content includes reworked left valves of gryphaeid oysters (Fig. 7I).

Interpretation: Based on its composition and alteration, this lithofacies is interpreted as a submarine-settled, tuffaceous sandstone (remobilized tuffaceous deposits *sensu* McPhie et al. 1993). Given its grain size, lamination, and fossil content, it may reflect sedimentation by currents.

Sedimentary logs and facies associations

This section describes three sedimentary logs (Fig. 1D) as well as their facies associations and paleoenvironmental interpretation. Outcrops have mixed composition varying from calcareous-rich (LRO, MCH) to volcanoclastic-rich lithofacies (SPR2); they are described from north to south. The detailed description of each sedimentary log and their beds, compiled in the field, has been provided as supplementary material (Tables SM-1 to SM-3).

La Rosita Section (LRO)—gravelly, mixed inner ramp

This locality comprises at least three grey-coloured, wedge-shaped small outcrops, exposed in a ca. 1 km radius, about 8 km to the south of Coyhaique (Figs. 1D; 5B–D; 4A). The central outcrop, here described (LRO), is better exposed and consists of a 17-m-thick succession slightly inclined to the SSW (strike/dip = 105/13; Figs. 5A–D). The outcrop displays several overhangs with diffuse contacts, after amalgamation and differential weathering of the strata (Fig. 5D). These rocks include mixed, volcanoclastic–bioclastic conglomerate and sandstone (lithofacies bGSm; bSGm; Fig. 5E, G, H–J), and subordinate bioclastic–volcanoclastic sandstone (bSp, Fig. 5I).

At the base, mixed rocks overlie meter-sized, volcanic boulders of the Foitzick Volcanic Complex with an erosive unconformity (De la Cruz et al. 1994, 2003; Fig. 5F). In addition, an angular unconformity, and local peperitic contact have been reported from adjacent, correlative outcrops (Bell et al. 1994; Suárez et al. 1996; Suárez and De la Cruz 1994a, b). The top of the LRO section is not exposed (Fig. 5B–D).

In the LRO section, the mixed succession is arranged in decimeter-thick, tabular beds, commonly amalgamated (avg. 0.3–0.4 m, max: 0.8–1.0 m, probably fused beds; Fig. 5C–D). Upsection, sediments are better sorted and their bedding is clearer (Fig. 5C). Coarsest, poorly sorted gravelly beds are usually thicker and more common in the lowermost part of the outcrop (bGSm; bSGm-g, Fig. 5E, G, J), changing to a gravelly–sandy alternation in the central part (bGSm; bSGm; Fig. 5C, D). The last third of the outcrop displays a thinning- and fining-upwards trend, dominated by gravelly sandstone with diffuse- and sharp, sinuous contacts (lithofacies bSGm; bSp; 0.3–0.5 m-thick; Fig. 5C); some beds are richer in volcanoclastics (microfacies Mf-4c, Table 1).

Macrofossils are reworked and fragmented, dominated by reworked oysters (rarely big-sized specimens of *Aetostreon* sp.1; Fig. 5H), but colonial corals were also found in the lowermost beds, some of them in life position (Bell et al. 1994; Townsend 1998; and here, see

Fig. 5J); belemnites are scarce and broken. Articulated- and encrusting oysters in life position have also been reported from this outcrop (*Exogyra* sp. *sensu* Bell et al. 1994; Townsend 1998), but they were not observed during this work.

Interpretation: The La Rosita outcrop depicts a relatively shallow marine environment, placed above the fair-weather wave-base. Its sub-environments comprise a deepening-upwards succession from a storm-influenced, gravelly upper shoreface towards a sandy lower shoreface (Hart and Plint 1995). These are here interpreted to represent a mixed volcanoclastic-carbonate inner ramp (*sensu* Burchette and Wright 1992; Fig. 14.3 in Flügel 2010). The fragmented fossil content, including sessile and free-living epifauna, reflects the development of local communities, though not forming reefs (“ahermatypic corals” *sensu* De la Cruz et al. 2003), and rather grew as discrete small crusts over the coastal gravel deposits.

These gravelly deposits represent the marine erosion over a rocky shoreline (coastal cliff), eroding an older volcanic terrain (Suárez et al. 1996). Based on the inferred “onlap” contact of these rocks above the volcanic complex (illustrated in Fig. 5 in Suarez and De La Cruz 1994a; also in Fig. 3.10 in Townsend 1998; Cover Photo in De la Cruz et al. 2003; and Fig. 5B here), also reported as locally peperitic (Bell et al. 1994; Suarez and De La Cruz 1994a, b), these rocks might reflect transgressive deposits settled over a volcanic flank (De la Cruz et al. 1994; Bell et al. 1994; Suárez et al. 1996; Suárez and De la Cruz 1994a, b). In particular, the gravelly facies (bGSm) may represent transgressive conglomerates (Suárez et al. 1996).

Muralla China Section (MCH)—wave- and storm-dominated inner-ramp

This section is located 2.8 km to the south-southeast of section LRO, near the northern end of a sub-horizontal sill, locally known as “Muralla China” (Figs. 1D; 4B; 6B–C). The succession comprises a wedge-shaped, steep outcrop formed of ca. 34 m of gravelly–sandy, bioclastic limestone dipping to the southeast (strike/dip = 060/20; Fig. 6A). The limestone conformably overlies pale grey-green-coloured, diffusely bedded, volcanic rocks of the Foitzick Volcanic Complex (*sensu* Bell et al. 1994; Suárez and De la Cruz 1994a, b, see Fig. 6A). Gravel-sized volcanic clasts found within the calcareous beds suggest erosion over this basal unit. The top of the MCH succession is not exposed (Fig. 6A).

In the MCH outcrop, the lower and uppermost beds are coarser grained, conformed of volcanoclastic–bioclastic, mixed gravelly–sandstone (lithofacies bSGm; Fig. 6E), and mega-rippled bioclastic limestone (lithofacies bLr-m;

Fig. 6D, F, G). The central part of the outcrop is relatively homogeneous and consists of well-sorted, wave-rippled bioclastic limestone (bLr-o; Fig. 6C, F, G). Bedding is tabular to wedge-shaped, displaying a subtle, fining- to coarsening-upwards trend (Fig. 6B). Bedding planes are commonly amalgamated, sinuous, and only recognized by tafoni superimposed on ripples (Fig. 6C, F). Sharp boundaries are subordinate, these are interpreted as erosive or reactivation surfaces (Fig. 6C).

The fossil content is fragmentary, though reworked, but articulated big-sized oysters (*Gryphaeidae* indet; *Aetostreon* sp.1.; Fig. 6M, N) and other small pectinids (*Entolium?* sp.; Fig. 6K), as well as bulb-shaped fish teeth (*Pycnodontidae* indet.), were found scattered in the middle part of the section (Fig. 6A, C). Near the top, complete, small- and medium-sized, oyster left-valves assigned to *Aetostreon* sp. and *A.* sp.2 (Fig. 6H) are abundant in mixed, gravelly floatstone beds. The latter were also found as small clusters, but detached from its original bed (*ex situ*; Fig. 6J). Exceptionally, some lenses of carbonized wood were observed (Fig. 6L) and, at the northern end of the outcrop, a lenticular bed of oyster-rich rudstone/coquinite was found (bRp; Fig. 6I).

Interpretation: Based on wave ripples (Walker and Plint 1992), mostly comminuted shells, and packstone–grainstone microfacies, these sediments suffered wave-reworking above the fair-weather wave-base, i.e., in the inner-ramp (Burchette and Wright 1992; Flügel 2010). This mixed inner ramp was affected by periodical storm-surges, as shown by mega-rippled limestone, coarse-grained coquinities, and layers with a bimodal distribution of bioclasts interpreted as tempestites (Kidwell et al. 1986; Flügel 2010; Fig. 6H). Storm-currents were strong enough to remobilize and rapidly bury big-sized, reclining oysters (*Aetostreon* spp.). These energetic events were periodic as shown by amalgamated layers and pinched-out bed-sets, enclosed by erosive surfaces (Fig. 6C).

This outcrop is described here for the first time. Regarding composition, thickness, and inferred age (Sect. “Stratigraphy and correlations”), the Muralla China limestone corresponds to one of the most remarkable Lower Cretaceous calcareous outcrop reported from the Aysén-Río Mayo Basin.

Salto Río Pollux Section (SRP2)—mixed, distal mid-ramp

This outcrop is located about 1 km to the south of the Muralla China Section (MCH), at the northern hand of Route 7, just before reaching the Pollux River (Fig. 1D). It is composed of ca. 9 m of dark-coloured, bioclastic muddy

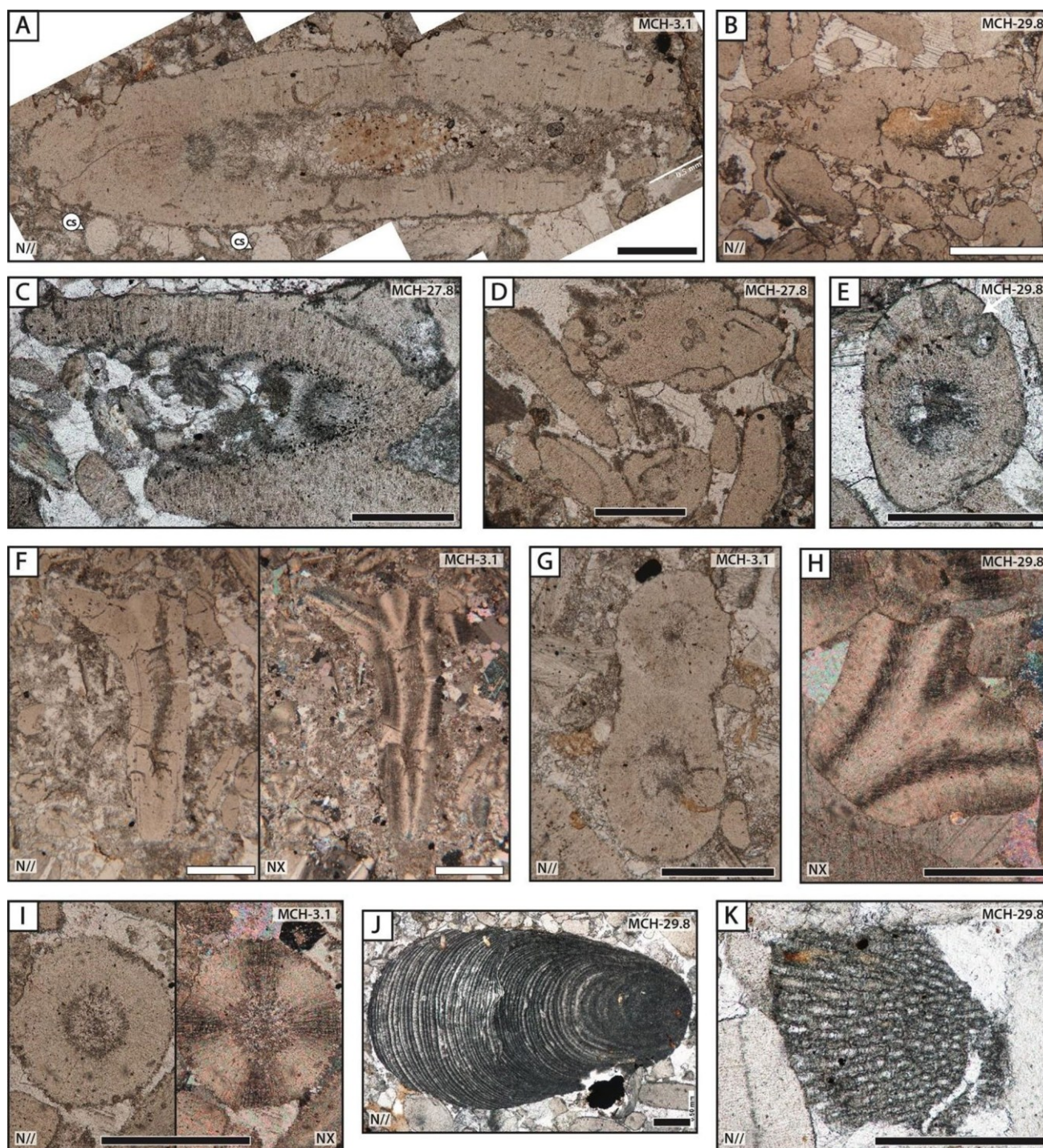
sandstone dipping towards the southeast (strike/dip = 041/10; Figs. 4C; 7A, B). Its base and top are not exposed; however, the outcrop is capped by the Muralla China sill (see 1.2; Fig. 7A–C) and, about 100 m to the east, this outcrop is separated from the black mudstones of the Katterfeld Formation by an inferred fault (Fig. 1D).

The Salto Río Pollux outcrop comprises bioclastic–volcaniclastic, muddy sandstones (lithofacies bSp), alternated with calcareous sandy beds (bSp-c; Fig. 7A). The former (bSp) are more abundant in the lower half of the outcrop, exposed as poorly defined, amalgamated beds (Fig. 7C, H). Some of them are rich in organic matter (microfacies Mf-4om; Fig. 7E). In contrast, calcareous beds (bSp-c), stand out as weathering-resistant guide beds (Fig. 7B–D). Bed-boundaries between these both lithofacies are sharp and sinuous (Fig. 7C, D). The middle point of the outcrop is marked by a 0.3 m-thick, fine interbedding of fossil-bearing, mixed sandstone (bSp) and tuffaceous sandstone (lithofacies tSp-b; Fig. 7C, H, I).

Bioclasts are abundant, dominated by bedding-concordant shell debris (mostly oysters; Fig. 7E). Complete macrofossils include scattered belemnite rostra (*Belemnopsis* sp.), and left valves of *Aetostreon* sp.2 (“*Aetostreon* sp. nov.” Rubilar 2000; Fig. 7F, I, J here), the latter also found conforming small clusters in life position (Fig. 7J).

Interpretation: Based on the matrix-rich, mixed sandstone (microfacies Mf-4), its bimodal fossil distribution (comminuted-complete), the amalgamation of its beds, and its sedimentary structures, these deposits reflect “event sedimentation” or “eventites” (Flügel 2010). They are interpreted as mixed calcareous–volcaniclastic tempestites settled in a mixed, distal mid-ramp (Wright and Burchette 1996; Flügel 2010), i.e., between the fair-weather- and the storm wave-base (Burchette and Wright 1992; Ramalho et al. 2013).

These tempestites show grain size differences between gravelly-grained shelly fragments and sandy-sized volcaniclastics, indicating a turbulent hydraulic sorting (Kidwell and Bosence 1991; Immenhauser 2009; Figs. 3I; 7E). The abundant comminuted shelly fragments were most likely swept off from the breaker- or swash area and were offshore-transported during storm-surges (Flügel 2010). As shown from the muddy matrix and well-preserved complete fossils, storm currents interrupted the relatively quiet background sedimentation, rapidly burying (or mildly reworking) the small, thin-shelled, recliner oysters in life position (*Aetostreon* sp.2; Fig. 7F, I–J) as well as other corporal fossils (e.g., belemnites; Fig. 7G). These small-sized *Aetostreon* sp.2 likely proliferated in a water–sediment interface affected by sporadic events of eutrophication, inferred from its organic matter content (Nori and Lathuilière 2003).



The high terrigenous content of the Salto Río Pollux beds reflects a major volcanoclastic supply (Table 1; Figs. 2G–K; 3M–O). Given the interbedding with tuffaceous beds (lithofacies tSp-b; Fig. 7C, H), and the similar composition of volcanic lithics and sedimentary matrix (Microfacies Mf-4; Fig. 3I, M–O), a remobilization of non-consolidated volcanoclastic

deposits is inferred (syneruptive?, McPhie et al. 1993; Schneider 2000). Previously, these volcanic deposits were classified as “volcanic coquinas” by Katz (1961). This author inferred a poorly-oxygenated, marine environment for these rocks, linked to a coeval, subaerial- and submarine volcanic eruptions. The former is supported by the fetid-odor and organic

• **Fig. 8** Red algae identified in the Toqui Formation (Manto Member). **A–I** *Archamphiroa jurassica* Steinmann (1930) **A** Longitudinal view displaying the internal hypothallium–perithallium contrast; note the alternation of dark–light arched layers in the hypothallium (apical part to the right). **B** Red algae-rich grainstone (microfacies Mf-3a), including several fragments of *A. jurassica*; note the bioerosion of bioclasts and dissolution-refill of the hypothallium. **C** Similar to **A**, longitudinal view of *A. jurassica* displaying the alternated layering (dark-coloured arches convex to the left). **D** Reworked, bioeroded, and micritized red algae fragments, possible source of the calcareous sediments (microfacies Mf-3a); note compaction (concave-convex contacts). **E** Club-shaped cavities in the peripheral zone of a reworked alga (cross-section), interpreted as bioerosion (white arrow). **F** Longitudinal view of *A. jurassica* displaying its non-geniculate ramification. **G** Cross-section of *A. jurassica* displaying the ramification (bifurcation) and hypothallium–perithallium contrast. **H** Longitudinal view displaying non-geniculate ramification, and the fan-shaped cell-arrangement in the hypothallium. **I** Circular cross-sections of thalli from *A. jurassica* are easy to confuse with echinoid spines; however, the red alga shows a fan-like extinction. **J** Reworked specimen of *Parachaetetes* sp. **K** Reworked specimen of “*Solenopora*” sp. Photographs from **C**, **E**, **J**, **K** courtesy of Prof. Dr. Ioan Bucur. Scale: black = 0.5 mm, white = 1 mm

matter content of these rocks (microfacies Mf-4; O’Brien and Slatt 1990; Ulmer-Scholle et al. 2014), and it could be linked to settling in a restricted environment or during a period of high biological productivity (Capelli et al. 2021). Regarding the volcanism, there is not enough evidence to support a sub-aqueous source.

Systematic paleontology

Oysters and red algae are the most abundant fossils found in the outcrops analyzed here. This section presents a detailed description of newly found fragments of the calcareous red alga *Archamphiroa jurassica*, identified here for the first time in the Lower Cretaceous of Chile (see “Calcareous-rich microfacies”; Fig. 2E, F; 8A–I). In addition, some oysters of the *Aetostreon* genus are also described (Fig. 9).

Archamphiroa jurassica

Class Rhodophyceae Rabenhorst 1863

Order ?Corallinales Silva and Johansen 1986

Genus *Archamphiroa* Steinmann 1930; emend. Bucur et al. 2009

Archamphiroa jurassica Steinmann 1930 (Pl. 1, Figs. 1–9)]; emend. Bucur et al. 2009 (neotype, Figs. 2–3).

Type material: The neotype was designated by Bucur et al. (2009) in algal wackestone of the Cotidiano Formation (see Fig. 1A, C). According to these authors, a neotype was

required given the loss of the original material, in which no holotype had been defined (see Steinmann 1930).

Type locality: Puesto Cotidiano (44°50’S; 71°39’W), at the isthmus connecting the La Plata and Fontana lakes in the Chubut province of Argentina (Fig. 1C). Originally defined by Steinmann (1930) at the Arroyo Negro, tributary of the Malargüe River in the Neuquén province of Argentina (ca. 35°S).

Material: Dozens of thallus fragments from the La Rosita (LRO, five thin sections; Fig. 4A) and Salto Río Pollux outcrops (SRP2, four thin sections; Fig. 4B); hundreds of thallus fragments from the Muralla China beds (MCH, six thin sections; Fig. 4C).

Description: Because of their small size, fragmentary preservation, strong cementation, and similar colour to that of the calcareous matrix-cement, thalli of *A. jurassica* are difficult to identify in hand samples. The following characteristics were used here for the assignation in thin section (based on Steinmann 1930; Bucur et al. 2009).

External: Thallus fragments are singular or frequently bifurcated, with rounded margins (Fig. 8A, C, E, F–I). Their cross-sections are circular, or ellipsoidal when obliquely cut (Fig. 8E, G, I); longitudinal views are ellipsoidal or sub-rectangular (Fig. 8A–C, H). When bifurcated, thalli are lambda-shaped, branches appear parallel-arranged, showing no hinge-like structure or constriction at the point of bifurcation (i.e., non-geniculate; Fig. 8F–H). Given their size and “dotted”, internal cell arrangement, thalli fragments might be confused with echinoids, though red algae display a clear fan-like extinction (Fig. 8H, I).

Internal: Thalli of *A. jurassica* are two-layered, with a central hypothallium covered by an outer perithallium (Fig. 8A, C, F–I). The hypothallium is multilayered coaxial, conformed of an alternation of dark- and pale-coloured arched cellular layers, convexly-oriented towards the apical part (Fig. 8A, C, F). Internally, the arches comprise elongated filaments, which diverge in an acute fan-shaped fashion (Fig. 8F, H). Filaments of the perithallium are oriented perpendicular to the thallus margin (Fig. 8A, E–G, I). In cross-section, the hypothallium appears darker or with a structureless cell arrangement, contrasting with the radial pattern observed in the perithallium (Fig. 8E, G, I).

In order to confirm peripheral cellular fusion, regarded as a diagnostic feature of this taxon, samples were observed using SEM, but without successful results. This may be linked to diagenetical alteration or incorrect preparation of the samples (see SEM-images as supplementary material).

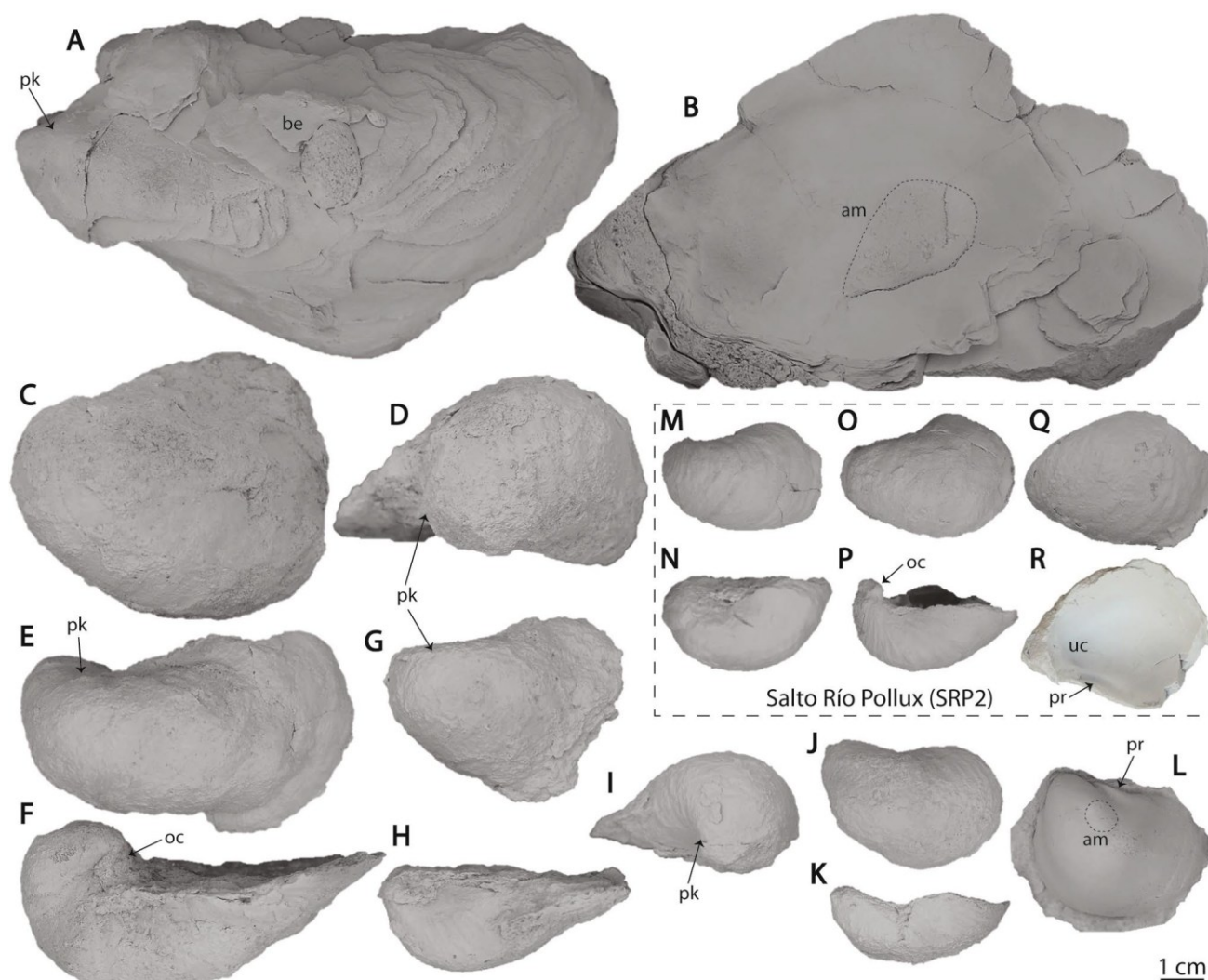


Fig. 9 *Aetostreon* spp. from the area south of Coyhaique. **A–L** Muralla China outcrop (MCH); **M–R**: Salto Río Pollux outcrop (SRP2). **A–B** (Sample MCH-14.8/1) *Aetostreon* sp.1, left valve, lateral view (A = external, B = internal); **C–D**: (Sample MCH-33/R/8) *Aetostreon* sp., external lateral- (C) and dorsal views (D). **E–F** (Sample MCH-33/R/2) *Aetostreon* sp., left valve, external lateral- (E) and posterior views (F); **G–I**: (Sample MCH-33/16) *Aetostreon* sp., left valve, external lateral- (G), posterior- (H), and dorsal views (I). **J–R**: *Aetostreon* sp.2. **J–K**: (Sample MCH-33/12) *Aetostreon* sp.2, exter-

nal lateral- (J) and posterior views (K); **L**: (Sample MCH/R/5) *Aetostreon* sp.2, internal mold; **M–N**: (Sample SRP2-3.2/9) *Aetostreon* sp.2, left valve, lateral external- (M) and posterior views (N); **O–P**: (Sample SRP2-2.7/6) *Aetostreon* sp.2, left valve, lateral external- (O) and posterior views (P); **Q–R**: (Sample SRP2-2.7/2) *Aetostreon* sp.2, left valve, lateral external- (Q) and internal views (R). Abbreviations: *am* adductor muscle scar (short dashed line); *be* bioerosion (long dashed line); *oc* opisthogryrate coiling; *pk* posterior keel; *pr* paradontal recess; *uc* umbonal cavity

Table 3 Measures of *Archamphiroa jurassica* taken in standards thin sections (summary)

	Max	Min	Avg	StdDev	Neotype*
ed	1.74	0.30	0.65	0.20	0.76
cd	0.72	0.12	0.26	0.09	0.23
prw	0.51	0.08	0.20	0.07	0.27

Ed external diameter, *cd* core diameter, *prw* width of the peripheral region, *Avg* average value, *StdDev* standard deviation. (*) Dimensional parameters (ed, cd, prw) as well as values for the neotype after Bucur et al. (2009, Table 1), included here for comparison purposes. Original data can be found in Table SM-5 (supplementary material)

Nevertheless, the assignment was confirmed by the Prof. Dr. Bucur (pers. com., 2020), with whom an algae-rich sample was shared.

Dimensions: The main size parameters for *A. jurassica* are summarized in Table 3 ($n = 128$, single measures are presented in Table SM-5 as supplementary material):

Remarks: Reproductive structures are absent. However, many thallus fragments show occasional circular, club-shaped, and irregular cavities as well as small, marginal

vermicular borings, caused by macro- and microborers (Fig. 8A–B, E).

Based on its cylindrical thallus shape and non-geniculate bifurcation, a fruticose to arborescent growth form is inferred for *Archamphiroa jurassica* (*sensu* classification of Woelkerling et al. 1993; see Fig. 10A, A').

Stratigraphic range: An early Callovian age was inferred for the beds bearing *Archamphiroa jurassica* in Central Argentina by Steinmann (1930), based on its association with Upper Jurassic brachiopods (“*Rhynchonella acuticosta*”) and corals (*Thamnasteria* sp.). In Southern Argentina, a late Tithonian age was suggested for the Cotidiano Formation by Bucur et al. (2009), unit bearing the *A. jurassica* neotype, type specimen defined by the same authors. The latter was based on the presence of *Steinmanella* (*Macrotrigonia* sp.) and *Megatrigonia* cf. *fontanaensis*, and on the close similarity of this fauna with the one found at Arroyo Pedregoso, which has been ammonite-dated to late Tithonian by Olivero (1982; based on *Berriasella* sp. and *Micracanthoceras ruedai*).

Outside southern Argentina, *Archamphiroa jurassica* Steinmann (1930) is now described from Coyhaique, Chile. This red alga is abundant in the mixed-calcareous outcrops here presented (see Sects. “La Rosita Section (LRO) - gravelly, mixed inner ramp” – “Muralla China Section (MCH) - wave and storm-dominated inner-ramp” above). The age of these outcrops is restricted to the late Berriasian/early Valanginian -Hauterivian? (see “Age of the deposits”). Therefore, this extends the range of *A. jurassica* to the Early Cretaceous, in particular, between the Tithonian-Valanginian (Hauterivian?).

***Aetostreon* spp.**

Superfamily Ostreoidea Rafinesque 1815

Family Gryphaeidae Vialov 1936

Subfamily Exogyrinae Vialov 1936

Tribe Nanogyrini Malchus 1990

Genus *Aetostreon* Bayle 1878

Type species: *Gryphaea latissima* Lamarck 1801, p. 399.

Diagnosis (modified from Stenzel 1971; Cooper 1995; Toscano and Lazo 2020): Medium- to large-sized, thick-shelled,

inequivalve. Opisthogyrate umbo, gyrostreoid or exogyroid ligament area. Left valve: convex and deep; right valve: flat or slightly concave. Left valve thickened in the crest zone of umbonal ridge, displaying a keel in the posterior third. Keel is rounded to acute, commonly surmounted by knobs. Shallow groove parallel to the keel separates a slightly more convex posterior flank. No ornamentation except for growth lines or occasionally radial wrinkles. Internally, adductor muscle scar usually subtruncate antero-dorsally, but sometimes rounded; paradontal apparatus well developed; chomata lacking.

Description: Oysters assigned to *Aetostreon* in this study display a marked morphological variation, interpreted here as evidence of the occurrence of at least two different species. Morphs are discernable based on their size and general shape of the valves, but specific relevant taxonomic information is unfortunately not preserved. Shells of *Aetostreon* sp.1 are big-sized, thick, with a subtriangular outline and a keel more pronounced in the dorsal third (Figs. 5H; 9A–B); internally, lack of an umbonal cavity, and the rounded adductor muscle scar is dorsally truncated (Fig. 9B). Overall, *Aetostreon* sp.1 resembles *A. latissimum* from the northern Neuquén Basin in Argentina (e.g., Lazo 2007; Rubilar and Lazo 2009; Aguirre-Urreta et al. 2011; Toscano and Lazo 2020). The lack of key diagnostic traits (i.e., ligament area, umbo), presently demands the use of an open nomenclature for them.

Specimens of *Aetostreon* sp.2 are smaller, and thinner than *A. sp.1*, their left valves are globular with a subovate outline, and the umbo is opisthogyrate, with a small- to big-sized attachment area (Fig. 9J–R), and well-preserved growth lines (Fig. 9M, O, P). The keel is more pronounced in the umbonal area, changing to a slightly more convex posterior flank in the rest of the valve (Fig. 9L–R). Internally, *Aetostreon* sp.2 displays a moderate umbonal cavity (Fig. 9L, R), a narrow, linear paradontal recess, a subcircular adductor muscle scar, and the lack of chomata (Fig. 9L, R); these features are very similar to “*Aetostreon* sp. nov.” of Rubilar (2000). A third type of *Aetostreon* displays intermediate size between both *Aetostreon* sp.1 and *A. sp.2*, with left valves elongated in a ventral or ventro-posterior direction (Fig. 9C, E), a subovate- to subtriangular outline (Fig. 9C, E, G), and a keel in the posterior third, more pronounced near the opisthogyrate umbo (Fig. 9D–E, G). Given their poor preservation and sediment-coverage, it is not clear whether these oysters represent juveniles of *Aetostreon* sp.1, bigger morphotypes of *Aetostreon* sp.2, or a third different species. Therefore, they are presented conservatively as *Aetostreon* sp. (Fig. 9C–I).

Stratigraphic range: Globally, *Aetostreon* have been reported from the Oxfordian-Albian, but mainly from the

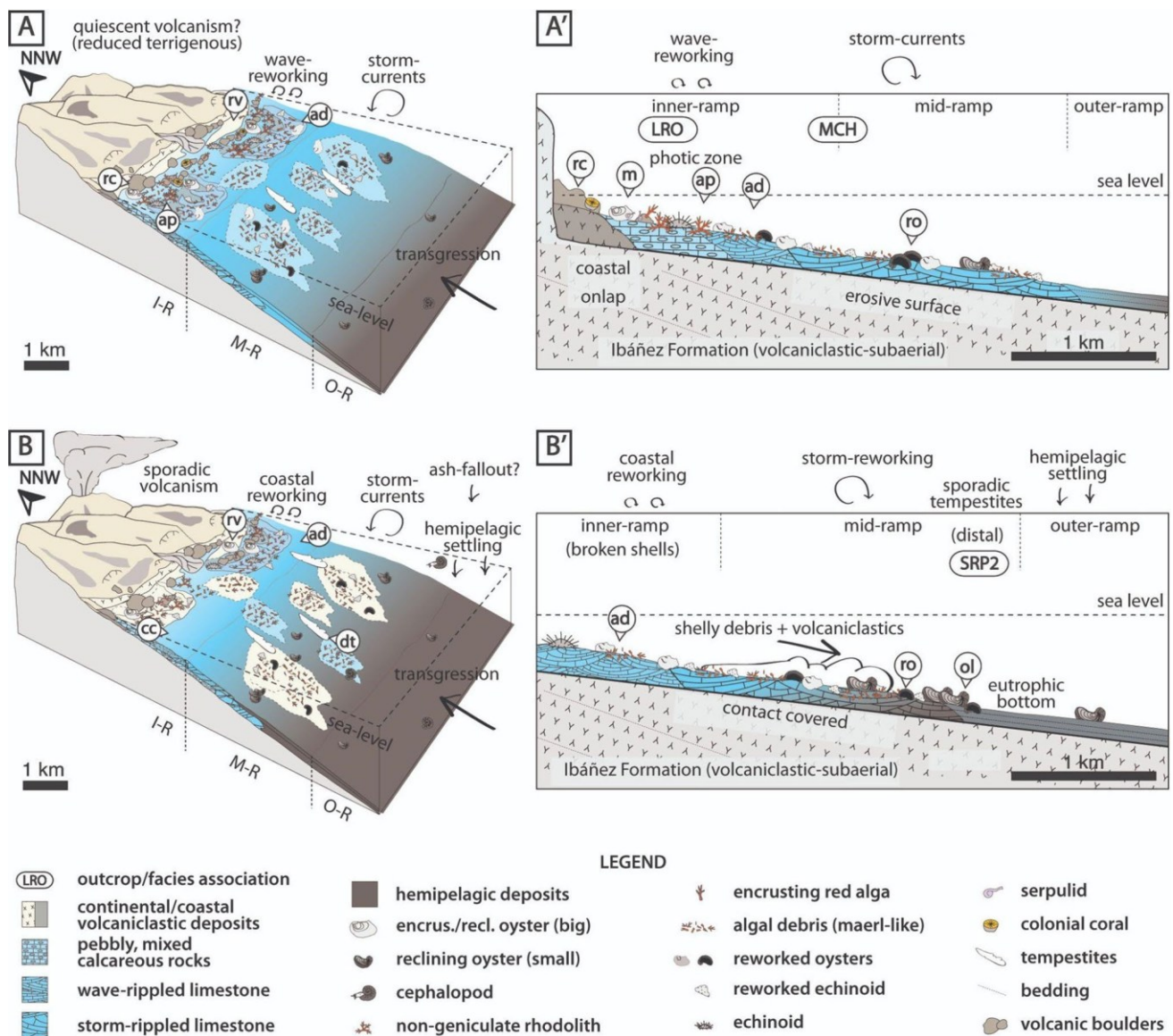


Fig. 10 Model for depositional environments and paleoecology of the Toqui Formation from the Coyhaique area (Modified from Rivas et al. 2021). Given the different composition and possible tectonic contacts between outcrops, which may reflect different timing of sedimentation (see “Discussion” in text), they are presented separated between calcareous-rich (LRO, MCH) and volcaniclastic-rich (SRP2). **A** Mixed, calcareous-volcaniclastic ramp model, during sedimentation of the LRO- and MCH beds. **A'** Cross-section displaying the shoreline-offshore arrangement of the facies associations, and the hypothetically, original habitat (communities) of the taxa here described as a fossil assemblage. **B** Mixed, calcareous-volcaniclastic ramp model, during sedimentation of the SRP2 beds. **B'** Cross-section displaying the shoreline-offshore arrangement of the facies associations. *I-R* inner ramp, *M-R* mid-ramp, *O-R* outer ramp, *ad* non-geniculate algal debris, as the result of near-coast wave and storm-

reworking, bioerosion, and grazing; they might resemble the current “maerl-type” deposits; *ap* algal pavements/meadows developed in the inner ramp, likely conforming non-geniculate rhodoliths; *cc* coastal carbonates; source of the eroded and crushed material, offshore-transported towards the deeper facies (SRP2); *dt* distal tempestites, formed by the offshore transport (mid-ramp) of shell-debris and sand-sized volcaniclastics during major storm-surges; *ol* small-sized, gryphaeid oysters in life position (isolated or in clusters; see Figs. 6, 7); *rc* rocky coast (source of gravel and encrusting organisms); *ro* reworked gryphaeid oysters; *rv* paralic/coastal resedimented volcaniclastics, interpreted as the main source of siliciclastic material in mixed lithofacies; *sv* syneruptive volcaniclastic input, eruption-fed (syneruptive) or after costal reworking of non-consolidated tuffaceous deposits. Scales are approximate, based on the current position of the outcrops (fossils not to scale)

Berriasian-Aptian range (Cooper 1995; Toscano and Lazo 2020, and references therein). In the Neuquén Basin of Argentina, several species of *Aetostreon* have been described in early-mid Berriasian (*A. subsinuatum*), late Berriasian-early Valanginian (*A. latissimum*; Toscano and Lazo 2020), late Valanginian (*A. pilmatuegrosum*; Rubilar and Lazo 2009), and late Valanginian-early Hauterivian units (*Aetostreon* sp.; Lazo 2007).

Discussion

Paleogeography

In the Aysén-Río Mayo Basin, several mixed- and calcareous outcrops have been identified (e.g., Płoszkiewicz and Ramos 1977; Ramos 1978; Olivero 1983, 1987; Scasso 1987; Covacevich et al. 1994; Bell et al. 1994; Suárez et al. 1996; Townsend 1998; Ramos and Lazo 2006; Suárez and De la Cruz 1994a, b, among many others). However, an unequivocal correlation of these deposits has been hindered, due to their discrete and discontinuous exposures, rapid lateral and vertical facies changes (Scasso 1989; Scasso and Kiessling 2002), and diachronism (Suárez et al. 2005, 2010a). The latter is linked to a marine incursion over an irregular topography, affected by extensional tectonics and active volcanism (Ramos 1981; Scasso 1987; 1989; Folguera and Iannizzotto 2004; Suárez et al. 2009, 2010a). In addition, during the Cenozoic, strong strike-slip tectonic disruption as well as Neogene glacial events have affected the Coyhaique area (Scalabrino 2009). This is evident in the study area, where the outcrops are disconnected, incomplete, and located at different elevations (Figs. 1C, D; 5B, 6A, 7B).

Nevertheless, based on composition, common fossil assemblages, inferred sedimentary environments, and contact relationship with the volcanic units, the outcrops La Rosita (LRO) and Muralla China (MCH) appear to be laterally correlative, and part of the same carbonate-rich, mixed inner ramp setting (Figs. 4A, B; 10A–A'). Volcaniclastic-rich strata from the uppermost LRO outcrop show a sporadic clastic input, whereas thicker bedded limestones of the MCH outcrop reflects a relatively stable carbonate sedimentation, either located in a more distant setting from the coastal volcaniclastic source, or deposited during a phase of quiescent terrigenous supply (Nelson 1988; James 1997; Dorobek, 2008; Fig. 10A). Both outcrops are carbonate-rich and assigned here to the Manto Member of the Toqui Formation (*sensu* Rivas et al. 2021).

As shown in Sects. “La Rosita Section (LRO) - gravelly, mixed inner ramp” – “Muralla China Section (MCH) - wave- and storm-dominated inner-ramp”, this ramp was developed during the marine transgression above a volcanic terrain (Fig. 10A, B), interpreted by several authors as an insular

volcanic flank (e.g., Bell et al. 1994; De la Cruz et al. 1994; Suárez et al. 1996; Townsend 1998; De la Cruz et al. 2003; Suárez et al. 2023). The latter may explain the preservation of gravel-rich facies, common in volcanic coasts affected by rapid shoreline translation (Felton 2002; Ramalho et al. 2013). The relationship between the previous outcrops (LRO, MCH) and the Salto Río Pollux (SRP2) section is unclear (Fig. 4B, C), given their contrasting lithologies, structural attitude, and inferred tectonic contacts. Although they share the same fossil content (but in different proportions, see Table 1), which may support a lateral correlation, the SRP2 succession bear intraclasts type 1 (reworked bioclastic limestone; Fig. 3B), and its composition reflects a deeper setting and a major volcaniclastic supply. Alternatively, based on the volcaniclastic-rich facies of the SRP2 outcrop, more compatible with the San Antonio Member of the Toqui Formation (*sensu* Rivas et al. 2021), it might represent a vertical transition in the facies, with sediments deposited in a (younger) period controlled by a terrigenous and probably syneruptive input (tuffaceous beds of lithofacies tSp- b; Fig. 10B–B'). An increased clastic supply may also be related to enhanced run-off, triggered by the change from dry to humid (and hotter?) conditions (Capelli et al. 2021).

Paleoenvironmental interpretation

“Cool-water” carbonate setting

Following the “cool-water” criteria of James (1997), and based on paleolatitude (non-tropical), platform morphology (ramp-type), and mode of life of benthic organisms (heterozoan association), a non-tropical, “temperate” or “cool-water” (*sensu lato*, Schlager 2003) setting is inferred for the study area, i.e., an open marine environment with water temperatures of < 18°–20 °C (“temperate-type” *sensu* Simone and Carannante 1988; James 1997; Schlager 2005). However, since factors other than temperature may strongly affect carbonate ecosystems and their grain associations (e.g., terrigenous input, trophic conditions, water chemistry, CO₂ saturation, among others, Kindler and Wilson 2010; Westphal et al. 2010; Michel et al. 2018), a “cool water” setting is used here in a broad sense (see contrasting examples in “Regional comparison”). Criteria supporting a cool-water setting for the rocks studied here are explained below.

As shown in “Age of the deposits”, the mixed rocks studied here appear to be restricted to the Lower Cretaceous. For that period, paleotectonic reconstructions of South America place the study area to south of 45°–50°S (e.g., Leinfelder et al. 2002; Scasso and Kiessling 2002; Seton et al. 2012; Matthews et al. 2016), i.e., in a non-tropical, high paleolatitude (Scasso and Kiessling 2002).

Facies, sedimentary structures and reworked bioclasts depict a shallow-marine environment for the mixed outcrops

of the Toqui Formation (refer to Sects. “Sedimentary logs and facies associations”). Wave- and storm-related structures reflect a relatively high-energy and a hydrodynamic control (Figs. 5C, 6C–G; 7D, E) regarded as typical for open shelves and ramp-type carbonate platforms lacking physical barriers (i.e., reefs, sand shoals; Burchette and Wright 1992; Wright and Burchette 1996; James 1997; Pedley and Carannante 2006; Flügel 2010).

Tropical carbonates usually accumulate in low latitudes (between ca. 30°N and S of the equator, Schlager 2003), in waters with temperatures higher than 20°–22 °C (Nelson 1988; James 1997; Schlager 2003). They are characterized by photo-autotrophic organisms with a dominant aragonitic mineralogy (e.g., green and red algae, hermatypic corals, and photosymbiotic interactions), and a biotic-abiotic precipitation of carbonate mud, cements, and non-skeletal allochems (Lees and Buller 1972; Nelson 1988; Schlager 2003; Kindler and Wilson 2010 and references therein). In contrast, limestones documented here are poor in carbonate mud and non-skeletal allochems (only sporadic intra-clasts), and the benthic fauna is dominated by calcareous red algae and calcitic-shelled heterotrophic organisms (see next Sect. “Paleoecology”), conforming a heterozoan association (*sensu* James 1997; Clarke 2009; Kindler and Wilson 2010).

Paleoecology

The fossil assemblage studied here is mostly composed of sessile organisms, including encrusters (red algae; serpulids; bryozoans; ahermatypic corals, oysters; Figs. 2; 5E, H, J), soft-bottoms recliners (gryphaeid oysters; Figs. 6J, M, N; 7F, J), vagile epifauna (echinoids, pectinids; Fig. 6K), and nektonic animals (fishes, belemnites; Fig. 7G). Most of these organisms are stenohaline and support an euhaline and shallow, open marine environment (e.g., Wray 1977; Scholle and Ulmer-Scholle 2003; Stenzel 1971; Toscano et al. 2018; Cawley et al. 2021). However, some of these organisms may also have an euryhaline physiology (e.g., bryozoans, oysters, red algae, serpulids *sensu* Scholle and Ulmer-Scholle 2003), thus, local brackish areas or zones with a variable salinity may also be feasible (Townsend 1998). This has been commonly reported from some volcanic coastlines with an alluvial influence (Ramalho et al. 2013).

Red algae are the most remarkable photo-autotrophic organisms found in these rocks of the Toqui Formation (Fig. 8); they might represent the main source of carbonate (Wray 1977; Flügel 2010; abraded-bioeroded algae in Fig. 8B, D). Algal content is reworked and found as broken branches or rounded bioclasts, abundant in wave-influenced sediments (inner ramp; lithofacies bLr). An original shallow-water setting in the photic zone is inferred for them (Michel et al. 2018), encrusting submerged rocky blocks (“solenoporoids”), or conforming semi-protected?,

low-relief meadows or “pavements” in coastal areas (see Fig. 5 in Henrich et al. 1995; Fig. 10A, A' here). The latter, rich in ramified non-geniculate algae (*A. jurassica*), is considered as wave-reworked and offshore-transported (Fig. 10A, A'). Red algae-rich grainstones like the ones described resemble the current “maerl-type” deposits, conformed by broken branches of non-geniculate, unattached rhodoliths, typically found today in high-latitude, shallow and cool-water settings of the North East Atlantic (Henrich et al. 1995; Ehrhold et al. 2021).

Ahermatypic corals flourished during the incipient transgression, encrusting subtidal gravel in a shallow-water setting; they disappeared upsection likely due to sediment stress (Risk and Edinger 2011; see Fig. 10A, A'). Echinoid plates and spines are rich in wave- and storm-reworked sediments. An epifaunal or semi-infaunal habit in the sandy sediments, grazing on the algal meadows is commonly recognized for them (Nebelsick and Bassi 2000; Kroh 2003; see Fig. 10A, A').

In the Aysén-Río Mayo Basin, oysters are mostly represented by exogyrids of the genre *Aetostreon* (Fig. 9), regarded as a homeomorph of *Gryphaea* (Stenzel 1971). Gryphaeids could live attached or free-lying (MacKerrow, 1981) in subtidal settings with soft-bottom and euhaline quiet water (Stenzel 1971; LaBarbera 1981). Analogous to *Gryphaea*, *Aetostreon* is also depicted as a soft-bottom recliner (Lazo 2007) living in shallow, low-energy inner-shelf settings with sandy-muddy, soft-bottoms (Cooper 1995; Lazo et al. 2005; Rubilar and Lazo 2009); in intertidal shelly mudstones (Cooper 1995); or forming biostromes in micritic mid-ramp settings (Rivas et al. 2021). In this study, big-sized articulated *Aetostreon* sp.1 from the LRO and MCH outcrops are found reworked in sandy limestones (lithofacies bLr), reflecting a local provenance (Figs. 5H, 6M–N, 9A–B). It is unclear if the oyster coquinites (lithofacies bRp) from the MCH outcrop may correspond to the same species (Fig. 6I), while in the LRO outcrop, Townsend (1998) reported life-positioned oysters encrusted in the basal volcanic blocks, but without providing a taxonomical assignation.

Smaller oysters from the MCH and SRP2 outcrops were tentatively classified as different species (*Aetostreon* sp. and *A. sp.2*; Fig. 9), though subtle morphological differences between specimens may represent morphotypes (Rubilar 2000). For example, the uppermost beds of the MCH outcrop bear a mixture of medium-sized (*Aetostreon* sp.; Fig. 9C–I) and small-sized oysters (*Aetostreon* sp.2; Fig. 9J–L); both appear as reworked and disarticulated valves, embedded in sandy limestone (Fig. 6H, J). In contrast, in the SRP2 outcrop, only small specimens were observed (*Aetostreon* sp.2 = “*Aetostreon* sp. nov.” Rubilar 2000, ex “*Gryphaea balli*” *sensu* Cecioni and Charrier

1974; Fig. 9M–R), in life position and reworked, embedded in shelly, muddy sandstone (lithofacies bSp; Fig. 7F, I–J).

In *Gryphaea*, their relatively heavy shells are unlikely to be distantly transported, serving as a good paleoecological indicator (Bayer et al. 1985). In addition, wider morphotypes may reflect an ecophenotypic adaptation to firmer substrates (e.g., sand-rich); this is also supported by the presence of bioeroded and reworked shells, more exposed to erosional events (Bayer et al. 1985). Therefore, in the MCH outcrop, small- and mid-sized *Aetostreon* spp. were likely transported from low-energy, muddy–sandy shallow-marine settings (see paragraph above), or they were adapted to bioclastic sandy bottoms of the carbonate inner ramp (Fig. 10A, A'). In the SPR2 beds, dominant small-sized *Aetostreon* sp.2 thrived in mud-rich soft-bottoms (LaBarbera 1981), with tendency to eutrophication (rich in organic matter; Nori and Lathuillière 2003), interpreted here as part of the mid-ramp (Fig. 10B, B').

Based on the previous, the fossil assemblage described here depicts an autochthonous-para-autochthonous assemblage in the inner-ramp (outcrops LRO, MCH; Fig. 10A, A'), but an autochthonous-allochthonous in the mid-ramp (outcrop SPR2; Fig. 10B, B').

Paleoclimate

The calcareous sedimentation in the Aysén-Río Mayo Basin was strongly diachronic, likely ranging from the Tithonian–Valanginian, or even Hauterivian (see Sect. “Stratigraphy and correlations”). Paleoclimate models for the Jurassic–Cretaceous transitions are usually contrasting. Some authors infer an equable warm climate, with a lower temperature gradient and absence of polar ice caps (Hay 2008; Föllmi 2012), while others depict episodic cooling or “cool-snaps” (Price 1999; Kessels et al. 2006; Donnadieu et al. 2011), or even seasonal growth of polar ice (Price 1999, 2009; Price et al. 2000; McArthur et al. 2007; Mutterlose et al. 2009; Hay and Floegel 2012; Tennant et al. 2017 among many others). Globally, the most remarkable J–K cool-spans are depicted as occurring during the late Tithonian, the mid-Valanginian, and across the Aptian–Albian boundary (Price 1999), though they have been called into question in more recent studies (Föllmi 2012; Jenkyns et al. 2012). This paradox is also extended to southern South America, where some models infer warm (> 25 °C), sea-surface temperatures in the Southern Ocean during the J–K transition (ca. 52°S; Jenkyns et al. 2012; Vickers et al. 2019); while others propose episodic cool intervals in the late Tithonian–earliest Berriasian, Valanginian, earliest Hauterivian, late Barremian, Aptian, and earliest Albian (Salazar and Stinnesbeck 2015; Brysch 2018).

In the Aysén-Río Mayo Basin (Fig. 1B), the paleoclimatic evidence for the existence of cold snaps is inconclusive. Overall, warm and humid conditions have been inferred for

the deposition of the Coyhaique Group (Tithonian–Aptian), but only based on the presence of limestone (Skarmeta 1976; Bell et al. 1994, 1996; Townsend 1998). However, as presented in “Paleoecology”, mixed rocks of the Toqui Formation exposed south of Coyhaique, and assigned to the late Berriasian/early Valanginian–Hauterivian? (see “Age of the deposits”; “Stratigraphy and correlations”), display typical features of “cool water” carbonates (see ““Cool-water” carbonate setting”).

Two events of global cooling are known from this period and are supported by evidence from Patagonia (Brysch 2018). The first one, across the Berriasian–Valanginian boundary, is marked by a glacioeustatic, long-term sea-level fall (Pucéat et al. 2003; Haq 2014). The second, in the Valanginian (Weissert and Erba 2004; Cavalheiro et al. 2021), corresponds to a positive carbon isotope excursion (“Weissert Event”; e.g., van de Schootbrugge et al. 2000; Meissner et al. 2015; Price et al. 2018), linked to a high rate of organic carbon burial (Erba et al. 2004; Price et al. 2018). Alternatively, these “episodes of environmental change” (*sensu* Föllmi 2012), among others during the Early Cretaceous, may represent short-termed humid periods alternated with long-termed arid greenhouse conditions (Föllmi 2012). For example, to the north, in the Neuquén basin (ca. 37°S), a shift to more humid conditions have been inferred during the early Berriasian–latest early Valanginian, prior to the onset of the Weissert Event (Capelli et al. 2021). There, humid conditions would have led to an enhanced runoff, triggering a shift from calcareous-rich to clastic-rich sedimentation (Capelli et al. 2021) as observed here (see ““Cool-water” carbonate setting”).

However, given the several unresolved problems regarding the global J–K paleoclimate models (Hay 2017), and the ambiguous, broad age range inferred for these outcrops of the Toqui Formation, more analytical data are required, to incorporate them in the global paleoclimatic scheme.

Regional comparison

The Toqui formation has been correlated with the upper Tithonian Cotidiano Formation, and with the Tithonian? – Hauterivian Tres Lagunas Formation from Argentina (45°S; see Sect. “Stratigraphy and correlations”). *Archamphiroa jurassica* has been reported from both the Cotidiano Fm. and from the outcrops presented here (Toqui Fm.), though both units differ in their carbonate depositional settings and inferred ages (see “Age of the deposits”). The Cotidiano Formation consists of biohermal limestone (“coral-stromatoporoid patch reefs”; Ramos 1978), analog to the “Photozoan Association” of James (1997), likely settled in a tropical–subtropical environment ($T > 22\text{ °C}$ *sensu* Ramos 1976; 1978), or in a warm-water ocean ($T > 18\text{ °C}$

sensu Kiessling et al. 1999; Leinfelder et al. 2002; Leinfelder et al. 2005). This contrast may be explained by the marked temporal gap between both deposits (Tithonian versus upper Berriasian–Hauterivian?), and potential deposition under differing paleoenvironmental conditions.

A similar problem arises when comparing the present outcrops of the Toqui Formation with those from the Tres Lagunas Formation. Even though both units display a mixed carbonate-clastic composition and partly coeval ages, their calcareous facies and depositional environments are clearly different. At its type locality (Laguna Salada), the Tres Lagunas Formation includes conglomerates, limestones (coquinites and coral-bioherms), tuffaceous beds, and sandstone–mudstone alternations (some calcareous or bioclastic); these rocks are discretely exposed showing abrupt vertical and lateral facies changes (Scasso 1987; 1989; Scasso and Kiessling 2002). Carbonate facies of the Tres Lagunas Fm. have been interpreted as coral patch-reefs and associated fore-reef deposits (Olivero 1983; Scasso 1987; 1989), likely developed in a warm-water setting during the Berriasian–Valanginian (Scasso 1989; Scasso and Kiessling 2002). These rocks depict a rimmed carbonate shelf (bioherms), contrasting with the wave- and storm-influenced, open-marine ramp deposits presented here (see Sects. 4, and 6.1). The cause behind these opposing depositional environments is not clear. Paleolatitude and temporality do not seem to be the controlling factors, and other variables must be considered; for example, their position within the basin (see paleo-reconstructions in Scasso 1989; Folguera and Iannizzotto 2004), but also coast morphology and hydraulic settings (rimmed shelf vs ramp profile), coeval volcanism (Scasso and Kiessling 2002), and terrigenous input or trophic conditions (e.g., coastal upwelling; Michel et al. 2018). The latter could have played a role in reef growth (Scasso and Kiessling 2002), as observed repeatedly in volcanic islands (Ramalho et al. 2013). Several other factors may favor the development of photozoan versus heterozoan benthic communities (e.g., temperature, salinity, water depth, CO₂ concentration, etc.; Nelson 1988; Pomar et al. 2004; Kindler and Wilson 2010; and references therein); their role in the study area is still unclear and needs to be addressed in future studies.

Conclusions

Three sections assigned to the Lower Cretaceous Toqui Formation, the lowermost member of the Coyhaique Group, are here investigated from an area south of Coyhaique in southern Chile (45°40'S). These rocks overlie the volcanic Ibáñez Formation, regarded to represent the early Valanginian in the study area, and their top is not exposed. In the study area, the sedimentological and microfacial analysis

of the Toqui formation reveals a mixed calcareous–volcaniclastic composition, rich in reworked bioclasts conforming a heterozoan-type fossil assemblage. Mixed lithofacies and associated sedimentary structures reflect the development of a wave- and storm-influenced mixed ramp. Based on their lithologies, two outcrops were assigned to the Manto Member (calcareous-rich LRO, MCH sections) and one to the San Antonio Member of the Toqui Formation (volcaniclastic-rich SRP2 section). The calcareous sedimentation is depicted as part of a retrograding coast above an active volcanic terrain with sporadic activity.

Bioclastic, mixed calcareous rocks of the Toqui Formation conform a “heterozoan” association (heterotrophic organisms + red algae), bearing gryphaeid oysters (*Aetostreon* spp.), non-geniculate calcareous red algae, and echinoids as major constituents. Red algae are controlled by *Archamphiroa jurassica*, identified here for the first time in the Lower Cretaceous of Chile and previously reported only from the Tithonian of Argentina.

Based on the inferred high paleolatitude of these rocks (south of 45°–50°S), their heterozoan fossil assemblage, and depicted depositional setting (open-marine, ramp-type), a “cool-water” non-tropical setting is inferred for the Aysén–Río Mayo Basin in the Coyhaique area during the late Berriasian/early Valanginian–Hauterivian? This contrasts with the depositional environments inferred for correlative reefal rocks in Argentina (Tres Lagunas Formation), which reflect “warm-water” settings. In the Aysén–Río Mayo Basin, the influence of sea-water key physical variables in the carbonate sedimentation, as well as the position of the carbonate platforms within the basin, and their interaction with the volcanism are still unclear.

Electronic supplementary material The online version of this article (<https://doi.org/10.1007/s10347-023-00669-4>) contains supplementary material, which is available to authorized users.

Acknowledgements We gratefully acknowledge Prof. Dr. Ioan Bucur (Babes-Bolyai University), and Dr. Stephen Kershaw (Brunel University London) for their help in the determination of microfossils. We appreciate the guidance of the Prof. Dr. Axel Munnecke (Universität Erlangen-Nürnberg), and Dr. Alexander Varychev (Universität Heidelberg) during the acquisition of SEM images. The authors would like to thank Valentina Maldonado, Benjamín Aldridge and Rayen Álvarez for their support during field work. We are grateful to Dr. Roberto Scasso (Universidad de Buenos Aires) and one anonymous reviewer for their careful revision and constructive remarks on the manuscript, and Enrique Bostelmann for his thoughtful observations.

Author contributions HR: software, formal analysis, investigation, data curation, writing—original draft, writing—review and editing, visualization. CS: conceptualization, methodology, writing—review and editing, supervision, funding acquisition. WS: resources, writing—review and editing, supervision, project administration.

Funding Open Access funding enabled and organized by Projekt DEAL. Financial support to this project was provided by the Chilean National Fund for Scientific and Technological Development

(FONDECYT de Iniciación 11140176), by the Chilean National Agency for Research and Development (ANID/DOCTORADO BECAS CHILE/2016–72170384), and by the German Academic Exchange Service (DAAD, STIBET/ “Studienabschlussbeihilfe Stipendium”).

Data availability statement The data that support the findings of this study are available as supplementary material of this article. This additional information includes: i) description of each sedimentary log and their beds, compiled in the field (Table SM-1 to SM-3); ii) description and modal composition of each thin section (Table SM-4); measurement of exemplars of *Archamphiroa jurassica* under the microscope (Table SM-5).

Declarations

Conflict of interest The authors have no competing interests to declare that are relevant to the content of this article.

Open Access This article is licensed under a Creative Commons Attribution 4.0 International License, which permits use, sharing, adaptation, distribution and reproduction in any medium or format, as long as you give appropriate credit to the original author(s) and the source, provide a link to the Creative Commons licence, and indicate if changes were made. The images or other third party material in this article are included in the article's Creative Commons licence, unless indicated otherwise in a credit line to the material. If material is not included in the article's Creative Commons licence and your intended use is not permitted by statutory regulation or exceeds the permitted use, you will need to obtain permission directly from the copyright holder. To view a copy of this licence, visit <http://creativecommons.org/licenses/by/4.0/>.

References

- Aguirre-Urreta MB, Ramos VA (1981) Estratigrafía y Paleontología de la Alta Cuenca del río Roble, Cordillera Patagónica—Provincia de Santa Cruz. In: VIII Congr. Geol. Argentino, Actas, Buenos Aires, Argentina, III, 101–133.
- Aguirre-Urreta MB, Suárez M, Bruce Z, De la Cruz R, Ramos VA (2000) Bioestratigrafía y amonoides de la Formación Katterfeld, (Cretácico Inferior) en Puerto Ibáñez, XI región, Chile. In: IX Congr. Geol. Chileno, Actas, Puerto Varas, Chile, 2, 183–187.
- Aguirre-Urreta MB, Lazo DG, Griffin M, Vennari V, Parras AM, Cataldo, C., Garberoglio, R. and Luci, L. (2011) Megainvertebrados del Cretácico y su importancia bioestratigráfica. In: Geología y Recursos Naturales de la Provincia del Neuquén, Asociación Geológica Argentina, Buenos Aires, Argentina, pp 465–488.
- Aguirre-Urreta MB (2002) Invertebrados del Cretácico Inferior. In: Geología y Recursos Naturales de Santa Cruz (Ed. MJ Haller). Relatorio del XV Congreso Geológico Argentino, El Calafate, Argentina, pp 439–459.
- Artemieva IM (2023) Back-arc basins: a global view from geophysical synthesis and analysis. *Earth Sci Rev* 236:104242
- Bayer U, Johnson ALA, Brannan J (1985) Ecological patterns in Middle Jurassic *Gryphaea*: The relationship between form and environment. In: Sedimentary and Evolutionary Cycles (Ed. U. Bayer and A. Seilacher), Springer, Berlin, Heidelberg, 1, 436–463.
- Bayle K (1878) Fossiles principaux des terrains: Explication carte géologique France. 158 pp.
- Bell CM, Suárez M (1997) The Lower Cretaceous Apeleg Formation of the Aisen basin, Southern Chile. Tidal sandbar deposits of an epicontinental sea. *Andean Geology* 24:203–225.
- Bell CM, Townsend MJ, Suárez M, De la Cruz R (1994) The depositional environments of the Lower Cretaceous Coyhaique Group, Aysén Basin, southern Chile (45°–46°S). In: VII Congr. Geol. Chileno, Actas. Concepción, Chile, pp 402–403.
- Bell CM, De la Cruz R, Suárez M, Townsend MJ (1996) The evolution of the Aysen Basin, an early Cretaceous epicontinental interior seaway in the southernmost South America. *Géodynamique andine: résumés étendus*. ORSTOM, Paris, pp 289–292.
- Blair TC, McPherson JG (1999) Grain-size and textural classification of coarse sedimentary particles. *J Sed Res* 69:6–19.
- Bourgeois J, Leithold EL (1984) Wave-worked conglomerates: Depositional processes and criteria for recognition. In: *Sedimentology of gravels and conglomerates* (Ed. E.H. Koster, R.J. Steel, and Canadian Society of Petroleum Geologists), Canadian Soc. Petrol. Geol., Calgary, Canada, 331–343.
- Brysch S (2018) Changes in climate and palaeoenvironment during the Late Jurassic–Early Cretaceous in southern South America and western Antarctica. PhD Thesis, Ruprecht-Karls-Universität Heidelberg.
- Bucur IL, Kiessling W, Scasso RA (2009) Re-description and neotypification of *Archamphiroa jurassica* Steinmann 1930, a calcareous red alga from the Jurassic of Argentina. *J Paleontol* 83:962–968.
- Burchette TP, Wright VP (1992) Carbonate ramp depositional systems. *Sed Geol* 79:3–57.
- Capelli IA, Scasso RA, Spangenberg JE, Kietzmann DA, Cravero F, Duperron M, Adatte T (2021) Mineralogy and geochemistry of deeply-buried marine sediments of the Vaca Muerta-Quintuco system in the Neuquén Basin (Chacabuco Melehue section), Argentina: Paleoclimatic and paleoenvironmental implications for the global Tithonian-Valanginian reconstructions. *J S Am Earth Sci* 107:103103.
- Carling P (1999) Subaqueous Gravel Dunes. *SEPM JSR*. <https://doi.org/10.1306/D4268A2C-2B26-11D7-8648000102C1865D>
- Cas RAF, Wright JV (1987) Volcanic successions: modern and ancient. a geological approach to processes, products and successions. Chapman & Hall, London, p 528.
- Cavalheiro L, Wagner T, Steinig S, Bottini C, Dummann W, Esegbue O, Gambacorta G, Giraldo-Gómez V, Farnsworth A, Flögel S, Hofmann P, Lunt DJ, Rethemeyer J, Torricelli S, Erba E (2021) Impact of global cooling on Early Cretaceous high pCO₂ world during the Weissert Event. *Nat Commun* 12:5411.
- Cawley JJ, Marramà G, Carnevale G, Villafañá JA, López-Romero FA, Kriwet J (2021) Rise and fall of pycnodontiformes: diversity, competition and extinction of a successful fish clade. *Ecol Evol* 11:1769–1796.
- Cecioni, G. and Charrier, R. (1974) Relaciones entre la Cuenca Patagónica, la Cuenca Andina y el Canal de Mozambique. *Ameghiniana*, XI, 1–38.
- Clarke J (2009) Carbonates, Cool Water. In: Gornitz V (ed) *Encyclopedia of paleoclimatology and ancient environments*. Springer, Netherlands, Dordrecht, pp 138–143.
- Clifton, H.E. (2006) A reexamination of facies models for clastic shorelines. In: *Facies Models Revisited* (Ed. H.W. Posamentier and R.G. Walker), *SEPM*, Tulsa, OK, 293–338.
- Cohen KM, Finney SC, Gibbard PL, Fan J-X (2013) The ICS international chronostratigraphic chart. *Episodes* 36:199–204.
- Collinson JD, Mountney NP, Thompson DB (2006) *Sedimentary structures*, 3rd edn. Terra, Harpenden, Hertfordshire, p 292.
- Cooper MR (1995) Exogyrid oysters (Bivalvia: Gryphaeoidea) from the Cretaceous of southeast Africa. *Durban Museum Novitates* 20:1–48.
- Covacevich V, De la Cruz R, Suárez M (1994) Primer hallazgo de fauna del Berriasiano inferior (Neocomiano) en la Formación Ibáñez, región XI, Aisen. In: VII Congr. Geol. Chileno, Actas, Concepción, Chile, I, 425–429.

- Cummings DI, Dumas S, Dalrymple RW (2009) Fine-grained versus coarse-grained wave ripples generated experimentally under large-scale oscillatory flow. *J Sed Res* 79:83–93
- De la Cruz R, Suárez M, Demant A (1994) Facies volcánicas del Mesozoico de Aisén (sector noreste), 44°–47° lat. S., Chile (Formaciones Ibáñez y Divisadero). In: VII Congr. Geol. Chileno, Actas, Concepción, Chile, I, 27–31.
- De la Cruz R, Suárez M, Covacevich V, Quiroz D (1996) Estratigrafía de la zona de Palena y Futaleufú (43°15'–43°45' latitud S), X Región, Chile. In: XIII Congr. Geol. Argentino y III Congr. Explor. Hidroc., Actas, Buenos Aires, Argentina, I, pp 417–424
- De la Cruz R, Suárez M, Belmar M, Quiroz D, Bell M (2003) Geología del área Coihaique-Balmaceda, Región Aisén del General Carlos Ibáñez del Campo. *SERNAGEOMIN*, Santiago, Chile, 40 pp.
- De la Cruz R, Welkner D, Suárez M, Quiroz D (2004) Geología del Área Oriental de las Hojas Cochrane y Villa O'Higgins, Región Aisén del General Carlos Ibáñez del Campo. *SERNAGEOMIN*, Santiago, Chile, 57 pp.
- Demant A, Suárez M, De la Cruz R, Bruguier O (2010) Early Cretaceous surtseyan volcanoes of the Baño Nuevo Volcanic Complex (Aysén Basin, Eastern Central Patagonian Cordillera, Chile). *Geol Acta* 8:207–219
- Donnadieu Y, Dromart G, Goddérès Y, Pucéat E, Brigaud B, Dera G, Dumas C, Olivier N (2011) A mechanism for brief glacial episodes in the Mesozoic greenhouse. *Paleoceanography*, 26:10
- Echaurren A, Folguera A, Gianni G, Orts D, Tassara A, Encinas A, Giménez M, Valencia V (2016) Tectonic evolution of the North Patagonian Andes (41°–44° S) through recognition of syntectonic strata. *Tectonophysics* 677–678:99–114
- Ehrhold A, Jouet G, Le Roy P, Jorjy SJ, Grall J, Reixach T, Lambert C, Gregoire G, Goslin J, Roubi A, Penaud A, Vidal M, Siano R (2021) Fossil maerl beds as coastal indicators of late Holocene palaeo-environmental evolution in the Bay of Brest (Western France). *Palaeogeogr Palaeoclimatol Palaeoecol* 577:110525
- Erba E, Bartolini A, Larson RL (2004) Valanginian Weissert oceanic anoxic event. *Geol.* 32, 149un
- Felton EA (2002) Sedimentology of rocky shorelines: 1. A review of the problem, with analytical methods, and insights gained from the Hulopoe Gravel and the modern rocky shoreline of Lanai. *Hawaii Sedimentary Geology* 152:221–245
- Fisher RV (1961) Proposed Classification of Volcaniclastic Sediments and Rocks. *Geol Soc America Bull* 72:1409
- Fisher RV (1966) Rocks composed of volcanic fragments and their classification. *Earth-Sci Rev* 1:287–298
- Fisher RV, Schmincke H-U (1984) Pyroclastic rocks. Springer, Berlin, p 472
- Flügel E (2010) Microfacies of carbonate rocks: analysis, interpretation and application, 2nd edn. Springer, Heidelberg; New York, 984 pp
- Folguera A, Iannizzotto NF (2004) The lagos La Plata and Fontana fold-and-thrust belt: long-lived orogenesis at the edge of western Patagonia. *J S Am Earth Sci* 16:541–566
- Föllmi KB (2012) Early Cretaceous life, climate and anoxia. *Cretac Res* 35:230–257
- Garzanti E (2019) Petrographic classification of sand and sandstone. *Earth Sci Rev* 192:545–563
- Gianni GM, Navarrete C, Echaurren A, Díaz M, Butler KL, Horton BK, Encinas A, Folguera A (2019) Northward propagation of Andean genesis: insights from early cretaceous synorogenic deposits in the Aysén-Río Mayo basin. *Gondwana Res* 77:238–259
- Gonzalez-Bonorio G, Suárez M (1995) Paleoambientes sedimentarios de la Formación Apeleg, Cretácico Inferior de la Cuenca de Aisen, Region XI. *Chile Andean Geol* 22:115–126
- Haller MJ, Lapido OR (1980) El Mesozoico de la Cordillera Patagónica Central. *Rev Asoc Geol Argentina*, XXXV, 230–247.
- Haller MJ, Lapido OR, Lizuaín A, Page R (1981) El mar tithononeocomiano en la evolución de la Cordillera Norpatagónica. In: Cuenas Sedimentarias del Jurásico y Cretácico de América del Sur, Com. Sudam. Jura. Cretac., 1, 221–237.
- Haller MJ, Lapido OR (1982) The Jurassic-Cretaceous volcanism in the septentrional Patagonian Andes. *Earth Sci Rev* 18:395–410
- Haq BU (2014) Cretaceous Eustasy Revisited. *Global Planet Sci* 113:44–58
- Hart BS, Plint AG (1989) Gravelly shoreface deposits: a comparison of modern and ancient facies sequences. *Sedimentology* 36:551–557
- Hart BS, Plint AG (1995) Gravelly shoreface and beachface deposits. In: Plint AG (ed) *Sedimentary facies analysis*. Blackwell, Oxford, UK, pp 75–99
- Hay WW (2008) Evolving ideas about the Cretaceous climate and ocean circulation. *Cretac Res* 29:725–753
- Hay WW (2017) Toward understanding cretaceous climate—an updated review. *Sci China Earth Sci* 60:5–19
- Hay WW, Floegel S (2012) New thoughts about the Cretaceous climate and oceans. *Earth Sci Rev* 115:262–272
- Hechem J, Figari E, Homocv J (1993) Secuencias deposicionales en el Neocomiano del lago Fontana, Chubut, Argentina. In: XII Congr. Geol. Argentino y II Congr. Explor. Hidroc., Actas, Mendoza, Argentina, II, 119–123.
- Henrich R, Freiwald A, Betzler C, Bader B, Schäfer P, Samtleben C, Brachert TC, Wehrmann A, Zankl H, Kühnmann DHH (1995) Controls on modern carbonate sedimentation on warm-temperate to arctic coasts, shelves and seamounts in the Northern Hemisphere: implications for fossil counterparts. *Facies* 32:71–108
- Hervé F, Calderón M, Faúndez V (2008) The metamorphic complexes of the Patagonian and Fuegian Andes. *Geol Acta* 6(1):43–45
- Iannizzotto NF, Folguera A, Leal PR, Iaffa D (2004) Control tectónico de las secuencias volcánicas neocomianas y paleogeografía en la zona del Lago La Plata (45°S). Sector interno de la faja plegada y corrida de los lagos La Plata y Fontana. *Rev Asoc Geol Argentina* 59:655–670
- Immenhauser A (2009) Estimating palaeo-water depth from the physical rock record. *Earth Sci Rev* 96:107–139
- Ippolitov AP, Desai B, Arkadiev VV (2015) First find of Parabelemnopsis, the alien belemnite from the southern hemisphere, in the upper Berriasian of Central Crimea. In: The International Scientific Conference on the Jurassic/Cretaceous boundary. Proceedings volume, Samara, Russia, 52–59.
- James NP (1997) The cool-water carbonate depositional realm. In: *Cool-Water Carbonates* (Ed. N.P. James and J. Clarke), *SEPM*, Tulsa, OK, 1–20.
- Jenkyns HC, Schouten-Huibers L, Schouten S, Sinninghe Damsté JS (2012) Warm middle jurassic-early cretaceous high-latitude sea-surface temperatures from the Southern Ocean. *Clim past* 8:215–226
- Katz H (1961) Sobre la ocurrencia de Cretáceo Superior marino en Coyhaique, Provincia de Aisén. *Anales De La Facultad De Ciencias Físicas y Matemáticas, Universidad De Chile, Santiago, Chile* 21:113–131
- Kendall AC, Tucker ME (1973) Radial fibrous calcite: a replacement after acicular carbonate. *Sedimentology* 20:365–389
- Kesjár D, Fözy I, Price G, Condon D, Salazar C, Pálffy J (2017) Integrated Lower Cretaceous stratigraphy from the Aisén Basin, Patagonia, Chile. In: 10th International Symposium on the Cretaceous - Abstracts (Ed. B. Sames), *Berichte der Geologischen Bundesanstalt, Vienna, Austria*, 120, 142.
- Kessels K, Mutterlose J, Michalzik D (2006) Early Cretaceous (Valanginian–Hauterivian) calcareous nannofossils and isotopes of the northern hemisphere: proxies for the understanding of Cretaceous climate. *Lethaia* 39:157–172

- Kidwell SM, Bosence DWJ (1991) Taphonomy and Time-Averaging of Marine Shelly Faunas. In: Allison PA, Briggs DEG (eds) Taphonomy: releasing the data locked in the fossil record. Plenum Press, New York, pp 115–193
- Kidwell SM, Fursich FT, Aigner T (1986) Conceptual framework for the analysis and classification of fossil concentrations. *Palaios* 1:228
- Kiessling W, Flügel E, Golonka J (1999) Paleoreef maps: evaluation of a comprehensive database of Phanerozoic reefs. *AAPG Bull* 83:1552–1587
- Kindler P, Wilson MEJ (2010) Carbonate grain associations: their use and environmental significance, a brief review. In: Carbonate systems during the Oligocene-Miocene climatic transition (Ed. M. Mutti, W.E. Piller, and C. Betzler), Blackwell Pub, Hoboken, NJ, 35–48.
- Kroh, A. (2003) Palaeobiology and biogeography of a Danian echinoid fauna of Lower Austria. In: Echinoderm research 2001: proceedings of the sixth European Conference on Echinoderm Research (Ed. J.-P. Feral and B. David), A.A. Balkema Publishers, Banyuls-sur-Mer, France, 69–75.
- LaBarbera M (1981) The Ecology of Mesozoic Gryphaea, Exogyra, and Ilymatogyra (Bivalvia: Mollusca) in a Modern Ocean. *Paleobiology* 7:510–526
- Lamarck JB (1801) *Système des animaux sans vertèbres*. Deterville, Paris, p 432
- Lazo DG (2007) Early Cretaceous bivalves of the Neuquén Basin, west-central Argentina: notes on taxonomy, palaeobiogeography and palaeoecology. *Geol J* 42:127–142
- Lazo DG, Cichowolski M, Rodríguez DL, Aguirre-Urreta MB (2005) Lithofacies, palaeoecology and palaeoenvironments of the Agrio Formation, Lower Cretaceous of the Neuquén Basin, Argentina. *J Geol Soc London Spec Publ* 252:295–315
- Leckie D (1988) Wave-formed, coarse-grained ripples and their relationship to hummocky cross-stratification. *J Sed Res*. <https://doi.org/10.1306/212F8E04-2B24-11D7-8648000102C1865D>
- Lees A, Buller AT (1972) Modern temperate-water and warm-water shelf carbonate sediments contrasted. *Mar Geol* 13:M67–M73
- Leinfelder RR, Schlagintweit F, Werner W, Ebli O, Nose M, Schmid DU, Hughes GW (2005) Significance of stromatoporoids in Jurassic reefs and carbonate platforms—concepts and implications. *Facies* 51:288–326
- Leinfelder RR, Schmid DU, Nose M, Werner W (2002) Jurassic reef patterns—The expression of a changing globe. In: Phanerozoic Reef Patterns (Ed. Wolfgang. Kiessling, Erik. Flügel, and Jan. Golonka), *SEPM (Society for Sedimentary Geology)*, 465–520.
- Leithold EL, Bourgeois J (1984) Characteristics of coarse-grained sequences deposited in nearshore, wave-dominated environments—examples from the Miocene of south-west Oregon. *Sedimentology* 31:749–775
- Malchus, N. (1990) Revision der Kreide-Austern (Bivalvia: Pteriomorpha) Ägyptens (Biostratigraphie, Systematik). *Berliner Geowissenschaftliche Abhandlungen*, **Reihe A**, 1–231.
- Masiuk V, Nakayama C (1978) Sedimentitas marinas mesozoicas del lago Fontana: Su importancia. In: VII Congr. Geol. Argentino, Actas, Neuquén, Argentina, II, 361–378.
- Matthews KJ, Maloney KT, Zahirovic S, Williams SE, Seton M, Müller RD (2016) Global plate boundary evolution and kinematics since the late Paleozoic. *Global Planet Change* 146:226–250
- MacKerrow WS (ed) (1981) *The Ecology of Fossils: an illustrated guide*. the MIT Press, Cambridge, Massachusetts, 384 pp.
- McArthur JM, Janssen NMM, Reboulet S, Leng MJ, Thirlwall MF, van de Schootbrugge B (2007) Palaeotemperatures, polar ice-volume, and isotope stratigraphy (Mg/Ca, $\delta^{18}O$, $\delta^{13}C$, $87Sr/86Sr$): the early cretaceous (Berriasian, Valanginian, Hauterivian). *Palaeogeogr Palaeoclimatol Palaeoecol* 248:391–430
- McPhie J, Doyle M, Allen RL (1993) Volcanic textures: a guide to the interpretation of textures in volcanic rocks. Centre Ore Depos. Explor. Stud. Univ, Tasmania, Hobart, 198 pp
- Meissner P, Mutterlose J, Bodin S (2015) Latitudinal temperature trends in the northern hemisphere during the Early Cretaceous (Valanginian–Hauterivian). *Palaeogeogr Palaeoclimatol Palaeoecol* 424:17–39
- Michel J, Borgomano J, Reijmer JJG (2018) Heterozoan carbonates: When, where and why? A synthesis on parameters controlling carbonate production and occurrences. *Earth Sci Rev* 182:50–67
- Mount J (1985) Mixed siliciclastic and carbonate sediments: a proposed first-order textural and compositional classification. *Sedimentology* 32:435–442
- Munneke A, Servais T, Vachard D (2000) A new family of calcareous microfossils from the silurian of Gotland, Sweden. *Palaeontology* 43:1153–1172
- Mutterlose J, Bornemann A, Herrle J (2009) The Aptian Albian cold snap: evidence for “mid” Cretaceous icehouse interludes. *N Jb Geol Paläont Abh* 252:217–225
- Myrow P (1992) Bypass-zone tempestite facies model and proximal-ity trends for an ancient muddy shoreline and shelf. *SEPM JSR*. <https://doi.org/10.1306/D426789D-2B26-11D7-8648000102C1865D>
- Myrow P (2005) Storms and Storm Deposits. In: Encyclopedia of Geology, Elsevier, 580–587.
- Nebelsick JH, Bassi D (2000) Diversity, growth forms and taphonomy: key factors controlling the fabric of coralline algae dominated shelf carbonates. *SP*, 178: 89–107.
- Nelson CS (1988) An introductory perspective on non-tropical shelf carbonates. *Sed Geol* 60:3–12
- Nori L, Lathuilière B (2003) Form and environment of *Gryphaea arcuata*. *Lethaia* 36:83–96
- O'Brien NR, Slatt RM (1990) *Argillaceous rock atlas*. Springer, New York, New York, NY
- Olivero EB (1983) Amonoideos y bivalvos berriasianos de la cantera Tres Lagunas, Chubut. *Ameghiniana* 20:11–20
- Olivero E (1987) Cefalópodos y bivalvos titonianos y hauterivianos de la Formación Lago La Plata, Chubut. *Ameghiniana* 24:181–202
- Olivero E, Aguirre-Urreta MB (2002) Sucesión de amonoideos de la Formación Katterfeld (Valanginiano-Hauteriviano) en su área tipo, Lago Fontana, Chubut. In: *XV Congr. Geol. Argentino, Actas*, El Calafate, Argentina, 6 pp.
- Olivero E (1982) Estratigrafía de la cuenca sur del Lago Fontana, Provincia del Chubut. PhD Thesis, Universidad de Buenos Aires
- Pankhurst RJ, Weaver SD, Hervé F, Larrondo P (1999) Mesozoic-Cenozoic evolution of the North Patagonian Batholith in Aysen, southern Chile. *J Geol Soc London* 156:673–694
- Pankhurst R, Hervé F, Fanning M, Suárez M (2003) Coeval plutonic and volcanic activity in the Patagonian Andes: the Patagonian Batholith and the Ibáñez and Divisadero formations, Aysén, Southern Chile. In: X Congr. Geol. Chileno, Actas, Concepción, Chile, 5 pp.
- Pedley M, Carannante G (2006) Cool-water carbonate ramps: a review. *J Geol Soc London Spec Publ* 255:1–9
- Pérez-López A, Pérez-Valera F (2012) Tempestite facies models for the epicontinental Triassic carbonates of the Betic Cordillera (southern Spain): tempestite models for the epicontinental Triassic, southern Spain. *Sedimentology* 59:646–678
- Petford N, Turner P (1996) Reconnaissance 40Ar-39Ar age and palaeomagnetic study of igneous rocks around Coyhaique, S. Chile (45°30'–47°S). In: Third ISAG, St Malo, France, 625–628.
- Plint AG (2010) Wave- and storm-dominated shoreline and shallow-marine systems. In: Facies models 4, 4. Version (Ed. N.P. James and R.W. Dalrymple), Geolog. Assoc. of Canada, St. Johns, 167–200.

- Ploszkiewicz JV, Ramos VA (1977) Estratigrafía y tectónica de la Sierra de Payaniyeu (Provincia del Chubut). Rev. Asoc. Geol. Argentina, XXXII: 209–226.
- Ploszkiewicz JV (1987) Descripción Geológica de la Hoja 47 c—“Apeleg”, Provincia del Chubut: Carta Geológico-económica de la República Argentina, Escala 1:200.000. *SEGEMAR Boletín*, 100 pp.
- Pomar L, Brandano M, Westphal H (2004) Environmental factors influencing skeletal grain sediment associations: a critical review of Miocene examples from the western Mediterranean: tropical foramol associations. *Sedimentology* 51:627–651
- Price G (1999) The evidence and implications of polar ice during the Mesozoic. *Earth Sci Rev* 48:183–210
- Price GD, Ruffell AH, Jones CE, Kalin RM, Mutterlose J (2000) Isotopic evidence for temperature variation during the early Cretaceous (late Ryazanian–mid-Hauterivian). *JGS* 157:335–343
- Price GD, Janssen NMM, Martinez M, Company M, Vandeveld JH, Grimes ST (2018) A high-resolution belemnite geochemical analysis of Early Cretaceous (Valanginian–Hauterivian) environmental and climatic perturbations. *Geochem Geophys Geosyst* 19:3832–3843
- Price GD (2009) Mesozoic Climates. In: *Encyclopedia of Earth Sciences Series: Encyclopedia of Paleoclimatology and Ancient Environments* (Ed. V. Gornitz), Springer Science+Business Media, 554–558.
- Pucéat E, Lécuyer C, Sheppard SMF, Dromart G, Reboulet S, Grandjean P (2003) Thermal evolution of Cretaceous Tethyan marine waters inferred from oxygen isotope composition of fish tooth enamels. *Paleoceanography*, 18: 7–1/7–12.
- Rabenhorst L (1863) Kryptogamen-Flora von Sachsen, Ober-Lausitz, Thüringen und Nord-Böhmen, mit Berücksichtigung der benachbarten Länder: erste Abtheilung: Algen im weitesten Sinne, Leber und Laubmoose. *Eduard Kummer*, Leipzig, 653 pp.
- Rafinesque C (1815) *Analyse de la Nature ou Tableau de l'University et des Corps Organisés*. *Juan Barravecchia*, Palermo.
- Ramalho RS, Quartau R, Trenhaile AS, Mitchell NC, Woodroffe CD, Ávila SP (2013) Coastal evolution on volcanic oceanic islands: a complex interplay between volcanism, erosion, sedimentation, sea-level change and biogenic production. *Earth-Sci Rev* 127:140–170
- Ramos VA (1978) Los arrecifes de la formación cotidiano (Jurásico Superior) en la cordillera patagónica y su significado paleoclimático. *Ameghiniana* 15:97–111
- Ramos ME, Suárez R, Boixart G, Ghigliione M, Ramos VA (2019) The structure of the northern Austral Basin: tectonic inversion of mesozoic normal faults. *J S Am Earth Sci* 94:102197
- Ramos VA, Lazo DG (2006) La Formación Tres Lagunas en las nacientes del arroyo Blanco al sur de lago La Plata—Chile. In: XI Congr. Geol. Chileno, Actas, Antofagasta, Chile, 2, 299–302.
- Ramos VA (1976) Estratigrafía de los lagos La Plata y Fontana, Provincia del Chubut, República Argentina. In: I Congr. Geol. Chileno, Actas, Santiago, Chile, 1, 43–64.
- Ramos VA (1981) Descripción Geológica de la Hoja 47 ab—“Lago Fontana”, Provincia del Chubut: Carta Geológico-económica de la República Argentina, Escala 1:200.000. *SEGEMAR Boletín*, 135 pp.
- Riccardi A (1977) Berriasian invertebrate fauna from the Springhill Formation of southern Patagonia. *N Jb Geol Paläont* 155:216–252
- Risk MJ, Edinger E (2011) Impacts of sediment on coral reefs. In: Hopley D (ed) *Encyclopedia of Modern Coral Reefs*. Springer, Netherlands, Dordrecht, pp 575–586
- Rivas H, Salazar C, Stinnesbeck W (2021) Facies and sequence stratigraphy of a mixed carbonate-volcaniclastic ramp in intra-arc settings: an example from the Toqui Formation (Lower Cretaceous), southern Chile (45°S). *J S Am Earth Sci* 109:103292. <https://doi.org/10.1016/j.jsames.2021.103292>
- Rubilar AE, Lazo DG (2009) Description of *Aetostreon pilmatuegrossum* sp. nov. from the Lower Cretaceous of Argentina (Neuquén Basin), and significance of the conservative left valve morphology in oysters of the genus *Aetostreon* Bayle. *Cretac Res* 30:727–748
- Rubilar AE (2000) *Aetostreon* sp. nov. del Neocomiano, sur de Chile y Argentina, y su afinidad morfológica con *Gryphaea* Lamarck. In: IX Congr. Geol. Chileno, Actas, Puerto Varas, Chile, 2, 249–253.
- Salazar C, Stinnesbeck W (2015) Redefinition, stratigraphy and facies of the Lo Valdés Formation (Upper Jurassic–Lower Cretaceous) in central Chile. *Boletín Del Museo Nacional De Historia Natural* 64:41–68
- Scalabrino B (2009) Déformation d'un continent au-dessus d'une dorsale océanique active en subduction. PhD Thesis, Université Montpellier 2 Sciences et Techniques du Languedoc
- Scasso RA, Kiessling W (2002) Earliest Cretaceous high latitude reefs in Tres Lagunas (Chubut Province, Argentina). In: *XV Congr. Geol. Argentino, Actas*, El Calafate, Argentina, 6 pp.
- Scasso RA (1987) Estratigrafía y ambientes de sedimentación del ciclo sedimentario del Jurásico Superior y Cretácico Inferior de la región sudoccidental del Chubut, con referencias a la columna estratigráfica general del área. PhD Thesis, Universidad de Buenos Aires
- Scasso RA (1989) La cuenca sedimentaria del Jurásico Superior y Cretácico Inferior de la región sudoccidental del Chubut. In: Chebli GA, Spalletti LA (eds) *Cuencas Sedimentarias Argentinas*, pp 395–417
- Schlager W (2003) Benthic carbonate factories of the Phanerozoic. *Int J Earth Sci* 92:445–464
- Schlager W (ed) (2005) Carbonate sedimentology and sequence stratigraphy. In: *SEPM concepts in sedimentology and paleontology*, vol 8. Society for Sedimentary Geology
- Schneider J-L (2000) Volcaniclastic sedimentation in submarine settings: products and processes. In: Leyrit H, Bordet P, Montenat C (eds) *Volcaniclastic rocks, from magmas to sediments*. Gordon and Breach Science Publishers, Amsterdam, pp 175–192
- Scholle PA, Imer-Scholle DS (2003) A colour guide to the petrography of carbonate rocks: grains, textures, porosity, diagenesis. AAPG, Tulsa, Ok, 474 pp.
- Seton M, Müller RD, Zahirovic S, Gaina C, Torsvik T, Shephard G, Talsma A, Gurnis M, Turner M, Maus S, Chandler M (2012) Global continental and ocean basin reconstructions since 200Ma. *Earth-Sci Rev* 113:212–270
- Shanmugam G (1997) The Bouma Sequence and the turbidite mind set. *Earth-Sci Rev* 42:201–229
- Shanmugam G (2002) Ten Turbidite Myths. *Earth-Sci Rev* 58:311–341
- Shanmugam G (2016) Slides, slumps, debris flows, turbidity currents, hyperpycnal flows, and bottom currents. In: *Encyclopedia of Ocean Sciences*, Elsevier, 228–257.
- Silva PC, Johansen HW (1986) A reappraisal of the order Corallinales (Rhodophyceae). *Brit Phycol J* 21:245–254
- Simone L, Carannante G (1988) The fate of foramol (“temperate-type”) carbonate platforms. *Sed Geol* 60:347–354
- Skarmeta J (1976) Evolución tectónica y paleogeografía de los Andes Patagónicos de Aisén (Chile), durante el Neocomiano. In: I Congr. Geol. Chileno, Actas, Santiago, Chile, B, 1–15.
- Steinmann G (1930) Sobre Archamphiroa jurásica. *Revista del Museo de la Plata*, 1–8.
- Stenzel, H.B. (1971) Oysters. In: *Treatise in Invertebrate Paleontology, Volumen 3, Mollusca 6 (Bivalvia)* (Ed. R.C. Moore), *Geological Society of America; University of Kansas*, 3, N953–N1224.
- Suárez M, De la Cruz R (1994a) Estratigrafía del Jurásico Superior - Cretácico Inferior de la Cordillera Patagónica Oriental (45°–46° latitud sur), Chile: Facies, Paleogeografía. *SERNAGEOMIN, Región de Aysén, Chile*, 98 pp
- Suárez M, De la Cruz R (1994b) Estratigrafía y paleogeografía meso-

- zoica de Aisén Nororiental. In: VII Congr. Geol. Chileno, Actas, Concepción, Chile, I, pp 538–542
- Suárez M, De la Cruz R (2001) Jurassic to miocene K-Ar dates from eastern central Patagonian Cordillera plutons, Chile (45°–48° S). *Geol Mag* 138:53–66
- Suárez M, De la Cruz R, Bell CM (1996) Estratigrafía de la región de Coyhaique (latitud 45°–46° S), Cordillera Patagónica, Chile. In: XIII Congr. Geol. Argentino y III Congr. Explor. Hidroc., Actas, I, pp 575–590
- Suárez M, De la Cruz R, Aguirre-Urreta MB, Fanning M (2005) Diachronic Tithonian-Valanginian marine transgression of the Coyhaique Group, Aysén Basin (43°–47°S), Chile. In: XVI Congr. Geol. Argentino, Actas, La Plata, Argentina, I, 305–308.
- Suárez M, De la Cruz R, Bell CM (2007) Geología del área Ñireguao-Baño Nuevo, Región Aisén del General Carlos Ibáñez del Campo. SERNAGEOMIN, Santiago, Chile, 56 pp
- Suárez M, De la Cruz R, Aguirre-Urreta B, Fanning M (2009) Relationship between volcanism and marine sedimentation in northern Austral (Aisén) Basin, central Patagonia: Stratigraphic, U-Pb SHRIMP and paleontologic evidence. *J S Am Earth Sci* 27:309–325
- Suárez M, De la Cruz R, Bell M, Demant A (2010a) Cretaceous slab segmentation in southwestern Gondwana. *Geol Mag* 147:193–205
- Suárez M, Demant A, Cruz RDL, Fanning CM (2010b) 40Ar/39Ar and U-Pb SHRIMP dating of Aptian tuff cones in the Aisén Basin, Central Patagonian Cordillera. *J S Am Earth Sci* 29:731–737
- Suárez M, Gressier JB, Rossel P, De la Cruz R (2023) Lower cretaceous missing volcanic arc. A migrating arc, central Patagonian cordillera, Chile: Detrital zircon U–Pb geochronology. *Int J Earth Sci (Geol Rundsch)* 112:907–923. <https://doi.org/10.1007/s00531-022-02272-4>
- Swift D, Figueiredo A Jr, Freeland GL, Oertel GF (1983) Hummocky cross-stratification and megaripples: A geological double standard? *SEPM JSR*. <https://doi.org/10.1306/212F8369-2B24-11D7-8648000102C1865D>
- Tarney J, Windley BF, Kröner A (1981) Marginal basins through geological time. *Phil Trans r Soc Lond A* 301:217–232
- Tennant JP, Mannion PD, Upchurch P, Sutton MD, Price GD (2017) Biotic and environmental dynamics through the Late Jurassic–Early Cretaceous transition: evidence for protracted faunal and ecological turnover: Jurassic–Cretaceous biotic and abiotic dynamics. *Biol Rev* 92:776–814
- Toscano AG, Lazo DG (2020) Taxonomic revision and palaeobiogeographic affinities of Berriasian-Valanginian oysters from the Vaca Muerta and Mulichinco formations, southern Mendoza, Neuquén Basin. *Argentina Cretaceous Research* 109:104358
- Toscano AG, Lazo DG, Luci L (2018) Taphonomy and paleoecology of lower cretaceous oyster mass occurrences from west-central argentina and evolutionary paleoecology of gregariousness in oysters. *Palaos* 33:237–255
- Townsend MJ (1998) The palaeogeography of the Lower Cretaceous Aysén Basin of southern Chile. PhD Thesis, University of Bristol
- Ulmer-Scholle DS, Scholle PA, Schieber J, Raine RJ (2014) A colour guide to the petrography of sandstones, siltstones, shales and associated rocks. American Association of Petroleum Geologists, Tulsa, OK, U.S.A, 526 pp.
- van de Schootbrugge B, Föllmi KB, Bulot LG, Burns SJ (2000) Paleooceanographic changes during the early Cretaceous (Valanginian–Hauterivian): evidence from oxygen and carbon stable isotopes. *Earth Planet Sci Lett* 181:15–31
- Vialov OS (1936) Sur la classification des huitres. In: Academie des Science de l'URSS, *Comptes Rendus (Doklady)*, 13, 17–20.
- Vickers ML, Bajnai D, Price GD, Linckens J, Fiebig J (2019) Southern high-latitude warmth during the Jurassic–Cretaceous: New evidence from clumped isotope thermometry. *Geology* 47:724–728
- Walker RG, Flint AG (1992) Wave- and storm-dominated shallow marine systems. In: *Facies models: response to sea level change*, 8. (Ed. R.G. Walker and N.P. James), Geological Association of Canada, Toronto, 219–238.
- Weissert H, Erba E (2004) Volcanism, CO₂ and palaeoclimate: a Late Jurassic–Early Cretaceous carbon and oxygen isotope record. *J Geol Soc* 161:695–702
- Westphal H, Halfar J, Freiwald A (2010) Heterozoan carbonates in subtropical to tropical settings in the present and past. *Int J Earth Sci (geol Rundsch)* 99:153–169
- Woelkerling W, Irvine L, Harvey A (1993) Growth-forms in non-geniculate coralline red algae (Coralliinales, Rhodophyta). *Aust Systematic Bot* 6:277
- Wray JL (1977) *Calcareous algae*. Elsevier Scientific Pub. Co.; Distributors for the United States and Canada, Elsevier/North Holland, Amsterdam, New York
- Wright VP (1992) A revised classification of limestones. *Sed Geol* 76:177–185
- Wright VP, Burchette TP (1996) Shallow-water carbonate environments. In: Reading HG (ed) *Sedimentary environments: processes, facies, and stratigraphy*, 3rd edn. Blackwell Science, Oxford, pp 325–394

Supplementary Material (Addendum)

Article Title: A “cool-water, non-tropical, mixed volcanoclastic-carbonate ramp from the Early Cretaceous of southern Chile (45°40’S).

Journal Name: Facies

Authors: Hermann Rivas ^{1, *}, Christian Salazar ², Wolfgang Stinnesbeck ¹

¹ Institut für Geowissenschaften, Universität Heidelberg, Im Neuenheimer Feld 234, 69120 Heidelberg, Germany.

Hermann Rivas

Email: hermann.rivas@geow.uni-heidelberg.de.

ORCID: [0000-0003-3642-1045](https://orcid.org/0000-0003-3642-1045).

ResearchGate account: https://www.researchgate.net/profile/Hermann_Rivas

Wolfgang Stinnesbeck

wolfgang.stinnesbeck@geow.uni-heidelberg.de

² Escuela de Geología, Facultad de Ciencias, Universidad Mayor, Manuel Montt #367, 7500994 Providencia, Chile.

Christian Salazar

Email: christian.salazar@umayor.cl

ORCID: [0000-0002-9436-4950](https://orcid.org/0000-0002-9436-4950)

* corresponding author

A1. Glossary of volcanic terms used in the manuscript.

1.1 Volcanic:

Fisher (1961) referred to “volcanic rocks” as a general term grouping three subdivisions based on the origin of the particles (autoclastic, pyroclastic, epiclastic), adding later the categories alloclastic and hyaloclastic (Fisher, 1966). In the same article, “volcanic” is used as a non-genetic adjective for epiclastic rocks containing volcanoclastic sediments, for example, “volcanic sandstone or volcanic breccia” (see Table 3 - “Proposed Classification of Volcanoclastic Rocks” of Fisher, 1961). In Fisher (1966), the author stated, when referring to “volcanic”: “I hold that it is an adjective which can apply as well to sediments derived from volcanic sources as to those produced directly by volcanic explosion.”. In summary, in the classifications here summarized, the term “volcanic” is used as a non-genetic adjective for epiclastic rocks* containing volcanoclastic sediments (e.g., “volcanic sandstone”).

However, in the manuscript presented here, the “volcanoclastic”, instead of “volcanic”, was preferred, when referring to rocks containing volcanoclastic sediments. This adjective has been regarded as being “widely used” (*sensu* Garzanti, 2019).

* “formed by weathering and erosion of older volcanic rocks” (*sensu* Fisher & Schmincke, 1984). See also below, in item iv) Tuffaceous, the definition of “epiclastic” *sensu* Cas & Wright (1987).

1.2 Volcanoclastic

Fisher (1966):

“Volcanoclastic is used to pinpoint and include the entire spectrum of fragmental volcanic rocks formed by any mechanism or origin, emplaced in any physiographic environment (on land, under water or under ice), or mixed with any other volcanoclastic type or with any non-volcanic fragment types in any proportion.”

The same concept was slightly paraphrased by Fisher & Schmincke (1984, p. 89): “The general term volcanoclastic introduced by Fisher (1961a) includes all clastic volcanic materials formed by any process of fragmentation, dispersed by any kind of transporting agent, deposited in any environment or mixed in any significant proportion with non-volcanic fragments.”

1.3 Pyroclastic

Cas & Wright (1987, p. 360): “Pyroclastic deposits are those which have a demonstrated pyroclastic mode of fragmentation and a demonstrated pyroclastic mode of deposition (fall, flow, surge).”.

The “pyroclastic mode of fragmentation” means that they are “produced by explosive or aerial ejection of material from a volcanic vent” (Wentworth & Williams *in* Fisher, 1966), “without reference to the causes of eruption or origin of the particles.” (Fisher & Schmincke, 1984).

1.4. Tuffaceous

In the literature, the adjective “tuffaceous” is usually restricted to reworked/remobilized pyroclastic deposits, in which their primary mode of fragmentation (i.e., pyroclastic) is still recognizable. Some examples:

Fisher (1961) used “tuffaceous” as a non-genetic adjective for “epiclastic” deposits or rocks containing pyroclastic material < 2 mm in size. Later, this term was better explained by Cas & Wright (1987, p. 360), when referring to redeposited and epiclastic deposits: “Epiclastic deposits... are clastic deposits which were fragmented by normal surface processes (weathering, physical abrasion, gravitational collapse) or were deposited by normal surface processes, irrespective of the mode of fragmentation, or both.”, and, subsequently, “If such a deposit (epiclastic) still clearly contains evidence of its pyroclastic fragmentation mode, then qualifying terms may be used, e.g. ‘tuffaceous sandstone’ or ‘tuffaceous mudstone’.”

A2. Additional Illustrations

2.1 SEM Images

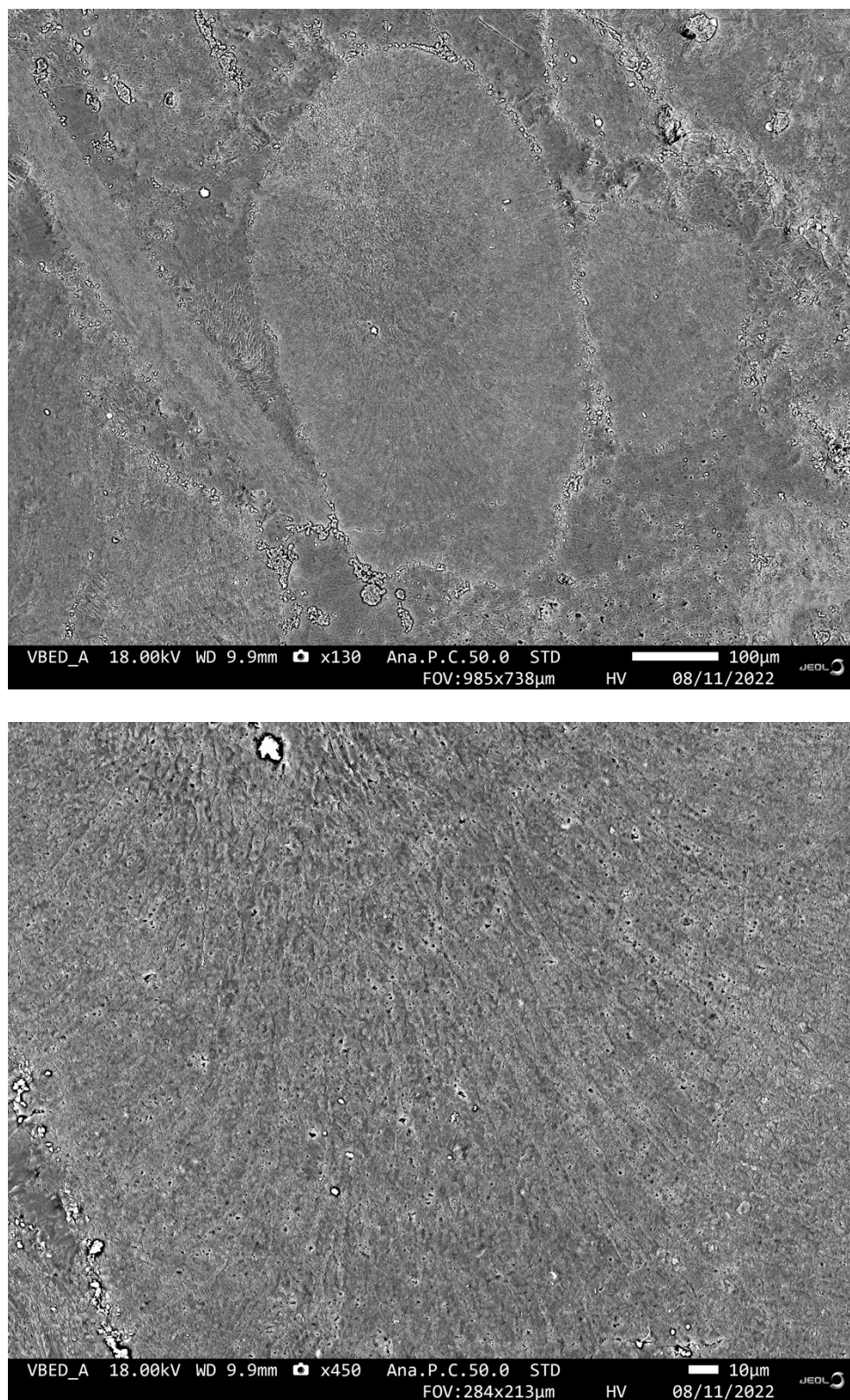


Figure 25. SEM pictures of *Archamphiroa jurassica*, prepared after methods of Munnecke et al. (2000); t (etching) = 45s.

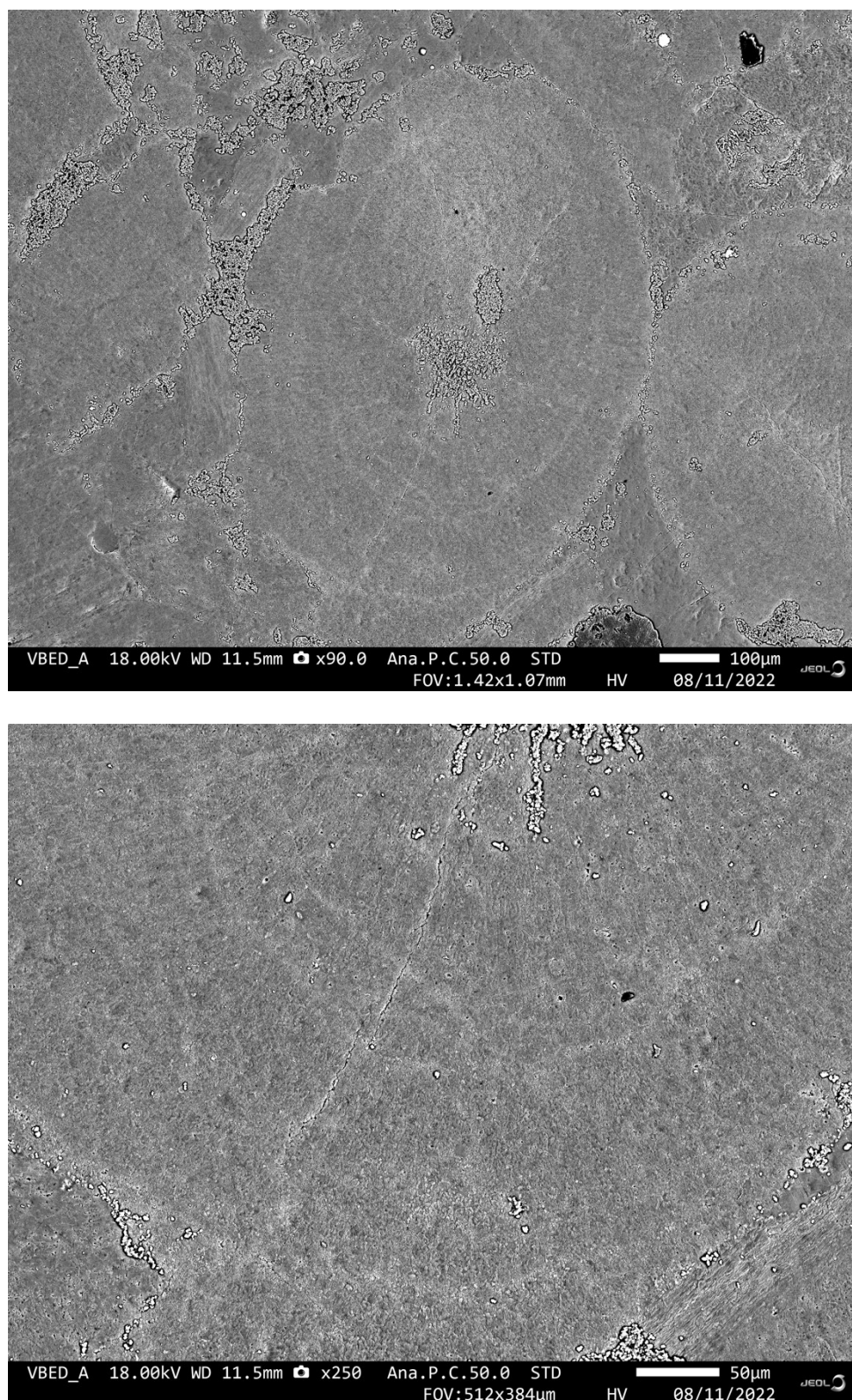


Figure 2. SEM pictures of *Archamphiroa jurassica*, prepared after methods of Munnecke et al. (2000); t (etching)= 60s.

A3. Additional tables

- **Tables SM-1 to SM-3. Sedimentary logs** (main information compiled in the field)
- **Table SM-4: Petrography**
- **Table SM-5: *Archamphiroa jurassica*** (microscopy)

* **Abbreviations:**

- Sandstones grain size: **VF** (very fine), **F** (fine), **M** (medium), **C** (coarse), **VC** (very coarse)
- Types of rock: **SH** (shale), **SL** (Siltstone), **SS** (sandstone), **CG** (conglomerate), **LS** (limestone)
- Types of contacts (CD = diffuse; CN = sharp; CA = amalgamated; CS = sinuous).
- (M) = Sample (“*muestra*” in Spanish)

* **Log description (template).**

Name of section: LOG NAME (CODE)							
Information related:							
Contact (top)	Sum. (top) Thickness	Thickness (m)	Lithology	Sedimentary structures	Fossils	Samples	Observations
Base:							
Bed 1							
Bed 2							
Bed 3							
etc...							
Top							

3.1 Table SM-1. La Rosita outcrop (LRO)

Name of section: LA ROSITA (LRO)								
- Outcrop located 1 km to the north of the NOLS Patagonia house, at the west side of the Route 7 (coming from Coyhaique).								
- $\rho/\mu = 105/13$ (SSW)								
Litho-facies	Contact (top)	Sum. (top) Thickness	Thickness (m)	Lithology	Sedimentary structures	Fossils	Samples	Observations
Base: Blocks of light-grey-colored volcanic blocks (Foitzick Volcanic Complex)								
bSGm bGSm	CN	1.5	1.5	Pebbly SS to sandy CG, matrix formed of C-VC grained SS. Bad sorting, beds matrix-supported and clast-supported, with thicknesses up to 40 cm. - Gravel clasts within 2 mm and 2.5 cm (media: 1 cm), sub-rounded to sub-angular, monomictic.	Diffuse parallel bedding	Fragmented bivalves (oysters), corals.	(M) LRO – 0.8 (M) LRO – 1.3	- Clasts composition: felsic igneous rock, cxls < 0.5 cm, pg massive and transparent, amp altered to chlorite. Similar composition compared to basal volcanic blocks. - Bioclasts of oysters, corals < 10 cm, poorly packed. - Sharp boundaries marked by contrasting pebble content.
bGSm	CN	1.85	0.35	Clast-supported conglomerate, whitish with grey matrix.	Parallel bedding	Fragmented bivalves (oysters), colonial corals	(M) LRO – 1.7	- Guide level (Conglomerate)

				<ul style="list-style-type: none"> - Felsic clasts, monomictic, greenish white in color, up to 15 cm (media: 2-5 cm) (50%). - Bioclasts (30%) 				<ul style="list-style-type: none"> - Oyster fragments up to 2 cm. Corals up to 0.5 cm (in life position) - Big gryphaeid oyster (not sampled, cemented).
bSGm >> bGSm	CN CD	7.06	5.21	C-VC calcareous SS to pebbly SS, good to regular sorting, clast-supported. - Intercalation of sandy conglomerate and pebbly SS, matrix of C-VC SS (same lithology than previous level).	Parallel bedding	Oyster fragments < 2 cm (media: 1 cm) Carbon fragments at 5.9 m.	(M) LRO – 3.9 (M) LRO – 5.9	<ul style="list-style-type: none"> - Bed thickness 30-80 cm (contacts are sharp to diffuse) - Clasts colors greenish white. - Clasts size decreases to the upper part (< 3 cm).
bSGm	CN	8.5	9.45	Sandy CG with clasts < 2 cm (media 1 cm). Matrix supported with same igneous felsic clasts.	Parallel bedding, some boundaries are sinuous	Bioclastic fragments.	(M) LRO – 8.5	<ul style="list-style-type: none"> - Lower bioclastic content, oyster fragments < 2 cm (< 10%). - Bed thickness varies between 0.3 – 1 m.
bSGm	CN	10	1.5	Sandy CG (clasts < 2 cm) intercalated with pebbly SS, VC SS in matrix, calcareous.	Parallel bedding	Bioclastic fragments	(M) LRO – 10	<ul style="list-style-type: none"> - Matrix of VC SS (0.2 – 0.3 mm). - Beds thickness between 0.3 -1 m.
bSGm >> bGSm	CN CD	15.5	5.5	Sandy CG (clasts < 2 cm) alternated with F grained conglomerate (clast up to 4 mm). - Clasts light green-colored, up to 1 cm, sub-rounded and calcareous matrix.	Parallel bedding, sinuous bed boundaries	Bioclastic fragments (< 5 %)	(M) LRO – 11.5 (M) LRO – 13	<ul style="list-style-type: none"> - To the upper part bed thickness varies between 30 - 50 cm.

								- Beds thickness between 0.3 -1 m (thicker likely amalgamated)
bSGm	CN	17	1.5	Like previous, but grain size decrease to C- VC SS, in part pebbly SS, with greater matrix percent (40 %).	Parallel bedding	Bioclastic fragments. Belemnite and oyster fragment.	(M) LRO – 16.5	
END Section LRO								

3.2 Table SM-2. Muralla China Outcrop (MCH)

Name of section: MURALLA CHINA (MCH)								
Information related: Outcrop of bedded limestones, in the higher part of the Muralla China area, directly to the north of the remarkable flat-topped sill. Rocks have a steep and white appearance.								
Strike/dip = 060/20 (SE)								
Litho-facies	Contact (top)	Sum. (top) Thickness	Thickness (m)	Lithology	Sedimentary structures	Fossils	Samples	Observations
Base: Ibáñez Group, volcanic (tuffaceous) rocks with light grey colors. The direct boundary is masked by loose sediment and vegetal coverage. Is it possible to observe an apparent concordant boundary from the road, however, the presence of exotic volcanic clasts might reflect reworking-erosive processes.								
bSGm	CN-S	0.7	0.7	Sandy-pebbly limestone, bioclastic, purplish gray. BC oysters. VC, light whitish green, < 2 cm (ca. 10%).	Subtle parallel bedding, in beds ca. 0.3 m thick.	Oyster fragments < 2 cm. (avrg. 1 cm) (ca. 50%), with some bigger, isolated fragments. - Coal fragments < 1cm (< 1 %).	(M) MCH -0.4	- Bigger oyster and smaller clasts show a horizontal position, conformably with the bedding.
bSGm	CN	2.4	1.7	Pebbly limestone, bioclastic (oyster fragments). Volcanic clasts idem previous (< 1cm).	Diffuse parallel bedding 0.2-0.3 m thick.	Oyster fragments (< 0.5 cm), disarticulated valves. (< 9 cm).	(M) MCH-1.8	Crops out as a ledge with rounded margin.
bLr-m	CN-S	5.1	2.7	Pebbly-bioclastic limestone, brownish gray (gray in exposure). Bioclasts < 1 cm. FLV, sharp-shaped (low roundness) ca. 1 cm.	Diffuse sinuous bedding, in 15-20 cm thick beds*.		(M) MCH-3.1	Symmetric ripples, with variable lambda (50-90 cm), towards the upper part, the lambda is lower (20-30cm).
Succession (repeated +- in a homogeneous manner, without marked lithological changes). Description/sampling each meter. Diffuse sinuous structures are still preserved, between diffuse bedding ca. 0.3 m thick.								
Laterally continuous tafoni layers indicate bed boundaries (rippled)								

bLr-o	CN	8.1	3.0	Bioclastic limestone, with oyster fragments.	Parallel bedding 0.3 m	Oyster fragments.	(M) MCH-7.1	
bLr-o	CN	10.1-11.7	2.0	Bioclastic limestone, with oyster fragments.	Parallel bedding 0.3-0.4 m - Diffuse sinuous bedding	Oyster fragments	(M) MCH-10.8	Sample was taken in the thickest area.
bLr-o	CN	12.8	1.0-2.7 (wedge)	***Wedge-shaped bed. Thicker to the south (2.7 m). Bioclastic limestone.	Diffuse parallel bedding (0.2 m). To the south, appear massive.	- Big-sized oyster	(M) MCH-12.1	Oyster reworked, both valves, found in oblique position, with hinge point to the top of the bed.
bLr-o	CD CA	14.8	2.0	M-C Sandy limestone, FLV < 1mm (< 5 %), bioclasts < 1 cm; avrg. < 2 mm (5-10%).		- Big oyster (isolated) - Small bivalve - Bioclasts – fragmented	(M) MCH-14.8	
bLr-o		15.8	1.0	M calcareous sandstone, sandy limestone. FLV <2- mm (5-7%). Bioclasts < 3 mm (<5%)	Diffuse parallel bedding 0.4 m. Laterally is exposed clearly. Last 0.7 m single bed.	Ichnofossil (ex situ)	(M) MCH-15.8	
bLr-o		16.8	1.0	M – C sandy limestone. FLV <2- mm (5-7%). Bioclasts < 3 mm (<5%)		Shell debris	(M) MCH-16.8	
bLr-o		17.8	1.0	M sandy limestone. FLV <2- mm (5-7%). Bioclasts < 3 mm (<5%)		Shell debris	(M) MCH-17.8	
bLr-o		18.8	1.0	C sandy limestone. FLV <2- mm (5-7%). Bioclasts < 3 mm (<5%)		Shell debris	(M) MCH-18.8	

bLr-o		19.8	1.0	F-M sandy limestone. FLV <2- mm (7%). Bioclasts non-observed.		Shell debris	(M) MCH-19.8	
bLr-o		20.8	1.0	C sandy bioclastic limestone. FLV ca. 2- mm (7%). Bioclasts < 2 cm, avrg <0.5cm (ca. 20%)		Fish teeth (Pycnodontidae indet.)	(M) MCH-20.8	
bLr-o		21.8	1.0	C Pebbly bioclastic limestone. FLV <7 mm; avrg 3mm (5%). Bioclasts < 5mm (10%)		Shell debris	(M) MCH-21.8	
bLr-o		22.8	1.0	M sandy bioclastic limestone. FLV < 2- mm (<5%). Bioclasts < 3-4 mm, avrg <0.5cm (ca. 10%)		Shell debris	(M) MCH-22.8	
bLr-o		23.8	1.0	M-C sandy bioclastic limestone. FLV < 2- mm (<5%). Bioclasts < 0.5 cm, avrg <1- 2mm (ca. 10%)		Small bivalves, disarticulated, complete.	(M) MCH-23.8	
bLr-o		24.8	1.0	C pebbly bioclastic limestone. FLV < 5mm; avrg 1-2 mm (<5%). Bioclasts < 0.5 cm, avrg <1-2mm(ca. 10%)		Shell debris	(M) MCH-24.8	
bLr-o		25.8	1.0	C pebbly bioclastic limestone. FLV < 1cm; avrg 1-2 mm (<5%). Bioclasts < 0.7 cm, avrg <2mm(ca. 10%)		Shell debris	(M) MCH-25.8	
bLr-o		26.8	1.0	C pebbly bioclastic limestone. FLV < 1.7cm; avrg 0.5-1cm (<5%). Bioclasts < 1 cm, avrg 5mm (ca. 10%)		Shell debris	(M) MCH-26.8	

bLr-o	CN	27.8	1.0	Sandy-pebbly limestone, gray, bioclasts <5mm, avrg 1-2 mm (C-VC sand to fine gravel sized).	Sinuuous parallel bedding. Lambda = 0.3-0.4 m.	Oyster fragments	(M) MCH-27.8	
bLr-o	CN	29.8	2.0	Sandy-pebbly limestone, purplish gray, bioclasts < 1.5 cm, avrg 1 mm (C-VC sand to fine gravel sized). FLV <2-4 mm (ca. 5%) Guide bed (crop out as a ledge)		Oyster fragments	(M) MCH-29.8	Last bed under the layer with entire oyster fossils - At ca. the same isoline, but in the northern end of the outcrop, exposure of coquinites (ca. 1-2 m-thick), rich in oyster shells embedded in brownish calcareous mudstone.
bLr-m	CN	31.5	0.9	Pebbly limestone to calcareous conglomerate, with FLV up to 5 mm and bioclastic fragments up to 2 cm (avrg. < 1 cm). - FLV accumulate in lense-shaped structures, with diffuse boundaries and 10 cm thick.	Internal parallel bedding, in layers 0.2-0.35 m, with a sharp and sinuous margin*.	Isolated oyster 8-10 cm.		Ripples of the sinuous boundary with lambda 0.2-0.3 m.
bSGm	CN	32.4	1.1	VC calcareous sandstone, idem color – with a dominance of greenish FLV (ca. 60 %) with whitish alteration. Bioclastic fragments (mm-sized).		Shell debris		
bSGm	CN	33.2	1.4	Conglomeratic calcareous sandstone, with sandy conglomerate lenses (ca. 0.2 m thick) and diffuse margins.		* Complete and fragmented oysters (app.	(M) MCH-33	- C-VC (2-3 mm) sand formed by FLV whitish-green clasts, monomictic. These are isolated or

						same sp.) (ca. 5 %)- + 1 belemnite. - Ichnofossils? - Coal fragments (mm-cm) up to dm (ex-situ).		in lenses with gradual/diffuse margins, clast-to matrix supported. *Disarticulated and isolated biggest valves, concave, filled with sedimentary matrix, in a concave-up position.
	END Section MCH.							

3.3 Table SM-3. Salto Río Pollux outcrop (SRP2)

Name of section: SALTO RIO POLLUX 2 (SRP2)								
Information related:								
- Outcrop located just before the crossroad to “El Fraile – Lago Frio”, coming from Coyhaique.								
- ρ/μ = 037/10 E; 045/11 SE.								
Litho-facies	Contact (top)	Sum. (top) Thickness	Thickness (m)	Lithology	Sedimentary structures	Fossils	Samples	Observations
Base: covered (not exposed). Nearby, in a lower position (towards the river thalweg), black mudstone of the Katterfeld position is exposed, likely in tectonic contact with this outcrop								
bSp	CN	0.5	0.5	Dark grey-black-coloured, bioclastic-sandy limestone. Grain size VF.	Apparently massive; brittle	Abundant shell debris		- Outcrop partially covered. - Bioclastic fragments < 3 mm (50 %)

bSp	CN	2.2	1.7	Same lithology than previous level. Limestone matrix VF in grain size, muddy appearance, with high organic matter (odor).	Diffuse parallel bedding (0.4-0.7 cm-thick) Brittle	Abundant shell fragments; belemnites, gryphaeid oysters, bivalves, echinoderm spines.	(M) SRP2 – 0.6 (M) SRP2 – 1.7	- Bedding with bed thickness of 40 – 70 cm (diffuse, amalgamated) - Some gryphaeid specimens only have 1 valve, also filled with sediment (reworking/remobilized).
bSp-c	CN (S)	2.55	0.35	Same lithology than previous level. Lower cemented layer	* More cemented layer, resistant (ledge).	Abundant shell debris		- Bioclasts are smaller (2 mm) and have a more crystalline appearance. - Boundary with the previous bed has a muddy composition. (S) = Sinuous basal contact
bSp	CN	5.15	2.6	Alternation of calcareous mudstone – muddy limestone.	Brittle	Abundant shell debris. Gryphaeid oysters, belemnite (lower part).	(M) SRP2 – 4.2	- Bioclastic fragments < 2 mm (50 %). - Gryphaeids concave-up (life position) - Bed thickness between 10 – 40 cm, fissile & brittle, more resistant in the upper part.
bSp-c	CN	5.45	0.3	Grey sandy limestone; with C-VC grain size clasts (40 – 50%). Upper cemented layer	* More cemented layer, resistant (ledge).	Abundant shell debris, gryphaeid oysters	(M) SRP2 – 5.45	- Mud % decreases in comparison with the previous level (harder exposure).
tSp-b	CN	5.85	0.4	Intercalation of whitish, M sized, sandstone with dark grey limestone. Green crystals in sandstone (glauconite? weathered felsic or pumice lithics?) Guide layer (white-colored)	Parallel bedding. Brittle	Gryphaeid oysters	(M) SRP2 – 5.85	- Bed thickness up to 5 cm.
bSp	CN	6.05	0.2	Black bioclastic limestone (F-M grained)	Apparently massive Brittle	Abundant shell fragments	(M) SRP2 – 6	- Bioclastic fragments < 2 mm (50 %)

bSp	CN	7.25	1.2	M grain size, calcareous sandstone.	Parallel bedding. Massive (internally); diffuse planar cross bedding? (unclear)		(M) SRP2 – 7.1	- Bed thickness variable between 10 – 20 cm.
bSp bSp-c	CN	9.15	1.9	Intercalation of grey, hard limestones with black, fissile limestones (shales?) Alternation cemented-uncemented	Bed thickness decreases upsection	Shell fragments	(M) SRP2 – 7.5	- Bed thickness start with 28 (lower part) to 6 cm (upper part). - Weathered black LS very similar to the previous bioclastic levels.
	CN	14.15	5	Greenish – brownish sill, with amphiboles (3 mm approx.) and pyroxenes < 1mm. Aphanitic texture.			(M) SRP2 – 9	- Sill apparently form part of the “Muralla China”.
bSp	CN	15.35	1.2	Sandy limestones (idem)	Bed inferred			Difficult to access (slope).
	CE	16.55	1.2	Sill (idem)				Another “arm” bifurcated from the same sill
END Section SRP2. - Top: Weathering surface (recent), covered with vegetation.								

3.4 Table SM-4. Petrography.

This table summarize the petrographical information of 18 thin sections here analyzed, including their microfacies as well as their estimated modal composition. Thin sections are grouped by locality. Abbreviations: Sort. = Sorting (vp = very poorly, p = poorly, r = regular, w = well, vw = very well); Round. = Roundness (a = angular, sa = sub-angular, sr = sub-rounded, r = rounded, L = lithic fragments, C = crystals); Grain Size (sand: VF = very fine, F = fine, M = medium, C = coarse, VC = very coarse-grained); Bioclasts (Bv = bivalve, Ec = echinoid, Al = red alga, Br = Bryozoans, In = Intraclasts, Se = serpulid, Ca = calcispheres, Wo = carbonized wood, Fo = foraminifer); Terrigenous (L = lithic fragments; F = feldspars; Q = total quartz, A = accessory minerals). I/F = proportion volcanic lithics (Intermediate:Felsic); Summary: Fr = framework; Ma = matrix; Ce = cement. **Observation:** values were estimated with percentual charts and they are, therefore, approximated.

Locality	Sample	Micro facies	Lithology	Grain-size	Sort.	Round.	Bioclasts/Allochems										Terrigenous					Summary		
							Bv	Ec	Al	Br	In	Se	Ca	Wo	Fo	Os	L	F	Q	A	I/F	Fr	Ma	Ce
La Rosita (LRO)	LRO 1.3	Mf-1	Sandy-gravelly, volcaniclastic-bioclastic packstone (wackestone patches)	M sand - pebble	p	sa	23	5	5	<1	<1	<1	<1	-	-	-	25	2	<1	-	9:1	60	30	10
	LRO 2.0	Mf-1	Gravelly-sandy, volcaniclastic-bioclastic pack-rudstone (grainstone patches)	M sand - cobble	vp	sa-sr	30	4	5	-	-	1	<1	-	-	-	20	2	<1	-	9:1	62	23	15
	LRO 3.9	Mf-1	Gravelly-sandy volcaniclastic-bioclastic packstone (grainstone patches)	M sand - pebble	p	sr>sa	15	10	15	-	-	-	-	-	-	-	30	4	1	Gl <1	9:1	75	10	15
	LRO 8.5	Mf-4cg	Gravelly, bioclastic-volcaniclastic, qFL sandstone (grainstone patches)	M-C sand - pebble	p	sr > sa	13	2	5	-	-	-	-	-	-	-	50	4	1	-	6:4	75	15	10

	LRO 13	Mf-1	Sandy, volcanoclastic- bioclastic, pack-wackestone	M-C sand - pebble	r	sa – sr	30	4	5	-	-	-	-	-	-	-	20	1	<1	-	-	60	10	30
Muralla China (MCH)	MCH 0.4	Mf-2	Sandy-gravelly, volcanoclastic-bioclastic float-wackestone (packstone patches)	M sand - cobble	vp	sa-sr	25	5	5	-	<1	-	-	<1	-	-	5	<1	<1	-	-	40	45	15
	MCH 3.1	Mf-3	Sandy bioclastic rudstone-grainstone (pack-wackestone patches)	F sand - pebble	vp	sa-r	15	5	30	-	2	-	-	-	-	<1	4	1	<1	-	-	55	15	30
	MCH 12.1	Mf-3	Sandy bioclastic grainstone (packstone patches)	M sand - pebble	r-w	sa-sr	20	5	25	-	2	-	-	-	<1	-	13	1	1	-	-	65	3	32
	MCH 27.8	Mf-3a	Red algae-rich grainstone (packstone patches)	M sand - pebble	w	sr-r	5	5	50	<1	-	-	-	<1	-	<1	3	<1	<1	-	-	63	3	34
	MCH 29.8	Mf-3a	Red algae-rich, fitted grainstone (rudstone patches)	M sand - pebble	w	sr-r	5	5	60	<1	-	-	-	-	-	-	3	<1	<1	-	-	73	3	24
Salto Río Póllux (SRP2)	SRP2 1.7	Mf-4om	Gravelly, muddy Bioclastic-volcaniclastic, qFL-FL sandstone	M-C sand - granule	p-r	sa-sr	30	2	3	-	<1	-	-	-	-	-	33	4	2	Bt 1	9:1	75	25	-
	SRP2 5.8	Mf-4 Mf-5	Alternation: bioclastic- volcaniclastic qFL and lQF sandstone	qFL: M-C lQF: F-M	r-w w-vw	L: sa-sr C: a-sa	17	2	1	<1	-	-	-	-	-	-	40	13	10	Bt 2	9:1	85	5	10
	SRP2 6.0	Mf-4m	Gravelly, muddy, bioclastic-volcaniclastic, qFL sandstone	M-C sand - granule	p-r	L: sa-sr C: a-sa	5	2	3	-	-	-	-	-	-	-	40	15	5	Bt 2	9:1	72	25	3
	SRP2 7.1	Mf-4c	Bioclastic-volcaniclastic, qFL sandstone	M-VC sand	w	sa-sr	18	2	5	-	-	-	-	-	-	-	45	10	5	Bt 1	6:4	86	4	10
	SRP2 7.5	Mf-4	Gravelly, bioclastic- volcaniclastic, qFL sandstone	M-C sand - granule	r	L: sr C: sa-sr	15	5	5	-	-	-	-	-	-	-	45	12	2	Bt 1	9:1	80	15	5

3.5 Table SM-5. *Archamphiroa jurassica*

Measurements of red alga *Archamphiroa jurassica* (in thin section).

Code	Sample	ed	cd	prw	Shape	Section	Photograph (name)	comments
1	LRO-001.3	0.733	0.277	0.24	circular	diffuse core + bioerosion	redalgae - echin - ostra	
2	LRO-001.3	0.807	0.445	0.238	elliptical + bifurcation	oblique section	redalgae1&cross-section	alga 1 (right) - partly eroded
3	LRO-001.3	0.683	0.345	0.283	elliptical + bifurcation	oblique section	redalgae1&cross-section	alga2 (left) - incomplete
4	LRO-001.3	1.135	0.61	0.265	elliptical + core growth	cross-section	redalgae3&oblique&growth	
5	LRO-001.3	0.49	0.228	0.176	sub-lenticular + bifurcation	longitudinal section	redalgae4&sagital¢er	
6	LRO-002	0.642	0.265	0.222	elliptical + bifurcation	cross-section	redalgae1&cross-section	
7	LRO-002	0.607	0.274	0.174	elliptical	cross-section	redalgae2&cross-section	
8	LRO-002	1.132	0.324	0.397	elliptical + peripheral growth	cross-section	redalgae3&cross-section	partly eroded
9	LRO-002	0.759	0.347	0.203	sub-elliptical	cross-section	redalgae4&cross-section	partly eroded
10	LRO-002	1.746	0.726	0.51	fan-shaped (incomplete)	longitudinal section	redalgae5&oblique	inferred measure (duplicated)
11	LRO-003.9	0.66	0.338	0.197	circular	cross-section	redalgae2&cross-section	partly eroded
12	LRO-003.9	0.585	0.215	0.143	elliptical + peripheral growth	cross-section	redalgae3&cross-section	
13	LRO-003.9	0.831	0.163	0.334	spearhead-shaped (apical?)	longitudinal section	redalgae6&oblique	ed inferred
14	MCH-004	1.009	0.413	0.264	toroidal incomplete	cross-section	redalgae1_10x	center altered + bioerosion
15	MCH-004	0.446	0.269	0.088	spearhead-shaped (basal?)	longitudinal section	redalgae2_10x	partly eroded
16	MCH-004	0.922	0.21	0.513	irregular + peripheral growth	cross-section	redalgae3_10x	ed inferred

17	MCH-3_1	0.564	0.278	0.149	elliptical & circular + bifurcation	cross-section	redalgae_cross-section	alga 1 (left)
18	MCH-3_1	0.494	0.208	0.127	elliptical & circular + bifurcation	cross-section	redalgae_cross-section	alga 2 (right)
19	MCH-3_1	0.612	0.19	0.182	sub-elliptical	cross-section	redalgae&echin_10x	
20	MCH-3_1	0.797	0.385	0.209	sub-elliptical	oblique section	redalgae1_10xNX	
21	MCH-3_1	0.734	0.252	0.216	sub-circular + bifurcation	cross-section	redalgae2_10xNX	
22	MCH-3_1	0.591	0.201	0.169	sub-circular + perithallum growth	cross-section	redalgae3_cross-section	
23	MCH-3_1	0.684	0.244	0.268	lenticular + core growth	longitudinal section	redalgae4_oblique	
24	MCH-3_1	0.667	0.376	0.218	elliptical + peripheral growth	oblique section	redalgae5_cross-section	partly eroded
25	MCH-3_1	0.926	0.404	0.235	elliptical + peripheral growth	longitudinal section	redalgae6_cross-section	
26	MCH-3_1	0.453	0.143	0.156	sub-circular + perithallum growth	cross-section	redalgae7_cross-section	
27	MCH-3_1	0.835	0.326	0.306	lenticular + core growth	longitudinal section	redalgae8_longitudinal	
28	MCH-3_1	0.693	0.294	0.132	elliptical	cross-section	redalgae9_cross-section	
29	MCH-3_1	1.035	0.477	0.299	elliptical + core growth	longitudinal section	redalgae10_cross-section&growth	
30	MCH-3_1	0.65	0.192	0.239	elliptical + peripheral growth	longitudinal section	redalgae11_growth	
31	MCH-3_1	0.644	0.295	0.161	sub-circular + perithallum growth	cross-section	redalgae12_cross-section	
32	MCH-3_1	1.047	0.457	0.252	lenticular + core growth	longitudinal section	redalgae13_longitudinal02	
33	MCH-3_1	0.859	0.418	0.182	ramified + bifurcation	longitudinal section	redalgae14_longitudinal02	
34	MCH-3_1	0.623	0.22	0.159	ramified + bifurcation	longitudinal section	redalgae16_bifurcation	
35	MCH-12_1	0.334	0.138	0.116	lenticular + core growth	longitudinal section	redalgae6&oblique	
36	MCH-27_8	0.754	0.308	0.224	horseshoe-shaped (core-altered)	longitudinal section	redalgae3¢er	
37	MCH-27_8	0.763	0.278	0.226	sub-lenticular + bifurcation	longitudinal section	redalgae4¢er	
38	MCH-27_8	0.544	0.2	0.143	circular	cross-section	redalgae5_cross-section	
39	MCH-27_8	0.479	0.279	0.089	sub-elliptical	cross-section	redalgae9&echin&oyster	partly eroded (core-altered)
40	MCH-27_8	0.717	0.35	0.164	irregular + bifurcation	cross-section	redalgae12&bifurcation	partly eroded (core-altered)
41	MCH-27_8	0.862	0.25	0.286	sub-elliptical	longitudinal section	redalgae13¢er_10x	partly eroded
42	MCH-27_8	0.938	0.222	0.347	lenticular	longitudinal section	redalgae14_longitudinal	core not clear

43	MCH-27.8	0.329	0.186	0.094	sub-elliptical	oblique section	redalgae15_cross-section	partly eroded
44	MCH-27.8	0.568	0.183	0.191	spearhead-shaped + bifurcation	cross-section	redalgae16_cross-section	
45	MCH-27.8	0.566	0.129	0.227	lenticular	longitudinal section	redalgae17_longitudinal	core not clear
46	MCH-27.8	0.373	0.167	0.119	sub-lenticular + bifurcation	cross-section	redalgae20&cross-section	
47	MCH-27.8	0.429	0.148	0.158	circular	cross-section	redalgae22&cross-section	core not clear
48	MCH-27.8	0.646	0.183	0.282	lenticular	longitudinal section	redalgae23&longitudinal	core dissolved
49	MCH-27.8	0.586	0.318	0.118	circular	cross-section	redalgae24&cross-section	core altered
50	MCH-27.8	0.372	0.161	0.118	circular	cross-section	redalgae27&fragments	core altered
51	MCH-27.8	0.775	0.503	0.136	elliptical + core growth	oblique section	redalgae28¢er	
52	MCH-27.8	0.545	0.132	0.168	elongated + bifurcation	cross-section + longitudinal	redalgae31&bifurcation	alga 1 (left)
53	MCH-27.8	0.555	0.174	0.144	elongated + bifurcation	cross-section + longitudinal	redalgae31&bifurcation	alga 2 (right)
54	MCH-27.8	1.116	0.38	0.368	elongated + perithallum growth	longitudinal section	redalgae32&longitudinal	ed inferred
55	MCH-27.8	0.303	0.127	0.089	circular	cross-section	redalgae33&cross-section	core not clear
56	MCH-27.8	0.447	0.229	0.145	sub-circular	cross-section	redalgae35&oblique	core not clear
57	MCH-27.8	0.424	0.157	0.129	sub-circular	cross-section	redalgae36_cross-section	core not clear
58	MCH-27.8	0.583	0.245	0.171	sub-circular + perithallum growth	cross-section	redalgae37_cross-section	core not clear
59	MCH-27.8	0.654	0.238	0.224	elliptical + peripheral growth	cross-section	redalgae38&cross-section	alga 1 (above)
60	MCH-27.8	0.595	0.219	0.175	elliptical	cross-section	redalgae38&cross-section	alga 2 (below)
61	MCH-27.8	0.495	0.171	0.147	elongated	longitudinal section	redalgae40&longitudinal	alga 1 (elongated)
62	MCH-27.8	0.406	0.161	0.107	circular	cross-section	redalgae40&longitudinal	alga 2 (circular)
63	MCH-27.8	0.746	0.224	0.253	elliptical	cross-section	redalgae41&cross-section	core dissolved
64	MCH-27.8	0.433	0.232	0.097	spearhead-shaped (apical?)	longitudinal section + core growth	redalgae42&internal-growth	
65	MCH-27.8	0.438	0.173	0.115	irregular + core growth	longitudinal section	redalgae46¢er	partly eroded
66	MCH-27.8	0.738	0.288	0.236	sub-circular + perithallum growth	cross-section	redalgae48¢er	core not clear
67	MCH-29.8	0.771	0.259	0.256	sub-elliptical	oblique section	redalgae1&oblique	ed inferred; partly eroded
68	MCH-29.8	0.612	0.224	0.168	sub-circular	longitudinal section	redalgae2&oblique	partly eroded

69	MCH-29.8	0.55	0.162	0.194	spearhead-shaped sub-elliptical + perithallum growth	cross-section + perithallum growth	redalgae3¢er	ed inferred; partly eroded
70	MCH-29.8	1.008	0.393	0.368	sub-elliptical + perithallum growth	cross-section	redalgae4¢er	
71	MCH-29.8	0.603	0.226	0.198	hemicircle sub-elliptical + perithallum growth	cross-section	redalgae5&cross-section	alga 1 (left)
72	MCH-29.8	0.591	0.317	0.14	sub-elliptical + perithallum growth	cross-section	redalgae5&cross-section	alga 2 (right)
73	MCH-29.8	0.503	0.185	0.163	irregular + bifurcation	longitudinal section	redalgae6&oblique	core not clear
74	MCH-29.8	0.499	0.223	0.138	elliptical	cross-section	redalgae7&cross-section	core not clear
75	MCH-29.8	0.977	0.408	0.357	ramified + bifurcation	longitudinal section	redalgae8&oblique	core dissolved
76	MCH-29.8	0.42	0.226	0.097	irregular + bifurcation	cross-section	redalgae9¢er	ed inferred (bifurcation)
77	MCH-29.8	0.872	0.333	0.3	ramified + bifurcation	cross-section + longitudinal	redalgae11¢er	
78	MCH-29.8	0.804	0.294	0.271	elongated + bioerosion	longitudinal section	redalgae13&cross-section	alga 1 (left)
79	MCH-29.8	0.669	0.308	0.181	circular	cross-section	redalgae13&cross-section	alga 2 (right)
80	MCH-29.8	0.836	0.337	0.226	elongated + core growth	longitudinal section	redalgae14&sagital	
81	MCH-29.8	0.377	0.14	0.119	sub-circular	cross-section	redalgae16&cross-section	core not clear
82	MCH-29.8	0.748	0.247	0.261	irregular	longitudinal section + core growth	redalgae18&sagital	irregular core-growth
83	MCH-29.8	0.572	0.239	0.156	sub-circular	cross-section	redalgae20&cross-section	alga 1 (left)
84	MCH-29.8	0.758	0.367	0.167	sub-elliptical + perithallum growth	longitudinal section	redalgae20&cross-section	alga 2 (right)
85	MCH-29.8	0.393	0.145	0.134	circular	cross-section	redalgae21&cross-section	alga 1 (left-circular)
86	MCH-29.8	0.521	0.21	0.16	sub-quadratic	longitudinal section	redalgae21&cross-section	alga 2 (right-elongated)
87	MCH-29.8	0.515	0.182	0.164	elliptical	cross-section	redalgae23&cross-section	
88	MCH-29.8	0.619	0.225	0.197	sub-elliptical	oblique section	redalgae24&cross-section	ed inferred
89	MCH-29.8	0.772	0.36	0.235	irregular + core growth	longitudinal section	redalgae25&oblique	partly eroded
90	MCH-29.8	0.647	0.31	0.155	elliptical + peripheral growth	cross-section	redalgae27&cross-section	
91	MCH-29.8	0.521	0.223	0.172	circular	cross-section	redalgae29&cross-section	core not clear
92	MCH-29.8	0.61	0.242	0.195	sub-elliptical	oblique section	redalgae31&cross-section	
93	MCH-29.8	0.789	0.212	0.329	sub-elliptical	longitudinal section	redalgae34&sagital	

94	MCH-29.8	0.542	0.204	0.208	elliptical	longitudinal section	redalgae36&sagital	
95	MCH-29.8	0.481	0.217	0.138	sub-rectangular	longitudinal section + core growth	redalgae38&sagital	partly eroded
96	MCH-29.8	0.723	0.236	0.216	sub-elliptical	oblique section	redalgae40_cross-section	alga (right)
97	MCH-29.8	0.762	0.21	0.276	elliptical + peripheral growth	oblique section	redalgae41_cross-section	ed inferred
98	MCH-29.8	0.502	0.229	0.173	circular	cross-section	redalgae42_cross-section	alga (above-circular)
99	MCH-29.8	0.539	0.228	0.146	sub-circular + perithallum growth	cross-section	redalgae43_cross-section	partly eroded
100	MCH-29.8	0.464	0.155	0.169	elliptical	cross-section	redalgae44_cross-section	alga 1 (left)
101	MCH-29.8	0.538	0.188	0.165	sub-circular + perithallum growth	cross-section	redalgae44_cross-section	alga 2 (right)
102	MCH-29.8	0.429	0.212	0.138	sub-circular + perithallum growth	cross-section	redalgae46_cross-section	partly eroded
103	MCH-29.8	0.555	0.303	0.125	elongated + core growth	longitudinal section + core growth	redalgae48_cross-section	alga 1 (above)
104	MCH-29.8	0.786	0.34	0.223	fan-shaped (incomplete)	cross-section	redalgae48_cross-section	alga 2 (below) - ed inferred
105	MCH-29.8	0.612	0.268	0.155	elongated + core growth	longitudinal section	redalgae49_cross-section	alga 1 (left)
106	MCH-29.8	0.807	0.376	0.18	elliptical	cross-section	redalgae49_cross-section	alga 2 (right)
107	MCH-29.8	0.446	0.178	0.148	sub-rectangular	longitudinal section	redalgae51_sagital	core not clear
108	MCH-29.8	0.59	0.232	0.179	sub-elliptical + perithallum growth	oblique section	redalgae52&cross-section	alga (left)
109	MCH-29.8	0.445	0.158	0.17	sub-circular	cross-section + perithallum growth	redalgae54&cross-section	alga (centered)
110	MCH-29.8	0.8	0.238	0.281	elongated + core growth	longitudinal section	redalgae56&sagital	ed inferred; partly eroded
111	MCH-29.8	1.083	0.447	0.338	spearhead-shaped (apical?)	longitudinal section + core growth	redalgae57&sagital	
112	MCH-29.8	0.677	0.227	0.225	lenticular - elongated	longitudinal section	redalgae63&sagital	partly eroded
113	MCH-29.8	0.462	0.192	0.181	circular	cross-section	redalgae64&cross-section	alga (left-circular)
114	MCH-29.8	0.548	0.202	0.153	elliptical	cross-section	redalgae67&cross-section	alga (left); core dissolved
115	MCH-29.8	0.652	0.192	0.201	circular	cross-section	redalgae69&cross-section	
116	MCH-29.8	0.583	0.241	0.157	sub-rectangular	longitudinal section	redalgae71&oblique	alga (right)
117	MCH-29.8	0.584	0.274	0.173	spearhead-shaped (apical?)	longitudinal section	redalgae76&cross-section	alga (left)
118	MCH-29.8	0.634	0.296	0.156	circular	cross-section	redalgae76&cross-section	alga (right)
119	MCH-29.8	0.733	0.285	0.219	elliptical	oblique section	redalgae78&cross-section	alga (lef)

120	MCH-29_8	0.754	0.226	0.249	sub-elliptical	cross-section	redalgae79&cross-section	
121	MCH-29_8	0.6	0.2	0.174	circular	cross-section	redalgae81&cross-section	alga (above-left-circular)
122	MCH-29_8	0.631	0.244	0.193	spearhead-shaped	oblique section	redalgae84&cross-section	alga 1 (left)
123	MCH-29_8	0.689	0.314	0.201	sub-elliptical	oblique section	redalgae84&cross-section	alga 2 (right)
124	MCH-29_8	0.533	0.209	0.161	sub-circular	cross-section	redalgae85&cross-section	core not clear
125	MCH-29_8	0.863	0.377	0.243	elliptical	cross-section	redalgae88&cross-section	ed inferred; partly eroded
126	MCH-29_8	1.065	0.403	0.355	sub-circular	cross-section	redalgae89&cross-section	core not clear
127	MCH-29_8	0.524	0.188	0.168	elliptical + bifurcation?	cross-section	redalgae91&cross-section	ed inferred; partly eroded
128	MCH-29_8	0.476	0.205	0.142	ramified + bifurcation	longitudinal section	redalgae93&sagital	
Max		1.746	0.726	0.513				
Min		0.303	0.127	0.088				
Avrg		0.658	0.263	0.202				
dDev		0.208	0.098	0.077				

8.3. Scientific Publication Nr. 3:

Deciphering the Early Cretaceous Patagonian “black shales”: paleoenvironmental analysis of the Katterfeld Formation, southern Chile (45°S)

Authors: Rivas, H., Salazar, Stinnesbeck, W., Encina, J., Pérez-Barría, L., Álvarez-Mena, K.

Status: Submitted – In Review in Sedimentology (Wiley)

Year: 2025

Author contribution (CRediT)

Hermann Rivas: Software, Formal analysis, Investigation, Data curation, Writing – original draft, Writing – review & editing, Visualization, Funding acquisition.

Christian Salazar: Conceptualization, Methodology, Writing – review & editing, Supervision, Funding acquisition.

Wolfgang Stinnesbeck: Resources, Writing – review & editing, Supervision, Project administration, Funding acquisition.

Javier Encina: Writing – original draft, Software

Leonardo Pérez-Barría: Writing – original draft, Investigation

Kevin Álvarez-Mena: Writing – original draft

Formblatt Kumulative Dissertation

Stand 14.02.2023

1. Publikation/Publication:

Vollständige bibliographische Referenz/Complete bibliographic reference:

Rivas, H., Salazar, C., Stinnesbeck, W., Pérez-Barría, L., Álvarez-mena, K. (2025). Deciphering the Early Cretaceous Patagonian “black shales”: paleoenvironmental analysis of the Katterfeld Formation, southern Chile (45°S). Sedimentology (submitted - in review)

2. Erst- oder gleichberechtigte Autorenschaft/First or equal authorship:**Ja/Yes**

Nein/No

3. Veröffentlicht/Published

Zur Veröffentlichung akzeptiert/Accepted

Q1/Q2*: 1.289

*SCImago Journal Rank (SJR) indicator

Ja/Yes ☒ Nein/NoIm Erscheinungsjahr oder im letzten verfügbaren Vorjahr/In the year of publication or the last prior year available: 2023**Eingereicht/Submitted**

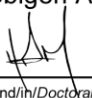
Noch nicht eingereicht/Not yet submitted

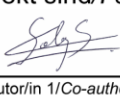
4. Beteiligungen/Contributions**

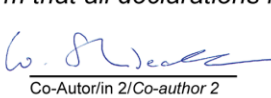
Contributor Role	Doktorand/in/ Doctoral student	Co-Autor/in 1/ Co-author 1	Co-Autor/in 2/ Co-author 2
Name, first name	Rivas, Hermann	Salazar, Christian	Stinnesbeck, Wolfgang
Methodology	<input type="checkbox"/>	<input checked="" type="checkbox"/>	<input type="checkbox"/>
Software	<input checked="" type="checkbox"/>	<input type="checkbox"/>	<input type="checkbox"/>
Validation	<input type="checkbox"/>	<input checked="" type="checkbox"/>	<input type="checkbox"/>
Formal analysis	<input checked="" type="checkbox"/>	<input type="checkbox"/>	<input type="checkbox"/>
Investigation	<input checked="" type="checkbox"/>	<input type="checkbox"/>	<input type="checkbox"/>
Resources	<input type="checkbox"/>	<input checked="" type="checkbox"/>	<input checked="" type="checkbox"/>
Data Curation	<input checked="" type="checkbox"/>	<input type="checkbox"/>	<input type="checkbox"/>
Writing-Original Draft	<input checked="" type="checkbox"/>	<input type="checkbox"/>	<input type="checkbox"/>
Writing-Review&Editing	<input checked="" type="checkbox"/>	<input checked="" type="checkbox"/>	<input checked="" type="checkbox"/>
Visualization	<input checked="" type="checkbox"/>	<input type="checkbox"/>	<input type="checkbox"/>
Supervision	<input type="checkbox"/>	<input checked="" type="checkbox"/>	<input checked="" type="checkbox"/>
Project administration	<input type="checkbox"/>	<input checked="" type="checkbox"/>	<input checked="" type="checkbox"/>
Funding acquisition	<input type="checkbox"/>	<input checked="" type="checkbox"/>	<input type="checkbox"/>

**Kategorien des CRediT (Contributor Roles Taxonomy, <https://credit.niso.org/>)

Hiermit bestätige ich, dass alle obigen Angaben korrekt sind/I confirm that all declarations made above are correct.

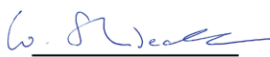
Unterschrift/Signature

 Doktorand/in/Doctoral student


 Co-Autor/in 1/Co-author 1


 Co-Autor/in 2/Co-author 2
Betreuungsperson/Supervisor:

Hiermit bestätige ich, dass alle obigen Angaben korrekt sind und dass die selbstständigen Arbeitsanteile des/der Doktoranden/in an der aufgeführten Publikation hinreichend und signifikant sind/I confirm that all declarations made above are correct and that the doctoral student's independent contribution to this publication is significant and sufficient to be considered for the cumulative dissertation.

 Wolfgang Stinnesbeck
 Name/Name


 Unterschrift/Signature

 20.03.2025
 Datum/Date

Deciphering the Early Cretaceous Patagonian “black shales”: paleo-environmental analysis of the Katterfeld Formation, southern Chile (45°S)

Hermann Rivas^{1,*}, Christian Salazar², Wolfgang Stinnesbeck¹, Javier Encina², Leonardo Pérez³, Kevin Álvarez-Mena³

¹ Institut für Geowissenschaften, Universität Heidelberg, Im Neuenheimer Feld 234, 69120 Heidelberg, Germany.

² Escuela de Geología, Facultad de Ciencias, Universidad Mayor, Manuel Montt 367, 7510041 Providencia, Chile.

³ Museo Regional de Aysén, Km. 3 camino a Coyhaique Alto, 5950000 Coyhaique, Chile.

*Corresponding author

E-mail addresses: hermann.rivas@geow.uni-heidelberg.de (H. Rivas); christian.salazar@umayor.cl (C. Salazar); wolfgang.stinnesbeck@geow.uni-heidelberg.de (W. Stinnesbeck); javier.encinak@mayor.cl (J. Encina); leonardo.perez@museoschile.gob.cl (L. Pérez); kevin.alvarez.geo@gmail.com (K. Álvarez-Mena).

Abstract

The Valanginian-Hauterivian Katterfeld Formation is one of the most important yet less studied Mesozoic “black shales” from southern South America (43°-47°S). The unit represents the deepest stage of marine transgression into the Aysén-Río Mayo Basin, a marginal basin developed during the Late Jurassic-Early Cretaceous (Tithonian-Aptian) along the southwestern margin of Gondwana. A paleoenvironmental model based on five facies associations (FA1-FA5), comprising 22 lithofacies and 17 microfacies, is here defined for the Katterfeld Formation and its stratigraphically adjacent units, exposed near Coyhaique, in the Aysén Region of southern Chile (45°S). The facies model shows distal volcanic apron- and prodelta deposits (FA1, FA2) of the Toqui Formation, covered by black mudstone (FA3) of the Katterfeld Formation with a transgressive surface. Mudstone is massive and brittle, including calcareous concretions and interbedded tuffaceous beds. “Black shale” microfacies consists of fossil-bearing, carbonaceous silty claystone to calcimudstone, depicting a hemipelagic sedimentation below the storm-wave base, under oxygen-poor conditions. Deposition of the Katterfeld Formation occurred in at least four phases. Its lowermost part displays a siliciclastic-calcareous, deepening-upwards trend from shelf to slope settings (FA3-A; mid?-upper Valanginian). The lower-middle layers show a siliciclastic-calcareous trend with a periodic volcanoclastic input (FA3-B; lower Hauterivian). The mid?-upper levels are rich in phosphate and microfossils, depicting upwelling-triggered high productivity (FA3-C; lower-mid Hauterivian). Towards the top, the formation shows a shallowing-upward trend to offshore-transition and prodelta settings (FA3-D, mid-upper Hauterivian). Sequence stratigraphy depicts a basal syn-rift sequence (FA3-A), followed by at least two transgressive system tracts (FA3-A; FA3-B). Phosphatic beds (FA3-C) might represent a maximum flooding surface. Upsection, the succession conforms a regressive system tract (FA3-D to FA5). The onset of mudstone sedimentation likely occurred during an interval of global humid conditions attributed to the Valanginian Weissert Event, whereas the relation between the high-productivity beds and the Hauterivian Faraoni Event remains unclear.

1. Introduction

Fine-grained sediments comprise more than the half of the Earth's sedimentary successions by volume (e.g., Potter et al., 2005; Kurosawa et al., 2023). Mud is a product of the weathering of older rocks, mixed with terrigenous, calcareous, and biogenic material (Potter et al., 2005). In deep marine settings (i.e., below the storm-wave base), mud deposition is important close to continental margins (Stow & Tabrez, 1998), where it is deposited by hemipelagic processes, including vertical settling and slow lateral advection (e.g., Stow & Tabrez, 1998; Stow & Smillie, 2020). Carbonaceous mudstones – also known as “black shales” – are a particular type of fine-grained rocks, characterized by their dark colour, high organic content, and poor benthic fauna (e.g., Arthur & Sageman, 1994). They provide insights into past climatic conditions, oceanographic processes, and marine biogeochemical cycles (Arthur & Sageman, 1994; Ulmer-Scholle et al., 2014). The deposition of black mudstone, rich in organic matter, is linked to periods of reduced oxygen in the oceans, usually corresponding with global events such as eustatic highs, bioevents, and significant climatic shifts (e.g., Föllmi et al., 2006; Föllmi, 2012; Trabucho-Alexandre, 2015).

“Black shales” are a remarkable component of the Cretaceous Patagonian basins (Arbe, 2002; Mpodozis et al., 2011; Richiano et al., 2019; Fig. 1), representing important regional sources of hydrocarbons (Richiano et al., 2015). In the Aysén-Río Mayo Basin of southern Chile and Argentina (43°-47°S/49°S; Bell et al., 1996; Suárez et al., 1996; Townsend, 1998; Fig. 1), fine-grained deposits are majorly represented by the Katterfeld Formation, defined at the boundary between both countries (Cerro Katterfeld; Ramos, 1976; 1981; Olivero, 1982; Fig. 1). In Chile, the Katterfeld Formation crops out as scattered and incomplete exposures between Palena and Villa O'Higgins (De La Cruz et al., 1996; 2004). Because of its relatively low hydrocarbon potential (Duhart, 1960), and in contrast to correlative units in adjacent basins (e.g., Río Mayer Fm., Zapata Fm.; Arbe, 2002; Mpodozis et al., 2011; Cuitiño et al., 2019), no detailed sedimentological study of the Katterfeld Formation has yet been undertaken. Most lithological information of the unit comes from regional or biostratigraphic studies (e.g., Ramos, 1976; Scasso, 1989; Suárez & De La Cruz, 1994; Suárez et al., 1996; Olivero & Aguirre-Urreta, 2002; Folguera & Iannizzotto, 2004).

Based on its dark colour and fine-grained composition, the Katterfeld Formation has been depicted as formed by “homogeneous” mudstone settled in anoxic offshore settings (Ramos, 1976; Suárez et al., 1996; De la Cruz et al., 2003). However, no facies model has yet been proposed for this unit. A detailed investigation of the Katterfeld Formation, addressing its facies, paleoenvironments, and sequence stratigraphy is

presented here. The depositional evolution in the basin and its relation with regional and global events is also discussed.

1.1. Geological Setting

The Katterfeld Formation is a marine sedimentary unit composed of carbonaceous mudstone; it forms part of the Lower Cretaceous fill of the Aysén-Río Mayo Basin in Central Patagonia (43°-47°S; Haller et al., 1981; Bell et al., 1996; Fig. 1). The Aysén-Río Mayo Basin (ARB) was a back-arc basin developed at the southwestern margin of proto-South America during the Jurassic-Cretaceous transition (Aguirre-Urreta & Ramos, 1981; Suárez et al., 2010; 2023). Back-arc extension had its focus to the east of the coeval volcanic arc, represented by the Patagonian Batholith (Pankhurst et al., 1999; Suárez & De La Cruz, 2001; Folguera & Iannizzotto, 2004; Suárez et al., 2023; Fig. 1).

The basin fill of the ARB comprises the volcanic products of the Mid-Upper Jurassic to Early Cretaceous volcanic arc (Lago La Plata Group; Ibáñez Formation; Suárez et al., 2009; 2010; 2023), which are overlain by a transgressive-regressive marine succession (Coyhaique Group) deposited during a Tithonian-Aptian Pacific marine incursion (Skarmeta, 1976; Charrier & Covacevich, 1978; Aguirre-Urreta & Ramos, 1981; Scasso, 1989; Haller & Lapido, 1980; Figs. 1; 2). In the Coyhaique Group, the earliest transgression includes mixed volcanoclastic-calcareous rocks of the Tithonian-Valanginian Toqui Formation (and correlative units in Argentina; see Rivas et al., 2021), settled discretely in shallow-marine carbonate platforms (Scasso, 1989; Rivas et al., 2021; 2023).

The Katterfeld Formation (Valanginian-Barremian), middle member of the Coyhaique Group (Fig. 2), represents the deepest marine stage in the Aysén-Río Mayo Basin (Olivero & Aguirre-Urreta, 2002; Suárez et al., 2007). It overlies the Toqui Formation with a gradual to sharp contact. The Katterfeld Formation consists of black carbonaceous mudstone with calcareous concretions, and sporadically interbedded sandy beds. It has been interpreted as deposited in outer shelf- to prodelta settings (Ramos & Palma, 1983; Scasso, 1987; 1989), under anoxic (De la Cruz et al., 2003) or euxinic conditions (Katz, 1961; Skarmeta, 1976; Skarmeta & Charrier, 1976).

The regressive stage in the basin is represented by the Apeleg Formation dated to the Hauterivian? Barremian-Aptian (Ramos, 1981; Olivero, 1982; Scasso, 1987; 1989; Suárez et al., 2010; 2015; 2023), i.e., the youngest member of the Coyhaique Group (Haller & Lapido, 1980; Haller et al., 1981; Fig. 2). The Apeleg Formation overlies the Katterfeld Formation with a

transitional contact. It is conformed by heterolithic and glauconitic sandy-gravelly

layers (Ploszkiewicz & Ramos, 1977; Gonzalez-Bonorino & Suárez, 1995) and reflects the progradation of coastal and continental environments during the regression (Ploszkiewicz, 1987; Scasso, 1987; 1989; Gonzalez-Bonorino & Suárez, 1995).

The inversion of the ARB occurred in the Aptian (Suárez et al., 2010; Suárez et al., 2015; Echaurren et al.,

2003). However, 15 km to the south, the Ibáñez Formation has been dated to the early Valanginian (Pankhurst et al., 1999; De la Cruz et al., 2003; Suárez et al., 2009; Fig. 2).

At Alto Baguales, these volcanic rocks conformably underlie tuffaceous mudstone assigned to the Toqui Formation (De la Cruz et al., 2003; Figs. 3; 4). This formation also includes discrete calcareous outcrops south of Coyhaique, with an inferred Valanginian age (De la Cruz et al., 2003; Rivas et al., 2023; Fig. 2). Regionally, a

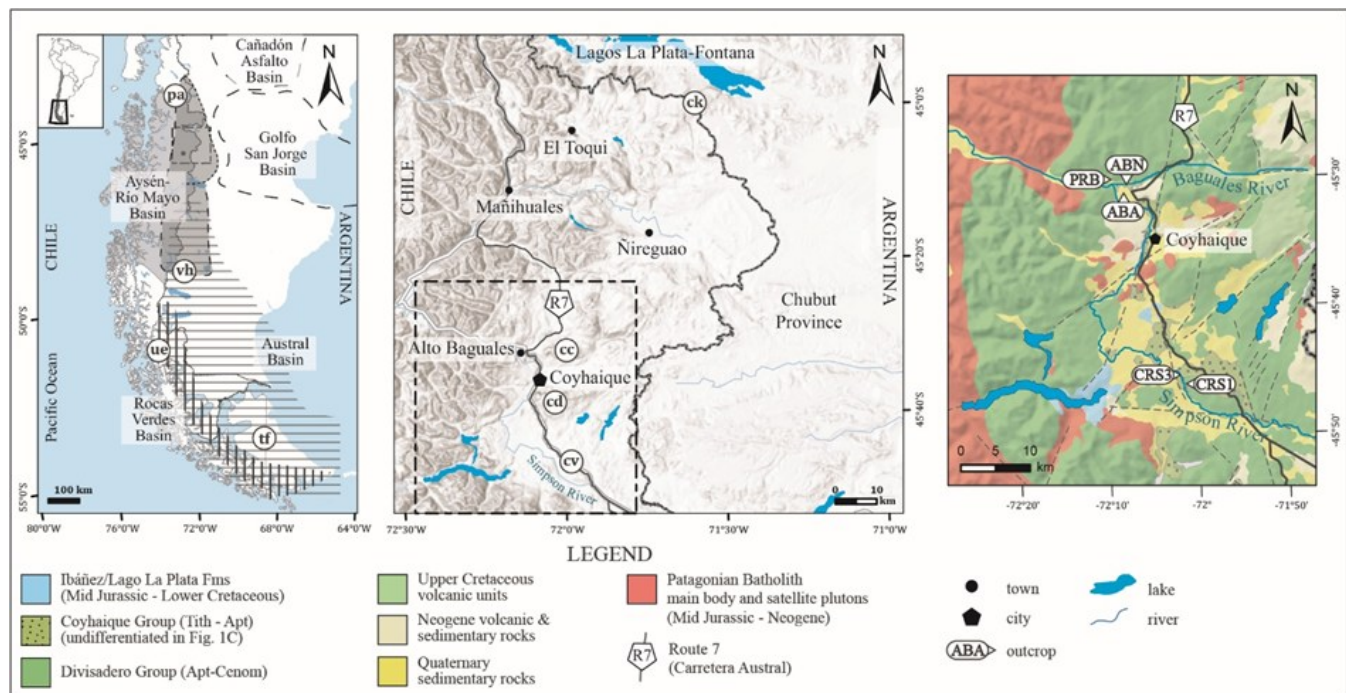


Figure 1. Location Map. Left: Location of the Aysén-Río Mayo Basin (ARB) and adjacent basins. Short-dashed Line: Outline of the ARB sensu Suárez et al. (2010); dotted line: Río Mayo Embayment sensu Aguirre-Urreta and Ramos (1981). Outlines of the adjacent basins after Calderón et al. (2013; Rocas Verdes Basin); Figari et al. (2015; Cañadón Asfalto Basin); Fosdick et al. (2020; Austral Basin); Ramos (2015; San Jorge Basin). Study area is indicated in the black square. Center: Study area (Coyhaique area). Right: Geology of the study area and location of sedimentary logs. Abbreviations of logs: ABA: Alto Baguales; ABN: Alto Baguales Norte; CRS1: Cañadón Río Simpson 1; CRS3: Cañadón Río Simpson 3; PRB: Puente Río Baguales. Localities mentioned in text: cc = Cerro Cinchao; cd = Cerro Divisadero; ck: Cerro Katterfeld (type locality of the Katterfeld Formation); cv = Cerro La Virgen; pa: Palena; ue: Última Esperanza Province; tf: Tierra del Fuego; vh: Villa O'Higgins. Modified from Rivas et al. (2021).

2016). The marine succession of the Coyhaique Group was capped by subaerial volcanic rocks of the Divisadero Group, representing a new pulse of arc volcanism starting in the Aptian (Skarmeta & Charrier, 1976; Scasso, 1989; Iannizzotto et al., 2004; Suárez et al., 2010; 2015; Fig. 2).

1.2. Local Stratigraphy

In the Coyhaique area, the oldest beds are the volcanic rocks of the Ibáñez Formation, dated regionally to the Kimmeridgian?-early Valanginian (De la Cruz et al., 2003; Suárez et al., 2009; Fig. 2). In the Alto Baguales area, this lithological unit comprises the “Tobas del Simpson” informal unit, lacking an absolute age (De la Cruz et al.,

Tithonian-Valanginian age has been suggested for the Toqui Formation (Suárez et al., 2005; 2015).

The Katterfeld Formation (Valanginian-Hauterivian) is a remarkable unit in the Coyhaique area, where it has been historically referred to as “black shales” or “black lutites of Coyhaique” (Fuenzalida & Latcham, 1935; Heim, 1940; Duhart, 1960). Its outcrops are scattered and incompletely exposed between the Río Baguales and the Cerro La Virgen (Fig. 1). The base and lower-mid part of the Katterfeld Formation crop out at Alto Baguales, where it sharply overlies the Toqui Formation (De la Cruz et al., 2003; Figs. 2-4). At its top, the Katterfeld Formation has a transitional contact with the Apeleg Formation, as exposed at the Río Simpson, westwards of Cerro La Virgen (Figs. 1; 3). Locally, the

Katterfeld Formation is intruded by a dike-and-sill swarm dated to the Late Cretaceous (De la Cruz et al., 2003; Suárez et al., 2023; Fig. 3).

The Apeleg Formation (Hauterivian-Aptian) is the youngest marine unit in the ARB; it is exposed at the flanks of the main hills surrounding the Coyhaique valley (Cerros Cinchao, Divisadero, La Virgen), underlying volcanic strata of the Divisadero Group (De la Cruz et al., 2003; Fig. 2). In this area the contact is covered, but an unconformity, and local conformity has been reported regionally (Suárez et al., 2015, 2023).

1.3. The Katterfeld Formation: Age and correlations

A Valanginian - Hauterivian age has been inferred for the Katterfeld Formation (Fig. 2). This age is based on benthic foraminifers, e.g. *Lenticulina nodosa*, and *Astacolus gibber* (Masiuk & Nakayama, 1978), as well as the ammonites *Kilianella* sp., *Thurmanniceras* sp., *Aegocrioceras* sp., *Crioceratites* spp., and *Favrella* spp. (Aguirre-Urreta et al., 2000; Olivero & Aguirre-Urreta, 2002; Fig. 2). Its lower boundary may extend to the Berriasian, because of its conformable contact with the underlying Toqui Formation (Tithonian-Valanginian; Covacevich et al., 1994; Suárez et al., 2010).

In the Coyhaique area, the lower portion of the Katterfeld Formation was assigned to the Valanginian (U-Pb 133.2 ± 1 Ma; Suárez et al., 2023). To the south, near Cerro La Virgen, tuffaceous beds within the Katterfeld Formation provided a Hauterivian age (U-Pb 129-127 Ma; Késjar et al., 2017; Fig. 2). However, its upper limit may be as young as Barremian, given its transitional contact with the overlying Apeleg Formation (Hauterivian-Aptian; Suárez et al., 2010; 2015).

Based on its composition, its inferred age, and the fossil assemblage (*Favrella* spp., *Lenticulina nodosa*, *Astacolus gibber*; Malumian & Masiuk, 1975; Masiuk & Nakayama, 1978; Malumian & Nañez, 1983), the Katterfeld Formation is litho- and partly chronostratigraphically correlative with the Río Mayer Formation (Berriasian-Albian; Richiano et al., 2015) from the northern Santa Cruz Province in Argentina, and with the subsurface units defined between Última Esperanza and Tierra del Fuego in Chile and Argentina (e.g., Erezcano-, Zapata-, and Pampa Rincón Formations; Arbe, 2002; Cuitiño et al., 2019).

A close affinity between the foraminiferal assemblage of the Katterfeld Formation with coeval South African species has also been proposed (Malumian & Masiuk, 1975; Masiuk & Nakayama, 1978).

2. Material and Methods

This study comprises four outcrops studied in the vicinity of Coyhaique ($45^{\circ}34'S$; $72^{\circ}03'W$; Fig. 1), in the Aysén Region of southern Chile. The outcrops are exposed between the Río Baguales and the Cerro La Virgen, covering most of the Katterfeld Formation, including its base and top. Sections are between 15 m and 128 m-thick; they comprise, from north to south: Puente Río Baguales (PRB), Alto Baguales Norte (ABN), Alto Baguales (ABA), and two sedimentary logs from the Río Simpson, near Cerro La Virgen (CRS1 and CRS3; Fig. 1). Rock samples were taken each 3-5 m, or at wider distance, when avoiding strongly weathered horizons. Microfacies of mudstone and sandstone were studied in 35 standard thin sections. A detailed version of the sedimentary logs (Fig. 3) is presented as supplementary material.

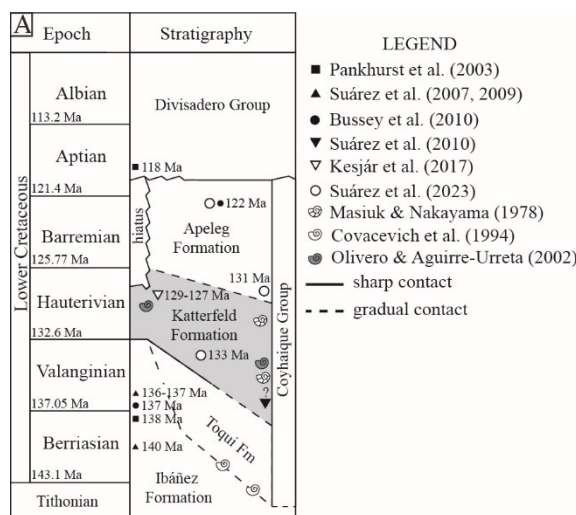


Figure 2. Chronostratigraphic chart for the Coyhaique Group. Main references addressing the relative and absolute age of the formations is presented as symbols. Modified from Rivas et al. (2021). Ages of chronostratigraphic units after International Chronostratigraphic Chart v2024/12.

2.1. Definitions and Guidelines

The classification of fine-grained rocks follows Potter et al. (2005), using “mudstone” as a generic term for fine-grained, argillaceous rocks, while “shale” is usually reserved for fissile argillaceous rocks, i.e., with a planar parting 0.5-1.0 mm-thick (Potter et al., 1980). “Hemipelagic” refers to a mixture of biogenic and terrigenous material with a coarse silt-size (5 microns) greater than 25% (adapted from Jackson, 1997 in Potter et al., 2005; Flügel & Munnecke, 2010). The term “pelagic” depicts mudstone with more than 70-75% of biogenic components, also known as “biogenic oozes” (Stow & Tabrez, 1998; Pickering & Hiscott, 2016).

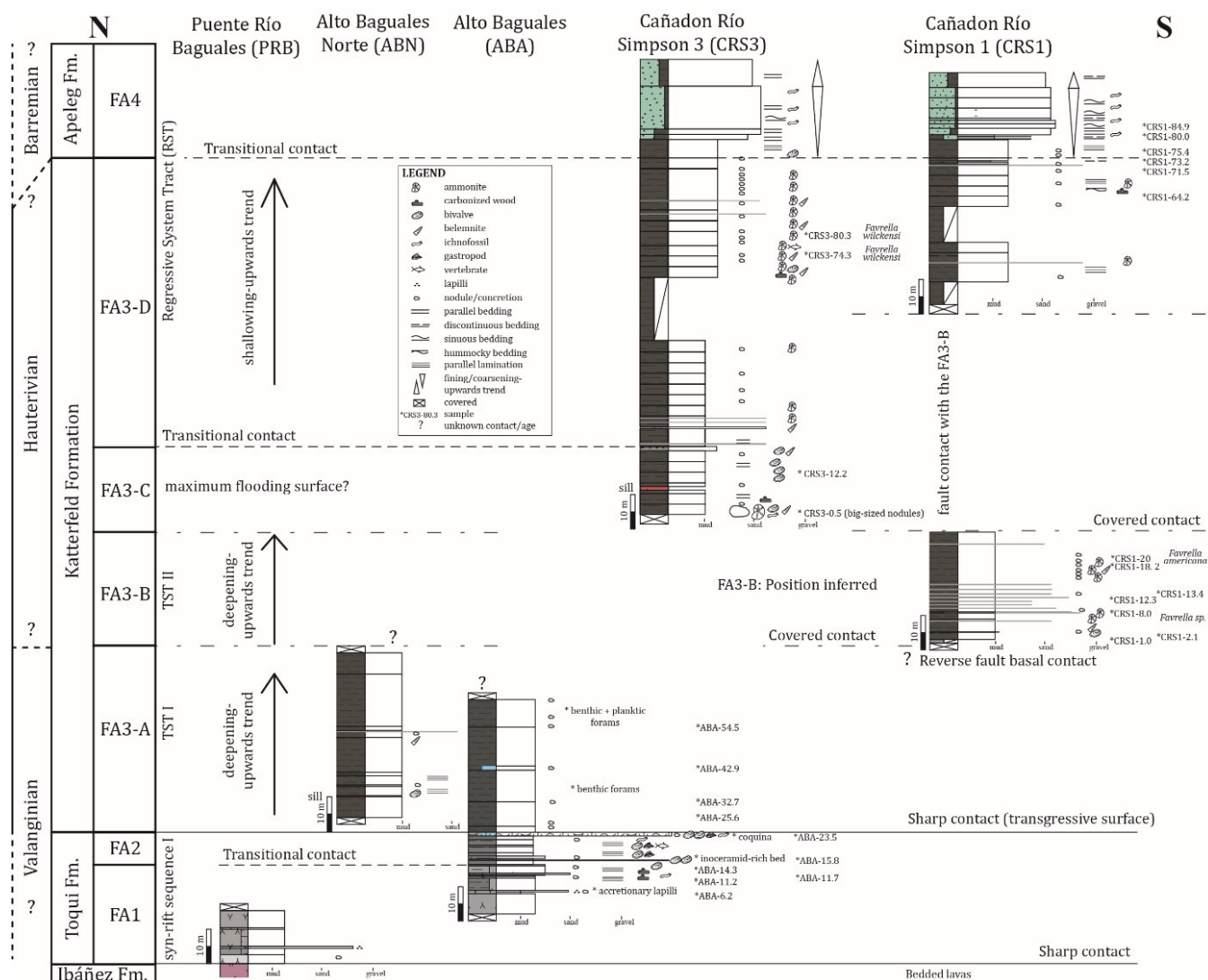


Figure 3. Correlation of sedimentary logs from the Coyhaique area.

For sandstone, we used the recommendations of Garzanti (2019). Rocks with a volcanic component are common in the Coyhaique Group. For these, “volcaniclastic” is a general term used for all clastic volcanic materials independent from fragmentation, dispersal, deposition, and mixture with epiclastic sediments (modified from Fisher, 1966; Fisher & Schmincke, 1984). “Tuffaceous” is restricted to reworked/remobilized pyroclastic deposits (Fisher, 1961; Cas & Wright, 1987). Chronostratigraphic units follow the International Chronostratigraphic Chart v2024/12 (Cohen et al., 2013; updated).

3. Facies associations: litho- and microfacies

Five facies associations are defined here for the Coyhaique Group in the area near the homonymous city (FA1 to FA5; Fig. 3). The Katterfeld Formation comprises four sub-facies associations (FA3-A to FA3-D). To

contextualize this unit, facies associations comprise its base (FA1; FA2), and top (FA4; FA5). Facies are presented in a base to top order (Fig. 3).

3.1. Facies Association 1 (FA1): Distal volcanic apron hemipelagites

3.1.1. Facies Association 1 (FA1): Lithofacies

The facies association 1 overlies decimeter- to meter-thick volcanic beds of the Ibáñez Formation (Fig. 3). It consists of pale gray-coloured, diffusely parallel-bedded, massive tuffaceous mudstone (lithofacies tMm), with minor siltstone to fine-grained sandstone (lithofacies tSm). Mudstone is brittle (blocky parting), and decimeter- to meter-thick, while silty-sandy beds form small ledges with slabby parting (Figs. 4A, 4B, 4C). A mid-grained lapillistone bed (lithofacies tG) was observed near the base of this association (Fig. 4E). Discrete, sinuous laminae of carbonaceous siltstone were also

observed (lithofacies Us; Fig. 4D). The carbonaceous content increases upsection, with the appearance of gray-coloured mudstone bearing carbonized plant fragments (<1 cm; Fig. 4F). Poorly-preserved ichnofossils, and small sedimentary nodules (diameter <3 cm) are scarce.

3.1.2. Facies Association 1 (FA1): Microfacies

These facies are controlled by tuffaceous silty claystone to clayey siltstone (microfacies V1; Figs. 4G, 4H). It appears commonly massive, sometimes diffusely laminated, or as the matrix of coarser-grained volcanoclastic microfacies. Mudstone is pale gray to brown-coloured (Fig. 4G), formed of devitrified glassy material (isotropic), usually altered to illite-sericite or by scattered calcite. The silt-sized component includes small crystals (feldspar microliths, quartz, opaque minerals, scarce micas), and pyroclasts (altered pumice and shard fragments). Subordinate interlaminated microfacies include:

- i) Fine-grained, tuffaceous sandstone (V2-f), composed of normal-graded, flattened to equant, argillized pumice and scarce quartz. It displays basal scouring on mudstone (V1; Fig. 4G).
- ii) Diffusely laminated, volcanoclastic, muddy sandstone (V2), formed of sericitized feldspar, volcanic quartz (broken, resorpted), and volcanic lithics (Figs. 4I, 4J).
- iii) Carbonaceous silty claystone with a wavy and discontinuous lamination (microfacies M1-s; bioturbated). It also appears as lenses within tuffaceous siltstone (Fig. 4H).

3.1.3. Facies Association 1 (FA1): Interpretation

Tuffaceous mudstone of the facies association 1 depicts hemipelagic sedimentation in a marine setting, below the storm wave base. These hemipelagites are analog to the facies association MVF of Rivas et al. (2021) and may represent a distal volcanic apron setting (Carey & Sigurdsson, 1984; Carey & Schneider, 2011), or a “pyroclastic prodelta” (Nemec, 1990; Rivas et al., 2021). An explosive (phreatomagmatic?) volcanic source is inferred for these sediments (Cas & Wright, 1987; McPhie et al., 1993); they settled subaqueously after fallout (structureless) or, as inferred from lamination, they were remobilized by sediment-laden plumes (Carey & Schneider, 2011; Henrich & Hüneke, 2011; Zavala & Pan, 2018). Laminated microfacies reflect sporadic ash-turbidites or distal tempestites (microfacies V2-t; McPhie et al., 1993; Flügel & Munneke, 2010), while sinuous carbonaceous laminae (M1) indicate subtle currents and a terrestrial influence (O'Brien & Slatt, 1990). The lack of

benthic fauna depicts stressful conditions, making colonization of the substrate inviable due to sediment in suspension (Housego & Rosman, 2016).

3.2. Facies Association 2 (FA2): Fossiliferous, mixed prodelta

3.2.1. Facies Association 2 (FA2): Lithofacies

The facies association 2 has a transitional contact with the FA1 (Figs. 3; 4B, 4C), with a gradual carbonaceous and calcareous enrichment. It comprises gray fossiliferous mudstone (fMp), and fossil-bearing, carbonaceous mudstone (lithofacies fMm/fMp). Mudstone is massive to diffusely laminated, and brittle with a platy-blocky parting (Fig. 5A). Discrete beds show fine lamination with fissile parting (lithofacies fMp-in). Bed-thickness varies between 0.3 and 1.8 m, with diffuse to sharp contacts noticeable from subtle changes in grain-size, fossils, or weathering (Figs. 4B; 5A). Sedimentary nodules are infrequent, and small-sized (diameter < 5 cm).

Fossil content is characterized by scattered bivalves and small gastropods, while carbonized plant remains and serpulids are scarce. Fossils are more abundant upsection, including complete and broken specimens. Three main lithofacies were defined in this facies association: 1) bioclastic-bearing (gastropods and/or bivalves; Fig. 5B), massive- to diffusely laminated mudstone (fMm, fMp, respectively); 2) inoceramid-rich, parallel-laminated mudstone (fMp-in; Fig. 5C); and 3) bivalve-rich, massive and bioturbated mudstone (coquina; fM-cq; Figs. 5D, 5E, 5F). The latter includes abundant bimodal fossils (complete and fragmented), including gryphaeids, isognomonids, trigoniids, and astarteids? (lithofacies fM-cq; Figs. 5E; 5F).

3.2.2. Facies Association FA2: Microfacies

Microfacies of the FA2 varies from fossiliferous, carbonaceous silty claystone (microfacies M1-f) to carbonaceous-micritic siltstone (microfacies M2-f). Lamination is diffuse, as identified by aligned shells and carbonaceous rip-up clasts (Figs. 6A, 6B). The framework is moderately to poorly-sorted, formed of terrigenous particles and bioclasts. The former (<5-10%) consist of quartz, feldspars, volcanic clasts, and opaque minerals; while bioclasts are conformed by bivalve fragments (inoceramids, oysters, and other bivalve groups preserved as voids; Figs. 6A; 6B, 6C), and calcispheres. Other allochems are scarce ($n < 5$), including ostracods, benthic foraminifers, bryozoans, micritic intraclasts, and fish remains. Sparse silt-sized microdolomite was also observed.

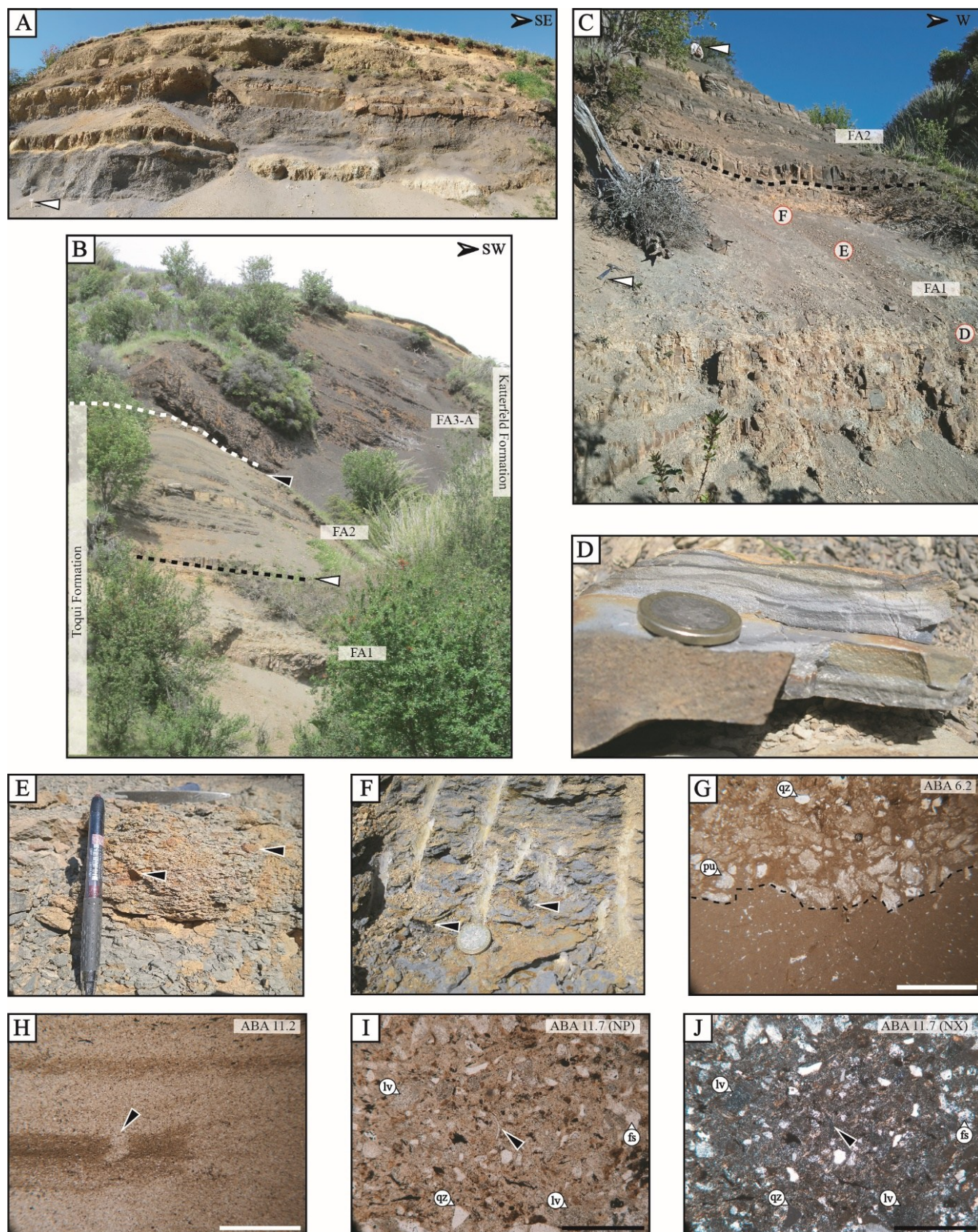


Figure 4. Facies Associations FA1 and FA2 (Toqui Formation). A: Bedded tuffaceous rocks of the FA1 at the Puente Río Baguales section (PRB). Road sign as scale, about 50 cm-long (white arrow). B: Section Alto Baguales (ABA), note the gradual transition between tuffaceous rocks of the FA1 and the mixed rocks of the FA2 (white dashed line), and the sharp contact with mudstone of the lowermost Katterfeld Formation (FA3-A; black dashed line). Outcrop is ca. 60 m-high, see person to scale in Fig. 4C. C: Detailed view of the association FA1 (lithofacies tMm) and its contact with FA2 (lithofacies fMp). Note the appearance of massive beds as ledges upsection (lithofacies fMm). Encircled letters make reference to the pictures shown in Fig. 7 below. Person and hammer to scale (white arrows). D: Tuffaceous mudstone (lithofacies tMm) interlaminated with sinuous layers of carbonaceous mudstone (lithofacies Us). E: Tuffaceous bed with accretionary lapilli (lithofacies tG; black arrows); pencil to scale.

Figure 4 (continuation). F: Tuffaceous mudstone with fragments of carbonaceous wood (lithofacies tMm); coin to scale G: Erosive contact between massive tuffaceous mudstone (microfacies V1) and normal-graded, ash-turbidites (microfacies V2-g). Note the compaction of pumice clasts. H: Tuffaceous siltstone (microfacies V1) with discontinuous alternations of bioturbated carbonaceous mudstone (Microfacies M1-s). I-J: Tuffaceous siltstone to fine grained sandstone (lithofacies V2-f; parallel- and crossed nicols, respectively). Note the devitrified grayish matrix, angular quartz particles, and broken shells (ostracod?). Abbreviations: fs = feldspar; lv = volcanic lithic; qz = quartz. Scale in microscopic pictures: 2 mm (white); 0.5 mm (black).

3.2.3. Facies Association 2 (FA2): Interpretation

In facies association 2 (FA2), faint lithological changes in mudstone represent fluctuations regarding the discharge, or the shifting of buoyant plumes (Reading & Collinson, 1996; Bhattacharya, 2006). These are commonly observed in a prodelta, or in a mud-dominated shelf setting (Johnson & Baldwin, 1996; Elliott, 2005), which are closely related (Bhattacharya, 2006). In FA2, massive mudstone (Mm) is interpreted as settled after suspension from collapsing buoyant plumes (hypo- and hyperpynites; Zavala & Pan, 2018), or resulting from “fluid-mud layers” concentrated at the sea floor (Bhattacharya & Walker, 1992). A structureless fabric may also derive from bioturbation, but sparse ichnofossils in this association rather reflect a high rate of sediment in suspension (Bhattacharya & Walker, 1992; Reading & Collinson, 1996; Bhattacharya, 2006).

Massive, bioclastic beds (fM), including broken and/or reworked shells, are interpreted as “muddy hyperpynal flow” deposits (Zavala & Pan, 2018), potentially linked to avulsion events onshore, which were strong enough to disturb benthic communities (Mutti et al., 1996; Mutti et al., 2000). Carbonaceous, laminated beds (fMp) depict sporadic periods with a low sedimentary rate, favoring the proliferation of benthic organisms (Lazo, 2006). Compared to the association 1 (FA1), a notable increase in both abundance and diversity of fossils in the prodelta setting of the facies association 2 (FA2); this reflect a notable improvement in oxic conditions and environmental stability (Potter et al., 2005). This may also depict progradation, or a shallowing-upwards transition to distal delta-front facies (Rodríguez & Arche, 2010).

Along the FA2, shell accumulations changed from mono-oligospecific assemblages (lithofacies fMm-bv) to a polyspecific, soft-bottom assemblage at the top (lithofacies fM-cq; Fig. 5D, 5E, 5F). Mixture of both articulated-disarticulated in the top guide-bed, and reworked epifaunal and infaunal organisms indicate a coastal (storm?) reworking. The latter is interpreted to represent a parautochthonous fossil association (*sensu* Kidwell & Bosence, 1991), but possibly comprising several sedimentation events (time-averaged?, e.g., Lazo, 2006). Shallow waters (tens of meters) are inferred from the presence of trigoniids, which populated near-shore environments (Francis & Hallam, 2003). In the FA2, at least one low oxygen event is inferred from laminated, carbonaceous mudstone rich in inoceramids (fMp-in;

Reading & Collinson, 1996; Lazo, 2006), which might also depict temperate waters (Dhondt, 1992).

3.3. Facies Association FA3: “Black shales” (shelf to slope hemipelagites)

The facies association 3 (FA3) overlies FA2 with a sharp contact (Figs. 4B; 5D). It consists of massive black mudstone (lithofacies Mm) with diffuse parallel bedding, as inferred from interbedded layers, and from horizons with aligned light brown-coloured ovoidal calcareous concretions (lithofacies Mm-c; Figs. 5D; 5G). Mudstone is rich in organic matter, as inferred from its dark colour and bitumen smell when cracked (“oil shales”, Potter et al., 2005). These rocks are strongly brittle (blocky parting), with exposure surfaces usually covered by reddish patinae after oxidation of sulphides (Fig. 5D). Relic pyrite is occasionally present as scattered small crystals (< 1 mm), as patches, or as irregular patinae.

Microscopically, the FA3 consists of carbonaceous silty claystone, and minor calcimudstone. Mudstone is structureless to diffusely laminated, with a patchy to peloidal matrix texture, rich in wispy- to amorphous organic matter particles. Microfossils are sparse (<10%), conformed mainly by benthic foraminifers, calcispheres, and ostracods (Fig. 6D). Exceptionally, some phosphatic beds are rich in microfossils (see FA3-C). The silty framework (10-20%) is formed of sub-angular quartz, feldspar, and sparse, rounded volcanoclastics. Opaques are scattered in the matrix, coupled to organic matter and pyrite framboids, or concentrated within particles.

Overall, the Facies Association 3 depicts hemipelagites settled in a low-energy setting, away from storm-wave influence (Reineck & Singh, 1973; Potter et al., 2005). This setting has been referred to as the “offshore zone” (Reading & Collinson, 1996), or “deep water” settings (Flügel & Munnecke, 2010), which comprises the distal shelf and upper slope (Reineck & Singh, 1973; Coniglio & Dix, 1992; Johnson & Baldwin, 1996).

Based on subtle lithological differences (colour, oxidation, parting), type and frequency of interbedded lithofacies, fossil content, and microfacies, four “black shales” sub-facies associations were defined. These are named after their inferred stratigraphic position, from base to top (“A”, “B”, “C”, “D”).

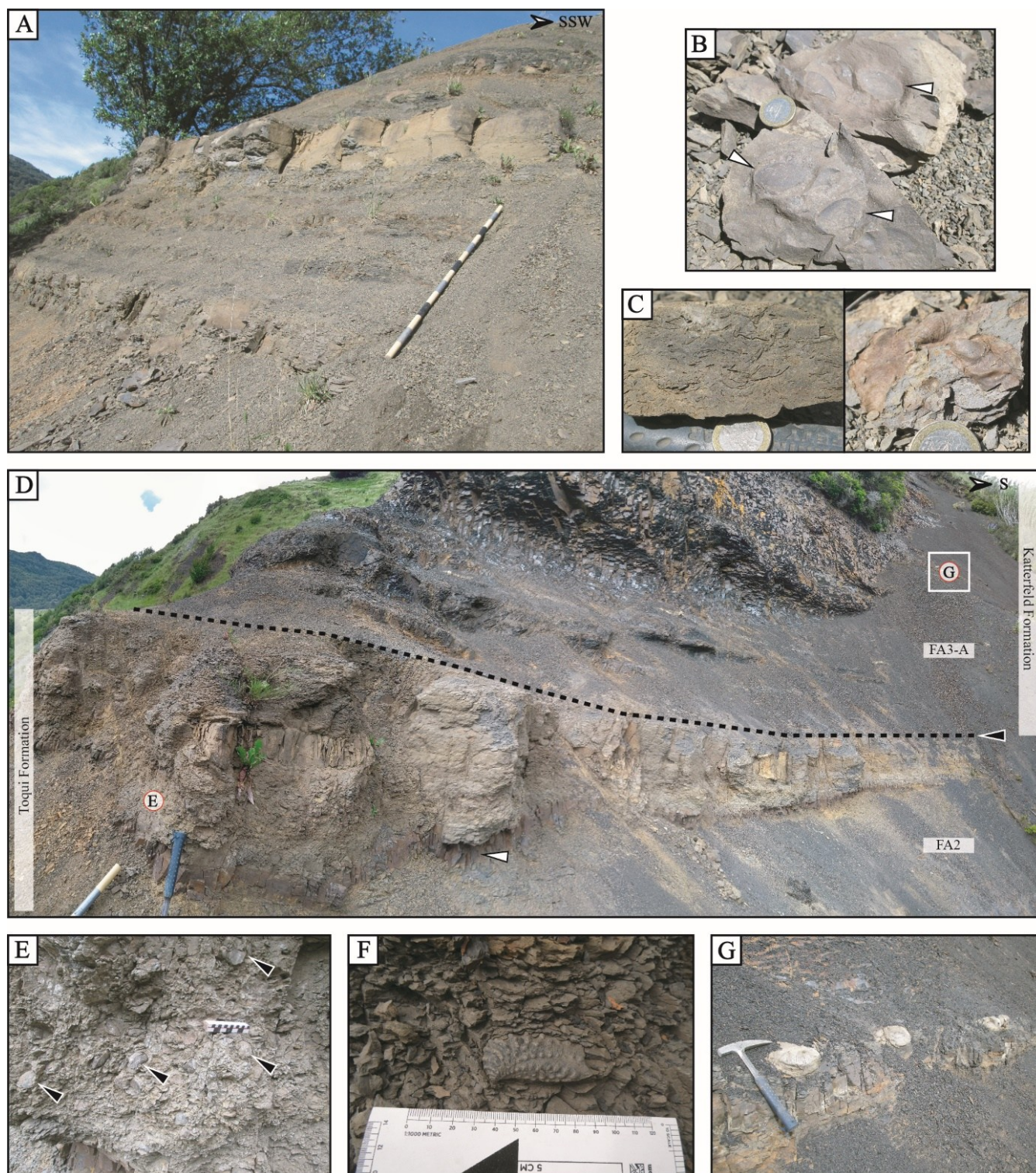


Figure 5. Facies Associations FA2 and FA3A (Toqui- and Katterfeld Formations, respectively) at the Alto Baguales outcrop (ABA). A: Alternation of thinly bedded and massive muddy beds of the FA2 (lithofacies fMp and fMm, respectively); Jacob's staff as scale (1.5 m-long). B: Bivalve-bearing, massive mudstone (lithofacies fMm); coin to scale. C: Inoceramid-rich coquina; left: cross-section; right: plan view (lithofacies fMp-in); coin to scale. D: Panoramic picture showing the sharp contact between the FA2 (Toqui Formation) and the FA3-A (lowermost Katterfeld Formation), see dashed line and black arrow. Note the concretionary horizons in the uppermost bed of the FA2 (coquina, lithofacies fM-cq). Basal laminated mudstone is marked with a white arrow (lithofacies fMp). E: Close-up view of the coquina (lithofacies fM-cq), reworked bivalve cast are indicated with black arrows. F: Close-up of the same guide-bed (coquina), displaying a reworked, but articulated steinmanellid. G: Calcareous horizons (lithofacies cMp) and aligned concretions (lithofacies Mm-c) from the mid-part of the association FA3-A; their position is represented with a white square in Fig. 5D.

3.3.1. Facies Association 3-A (FA3-A): Lithofacies

Black mudstone of facies association 3-A occupies the lowermost stratigraphic position, sharply

covering the fossiliferous rocks of the FA2 in the Alto Baguales area (Figs. 4B; 5D). The FA3-A consists of diffusely bedded, black mudstone (lithofacies Mm) with rare calcareous beds (ca. 0.3-0.4 m-thick, lithofacies cMp),

and sparse thin tuffaceous layers (< 50 mm-thick; max 0.30 m-thick, lithofacies tSm). These rocks are strongly brittle, breaking into sharp, wedge-shaped pieces with an orange-reddish oxidation (Figs. 4B; 5D). Calcareous concretions are mid-sized (< 0.20 m in diameter; max: up to 0.40 m), and sparsely distributed (> 5-10 m distance; Fig. 5G). In the Alto Baguales area (section ABN; Fig. 3), this association is locally intruded by a dike swarm (De la Cruz et al., 2003; Suárez et al., 2023).

Fossils are scarce in the FA3-A (less than 10 fossils found in this study), including scattered belemnite rostra, poorly preserved ammonite impressions, and bivalves. Some fissile beds (Mp) bear concentrations of small pectinids (*Entolium* sp., length < 20 mm).

3.3.2. Facies Association 3-A (FA3-A): Microfacies

Microscopically, the FA3-A consists of fossil-poor, carbonaceous silty claystone (M1; Figs. 6D, 6F) to silty calcimudstone (M2; Figs. 6G, 6H). Mudstone is structureless to diffusely laminated, sometimes strongly sericitized (e.g., sample ABA 25.6) and locally strongly micro-dolomitized (“pseudo siltstone texture”; microfacies M1-c; Fig. 6F). Dispersed terrigenous (10-20%), and organic matter particles are abundant; the latter usually associated with opaque minerals. Fossils include articulated- or fragmented ostracods (Fig. 6D), calcspheres (Fig. 6G), recrystallized radiolarians, and broken bioclasts (bivalves?). Benthic foraminifers are rare ($n < 5$; *Lenticulina?* sp.; Fig. 6G); these also appear in association with planktic foraminifers in a calcimudstone sample near the top of the association (microfacies M2-pf; Fig. 6H). A tuffaceous-carbonaceous bed from the FA3-A shows sandy-clayey siltstone (microfacies V2) rich in shards, volcanic quartz, feldspars, lithics, and scarce ostracods (Fig. 6E).

3.3.3. Facies Association 3-A (FA3-A): Interpretation

In the facies association 3-A (FA3-A), a structureless fabric and dispersal of terrigenous components (“floating”) may indicate transport as a “gel-like” fluid mud (e.g. “Microfacies 3” of Flint, 2014). Flow cohesion was high enough to transport coarser particles, including complete and broken ostracods shells. Cohesion reflects rapid settling of flocculated aggregates, common in mud-laden flows (Pickering & Hiscott, 2016), as inferred for distal storm- or turbidity currents (Ulmer-Scholle et al., 2014). The appearance of planktic foraminifers upsection may depict a deepening-upwards trend to slope facies, or the onset of an open marine setting.

Carbonaceous and pyrite content in the FA3-A reflect burial of organic matter in poorly oxygenated environments (O’Brien & Slatt, 1990; Potter et al., 2005).

A dysoxic setting is supported by the scarce and poorly diverse benthic fauna (Potter et al., 2005; Flügel & Munnecke, 2010), characterized by small-sized pectinids (*Entolium* sp.) and other scarce bivalves. Oxygen-poor conditions prevailed during diagenesis, promoting the growth of organogenic dolomite (Mazzullo, 2000; Scholle & Ulmer-Scholle, 2003; Fig. 6F). Volcaniclastic input was present, but it was infrequent during deposition of this association.

3.4. Facies Association 3-B (FA3-B): Shelf hemipelagites with volcanic supply

3.4.1. Facies Association 3-B (FA3-B): Lithofacies

Base and top of facies association FA3-B are covered (Figs. 3; 7A). Nevertheless, at Río Simpson, the FA3-B is present above the overlying facies association FA3-C (FA3-C) with a reverse fault contact (Fig. 7B). Mudstone of FA3-B is black- to dark-gray coloured, strongly brittle (polyhedral blocky parting), and covered with reddish-brown patina (Figs. 7A, 7B). Bedding is diffuse (lithofacies Mm), with numerous tuffaceous layers (Figs. 7A, 7B), concretions, and fossils. Concretions are mid-sized (0.2-0.4 m in diameter). Calcareous beds (lithofacies cMp) are rare and exposed as small ledges (0.1-0.3 m-thick) with a slabby-parting (Fig. 7C).

Tuffaceous sandy beds (tSm) are fine- to coarse-grained, pale-coloured (but usually oxidized), and arranged in centimeter- to decimeter-thick beds (usually 50-100 mm-thick, up to 0.60 m-thick). These layers display sharp contacts and a strong weathering (argillization with a “floury” texture; Fig. 7A; 7F). Internally, tuffaceous lithofacies are structureless (effaced) or show a diffuse parallel lamination (tSp). A single well-preserved volcaniclastic guide-bed (Bed T2; 0.30 m-thick) was found; it displays structures interpreted as incomplete Bouma sequences (Bouma Tc to Tf, Tb; Figs. 7D, 7E).

In the FA3-B, fossils are more diverse and abundant, dominated by ammonites (*Favrella americana*, *Favrella* sp.; Figs. 7G; 8A), and belemnites (*Belemnopsis?* sp.; Fig. 7H). Other fossils include bivalves (*Gryphaeids*), nautiloids (*Cymatoceras* sp.), and brachiopods (*Discinisca* sp.). Fossils are scattered along the succession, but many appear embedded within concretions (e.g., ammonites).

3.4.2. Facies Association 3-B (FA3-B): Microfacies

Mudstone of the FA3-B grades from bioclast-bearing, carbonaceous-calcareous, silty-sandy claystone (microfacies M1; Fig. 7J), to calcimudstone upsection

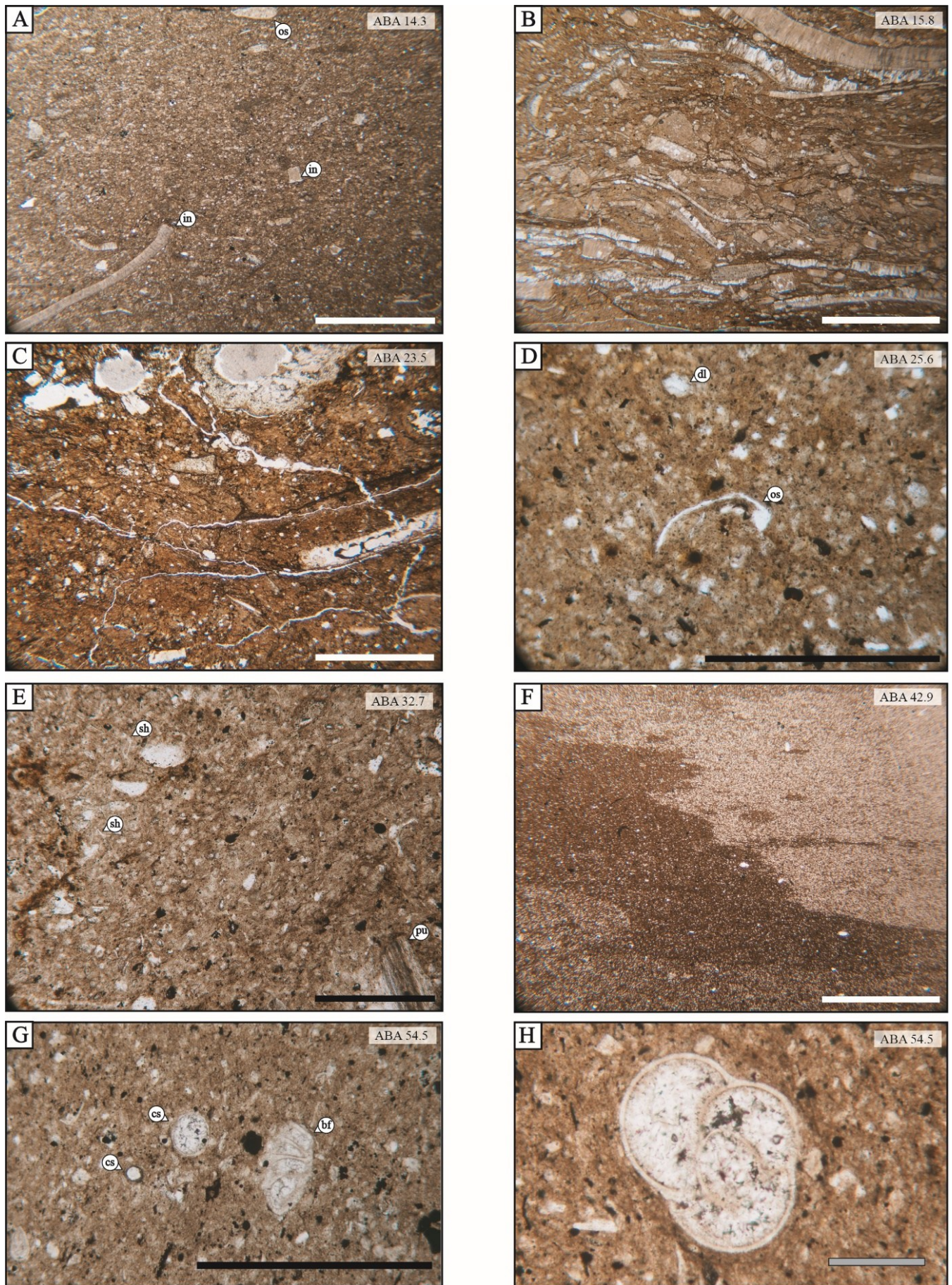


Figure 6. Petrography and microfacies of facies associations FA2 and FA3-A. Facies Association FA2: A-C. A: Bioclastic, carbonaceous-calcareous siltstone (microfacies M1-f). Note a diffuse lamination (aligned bioclasts). Microfossils include inoceramid shells and ostracods. B: Inoceramid-rich, carbonaceous claystone of lithofacies fMp-in (microfacies M1-f). Framework consists mostly of parallel-settled, inoceramid shells.

Figure 6 (continuation). C: Matrix-supported, bioclastic, sandy silty claystone of lithofacies fM-cq (microfacies M1-f; M2-f). Matrix appears bioturbated and oxidized. Calcareous fossils are partly dissolved as voids, or filled by illuviation cutans. Facies Association FA3-A: D-H. D: Massive, carbonaceous silty claystone (microfacies M1). Note “floating” reworked and disarticulated ostracod shells. E: Mixed tuffaceous-carbonaceous, clayey-sandy siltstone (microfacies VM-f). This sample consist of a mixture of tuffaceous and carbonaceous sediments (bioturbation?). Note the presence of juvenile pyroclasts (shards, pumice). F: Bioturbated, carbonaceous silty claystone. Claystone is strongly microdolomitized (lighter-coloured patches) showing a “pseudo-silty” texture (microfacies M1-c). G: Silty, carbonaceous-calcareous wackestone (microfacies M2-f). Note scattered calcispheres and a benthic foraminifer (*Astacolus?* sp.). H: Close-up of the same sample showing the appearance of planktic foraminifer (*globigeriniid?*). Note the scattered microdolomite rhombs around the microfossil. Scale of microscopic pictures: 2 mm (white); 0.5 mm (black); 0.1 mm (gray). Abbreviations: bf = benthic foraminifer; cs = calcispheres; dl = microdolomite; in = inoceramid; os = ostracod; sh = shard.

(microfacies M2; Fig. 7N). Mudstone is brown-coloured, structureless or with a diffuse planar fabric (aligned allochems; Figs. 7J, 7M). Its framework consists of volcanoclastics (5-10%), and sparse microfossils (up to 5 %), including benthic foraminifers (mostly *Lenticulina* sp., *Epistomina* sp.; microfacies M2-for; Figs. 8C, 8D), phosphatic allochems, radiolarians?, and calcispheres (Fig. 7N). Calcareous microfacies comprise foram-rich calcimudstone to sandy wackestone (microfacies M2-bf); and calcisphere-bearing wackestone to calcimudstone (microfacies M2-ccs; Fig. 7N). Benthic foraminifers (rotaliines) and calcispheres are the most common microfossils (about 5%; Figs. 7J; 7M, respectively), and planktic foraminifers were observed towards the top (Fig. 8E). Scattered microdolomite was identified in some samples (Fig. 7J).

Volcanoclastic sandstone is medium-coarse grained with a clayey matrix (sericitized), partly mixed with carbonaceous sediment (microfacies VM-f; Fig. 7I). The composition of framework is equivalent in all samples (feldspars, volcanic quartz, volcanic lithics, sparse micas), but differing in texture (clasts size, proportion, fabric). Sandstone shows a diffuse- to sharp parallel lamination (e.g., VM-f; Fig. 7I), sometimes secondary (fiamme texture; microfacies V2-t; Fig. 7L). Normal grading was observed in the guide-bed T2 (microfacies V2-g; Fig. 7K). Besides microfacies VM-f (bioclast-bearing; Fig. 7I; 8C), fossils are scarce in volcanoclastic rocks (<5 %); they include fragmented bivalves, carbonized wood, benthic foraminifera (Fig. 7I), and phosphatized microfossils (acritarchs?, calcispheres).

3.4.3. Facies Association 3-B (FA3-B): Interpretation

Mudstone of the Facies Association 3-B (FA3-B) is interpreted to represent shelf hemipelagites with periodic volcanic supply. Current influence is inferred from planar microfabric in mudstone (e.g., facies SMF-3 from Flügel & Munnecke, 2010), and clast-rich lenses (lag deposits; Fig. 7J); while massive, fossil-poor massive microfacies are interpreted as “mud-laden” flow deposits (Pickering & Hiscott, 2016). Tuffaceous layers show a low degree of mixing, representing a sudden input of sediment-gravity flow deposits (“eventites”, e.g., distal tempestites, ash-turbidites; Flügel & Munnecke, 2010). These sediments were remobilized from coeval

pyroclastic deposits (McPhie et al., 1993). Given the lack of evidence for a hot emplacement, fiamme texture is interpreted as diagenetic in origin (Bull & McPhie, 2007).

Analogous to FA3-A, the appearance of calcareous microfacies upsection reflects a low terrigenous input, possibly indicating a deepening-upwards trend (Cattaneo & Steel, 2003). Microfossils are poor in diversity and controlled by calcareous benthic foraminifers; these show an association of *Epistomina* sp. and *Lenticulina* sp., reflecting a mixture of inner- and outer neritic species, respectively (McMillan, 2008). The dominance of *Epistomina* sp. might indicate a stressful or oxygen-poor setting, as interpreted for the coeval Río Mayer Formation to the south by Malumian & Nañez (1983). The latter is also supported by the presence of gryphaeids, which had a soft-bottom reclining ecology thriving in low-energy, muddy soft-bottoms (Stenzel, 1971; LaBarbera, 1981). It is well known that they were able to tolerate eutrophic conditions (Nori & Lathuilière, 2003).

3.5. Facies Association 3-C (FA3-C): Outer-shelf pelagites, algal bloom pelagites

3.5.1. Facies Association 3-C (FA3-C): Lithofacies

The facies association 3-C (FA3-C) is exposed at the margin of the Río Simpson near the Cerro La Virgen (Fig. 9A). Its basal contact is not exposed; however, an intermediate stratigraphic position is inferred from the overlying facies (FA3-D; Fig. 3). The FA3-C consists of parallel-bedded, carbonaceous- and calcareous mudstone (lithofacies Mp, cMp, respectively), arranged in sharp, relatively less brittle, decimeter-thick beds (Fig. 9A). Outcrops of the FA3-C are dark gray to black-coloured, with orange oxidation patches (Fig. 9A). Mudstone splits in platy-wispy fragments, or in slabs in calcareous beds (Figs. 9B, 9C). This association is locally intruded by sills (Fig. 9A).

Sparse ammonites, belemnites, concave-up gryphaeid oysters, carbonized wood fragments (Fig. 9F) and small pectinids (*Entolium* sp., length < 20 mm) are present. Locally, calcareous mudstone of the FA3-B bears big-sized concretions (diameter > 0.5-1.0 m; lithofacies cMp-c; Fig. 9B, 9D). In addition to ichnofossils (*Planolites* isp.; Fig. 9C), these beds bear large ammonite



Figure 7. Facies Association FA3-B at the Cañadón Río Simpson 1 section (CRS1). A: Panoramic view of the outcrop, showing the FA3-B in the foreground and its inferred faulted contacts with the adjacent facies associations. Note the periodicity of the interbedded pale-coloured tuffaceous layers (lithofacies *tSm*; white arrows). Encircled letters make reference to the pictures shown in Fig. 7 below. Vertical scale ca. 5 m. B: Reverse fault contact between the FA3-B and the FA3-C. Photo was taken in front of the outcrop Cañadón Río Simpson 3 (CRS3). Outcrop is about 15 m-high.

Figure 7 (continuation). C: Calcareous/concretionary bed of lithofacies cMp, exposed as a ledge. D: Sandy volcanoclastic bed exposed as a ledge (guide-bed) and interpreted as a turbidite (lithofacies tSp; microfacies V2). See scale in following picture (Fig. 5 E). E: Close-up of the same bed showing the interpreted Bouma divisions and normal-grading (lithofacies tSp). Scale bar = 7 cm. F: Sharp-bedded tuffaceous layer (lithofacies tSm). Note its oxidation and “floury” texture after alteration. Scale bar = 7 cm. G: Compacted ammonite (*Favrella* sp.) preserved in a less brittle layer of lithofacies Mm. Scale = 5 cm. H: Bed-conformable belemnite rostrum (*Belemnopsis?* sp.) found in lithofacies Mm. Scale = 7 cm. I: Bioclastic-bearing, mixed tuffaceous-carbonaceous clayey sandstone (microfacies VM-f). Note its diffuse parallel lamination (aligned clasts). J: Foram-bearing, carbonaceous silty mudstone (microfacies M1) from lithofacies cMp (Fig. 7C). Concentration of calcareous particles around the bivalve shell (benthic-foraminifer inclusive) is interpreted as a lag deposit. Mudstone is strongly microdolomitized displaying a “pseudo-silty” texture. K: Microscopic picture of lithofacies tSp (microfacies V2; Fig. 7E). Note the normal grading between the basal- (left, parallel nicols) and upper sections (right, crossed nicols). L: Altered tuffaceous sandstone with diagenetical fiamme texture (microfacies V2-t). Matrix has been devitrified and partly altered to clay minerals. Left: parallel nicols; right: crossed nicols. M: Silty, carbonaceous calcimudstone (microfacies M2-for). Note the diffuse parallel lamination (aligned clasts and brown-coloured organic matter), and the presence of bacterial structures (dark-coloured spots). N: Massive, calcisphere-bearing, wackestone to calcimudstone (microfacies M2-css). Note the “floating” allochems embedded in the matrix. Scale of microscopic pictures: 2 mm (white); 0.5 mm (black).

phragmocones (diameter up to >1 m), usually embedded in concretions (Fig. 9D, 9E).

3.5.2. Facies Association 3-C (FA3-C): Microfacies

The FA3-C displays fossil-rich, carbonaceous-calcareous, sandy-silty claystone (M1; Fig. 9G) to fine-grained sandstone (M3-f; Fig. 9H). Sandy laminae are sharp and discontinuous; they are interpreted as lag deposits (Fig. 9G). Mudstone (M1-f) is diffusely to sharply laminated, with a framework rich in terrigenous particles (5-20 %) and microfossils (5-30 %). Most fossils are

circular in cross-section and are strongly phosphatized (Fig. 9I-9L); they are here interpreted as acritarchs, though some bioclasts resemble dinoflagellate cysts (tasmanitids?; microfacies M1-ac Fig. 9I, 9L), or palynomorphs (miospores?). Calcispheres are less abundant, while benthic foraminifers (Fig. 9J), carbonized wood, disarticulated ostracods, and broken bivalves are rarely found.

3.5.3. Facies Association 3-C (FA3-C): Interpretation

Sharp bed contacts and bioturbation in the facies association FA3-C might reflect periods of low rate in the hemipelagic sedimentation (Scott et al., 2003), as commonly inferred for pelagites (Ulmer-Scholle et al., 2014). However, a sporadic enhanced terrigenous supply can be inferred from the mixture of mudstone and coarser-grained sediments bearing vegetal remains. These diffusely laminated, fossiliferous beds (Fig. 9H) might indicate sediment transport as plankton-rich mud-laden flows. Planar fabric and lag deposits are commonly observed in distal turbidites or tempestites, reflecting a rapid tractive transport (Ulmer-Scholle et al., 2014; Flügel & Munnecke, 2010).

The abundance of plankton in FA3-C (microfacies M3-ac) indicates periods of high coastal productivity (algal blooms). The latter is known to occur when nutrient supply is elevated, usually triggered by coastal

upwelling, an enhanced terrestrial input (runoff), or during a marine transgression (Stow et al., 1996; Slomp & Van Cappellen, 2007; Flügel & Munnecke, 2010). Phosphate-enrichment of these rocks support the hypothesis of increased coastal upwelling (Baturin & Vitaliano, 1982; Flügel & Munnecke, 2010; Hesse & Schacht, 2011; Zell & Stinnesbeck, 2016). In this scenario, plankton thrives in the photic zone, and its decay and burial as organic-rich facies occurs offshore on the sea bottom under local anoxic conditions (OM production > decay; Potter et al., 2005). These environments are usually found in outer shelf to upper slope settings (Hesse & Schacht, 2011).

Big-sized concretions are a remarkable feature in FA3-C. Concretions form during the early diagenesis, a few meters below the sediment-water interface (Potter et al., 2005; Marshall & Pirrie, 2013), by chemical reactions between decaying organic matter and the calcium present in pore water (Yoshida et al., 2015, 2018). Organic matter for the formation of big-sized concretions in FA3-B (lithofacies cMp-c) may have resulted from the plankton-rich pelagites (microfacies M3-ac).

Ammonites and belemnites are the most abundant fossils in the Katterfeld Formation, particularly in the facies associations 3-B to 3-D (FA3-B to FA3-D), including several well-preserved phragmocones. Given the nektonic ecology of these fossil cephalopods, their shell remains only indicate oxygenated conditions in the water column. They were likely unaffected by oxygen-deficient conditions on the sea floor. In the Katterfeld Formation, phragmocones are well preserved and lack encrustation, reflecting a rapid sinking towards oxygen-poor conditions (Lazo, 2004), falling near their original habitat (Yacobucci, 2018). The settling of large phragmocones (FA3-B), has been linked to an allochthonous origin after post-mortem drift (Chamberlain et al., 1981). However, the preservation of autochthonous big-sized phragmocones may also be possible after taphonomical processes (Maeda & Seilacher, 1996; Yacobucci, 2018).

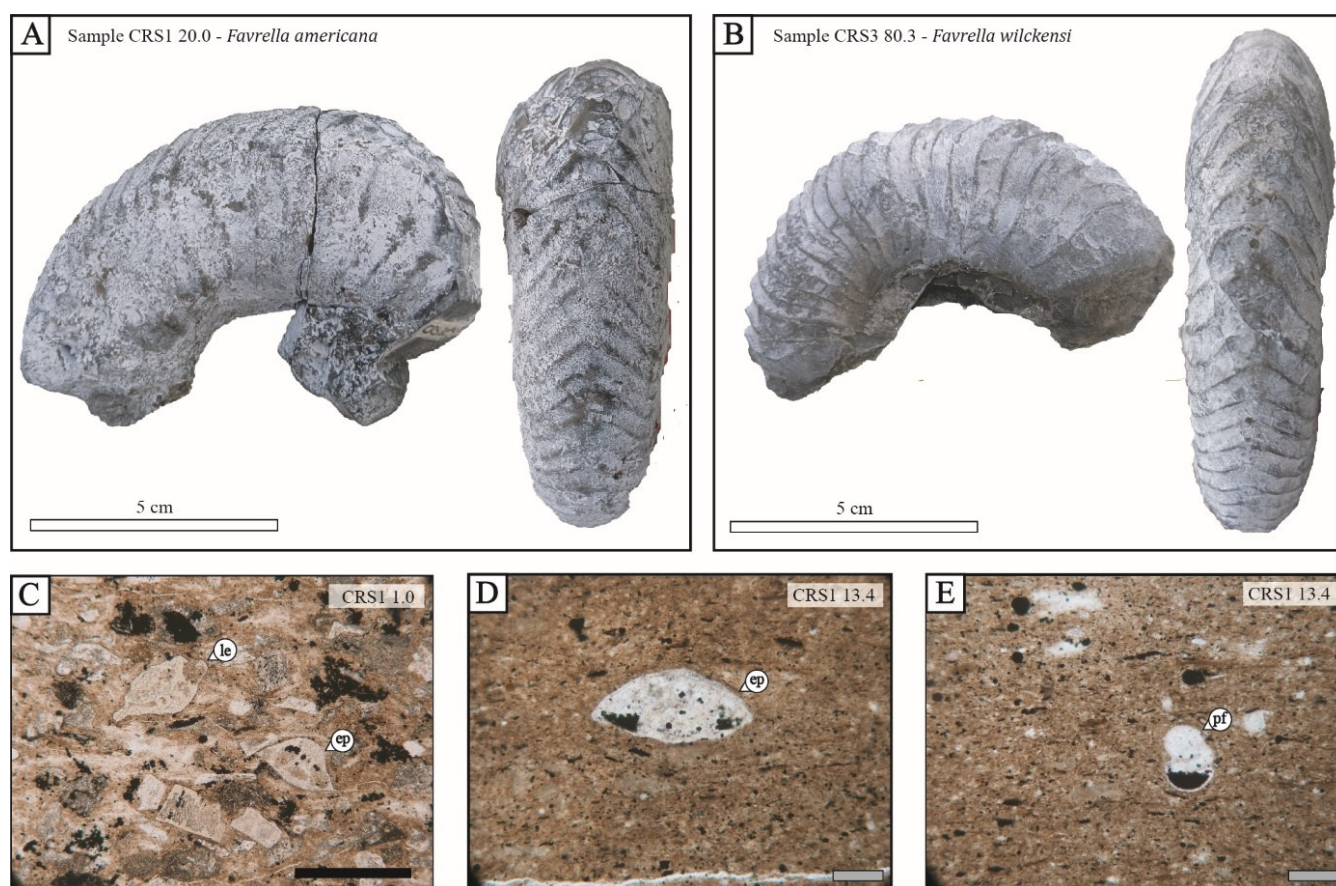


Figure 8. Guide fossils from facies associations FA3-B and FA3-C. A: *Favrella americana* from the upper part of the FA3-A (Fig. 3). B: *Favrella wilckensi* from the uppermost FA3-C (Fig. 3). C: Benthic foraminifers from the FA3-B; *Lenticulina* sp. (le) and *Epistomina* sp. (ep), from microfacies VM-f D: Benthic foraminifer from the FA3-B; *Epistomina* sp. (ep). E: Planktic foraminifer from the FA3-B; globigeriniid? Both Fig. 5D and 5E are from microfacies M2-for.

3.6. Facies Association 3-D (FA3-D): Shelf hemipelagites to offshore-transition

3.6.1. Facies Association 3-D (FA3-D): Lithofacies

The facies association 3-D (FA3-D) overlies FA3-B with a covered, but inferred fault contact. FA3-D consists of carbonaceous mudstone (lithofacies Mm) to silty mudstone (lithofacies Um) with a pale colour (dark gray to gray), and less pronounced oxidation (reddish-brown; Fig. 10A). The mudstone presents a “gritty” texture and rounded-blocky parting, reflecting a greater silt content (Fig. 10B). Calcareous and tuffaceous beds are less frequent (lithofacies cMp; tSm), but concretions are common, appearing each ca. 1-3 m (lithofacies Mp-c; Fig. 10B, 10C). Concretions are ovoidal, small- to mid-sized (0.20-0.40 m in diameter), and frequently show septarian cracks and voids (Fig. 10C). Tuffaceous beds are highly altered (argillized), and between 5-20 cm-thick (lithofacies tSm). Discrete silty- to fine sandy beds (lithofacies Up), some of them displaying parallel- and hummocky cross-lamination (lithofacies Uh), are present towards the top (Fig. 10D).

Ammonites and belemnites fossils are common in the FA3-D, with the former usually associated with

concretions. Ammonites are majorly represented by *Favrella wilckensi* (Fig. 8B). Other fossils are scarce and were only found in the uppermost beds of the association; they include poorly preserved ichnofossils, trigoniids, and coal fragments. Exceptionally, an ex-situ ichthyosaur vertebra was found at about the middle portion of this association.

3.6.2. Facies Association 3D (FA3-D): Microfacies

Facies association 3-D (FA3-D) consists of finely laminated, carbonaceous silty claystone and clayey siltstone, sometimes calcareous (microfacies M1-p; Fig. 10E). Lamination is parallel, continuous to discontinuous, and locally crossed with a low angle (Figs. 9E, 9G). Siltstone is formed of quartz, feldspars, opaque minerals, organic matter, and scattered calcite. Minor components (<1 to 5%) include volcanic lithics, micas, and rounded glauconite grains. Microfossils are negligible (<<5%), and only a couple of calcispheres, benthic foraminifers, and carbonized wood fragments were found. Bioturbation is moderate to strong (Fig. 10F). Tuffaceous beds are analogous to FA3-C (microfacies V2).

Table 1. Facies associations and associated litho- and microfacies. Abbreviations: Framework: VF = very fine grained, M = medium-grained, C = coarse-grained, Sa = Sand, Si = Silt. Matrix: C-Mud = carbonaceous mud; Mcr = Micrite. Thickness: cm = centimetric, dm = decimetric, m = metric. Fossils: amm = ammonites, bel = belemnites, biv = bivalves, bra = brachiopods, gas = gastropods, ich = ichnofossils, ino = inoceramids, pla = carbonized plants, ver = vertebrate remains, n/o = non observed.

Facies Association	Lithofacies	Symbol	Micro facies	Frame-work	Matrix	Thickness	Structures/Observations	Fossils	Interpretation
FA1	Tuffaceous mudstone	tMm	V1	Coarse-ash	ash	dm-m	Massive; brittle (blocky parting)	(pla)	Subaqueous settled, fallout deposits
	Tuffaceous sandstone to siltstone	tSm	V2	VF-M; M-C Sand	ash	cm-dm	Massive, grading, low-angle cross-bedding, slabby parting	n/o	Ash turbidites or debrites
	Lapillistone	tG	N/A	Lapilli	ash	dm	Accretionary lapilli	n/o	Remobilized, phreatomagmatic deposits
	Laminated carbonaceous siltstone	Us	M1	Silt	C-Mud	mm	Sinuuous lamination; rip-up clasts in tSm	pla	Current-reworked carbonaceous hemipelagites
FA2	Fossil-bearing carbonaceous mudstone	fMm fMp	M1, M2	Sand-Pebble	C-Mud	Dm	Massive (fMm) to parallel-bedded (fMp), brittle-blocky parting	biv; gas	Muddy hyperpycnal deposits
	Inoceramid-rich, carbonaceous mudstone	fMp-in	M1-f	Sand-Pebble	C-Mud		Parallel lamination, fissile (fMp)	biv (ino)	Carbonaceous hemipelagites, oxygen-poor setting
	Fossiliferous, carbonaceous-calcareous mudstone	fM-cq	M1-f	Sand-Pebble	C-Mud	dm-m	Massive; bivalves reworked and some in life-position	biv, bra, gas	Fossiliferous tempestites
FA3 general (FA3-A, FA3-B, FA3-C, FA3-D)	Massive, carbonaceous mudstone	Mm	M1	Si	C-Mud	dm-m	Massive to diffusely lamination; wedgy-parting	amm, bel, biv	Carbonaceous hemipelagites to pelagites

Table 1 (continuation).

Facies Association	Lithofacies	Symbol	Micro facies	Frame-work	Matrix	Thickness	Structures/Observations	Fossils	Interpretation
FA3 general (FA3-A, FA3-B, FA3-C, FA3-D)	Carbonaceous mudstone with concretions	Mm-c	N/A	Si	C-Mud	dm – m	Massive, diffuse lamination/bedding, ovoidal sedimentary concretions, wedgy parting	amm, biv	Carbonaceous hemipelagites, some bearing free-fallen ammonites (hiatuses, reworking?)
	Parallel-bedded carbonaceous mudstone	Mp	M1 M2	Si	C-Mud	cm – dm	Parallel lamination/bedding; platy to wispy parting (fissile rare)	amm, bel, biv	Carbonaceous hemipelagites, hiatus or low sedimentary rate?
	Calcareous, carbonaceous mudstone	cMp	M1-c	Si	C-Mud	dm	Tabular bedding; slabby parting	amm, ich	Diagenetical concretionary horizons (sedimentation hiatuses?)
	Tuffaceous sandstone to siltstone	tSm	V2	VF-M; M-C Sand	Ash	cm-dm	Massive, grading, low-angle cross-bedding, slabby parting, floury texture (weathered)	n/o	Tuffaceous sediment gravity flow deposits; ash-fallout deposits?
FA3-B	Parallel-laminated, graded, tuffaceous sandstone	tSp	V2	VF-MSa	ash	cm- dm	Parallel lamination (Bouma Tc-Te, Tb; normal grading)	n/o	Ash turbidites; fall out deposits?
FA3-D	Carbonaceous silty mudstone	Um	M1-p	Si	C-Mud Mcr	dm	Gritty texture, rounded-blocky parting,	amm, bel, biv, pla, ver	Distal shelf to prodelta hemipelagites
	Laminated siltstone to fine sandstone	Up (Uh)	M1-p	Si, FSa	C-Mud Mcr	dm	Parallel lamination (Up); hummocky cross lamination (Uh)	ich?	Distal tempestites
FA4	Massive siltstone	Um	M1	Si	C-Mud Mcr	dm	Massive, slabby parting	n/o	Sedimentary gravity flow (hyperpycnite?)
	Parallel-bedded silty mudstone	Mp	M1 M1-p	Si	C-Mud Mcr	cm	Parallel bedding/lamination	ich	Sediment-laden flow deposits

Table 1 (continuation).

Facies Association	Lithofacies	Symbol	Micro facies	Frame-work	Matrix	Thickness	Structures/Observations	Fossils	Interpretation
FA4	Laminated tuffaceous mudstone	tMp	V2 V2-t	Si-Sa	Ash	cm-dm	Diffuse parallel lamination	n/o	Current-reworked, tuffaceous deposits
FA5	Heterolithic sandstone-mudstone	SMh	N/A	Sa	C-Mud	cm-dm	Lenticular to flaser bedding, thickening-upwards trend, double mud-drapes, bioturbation	ich	Alternation current dunes and slack-water mudstone
	Tabular glauconitic sandstone	Sp	N/A	F-M Sand	C-Mud	dm-m	Amalgamated, tabular parallel-bedding; parallel- and low-angle cross-lamination; flasers, mud-drapes; rip-up clasts	ich	Deltaic, tidal bars or sand sheets
	Sandstone - mudstone couplets	SMp	N/A	F-M Sand		cm-dm	Parallel-bedding; sinuous bedding planes; scour-marks; rip-up clasts	ich	Deltaic, frontal splay deposits
	Rippled, bioturbated sandstone-siltstone	SMr	N/A	Sa, Si	C-Mud	Cm	Fine parallel bedding; ripples contacts; bioturbation	ich	Wave-reworked, deltaic interbar complexes

Table 2. Microfacies and their associated facies associations. Abbreviations: Framework: VF = very fine grained, F = fine-grained, M = medium-grained, C = coarse-grained, VC = very coarse-grained, Sa = Sand, Si = Silt. Matrix: dev = devitrified, C-Mud = carbonaceous mud; Mcr = Micrite. Composition: Bio = Bioclasts, Bt = Biotite, Fel = Feldspars, Lv = Volcanic lithics, Pmc = Pumice, OM = organic matter, Opq = opaque minerals, Qz = quartz, Shd = Shards. Abundance: Qz = > 20 %, Qz < 10 %, (Qz) = not present in all samples. Var = Variant. Microfossils: acr = acritarchs, alg = algal structures, bio = bioclasts (undetermined), biv = bivalves, bry = bryozoans, ccs = calcispheres, for = foraminifer (b-for = benthic, p-for = planktic), ich = ichnofossils, ino = inoceramids, ost = ostracods, pal = palynomorphs, pho = phosphatic microfossils, pla = carbonized plants, rad = radiolarians, ver = vertebrate fragments.

Type	Micro facies	Facie Assoc.	Composition	Frame work	Matrix	Composition	Sedimentary structures	Fossils	Interpretation
Volcaniclastic	V1	FA1	Tuffaceous mudstone (claystone to siltstone)	Si VF Sa	Fine ash (dev)	Si: Qz, Pmc, OM, Opq	Massive; diffuse parallel lamination; (bioturbation)	ich	Subaqueous-settled, ash-fallout deposits
	V2 V2-g V2-t	FA1 FA3-A FA3-B FA3-D	V2-f: Tuffaceous sandstone to muddy sandstone	VF-M Sa	Ash (dev)	(Pmc); Qz; Fel, (Lv), Opq	Normal-grading; “cut-and-fill” structures; (rip-up clasts; diffuse parallel lamination; fiamme texture)	[bio*]	Ash turbidites or fallout deposits?
		FA3-B FA3-D	V2: M-VC volcanic sandstone to muddy sandstone, sometimes carbonaceous (Var2); V2-t: pumice rich	M to VC Sa	Ash (dev)	Var1: Lv; Pmc, Fel, Qz; Opq; (Bt) Var2: Shd, Pmc, Qz, Fel, Lv, Bio	Parallel lamination; grading; [“fiamme”-texture] Var2: Mixing with carbonaceous sediments	Var2: ost	Remobilized sandy debrites, sometimes mixed/reworked with carbonaceous sediments (Var2). Diagenetical compaction (fiamme).
	VM-f	FA3-B	Fossil-bearing, tuffaceous-carbonaceous muddy sandstone to sandy claystone	Si VF-M Sa	Ash, C-Mud	Fel, Lv, Opq, Qz, Bt	Diffuse parallel lamination	biv (acr, b-for, ccs, pla)	Remobilized/reworked volcaniclastic deposits (tempestites?)
Fine-grained siliciclastic	M1 M1-f	FA2 FA3-A	Carbonaceous, bioclasts-bearing, silty sandy claystone, sometimes fossiliferous (M1-f)	Si, FSa	C-Mud Mcr	Lv, Bio	Massive; diffuse parallel fabric; sometimes sparse microdolomite	i) ino, bry; or ii) b-for, pho, ccs, rad (also, biv, ost, bry, ver, p-for)	Carbonaceous hemipelagites, locally affected by weak currents. Distal shelf to slope setting.
	M1-ac	FA3-C	Acritarch-rich carbonaceous-calcareous, sandy-silty claystone	Si, Sa	C-Mud, Mcr	Bio; Qz, Fel, Opq	Sharp to diffuse, parallel lamination	acr, alg, pal, ccs, b-for, ost, pla, biv	Plankton-rich pelagites, algal bloom?

Tabelle 2 (continuation).

Type	Micro facies	Facie Assoc.	Composition	Frame work	Matrix	Composition	Sedimentary structures	Fossils	Interpretation
Fine-grained siliciclastic	M1-s M1-p	FA1 FA3-D FA4	Laminated, carbonaceous silty claystone to clayey siltstone	Si	C-Mud	Qz, Fel, Opq	Discontinuous parallel and sinuous lamination (M1-s); parallel- to cross-lamination (M1-p); bioturbation	ich (css, b-for, bio, ich, pla)	Current-reworked carbonaceous hemipelagites; hyperpycnites?
	M1-c	FA3-A FA3-B	Dolomitized, carbonaceous silty claystone	Si	C-Mud	Qz, Bio, Fel, Lv, Opq	“pseudo-siltstone” texture (pervasive microdolomite)	ccs	Hemipelagites affected by diagenetical, organogenic dolomitization (oxygen poor setting)
	M2 M2-f M2-for M2-ccs	FA3-A FA3-B	M2-f: fossiliferous, carbonaceous silty calcimudstone M2-for: Foraminifer-bearing, carbonaceous, calcimudstone to sandy wackestone M2-ccs: Calcisphere-rich, carbonaceous, silty-sandy calcimudstone to wackestone	Si, FSa	Mcr C-Mud	Bio, Qz, Fel, Opq	Massive; diffuse parallel fabric	b-for; ccs	Calcareous hemipelagites, locally affected by weak currents; deeper, siliciclastic-poor setting; minor events of high productivity?
	M3-f	FA3-C	Fossil-rich, fine-grained sandstone	FSa	C-Mud	Bio, Qz, Fel, Lv, Opq	Sharp, continuous to discontinuous, parallel lamination, clast-supported	acr, alg?, pal?, ccs	Current-formed, lag deposits
Sandy facies	M4	FA5	Glaucinitic, litho-feldspatho-quartzose sandstone	M/CSa	C-Mud Mcr	Qz, Fel, Lv	Continuous to discontinuous lamination; mud drapes; bioturbation	ich	Alternation between tractive transport and mud settling.

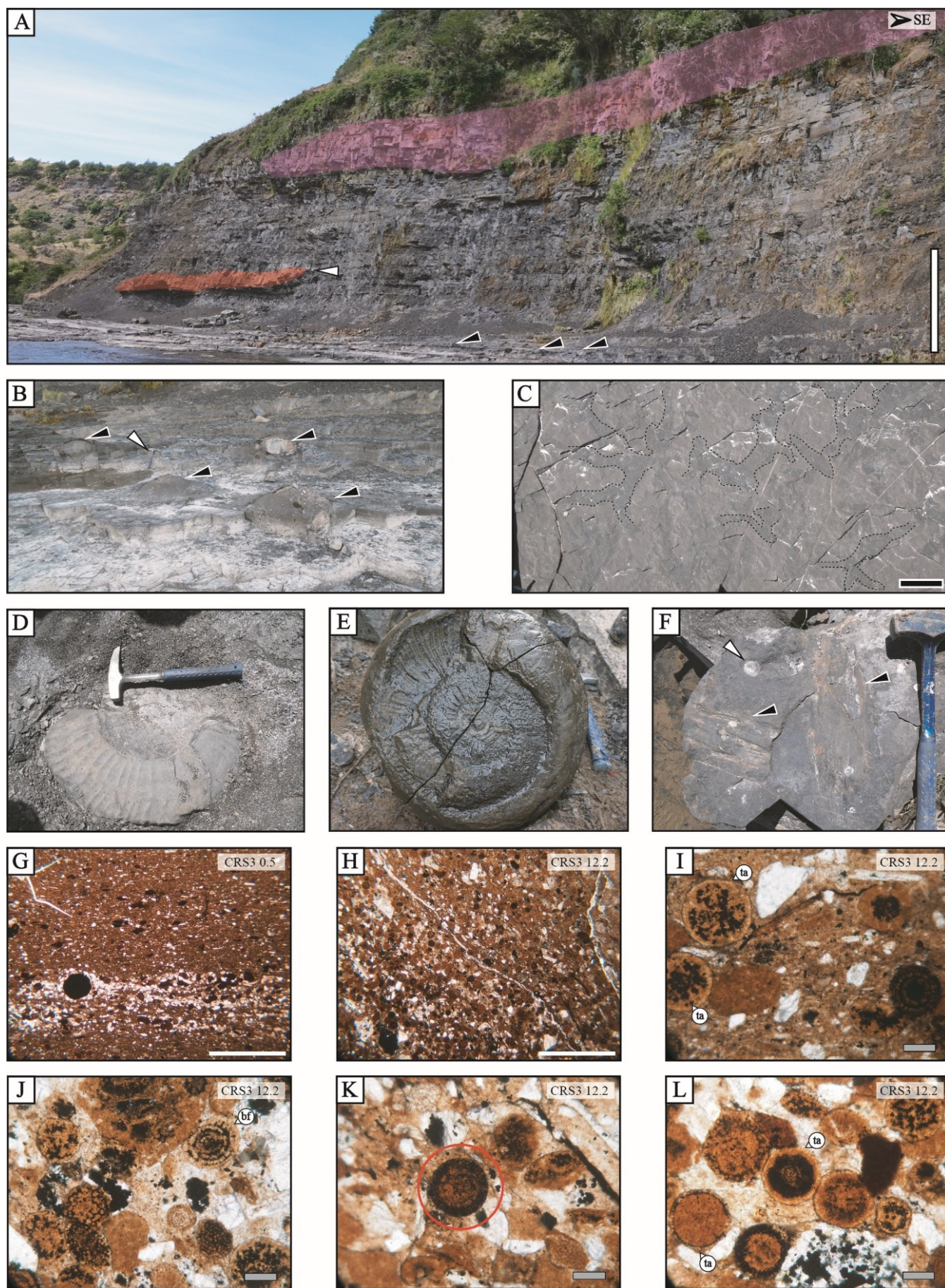


Figure 9. Facies Association FA3-C (mid-upper Katterfeld Formation) at the lower part of the Cañadón Río Simpson 3 section (CRS3; Fig. 3). A: Panoramic view of the FA3-C. Note its relatively marked parallel bedding and the sill intrusion in the lower part of the outcrop (red area + white arrow), plus an inferred sill in the uppermost part of the outcrop (pink coloured). Some big-sized calcareous concretions are marked with black arrows. Scale about 5 m. B: Aligned, big-sized calcareous concretions from the lowermost FA3-C (lithofacies Mm-c). Note the sharp parallel bedding; hammer to scale (white arrow).

Figure 9 (continuation). C: Plan view of the lowermost FA3-C with ichnofossils (*Planolites isp.*). Scale = 5 cm. D: Big-sized ammonite shell fragment from the lowermost FA3-C (lithofacies Mm-c). Hammer to scale. E: Cast and external mold of a big-sized ammonite embedded in a calcareous concretion from the lowermost FA3-C (lithofacies Mm-c). Hammer to scale. F: Carbonized wood (black arrows) and oyster shell fragment from lithofacies Mm-c (white arrow). Hammer to scale. Carbonaceous silty claystone bearing phosphatized microfossils (microfacies M1-ac). Note the alternation between diffuse- (aligned allochems) and sharp parallel lamination; the latter interpreted as lag deposits. H: Diffusely parallel laminated, acritarch-rich, carbonaceous clayey siltstone to very-fine sandstone (microfacies M3-f). I: Close-up of Fig. 9H, showing microfossils in detail. Microfossils with a circular cross-section and porous external wall are interpreted as tasmanitids. J: Mixture of indetermined phosphatic microfossils, the one with a spiral coiling is interpreted as a benthic foraminifer. K: Detailed view of a phosphatic microfossil displaying a radial internal structure (red circle). Possible altered tasmanitids or palynomorph? L: Close-up views from the CRS3-13.2 (Fig. 9H), showing several tasmanitids and possible palynomorphs? Abbreviations: bf = benthic foraminifer; ta = tasmanitid. Scale in microscopic pictures: 2 mm (white); 0.1 mm (gray).

3.6.3. Facies Association 3-D (FA3-D): Interpretation

Facies Association 3-D (FA3-D) depicts a shallowing-upwards succession, grading from an offshore setting (lithofacies Mm) towards an offshore-transition zone or distal prodelta (lithofacies Um, Up) influenced by storms (lithofacies Uh). The transition is marked by a coarsening-upwards trend (clay to silt), and by the appearance of distal tempestites (lithofacies Up; Uh). A terrestrial influence and the onset of oxic-/suboxic conditions is inferred from trigoniids, bivalves which lived in water depth of a few tens of meters, at most (Francis & Hallam, 2003), charcoal remains, and bioturbation (Potter et al., 2005). Tuffaceous beds are sparse in FA3-D and only occur in the middle-upper part of the association, possibly depicting a waning volcanic phase.

A common feature in FA3 is the concentration of concretions, many of them septarian, in discrete horizons (Fig. 5G; 7A; 9B; 10A, 10B). This may reflect lags or hiatuses in the sedimentation or even short-term erosion events (Marshall & Pirrie, 2013). Septarian nodules, abundant in FA3-D (Fig. 10B), have been interpreted as formed during sediment compaction after a rapid burial (Astin, 1986), but microbial decay may also be a plausible cause of their origin (Marshall & Pirrie, 2013).

3.7. Facies Association 4 (FA4) – Prodelta

3.7.1. Facies Association 4 (FA4): Lithofacies

Facies association 4 is exposed as steep muddy outcrops with negligible oxidation, overlying the FA3-D with a sharp contact (Figs. 3; 10A; 10B; 11A; 11B). It consists of parallel-bedded silty mudstone (lithofacies Mp) with small, flattened, and non-calcareous concretions (lithofacies Mp-c; concretions < 0.20 m in diameter; Fig. 11C). At its base, the contact between the FA3-D and the FA4 is marked by decimeter-thick, massive siltstone with slabby parting (Um), which alternates with centimeter- to decimeter-thick beds of diffusely laminated, tuffaceous muddy sandstone (lithofacies tMp; Figs. 11A; 11B). Upsection, mudstone is brittle, dark grey coloured, and diffusely laminated (Mp; Fig. 11A; 11B; 11C).

3.7.2. Facies Association FA4: Microfacies

Facies association 4 (FA4) grades from carbonaceous-calcareous, silty claystone to clayey siltstone. Claystone is interlaminated with thin silty lenses and laminae (a few grains-thick, microfacies M1-p; Fig. 11I). Silty laminae are continuous to discontinuous, and locally bioturbated (Fig. 11C). The degree of bioturbation increases upsection.

3.7.3. Facies Association FA4: Interpretation

In facies association 4 (FA4), the interbedding of massive mudstone and laminated siltstone indicates changing flow conditions between fluid mud- and sediment-laden currents, which are typically present in prodeltaic settings (Elliott, 2005). Basal massive beds are interpreted as sediment gravity flow deposits (hyperpicnites?), some of them volcanoclastic (lithofacies tMp). Compared to FA3-D, an increased sediment rate is inferred from parallel lamination of the sediments (Potter et al., 2005), the flattening of nodules, and the local absence of ichnofossils (Elliott, 2005; Lin & Bhattacharya, 2021).

3.8. Facies Association 5 (FA5): Tide-influenced delta front

3.8.1. Facies Association 5 (FA5): Lithofacies

The facies association 5 (FA5) overlies FA4 with a sharp contact (Fig. 10A; 11A; 11B). The succession comprises a coarsening -upwards succession (from heterolithic-lenticular to sandy beds), upsection changing locally to a fining-thinning trend (heterolithic-flaser; Figs. 3; 11A; 11G). Bedsets of the FA5 are strongly bioturbated, as observed in exposed ledges and fallen blocks (Fig. 11D; 11G; 11H). Provisionally, this association comprises at least four main lithofacies (from base to top):

- i) Finely bedded, lenticular to flaser heterolithic rocks (SMh), with sporadic double mud-drapes (Fig. 11D).
- ii) Amalgamated, tabular- sandstone (Sp), sharply overlying the heterolithic facies (Fig. 11A; 11D). Sandstone is internally massive, but some beds show parallel- and planar crossed-lamination (Fig. 11E. 11F).

Bedding planes are identified by flasers and mud drapes (sometimes double).

iii) Tabular sand-mud couplets (SMp), interbedded with lithofacies Sp (Fig. 11E). In couplets, sandy beds are decimeter-thick, while muddy layers are centimeter-thick. Rip-up clasts are present.

iv) The uppermost beds of FA5 comprise strongly bioturbated, finely bedded, rippled sandstone and siltstone, locally heterolithic (SMr; Fig. 11G).

Ichnofossils are abundant, commonly preserved as negatives in the lower surface of sandy beds (Fig. 11H). Traces are dominated by at least two morphotypes of *Thalassinoides* isp., associated with *Lockeia* isp. and *Gyrochorte* isp. Less abundant, *Spongiomorpha* isp., *Ophiomorpha* isp., *Palaeophycus* isp., *Chondrites*? isp. and *Helminthopsis* isp. were identified in fallen blocks.

3.8.2. Facies Association 5 (FA5): Microfacies

Sandstone of FA5 is mid- to coarse-grained, and glauconitic (M4; Fig. 11J; 11K). Its classification varies between litho-feldspatho-quartzose and quartzose-feldspatho-lithic (*sensu* Garzanti, 2018). Clasts are moderately- to well-sorted, and sub-angular to sub-rounded. Rounded glauconite comprises about 5% of the samples. The matrix is carbonaceous, clayey to micritic, with some intergranular spar cement of apparently secondary origin (10-25%). Mudstone appears as irregular mud drapes, laminae, and burrows filled by carbonaceous, silty-sandy claystone (Fig. 11K).

3.8.3. Facies Association 5 (FA5): Interpretation

In facies association 5 (FA5), heterolithic beds (SMh) represent a changing flow regime between current-transport and slack water periods (Reineck & Singh, 1973), commonly observed in proximal prodelta and distal delta front settings (Coates & MacEachern, 2007; Lin & Bhattacharya, 2021; Kumar et al., 2022). The presence of glauconite indicates a shallow marine environment (Ulmer-Scholle et al., 2014), while its sedimentary structures (e.g., heterolithic bedding, double mud drapes, rip-up clasts) reflect a tidal-modulation (Bhattacharya, 2006; Longhitano et al., 2012; Kumar et al., 2022).

Tabular sandstone (lithofacies Sp) is interpreted as prograding, compound tidal bars or sand-sheets of the delta front (Kumar et al., 2022; Bhattacharya, 2010). These bars were deposited during major pulses of tractive transport, eroding mudstone from the slack water phase. Its alternation with sand-mud couplets (lithofacies SM) may correspond to frontal splay deposits (Kumar et al.,

2022; Lin & Bhattacharya, 2021). At the top, finely bedded layers (SMr), affected by intense bioturbation and wave-reworking, possibly depict heterolithic interbar complexes developed after bar migration (Kumar et al., 2022). Thriving of benthic fauna occurred during the muddy slack-water phases.

Compared to the facies associations FA3, where bioturbation is rare (e.g. *Planolites*? isp.) and even widely absent, the facies associations FA4 and FA5 show an abundance and diversity of ichnofossils. Here the ichnoassemblage is dominated by *Thalassinoides* isp., *Lockeia* isp. and *Gyrochorte* isp.; these traces depict domicile and grazing ethologies (Seilacher, 2007; Buatois & Mángano, 2011; Knaust, 2017), associated with deposit feeders and active predators (e.g.; crustaceans, bivalves, and annelids, respectively; Buatois & Mángano, 2011; Fürsich et al., 2017). This contrasting ichnodiversity between muddy- and sandy facies associations (FA3 vs FA5, respectively) is linked to physicochemical changes in the environment (MacEachern et al., 2005), related to oxygen levels, sedimentation rate, and water salinity. This ecological and sedimentological change is attributable to the transition from shelf to delta environments, as also observed in others studies in the region (Álvarez-Mena et al., 2023; Carmona et al., 2009).

4. Discussion

4.1. Local Paleoenvironmental Evolution

4.1.1. Base of the Katterfeld Formation: Distal volcanic apron and prodelta

Black mudstone of the Katterfeld Formation overlies distal volcanic apron and prodeltaic deposits of the Facies Associations 1 (FA1) and 2 (FA2), respectively. This contact is well exposed at Alto Baguales (section ABA; Figs. 1; 3; 4B; 5D); where the marine succession represents the first evidence of the Cretaceous transgression in the Coyhaique area. The associations depict prograding subaqueous fans around volcanic islands (Carey & Schneider, 2011), which evolved into small mixed carbonate-siliciclastic platforms (Rivas et al., 2021). In the Aysén-Río Mayo Basin, coastal volcanism and shallow-water carbonate settings represent the early transgressive phase (Skarmeta & Charrier, 1976; Bell et al., 1996; Folguera & Iannizzotto, 2004; Suárez et al., 2009; 2010; Rivas et al., 2021). The gradual transition from tuff-dominated deposits (FA1) to small, carbonate- and mixed platforms (FA2) may hereby depict a waning volcanic phase, as observed in other parts of the basin (Scasso, 1989; Rivas et al., 2021; 2023).

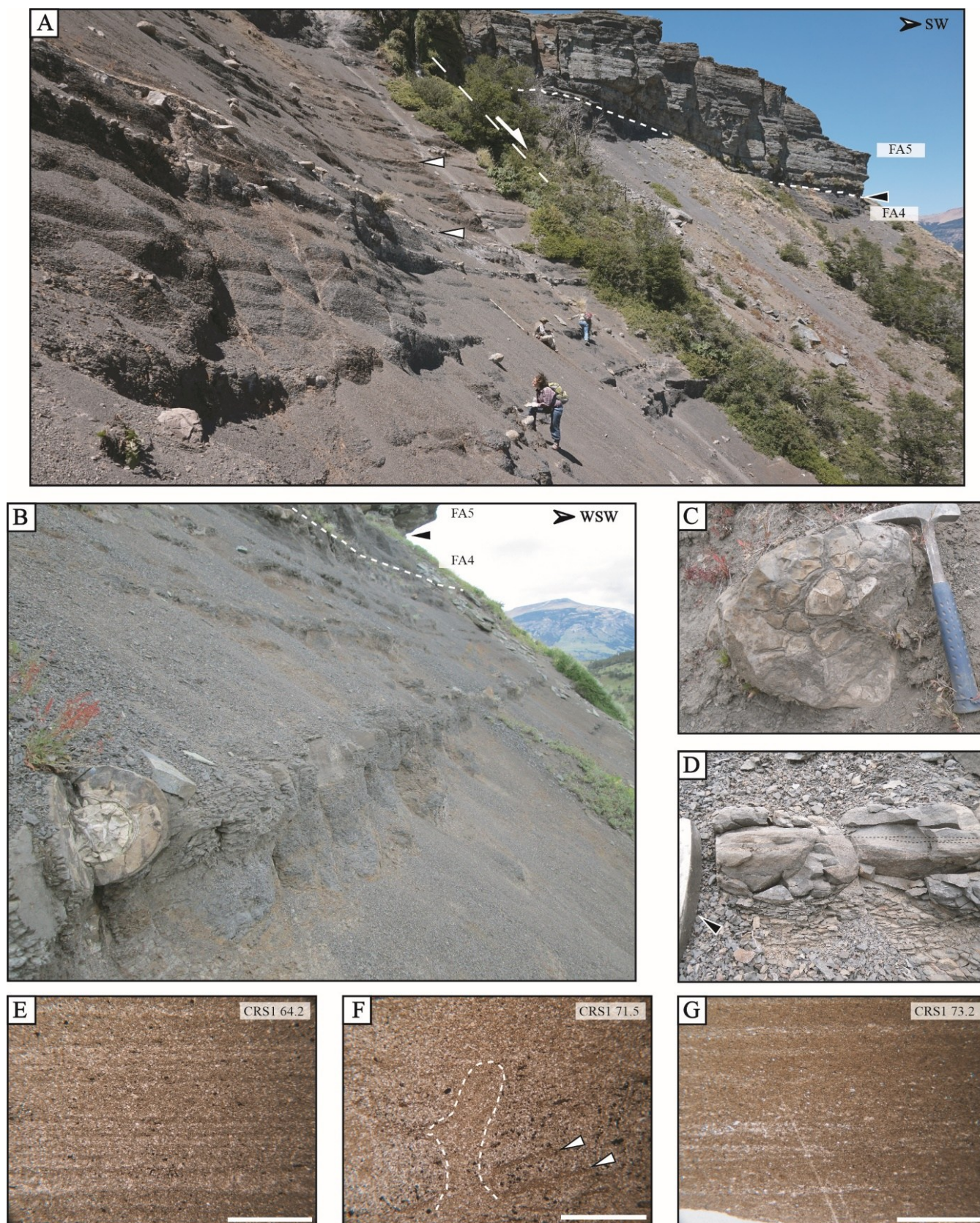


Figure 10. Facies Association FA3-D (uppermost Katterfeld Formation) and adjacent facies associations at the upper part of the Cañadón Río Simpson 3 section (CRS3, Fig. 3). A: Panoramic view of the outcrop, showing the diffuse parallel bedding of the FA3-D; tuffaceous beds are marked with white arrows; concretions are visible along the outcrop. People to scale. B: Close up of the bedding, texture/parting of silty beds (lithofacies Um) and horizons with aligned concretions (lithofacies Mm-c) at the Cañadón Río Simpson 1 section (CRS1). Scale: Concretion in the foreground is about 40 cm in diameter. C: Septarian concretion; hammer to scale. Laminated siltstone exposed as a ledge from the upper part of the FA3-D. D: Silty to fine-grained sandy bed of lithofacies Up, showing a low-angle cross-lamination interpreted as "hummocky-type". E: Parallel-to low-angle cross-laminated, carbonaceous silty claystone and clayey siltstone (microfacies M1-p). F: Bioturbated, diffusely laminated, clayey carbonaceous siltstone (microfacies M1-p). Rip-up clasts are marked with white arrows. G: Carbonaceous claystone finely laminated with discontinuous layers of silty claystone (microfacies M1-p). Laminations is irregular and discontinuous.

Given their composition and stratigraphic position (see above), the facies associations 1 and 2 are here assigned to the volcanoclastic San Antonio Member of the Toqui Formation (*sensu* Rivas et al., 2021). A possible source for these volcanoclastic sediments may be the Foitzick Volcanic Complex, a local member of the Ibáñez Formation exposed about 15 km south of the study area, and dated to the early Valanginian (U-Pb 138.3 ± 1.3 Ma; Pankhurst et al., 2003; U-Pb 139.1 ± 1.4 Ma; Suárez et al., 2009).

4.1.2. Katterfeld Formation: “Black shales” (shelf hemipelagites)

Despite being depicted as a “homogenous” unit (Bell et al., 1994; Suárez et al., 1996; Suárez et al., 2007), litho- and microfacies of the Katterfeld Formation in the Coyhaique area show at least four depositional phases (facies associations 3-A to 3-D).

The first phase, i.e. the lowermost Katterfeld Formation (FA3-A), is exposed at Alto Baguales (sections ABA, ABN; Figs. 3; 4B; 5). It reflects an abrupt sea level rise towards a poorly oxygenated shelf setting. Hemipelagic sedimentation was controlled by mud-laden flows. Beds are poor in fossils, even though a subtle deepening-upwards trend towards upper slope facies and open marine conditions is suggested by the appearance of calcareous microfacies and the presence of planktic foraminifers. The age of the basal Katterfeld Formation is insufficiently known in the Coyhaique area, but Suárez et al. (2023) suggest a Valanginian age.

The second phase (lower-middle? beds of the Katterfeld Formation) is exposed in the Río Simpson section (CRS1, lower part; Figs. 3; 7); it is characterized by carbonaceous hemipelagites interbedded with tuffaceous layers (Fig. 7A). Sedimentation was controlled by gravity flows during a period of explosive volcanism (facies association 3-B; FA3-B). An early Hauterivian age is inferred for this member based on the presence of *Favrella americana* (Olivero & Aguirre-Urreta, 2002), as well as the stratigraphic position of the unit, underlying the well-dated mid-Hauterivian beds of FA3-C (Késjar et al., 2017). A likely source of volcanoclastic sediments during deposition of FA3-B may have been the Valanginian-Hauterivian volcanic arc, which was contemporaneously emplaced along the western-southwestern margin of the basin (“Missing Volcanic Arc” *sensu* Suárez et al., 2015; 2023). Analogous to FA3-A, the carbonate enrichment upsection may also depict a deepening-upwards trend.

The third phase (middle?-upper portion of the Katterfeld Formation) is characterized by the phosphatic, microfossil-rich (hemi)-pelagites of facies association 3-C (FA3-C), as exposed at Río Simpson (Section CRS3, lower

portion; Figs. 3; 9). These sediments represent at least one event of high marine productivity in the basin (algal bloom); they are tentatively dated to the mid-Hauterivian, based on U-Pb 129-127 Ma ages of Késjar et al., 2017 for this outcrop; Palfy, pers. comm., 2024). The algal bloom sediments identified here support the hypothesis of Késjar et al. (2017) based on chemical data, that FA3-C represents deposits related to strong upwelling in the area. Phosphate-rich sediments and big-sized concretions (Fig. 9), may represent an event of oxygenation (Capelli et al., 2021), or condensation in the deeper parts of the basin during the ongoing transgression (Föllmi et al., 2006).

The fourth phase (uppermost Katterfeld Formation) crops out in the Río Simpson area (sections CR1 and CRS3, upper portions; Figs. 3; 10) and corresponds to a shallowing-upwards trend leading to offshore-transition and finally distal prodelta settings (facies association 3-D; FA3-D). These silt-dominated facies depict tractive transport and an increase in sedimentary rates. Upsection, the appearance of tempestites reflects reworking above the storm wave base, while hiatuses or erosive events are inferred from the presence of concretion-rich horizons. This stage is here dated to the mid-late Hauterivian based on the presence of *Favrella wilckensi* (Olivero & Aguirre-Urreta, 2002), and on its stratigraphic position overlying the FA3-C (mid-Hauterivian).

4.1.3. Top of the Katterfeld Formation: Tide-influenced delta

The top of the Katterfeld Formation is well exposed at Río Simpson, near the Cerro La Virgen (sections CRS1, CRS3; upper portion; Figs. 1; 3; 11). Here, black shelfal mudstone (Facies Association FA3-D) is capped by prograding prodelta- to delta-front facies (facies associations 4 and 5, respectively; Figs. 3; 11). These tidal-influenced coastal deposits mark a change to oxic conditions, as indicated by a thriving benthic faunal association including abundant and diverse ichnofossils (Doyle et al., 2005). Deltaic facies are here assigned to the Apeleg Formation, representing the last marine stage of the Cretaceous sea in the area (Płoszkiewicz & Ramos, 1977; Scasso, 1989; Gonzalez-Bonorino & Suárez, 1995; De la Cruz et al., 2003; Fig. 2). Regionally, deposits of the Apeleg Formation prograded from the east and northeast during the Hauterivian-Aptian (e.g., Ramos, 1981; Scasso, 1987; 1989; Gonzalez-Bonorino & Suárez, 1995; Bell & Suárez, 1997; Suárez et al., 2015).

4.2. Global Paleoenvironmental inferences

In the Coyhaique area, rocks of the Aysén-Río Mayo Basin comprise the Lower Cretaceous (De la Cruz et

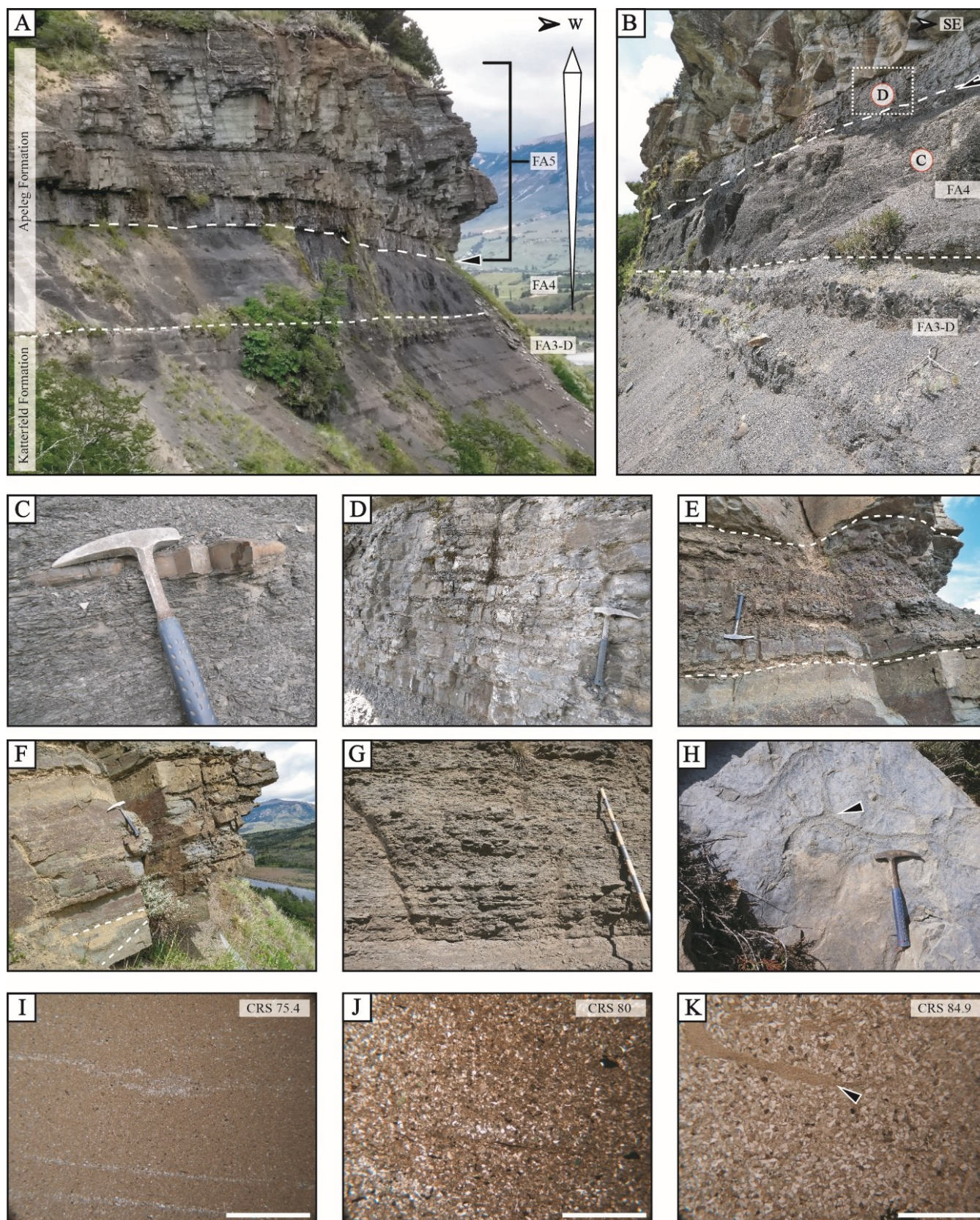


Figure 11. Facies associations FA3-D, FA4 and FA5 exposed at the upper part of the Cañadón Río Simpson 1 section (CRS1). A: Panoramic view showing the gradual contact between the Katterfeld Formation (FA3-D), and the prodelta sediments of the Apeleg Formation (FA4; short-dashed line). The sharp contact between prodelta and delta-front deposits is marked with a long-dashed line and a black arrow. Scale: area between dashed lines (FA4) is about 5 m-thick. B: Close-up of Fig. 11A. Encircled letters make reference to the pictures shown in Fig. 11 below. C: Finely laminated-bedded mudstone (lithofacies Mp) with flat concretions of the FA4 (lithofacies Mp-c). Hammer to scale. D: Lowermost heterolithic facies (lithofacies SMh) of the association FA5. Hammer to scale. E: Sand-mud couplets (lithofacies SMP), sandwiched between two tabular beds of amalgamated sandstone (lithofacies Sp). F: Tabular, amalgamated sandy beds showing parallel bedding and cross-lamination (lithofacies Sp). G: Strongly bioturbated, rippled, heterolithic beds of the uppermost FA5 (lithofacies SMr). Jacob's staff to scale (each division = 10 cm). H: Plan view of a fallen block of the association FA5 (lithofacies Sp), showing a well-preserved exemplar of *Thalassinoides* isp. I: Diffusely laminated, calcareous claystone with thin silty claystone lamina of the FA4 (microfacies M1-p). J: Bioturbated, very fine sandstone with clayey siltstone patches (microfacies M4). This sample is from the heterolithic lithofacies (SMh). K: Well-sorted, glauconitic, fine- to mid-grained sandstone (microfacies M4) from lithofacies Sp. Note the silty claystone lens (black arrow), interpreted as a mud flake. Scale in microscopic pictures: 2 mm (white).

al., 2003; Suárez et al., 2009; 2010). Deposition of the Katterfeld Formation (Valanginian-Hauterivian, Barremian?; see section 1.3) was contemporaneous with two global “episodes of environmental change”, i.e. the Valanginian Weissert Event and the Hauterivian Faraoni Event; Föllmi et al., 2006; 2012).

4.2.1. The Valanginian Weissert Event

The Weissert Event corresponds to an episode of environmental change marked by a positive $\delta^{13}\text{C}$ excursion (Weissert et al., 1998; Erba et al., 2004). This excursion was likely caused by an increase in atmospheric pCO_2 expelled during magmatism of the Paraná-Etendeka Large Igneous Province (Erba et al., 2004; Martinez et al., 2015; Cavalheiro et al., 2021). The Weissert Event is widely known from the Tethys area (e.g.; Weissert et al., 1998; Erba et al., 2004; Föllmi et al., 2006; Shmeit et al., 2022), but it had a global fingerprint as evidenced by isotopic values from the Pacific- and Austral regions (Erba et al., 2004; Cavalheiro et al., 2021) as well as from the Neuquén Basin in Argentina (Gómez Dacal et al., 2018; Capelli et al., 2021). This positive isotopic excursion is usually linked to a carbonate crisis, to “platform drowning” (Weissert et al., 1998; Erba et al., 2004), and to deposition of carbonaceous mudstone (“black shales”) after a sea-level rise (Föllmi et al., 2006). The Weissert Event has therefore been interpreted as an oceanic anoxic event (Erba et al., 2004).

The Weissert Event has been assigned to the mid-late Valanginian (ca. 133.9–132.6 Ma; Cavalheiro et al., 2021), but in Argentina, it has been reported for rocks dated to the late early Valanginian (“mid Valanginian”; Aguirre-Urreta et al., 2008; Gómez Dacal et al., 2018; Capelli et al., 2021). In the Neuquén Basin, this event coincides with a paleoenvironmental change from carbonate to siliciclastic-carbonate sedimentation (Capelli et al., 2021), even though organic-rich facies are absent (Gómez Dacal et al., 2018). The change in lithology was likely triggered by enhanced runoff following a shift from arid to humid conditions (Capelli et al., 2021). The latter intensified the hydrological cycle during greenhouse conditions, as globally reported (Weissert, 1989; Föllmi, 2012; Martinez et al., 2015).

This carbonate-to-siliciclastic shift in sedimentation is also observed in the Aysén-Río Mayo Basin (ARB), represented by the boundary between the Toqui and Katterfeld Formations (e.g.; Olivero & Aguirre-Urreta, 2002; Rivas et al., 2021; and section ABA here, contact between FA2-FA3-A), dated to around the mid-late Valanginian (133.2 ± 1 Ma Suárez et al., 2023; i.e.; lowermost Katterfeld Fm. according to the facies model presented here). Therefore, the onset of “black shale” sedimentation in the ARB was apparently coeval with

enhanced regional humid conditions (Capelli et al., 2021) and it coincides with the inferred timespan of the Weissert Event (Cavalheiro et al., 2021).

4.2.2. The Hauterivian Faraoni Event

The Faraoni Event is dated to the late Hauterivian (Baudin, 2005; Baudin & Riquier, 2014) and is characterized by black shale sedimentation associated with a minor positive carbon isotopic excursion; it is depicted as a brief oceanic anoxic event (Baudin, 2005; Baudin & Riquier, 2014). This event has been reported primarily from the Tethyan area; however, based on coeval carbonaceous deposition in the Pacific and African regions, its global presence cannot be excluded (Baudin & Riquier, 2014). “Faraoni-equivalent” levels have also been reported from the Neuquén Basin in Argentina (Archuby et al., 2011), though their correlation remains to be confirmed (Guler et al., 2013).

In the Aysén-Río Mayo Basin, a positive carbon isotopic excursion has been reported from the upper Hauterivian unit of the Katterfeld Formation at the Río Simpson, which was linked to the late Hauterivian Tethyan event by Késjar et al. (2017). Rocks of the Katterfeld Formation from the Río Simpson outcrops (sections CRS1; CRS3, see chapters 3.6 and 4.1.2) are tentatively assigned here to the upper Hauterivian and are included in facies association 3-D (FA3-D). However, these carbonaceous rocks show a shallowing-upwards trend to offshore transition facies, depicting a relatively high sediment supply and a gradual shift to more oxic conditions, which is not consistent with an anoxic event (see Baudin & Riquier, 2014). This trend may have been shaped by local conditions during the regression (possibly basin inversion?). A correlation with the Faraoni Event should thus be examined in the units exposed to the south, such as the Río Mayer Formation, where the deep-marine environment persisted further into the Early Cretaceous (e.g., Richiano et al., 2012; 2015; Aramendía et al., 2018; Cuitiño et al., 2019).

A high productivity event is recorded by microfossil- and phosphate-rich mudstone of the facies association 3-B (FA3-B). In this case, phosphorous accumulation may reflect an elevated nutrient supply from deep waters during decreased oceanic circulation (Slomp & Van Cappellen, 2007), and/or terrigenous supply under humid conditions (Weissert, 1989; Föllmi, 2012). High amount of P burial has been depicted as favored by oxygenated bottom waters (Bodin et al., 2006), even though P-accumulation in shelf settings may also coincide or follow oceanic anoxic events (OAE; Slomp & Van Cappellen, 2007). Phosphogenesis is common in current suboxic to anoxic marine settings in upwelling regions (Arning, 2008). This may confirm the hypothesis

of Késjar et al. (2017), who proposed local bottom-water upwelling in the basin during the Hauterivian sea-level rise. Upwelling during the deposition of the Katterfeld Formation may have occurred around the mid-Hauterivian (see chapter 4.1.2.). This phenomenon may correlate to an event of platform demise reported from the Tethys area and there dated to the mid-Hauterivian. Nevertheless, the latter has not been assigned to an oceanic anoxic event and it may have had a local trigger (Föllmi et al., 2006). Still, given the local faulting in the area, and since radiometric ages of these rocks are not well constrained, more evidence is needed to establish a potential correlation.

4.3. Sequence Stratigraphy

The Aysén-Río Mayo Basin (ARB) has been interpreted as a marginal basin formed after back-arc extension in the proto-Patagonian Cordillera (Folguera & Iannizzotto, 2004; Suárez et al., 2010; 2023). Its basin fill, i.e., the Coyhaique Group (Haller & Lapido, 1980), depicts a transgressive-regressive (T-R) sequence (Suárez et al., 2005; 2010; Rivas et al., 2021). Sequence stratigraphical models for extensional basins differ from the “classical” systems developed for passive margins, which are majorly controlled by eustasy (Catuneanu et al., 2009; Catuneanu, 2017). Rift basins are nevertheless characterized by tectonic-triggered, short pulses of fast creation of accommodation space, alternating with longer intervals of tectonic quiescence. This leads to a repetition of transgressive- and highstand system tracts forming coarsening-upwards “syn-rift” sequences (Martins-Neto & Catuneanu, 2010).

In the Aysén-Río Mayo Basin, sea level rise towards deep marine deposits of the Katterfeld-Formation (Valanginian-Hauterivian), does not correlate well with the global eustatic curve. The latter shows a long-term global sea-level fall starting in the late Berriasian, reaching a low in the mid-Valanginian (Haq, 2014), or early Hauterivian (Müller et al., 2008), i.e., coeval to the sedimentation of the Katterfeld Formation. The post-Valanginian sea-level rise reached a maximum either in the early Barremian (Haq, 2014), or in the mid Aptian (Müller et al., 2008), i.e., correlating with the deposition of the Apeleg Formation (Hauterivian-Aptian). This paradox is interpreted as caused by local tectonics in the initial creation of accommodation space in the basin. The latter was likely enhanced by post-rift thermal subsidence (Richiano et al., 2012; Barberón et al., 2015), as inferred from the regional expression of black mudstone in the basin (Bell et al., 1996).

In the Coyhaique Group, the early transgression is represented by the Toqui Formation and correlative units (Suárez & De la Cruz, 1994; Suárez et al., 2007;

Suárez et al., 2009, 2010; see review in Rivas et al., 2021). These rocks comprise several local syn-rift sequences deposited during the gradual flooding of the former volcanic area (Scasso, 1989; Rivas et al., 2021). In the study region (ABA outcrop), a basal syn-rift sequence (Synrift sequence I) is inferred from the distal volcanic apron to prodelta transition (associations FA1 and FA2).

The syn-rift sequence I is sharply covered by black mudstone of the Katterfeld Formation (outcrop ABA; boundary FA2 and FA3-A), depicting a transgressive surface (Martins-Neto & Catuneanu, 2010). The deepening-upwards trend in the association 3-A (FA3-A) is marked by the appearance of planktic foraminifers, and is here interpreted as part of the Transgressive System Tract I (TST I). A similar depositional pattern is observed in the FA3-B in the south (section CRS), with a siliciclastic to calcareous transition and the appearance of planktic foraminifers. Since a different stratigraphical position has been inferred for the two facies associations, the deepening-upwards trend of the FA3-B corresponds to the Transgressive System Tract II (TST II).

In the area studied here exposure of the Katterfeld Formation is discontinuous. Therefore, some sequence stratigraphic key features had to be indirectly deduced. For example, high productivity beds are usually linked to a maximum flooding surface (Potter et al., 2005). Therefore, a (local?) maximum flooding stage is here interpreted to occur associated with the deposition of phosphatic pelagites characterizing the facies association 3-C (FA3-C). Upsection, the onset of a shallowing-upwards trend towards offshore-transition (association FA3-D), prodelta, and finally delta front deposits (associations FA4 and FA5, respectively), reflects a gradual fill of the accommodation space, interpreted as a regressive system tract (RST). The rapid progradation of the deltaic systems of the Apeleg Formation indicates fast reduction in accommodation space, likely enhanced by the onset of basin inversion during the Aptian (Scasso, 1989; Suárez et al., 2015; Aramendía et al., 2018).

5. Conclusions

This sedimentological investigation carried out in the “homogeneous black shales” of the Katterfeld Formation (Valanginian-Hauterivian) reveals a rich depositional evolution of this stratigraphic unit. The Katterfeld Formation represents the deepest stage of marine transgression in the back-arc Aysén-Río Mayo Basin, developed during the Late Jurassic-Early Cretaceous (Tithonian-Aptian) in Central Patagonia (Chile and Argentina), southern South America (43°-47°S).

Five facies associations were defined for the Coyhaique Group, i.e. the marine sedimentary fill of the

Aysén-Río Mayo Basin, in the Coyhaique area, i.e. in Aysén Region of southern Chile (45°S). The lowermost facies associations depict a distal volcanic apron- and mixed prodeltaic setting, assigned to the Toqui Formation (FA1, FA2). These deposits are covered by shelf- to slope hemipelagites of the Katterfeld Formation (FA3) with a transgressive surface. Hemipelagites gradually underlie prodelta and tidal-influenced delta front deposits of the Apeleg Formation (FA4, FA5).

Litho- and microfacies of the carbonaceous mudstone of the Katterfeld Formation show at least four stages in its sedimentation (sub-facies associations FA3-A to FA3-D). The lowermost Katterfeld Formation displays a deepening-upwards trend from shelf to slope hemipelagites (FA3-A; upper? Valanginian). Its lower-middle? part consists of hemipelagites with a periodic, explosive volcanoclastic input (FA3-C; lower Hauterivian). The middle?-upper part of the lithological unit is characterized by plankton-rich pelagites linked to an event of high productivity occurring tentatively in the mid Hauterivian (FA3-B). Towards the top, the layers display a shallowing upwards trend to an offshore-transition and prodelta setting (FA3-D; mid?-upper Hauterivian).

Overall, carbonaceous hemipelagites of the Katterfeld Formation depict a poorly-oxygenated, low energy setting, emplaced below the storm- and wave base, indicating distal shelf and upper slope depositional environments. The deep-water setting in the Aysén-Río Mayo Basin was coeval to an interval of low global eustasy (Haq, 2014), reflecting a regional tectonic control in the sedimentation of the Katterfeld Formation. Sequence stratigraphy depicts a basal syn-rift sequence (FA3-A), followed by at least two transgressive system tracts (FA3-A; FA3-B). Highly productive beds of the FA3-C might represent a local maximum flooding surface. Upsection, the succession progrades as a regressive system tract (FA3-D; FA4; FA5).

The onset of black mudstone deposition in the basin likely occurred under humid conditions and it is here suggested to be coeval to the Valanginian global anoxic event (Weissert Event). The uppermost part of the Katterfeld Formation shows a shallowing-upwards trend, and there is no obvious correlation between sedimentation of this unit and the late Hauterivian Faraoni oceanic anoxic event. A remarkable high productivity event is reported here for the first time in the mid-Hauterivian of the Aysén-Río Mayo Basin, which might support an enhanced runoff under humid conditions. The Katterfeld Formation is partly correlative litho-, chrono- and biostratigraphically with the Río Mayer Formation, and with the Lower Cretaceous fine-grained units from the Rocas Verdes Basin defined in subsurface (e.g. Pampa Rincón Formation, Zapata Formation).

6. Acknowledgments

The authors would like to thank Valentina Maldonado, Benjamín Aldridge, Rayen Álvarez, Benjamín Gómez, María José Maiza, Juan Arbea, Melany Muñoz, César Pailacheo, Pascale Ergas, and Grisel Rivera for their support during field work; and Theresa Huber for her guidance and assistance during laboratory analyses. We are grateful to Dr. Huber Rivera, Prof. Dr. Jozsef Palfy, and Dr. Istvan Fózy for providing helpful information regarding the rocks studied here. We gratefully acknowledge José Antonio Bernabé, Mirta Ramírez, and José Bernabé Jr. from the Fundo San Carlos for allowing the access to the outcrops at the Río Simpson, near Cerro La Virgen.

7. Funding

Financial support to this project was provided by the Chilean National Fund for Scientific and Technological Development (FONDECYT de Iniciación 11140176), by the Chilean National Agency for Research and Development (ANID/DOCTORADO BECAS CHILE/2016–72170384), and by the German Academic Exchange Service (DAAD, STIBET/ “Studienabschlussbeihilfe Stipendium”). Laboratory analyses were partly funded by the Postgraduate Research Grant of the International Association of Sedimentologists (IAS).

8. References

- Aguirre-Urreta, M.B., Price, G.D., Ruffell, A.H., Lazo, D.G., Kalin, R.M., Ogle, N. and Rawson, P.F. (2008) Southern Hemisphere Early Cretaceous (Valanginian-Early Barremian) carbon and oxygen isotope curves from the Neuquén Basin, Argentina. *Cretaceous Research*, 29, 87–99.
- Aguirre-Urreta, M.B. and Ramos, V.A. (1981) Estratigrafía y Paleontología de la Alta Cuenca del río Roble, Cordillera Patagónica - Provincia de Santa Cruz. In: VIII Congr. Geol. Argentino, Actas, Buenos Aires, Argentina, III, 101–133.
- Aguirre-Urreta, M.B., Suárez, M., Bruce, Z., De la Cruz, R. and Ramos, V.A. (2000) Bioestratigrafía y amonoides de la Formación Katterfeld, (Cretácico Inferior) en Puerto Ibáñez, XI región, Chile. In: IX Congr. Geol. Chileno, Actas, Puerto Varas, Chile, 2, 183–187.
- Álvarez-Mena, K., Pérez-Barría, L., Rivas, H. and Varela, J.P. (2023) Cerro Mirador, Ñirehuao: Un hotspot de icnología marina en el Cretácico Inferior de la Formación Apeleg (Aysén, Chile). In: XVIII Reunión Argentina de Sedimentología: IX Congreso Latinoamericano de Sedimentología, Actas, La Plata, Argentina, 205.
- Aramendía, I., Ramos, M.E., Geuna, S., Cuitiño, J.I. and Ghiglione, M.C. (2018) A multidisciplinary study of the Lower Cretaceous marine to continental transition in the northern Austral-Magallanes basin and its geodynamic significance. *Journal of South American Earth Sciences*, 86, 54–69.
- Arbe, H.A. (2002) Análisis Estratigráfico del Cretácico de la Cuenca Austral. In: *Geología y Recursos Naturales de Santa Cruz* (Ed. M.J. Haller), El Calafate, Argentina, II–6, 103–128.
- Archuby, F.M., Wilmsen, M. and Leanza, H.A. (2011) Integrated stratigraphy of the Upper Hauterivian to Lower Barremian Agua de la Mula Member of the Agrio Formation, Neuquén Basin, Argentina. *Acta Geologica Polonica*, 61, 1–26.
- Arning, E. (2008) Phosphogenesis in Coastal Upwelling Systems - Bacterially-Induced Phosphorite Formation. Dissertation (Dr. rer. nat.), Universität Bremen

- Arthur, M.A. and Sageman, B.B. (1994) Marine Black Shales: Depositional Mechanisms and Environments of Ancient Deposits. *Annu. Rev. Earth Planet. Sci.*, 22, 499–551.
- Astin, T.R. (1986) Septarian crack formation in carbonate concretions from shales and mudstones. *Clay Minerals*, 21, 617–631.
- Barberón, V., Ronda, G., Leal, P.R., Sue, C. and Ghiglione, M.C. (2015) Lower Cretaceous provenance in the northern Austral basin of Patagonia from sedimentary petrography. *J. S. Am. Earth Sci.*, 64, 498–510.
- Baturin, G.N. and Vitaliano, D.B. (1982) Phosphorites on the sea floor: origin, composition and distribution. Elsevier, Amsterdam Oxford New York.
- Baudin, F. (2005) A Late Hauterivian short-lived anoxic event in the Mediterranean Tethys: the 'Faraoni Event'. *Comptes Rendus. Géoscience*, 337, 1532–1540.
- Baudin, F. and Riquier, L. (2014) The Late Hauterivian Faraoni 'Oceanic Anoxic Event': an update. *Bulletin de la Société Géologique de France*, 185, 359–377.
- Bell, C.M., De la Cruz, R., Suárez, M. and Townsend, M.J. (1996) The evolution of the Aysen Basin, an early Cretaceous epicontinental interior seaway in the southernmost South America. In: *Géodynamique andine: résumés étendus*, ORSTOM, Paris, 289–292.
- Bell, C.M. and Suárez, M. (1997) The Lower Cretaceous Apeleg Formation of the Aisen basin, Southern Chile. Tidal sandbar deposits of an epicontinental sea. *Andean Geology*, 24, 203–225.
- Bell, C.M., Townsend, M.J., Suárez, M. and De la Cruz, R. (1994) The depositional environments of the Lower Cretaceous Coyhaique Group, Aysén Basin, southern Chile (45°–46°S). In: *VII Congr. Geol. Chileno*, Actas, Concepción, Chile, I, 402–403.
- Bhattacharya, J. (2006) Deltas. In: *Facies Models Revisited* (Ed. H.W. Posamentier and R.G. Walker), SEPM, Tulsa, OK, 237–292.
- Bhattacharya, J.P. (2010) Deltas. In: *Facies models 4*, 4. Version (Ed. N.P. James and R.W. Dalrymple), Geol. Assoc. of Canada, St. Johns, 233–264.
- Bhattacharya, J.P. and Walker, R.G. (1992) Deltas. In: *Facies models: response to sea level change* (Ed. R.G. Walker and N.P. James), Geological Association of Canada, Stittsville, Ontario, 157–178.
- Bodin, S., Godet, A., Föllmi, K.B., Vermeulen, J., Arnaud, H., Strasser, A., Fiet, N. and Adatte, T. (2006) The late Hauterivian Faraoni oceanic anoxic event in the western Tethys: Evidence from phosphorus burial rates. *Palaeogeography, Palaeoclimatology, Palaeoecology*, 235, 245–264.
- Buatois, L.A. and Mángano, M.G. (2011) *Ichology: organism-substrate interactions in space and time*. Cambridge university press, Cambridge.
- Bull, K.F. and McPhie, J. (2007) Fiamme textures in volcanic successions: Flaming issues of definition and interpretation. *Journal of Volcanology and Geothermal Research*, 164, 205–216.
- Capelli, I.A., Scasso, R.A., Spangenberg, J.E., Kietzmann, D.A., Cravero, F., Duperron, M. and Adatte, T. (2021) Mineralogy and geochemistry of deeply-buried marine sediments of the Vaca Muerta-Quintuco system in the Neuquén Basin (Chacabuco Melehue section), Argentina: Paleoclimatic and paleoenvironmental implications for the global Tithonian-Valanginian reconstructions. *Journal of South American Earth Sciences*, 107, 103103.
- Carey, S. and Sigurdsson, H. (1984) A model of volcanogenic sedimentation in marginal basins. *J. Geol. Soc. London Spec. Publ.*, 16, 37–58.
- Carey, S.N. and Schneider, J.-L. (2011) Volcaniclastic Processes and Deposits in the Deep-Sea. In: *Developments in Sedimentology*, Elsevier, 63, 457–515.
- Carmona, N.B., Buatois, L.A., Ponce, J.J. and Mángano, M.G. (2009) Ichology and sedimentology of a tide-influenced delta, Lower Miocene Chenque Formation, Patagonia, Argentina: Trace-fossil distribution and response to environmental stresses. *Palaeogeography, Palaeoclimatology, Palaeoecology*, 273, 75–86.
- Cas, R.A.F. and Wright, J.V. (1987) *Volcanic successions: Modern and Ancient. A geological approach to processes, products and successions*. Chapman & Hall, London, 528 pp.
- Cattaneo, A. and Steel, R.J. (2003) Transgressive deposits: a review of their variability. *Earth-Sci. Rev.*, 62, 187–228.
- Catuneanu, O. (2017) Sequence Stratigraphy: Guidelines for a Standard Methodology. In: *Stratigraphy & Timescales*, Elsevier, 2, 1–57.
- Catuneanu, O., Abreu, V., Bhattacharya, J.P., Blum, M.D., Dalrymple, R.W., Eriksson, P.G., Fielding, C.R., Fisher, W.L., Galloway, W.E., Gibling, M.R., Giles, K.A., Holbrook, J.M., Jordan, R., Kendall, C.G.St.C., Macurda, B., Martinsen, O.J., Miall, A.D., Neal, J.E., Nummedal, D., Pomar, L., Posamentier, H.W., Pratt, B.R., Sarg, J.F., Shanley, K.W., Steel, R.J., Strasser, A., Tucker, M.E. and Winker, C. (2009) Towards the standardization of sequence stratigraphy. *Earth-Science Reviews*, 92, 1–33.
- Cavalheiro, L., Wagner, T., Steinig, S., Bottini, C., Dummman, W., Esegue, O., Gambacorta, G., Giraldo-Gómez, V., Farnsworth, A., Flögel, S., Hofmann, P., Lunt, D.J., Rethemeyer, J., Torricelli, S. and Erba, E. (2021) Impact of global cooling on Early Cretaceous high pCO₂ world during the Weissert Event. *Nat Commun*, 12, 5411.
- Chamberlain, J.A., Ward, P.D. and Weaver, J.S. (1981) Post-mortem ascent of Nautilus shells: implications for cephalopod paleobiogeography. *Paleobiology*, 7, 494–509.
- Charrier, R. and Covacevich, V. (1978) Paleogeografía y bioestratigrafía del Jurásico Superior y Neocomiano en el sector austral de los Andes Meridionales Chilenos (42°–56° latitud sur). In: *II Congr. Argentino de Paleont. Estrat. y I Cong. Latinoam. Paleont.*, Actas, Buenos Aires, Argentina, V, 153–175.
- Coates, L. and MacEachern, J.A. (2007) The Ichnological signatures of river- and wave-dominated delta complexes: Differentiating deltaic and non-deltaic shallow marine successions, Lower Cretaceous Viking Formation and Upper Cretaceous Dunvegan Formation, West-Central Alberta. In: *Applied Ichnology*, SEPM Society for Sedimentary Geology, 349–374.
- Cohen, K.M., Finney, S.C., Gibbard, P.L. and Fan, J.-X. (2013) The ICS International Chronostratigraphic Chart. *Episodes*, 36, 199–204.
- Coniglio, M. and Dix, G.R. (1992) Carbonate Slopes. In: *Facies models: response to sea level change* (Ed. R.G. Walker and Noel P. James), Geological Association of Canada, Stittsville, Ontario, 349–374.
- Covacevich, V., De la Cruz, R. and Suárez, M. (1994) Primer hallazgo de fauna del Berriasiano inferior (Neocomiano) en la Formación Ibáñez, región XI, Aisén. In: *VII Congr. Geol. Chileno*, Actas, Concepción, Chile, I, 425–429.
- Cuitiño, J.L., Varela, A.N., Ghiglione, M.C., Richiano, S. and Poiré, D.G. (2019) The Austral-Magallanes Basin (southern Patagonia): A synthesis of its stratigraphy and evolution. *Latin American Journal of Sedimentology and Basin Analysis*, 26, 155–166.
- De la Cruz, R., Suárez, M., Belmar, M., Quiroz, D. and Bell, M. (2003) Geología del Área Coihaique-Balmaceda, Región Aisén del General Carlos Ibáñez del Campo. *SERNAGEOMIN*, Santiago, Chile, 40 pp.
- De la Cruz, R., Suárez, M., Covacevich, V. and Quiroz, D. (1996) Estratigrafía de la zona de Palena y Futaleufú (43°15'–43°45' latitud S), X Región, Chile. In: *XIII Congr. Geol. Argentino y III Congr. Explor. Hidroc.*, Actas, Buenos Aires, Argentina, I, 417–424.
- De la Cruz, R., Welkner, D., Suárez, M. and Quiroz, D. (2004) Geología del Área Oriental de las Hojas Cochrane y Villa O'Higgins, Región Aisén del General Carlos Ibáñez del Campo. *SERNAGEOMIN*, Santiago, Chile, 57 pp.
- Dhondt, A.V. (1992) Cretaceous inoceramid biogeography: a review. *Palaeogeography, Palaeoclimatology, Palaeoecology*, 92, 217–232.
- Doyle, P., Poiré, D.G., Spalletti, L.A., Pirrie, D., Brenchley, P. and Matheos, S.D. (2005) Relative oxygenation of the Tithonian — Valanginian Vaca Muerta—Chachao formations of the Mendoza Shelf, Neuquén Basin, Argentina. *SP*, 252, 185–206.
- Duhart, J. (1960) Resultado de Estudios Geológicos en parte N.E de la Provincia de Aysen. Instituto de Investigaciones Geológicas, Punta Arenas.
- Echaurren, A., Folguera, A., Gianni, G., Orts, D., Tassara, A., Encinas, A., Giménez, M. and Valencia, V. (2016) Tectonic evolution of the North Patagonian Andes (41°–44° S) through recognition of syntectonic strata. *Tectonophysics*, 677–678, 99–114.
- Elliott, T. (2005) Deltas. In: *Encyclopedia of Geology*, Elsevier, 528–539.
- Erba, E., Bartolini, A. and Larson, R.L. (2004) Valanginian Weissert oceanic anoxic event. *Geol.*, 32, 149.
- Fisher, R.V. (1966) Rocks composed of volcanic fragments and their classification. *Earth-Sci. Rev.*, 1, 287–298.
- Fisher, R.V. (1961) Proposed Classification of Volcaniclastic Sediments and Rocks. *Geol. Soc. America Bull.*, 72, 1409.
- Fisher, R.V. and Schmincke, H.-U. (1984) *Pyroclastic Rocks*. Springer, Berlin, 472 pp.
- Flügel, E. and Munnecke, A. (2010) *Microfacies of carbonate rocks: analysis, interpretation and application*, 2. ed. [erw.]. Springer, Berlin Heidelberg, 984 pp.
- Folguera, A. and Iannizzotto, N.F. (2004) The lagos La Plata and Fontana fold-and-thrust belt: long-lived orogenesis at the edge of western Patagonia. *Journal of South American Earth Sciences*, 16, 541–566.
- Föllmi, K.B. (2012) Early Cretaceous life, climate and anoxia. *Cretaceous Research*, 35, 230–257.
- Föllmi, K.B., Godet, A., Bodin, S. and Linder, P. (2006) Interactions between environmental change and shallow water carbonate buildup along the northern Tethyan margin and their impact on the Early Cretaceous

- carbon isotope record. *Paleoceanography*, 21, 2006PA001313.
- Francis, A.O. and Hallam, A. (2003) Ecology and evolution of Jurassic trigoniid bivalves in Europe. *LET*, 36, 287–304.
- Fuenzalida, H. and Latcham, R. (1935) Observaciones geológicas del territorio del Aysén. *Boletín del Museo Nacional de Historia Natural, Chile*, 14, 31–36.
- Fürsich, F.T., Alberti, M. and Pandey, D.K. (2017) Behavioural variants of the trace fossil Gyrochorte. doi: 10.5282/UBM/EPUB.40455
- Garzanti, E. (2019) Petrographic classification of sand and sandstone. *Earth-Science Reviews*, 192, 545–563.
- Gómez Dacal, A.R., Gómez Peral, L.E., Spalletti, L.A., Sial, A.N., Siccardi, A. and Poiré, D.G. (2018) First record of the Valanginian positive carbon isotope anomaly in the Mendoza shelf, Neuquén Basin, Argentina: palaeoclimatic implications. *andgeo*, 45, 111.
- Gonzalez-Bonorino, G. and Suárez, M. (1995) Paleoambientes sedimentarios de la Formación Apeleg, Cretácico Inferior de la Cuenca de Aisen, Region XI, Chile. *Andean Geol.*, 22, 115–126.
- Guler, M.V., Lazo, D.G., Pazos, P.J., Borel, C.M., Ottone, E.G., Tyson, R.V., Cesaretti, N. and Aguirre-Urreta, M.B. (2013) Palynofacies analysis and palynology of the Agua de la Mula Member (Agrio Formation) in a sequence stratigraphy framework, Lower Cretaceous, Neuquén Basin, Argentina. *Cretaceous Research*, 41, 65–81.
- Haller, M.J. and Lapido, O.R. (1980) El Mesozoico de la Cordillera Patagónica Central. *Rev. Asoc. Geol. Argentina*, XXV, 230–247.
- Haller, M.J., Lapido, O.R., Lizuain, A. and Page, R. (1981) El mar tithono-neocomiano en la evolución de la Cordillera Norpatagónica. In: *Cuencas Sedimentarias del Jurásico y Cretácico de América del Sur*, Com. Sudam. Jura. Cretac., 1, 221–237.
- Haq, B.U. (2014) Cretaceous eustasy revisited. *Global Planet. Sci.*, 113, 44–58.
- Heim, A. (1940) Geological Observations in the Patagonian Cordillera (Preliminary Report). *Eclogae Geologicae Helveticae*, 33, 25–51.
- Henrich, R. and Hüneke, H. (2011) Hemipelagic advection and periplatform sedimentation. In: *Developments in Sedimentology*, Elsevier, 63, 353–396.
- Hesse, R. and Schacht, U. (2011) Early Diagenesis of Deep-Sea Sediments. In: *Developments in Sedimentology*, Elsevier, 63, 557–713.
- Housego, R.M. and Rosman, J.H. (2016) A model for understanding the effects of sediment dynamics on oyster reef development. *Estuar. Coast.*, 39, 495–509.
- Iannizzotto, N.F., Folguera, A., Leal, P.R. and Iaffa, D. (2004) Control tectónico de las secuencias volcánicas neocomianas y paleogeografía en la zona del Lago La Plata (45°S). Sector interno de la faja plegada y corrida de los lagos La Plata y Fontana. *Rev. Asoc. Geol. Argentina*, 59, 655–670.
- Johnson, H.D. and Baldwin, C.T. (1996) Shallow Clastic Seas. In: *Sedimentary Environments: Processes, Facies and Stratigraphy*, Blackwells, Cornwall, 232–280.
- Katz, H. (1961) Sobre la ocurrencia de Cretáceo Superior marino en Coyhaique, Provincia de Aysén. In: *Anales de la Facultad de Ciencias Físicas y Matemáticas*, Universidad de Chile, Santiago, Chile, 21, 113–131.
- Késjar, D., Fözy, I., Price, G., Condon, D., Salazar, C. and Pálffy, J. (2017) Integrated Lower Cretaceous stratigraphy from the Aysén Basin, Patagonia, Chile. In: *10th International Symposium on the Cretaceous - Abstracts* (Ed. B. Sames), *Berichte der Geologischen Bundesanstalt*, Vienna, Austria, 120, 142.
- Kidwell, S.M. and Bosence, D.W.J. (1991) Taphonomy and Time-Averaging of Marine Shelly Faunas. In: *Taphonomy: releasing the data locked in the fossil record* (Ed. P.A. Allison and D.E.G. Briggs), Plenum Press, New York, 115–193.
- Knaust, D. (2017) Atlas of trace fossils in well core: appearance, taxonomy and interpretation. Springer, Cham, 209 pp.
- Kumar, P., Devi, K.L., Chakraborty, P.P. and Rajkumar, H.S. (2022) Depositional architecture of sub-aqueous part of a tide-dominated delta and its palaeogeographic implications: Laisong Formation (Barail Group), Indo-Myanmar Ranges, western Manipur. *J Earth Syst Sci*, 131, 103.
- Kurosawa, S., Furota, S., Mitsui, M., Sawada, K., Seike, K., Furukawa, N. and Ito, M. (2023) Downslope variation in hemipelagic sedimentation in an active margin basin: An example from the lower Pleistocene Kiwada and Takamizo formations on the Boso Peninsula, Japan. *Sedimentology*, 70, 705–727.
- LaBarbera, M. (1981) The Ecology of Mesozoic Gryphaea, Exogyra, and Ilymatogyra (Bivalvia: Mollusca) in a Modern Ocean. *Paleobiology*, 7, 510–526.
- Lazo, D.G. (2006) Análisis tafonómico e inferencia del grado de mezcla temporal y espacial de la macrofauna del Miembro Pilmatué de la Formación Agrio, Cretácico Inferior de cuenca Neuquina, Argentina. *Ameghiniana*, 43, 311–326.
- Lazo, D.G. (2004) Análisis de concentraciones fósiles del Cretácico Inferior de Cuenca Neuquina (PhD Thesis). Tesis Doctoral, Universidad de Buenos Aires
- Lin, W. and Bhattacharya, J.P. (2021) Storm-flood-dominated delta: A new type of delta in stormy oceans. *Sedimentology*, 68, 1109–1136.
- Longhitano, S.G., Mellere, D., Steel, R.J. and Ainsworth, R.B. (2012) Tidal depositional systems in the rock record: A review and new insights. *Sedimentary Geology*, 279, 2–22.
- MacEachern, J.A., Bann, K.L., Bhattacharya, J.P. and Howell, C.D. (2005) Ichnology of deltas: Organism responses to the dynamic interplay of rivers, waves, storms, and tides. In: *River Deltas-Concepts, Models, and Examples* (Ed. L. Giosan and J.P. Bhattacharya), SEPM (Society for Sedimentary Geology),
- Maeda, H. and Seilacher, A. (1996) Ammonoid Taphonomy. In: *Ammonoid Paleobiology* (Ed. N.H. Landman, K. Tanabe, and R.A. Davis), Springer US, Boston, MA, 13, 543–578.
- Malumian, N. and Masiuk, V. (1975) Foraminíferos de la Formación Pampa Rincón (Cretácico Inferior), Tierra del Fuego, Argentina. *Revista Española de Micropaleontología*, VII, 579–600.
- Malumian, N. and Nañez, C. (1983) Foraminíferos de ambiente anóxico de la Formación Río Mayer (Cretácico Inferior), Provincia de Santa Cruz. *Ameghiniana*, XX, 367–393.
- Marshall, J.D. and Pirrie, D. (2013) Carbonate concretions—explained. *Geology Today*, 29, 53–62.
- Martinez, M., Deconinck, J.-F., Pellenard, P., Riquier, L., Company, M., Reboulet, S. and Moiroud, M. (2015) Astrochronology of the Valanginian–Hauterivian stages (Early Cretaceous): Chronological relationships between the Paraná–Etendeka large igneous province and the Weissert and the Faraoni events. *Global and Planetary Change*, 131, 158–173.
- Martins-Neto, M.A. and Catuneanu, O. (2010) Rift sequence stratigraphy. *Mar. Petrol. Geol.*, 27, 247–253.
- Masiuk, V. and Nakayama, C. (1978) Sedimentitas marinas mesozoicas del lago Fontana: Su importancia. In: *VII Congr. Geol. Argentino*, Actas, Neuquén, Argentina, II, 361–378.
- Mazzullo, S.J. (2000) Organogenic Dolomitization in Peritidal to Deep-Sea Sediments. *Journal of Sedimentary Research*, 70, 10–23.
- McMillan, I.K. (2008) Aragonitic-walled benthic foraminifera (Epistomina) in the Cretaceous “mud belt” off southern Africa, and postmortem cross-shelf transport of tests. *African Natural History*, 4, 17–24.
- McPhie, J., Doyle, M. and Allen, R.L. (1993) Volcanic textures: a guide to the interpretation of textures in volcanic rocks. *Centre Ore Depos. Explor. Stud. Univ. Tasmania*, Hobart, 198 pp.
- Mpodozis, C., Mella, P. and Pavda, D. (2011) Estratigrafía y megasecuencias sedimentarias en la Cuenca Austral-Magallanes, Argentina y Chile. In: *VIII Congreso de Exploración y Desarrollo de Hidrocarburos*, Actas, Instituto Argentino del Petróleo y el Gas, Mar del Plata, Argentina, 35, 97–137.
- Müller, R.D., Sdrolias, M., Gaina, C., Steinberger, B. and Heine, C. (2008) Long-Term Sea-Level Fluctuations Driven by Ocean Basin Dynamics. *Science*, 319, 1357–1362.
- Mutti, E., Davoli, G., Tinterri, R. and Zavala, C. (1996) The importance of ancient fluvio-deltaic systems dominated by catastrophic flooding in tectonically active basins. *Mem. Sci. Geol.*, 48, 233–291.
- Mutti, E., Tinterri, R. and Di Biase, D. (2000) Delta-front associations of ancient flood-dominated fluvio-deltaic systems. *Mem. Sci. Geol.*, 13, 165–190.
- Nemec, W. (1990) Aspects of Sediment Movement on Steep Delta Slopes. In: *Coarse-Grained Deltas* (Ed. A. Colella and D.B. Prior), Wiley-Blackwell, Oxford, 29–73.
- Nori, L. and Lathuilière, B. (2003) Form and environment of Gryphaea arcuata. *Lethaia*, 36, 83–96.
- O'Brien, N.R. and Slatt, R.M. (1990a) Argillaceous Rock Atlas. Springer New York, New York, NY.
- O'Brien, N.R. and Slatt, R.M. (1990b) Argillaceous Rock Atlas.
- Olivero, E. (1982) Estratigrafía de la cuenca sur del Lago Fontana, Provincia del Chubut. PhD Thesis, Universidad de Buenos Aires
- Olivero, E. and Aguirre-Urreta, M.B. (2002) Sucesión de amonoideos de la Formación Katterfeld (Valanginiano-Hauteriviano) en su área tipo, Lago Fontana, Chubut. In: *XV Congr. Geol. Argentino*, Actas, El Calafate, Argentina, 6 pp.
- Pankhurst, R., Hervé, F., Fanning, M. and Suárez, M. (2003) Coeval plutonic and volcanic activity in the Patagonian Andes: the Patagonian Batholith and

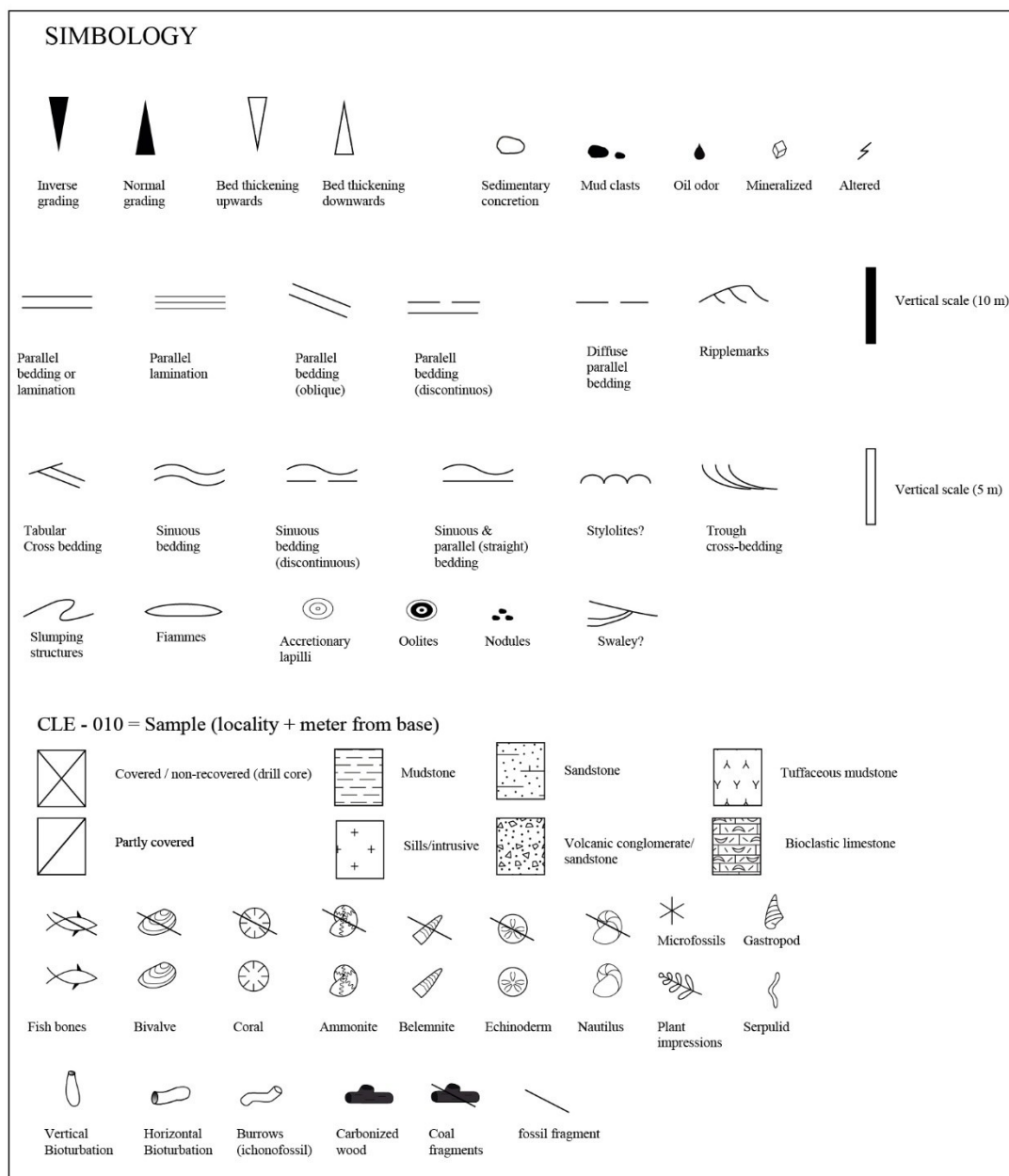
- the Ibáñez and Divisadero formations, Aysén, Southern Chile. In: X Congr. Geol. Chileno, Actas, Concepción, Chile, 5 pp.
- Pankhurst, R.J., Weaver, S.D., Hervé, F. and Larrondo, P. (1999) Mesozoic-Cenozoic evolution of the North Patagonian Batholith in Aysén, southern Chile. *J. Geol. Soc. London*, 156, 673–694.
- Pickering, K.T. and Hiscott, R.N. (2016) Deep-marine systems: processes, deposits, environments, tectonics and sedimentation. John Wiley & Sons Inc, Chichester, West Sussex; Hoboken, NJ, 657 pp.
- Plint, A.G. (2014) Mud dispersal across a Cretaceous prodelta: Storm-generated, wave-enhanced sediment gravity flows inferred from mudstone microtexture and microfacies. *Sedimentology*, 61, 609–647.
- Ploszkiewicz, J.V. (1987) Descripción Geológica de la Hoja 47 c - "Apeleg", Provincia del Chubut: Carta Geológico-económica de la República Argentina, Escala 1:200.000. SEGEMAR Boletín, 100 pp.
- Ploszkiewicz, J.V. and Ramos, V.A. (1977) Estratigrafía y tectónica de la Sierra de Payaniyeu (Provincia del Chubut). *Rev. Asoc. Geol. Argentina*, XXXII, 209–226.
- Potter, P.E., Maynard, J.B. and Depetris, P.J. (2005) Mud and Mudstones: Introduction and Overview. Springer, Berlin; New York, 297 pp.
- Potter, P.E., Maynard, J.B. and Pryor, W.A. (1980) *Sedimentology of Shale*. Springer New York, New York, NY.
- Ramos, V.A. (1976) Estratigrafía de los lagos La Plata y Fontana, Provincia del Chubut, República Argentina. In: I Congr. Geol. Chileno, Actas, Santiago, Chile, 1, 43–64.
- Ramos, V.A. (1981) Descripción Geológica de la Hoja 47 ab - "Lago Fontana", Provincia del Chubut: Carta Geológico-económica de la República Argentina, Escala 1:200.000. SEGEMAR Boletín, 135 pp.
- Ramos, V.A. and Palma, M. (1983) Las lutitas pizarreñas fosilíferas del Cerro Dedo y su evolución tectónica; Lago La Plata, Provincia del Chubut. *Rev. Asoc. Geol. Argentina*, XXXVIII, 148–160.
- Reading, H.G. and Collinson, J.D. (1996) Clastic Coasts. In: *Sedimentary Environments: Processes, Facies and Stratigraphy* (Ed. H.G. Reading), Blackwells, Cornwall, 154–231.
- Reineck, H.-E. and Singh, I.B. (1973) *Depositional Sedimentary Environments*. Springer Berlin Heidelberg, Berlin, Heidelberg.
- Richiano, S., Gómez-Peral, L.E., Varela, A.N., Gómez Dacal, A.R., Cavarozzi, C.E. and Poiré, D.G. (2019) Geochemical characterization of black shales from the Río Mayer Formation (Early Cretaceous), Austral-Magallanes Basin, Argentina: Provenance response during Gondwana break-up. *Journal of South American Earth Sciences*, 93, 67–83.
- Richiano, S., Varela, A.N., Cereceda, A. and Poiré, D.G. (2012) Evolución paleoambiental de la Formación Río Mayer, Cretácico Inferior, Cuenca Austral, Provincia de Santa Cruz, Argentina. *Latin American Journal of Sedimentology and Basin Analysis*, 19, 3–26.
- Richiano, S., Varela, A.N., Gómez-Peral, L.E., Cereceda, A. and Poiré, D.G. (2015) Composition of the Lower Cretaceous source rock from the Austral Basin (Río Mayer Formation, Patagonia, Argentina): Regional implication for unconventional reservoirs in the Southern Andes. *Marine and Petroleum Geology*, 66, 764–790.
- Rivas, H., Salazar, C. and Stinnesbeck, W. (2021) Facies and sequence stratigraphy of a mixed carbonate-volcaniclastic ramp in intra-arc settings: An example from the Toqui Formation (Lower Cretaceous), southern Chile (45°S). *J. S. Am. Earth Sci.*, 109, 103292.
- Rivas, H., Salazar, C. and Stinnesbeck, W. (2023) A "cool-water", non-tropical, mixed volcaniclastic-carbonate ramp from the Early Cretaceous of southern Chile (45°40'S). *Facies*, 69, 14.
- Rodríguez, J.P. and Arche, A. (2010) Deltas. In: *Sedimentología. Del proceso físico a la cuenca sedimentaria* (Ed. A. Arche), Consejo Superior de Investigaciones Científicas (CSIC), Madrid, 561–618.
- Scasso, R.A. (1989) La Cuenca Sedimentaria del Jurásico Superior y Cretácico Inferior de la Región Sudoccidental del Chubut. In: *Cuencas Sedimentarias Argentinas* (Ed. G.A. Chebli and L.A. Spalletti), 395–417.
- Scasso, R.A. (1987) Estratigrafía y ambientes de sedimentación del ciclo sedimentario del Jurásico Superior y Cretácico Inferior de la región sudoccidental del Chubut, con referencias a la columna estratigráfica general del área. PhD Thesis, Universidad de Buenos Aires.
- Scholle, P.A. and Ulmer-Scholle, D.S. (2003) A colour guide to the petrography of carbonate rocks: grains, textures, porosity, diagenesis. AAPG, Tulsa, OK, 474 pp.
- Scott, E.D., Bouma, A.H. and Bryant, W.R. (2003) *Siltstones, mudstones and shales*. SEPM (Society for Sedimentary Geology), Tulsa, OK.
- Seilacher, A. (2007) *Trace fossil analysis*. Springer, Berlin, 226 pp.
- Shmeit, M., Giraud, F., Jaillard, E., Reboulet, S., Masrour, M., Spangenberg, J.E. and El-Samrani, A. (2022) The Valanginian Weissert Event on the south Tethyan margin: A dynamic paleoceanographic evolution based on the

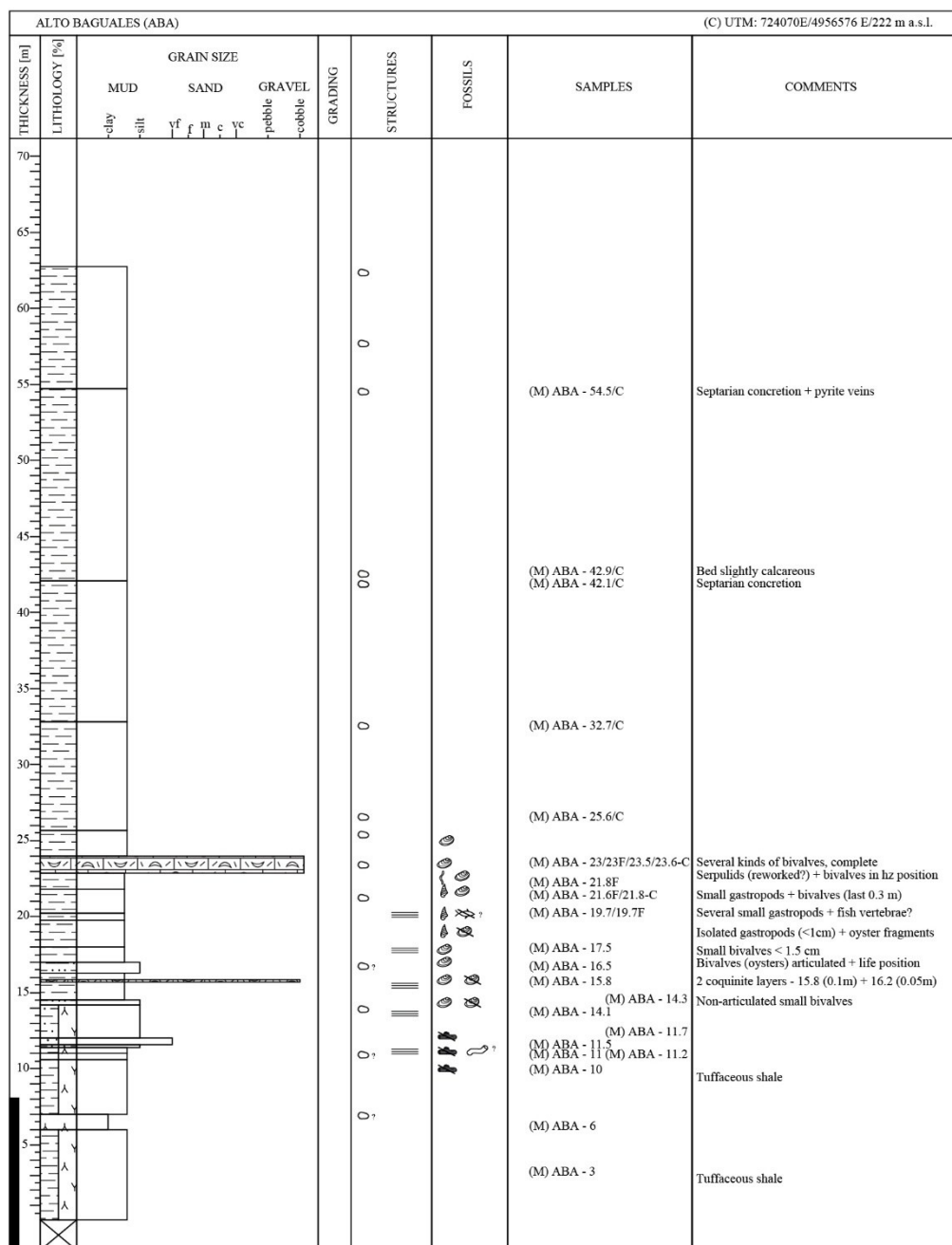
- study of calcareous nannofossils. *Marine Micropaleontology*, 175, 102134.
- Skarmeta, J. (1976) Evolución tectónica y paleogeográfica de los Andes Patagónicos de Aysén (Chile), durante el Neocomiano. In: I Congr. Geol. Chileno, Actas, Santiago, Chile, B, 1–15.
- Skarmeta, J. and Charrier, R. (1976) Geología del sector fronterizo de Aysén entre los 45° y 46° de latitud sur, Chile. In: VI Congr. Geol. Argentino, Actas, Asociación Geológica Argentina, Buenos Aires, Argentina, I, 267–286.
- Slomp, C.P. and Van Cappellen, P. (2007) The global marine phosphorus cycle: sensitivity to oceanic circulation. *Biogeosciences*, 4, 155–171.
- Stenzel, H.B. (1971) Oysters. In: *Treatise in Invertebrate Paleontology*, Volumen 3, Mollusca 6 (Bivalvia) (Ed. R.C. Moore), Geological Society of America; University of Kansas, 3, N953–N1224.
- Stow, D. and Smillie, Z. (2020) Distinguishing between Deep-Water Sediment Facies: Turbidites, Contourites and Hemipelagites. *Geosciences*, 10, 68.
- Stow, D.A.V., Reading, H.G. and Collinson, J.D. (1996) Deep Seas. In: *Sedimentary Environments: Processes, Facies and Stratigraphy* (Ed. H.G. Reading), Blackwells, Cornwall, 154–231.
- Stow, D.A.V. and Tabrez, A.R. (1998) Hemipelagites: processes, facies and model. *SP*, 129, 317–337.
- Suárez, M. and De la Cruz, R. (2001) Jurassic to Miocene K–Ar dates from eastern central Patagonian Cordillera plutons, Chile (45°–48° S). *Geol. Mag.*, 138, 53–66.
- Suárez, M. and De la Cruz, R. (1994a) Estratigrafía del Jurásico Superior - Cretácico Inferior de la Cordillera Patagónica Oriental (45°–46° latitud sur), Chile: Facies, Paleogeografía. SERNAGEOMIN, Región de Aysén, Chile, 98 pp.
- Suárez, M. and De la Cruz, R. (1994b) Estratigrafía y paleogeografía mesozoica de Aysén Nororiental. In: VII Congr. Geol. Chileno, Actas, Concepción, Chile, I, 538–542.
- Suárez, M., De La Cruz, R., Aguirre-Urreta, M.B. and Fanning, M. (2009) Relationship between volcanism and marine sedimentation in northern Austral (Aysén) Basin, central Patagonia: Stratigraphic, U–Pb SHRIMP and paleontologic evidence. *J. S. Am. Earth Sci.*, 27, 309–325.
- Suárez, M., De la Cruz, R., Aguirre-Urreta, M.B. and Fanning, M. (2005) Diachronic Tithonian-Valanginian marine transgression of the Coyhaique Group, Aysén Basin (43°–47°S), Chile. In: XVI Congr. Geol. Argentino, Actas, La Plata, Argentina, I, 305–308.
- Suárez, M., De la Cruz, R. and Bell, C.M. (1996) Estratigrafía de la región de Coyhaique (latitud 45°–46° S), Cordillera Patagónica, Chile. In: XIII Congr. Geol. Argentino y III Congr. Explor. Hidroc. Actas, I, 575–590.
- Suárez, M., De la Cruz, R. and Bell, C.M. (2007) Geología del área Ñireguao-Baño Nuevo, Región Aysén del General Carlos Ibáñez del Campo. SERNAGEOMIN, Santiago, Chile, 56 pp.
- Suárez, M., De la Cruz, R., Bell, M. and Demant, A. (2010) Cretaceous slab segmentation in southwestern Gondwana. *Geol. Mag.*, 147, 193–205.
- Suárez, M., De la Cruz, R., Etchart, H., Marcelo, M. and Mark, F. (2015) Síntesis de la cronología magmática Meso-Cenozoica de Patagonia Central, Aysén, Chile: edades U–Pb SHRIMP. In: XIV Congr. Geol. Chileno, Actas, La Serena, Chile, 789–792.
- Suárez, M., Gressier, J.B., Rossel, P. and De la Cruz, R. (2023) Lower cretaceous missing volcanic arc. A migrating arc, central Patagonian cordillera, Chile: Detrital zircon U–Pb geochronology. *Int J Earth Sci (Geol Rundsch)*, 112, 907–923.
- Townsend, M.J. (1998) The palaeogeography of the Lower Cretaceous Aysén Basin of southern Chile. PhD Thesis, University of Bristol.
- Trabucho-Alexandre, J. (2015) Organic Matter-Rich Shale Depositional Environments. In: *Fundamentals of Gas Shale Reservoirs*, 1st edn. (Ed. R. Rezaee), Wiley, 21–45.
- Ulmer-Scholle, D.S., Scholle, P.A., Schieber, J. and Raine, R.J. (2014) A colour guide to the petrography of sandstones, siltstones, shales and associated rocks. American Association of Petroleum Geologists, Tulsa, OK, U.S.A., 526 pp.
- Weissert, H. (1989) C-isotope stratigraphy, a monitor of paleoenvironmental change: A case study from the early cretaceous. *Surv Geophys*, 10, 1–61.
- Weissert, H., Lini, A., Föllmi, K.B. and Kuhn, O. (1998) Correlation of Early Cretaceous carbon isotope stratigraphy and platform drowning events: a possible link? *Palaeogeography, Palaeoclimatology, Palaeoecology*, 137, 189–203.
- Yacobucci, M.M. (2018) Postmortem transport in fossil and modern shelled cephalopods. *PeerJ*, 6, e5909.
- Yoshida, H., Ujihara, A., Minami, M., Asahara, Y., Katsuta, N., Yamamoto, K., Sirono, S., Maruyama, I., Nishimoto, S. and Metcalfe, R. (2015) Early post-mortem formation of carbonate concretions around tusk-shells

- over week-month timescales. *Sci Rep*, 5, 14123.
- Yoshida, H., Yamamoto, K., Minami, M., Katsuta, N., Sin-ichi, S. and Metcalfe, R. (2018) Generalized conditions of spherical carbonate concretion formation around decaying organic matter in early diagenesis. *Sci Rep*, 8, 6308.
- Zavala, C. and Pan, S. (2018) Hyperpycnal flows and hyperpycnites: Origin and distinctive characteristics. *Lithologic Reservoirs*, 30, 1–27.
- Zell, P. and Stinnesbeck, W. (2016) Paleobiology of the Latest Tithonian (Late Jurassic) Ammonite *Salinites grossicostatum* Inferred from Internal and External Shell Parameters. *PLoS ONE*, 11, e0145865.

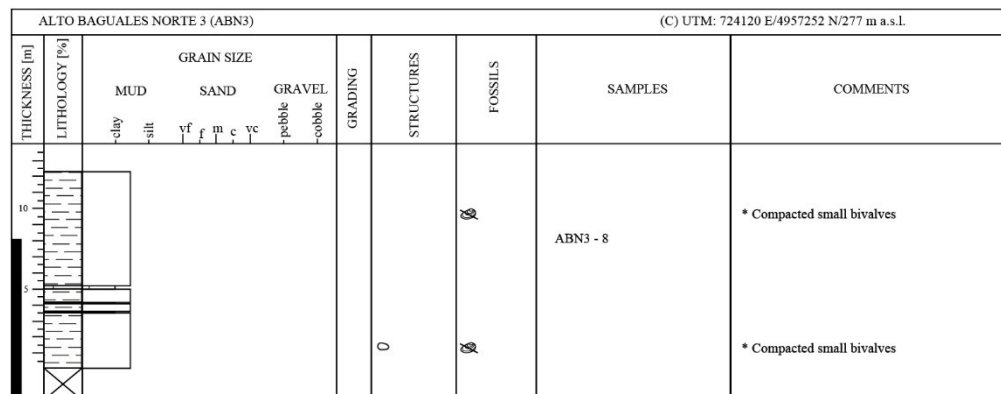
9. Supplementary Material

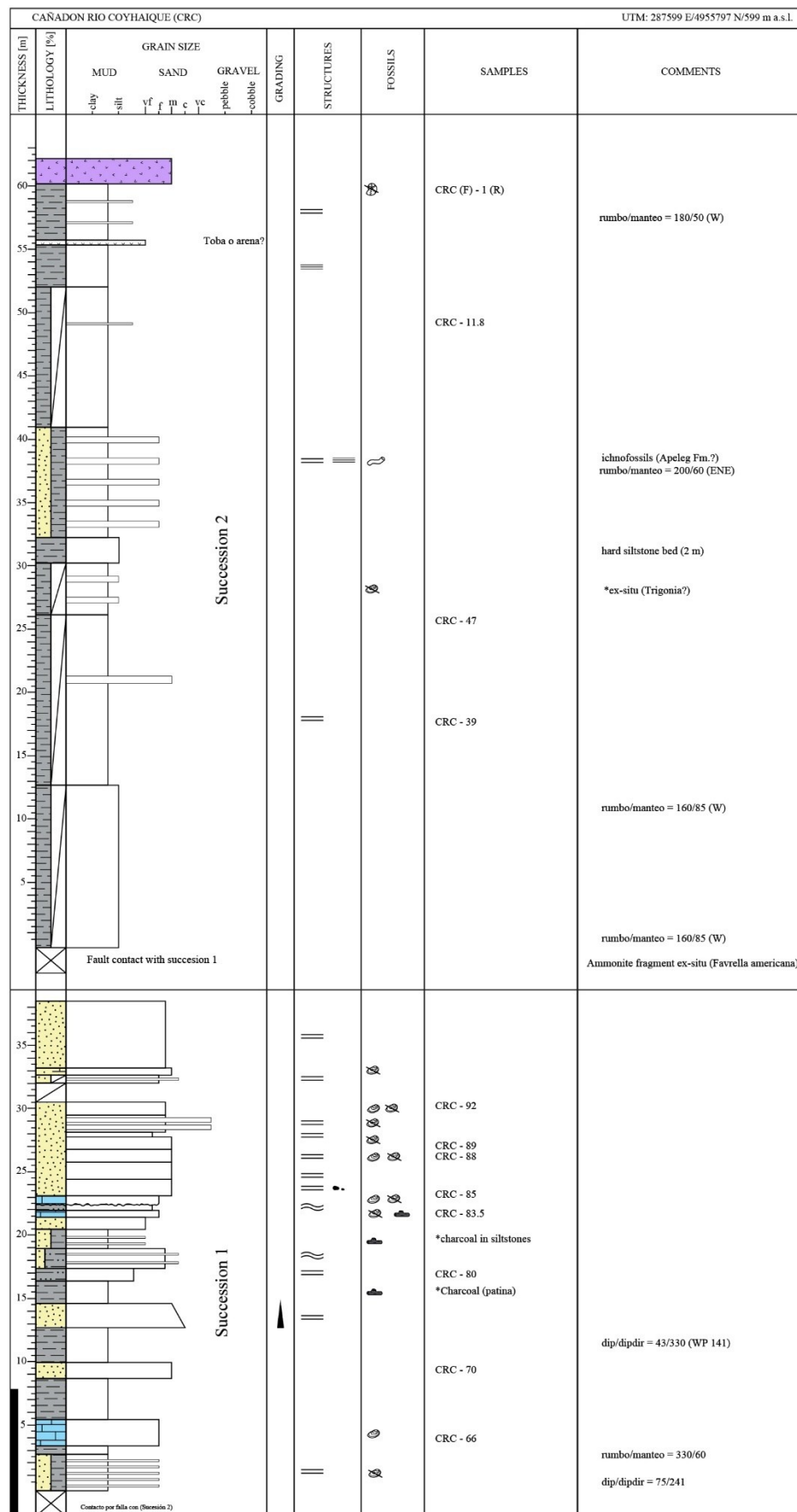
9.1. Sedimentary logs

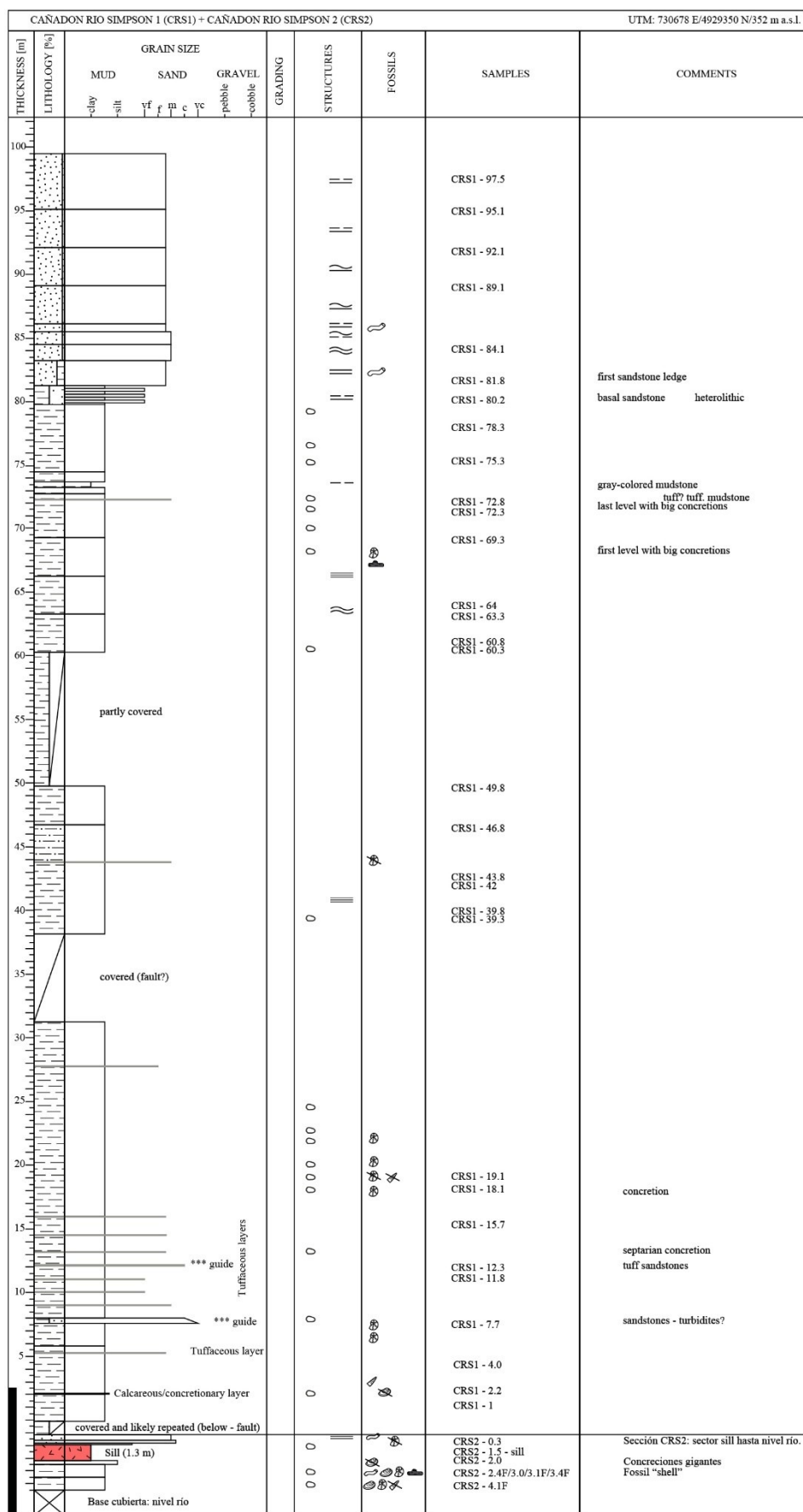


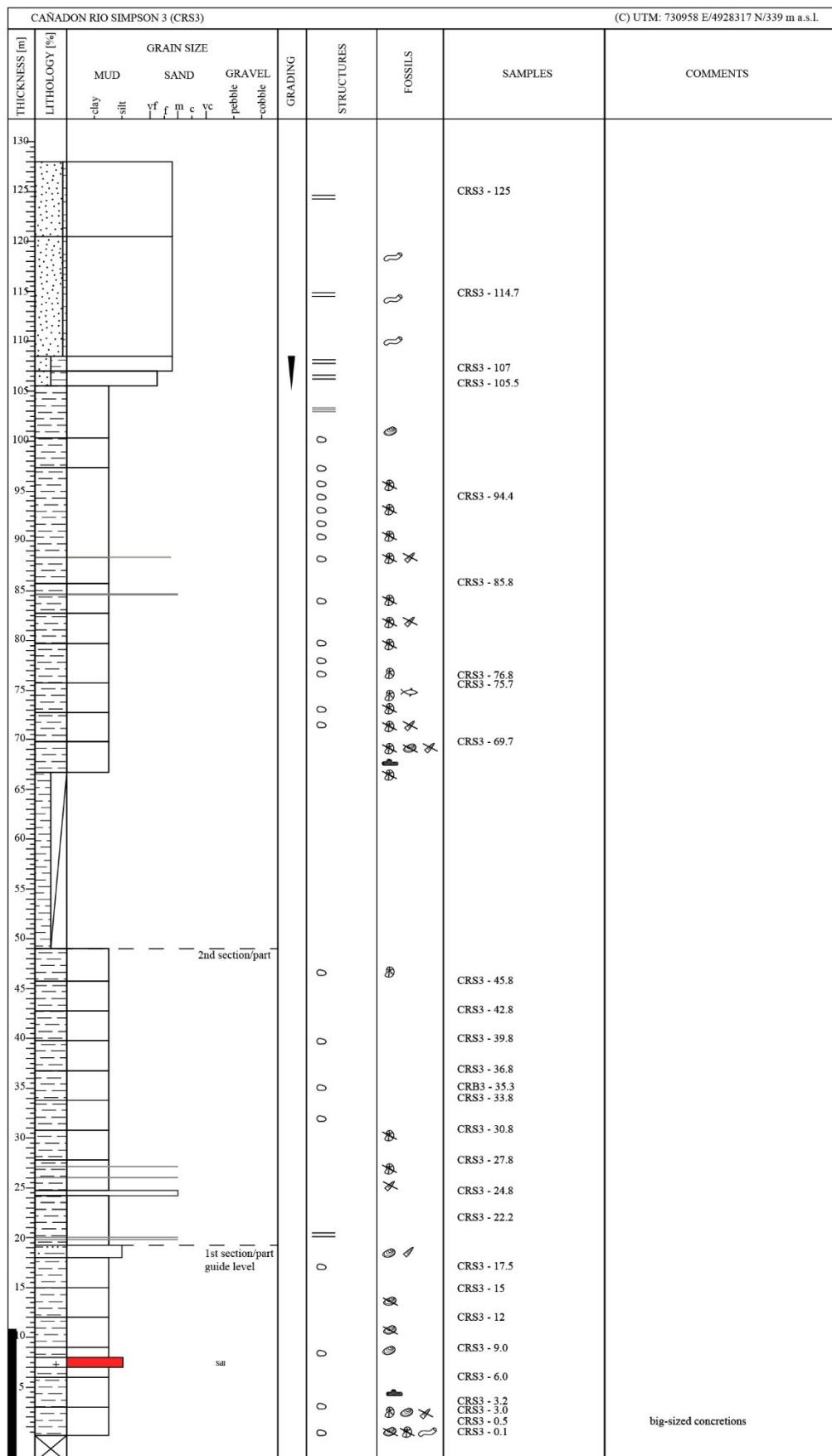


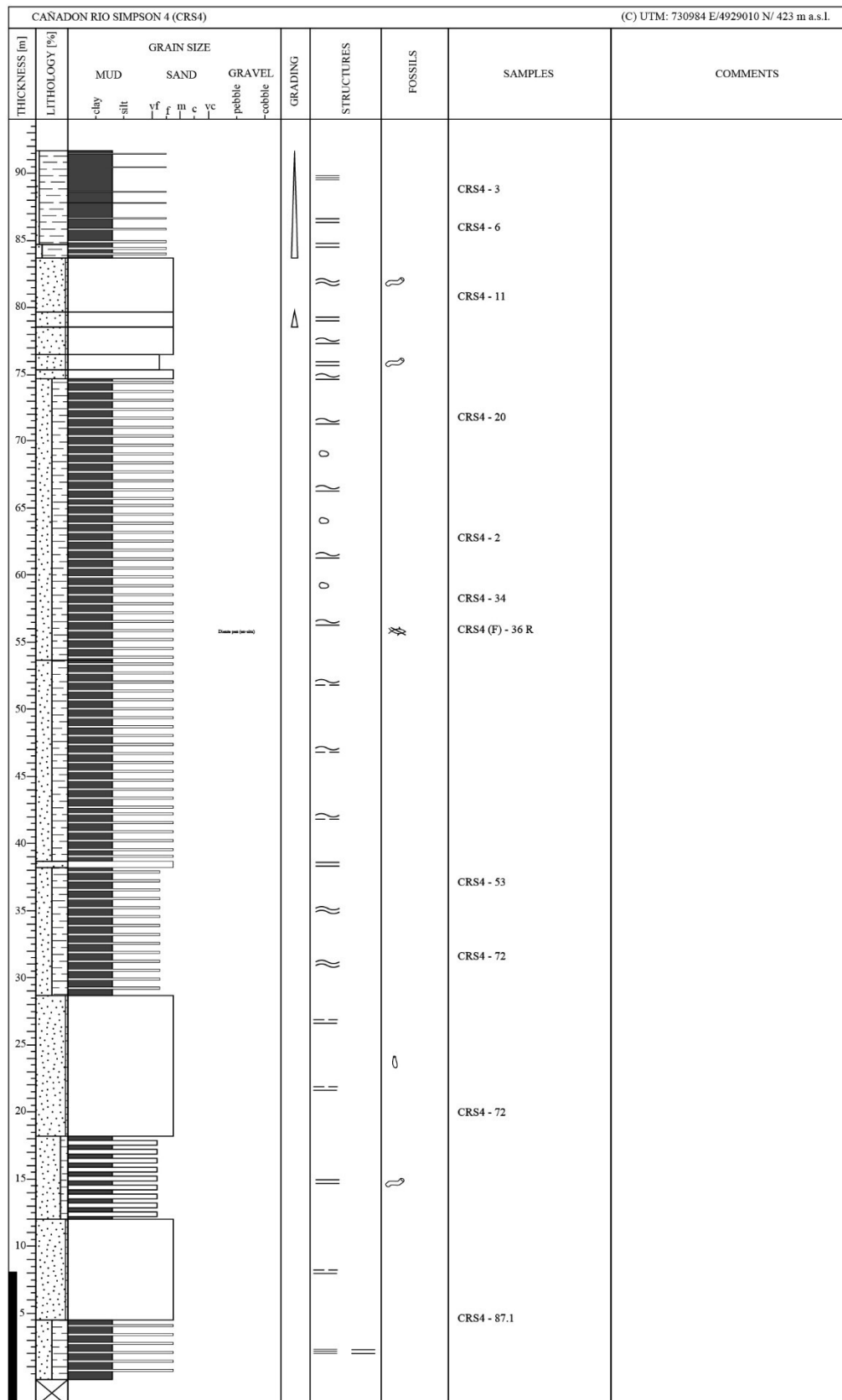
ALTO BAGUALES NORTE (ABN)										(C) UTM: 724358 E/4957395 N/219 m a.s.l				
THICKNESS [m]	LITHOLOGY [%]	GRAIN SIZE								GRADING	STRUCTURES	FOSSILS	SAMPLES	COMMENTS
		MUD		SAND			GRAVEL							
		-clay	-silt	vf	f	m	c	vc	-pebble	-cobble				
45														
40													ABN - 40	
35														
30														
25													ABN - 25.5	
20														
15														
10													ABN - 9	
5													ABN - 6.3	









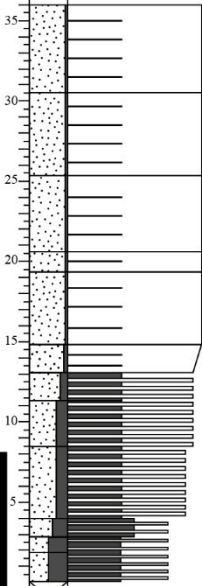


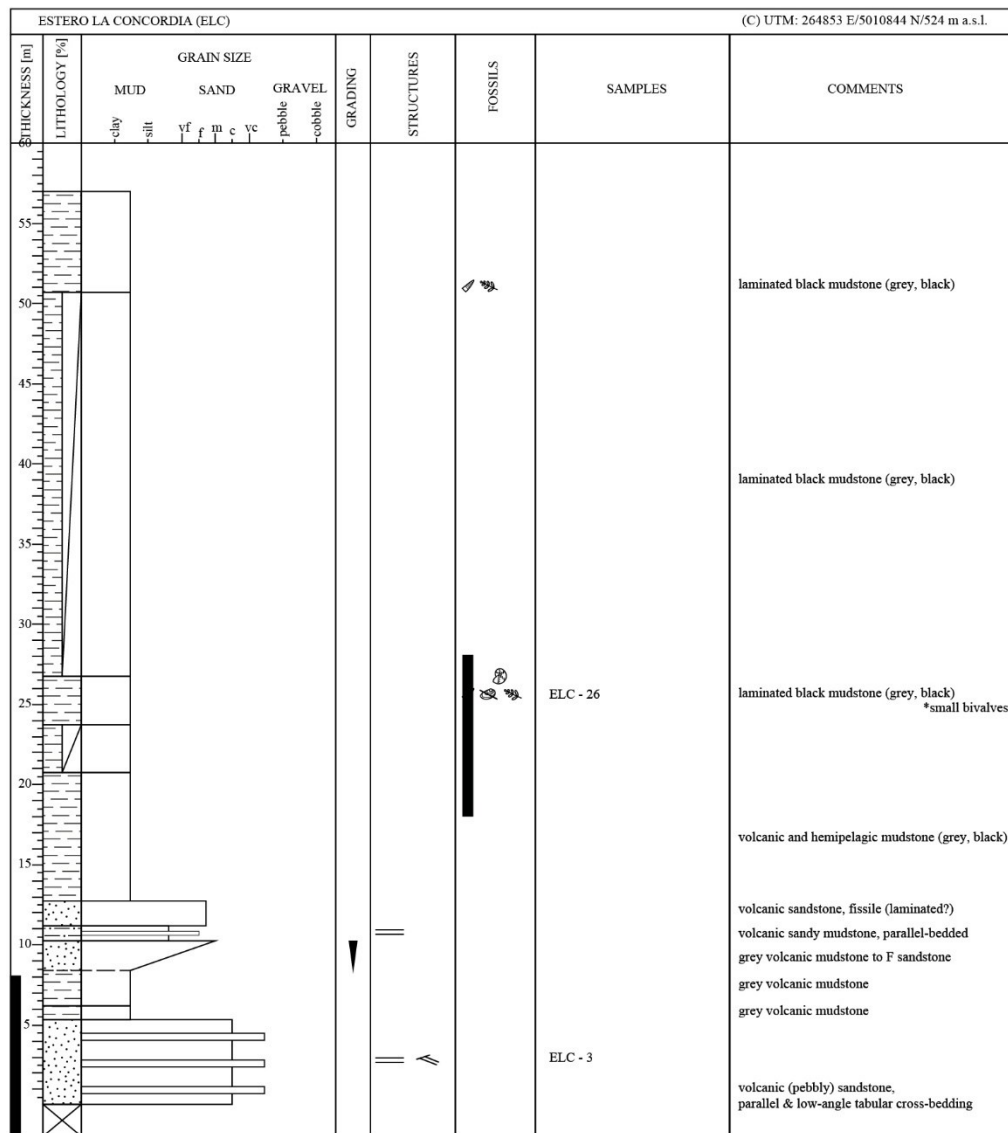
CASA DE BENJA (CDB)										(C) UTM: 729404 E/4951839 N/301 m a.s.l.		
THICKNESS [m]	LITHOLOGY [%]	GRAIN SIZE						GRADING	STRUCTURES	FOSSILS	SAMPLES	COMMENTS
		MUD		SAND			GRAVEL					
		-clay	-silt	v f	f m	c v	-pebble	-cobble				
60												
55												
50												
45												
40												
35												
30												
25												
20												
15												
10												
5												

CEMENTERIO (CMT)										(C) UTM: 730277 E/4949833 N/247 m a.s.l.				
THICKNESS [m]	LITHOLOGY [%]	GRAIN SIZE								GRADING	STRUCTURES	FOSSILS	SAMPLES	COMMENTS
		MUD		SAND			GRAVEL							
		-clay	-silt	vf	f	m	c	vc	-pebble	-cobble				
30														
25														
20														
15														
10														
5														

CERRO CINCHAO 1 (CCH1)										(C) UTM: 728047 E/4953914 N/290 m a.s.l.				
THICKNESS [m]	LITHOLOGY [%]	GRAIN SIZE								GRADING	STRUCTURES	FOSSILS	SAMPLES	COMMENTS
		MUD		SAND			GRAVEL							
		-clay	-silt	vf	f	m	c	vc	-pebble	-cobble				
30														
25														
20														
15														
10														
5														

CERRO CINCHAO 2 (CCH2)										(C) UTM: 728016 E/4953792 N/290 m a.s.l.				
THICKNESS [m]	LITHOLOGY [%]	GRAIN SIZE								GRADING	STRUCTURES	FOSSILS	SAMPLES	COMMENTS
		MUD		SAND				GRAVEL						
		-clay	-silt	vf	f	m	c	vc	-pebble	-cobble				
30														
25											0		CCH2 - 26	
20													CCH2 (F) - 20 R (ex - situ)	
15													CCH2 - 16.3	
10														
5													CCH2 - 5.7	

CRUCE LAGO ELIZALDE (CLE)										(C) UTM: 728416 E/4935244 N/402 m a.s.l.				
THICKNESS [m]	LITHOLOGY [%]	GRAIN SIZE								GRADING	STRUCTURES	FOSSILS	SAMPLES	COMMENTS
		MUD		SAND			GRAVEL							
		-clay	-silt	v	f	m	c	vc	-pebble	-cobble				
35														
30													CLE - 30.6	
25														
20													CLE - 20.1	
15													CLE - 15.8	
10													CLE - 13.8 CLE - 13.1	
5													CLE - 10	
													CLE - 0.9	



ESTERO SAN ANTONIO (ESA)										(C) UTM: 267789 E/5007784 N/ 790 m a.s.l.			
THICKNESS [m]	LITHOLOGY [%]	GRAIN SIZE						GRADING	STRUCTURES	FOSSILS	SAMPLES	COMMENTS	
		MUD		SAND			GRAVEL						
		-clay	-silt	vf	f	m	c	vc	-pebble	-cobble			
25													
20													
15													
10											ESA - 10	floatstone	
5											ESA - 6.65		
											ESA - 6.6 R	rudstone floatstone	
											ESA - 1.7	Oyster fragments, replaced by mineralization *Main mantle (mineralized)	

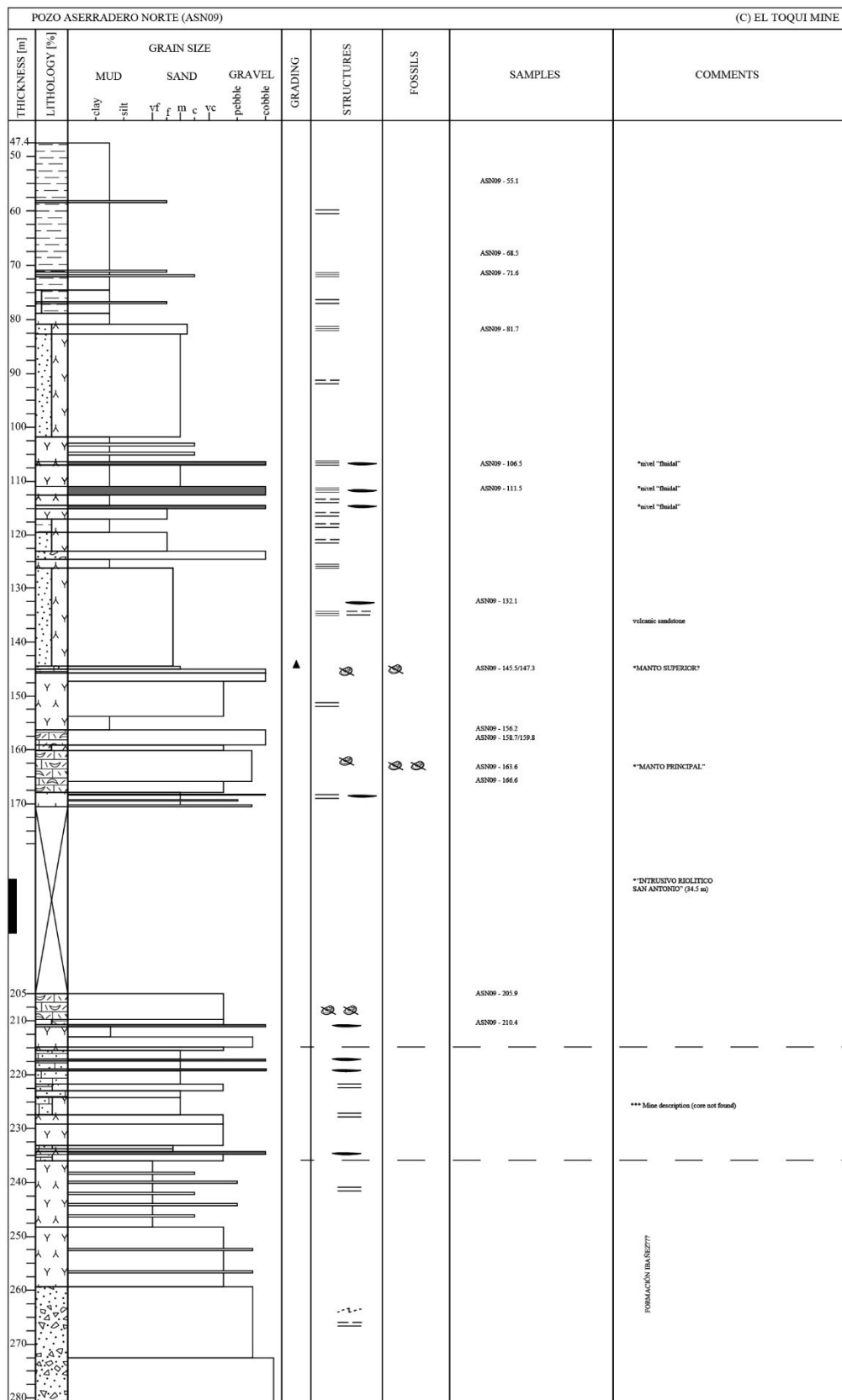
LA ROSITA (LRO)										(C) UTM: 727428 E/4940522 N/296 m a.s.l.				
THICKNESS [m]	LITHOLOGY [°a]	GRAIN SIZE								GRADING	STRUCTURES	FOSSILS	SAMPLES	COMMENTS
		MUD		SAND				GRAVEL						
		-clay	-silt	v f	f	m	c	v c	-pebble	-cobble				
20														
15												Ø ×	LRO - 16.5	
10												Ø	LRO - 13 LRO - 11.5	
5												Ø	LRO - 10	
												Ø	LRO - 8.5 LRO - 5.9	
												Ø	LRO - 3.9	
												Ø Ø	LRO - 1.7 LRO - 0.8	

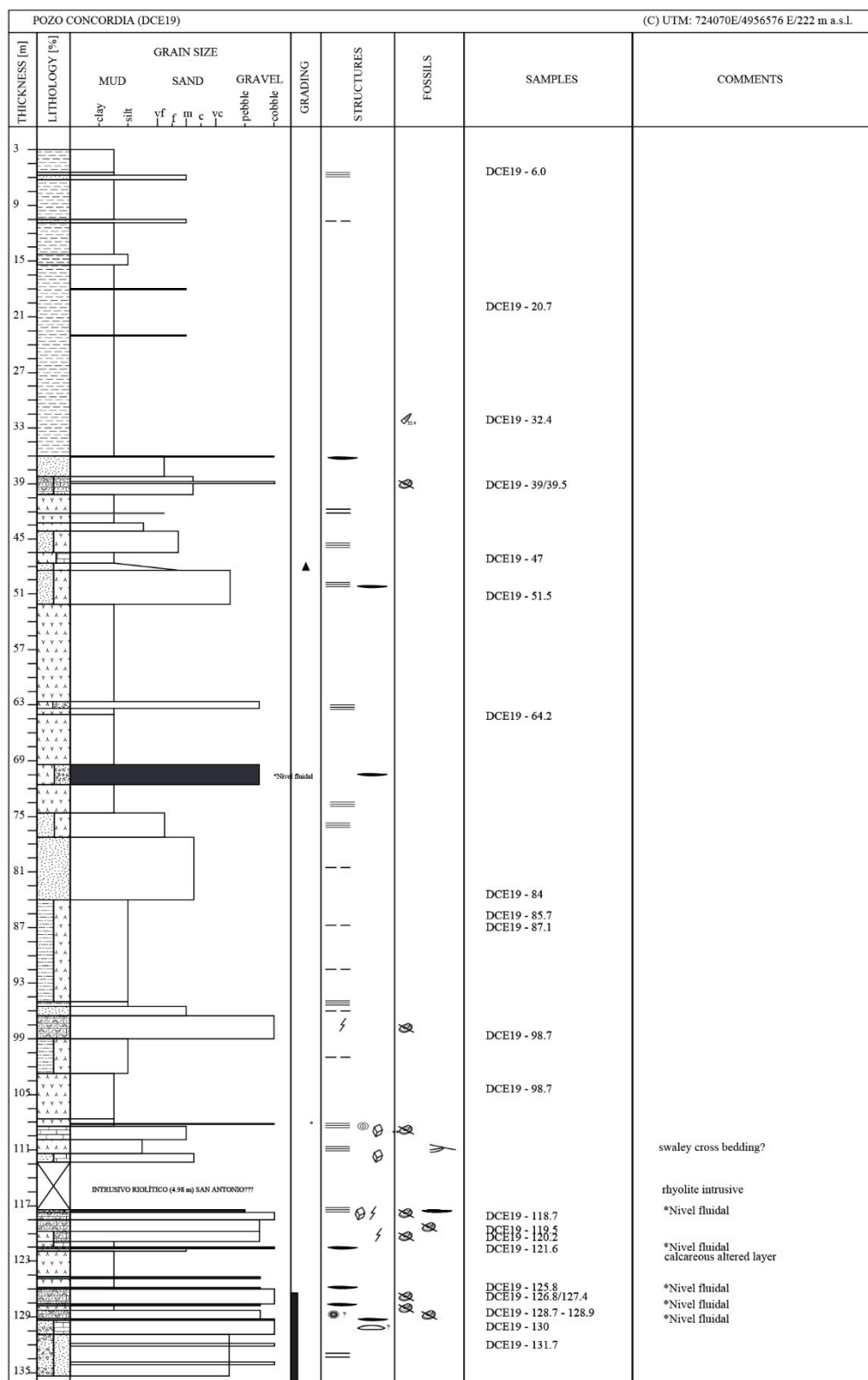
[illegible]

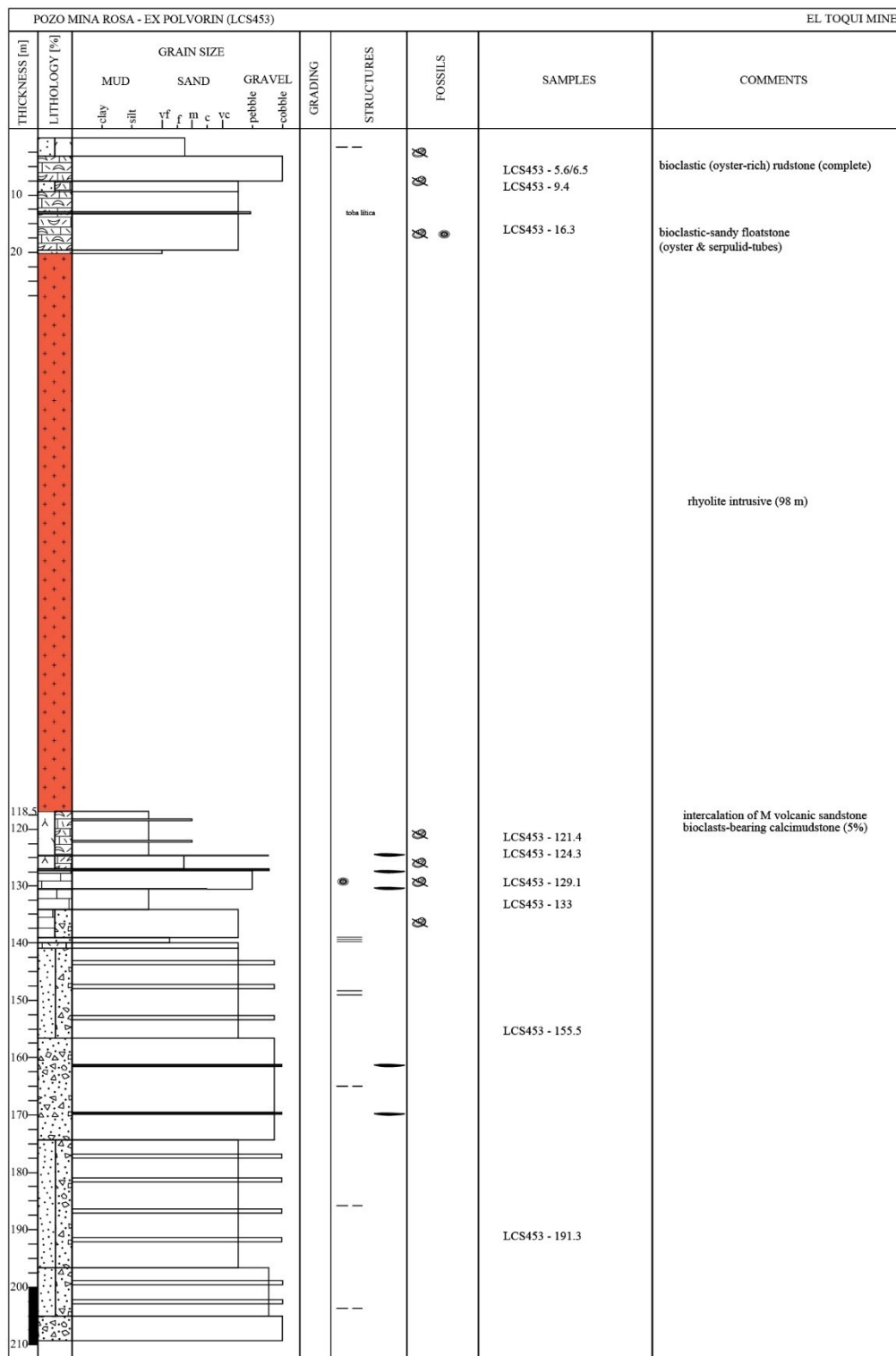
NIREHUAO NORTE (NIN)										(C) UTM: 285620 E/4988717 N/517 m a.s.l.		
THICKNESS [m]	LITHOLOGY [%]	GRAIN SIZE						GRADING	STRUCTURES	FOSSILS	SAMPLES	COMMENTS
		MUD		SAND			GRAVEL					
		clay	silt	vf	f	m	c	vc	pebble	cobble		
35												

(C) UTM: 728944E/4938097 N

MURALLA CHINA (MCH)														
THICKNESS [m]	LITHOLOGY [%]	GRAIN SIZE								GRADING	STRUCTURES	FOSSILS	SAMPLES	COMMENTS
		MUD		SAND				GRAVEL						
		clay	silt	vf	f	m	c	vc	pebble	cobble				
35													(M) MCH-34/34R	Several oyster, almost only biggest valves
30													(M) MCH-28.8	
													(M) MCH-27.8	
													(M) MCH-26.8	
													(M) MCH-25.8	
25													(M) MCH-24.8	
													(M) MCH-23.8	
													(M) MCH-22.8	
													(M) MCH-21.8	
													(M) MCH-20.8	Round & small fish teeth
20													(M) MCH-19.8	
													(M) MCH-18.8	
													(M) MCH-17.8	
													(M) MCH-16.8	
													(M) MCH-15.8	Big oyster - incomplete
15													(M) MCH-14.8/14.8F	Big oyster - almost complete
													(M) MCH-12.1	Wedge-shaped bed
10													(M) MCH-10.8	
													(M) MCH-7.1	
5														
													(M) MCH-3.1	
													(M) MCH-1.8/1.8F	oyster fragments
1													(M) MCH - 0.4	pebbly limestone - bioclastic









[illegible]

RIO NORTE (RNO)											(C) UTM: 724070E/4956576 E/222 m a.s.l.				
THICKNESS [m]	LITHOLOGY [%]	GRAIN SIZE									GRADING	STRUCTURES	FOSSILS	SAMPLES	COMMENTS
		MUD		SAND					GRAVEL						
		-clay	-silt	v f	f	m	c	v c	-pebble	-cobble					
25												==			
20												==			
15															
10															*wedge/acuflamiento
5												==		RNO - 6	

238

SALTO RIO POLUX 2 (SRP2)										(C) UTM: 728936 E/4937053 N/361 m a.s.l					
THICKNESS [m]	LITHOLOGY [%]	GRAIN SIZE									GRADING	STRUCTURES	FOSSILS	SAMPLES	COMMENTS
		MUD		SAND					GRAVEL						
		-clay	-silt	v f	f	m	e	v c	-pebble	-cobble					
20															
15															
10															
5															

9.2. Description of outcrops

Name of section: ALTO BAGUALES (ABA)							
Information related: (Monday 06.02.2017) (C) UTM: 724070E/4956576 E/222 m a.s.l. - ρ/μ = N60W/14 E. - Outcrop of black shale, sub-horizontal, weathered in exposition (orangey oxidation colour), brittle and fissile.							
Contact (top)	Sum. (top) Thick.	Thick-ness (m)	Lithology	Sedimentary structures	Fossils	Samples	Observations
Base: covered by vegetation, but is clear than this unit overlies the thick-bedded, volcanic rocks of the Ibáñez Group in the area, in an apparently slight angular unconformity. To the east is exposed the mountain range conforming the Patagonian Batholith.							
CN Layer 1	6	6	*OPC (outcrop partially covered) - Tuffaceous shales, grey (greenish-gray exposure), aphanitic texture. Very fragmented/several fractures. - fissile texture and a marked oxidation (FeOx patina).	Massive app.		(M) ABA - 3	(F) 304 Brittle and covered (first layer above the vegetation-covered zone)
CG Layer 2	7	1	VF tuffs (aphanitic txt), grey coloured but with orange patina, similar to previous but apparently with better preservation (more cemented?) Last 0.2-0.3 m F/MGr - cgr' - cl (apparently, layer rich in fine-middle accretionary lapilli)	Better preserved as adjacent beds. Bedding Accretionary lapilli at the top		(M) ABA - 6	- This bed stands out as a ledge (F) 305-306 (Guide Bed G1)
CN Layer 3	10.6	4.6	Tuffaceous shale, idem to the first layer. Dark grey colour (exposition light grey-yellowish). Brittle and, in some areas, wet and weathered (darker-coloured) - Small gravel clasts FGr (< 3 mm; < 5%), near the top of the bed.	Brittle exposure	- Small carbonaceous pieces mm-cm (< 2cm), near the top of the bed	(M) ABA-10	- Oxidation in patina, between and following the fracture joints (diagonal). Close relationship between carbonaceous areas and OxFé. (F) 307-309

CN Layer 4	11	0.4	Tuffaceous shale, grey-orange. Less weathered or with “concretional” areas.	Massive.		(M) ABA-11	Crops out as a small ledge
CN Layer 5	11.4	0.4	Sinuuous-laminated, tuffaceous siltstone	Sub-parallel lamination, sinuous near the top. - Possible ichnofossil.	- Small carbonaceous pieces mm-cm (< 1cm).	(M) ABA-11.2	Weathering less marked (better preservation) (F) 313-319
CN Layer 6	11.55	0.15	Siltstone-VF SS, light greenish gray.	Massive app.	- Small carbonaceous pieces mm-cm (< 1cm) (<5%)	(M) ABA-11.5	Brittle layer This layer may be good for dating with zircons (because of its grain-size)
CN Layer 7	12	0.45	VF SS, tuffaceous, grey.	Massive app.	- Small carbonaceous pieces mm-cm (< 1cm) (<5%)	(M) ABA-11.7	(F) 320-321 (boundary between siltstone and VF SS). Sandstone crops out as a ledge (Guide Bed G2)
CN Layer 8	14.2	2.2	*OPC Tuffaceous siltstone-VF SS. Fissile-weathered area.	Parallel lamination app. (fissile parting) Ovoidal nodules 1.5-3 cm, near the top.		(M) ABA-14.1	Covered by loose-sediment. Highly weathered bed
CN Layer 9	14.5	0.4	Siltstone, dark grey.	Sub-horizontal parting In the middle part: parallel lamination, discontinuous and slightly sinuous	Several bivalves, small, poorly preserved and compacted. Trigonidae indet.	(M) ABA-14.3	Bed rich in compacted/deformed bivalves: Bivalve valves, non-articulated. Concentric ornamentation. Fragments of this bed are usually found reworked downsection. (F) 322-331
CN Layer 10	16.3	1.8	Mudstone, dark grey. Lower (50 cm): dark grey, massive, but brittle	Fissile (long & sharp pieces).	Numerous non-articulated bivalves.	(M) ABA-15.8	(F) 332-353 -358 * (inoceramid-rich bed)

			Middle: Coquinite layer at 15.8 m (10 cm), and 16.2 m (5 cm). Upper (1 m): parallel lamination	Stepped bedding in layers 0.3 m thick.	Apparently, of the same sp.*		
CN Layer 11	17	0.7	Calcareous siltstone, grey. Last 0.3 m, more resistant to weathering (concretionary layer?).	Massive, blocky-parting in zones.	Bimodal: Several broken and complete bivalve shells (oysters; < 5 %).	(M) ABA-16.5C*	Guide Bed G3 strike/dip = 030/15 (SE). * rock + concretion (F) SAM_3253-3257 + IMG_0358-0361
CN Layer 12	18	1	Shale, grey-coloured. Last 10 cm with abundant OxFe.	Brittle Parallel lamination.	Small bivalves < 1.5 cm.	(M) ABA-17.5	
CN Layer 13	19.7	1.7	Shale, dark gray-gray-coloured.	Brittle	Small isolated gastropods (< 1 cm) and oyster fragments.		
CN Layer 14	20.2	0.5	Shale, grey	Parallel lamination.	Several snails/gastropods in horizontal position + possible reptile vertebrae.	(M) ABA-19.7 F (M) ABA-19.7	This bed is lighter-coloured than the adjacent beds
CN Layer 15	21.8	1.6	Shale, dark grey. OxFe patina between clasts/peds.	Fissile. Sphere-shaped concretions	Last 0.3 m: isolated gastropods and bivalves (< 1 cm).	(M) ABA-21.6 F (M) ABA-21.8 + concretion	
CN Layer 16	22.9	1.1	Shale, dark grey (exposition colour, light grey). Oxidation/weathering is more intense.	Fissile	Serpulids, reworked app. - Bivalves, articulated, in hz position.	(M) ABA-21.8F	
CN-E? Layer 17	24	1.1	1) * Mudstone, calcareous, dark grey (0.15 m), it crops out as a ledge/resistant layer.	Calcareous concretions in the middle layer.	* small gastropods + <i>Discinisca</i> sp.?	(M) ABA-23 (basal mudstone)	Guide bed G4. Basal mudstone and coquinite with a sharp contact

			2) - Coquinite, high bivalve concentration and big concretions (0.6 m) - Shale, grey, fissile (0.35)		1. Bivalves < 1 cm, Trigonidae indet. 2. Several kinds of bivalves. 3. Trigonidae indet, non-articulated.	(M) ABA-23.6 (concretion) (M) ABA-23.5 (sediment) (M) ABA- 23 F	
CN	25.5	1.5	Black shale idem. Very weathered.		Oyster.	(M) ABA(F)-24 – 25.6	
CN	25.7	0.2	Zone with calcareous concretions	Oval calcareous concretions up to 0.2 m.	Bivalve fossils.	(M) ABA(F) – 25.7 * (M) ABA – 25.6C	* Collected on December 2018 (rock + concretion)
CN	32.7	7	Black shale idem. Weathered (oxidation colour).				
CN	32.9	0.2	Zone with calcareous concretions.	Oval calcareous concretions up to 0.2 m.		* (M) ABA-32.7	* Collected on December 2018 (rock + concretion)
CN	41.9	9	Black shale idem.				
CN	42.1	0.2	Zone with calcareous concretions.	Calcareous concretions up to 0.4 m		* (M) ABA-42.1 * (M) ABA-42.9	* Collected on December 2018 (ABA-42.1: septarian concretion; ABA-42.9: calcareous layer)
CN	54.5	12.4	Black shale idem.			* (M) ABA-54.5	* Collected on December 2018 (rock + concretion)
CN	55.7	0.2	Zone with calcareous concretions.	Calcareous concretions up to 0.6 m, isolated.			
CN	57.7	3	Black shale idem.				
CN	57.8	0.1	Zone with calcareous concretions.	Calcareous concretions up to 0.1 m, isolated.			

CN	62.8	5	Black shale idem. - Concretions at 68 m.	Calcareous concretions up to 0.2 m. These are hollow.			
<p>END Section ABA.</p> <p>Top: erosive boundary with sandy-pebbly quaternary deposits, with soil development.</p> <p>(F) 3251 – 3274</p> <p>(C) UTM: 724127E/4956525 N/268 m a.s.l.</p>							

Name of section: ALTO BAGUALES NORTE (ABN) - directly before the bridge above the Baguales River							
Information related: (Sunday 17.01.2016) (C) UTM: 724358 E/4957395 N/219 m a.s.l. (WP 124) - $\rho/\mu = 040/10$ (SE) - dip/dipdir = 10/135							
Contact (top)	Sum. (top) Thick.	Thick-ness (m)	Lithology	Sedimentary structures	Fossils	Samples	Observations
Base: covered by the vegetation and intersected by the road. But, going down to the river level, crops out some isolated black shale outcrops. Therefore, it is assumed that the whole hillside is composed by this kind of rocks. (total thickness should be greater than measured).							
CN	6	6	Black shale, brittle. - First 2 m partly covered.				- This basal part is partly covered by the eroded sediment (black shale fragments, brittle)
CN	6.4	0.4	Aphanitic – MF grain size rock, possible igneous (sill? Tuff?). Colour light grey (fresh) and orangey (exposed).			(M) ABN – 6.3	- Sharp boundary between this bed and surrounding shale. Hypabyssal intrusive (sill)
CN	12	5.6	Black shale, fissile. - At 9 m, a bed of 0.4 m of calcareous shale/mudstones.	Possibly parallel lamination. - Calcareous concretions isolated < 10 cm	Bivalve fragments < 2 cm. Dispersed (<1 %)	(M) ABN (F) – 6.4 (M) ABN - 9	(F) 1309 – 1310 (concretions)
CN	13	1	Calcareous black shale, idem at 9 m. - It is exposed in beds up to 30 cm, although it is internally fissile.				
CN	23	10	Black shale idem.		Belemnites	(M) ABN (F) – 21.5 (M) ABN (F) - 22	- ρ (belemnites): 210 (21.5 m), 140 (22 m).
CN	25	2	Black shale idem. - Calcareous concretions dispersed.	- Calcareous concretions			

			- At 24.6 layer of tuffaceous sandstone (5 cm), very weathered.				
CN	26.2	1.2	Calcareous shale			(M) ABN – 25.5	
CN	41.2	15	Black shale idem			(M) ABN - 40	
CN	47.2	6	Black shale idem				
<p>END Section ABN</p> <p>Top: erosive boundary with Quaternary deposits. (C) UTM: 724386 E/4957325 N/ 284 m a.s.l.</p>							

Name of section: Cañadón Río Simpson 1 (CRS1)							
Information related: (Monday 11/01/16) - Outcrop located inside the Fundo San Carlos. (Family Bernabé – Ramírez) (C) UTM: 730678 E/4929350 N/352 m a.s.l.							
Contact (top)	Sum. (top) Thick.	Thick-ness (m)	Lithology	Sedimentary structures	Fossils	Samples	Observations
Base: starting the measure of the section above a sill level exposed in the river valley (being eroded by the river). Sandy and shaly layer < 1 m thick (different bedding), in the NE riverside of the Simpson River. $\rho/\mu = 315/29$ (NE) sandy bed with concretions.							
CN	2.2	2.2	Black shale, fissile, brittle	Ap. massive.		(M) CRS – 1.0	
CN	2.3	0.1	Calcareous shale (mudstone), light brown in colour (exposition)/dark grey (fresh)	Concretionary layer. Concretions present several herringbone-shaped structures (septarian?)	Bivalve fragment, isolated (< 1 cm).	(M) CRS – 2.2 (M) CRS – 2.1C* (M) CRS -2.2C*	* December 2018: ex samples CRS1-X13 (herringbone)/X15. Concretionary-calcareous layer, continuous.
CN	5.3	3.0	Black shale, fissile, brittle. 2 thin beds (lamina) of calcareous shale (mudstone) at 3.1 and 4.9 m.		Isolated belemnites at 0.4-0.5 m from the base. - Compacted ammonite	(M) CRS – 4.0 (M) CRS-2.7F* (M) CRS1(F)-2.7R	* December 2018: ex sample CRS1-X14F (belemnites) - Belemnites strike: 160; 120; 245; 270; 330 (2); 290; 060. * (M) CRS1(F)-2.7R: 3 oysters (gryphaeid-like) + 6 ammonite whorl-fragments
CN	5.35	0.05	Tuffaceous layer, F-M grain sized, light grey to orange in colour (high weathered). Floury texture.				- The entire outcrop has a remarkable deformed/faulted aspect. With sector with metric displacement (normal faulting). - The relationship between the lower shaly levels at the river, and the upper sandy level in the upper part of the hillside is unclear.
CN	5.8	0.5	Black shale (idem)				

CN	7.6	1.8	Black shale (idem)		Ammonite in-situ		(F) 860 – 865 (ammonite in-situ, inside brecciated block). (F) 853 – 859 (normal fault)
CN	7.9	0.3	<p>(GUIDE LEVEL – Thick superior)</p> <p>- (4 cm): C-VC sandstone, muddy matrix. Intercalation of 1 muddy lens/laminae of 0.6 cm thick., immediately over the lens, C SS. Inclined lamination (cross lamination?)</p> <p>- (3 cm): grey mudstone with parallel lamination. It finishes with a black mudstone layer, 3 mm thick.</p> <p>- (4 cm): Not always exposed. Concretionary horizon between muddy layer and upper sandstones.</p> <p>- (13 cm): Intercalation M and C SS in beds < 2 cm (avrg. 1 cm). Parallel lamination. CRS1-X16</p> <p>- (7 cm –upper) M-C crystal SS idem, but brittle and tuffaceous texture.</p> <p>- SS grey in colour, with ca. 20 % biotite.</p>	<p>Parallel bedding (overall)</p> <p>- Inclined-cross bedding? In the lower C-VC sandstone (35° al E)</p>		<p>(M) CRS – 7.7</p> <p>(M) CRS (F) – 8</p> <p>(M) CRS-8.0</p>	<p>* December 2018: sandy guide layer. Sample CRS-8.0 (ex CRS1-X16) was taken from the thicker succession in the middle (13 cm)- turbidites?</p> <p>(F) 719-726</p>
CN	12.2	4.3	<p>Black shale (idem)</p> <p>- Layer of M SS idem (no calcareous) 10 cm thick, at 9 m.</p> <p>- Layers of MF tuffaceous SS/tuff, 5 cm thick, white in colour, at 10.2 and 11 m.</p>			(M) CRS 11.8	
CN	12.35	0.15	C-grained SS, good sorting, poli, tuffaceous matrix. Weathered and brittle			<p>(M) CRS – 12.3</p> <p>(M) CRS-12.3</p>	<p>*December 2018: Next thick and relatively resistant white guide layer. Ex sample CRS1-X17.</p> <p>(F) 727-729</p>

CN	16	2.7	Black shale (idem). - Layers of F-M tuffaceous SS (5 cm thick) at 13.35, 14.45 and 16 m.	Septarian concretions at 13.4 m.		(M) CRS – 15.7 (M) CRS-13.4C	(F) 870 – 871 * December 2018: horizon with septarian concretions about 10 cm over the first tuffaceous layer. Ex sample CRS1-X18.
CN	18.1	2.1	Black shale (idem)	Calcareous concretions at 18.1 m, isolated.	Ammonites in concretions	(M) CRS (F) – 18* (M) CRS – 18.1 (M) CRS – 18C	- Concretions disposed subhorizontally, oval, up to 30 cm width and up to 1 m length. (F) 872 – 873 (concretions). * New findings on Fieldtrip 2017. * December 2018: Horizon with concretions, about 3 tuffaceous layer higher from the sample CRS1-X18. The concretions are about 2 m over the last tuffaceous horizon in this part of the outcrop (ex-sample CRS1-X19) (F) 730-732
CN	19.1	1	Black shale	Calcareous concretions at 19.1 m (idem), isolated	Fragmented ammonites and belemnites	(M) CRS (F) – 19.1	
CN	21.8	2.7	Black shale	Calcareous concretions at 20 and 21.8 m, isolated		(M) CRS (F) – 20*	- Septarian concretions, with radial, inner, carbonate veins. * New findings on Fieldtrip 2017.
CN	24.7	2.9	Black shale	Calcareous concretions at 22 and 24.7 m, isolated		(M) CRS (F) – 22*	- Concretions reduces size < 0.5 m. * New findings on Fieldtrip 2017.
CN	27.8	3.1	Black shale - Layer of F calcareous SS, weathered (10 cm thick). Light grey in colour, orange weathering exposition colour.				

	31.3	3.5	Black shale (idem)				
<p>END CRS (basal part), to the upper part, covered with vegetation. Continued next day. (C) UTM: 731138 E/4928134 N/366 m a.s.l.</p> <p>* Log continue next day (Tuesday 12.01.2016) - Outcrop of the same black shale with concretions of the previous level, after a covered zone. - Continue some meters in direction upstreams. (C) UTM: 731180 E/4928089 N/378 m a.s.l.</p>							
CC	38.2	6.9	Covered zone with vegetation and soil formation. Some non-in-situ of green SS blocks, with ichnofossils between bedding planes, have fallen in this area.				- $\rho/\mu = 340/20$ (E)
CN	43.8	5.6	Basal zone of the continuing previous measured section. - Black shale, brittle (fragments < 1cm and < 5 cm), fissile. - Sedimentary concretions at 39.3 m composed of calcareous mudstones, oval shape, isolated.	Ap. massive. Masked parallel lamination/bedding by the fissile texture - Sedimentary calcareous concretions (70 x 90 cm app.)		(M) CRS – 39.3 (M) CRS – 39.8 (M) CRS – 42.0	- Shale colour black to dark grey, in fracture planes orangey and between fissile fragments (exposure colour). (F) 892 – 896 (shale + concretions)
CN	43.85	0.05	Thin layer of M SS, light grey in colour to light orange (oxidated/weathered).	Ap. massive. Separable in horizontal planar layers.		(M) CRS – 43.8	
CN	46.8	3	Sandy shale, with clasts of MF –F size (sand) (app. 10% sand). Fissile, grey in colour.	Ap. massive.	Ammonite fragments	(M) CRS (F) – 44 (M) CRS - 46.8	
CN	49.8	3	Black shale (idem)			(M) CRS – 49.8	
CN	60.3	10.5	Covered section (rock gravitational debris)				

			Possibly black shale, as upside outcrops the same lithology.				
CN	63.3	3	Black shale, Concretions at 60. 8 m (< 15 cm)	Calcareous concretions		(M) CRS – 60.3 (M) CRS – 60.8 (M) CRS – 63.3	
CN	66.3	3	Black shale (idem), less weathered, brittle fragments are a bit bigger (cm in size) - At 64 m, layer (5 cm) of intercalation of shale with MF SS with MF, sinuous lamination	Layer with parallel sinuous lamination (bed 5 cm thick).		(M) CRS - 64	(F) 899 – 901 (shale with // lamination)
CN	69.3	3	Black shale (idem)		Carbonized plant fragments (20x 6 cm) - Ammonite	(M) CRS 69.3 (M) CRS1-68C* (M) CRS1-68F	(F) 902 – 905 (carbon) * December 2018: First level with big concretions in the upper part of the formation (near the contact), some septarian. (ex samples-CRS1-X01) (F) 648-652 (diciembre-2018)
CN	*(71.5) 72.8	3.5	Black shale, from this area, is exposed fissile but less brittle. From the last big concretion (71.5 m), <u>the outcrop is more resistant to weathering.</u> Possibly composition varies to mud-siltstone. - (5 cm) layer of M SS, grey, tuffaceous, highly weathered (OxFe) at 72.3 m. - Concretions at 71. 5 m (up to 30 cm) and at 72.8 m (up to 20 cm)	Calcareous concretions * From the last big concretion horizon (at 71.5 m), the outcrop is exposed very steep, and parallel lamination/bedding is more evident.	Diffuse parallel bedding	(M) CRS – 72.3 (M) CRS – 72.8 (M) CRS1-70CC (M) CRS1-71.5C (M) CRS1-72.2C (M) CRS1-72.3***	* 71.5 m -> last level of shelf mudstone (Katterfeld) (F) 906 – 913 (concretions + black shale + tuffaceous SS) * December 2018: Intermediate concretion area between the two big-sized concretions horizons. (F) 653-656 (diciembre-2018) * Last big concretion horizon, near the contact (71.5 m), some septarian. (F) 657-661 (ex samples-CRS1-X02, 03, 04, 05) *** Tuffaceous layer, weathered. (F) 670-671

* From this point, the sedimentary concretions start to flatten.							
CN	74.5 Up	1.7	Black shale-siltstone? steep outcrop. - Grey mudstones at 73.3 (0.4 m thick).	Parallel bedding. Internally diffuse lamination		(M) CRS1-73.3	Start of the transition Katterfeld-Apeleg at ca. 71.5 m (last horizon with big concretions) ***** Zona con estratificación paralela, niveles que resaltan como cornisa. * December 2018: Sampling of the grey mudstone layer, brittle and less resistant to weathering (concave surface). (ex samples-CRS1-X06) (F) 662-664; 672-674 (diciembre-2018)
CN	79.8 Up	5.3	Black shale-siltstone? steep outcrop. - Isolated concretions at 75.3 m (lenticular in shape) and at 76.7 m	Calcareous concretions		(M) CRS – 75.3 (M) CRS – 78.3 (M) CRS1-75.4C (M) CRS1-76.7C (M) CRS1-78C (M) CRS1-79.1C	(F) 914 – 916 (outcrop + grey shale) * December 2018: Relatively flat-oblate concretion area. Last concretions before the contact with the heterolithic area. (ex samples-CRS1-X07, 08, 09, 10) (F) 665-669 (F) 672-674 (X07) + 675-676 (X09) + 680-681(X10, uppermost part of the outcrop) (diciembre-2018)
*** Lithological change!!! Black shale to sandstones! (F) 678-679 contact laminated mudstone (prodelta) and heterolithic beds (distal delta front)							
CN	81.4	1.6	MF SS, possibly silty, in beds up to 12 cm (basal layer; avrg 6-7 cm), intercalated with fissile shale beds up to 3 cm. - SS greenish grey (glauconitic?), shale in dark grey.	Parallel and discontinuous lamination (observed in transversal section) – lenticular. Heterolithic bedding (? not sure)		(M) CRS – 80.2 (M) CRS1-80	(F) 929 – 930 (lamination). * December 2018: Sampling of the basal sandy layer. (ex sample-CRS1-X11) (F) 677-679 (stratigraphic contacts) + 682 + 705-706 (diciembre-2018)
*** From here start the zone of the big, resistant, greenish, sandy ledges (sand platforms). Typical from the Apeleg Fm.							
CN	83.3	1.9	***	Horizontal bedding.	Ichnofossils in the lower	(M) CRS – 81.8 (M) CRS1 - 82	*** Lithological change, contact with thick SS level.

			<ul style="list-style-type: none"> - Thick layer of F-M SS, greenish, in beds of 15 – 70 cm, with interlayers of fissile mudstone (< 5 cm) with ichnofossils in its basal bed boundary (upper face). - The interface between layers is formed by shale-silt, fissile sediment. (upper organic matter content). 		<p>upper face of the basal bed plane. Very numerous in this plane (60 - 70% fossils). Some are observed in the plane direct the boundary with the heterolithic bed, and 0.4 m upper.</p>		<ul style="list-style-type: none"> - These rocks are similar with the observed in the CLE section. (F) 1081 – 1088 (outcrop + ichnofossils) (F) 920 -928 - ρ/μ = 225/05 (SE) * December 2018: (ex sample-CRS1-X012) (F) 682-706 (diciembre-2018)
CN	84.5	1.2	<p>M SS, green – greenish grey in colour.</p> <ul style="list-style-type: none"> - Bedding in beds of 40 cm, with sharp to sinuous boundaries between beds. 	Parallel bedding		(M) CRS – 84.1	<ul style="list-style-type: none"> - Evidence of yellow-orangey mottles (weathering). (F) 1096 – 1100 (mottles/nodules + boundaries). (F) 1089 – 1095 (ex-situ block with ichnofossils).
CN	85.5	1	Intercalation of tabular beds of M SS (idem), up to 25 cm thick, with layers of MF SS/siltstone, grey in colour (up to 5 cm thick).	Parallel bedding			
CN	86.1	0.6	Green, F- M SS (glaucconitic?), tabular and massive (internally). Patina of mudstone/organic matter within bedding planes. (horizontal and slightly oblique)	Parallel bedding	<p>Ichnofossils in the top of this level, boundary with the next bed (40 % of the boundary covered).</p>		(F) 1101 – 1103 (ichnofossils in a ex-situ block).

CN	89.1	3	F-M SS (idem) with bed thickness between 0.5 – 0.7 m. At 89.8 m there is a 30 cm intercalation zone of F-M SS with mudstone lamina up to 0.3 cm thick.	Parallel bedding. Sharp to slightly sinuous bed boundaries.		(M) CRS – 89.1	
CN	92.1	3	F-M SS (idem).			(M) CRS – 92.1	
CN	95.1	3	F-M SS (idem). It breaks in layers of 3-5 cm (weathering?).	Parallel bedding? Or weathering?		(M) CRS - 95.1	(F) 951 – 954 (weathering or diffuse parallel bedding?)
CN	99.5	4.4	M SS (idem).			(M) CRS – 97.5	
<p>END Section CRS (15:45).</p> <p>(C) UTM: 731295 E/4927892 N/424 m a.s.l.</p> <p>*** Obs: Upper section very steep and hard to measure/access.</p>							

Name of section: CAÑADON RIO SIMPSON 3 (CRS3)							
Information related: (Wednesday 13.01.16, starting at 11:00). - Walking downstream after a zone where a sill is exposed at the river level with giant's kettle ("marmitas de gigante") morphologies, it crops out a remarkable wall of black shale in the river side northeastern riverside. - There is more than one event of intrusion, appreciated in the contact relationships between intrusives. The main body is more resistant within the outcrop, standing out as a sharp, tabular bed. (C) UTM: 730958 E/4928317 N/339 m a.s.l. (F) 998 – 1003 (sills between shale). - The shales are slightly dipping to the NE. - $\rho/\mu = 315/20$ (NE)							
Contact (top)	Sum. (top) Thick.	Thick-ness (m)	Lithology	Sedimentary structures	Fossils	Samples	Observations
Base: Covered by the river. Possibly cut by the sill/dike under, or shale continue below the river level. - Measure start over a 1 m thick sill.							
CN	3	3	Black shale, massive, brittle and fissile.	Big calcareous concretions in the first 0.5 m, dispersed.	Bioclasts < 1 cm at 1.5 m (ca. 5 %). Ammonites at 1.8 m. In-situ and ex-situ fossil (Gryphaea, ammonites).	(M) CRS3 – 0.1 (M) CRS3 (F) – 1.0 (M) CRS3 (F) – 1.5 (M) CRS3 (F) – 1.8 (M) CRS3 (F) – 1.8 R (M) CRS3 – 3.0* (M) CRS3-0.5C	- Pyr disseminated at 0.1 m. (F) 1126 – 1129 - Oval calcareous concretions similar to CRS3. They appear parallel to the bedding plane, in some parts covering up to 50 % of the bed surface. Are exposed in this way because of the hydraulic erosion of the river. - External mould of a big ammonite in concretion (14 cm whorl height). (F) 1149 – 1155 (concretions – fossils). (F) 1008 – 1011/1137 (fossil) * Finding in 2017. * December 2018: sampling of giant concretions, located in the base of the sedimentary log (ex-sample CRS1-X20). (F) 733-738

CN	6	3	Black shale (idem). - Isolated concretions at 3.2 m	Sedimentary concretions up to 0.3 x 0.6 m.	Carbon fragment (2 cm) at 4.5 (patina)	(M) CRS3 – 3.2 (M) CRS3 – 6.0	(F) 1130 – 1131 (concretions).
CN	9	3	Black shale (idem). - Sill at 7.1 m (1 m thick).	Sedimentary concretion, lenticular, at 8.8 m (1 m x 0.25 m), and at 9.0 m (30 cm)	Gryphaea at 9 m.	(M) CRS3 – 9.0 (sh) (M) CRS3 – 9.0 (cc)	- Intrusion of a sill, discontinuous, at 7.1 m (1 m thick x 20-30 m wide). (F) 1142 – 1148 (outcrop) (F) 1016 – 1018 (intrusive/sill).
CN	12	3	Black shale (idem).		Bioclasts (compacted bivalve fragments) < 0.5 cm (ca. 5 %). small pectinids (Entolium sp.)?	(M) CRS3 -12	* compare the pectinids with the ones from ABA (also Entolium sp.)
CN	15	3	Black shale (idem)		Bioclasts are less abundant (in traces).	(M) CRS3 - 15	
CN	18	3	Black shale (idem)	Oval concretions at 17.5 m (0.5 x 0.3 m)		(M) CRS3 – 17.5	
CN	19.2	1.2	Siltstone, black to dark grey in colour, resistant to weathering (no fissile).	App. massive	Gryphaea, belemnite	(M) CRS3 (F) – 18.2	(F) 1026 – 1031 (fossils) (F) 1036 – 1040 (outcrop)

*** Break of the section, due that the vegetation covers the outcrop.

- Upper correlative stratigraphical level reached to the SE, where crops out a black shale succession, below a thick succession of green sandstones.

END (first part):

(C) UTM: 730989 E/4928456 N/371 m a.s.l. (WP 80)

- Next description was measured ca. 200 m downstream, searching the last bed described, between the contact shale-siltstones.

START (second part):

(C) UTM: 731036 E/4928539 N/374 m a.s.l. (WP 81).

- At this point, the rock succession is reached almost completely, except from some parts covered with vegetation, the transition from black shale cropping out in the stream of the river to the green sandstones of the recent erosion surface. The boundary between both units is sharp and possibly gradual.

- $\rho/\mu = 205/10$ (SE)

(F) 1160 – 1163 (outcrop).

CN	24.2	5	Black shale (idem). - Layers of M SS, light grey in colour, orangey in exposition (weathering). These beds are ca. 4 cm thick and are exposed in 3 level in the basal half if this part, separated by 0.4 – 0.6 m.	Parallel bedding.		(M) CRS3 – 22.2	(F) 1164 - 1166
CN	24.8	0.6	M SS, light gray in colour, idem thin previous SS in last layer.	Ap. massive.		(M) CRS3 – 24.8	
CN	27.8	3	Black shale (idem). - M SS layers (idem), 5 cm thick, at 26 and 27.2 m.		Belemnite fragment at 25 m. Ammonite fragment at 27 m.	(M) CRS3 – 27.8	
CN	30.8	3	Black shale (idem).		Ammonite fragment at 30.3 m.	(M) CRS3 – 30.8	
CN	33.8	3	Black shale (idem). - Concretions at 32.1 m	Calcareous concretions up to 20 cm height.		(M) CRS3 – 33.8	
CN	36.8	3	Black shale (idem) - Concretions at 35.3 m	Calcareous concretions up to 0.6 m height		(M) CRS3 – 35.3 (M) CRS3 – 36.8	
CN	39.8	3	Black shale (idem) - Concretions at 39.8 m	Calcareous concretions up to 0.1 m height		(M) CRS3 – 39.8	
CN	42.8	3	Black shale (idem)			(M) CRS3 – 42.8	
CN	45.8	3	Black shale (idem)			(M) CRS3 – 45.8	

CN	49	3.2	Black shale (idem) - Concretions at 46.6 m	Calcareous concretions up to 25 cm height.	Ammonite	(M) CRS3 (F) – 46.6	
<p>END Section (part 2): (C) UTM: 731055 E/4928520 N/390 m a.s.l. (WP 092).</p> <p>START Section (part 3): - About 200 m downstream following the same level elevation level. (C) UTM: 731103 E/4928744 N/396 m a.s.l. (WP 095). Thursday 14.01.16 (Starting at 11:10)</p>							
CN	53.2	4.2	Covered section due to shale fragmentation and gravitational settling from the upper part. - Possibly same lithology as previous (black shale).		Ammonite fragments (ex- situ)	(M) CRS3 (F) – 50 R	
CC	57.7	4.5	Partially covered section. - Black shale, idem.		Ammonite and Trigonia fragments (ex- situ).	(M) CRS3 (F) – 57.7	
CN	66.7	9	- Partially covered section - Black shale, idem.		Ammonite fragments.		
<p>Starting of uncovered section. After part covered with scattered gravitational shale fragments. (C) UTM: 731138 E/4928711 N/406 m a.s.l. (F) Fallen block of SS with ichnofossils (Thalassinoides isp.)</p>							
CN	69.7	3	Black shale (idem)		Fragments of bivalve, ammonite, belemnite, carbon?	(M) CRS3 (F) – 69.7 (M) CRS3 – 69.7	
CN	72.7	3	Black shale, idem	Isolated concretions up to 0.3 m.	Ammonite and belemnite fragments.	(M) CRS3 (F) – 72.7	- Fossils with bad preservation. (F) 1197 – 199 (belemnite)
CN	75.7	3	Black shale idem - Concretions at 73.7 m	Calcareous concretions up to 0.5 m with	Ammonite fragments at 73.7, 74 and 75	(M) CRS3 (F) – 73.7	- Vertebra up to 2 cm diameter.

				ammonite fragments inside	m. within concretions Ichthyosaur vertebra at 75 m	(M) CRS3 (F) – 74 (M) CRS3 (F) – 75 (M) CRS3 – 75.7	
CN	76.8	1.1	Black shale, idem. - Concretions at 76.8 m	Calcareous concretions up to 0.4 - 0.5 m	Ammonite in concretion (compacted)	(M) CRS3 – 76.8 (M) CRS3 (F) – 76.8	
CN	79.8	3	Black shale, idem. - Zone with numerous calcareous concretions at 78.3 and 79.8 m.	Calcareous concretions up to 0.4 m.	Ammonite fragments within concretions.	(M) CRS3 (F) - 78.3 (M) CRS3 (F) – 79.8	
CN	82.8	3	Black shale, idem		Ammonite and belemnite fragments.	(M) CRS3 (F) – 81.3 (M) CRS3 (F) – 82.3	
CN	85.8	3	Black shale, idem - Layer of tuffaceous SS at 84.6 m (20 cm). - Concretions at 84.3 m	Calcareous concretions up to 0.4 m with ammonites.	Ammonite fragments within concretions.	(M) CRS3 – 85.8 (M) CRS3 (F) – 84.3	
CN	88.4	2.6	Black shale idem. - Concretions at 88.1 m - Layer of F-M SS, tuffaceous at 88.4 m (5 cm thick).	Calcareous concretions with ammonite and belemnite fragments.	Ammonite and belemnite fragments.	(M) CRS (F) – 88.1	
CN	97.4	9	Black shale idem. - Concretions each 1.5 – 2 m with ammonite fragments.	Calcareous concretions with ammonite fragments.	Ammonite fragments in concretions.	(M) CRS3 (F) – 88.7 (M) CRS3 (F) - 90 (M) CRS3 – 94.4	
CN	100.4	3	Black shale idem. - Concretions at 100.4 m	Calcareous concretions	Trigonia in-situ	(M) CRS3 (F) – 101.2	

CN	105.5	1.1	Black shale idem	Parallel lamination		(M) CRS3 – 105.5	Start transition to Apeleg Fm. (F) 1224 – 1228 (laminated shale).
CN	108.5	3	Starts with VF-F SS, greenish grey in colour, with parallel lamination with dark grey shale. (1.5 m). - Continue with intercalation of beds up to/circa 10 cm thick of F-M SS, green-grey colour, glauconitic? with levels of the same shaly beds up to 5-10 cm thick.	Parallel lamination. - Thickening-upwards succession.		(M) CRS3 - 107	
<p>*** Sharp boundary with overlying beds of F-M SS, greenish grey in colour (glauconitic?), app. Internally massive. Very similar to the sandy levels described in CRS1. (C) UTM: 731194 E/4928684 N/457 m a.s.l. (WP 105).</p> <p>*** Displacement following guide level (contact/boundary) towards the next point (continuation): (C) UTM: 731228 E/4928838 N/440 m a.s.l. (WP 106)</p>							
CN	120.5	12	F-M SS, greenish grey in colour, glauconitic? - Tabular bodies up to 0.7 m	App. Internally massive.	Ichnofossils between/within the bedding planes.	(M) CRS3 -114.7	
CN	128	7.5	F-M SS, idem. - Beds up to 3 cm, separated by a dark shaly boundary.	Parallel bedding in beds up to 3 cm.		(M) CRS3 - 125	- Bedding plane black to dark grey in colour (organic matter). (F) 1242 – 1244 (fine bedding). (F) 1229 – 1231 (outcrop)
<p>END Section CRS3.</p> <p>Top: Actual soil surface/grass+woods.</p> <p>(C) UTM: 731234 E/4928789 N/467 m a.s.l.</p>							

Name of section: ESTERO LA CONCORDIA (ELC)							
Information related: (Friday 22.01.2016)							
- Outcrop of black shale in the riverbanks of the La Concordia stream, in the base/riverbed, crops out rocks composed of calcareous sandstones.							
- $\rho/\mu = 230/25$ (NW)							
(C) UTM: 264853 E/5010844 N/524 m a.s.l.							
Contact (top)	Sum. (top) Thick.	Thick-ness (m)	Lithology	Sedimentary structures	Fossils	Samples	Observations
Base: Covered. Riverbed of the La Concordia stream, and downwards to the north, riverbed of El Toqui River.							
CN	5.4	5.4	C SS, colour grey, calcareous, abundant Qz (quartz-sandstone?). Beds up to 35 cm, some with sedimentary structures. - Intercalation with beds of VC to pebbly SS, with clasts up to 2 cm (prom: < 5 mm)	Parallel bedding. - Low angle tabular cross bedding (< 5°) (in pebbly SS).	Some ex-situ fossils transported by the river (ammonites and oyster fragments).	(M) ELC - 3	- Present mineralization of pyr + sph disseminated (1%) - Cxls ang to sub-red. Good to regular sorting.
CN	6.2	0.8	Mudstone, colour grey.	Fissile.			
CN	10.2	4	Mudstone idem, less fissile, beds more resistant to weathering. - To the top grades to F-M SS, bad sorting, colour grey, and over this to M SS, idem characteristics.	Inverse gradation.			
CN	11.2	1	Sandy mudstone, fissile, clasts sized F SS in a black matrix. - Intercalation with F SS in beds up to 5 cm.	Fissile - Parallel bedding.			
CN	12.7	1.5	F-M SS, colour light grey, fissile, poli.	Fissile (less grade than shale).			
CN	20.7	8	Black and grey shale.	Fissile Parallel bedding			- Weathered rocks with O _x Fe mineralization in patina.
CN	23.7	3	Covered section. Possibly black shale, because of the adjacent lithology.				

CN	26.7	3	Black to dark grey shale.	Fissile	Belemnites ex-situ and in-situ. - Small bivalves shells and plant impressions.	(M) ELC (F) -23 R (M) ELC (F) – 26 (M) ELC - 26	- Fissile, but less brittle. - Pyr mineralization between beds boundaries, patina < 1 mm thick.
CN	50.7	24	* PCO - In a similar or correlative direction crops out black shale in the riverbank.				- Outcrop is covered by quaternary, or extracted deposits to road construction near following the ρ/μ measured. But the lithology crops out in the riverbank very steep.
CN	57	6.3	Black shale, idem, separated in slaty plates. The shale is exposed softened and bright in some sedimentary planes (fillites?)		Belemnite of at least 2 species (2 different sizes) - Vegetal/plant impressions.	(M) ELC (F) – 50.7a (M) ELC (F) – 50.7b	(F) 1574 – 1595 (outcrop + fossils)
<p>END Section ELC. Top: covered by vegetation. (C) UTM: 264768 E/5010811 N/562 m a.s.l. (WP 157)</p>							

Name of section: ESTERO SAN ANTONIO (ESA)							
Information related: (Thursday 18.02.2016) - Log measured in the old entrance to San Antonio Mine, following an inner road in the Toqui District Mine, upstream of the Estero San Antonio (San Antonio Stream/River). This place is located in the NW hillside of the Cerro San Antonio. - (C) UTM: 267789 E/5007784 N/ 790 m (2016). - $\rho/\mu = 340/15$							
Contact (top)	Sum. (top) Thick.	Thick-ness (m)	Lithology	Sedimentary structures	Fossils	Samples	Observations
Base: rhyolite intrusive, light greenish grey to white. "Qz eyes up to 2 mm" (San Antonio Rhyolite Porphyry). It has been proved that this intrusive is a sill (laccolith), some drill cores have found bedded rocks under this thick intrusive. - Unconformable boundary (intrusive-sedimentary).							
CN-G	4.8	4.8	"Main mantle": Coquina replaced by mineralization (Bl + Pyr + Po), purple to orange colour.		Fossils components of the coquina, replaced by the skarn mineralization.	(M) ESA – 1.7	(F) 2077 – 2079 (outcrop) * The boundary between this mineralized area and the sterile upper limestone is very irregular and transitional.
* From here downwards, begin the sterile main mantle. Lower mineralization but almost all the samples are recrystallized.							
CG	5.3	0.5	Coquinite limestone layer with many fragments, apparently monospecific (oysters). Bioclastic up to 4-5 cm (5-10%) (avrg. 1-2 cm (30%)). - Mafic minerals or alteration spot M-C grain-sized (5%). Clast-supported; matrix conformed of calcimudstone and smaller bioclasts fragments.		Oyster fragments. Apparently, monospecific and non-incrusting.		* Layer (1) – dic.2018. (F) 178-180.
CG	5.8	0.5	Coquinite limestone, similar to previous bed. Higher amount of biggest bioclasts, with some almost complete (50-60%).		Oyster bioclasts, idem.		* Layer (2) – dic.2018 (F) 181-182

			- Clast-supported; matrix conformed of calcimudstone and smaller bioclasts fragments (1-2 cm).		- Serpulid tubes between bioclasts (0.5 cm diameter) (<5%).		
CG	6.1	0.3	Bioclastic limestone, smaller and very fragmented bioclasts 1-2.5 cm (15%), max 3 cm, bigger bioclasts < 5 %. Bigger bioclasts are more common in the basal area of the bed, as well as, serpulids. - Matrix-supported.	Calcite veins up to 1.7x5cm.	Oyster fragments. Serpulids, grouped and isolated (0.3 cm diameter).		* Layer (3) – dic.2018 (F) 183-185
CG	6.4	0.3	Bioclastic limestone, 60 % bioclasts, some of them almost complete and articulated, with sedimentary filling; also fragments (1-2 cm), some of them with bioerosion evidence.		Oyster (complete and fragmented). - Bioerosion.		* Layer (4) – dic.2018 (F) 183-205
CG	6.7	0.3	Bioclastic limestone (10-20%), smaller bioclasts, almost only serpulids (10-20%) and minor oyster fragments. Matrix-supported.	Diffuse rippled bedding.	Serpulids, isolated or grouped, up to 3.5 mm diameter. - Abundant oyster fragments.	(M) ESA –(F) – 6.5 (M) ESA – 6.6 (M) ESA (F) – 6.6 R	* Layer (5) – dic.2018 (F) 216 – 219 + 237-238 - Fossils percent varies between conglomerate levels 40-50 cm thick, with 20% fossils, to 50 – 60 % fossils. (F) 2091 – 2101 (coquina + oysters). ** Serpulids are more common in zones where the oysters are less abundant (10 – 20 %).
CG	6.9	0.3	Bioclastic limestone, big-sized oyster, most of them complete and articulated (30%), up to 8 cm. Matrix-supported.		Oyster articulated. - Serpulids (3-4 mm diameter).		* Layer (6) – dic.2018 (F) 220-227

CG	7.2	0.3	Bioclastic limestone (5 %bioclasts), fragmented oysters 2-3 cm, longer and flat fragments in a position +- parallel with the bedding.	Weathering formed a small tafoni < 10 cm.			* Layer (7) – dic.2018 (F) 228 -232
CN	7.28	0.08	Tuff, light grey	Massive	No fossils. Oyster lye in life position, over the upper surface of this layer.	(M) ESA – 6.65 + new sample taken in 2018.	* This layer was sampled for dating (dic.2018) (F) 233-240
CN	9.88	1.8	Coquinite limestone with big-sized oysters (50-60%), up to 11 cm.		Oysters apparently complete. Closed grouped, possibly self-incrusting.	(M) ESA (F) – 9.5	* Layer (8) – dic.2018 (F) 2108 – 2109 (limestones).
CN	9.95	0.07	Aphanitic, light grey tuff.	Massive			
CN	10.65	0.7	Coquinite, bioclastic limestone idem last layer, only separated by the thin aphanitic tuff.		Oysters apparently complete. Closed grouped, possibly self-incrusting.		* Layer (9) – dic.2018
CN	35.65	25	Pumiceous tuffs, banded/laminated, green to light green. - Lower part shows a succession of very fined bedded, aphanitic greenish tuffs. - To the upper part of this succession, intercalations of, lapilli and lithic tuffs up to gravel size (<	Banding/lamination. - Starts with very fine parallel bedding/lamination To the top, bedding is sinuous, possible cross-bedding?	-	(M) ESA – 10	(F) 2109 – 2131 (tuffs + boundary limestone-tuff).

			2 cm). Bedding is thicker, more marked and sinuous.				
*** (C) UTM: 267805 E/5007773 N/792 m a.s.l. (WP 173). (Boundary between limestones – tuffs, sampling of (M) ESA – 10).							
END Section ESA. (C) UTM: 267805 E/5007773 N/792 m a.s.l. (WP 174).							

Name of section: LA ROSITA (LRO)							
Information related: (Starting at 10:20) - (C) UTM: 727428 E/4940522 N/296 m. - $\rho/\mu = 105/13$ (SSW)							
Contact (top)	Sum. (top) Thick.	Thick-ness (m)	Lithology	Sedimentary structures	Fossils	Samples	Observations
Base: covered by vegetation							
CN	1.5	1.5	Pebbly SS to sandy CG, matrix formed of C-VC grained SS. Bad sorting, beds matrix-supported and clast-supported, with thicknesses up to 40 cm. - Gravel clast within 2 mm and 2.5 cm (media: 1 cm), sub-rounded to sub-angular, monomictic.	Diffuse parallel bedding	Fragmented bivalves (oysters), corals.	(M) LRO – 0.8 (M) LRO – 1.3	- Clasts composition: felsic igneous rock, cxls < 0.5 cm, pg massive and transparent, amp altered to chlorite. - Bioclasts of oysters, corals < 10 cm, poor packaged (empaquetados). - Sharp boundaries between layers due to a marked dominance of clasts in the conglomeratic layers. (F) 704 - 709
CN	1.85	0.35	Clast-supported conglomerate, whitish with grey matrix. - Felsic clasts, monomictic, greenish white in colour, up to 15 cm (media: 2-5 cm) (50%). - Bioclasts (30%)	Parallel bedding	Fragmented bivalves (oysters), corals (colonial).	(M) LRO – 1.7 (M) LRO (F) – 1.7	- Guide level (Conglomerate) - Oyster fragments up to 2 cm. Corals up to 0.5 cm. (F) 710 - 714/1029-1031/1021-1022-1024
CN	7.06	5.21	C-VC calcareous SS to pebbly SS, good to regular sorting, clast-supported.	Parallel bedding	Oyster fragments < 2 cm (media: 1 cm)	(M) LRO – 3.9 (M) LRO - 5.9	- Bed thickness 30-80 cm. - Clasts colour is greenish white. - Clasts size decreases to the upper part (< 3 cm).

			- Intercalation of sandy conglomerate to pebbly SS, matrix of C-VC SS (same lithology than previous level).		Carbon fragments at 5.9 m.		
<p>OBS:</p> <ul style="list-style-type: none"> - Approximately 30 m moving to the west of this point, there are big blocks of felsic igneous rocks (up to 1.7 m x 0.8 m). And these blocks are in a layer 0.8 m thick, stratigraphically below the pebbly sandstones. The composition of these blocks is the same as previously seen (felsic dominant). - Bioclastic fragments within the sandy conglomerate, which overlie the bed with igneous clasts. Oyster fragments of cm-size. - These blocks are probably correlated with the lower conglomeratic bed (1.5 -1.85). Does the thickness increase laterally to the west? - Are these rocks evidence of the boundary between Toqui and Ibañez formations? - Possible decreasing of thickness of the beds (wedging) to the west, slightly with a dipping of 5°. <p>(F) 1042-1053 (outcrop – blocks)</p> <p>(M) LRO – 2.0 (just over the contact with the big blocks)</p>							
CN	8.5	9.45	Sandy CG with clasts < 2 cm (media 1 cm). Matrix supported with same igneous felsic clasts.	Parallel bedding	Bioclastic fragments.	(M) LRO – 8.5	- The bioclastic content reduces: Oyster fragments < 2 cm (< 10%). - Bed thickness varies between 0.3 – 1 m.
CN	10	1.5	Same lithology as previous level, intercalated with pebbly SS, VC SS in matrix, calcareous.	Parallel bedding	Bioclastic fragments	(M) LRO – 10	- Matrix of VC SS (0.2 – 0.3 mm). - Beds thickness between 0.3 -1 m.
CN	15.5	5.5	F grained conglomerate, clast up to 4 mm. Same lithology as previous. - Clasts light green in colour, up to 1 cm, sub-rounded and calcareous matrix.	Parallel bedding	Bioclastic fragments (< 5 %)	(M) LRO – 11.5 (M) LRO – 13	- To the upper part bed thickness varies between 30 - 50 cm. - Beds thickness between 0.3 -1 m.
CN	17	1.5	Grain size decrease to C-VC SS, in part pebbly SS, with greater matrix percent (40 %).	Parallel bedding	Bioclastic fragments. Belemnite and oyster fragment.	(M) LRO – 16.5 (M) LRO (F) – 16.5	
<p>END Section LRO.</p> <p>(C) 727349 E/4940512N/337 m a.s.l.</p>							

Name of section: MURALLA CHINA (MCH)							
Information related: Outcrop of bedded limestones, in the higher part of the Muralla China area, in the northern flank of the remarkable flat-topped sill. UTM: 728944E/4938097 N (18G). Strike/dip = 060/20 (SE) limestones.							
Contact (top)	Sum. (top) Thick.	Thick-ness (m)	Lithology	Sedimentary structures	Fossils	Samples	Observations
Base: Ibáñez Group, volcanic (tuffaceous) rocks with light grey colours. The direct boundary is masked by loose sediment and vegetal coverage. Is it possible to observe an apparent concordant boundary from the road, however, the presence of exotic volcanic clasts could be evidence of reworking-erosive processes.							
CN-S	0.7	0.7	Sandy-pebbly limestone, bioclastic, purplish gray. BC oysters. VC, light whitish green, < 2 cm (ca. 10%).	Subtle parallel bedding, in beds ca. 0.3 m thick.	Oyster fragments < 2 cm. (avrg. 1 cm) (ca. 50%), with some bigger, isolated fragments. - Coal fragments < 1cm (< 1 %).	(M) MCH -0.4,	- Bigger oyster and smaller clasts show a horizontal position, conformably with the bedding. (F) 39-44.
CN	2.4	1.7	Pebbly limestone, bioclastic (oyster fragments). Volcanic clasts idem previous (< 1cm).	Diffuse parallel bedding 0.2-0.3 m thick.	Oyster fragments (< 0.5 cm), as well as, disarticulated valves. (< 9 cm).	(M) MCH-1.8/1.8 F.	* Crops out as a ledge, with round margin. (F) 45-51
CN-S	5.1	2.7	Pebbly-bioclastic limestone, brownish gray (gray in exposure). Bioclasts < 1 cm. FLV, sharp-shaped (low roundness) ca. 1 cm.	Diffuse sinuous bedding, in 15-20 cm thick beds*.		(M) MCH-3.1	* Symmetric ripples, with variable lambda (50-90 cm), towards the upper part, the lambda is lower (20-30cm). (F) 52-60
Succession (repeated +- in a homogeneous manner, without great lithological changes). Sampling each 2-3 m. Diffuse sinuous structures are still preserved, between diffuse bedding ca. 0.3 m thick. Almost continuous tafoni layers, indicate bed boundaries.							

CN	8.1	3.0	Bioclastic limestone, with oyster fragments.	Parallel bedding 0.3 m	Oyster fragments.	(M) MCH-7.1	(F) 061-073
CN	10.1-11.7	2.0	Bioclastic limestone, with oyster fragments.	Parallel bedding 0.3-0.4 m - Diffuse sinuous bedding	Oyster fragments	(M) MCH-10.8	(F) 074-078
CN	12.8	1.0-2.7 (wedge)	***Wedge-shaped bed. Thicker to the south (2.7 m). Bioclastic limestone. - Apparently, clastic composition is richer to the south (FLV).	Diffuse parallel bedding (0.2 m). To the south, appear massive.		(M) MCH-12.1	* Sample was taken in the thickest area. (F) 079-090
CG	14.8	2.0	M-C Sandy limestone, FLV < 1mm (< 5 %), bioclasts < 1 cm; avrg. < 2 mm (5-10%).		- Big oyster (isolated) - Small bivalve - Bioclasts – fragmented	(M) MCH-14.8/F	*** Oyster ex-situ, both valves, found in oblique position, with hinge point to the top of the bed. (F) 150-154+158-159
	15.8	1.0	M calcareous sandstone, sandy limestone. FLV <2- mm (5-7%). Bioclasts < 3 mm (<5%)	Diffuse parallel bedding 0.4 m. Laterally is exposed clearly. Last 0.7 m single bed.	Ichnofossil (ex situ)	(M) MCH-15.8 (M) MCH - 15.4	(F) 092-094
	16.8	1.0	M –C sandy limestone. FLV <2- mm (5-7%). Bioclasts < 3 mm (<5%)			(M) MCH-16.8	
	17.8	1.0	M sandy limestone. FLV <2- mm (5-7%). Bioclasts < 3 mm (<5%)			(M) MCH-17.8	
	18.8	1.0	C sandy limestone. FLV <2- mm (5-7%). Bioclasts < 3 mm (<5%)			(M) MCH-18.8	
	19.8	1.0	F-M sandy limestone. FLV <2- mm (7%). Bioclasts non-observed.			(M) MCH-19.8	

	20.8	1.0	C sandy bioclastic limestone. FLV ca. 2- mm (7%). Bioclasts < 2 cm, avrg <0.5cm (ca. 20%)		Possible fish teeth. <i>Pogonias?</i> sp.	(M) MCH-20.8	* Rounded, very small fish teeth (Pycnodontidae indet.)
	21.8	1.0	C pebbly bioclastic limestone. FLV <7 mm; avrg 3mm (5%). Bioclasts < 5mm (10%)			(M) MCH-21.8	
	22.8	1.0	M sandy bioclastic limestone. FLV < 2- mm (<5%). Bioclasts < 3-4 mm, avrg <0.5cm (ca. 10%)			(M) MCH-22.8	
	23.8	1.0	M-C sandy bioclastic limestone. FLV < 2- mm (<5%). Bioclasts < 0.5 cm, avrg <1-2mm (ca. 10%)		Small bivalves, disarticulate, complete.	(M) MCH-23.8	
	24.8	1.0	C pebbly bioclastic limestone. FLV < 5mm; avrg 1-2 mm (<5%). Bioclasts < 0.5 cm, avrg <1-2mm (ca. 10%)			(M) MCH-24.8	
	25.8	1.0	C pebbly bioclastic limestone. FLV < 1cm; avrg 1-2 mm (<5%). Bioclasts < 0.7 cm, avrg <2mm (ca. 10%)			(M) MCH-25.8	
	26.8	1.0	C pebbly bioclastic limestone. FLV < 1.7cm; avrg 0.5-1cm (<5%). Bioclasts < 1 cm, avrg 5mm (ca. 10%)			(M) MCH-26.8	
	27.8	1.0	C pebbly bioclastic limestone. FLV < 1.7cm; avrg 0.5-1cm (<5%). Bioclasts < 1 cm, avrg 5mm (ca. 10%)		Small bivalves, disarticulated, complete.	(M) MCH-27.8 (M) MCH-27.8	
CN	29.8	2.0	Sandy-pebbly limestone, purplish gray, bioclasts < 1.5 cm, avrg 1 mm (C-VC sand to fine gravel sized). FLV <2-4 mm (ca. 5%)		Oyster fragments	(M) MCH-35.8 (M) MCH-29.8	Last bed under the layer with entire oyster fossils.

CN	31.5	0.9	Pebbly limestone to calcareous conglomerate, with FLV up to 5 mm and bioclastic fragments up to 2 cm (avrg. < 1 cm). - FLV accumulate in lens-shaped structures, with diffuse boundaries and 10 cm thick.	Internal parallel bedding, in layers 0.2-0.35 m, with a sharp and sinuous margin*.	Isolated oyster 8-10 cm.	(M) MCH-36 F (M) MCH-30.8 (M) MCH-30	* Ripples of the sinuous boundary with lambda 0.2-0.3 m. (F) 115-118 + 142-143
CN	32.4	1.1	VC calcareous sandstone, idem colour – with a dominance of greenish FLV (ca. 60 %) with whitish alteration. Bioclastic fragments (mm-sized).				
CN	33.2	1.4	Conglomeratic calcareous sandstone, with sandy conglomerate lenses (ca. 0.2 m thick) and diffuse margins.		* Complete oyster specimens and fragments (app. same sp.) (ca. 5 %)- + 1 belemnite. - Ichnofossils indet. - Coal fragments (mm-cm) up to dm (ex-situ).	(M) MCH-33/33F (M) MCH-33	(F) 119-141 Obs: - C-VC (2-3 mm) sand formed by FLV whitish-green clasts, monomictic. These are isolated or in lenses with gradual/diffuse margins, clast-to matrix supported. * Almost only disarticulated and isolated biggest valves, concave, filled with sedimentary matrix, in a upwards concave position-U.
END Section MCH. UTM: 729006E/4938099N.							

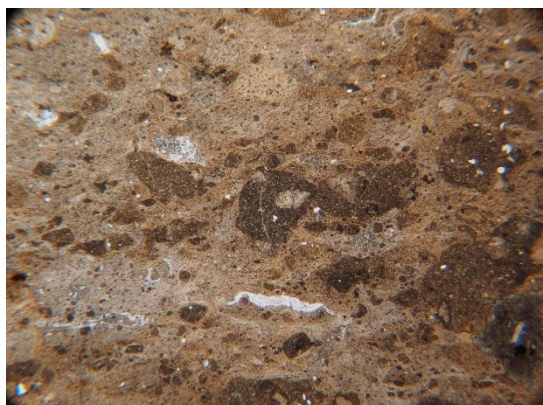
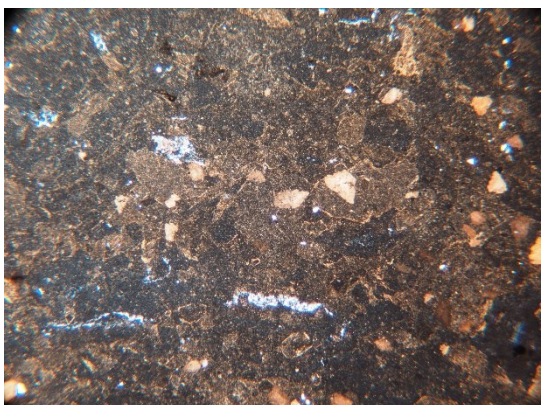
Name of section: PUENTE RIO BAGUALES (PRB)							
Information related: It crops out besides the road between Coyhaique and Aysén, on both sides, just crossing the bridge over the Baguales River. - UTM: 723900E/4957542N (18G).							
Contact (top)	Sum. (top) Thick.	Thick-ness (m)	Lithology	Sedimentary structures	Fossils	Samples	Observations
Base: These successions overlie the thick and well stratified rocks assigned to the Ibañez Group, these are well exposed in the lower area, near the riverbeds of the nearby rivers and creeks (especially in the Simpson-Baguales confluence). The basal contact is covered by vegetation, but it seems to be concordant (even when the lithological changes & alteration is quite noticeable).							
CN	2.6	2.6	Very fine-grained tuffaceous sandstone, pale-light gray, with scattered diffuse gray spots. Irregular, black and flat lenses, concordant (fiammes?), not very common, but noticeable.			(M) PRB – 1.0 D* (M) PRB – 1.5	* Sample collected for dating (tuff).
CN	4.4	1.8	VF pumiceous tuff (or tuffaceous mudstone?), grey. - Presence of scattered anhedral pyr (ca. 1 cm). - Several fractures with OxFE patina.	Fissile. Reniform and oblate concretions (4.5 cm diameter).		(M) PRB – 3.0 + C	Sample includes small reniform concretion
CN	5.0	0.6	VF tuffaceous sandstone, light gray, with dark grey circular nodules (2mm-1.5 cm). The nodules are observed in the central 0.3 m (less brittle).			(M) PRB – 4.7	
CN	10.0	5.0	Tuffaceous mudstone, grey. OxFE in patina			(M) PRB -7.0	
CN	10.4	0.4	Ash-tuff, light grey.	Massive		(M) PRB – 10.2	It crops out as a ledge.
CN	15.4	5.0	Ash-tuff, grey. Brittle, idem as bed 5-10 m. Very fractured, with OxFE in patina.			-	

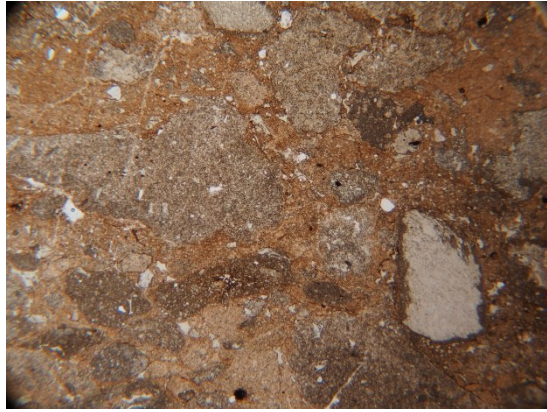
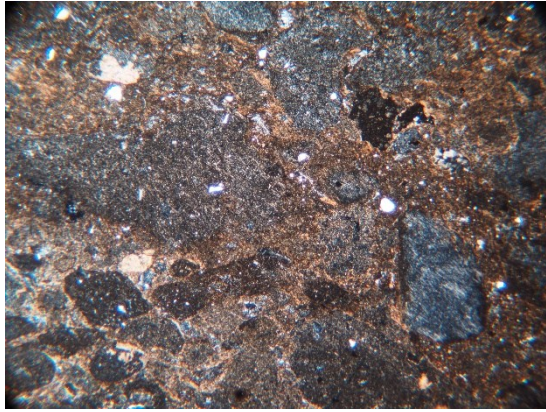
Top: Underlie Quaternary alluvial deposits with an erosive contact.

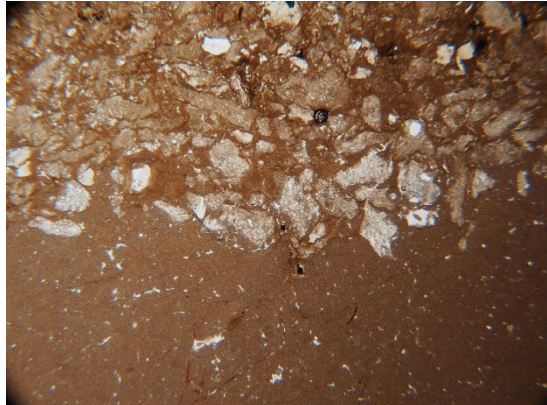
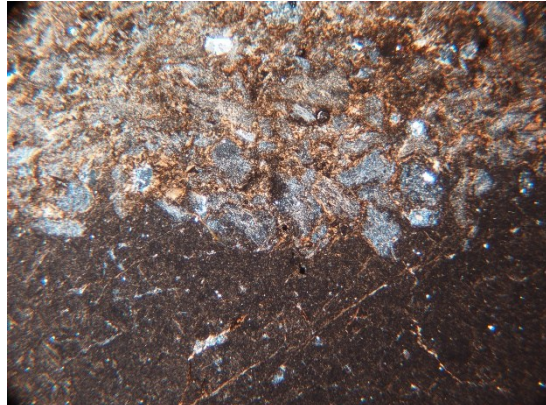
Name of section: SALTO RIO POLUX 2 (SRP2)							
Information related: - Outcrop located just before the crossroad to “El Fraile – Lago Frio”, coming from Coyhaique, in the beginning of the sharp slope turn. - (C) UTM: 728936 E/4937053 N/361 m a.s.l. (base not exposed). - $\rho/\mu = 037/10$ E; $045/11$ SE.							
Contact (top)	Sum. (top) Thickness	Thick-ness (m)	Lithology	Sedimentary structures	Fossils	Samples	Observations
- Base: covered by vegetation. It is possible to reach until the road. Maybe this lithologies continuous below to the Pólux River valley, but the land is covered (except in the waterfall, where black shale crops out below a sill)							
CN	0.5	0.5	Dark grey-black, bioclastic limestone. Grain size VF.	Apparently massive.	Numerous bioclastic fragments.		- Outcrop partially covered. - Bioclastic fragments < 3 mm (50 %)
CN	2.2	1.7	Same lithology than previous level. Limestone matrix VF in grain size, muddy appearance, with high organic matter (odor)		Plenty of invertebrate fragments. Mesoscopic rests of belemnites, <i>Gryphaea</i> , bivalves, echinoderm spines.	(M) SRP2 – 0.6 (M) SRP2 (F) – 0.8 (M) SRP2 – 1.7	- Possible bedding with bed thickness of 40 – 70 cm. - Some <i>Gryphaea</i> specimens only have 1 valve have been filled with sediment (reworking). - Belemnites (ρ): 065 (reverse)/105/035 (reverse)/095/075/090/068 (F) 639 – 641 (outcrop)/ 645 - 649
CN (S)	2.55	0.35	Same lithology than previous level.		Numerous bioclastic fragments.		- Bioclasts are smaller (2 mm) and have a more crystalline appearance. - Boundary with the previous bed has a muddy composition.
CN	5.15	2.6	Calcareous mudstone – Muddy limestone		Numerous bioclastic fragments.	(M) SRP2 (F) – 2.6	- Bioclastic fragments < 2 mm (50 %). - <i>Gryphaea</i> fossils are placed concave-up. - Belemnites (ρ): 190


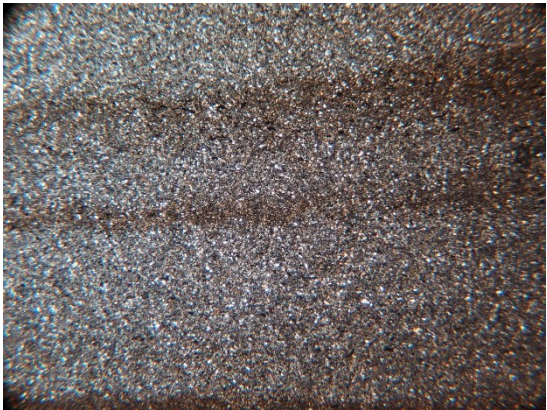
					Mesoscopic fossils: <i>Gryphaea</i> , belemnite (lower part).	(M) SRP2 (F) – 2.7 (M) SRP2 (F) – 3.2 (M) SRP2 – 4.2	- Bed thickness between 10 – 40 cm, fissile & brittle, more resistant in the upper part.
CN	5.45	0.3	Grey sandy limestone; with C-VC grain size clasts (40 – 50%).			(M) SRP2 – 5.45 (M) SRP2 (F) – 5.45	- Mud % decreases in comparison with the previous level (harder exposure). - <i>Gryphaea</i> fossil.
CN	5.85	0.4	Intercalation of whitish, M sized, SS with dark grey LS. Green crystal in the SS (glauconite?)	Parallel bedding.	<i>Gryphaea</i> .	(M) SRP2 – 5.85 (D)	- Bed thickness up to 5 cm.
CN	6.05	0.2	Black bioclastic limestone.	Ap. massive	Numerous bioclastic fragments.	(M) SRP2 – 6	- Bioclastic fragments < 2 mm (50 %)
CN	7.25	1.2	M grain size, calcareous SS.	Parallel bedding. Massive (internally)		(M) SRP2 – 7.1	- Bed thickness variable between 10 – 20 cm. (F) 667 – 771 (panoramic)
CN	9.15	1.9	Intercalation of grey, hard limestones with black, fissile limestones. (shales?)	Bed thickness decreasing to upper part.		(M) SRP2 – 7.5	- Bed thickness start with 28 (lower part) to 6 cm (upper part). - Weathered black LS very similar with the previous bioclastic levels.
CN	14.15	5	Greenish – brownish sill, with amphiboles (3 mm approx.) and pyroxenes < 1mm. Aphanitic texture.			(M) SRP2 – 9	*** - The sill apparently form part of the “Muralla China”, a significant subhorizontal intrusive body cropping out near the area of study.
CN	15.35	1.2	Limestones (idem)				***
CE	16.55	1.2	Sill (idem)				***
<p>END Section SRP2.</p> <p>*** For safety reasons, the thickness of the last 3 beds was estimated using trigonometry.</p> <p>- Top: Weathering surface (recent), covered with vegetation.</p> <p>(C) UTM: 728968 E/4937043 N/368 m a.s.l.</p>							

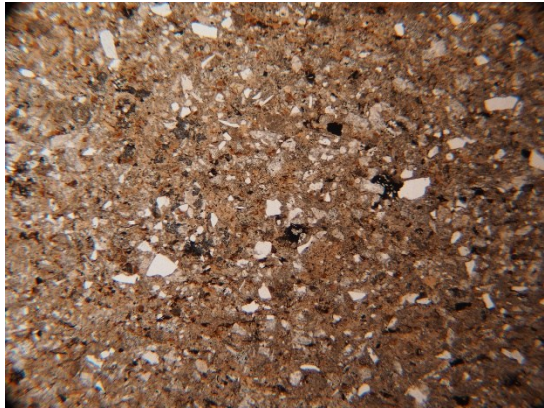
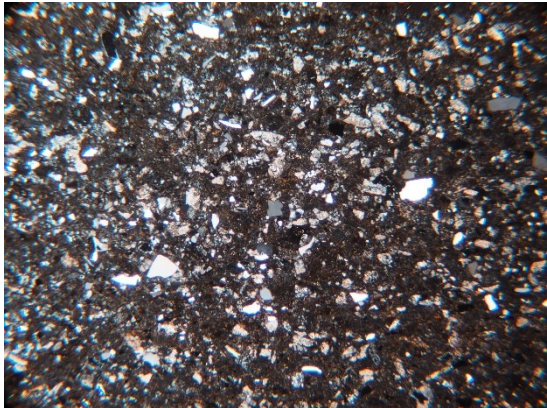
9.3. Thin sections descriptions



Sample: PRB-1.5		Locality: Puente Río Baguales (PRB)	
NP		NX	
			
		<div>2 mm</div>	
Composition:	Volcaniclastic		
Classification:	M-C tuffaceous muddy sandstone, minor pebbly.		
Framework:	<p>1) LVF (Lithic Volcanic Fragments): (20-30%), dark-brown-colored (minor pale-colored), mono-oligomictic, subang-subred (most subround-round, minor “rugged”), regular-sorted. Coarse-ash sized altered tuff clasts, apparently felsitic texture (scarce porphyritic); fragments of lapilli-sized, reworked vitreous tuffs, bearing silt- to F sand-sized volcanic Qz (1%) and subround pumice (<1%).</p> <p>2) Volcanic Qz: F-M sand-sized</p> <p>3) Pumice fragments: F-C ash-sized</p>		
Matrix:	Fine-ash (dev)		
Structures:	<p>Diffuse parallel lamination, inferred by compaction and aligned “fiamme”</p> <p>Fiamme texture, formed by elongated and rugged areas with a granophyric texture of Qz – Kfel (very small grains). These fiamme are sometimes associated with relict devitrified pumice.</p>		
Alteration/Observations:	<p>A: Volcanic clasts: devitrified +- illite. Some displaying illite in margins (formed by several fragments? – armoured lapilli?</p> <p>Some isolated small-sized clasts displays a devitrified margin, possibly “chilled”</p> <p>Some areas display closed-spaced clasts -> “jigsaw” texture?</p>		
Interpretation:	Remobilized hyaloclastite? Texture is similar to the “Subaqueously (shallow) emplaced pyroclastic flow deposits of the Pitts Head Tuff” (McPhie et al., 1993; p. 139)		

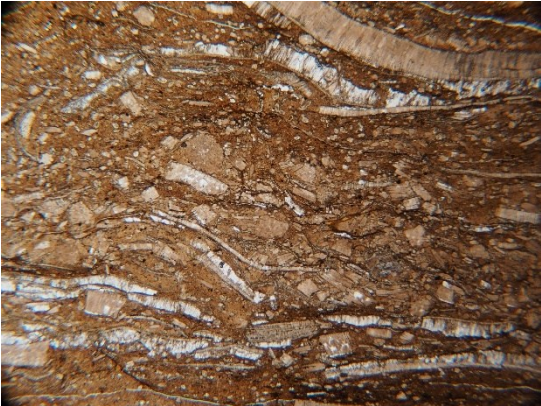
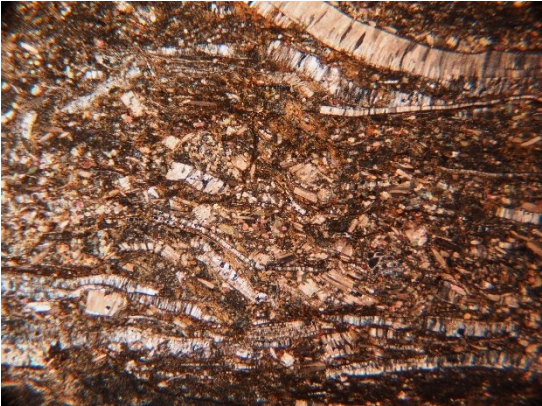
Sample: PRB-4.7		Locality: Puente Río Baguales (PRB)	
NP		NX	
		 <div>2 mm</div>	
Composition:	Volcaniclastic		
Classification:	Matrix-to clast-supported, normal-graded, tuffaceous conglomerate.		
Framework:	<p>1) LVF (55%): Regular-bad sorted, ang-subred - Vitreous tuff clasts (45%): granule-pebble-sized, dark-brown-coloured, internally matrix-supported (10-25% clasts). Framework: Shards > pumice > Qz. Pumice and shards are devitrified.</p> <p>2) Pumice (5%): Vesicular, ang-subang, M-sand-sized (coarse-ash), similar to the ones included in 1). Altered/dissolved -> 2° porosity.</p> <p>3) LVF porphyritic? (5%): subround, M-sand-sized. Devitrified, Pg-microliths also replaced by silica pseudomorphs.</p> <p>4) Volcanic Qz (1-2%): F-sand-sized, subhedral, subang-subround, minor resorption textures</p>		
Matrix:	Vitreous (fine-ash-sized), devitrified + illite. Brownish-orange-colored (FeOx).		
Structures:	It displays a coarse-tail normal-grading from tuffaceous conglomerate to pebbly tuffaceous sandstone.		
Alteration/Observations:	<p>A: Secondary porosity developed in pumice altered pumice fragments, voids filled by illuviation cutans (clay minerals + OM), chalcedony, calcite, and minor FeOx patinae.</p> <p>Devitrification of original vitreous material. Usually replaced by silica and illite. Plagioclase crystals in some porphyritic clasts are also replaced.</p>		
Interpretation:	Explosive felsic volcanism, possibly phreatomagmatic. Vitreous tuffs clasts are clearly remobilized -> hyaloclastite?		



Sample: ABA-6		Locality: Alto Baguales (ABA)	
NP		NX	
			
Composition:		Volcaniclastic	
Classification:		Tuffaceous mudstone alternated with F-grained tuffaceous sandstone	
Framework:		1) Tuffaceous mudstone: brown-colored (FeOx), formed by altered VF-ash (devitrified and irregular patches of illite). It includes minor silt-sized shards & VF-grained pumice (3%), and volcanic qz (<1%). 2) Tuffaceous sandstone: well-sorted, normal-graded. Composed of: - Pumice (85%): dev, ang-subang, also elongated and compacted. - Qz: Polycrystalline, possibly formed by replacement of pumice? Scarce monocrystalline.	
Matrix:		Fine-ash, altered to illite	
Structures:		Normal grading of tuffaceous sandstone, with bigger & equant pumice near the base and smaller & elongated to the top. Contact between 1) and 2) displays cut-and-fill structures. Lenticular rip-up clasts of 1) in 2)	
Alteration/Observations:		A: Devitrification and illite-replacement of ashy material.	
Interpretation:		Ash turbidites (sand) in an ash-fallout background sedimentation. Ash derived from felsic volcanism (pumice).	

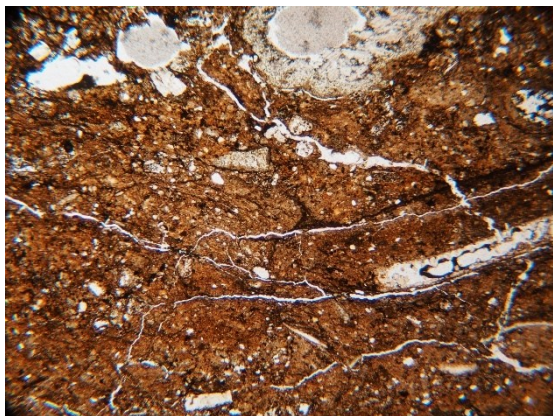
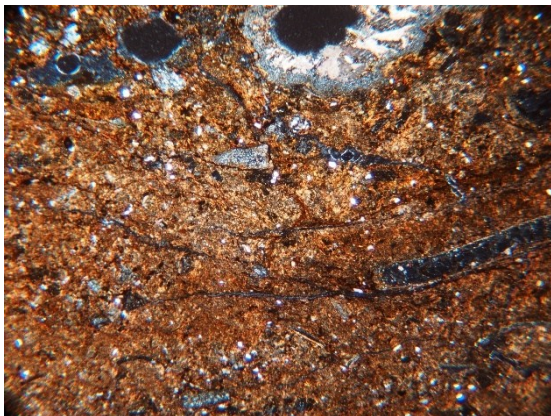
Sample: ABA-11.2		Locality: Alto Baguales (ABA)	
NP		NX	
			
Composition:		Volcaniclastic	
Classification:		Alternation of laminated tuffaceous siltstone and minor carbonaceous silty claystone	
Framework:		<p>1) Tuffaceous siltstone: super well-sorted, apparently internally massive. Composed of:</p> <ul style="list-style-type: none"> - Qz: subang-round, subh-anh, mono- and polycrystalline (2-3 crystals). - Ash: very fine, altered: devitrification > illite-replacement. <p>Qz + Ash = ca. 85%</p> <ul style="list-style-type: none"> - Organic matter (OM) (5%): ang-subang, brown-orange-colored (minor greenish), isopachous. - Opaques (3%): scattered, as granules or elongated-shaped (filament-like). - Other: mica (<1%), heavy minerals (scarce). <p>2) Silty carbonaceous claystone: dark-brown-coloured, internally fine laminated. Orange-brown-colored clay (80%), extinction in 45°.</p> <ul style="list-style-type: none"> - Qz (5-10%): idem to 1) - Opaques (5%): In botryoidal habit (cumulus), also isolated and elongated. 	
Matrix:		Fine-ash, altered to illite	
Structures:		<p>Thick parallel lamination between 1) and 2). Lamination is continuous and discontinuous, slightly sinuous. Lamination of 1) is thicker than 2)</p> <p>Parallel lamination of 2) inferred from aligned elongated opaques.</p>	
Alteration/Observations:		A: Lamination is bioturbated, burrows cutting 2) and filled by 1).	
Interpretation:		Bottom currents in the mid-outer-ramp? Siltstone possibly linked to ash-turbidites?	



Sample: ABA-11.7		Locality: Alto Baguales (ABA)	
NP		NX	
			
Composition:		Volcaniclastic	
Classification:		VF-F-grained volcanic sandstone	
Framework:		1) *Feldspars? (30%): Subhedral-euhedral, reg-well sorted. 2) Volcanic Qz (10-15%): anhedral or wedge-shaped (broken crystals), subang-subred, regular-well sorted, clean crystals. Some display resorbtion texture. Pseudomorphs: replaced by chal + illite + white mica. 3) LVF (10-15%): Subang-subround, altered (dev + illite), concentrate opaque minerals. 4) OM (10%): Ang-subround, also irregular shapes. Brown-orange-colored. 5) Opaques (3-5%): idem other samples. 6) Other: Scarce porous clasts (ca. 4 observed, they resemble bryozoarians, but smaller)	
Matrix:		Fine-ash (devitrified + illite) + carbonaceous clay	
Structures:		Diffuse parallel lamination. Parallel arrangement of lenticular zones richer in OM (carbonaceous). Also inferred from compaction.	
Alteration/Observations:		Not sure if feldspar minerals or pumice. This kind of alteration has been previously observed in both. Feldspar was chosen based on the euhedral shape of the clasts.	
Interpretation:		Sediment gravity-flow deposit (eventite)	

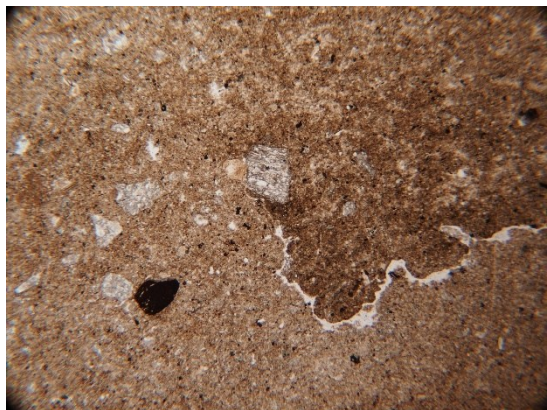
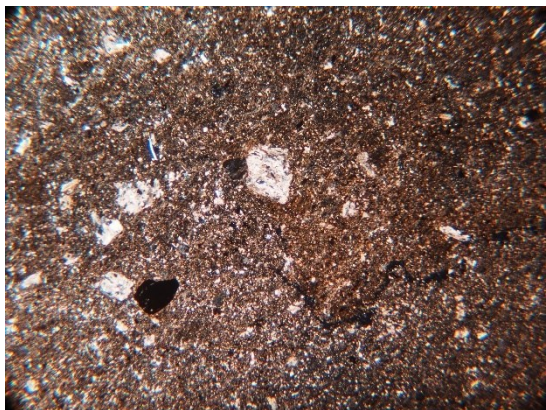
Sample: ABA 14.3		Locality: Alto Baguales (ABA)	
NP		NX	
			
Composition:		Mixed: Calcareous – epiclastic	
Classification:		Bioclastic, carbonaceous-calcareous siltstone	
Framework:		<p>1) Bioclasts (10-20%):</p> <ul style="list-style-type: none">- Inoceramid fragments: elongated, display a columnar internal structure. Also as isolated calcite crystals (derived from fragmented shells).- Ostracods: 1 well preserved (both valves, not compacted), usually as isolated and broken valves.- Pelagic bivalves?: thin, elongated or curved recrystallized bioclasts. Not sure if pelagic bivalves or inoceramid fragments.- Calcispheres: display a circular or ovoidal cross-section, diameter: ca. 0.025 mm, same size. Structure: two layers (external-thinner, internal-thicker), central void (usually filled by chalcedony or rarely calcite). Some display a gradually thinner side, with an apparently overlapping of the layer? Layers do not display a calcitic optical behaviour, are organic or micritic in composition?- Foram: 1 observed, chambered, broken or bad preserved. <p>II) Terrigenous:</p> <ul style="list-style-type: none">- Qz (5%): silt-sized, anhedral, ang-subang.- LVF (1%): silt-VF sand-sized, subround, dev + illite. Usually recognized by concentration of opaques.- Opaques (1-2%): rounded (botryoids), scattered or grouped.	
Matrix:		Carbonaceous micrite; carbonaceous clay	
Structures:		Diffuse parallel lamination: parallel arrangement of rip-up clasts of darker carbonaceous silty claystone (arranged in one horizon).	
Alteration/Observations:		<p>A: Dolomitization. Scattered, silt-sized crystals (microdolomite), rhomb-shaped. Usually its core is calcareous and the margin replaced by silica. Easy to confuse with other framework components.</p> <p>Compaction: broken ostracods.</p>	
Interpretation:		Reworked, mixed calcareous-carbonaceous hemipelagites.	


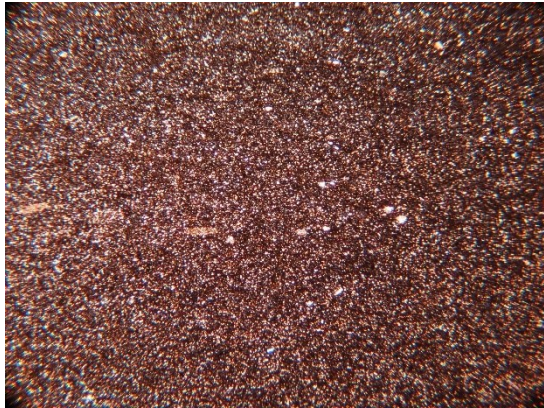
Sample: ABA 15.8		Locality: Alto Baguales (ABA)	
NP		NX	
			
Composition:		Mixed: Calcareous – Epiclastic	
Classification:		Inoceramid-rich carbonaceous claystone	
Framework:		<p>1) Inoceramid shells (40-50%): elongated, sinuous or curved. Original layering (ghost) displays a columnar calcite composition, usually broken in columns or with a turtle-carapace pattern.</p> <p>2) Bryozoans (<1%): calcareous, formed by small colonial chambered/fenestrated fossils, with a hexagonal or rounded section. Septa dividing the fenestra are thin, possibly layered?</p> <p>3) Oysters (<1%): only one fragment observed. Foliated internal microstructure.</p> <p>4) Opaques (<1%): scattered, rare framboids.</p>	
Matrix:		Carbonaceous claystone. Brown-colored.	
Structures:		Parallel lamination, inferred from arrangement of inoceramid shells.	
Alteration/Observations:		<p>A: Compaction (solution seams).</p> <p>Dolomite (10%): as isolated crystals, VF-F sand-sized, ídem to previous thin section (ABA 14.3) but with bigger crystals. Dolomite crystals display a calcareous core and replaced siliceous margin. They only occur within the matrix (interclastic).</p>	
Interpretation:		Reworked fossiliferous hemipelagites, possibly by storm currents. Oxygen-poor setting (inoceramids).	

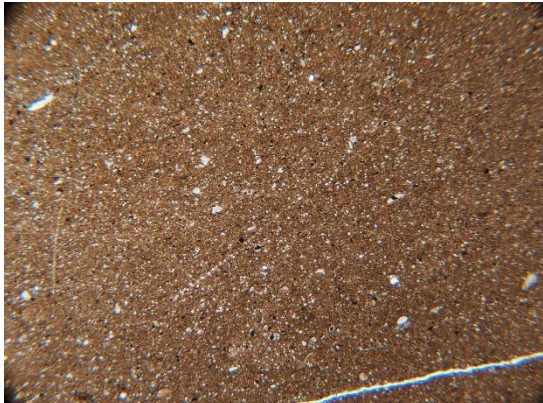
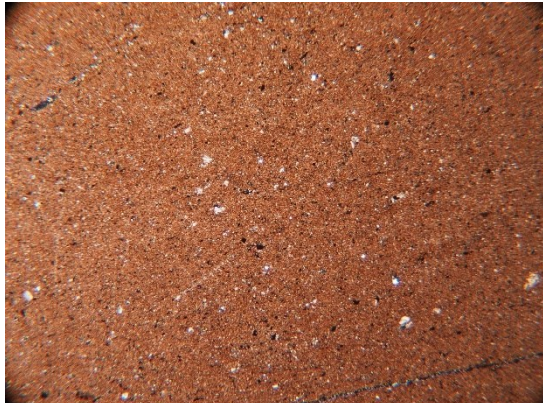
Sample: ABA 16.5		Locality: Alto Baguales (ABA)	
NP		NX	
			
Composition:		Mixed: calcareous-epiclastic	
Classification:		Calcsphere-bearing, clast-supported, micritic siltstone	
Framework:		<p>1) Bioclasts:</p> <ul style="list-style-type: none"> - calcispheres: two types: <ul style="list-style-type: none"> a) (15%) circular to ellipsoidal cross-section, sometimes double (similar to the ones observed in EPE sections), recrystallized to spar-calcite. b) (<1%) similar to previous, but with a two-layered, darker thin margin (analogous to the ones of ABA-14.3). - Inoceramid fragments (15%): small shell fragments and isolated columnar calcite crystals (mostly). - Pelagic bivalves? (1%): elongated or rectangular fragments, formed by spar-calcite. Also possible recrystallized external thin layers of inoceramid? - Ostracods (<1%): isolated, curved fragmented shells. - Intraclasts: Isolated, lens-shaped clasts formed by dark-brown-colored, bioclast-calcisphere-bearing calcimudstone. - Foraminifers: Isolated benthic? Forams (about 3 observed). Calcareous and recrystallized, usually clear by concentration of opaques (framoids, intraclastic). - Bone fragment: (one observed) orangey-brown colored, isopachous. Internal organic texture, possible fossil fish or crab-crustacean fragment. <p>2) Terrigenous</p> <ul style="list-style-type: none"> - Qz (10%): anh, ang-subang, wedge-shaped, also columnar. - LVF (<1%): subround-round, felsitic, partly altered to calcite. 	
Matrix:		Micrite	
Structures:		Diffuse parallel lamination inferred from arrangement of calcimudstone intraclasts and elongated shell fragments.	
Alteration/Observations:		N/A	
Interpretation:		Tempestites? Distal carbonate mid-ramp to outer-ramp?	

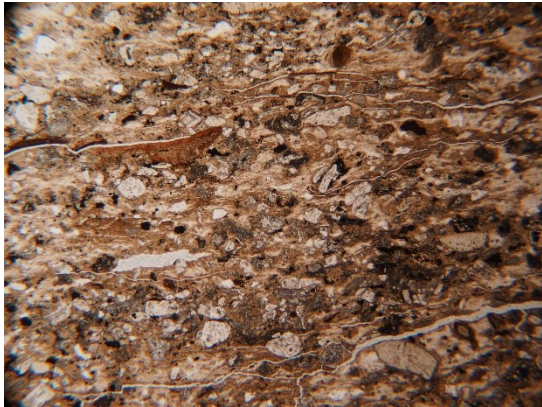
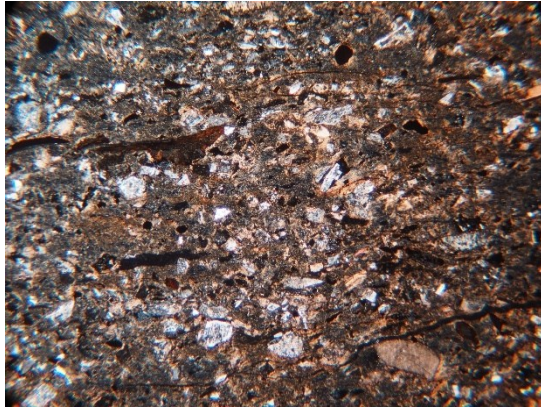
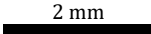
Sample: ABA 23.5		Locality: Alto Baguales (ABA)	
NP		NX	
			
Composition:		Mixed: Calcareous – Epiclastic	
Classification:		Bioclastic, matrix-supported, sandy-silty claystone	
Framework:		<p>1) Bioclasts:</p> <ul style="list-style-type: none">- Bioclasts (app. Bivalves, 15-20%): big-sized, curved and elongated fragments. Bad preservation, many dissolved and preserved as voids, partly filled by chal+calc, OM or FeOx. Some fragments recognized: inoceramid (trigonia?), oyster- Calcspheres (<1%): recrystallized to spar calcite.- Pelagic bivalves or ostracods? (<1%): isolated small curved valves. <p>2) Terrigenous:</p> <ul style="list-style-type: none">- Qz (5%): anh, ang-subround, wedge-shaped, also circular and elongated crystals.- Opaques (ca. 5%): Usually in pressure seams (elongated fiber-shaped), also scattered as irregular, rounded or wedge-shaped cumulus.	
Matrix:		Carbonaceous clay + FeOx (2°)	
Structures:		Apparently massive	
Alteration/Observations:		Dissolution, recrystallization, void fill by alteration minerals (chal, calc, FeOx, MnOx).	
Interpretation:		Reworked and bioturbated, carbonaceous and fossiliferous deposits (hemipelagites?). Possibly tempestitute.	

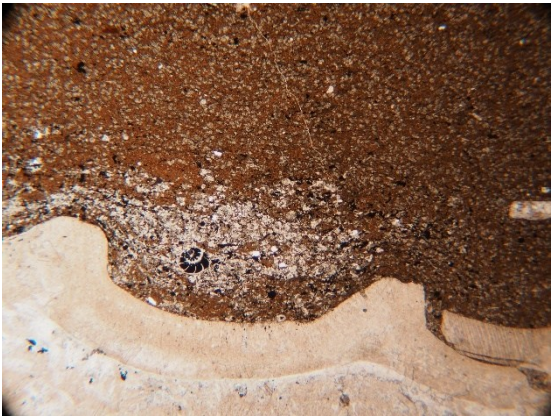

Sample: ABA 25.6		Locality: Alto Baguales (ABA)	
NP		NX	
			
Composition:		Epiclastic	
Classification:		Carbonaceous silty claystone	
Framework:		Framework (ca. 3%): <ul style="list-style-type: none">- Qz (ca. 1 %): F-sand -sized, isolated anhedral crystals, angular. Some porous are also inferred as lost qz crystals.- Ostracods (<1%): Isolated valves (dissolved to 2° porosity).- Porous (2°): inferred as formed after dissolution of silt-sized microdolomite. The border is preserved as siliceous, core dissolved.- Forams: Ovoidal and chambered (n< 5), filled by reddish or opaques fromboids.- Radiolarians?: Dissolved, one isolated broken fragment with “spines”.- Opaques (1-2%): Scattered, spotted as minor fromboids.	
Matrix:		Carbonaceous clay	
Structures:		Massive	
Alteration/Observations:		Dissolution of most silt-sized particles. Oxidation by FeOx.	
Interpretation:		Carbonaceous hemipelagites.	

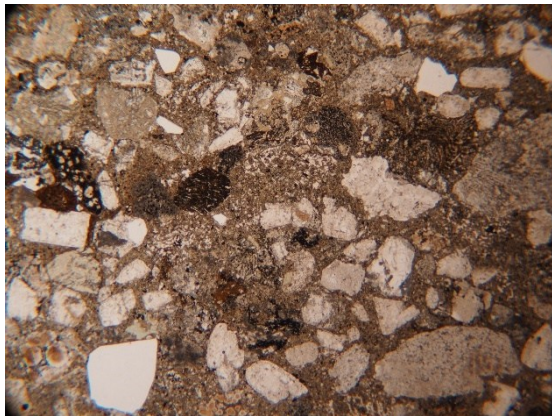
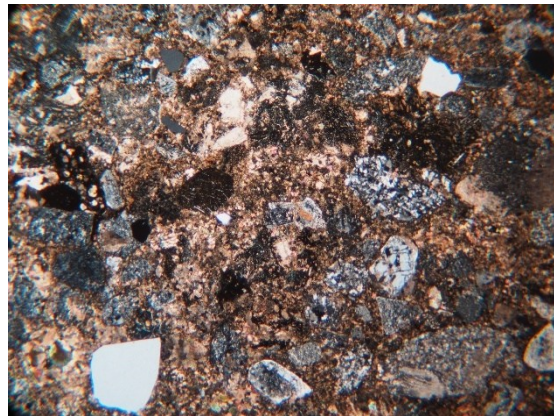
Sample: ABA 32.7		Locality: Alto Baguales (ABA)	
NP		NX	
			
Composition:	Mixed: Tuffaceous – Epiclastic		
Classification:	Tuffaceous-carbonaceous, clayey-sandy siltstone		
Framework:	<ul style="list-style-type: none">- Glass shards (20%): siliceous (microcryst), silt-sized, elongated, curved and cusate-shaped, many replaced by calcite.- Qz (ca. 3 %): VF-F sand (2%), silt-size (<1%), anh-subh, volcanic (rounded, resorbtion, broken crystals).- K-Fel (2-3%): VF-F-sized, subh-euh, altered (replaced by chal + calc).- LVF (<1%): VF-F-sand sized, subround, isotropic & some concentrated opaques.- Biotite? (<1%): Straight extinction, a couple of isolated crystals, VF-sized.- Microfossils (<1%): isolated compacted ostracods or valves, also foram (1) and scarce circular microfossils (radiolarians?).		
Matrix:	Fine ash, devitrified, slightly carbonaceous.		
Structures:	Parallel lamination (thick), alternation of tuffaceous and carbonaceous claystone.		
Alteration/Observations:	Spotted, scattered calcite-dolomite replacing glass-shards.		
Interpretation:	Mixed sedimentation after tuffaceous sediment-gravity flow or bioturbation.		

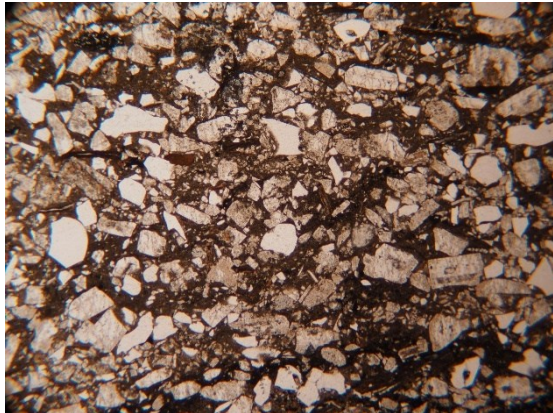
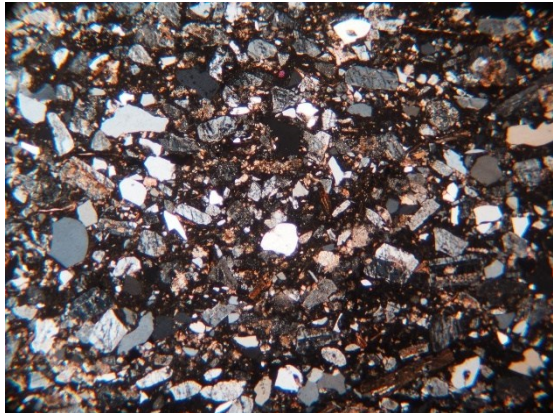
Sample: ABA 42.9		Locality: Alto Baguales (ABA)	
NP		NX	
			
Composition:			
Classification:		Carbonaceous silty claystone - alternation with micritic facies? (strongly dolomitized)	
Framework:		<p>Epiclastic?</p> <p>1) "Clayey siltstone": very-well sorted, ang-subang microdolomite crystals (50%)? -> altered dolomitized claystone or calcimudstone? - Qz (<1%): silt-sized, ídem anterior.</p> <p>2) Carbonaceous silty claystone (lenses) - ídem previous but with a smaller amount of microdolomite crystals (15-20%). Dark-brown-colored.</p>	
Matrix:		Carbonaceous clay	
Structures:		<p>Diffuse parallel lamination between 1) and 2). Lamina have an irregular thickness (variable), and display bioturbation of 1) in 2).</p> <p>Also, isolated lenses (rip-up clasts?) of 2) in 1).</p>	
Alteration/Observations:		In 1) apparent silt-sized qz crystals display the same optical behavior, or likely too small to be distinguished. Possibly dissolved microdolomite or replaced by chalcedony. They have a euhedral rhomboidal shape	
Interpretation:		Carbonaceous hemipelagites with organogenic dolomitization (anoxic setting).	

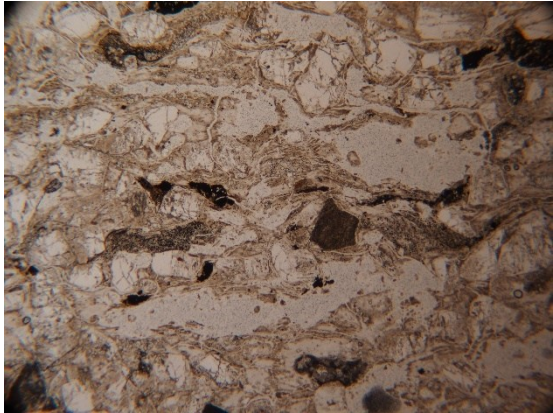
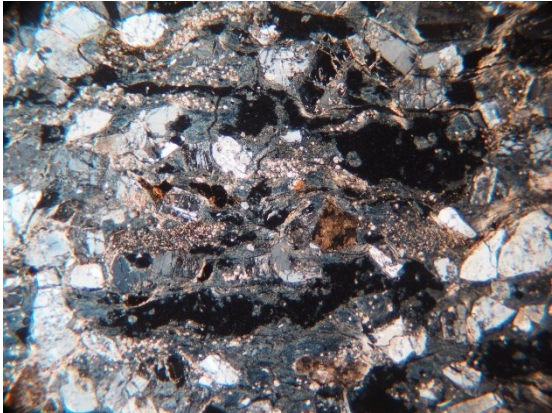
Sample: ABA 54.5		Locality: Alto Baguales (ABA)	
NP		NX	
			
Composition:		Calcareous-carbonaceous	
Classification:		Silty, carbonaceous wackestone	
Framework:		1) Bioclasts (5%): - Forams (ca. 1 %): VF-sand-sized, elongated and chambered (pelagic?), circular (like a big calcisphere,) and ovoidal cross-sections. One fragment displays spines. - Calcispheres (<1%) - Ostracods? (<1%): fragments - Non-determined bioclasts (ca. 1%): formed by spar-calcite. Possibly forams fragments. 2) Terrigenous: - Qz (<1%): silt-sized, ídem previous thin sections. - Opaques (1-2%): Silt to VF-sand-sized, scattered and irregularly-shaped. Also, as framboids within calcareous fragments or crystals and filling forams chambers.	
Matrix:		Micrite, slightly carbonaceous.	
Structures:		Massive	
Alteration/Observations:		Microdolomite (ca. 10%), dissolved or replaced by silica, or filled by opaque minerals. Presence of benthic and planktic foraminifers	
Interpretation:		Calcareous hemipelagites.	


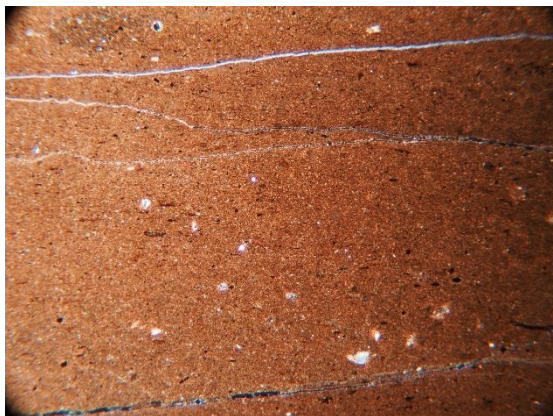
Sample: CRS1-1.0		Locality: Cañadón Río Simpson 1 (CRS1)	
NP		NX	
			
			
Composition:	Mixed: Tuffaceous/carbonaceous/calcareous		
Classification:	Bioclastic, carbonaceous-tuffaceous clayey sandstone		
Framework:	<p>1) Feldspar (15%): euh-subh; “dirty”, p.r. to calc+sil, reg-well-sort, twinned.</p> <p>2) LVF(5%): fg & microporphyric, ang-rnd, concentrate opaques, dev., VF-F-sand. reg-sort, alt to calc.</p> <p>3) Opaques (5%): irregular cumulus in matrix, LVF, rnd - wedge - elongated. scattered, framb?</p> <p>4) Qz (<1%): anh, ang-subang, wedge>rounded-shaped</p> <p>5) Bt (<1%): isolated elongated crystals</p> <p>Allochems (10%)</p> <p>1) Cortoids (ca. 5%): rectangular, extinction as 1 crystal (echin?) or part of bvv, margin replaced by silica.</p> <p>2) Foram (2-3%): chambered, complete > fragments, VF-F sand, at least 3 spp.</p> <p>3) Biv (1-2%): big-sized, two-layered partly recryst.</p> <p>4) Phosphatic microfossils (1%): orange-brown-colored, wedge-elong-rounded, isotropic. Acritarchs???</p> <p>5) Wood (<1%): fragments, comb-shaped</p>		
Matrix:	Tuffaceous/carbonaceous mudstone		
Structures:	<p>Matrix-supported</p> <p>Diffuse parallel lamination (elongated fragments)</p>		
Alteration/Observations:	Recrystallization; Feld (calcite); silicification in cortoids; Forams (some replaced by silica).		
Interpretation:	Tuffaceous sediment gravity-flow, sandy debrite?		

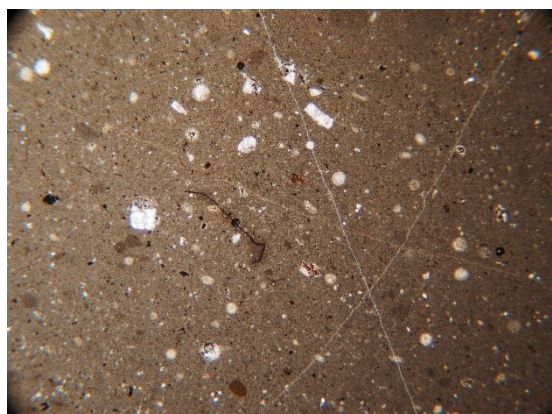
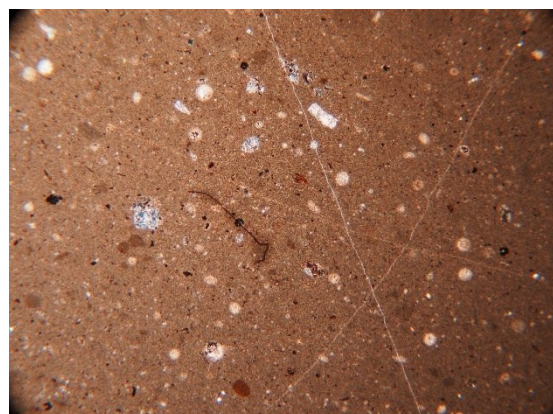
Sample: CRS1-2.1		Locality: Cañadón Río Simpson 1 (CRS1)	
NP		NX	
			
Composition:			
Classification:		Foram-bearing, carbonaceous calcimudstone, with small lenses of foram-wackestone	
Framework:		<p>I) Bioclasts (3%)</p> <p>1) Forams (2%): At least 2 types (planispiral; lens-shaped), VF Ssa</p> <p>2) Bivalves (1%): only 1 big fragment (ribs, recryst.); also scarce small and thin shells (recryst)</p> <p>3) Wood (Tz): silt-sized, 1 fragment</p> <p>4) OM (1%): circular/ellipsoidal concentration of opaques, or secondary replacement</p> <p>II) Terrigenous</p> <p>1) Feldspar (<1%): scatter., euh, partly repl (calc+ sil), VF-SSa</p> <p>2) Qz (<1%): silt-sz, anh, subang-subred</p> <p>3) Opq (1%): scatter, also intraclastic, spotted-elongated-cumulus</p>	
Matrix:		Carbonaceous mudstone (partly microdolomitized)	
Structures:		<p>Diffuse parallel lamination: fossils and coarse material are concentrated in isolated lenses.</p> <p>(lenses of coarse-gr material, or aligned opaques)</p>	
Alteration/Observations:		<p>A: Microdolomitization (pervasive, 40-50%), silt-sz, rhomb-shaped (possible to confuse with siltstone-sz, altered clasts) - “organogenic dolomite”</p> <p>Forams similar to the ones in CRS 1</p>	
Interpretation:		Carbonaceous hemipelagites with organogenic dolomitization (anoxic setting). Subtle bottom currents (lag deposits).	



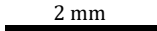
Sample: CRS1-8a		Locality: Cañadón Río Simpson 1 (CRS1)	
NP		NX	
		 2 mm	
Composition:	Mixed siliciclastic - calcareous		
Classification:	C-VC Volcanic sandstone (litharenite - lithic arkose)		
Framework:	1) LVF (40-50%): subang-subred, poli, dark-colored (altered). i) Lithics (30-40%): poli, microporphy, vitro> trachy, pg replaced by brown mica. Groundmass: dev, calc or chl, opq. ii) Pumice (10%): dev (qz poli), also altered to calc, chl. Some preserve vesicles, 1 fg with perlitic fracture. 2) Feldspar (10%): sub-ahn, reg-sort, altered (patchy: sil, wm, sil), some twinned. 3) Quartz (10%): subang-subround, anh, fractured, some resorption txt. 4) Opaques (1-2%): scatter, silt-VF-SSa, usually within LVF 5) Biotite (Tz)		
Matrix:	Volcanic mudstone (altered, devitrified)		
Structures:	Regular-good sorting; parallel bedding (thin), layers separated by volcanic mudstone; Normal grading, inverse-normal grading		
Alteration/Observations:	Variable: brown-black (opq), gray (vitreous), orange (FeOx), translucent (altered by calc), greenish (chl) Matrix altered to calc, clay minerals (argillization)		
Interpretation:	Sediment-gravity flow deposits (sandy debrite to coarse-grained turbidite?)		

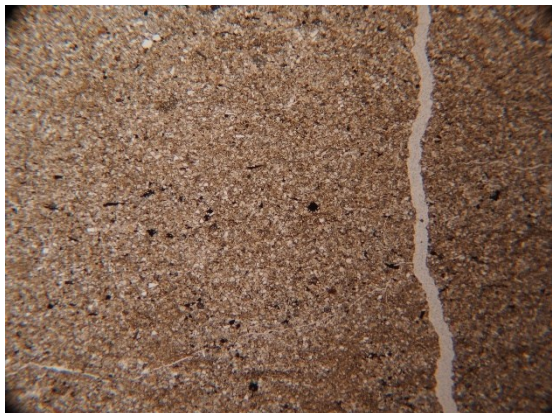
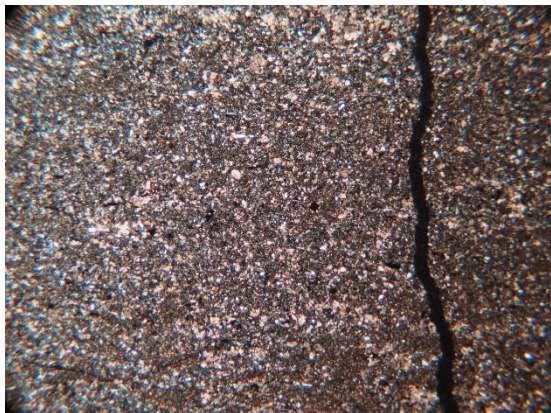
Sample: CRS1-8c		Locality: Cañadón Río Simpson 1 (CRS1)	
NP		NX	
		 2 mm	
Composition:	Volcaniclastic		
Classification:	M volcanic sandstone with small lenses of wacke (muddy sandstone)		
Framework:	1) Feldspar (30-40%): euh-subh, minor anh, broken/fract, reg-bad sort. 2) Qz (10-15%): anh, volcanic, reg-sort, subang-subreg, resorption 3) LVF (5%): subang-subred, oligo, altered (illit (gm), calc(pg)), it concentrates opq, smaller than Qz and Feld -> FSa grained. 4) Opaques (2-3%): very bad sort, silt-FSSa, also in cumulus. In one part of the thin-section, opq replaced almost the whole matrix.		
Matrix:	Silty volcanic mudstone, brown colored, same composition as the framework, but smaller		
Structures:	Diffuse parallel lamination: arrangement of Bt, imbrication of elongated crystals (feldspar)		
Alteration/Observations:	In comparison with 8a, 8c is richer in qz (volcanic) & feldspar, and poor in LVF. 8a is the lower part of the volcaniclastic bed		
Interpretation:	Sediment-gravity flow deposits (sandy debrite to coarse-grained turbidite?). Volcanic triggered or influenced.		



Sample: CRS1-12.3		Locality: Cañadón Río Simpson 1 (CRS1)
NP		NX
		
Composition:	Tuffaceous	
Classification:	M-C Tuffaceous muddy sandstone (wacke)	
Framework:	<p>1) Feldspar (20-30%): euh-subh, fract, alt (partly illite-wm > calc), twinned.</p> <p>2) LVF (5%): subang-subround, microporphyric, felsitic?, usually dev or replaced by calc (>> illite), darker (opq, FeOx)</p> <p>3) Bt (Tz): scatter, small crystals, some compacted.</p> <p>4) Opq (1-2%): Big, irregular concentration in matrix, also within LVF. Minor in matrix small & scatter.</p>	
Matrix:	Vitreous but devitrified, secondary alteration of ash or pumice clasts to illite (fiamme-like texture)	
Structures:	<p>Diagenetical fiamme-like texture</p> <p>Apparent parallel lamination (compaction)</p>	
Alteration/Observations:	Calc: clear, silt-VF-Ssa crystals, within matrix >> within Feld or LVF.	
Interpretation:	Subaqueous settled, coarse ash fallout deposits (though not graded -> sandy debrite?)	

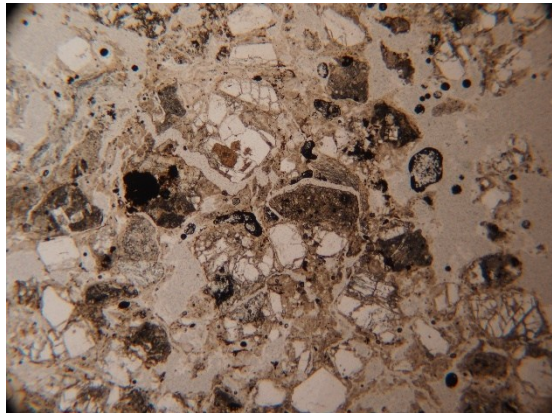
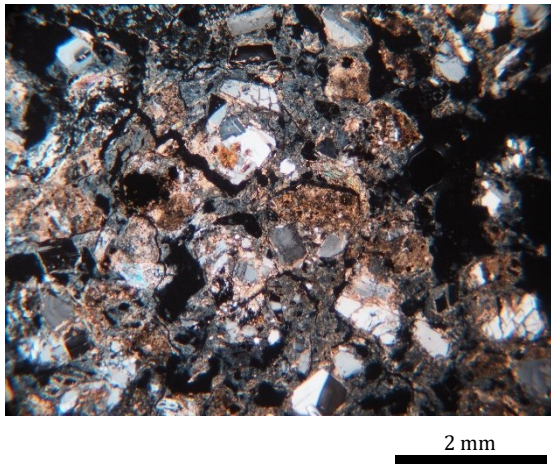
Sample: CRS1-13.4		Locality: Cañadón Río Simpson 1 (CRS1)	
NP		NX	
			
Composition:		Mixed calcareous-carbonaceous	
Classification:		Silty, carbonaceous calcimudstone	
Framework:		<p>Bioclasts</p> <p>1) Forams (1-2%): scatter, chambered, usually broken, replaced by calc or recryst. VF-F-Ssa, at least 3 spp. Opq in cumulus within.</p> <p>2) Calcspheres (Tz): several spp (at least 3), very small-silt-sized (40x).</p> <p>Terrigenous</p> <p>1) Qz (1-2%): silt-sized, anh, fragmented.</p> <p>2 Opq (2-3%): very small (silt-sized), circular cross-section (botryoids?), scattered or arranged in small lenses or cumulus (VF-SSa).</p> <p>3) WM (Tz)</p> <p>4) Glauconite (Tz): 1 cryst, subang, silt-sized</p>	
Matrix:		Micrite > carbonaceous clay	
Structures:		Diffuse parallel lamination	
Alteration/Observations:		<p>Possible bioturbation: darker and irregular or lens-shaped zones.</p> <p>Presence of benthic and pelagic foraminifers (benthic>planktic)</p>	
Interpretation:		Calcareous hemipelagites.	


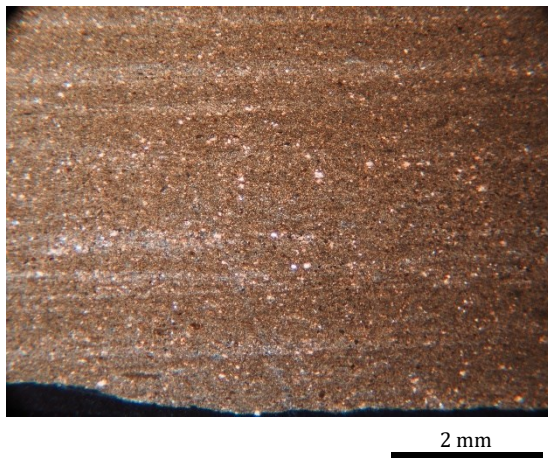
Sample: CRS1-18.2		Locality: Cañadón Río Simpson 1 (CRS1)	
NP		NX	
			
Composition:	Calcareous		
Classification:	Calcsphere-bearing wackestone to calcimudstone		
Framework:	<p>Bioclasts (5-7%):</p> <p>1) Calcspheres: at least 2 spp: i) big ones (4-5%): 2.5x rounded, recryst (spar calc, drusy), ghost txt, some with opq, fine grained at margin; ii) small ones (<1%): 20x-40x, clear margin not recryst. Or OM relatively well-preserved?</p> <p>2) Forams (<1%): at least 3 spp, scattered, filled with opq, benthonic</p> <p>3) Intraclasts (1-2%): darker, subang-subround fragments, diffuse margin but same composition, VF-FSSa</p> <p>4) OM (2%): irregular, spotted, fiber- or sphere-shaped, reddish, not altered (translucid), app. plant fragments.</p> <p>Terrigenous:</p> <p>1) Feldspar (1%): euh-subh, alt (sil+calc), VF-SSa</p> <p>2) Qz (<1%): silt-sized</p> <p>3) FLV (<1%) subang-subred, alt (dev+calc), VF-SSa</p> <p>4) Opaques (<1%): botryod-shaped, or grouped in irregular wedge-shaped cumulus</p>		
Matrix:	Micrite		
Structures:	Massive		
Alteration/Observations:	Recrystallized (big calcspheres); Pg (calc+sil); calcite veins		
Interpretation:	Calcareous hemipelagites. Analog to Carbonate outer ramp, facies FZ 2-3 (sensu Flügel 2010)		



Sample: CRS1-64.2		Locality: Cañadón Río Simpson 1 (CRS1)	
NP		NX	
			
			
Composition:	Mixed siliciclastic-calcareous		
Classification:	Laminated, carbonaceous silty claystone & clayey siltstone		
Framework:	<p>Silty claystone (SC)</p> <p>1) Qz (2-3%):</p> <p>2) Feld (2%)</p> <p>3) Calcite: scatte, irreg-shaped, not well-defined crystals (confusable with matrix) -> possible 2° (alt)</p> <p>4) Opq (1-2%): elongated & parallel arranged, wispy-shaped, scattered. Also rounded & framboidal (small)</p> <p>Clayey siltstone (CS)</p> <p>1) Qz (3%): anh, irreg, wedge, rectangular-shaped</p> <p>2) Feld (3-5%): subh, alt (calc)</p> <p>3) Calc (10%): scattered, irregular, within Feld</p> <p>4) Opq: ídem previous, though cumulus are bigger</p> <p>OM (both, 3%): scattered, irregular-shaped, diff to sharp, brown colored</p> <p>5) Other (Tz): Bt; Glauc</p>		
Matrix:	Carbonaceous clay		
Structures:	<p>Parallel lamination, slightly sinuous; one layer displays downlap.</p> <p>Laminae CS thinner than SC</p> <p>Fossils: wood (comb-shaped); calcispheres (scarce)</p>		
Alteration/Observations:	<p>A: Calcification (Feld) + spotted carbonate</p> <p>O: Clayey siltstone = pale-colored lamina, richer in calcite</p>		
Interpretation:	Finely laminated mudstone, after current- triggered bedload transport of flocculated mud (Ullmer-Scholle et al., 2014).		



Sample: CRS1-68		Locality: Cañadón Río Simpson 1 (CRS1)	
NP		NX	
			
Composition:		Siliciclastic (partly calcified)	
Classification:		Clayey, carbonaceous siltstone (tuffaceous?)	
Framework:		Framework (60-70%) 1) Qz (15%): anh, ang-subred, wedge or elong-shp 2) Feld (15%): eubh-euh, alt (dirty txt -> sil, ill > calc) 3) Opq (2-3%): irreg, scatt, framb or cumulus, also elong/euh (pyyr?). It may reach up to 15 % in richer areas 4) OM (2%) 5) WM (<1%): isolated crystals (platty) 6) Bt (Tz): Bt<WM 7) Glauc (<1%): scarce, isolated, subang 8) LVF (1%)	
Matrix:		Carbonaceous clay/ash (dev)?	
Structures:		Diffuse parallel lamination (arrangement elongated clasts; parallel intraclasts, carbonaceous claystones)	
Alteration/Observations:		Calcification (scattered>> within Feld) - 2° replacement	
Interpretation:		Current-reworked or bioturbated mudstone.	

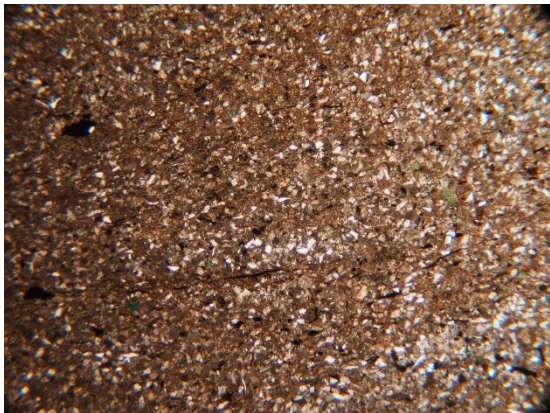
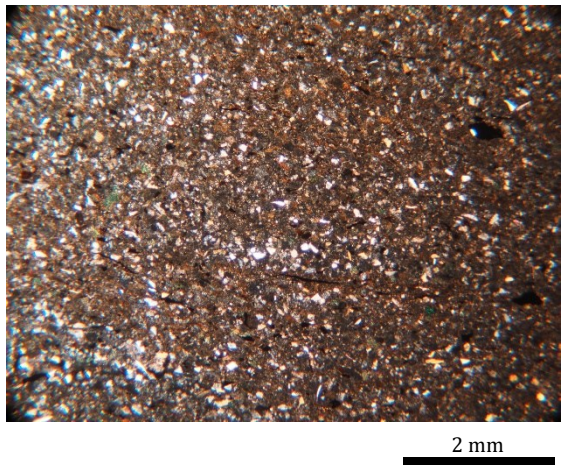
Sample: CRS1-71.5		Locality: Cañadón Río Simpson 1 (CRS1)	
NP		NX	
			
Composition:		Siliciclastic	
Classification:		Bioturbated clayey carbonaceous siltstone	
Framework:		1) Qz (15%) 2) Feld (15-20) 3) Calc: 2°, also reworked? 4) LVF (1%) 5) Glauc (<1%): subang-subred 6) WM 7) Opq (5-10%), scatter, also concentrated in carbon-rich hz (OM) 8) OM: brown-org-colored, usually elongated	
Matrix:		ídem CRS1-68, though: - lower CaCO3 content - higher OM content	
Structures:		Bioturbation (lamination interrupted). Burrows filled by carbonaceous claystone Parallel lamination (“wavy”)	
Alteration/Observations:		Calcification? not sure if 1° (clasts) or 2° (alt or feld)	
Interpretation:		Bioturbated, current-reworked siltstone. Bedload transport + erosion of muddy layers (flakes).	

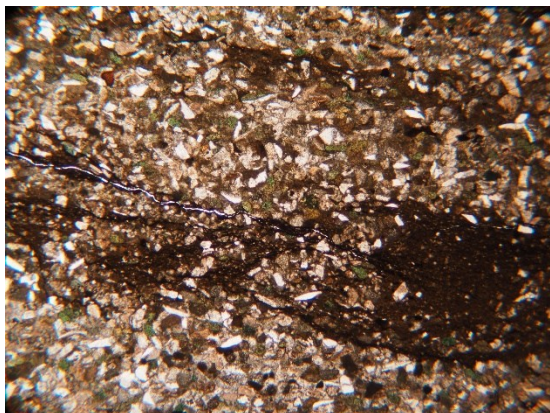
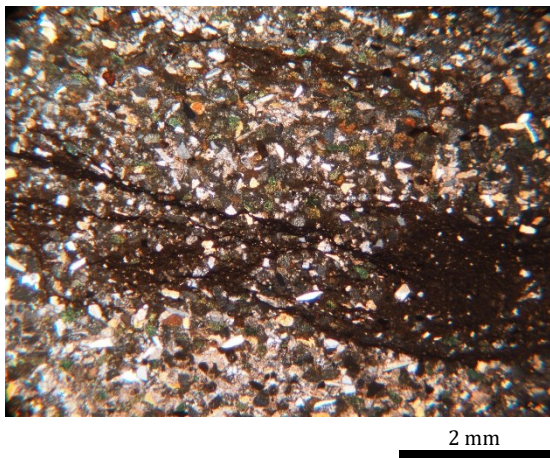
Sample: CRS1-72.3		Locality: Cañadón Río Simpson 1 (CRS1)	
NP		NX	
			
Composition:	Tuffaceous		
Classification:	M tuffaceous sandstone (lithic arkose)		
Framework:	1) Feld (15-20%): broken (fract filled by calc), clean cryst, twinned, euh-subh, well-sorted 2) LVF (15-20): darker, ang-subred, well-reg sort, mporpphy, somewith vesicles, alt (calc + illi: gm), also dev 3) Qz (5%): F-M-Ssa, broken, subang, mono & poli (or subcrystals) 4) Pumice (40-50%): inferred as altered to 2° matrix (fiamme-like txt), highly weathered 5) Bt (<1%): possibly replacement of Hb?		
Matrix:	Devitrified ash (illite; clay minerals)		
Structures:	Massive? or parallel lamination after diagenetical compaction?		
Alteration/Observations:	Highly weathered (clay mxs); dev of glassy material + calc + illite/WM + FeOx (spotted/patina)		
Interpretation:	Strongly altered (argillized), subaqueous settled, coarse ash fallout deposits or eventite?		

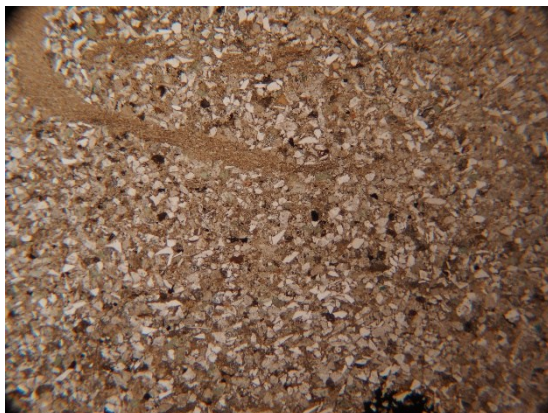
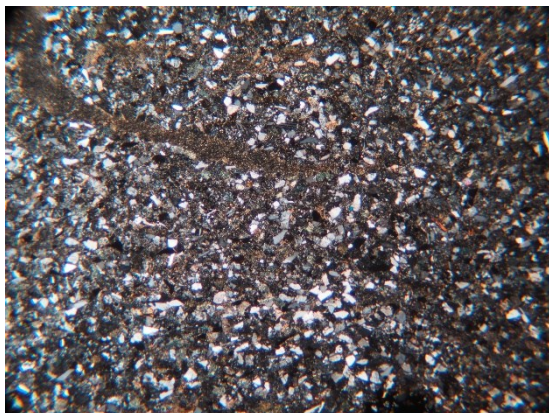
Sample: CRS1-73.3		Locality: Cañadón Río Simpson 1 (CRS1)	
NP		NX	
			
Composition:	Siliciclastic		
Classification:	Fine laminated carbonaceous-micritic claystone & silty claystone (minor)		
Framework:	<p>Carbonaceous claystone (dark-colored)</p> <ul style="list-style-type: none">1) Qz (5%): subang-subred, minor elong2) Calc: Qz > Calc, 2°cement? scatter/spotted3) Feld (<1%): rect, twn4) OM (5-10%): scatte, round to elong5) Opq (2%): scatte, also wispy/elong6) Glauc (Tz) <p>Silty claystone (pale-colored) idem previous, but > % clasts (20%), also bigger clasts (some up to VF-SSa)</p>		
Matrix:	Carbonaceous clay + micrite		
Structures:	Discontinuous & continuous fine parallel lamination, one layer with downlap (cross-lamination)		
Alteration/Observations:	N/A		
Interpretation:	Finely laminated mudstone, after current- triggered bedload transport of flocculated mud (Ullmer-Scholle et al., 2014).		

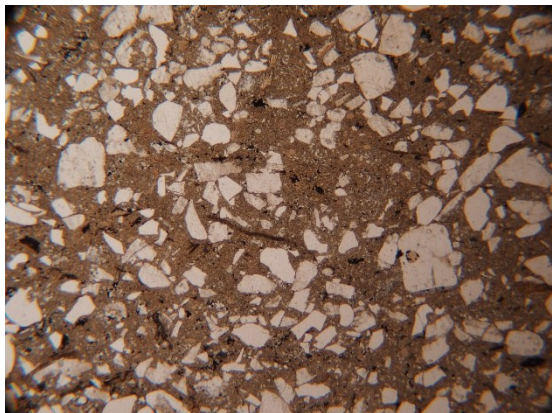
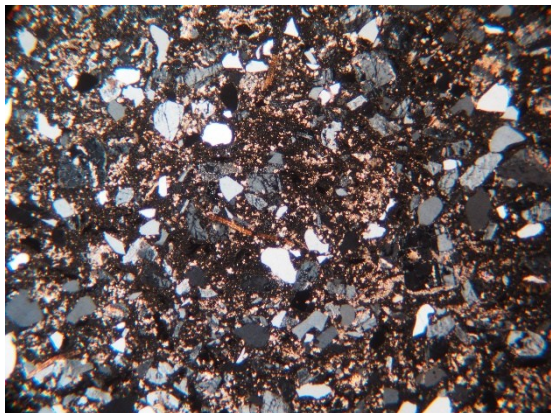
Sample: CRS1-75.4		Locality: Cañadón Río Simpson 1 (CRS1)	
NP		NX	
			
Composition:		Mixed siliciclastic-calcareous	
Classification:		Laminated, calcareous claystone & silty claystone	
Framework:		Terrigenous 1) Qz (2%): ang-subred, anh 2) Calc (2%): ang-round, bioclast frg? usually elong/lens-shaped 3) OM (3%): dark bn-colored, irreg, wedge/wispy, FeOx, also comb-shaped (wood?) 4) Opq (5%): irreg, wispy-shp, also round (framb), scatte, minor cumulus 5) Glauc (<1%); WM (<1%) Bioclasts (<1%) 1) Foram: 1 observed 2) calcispheres: scattered (<1%) 3) shard/spicule-like calcite frag (<1%): possible elong calcitic fragments or broken allochems?	
Matrix:		Carbonaceous clay + micrite	
Structures:		Parallel lamination, though discontinuous (in contrast to CRS-73.3) Scour-and-fill structures	
Alteration/Observations:		Calcite as cement?	
Interpretation:		Alternation of hemipelagic mudstone, or mud-laden flow deposits with silty bedload deposits.	

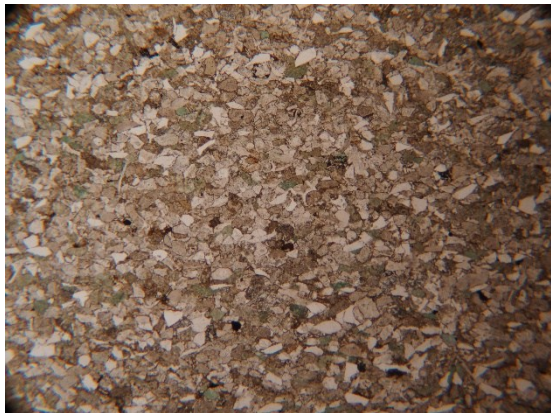

Sample: CRS1-79.1		Locality: Cañadón Río Simpson 1 (CRS1)	
NP		NX	
			
Composition:		Mixed siliciclastic-calcareous	
Classification:		Laminated, calcareous claystone & silty claystone	
Framework:		1) Qz (3%): anh, ang-subred, reg-sort 2) Feld (2-3%): partly altered to wm-calc, subh 3) LVF (1%) dev to polycryst qz, opqs 4) Calc: subang-subred, reworked? 5) WM; Glauc < 1% 6) OM (1%): idem prev 7) Opq (2-3%): idem	
Matrix:		Laminated, calcareous claystone & silty claystone	
Structures:		Bioturbation Parallel lamination, discontinuous (bioturbation)	
Alteration/Observations:		Minor calcite spotted/as patches	
Interpretation:		Bioturbated carbonaceous siltstone. Diffuse lamination reflects current transport.	

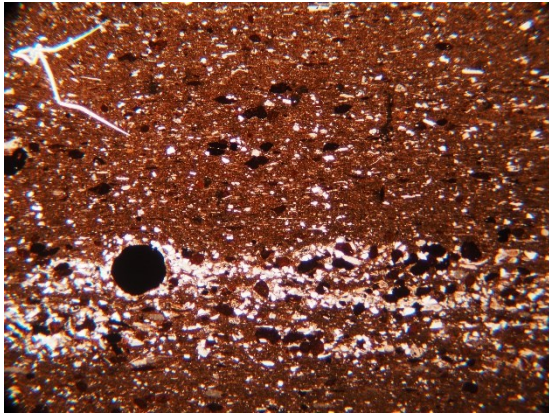
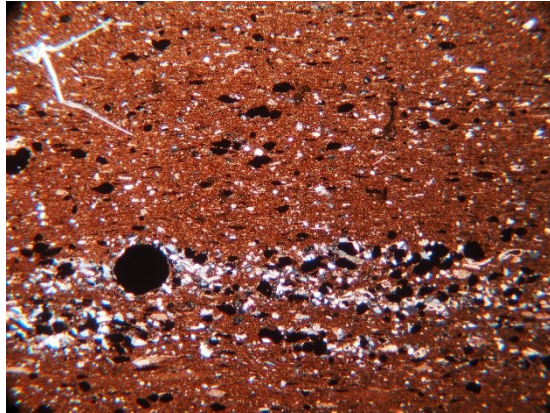
Sample: CRS1-80.2		Locality: Cañadón Río Simpson 1 (CRS1)	
NP		NX	
			
Composition:		Siliciclastic	
Classification:		Bioturbated VF sandstone to clayey siltstone	
Framework:		Clayey siltstone 1) Qz (10%): elong to subtriang, wedge, anh 2) Feld (15%): subh-anh, mottled txt, some partly alt (calc) 3) OM (15%): subang-subred, bn-org colored, bright at NX (alt to clay mls?) 4) Opq (5%); shard, wedge, wispy-shp, also elong and // arranged 5) Glauc (2-3%): subang-subred 6) WM (<1%) Silty claystone Framework: 20-25%, ídem sample CRS1-79.1	
Matrix:		Carbonaceous clay (richer in silty claystone, obviously)	
Structures:		Relict or diffuse parallel lamination, disturbed by pervasive bioturbation	
Alteration/Observations:		Bioturbation	
Interpretation:		Bioturbated, subtidal sandy deposits.	

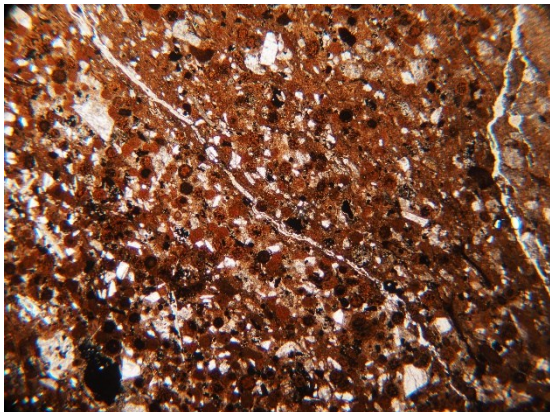
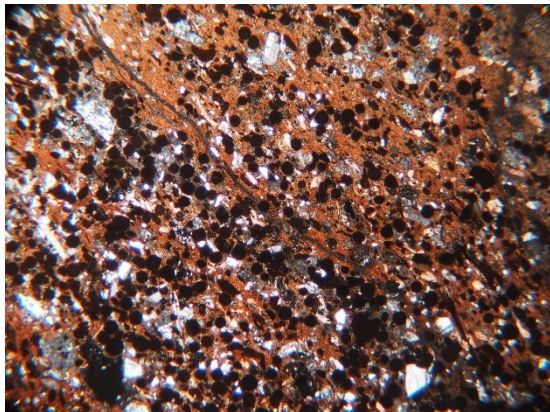
Sample: CRS1-84.1		Locality: Cañadón Río Simpson 1 (CRS1)	
NP		NX	
			
Composition:	Epiclastic		
Classification:	Glaucinitic, litho-feldspatho-quartzose sandstone.		
Framework:	1) Qz (40%): elong to subtriang, wedge, anh 2) Feld (20%): subh-anh, mottled txt, some partly alt (calc) 3) Lv (10%): rounded 4) Glauc (15%): subang-subred 5) Opq (1%); wedge, wispy-shp, also elong and // arranged 6) Phos? (2%) 6) Amph? (<1%) 6) WM (<1%)		
Matrix:	Carbonaceous + calcareous mudstone		
Structures:	Parallel lamination Mud flakes Bioturbation Regular to well sorting		
Alteration/Observations:	Calcification (Calcareous cement)		
Interpretation:	Bioturbated, subtidal sandstone. Mudflakes might reflect a tidal setting.		

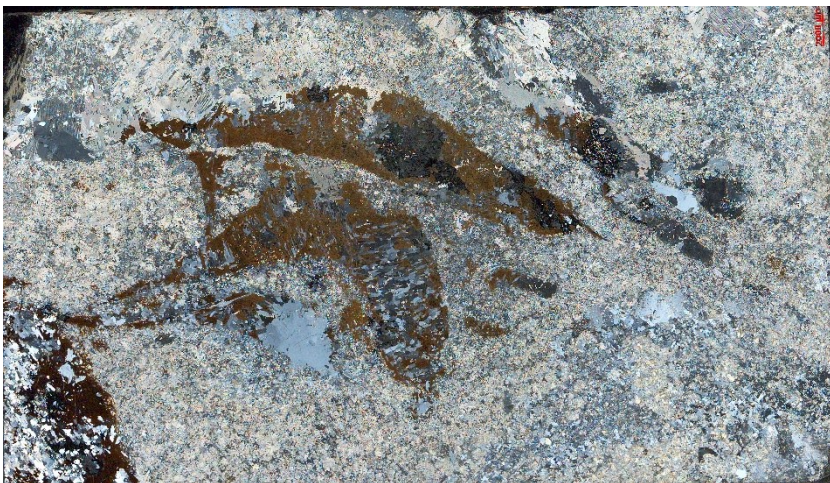
Sample: CRS1-84.9		Locality: Cañadón Río Simpson 1 (CRS1)	
NP		NX	
			
Composition:		Epiclastic	
Classification:		Glaucinitic, litho-feldspatho-quartzose sandstone.	
Framework:		1) Qz (30%): elong to subtriang, wedge, anh 2) Feld (25%): subh-anh, mottled txt, some partly alt (calc) 3) Lv (15%): sub-rounded 4) Glauc (10%): subang-subred 5) Opq (1%); wedge, wispy, and irregularly-shaped 6) Phos? (<1%): rounded 6) Amph? (<1%): anh to subh 6) WM (<1%): flakes	
Matrix:		Carbonaceous + calcareous mudstone	
Structures:		Diffuse parallel lamination Mud flakes or bioturbation? Well-sorted	
Alteration/Observations:		Calcification (Calcareous cement)	
Interpretation:		Subtidal sandstone, mud flakes might reflect a tidal setting.	


Sample: CRS-86.2		Locality: Cañadón Río Simpson 1 (CRS1)	
NP		NX	
		 <div>2 mm</div>	
Composition:	Epiclastic		
Classification:	Quartzo-feldspathic muddy sandstone (wacke)		
Framework:	1) Feld (40%): subh-anh, mottled txt, some partly alt (calc) 2) Qz (20%): anh to subh, angular-broken fragments 3) Lv (1%): sub-rounded 4) Opq (1%); wispy-shp, also elong and // arranged 5) Amph? (<1%) 6) WM (<1%): flakes		
Matrix:	Tuffaceous mudstone		
Structures:	Massive, poorly-sorted		
Alteration/Observations:	Calcification (Calcareous cement, spotted spar calcite)		
Interpretation:	Subaqueous-settled, volcanic-triggered, sediment-gravity flow deposits.		

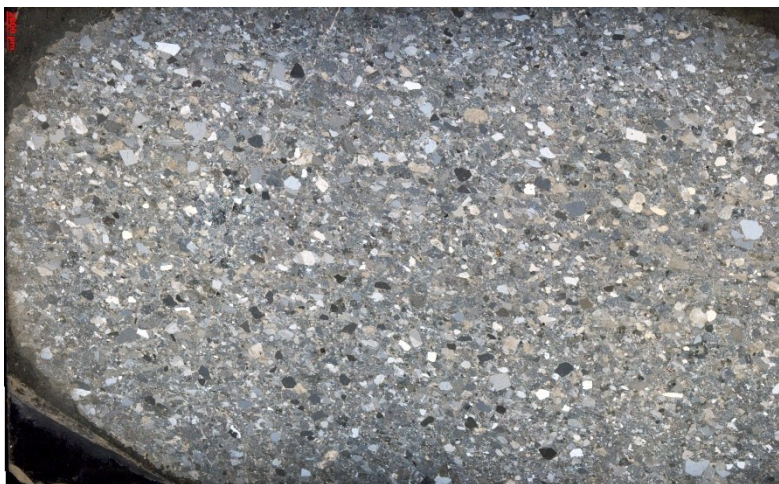
Sample: CRS1-97.5		Locality: Cañadón Río Simpson 1 (CRS1)	
NP		NX	
			
Composition:		Epiclastic	
Classification:		Glaucinitic, feldspatho-litho-quartzose sandstone.	
Framework:		1) Qz (40%): elong to subtriang, wedge, anh 2) Lv (35%): rounded, partly altered, felsitic texture. Some clasts resemble chert texture. 3) Feld (10%): subh-anh, mottled txt, some partly alt (calc) 4) Lm (5%): rounded, polycrystalline qz (quartzite) 5) Glauc (5%): subang-subred 6) Opq (1%); wedge, wispy, and irregularly-shaped 7) Amph? (<1%): anh to subh	
Matrix:		N/A	
Structures:		Apparently massive, very well-sorted.	
Alteration/Observations:		Calcification (Calcareous cement, spotted spar calcite)	
Interpretation:		Subtidal sandstone. Compared to previous samples, new sedimentary sources have been captured during sedimentation (unroofing?).	

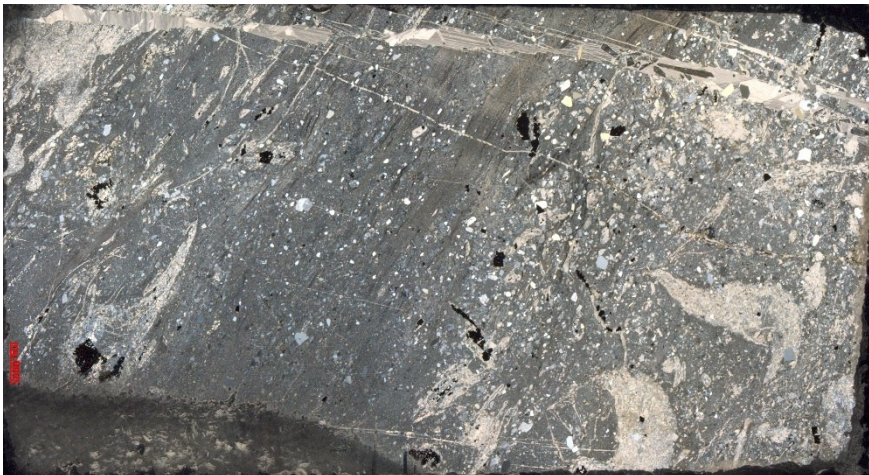
Sample: CRS3-0.5		Locality: Cañadón Río Simpson 3 (CRS3)	
NP		NX	
			
Composition:		Carbonaceous-phosphatic	
Classification:		Microfossil-bearing, carbonaceous, silty claystone	
Framework:		1) Qz (20%): ang to subround 2) Feld (5%): ang to subround 3) Phosphatic allochems (10%): rounded to subangular, opaque to isotropic. Possibly acritarchs. 4) Calcispheres (<1%) 5) WM (<1%):	
Matrix:		Carbonaceous mudstone	
Structures:		Parallel lamination Lag deposits	
Alteration/Observations:		Phosphatization Partly calcification of feldspars.	
Interpretation:		Carbonaceous hemipelagites. Lag deposits reflect bedload transport, while laminated zones might indicate a relatively fast deposition via storms or turbidites (Ullmer-Scholle et al., 2014).	


Sample: CRS3-12.2		Locality: Cañadón Río Simpson 3 (CRS3)	
NP		NX	
			
Composition:		Carbonaceous-phosphatic	
Classification:		Tasmanitid-rich, carbonaceous, clayey sandstone	
Framework:		Siliciclastic: 1) Feld (15%): euh to subh 2) Qz (5%): anh, angular 3) Lv (5%): subround-round 3) Opq (1%): subround Microfossils 1) Tasmanitids (40%): circular cross-section, concentric lamination (external ring + nucleus) 2) Acritarchs (20%) 3) Benthic forams (5%) 4) Calcispheres (5%):	
Matrix:		Carbonaceous mudstone	
Structures:		Parallel lamination Lag deposits	
Alteration/Observations:		Phosphatization Calcification/argillization of feldspars (partial)	
Interpretation:		Carbonaceous hemipelagites. Lag deposits reflect bedload transport, while laminated zones might indicate a relatively fast deposition via storms or turbidites (Ullmer-Scholle et al., 2014).	


Sample: DCE19-039.5		Locality: El Toqui Mine (Pozo DCE19)	
NX		<div></div> <div>5 mm</div>	
Composition:	Calcareous		
Classification:	Oysters-bearing floatstone		
Framework:	M-C Pebble-sized Bioclasts (oysters): 50%		
Matrix:	Spar calcite (secondary)		
Structures:	Bioclasts apparently aligned		
Alteration/Observations:	Replacement of fossils and calcareous matrix (OxFe, Qz, opaque minerals) - Skarn alteration		
Interpretation:	Marmorized & silicified floatstone		


Sample: DCE19-0.64.2		Locality: El Toqui Mine (Pozo DCE19)	
NX		<div></div>	
Composition:	Mixed volcanoclastic-calcareous		
Classification:	Calcified crystal tuff, or tuffaceous sandy mudstone		
Framework:	VF-F sand-sized Qz: 20% Calcite:10% (possibly secondary after feldspar)		
Matrix:	Ash devitrified + argillized		
Structures:	Discontinuous lamination		
Alteration/Observations:	Calcification + Opaque mineralization		
Interpretation:	Calcareous, volcanoclastic muddy sandstone ("wacke")		


Sample: DCE19-084		Locality: El Toqui Mine (Pozo DCE19)	
NX		<div></div>	
Composition:	Volcaniclastic		
Classification:	Feldspathic litharenite		
Framework:	F-VC sand-sized LVF (microporphyric, felsitic): 40% Pg + KFeI:20% Qz: 30%		
Matrix: 10%	Ash (devitrified)		
Structures:	Clast supported Massive – diffuse lamination		
Alteration/Observations:	N/A		
Interpretation:	Volcaniclastic turbidite or sandy debrite		


Sample: DCE19-085.7		Locality: El Toqui Mine (Pozo DCE19)		
NX				
Composition:	Volcaniclastic			
Classification:	Silty tuffaceous mudstone + volcaniclastic qz-wacke			
Framework:	F-M Pebble-sized (bioclasts) F-C sand-sized (terrigenous) Reworked bioclast (bivalves) Qz (red, subh-anh, reg.sor): 105% Pg (euh-subh, poly, zoned, alter): 10% KFel (tartan): 5% LVF: 1% Opaq.			
Matrix:	Clay			
Structures:	Normal grading Sharp boundaries (erosive?) Parallel lamination (thin)			
Alteration/Observations:	Pressure seams (compaction) Recrystallization of bioclasts Calcification (veins)			
Interpretation:	Cxl tuff + sandy tuffs (turbidites Ta-b)			

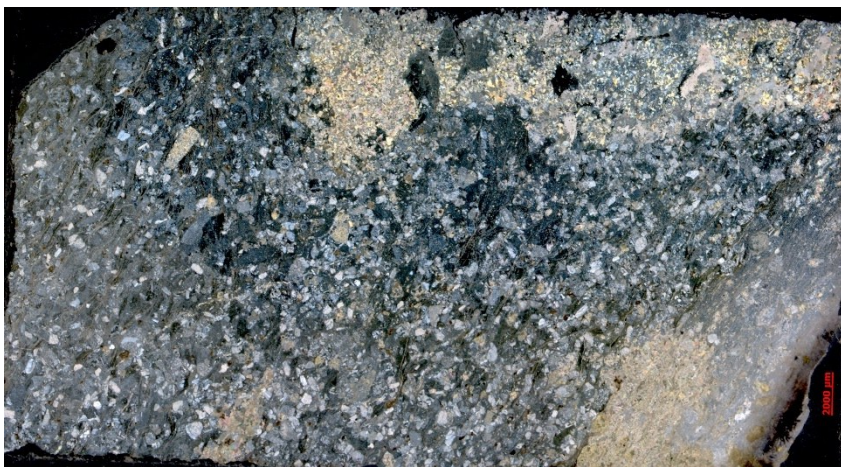
Sample: DCE19-098.7		Locality: El Toqui Mine (Pozo DCE19)	
NX		<div></div>	
Composition:		Calcareous	
Classification:		Marble (marmorized floatstone?)	
Framework:		Granule- F Pebble-sized Bioclasts (indet.), possibly oysters Bioclasts (ghost)	
Matrix/Cement		Spar-calcite	
Structures:		Massive	
Alteration/Observations:		Skarn mineralization (Garnet, Wollastonite) Replacement of bioclasts	
Interpretation:		Marble	


Sample: DCE19-108.3		Locality: El Toqui Mine (Pozo DCE19)		
NX				
Composition:				Tuffaceous – volcaniclastic
Classification:				Subaqueous settled lapillistone + banded tuffaceous mudstone
Framework:				C-F/VF sand-sized (regular sorting) Accretionary lapilli + clay matrix Pg (euh-subh, zoned): 70% Qz (subhedral): 15%
Matrix:				Ash (isotropic) Clay (secondary after ash)
Structures:				Parallel lamination Sharp/erosive contacts Normal grading (mudstone) + inverse grading (lapilli)
Alteration/Observations:				Argillization/sericitization
Interpretation:				Banded tuffaceous turbidites (Ta-b) + accretionary lapilli


Sample: DCE19-118.7		Locality: El Toqui Mine (Pozo DCE19)	
NX		<div></div> <div>5 mm</div>	
Composition:	Calcareous		
Classification:	Sparstone after oyster-bearing floatstone		
Framework:	Granule- F Pebble-sized bioclasts Bioclasts (ghost structures, oysters?): 25%		
Matrix:	Spar calcite		
Structures:	Diffuse parallel lamination		
Alteration/Observations:	Recrystallization + silicification of fossils Skarn mineralization (Garnet; Wollastonite, opaques)		
Interpretation:	Marmorized floatstone		

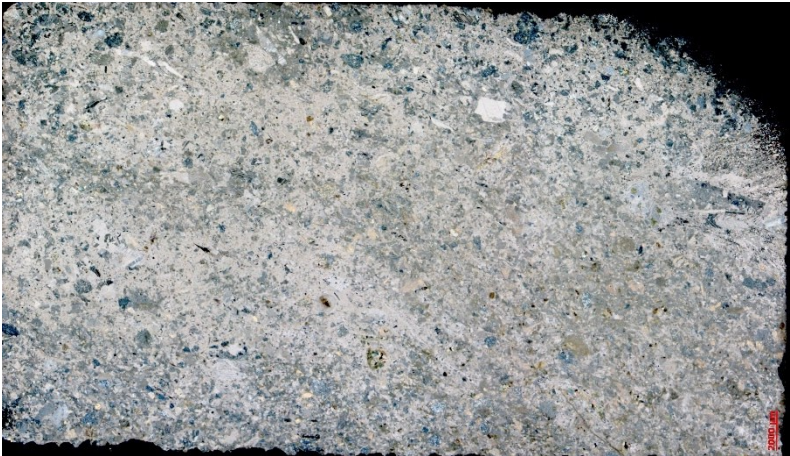
Sample: DCE19-119.5		Locality: El Toqui Mine (Pozo DCE19)	
NX		<div></div> <div>5 mm</div>	
Composition:	Calcareous		
Classification:	Recrystallized bioclastic wackestone/floatstone?		
Framework:	M Pebble-sized bioclasts (<10%) C-VC Sand-sized (peloids) Bivalves (recryst.), oysters?: 15% Echinoids: 1% Peloids (intraclasts, pellets?): <5% Micritized grains (algae?): 1%		
Matrix:	Microspar		
Structures:	Stylolites + horsetail structures (pressure seams)		
Alteration/Observations:	Recrystallization of bioclasts		
Interpretation:	Reworked bioclastic limestone (autoparabiostrome?)		

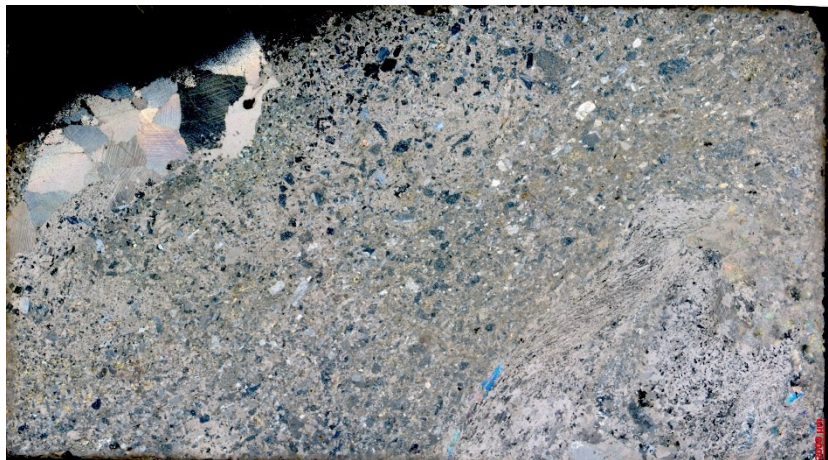
Sample: DCE19-120.2		Locality: El Toqui Mine (Pozo DCE19)	
NX		<div></div>	
xComposition:		Calcareous	
Classification:		Marmorized bioclastic floatstone	
Framework:		Granule – F Pebble-sized bioclasts Bivalves (ghost, curved, thin shells): 15%	
Matrix:		Microspar	
Structures:		Recrystallized, oriented bioclasts	
Alteration/Observations:		Recrystallization + silicification of bioclasts Skarn mineralization (garnet)	
Interpretation:		Recrystallized/marmorized floatstone	

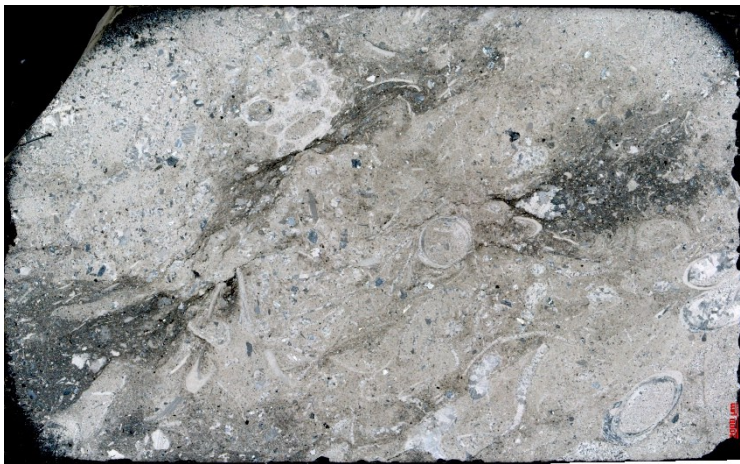
Sample: DCE19-121.6		Locality: El Toqui Mine (Pozo DCE19)	
NX		<div></div>	
Composition:	Volcaniclastic		
Classification:	Volcaniclastic lithic-feldspathic wacke		
Framework:	M-C Sand-sized Pg (subh-euh, zoned, altered):40 KFel (sanidine); Opaq.: 20 LVF (microporphyric, felsit):20		
Matrix:	Clay (secondary after ash)		
Structures:	Pressure seams (stylolites)		
Alteration/Observations:	Sericitization of feldspar Skarn mineralization: epidote + garnet		
Interpretation:	Volcaniclastic sediment gravity-flow		


Sample: DCE19-122.6		Locality: El Toqui Mine (Pozo DCE19)		
NX				
Composition:	Tuffaceous			
Classification:	Tuffaceous feldspathic wacke			
Framework:	Granule-F pebble-sized (LVF) – poorly sorted F-C Sand (crystals) LVF (microporphyric, trachytic):10% Pg (euh>subh): 20% K-Fel (sanidine): 15%			
Matrix:	Clay (secondary after pumice)			
Structures:	Fiamme texture (diagenetical)			
Alteration/Observations:	Pressure seams-stylolites Sericitization (feldspar) + argillization of matrix (ash/pumice)			
Interpretation:	Volcaniclastic sediment gravity-flow			


Sample: DCE19-125.8		Locality: El Toqui Mine (Pozo DCE19)	
NX		<div></div>	
Composition:	Tuffaceous		
Classification:	Volcaniclastic lithic wacke		
Framework:	C-sand to granule-sized Poorly-sorted LVF (polymict, microporphyric, felsit, trachy, aphanit): 30% LIF (graphic, phaneritic): <5% Pg+Sanidine: <5%		
Matrix:	Clay (secondary) – devitrification of ash		
Structures:	Pressure seams Fiamme texture (diagenetical)		
Alteration/Observations:	Sericitization + argillization of matrix		
Interpretation:	Volcaniclastic sediment gravity-flow (proximal)		


Sample: DCE19-126.8		Locality: El Toqui Mine (Pozo DCE19)
NX <div data-bbox="397 275 1190 728">  </div>		
Composition:	Mixed calcareous - siliciclastic	
Classification:	Sandy bioclastic limestone	
Framework:	C-VC sand-sized Bivalves 10% Calcareous red algae:<1% Carbonate grains: <5% Echinoderms: 1% LVF (rounded to sub-ang, vitrophyric, trachytic, felsitic):15%	
Matrix:	Micrite + Microspar	
Structures:	Diffuse lamination (thin)	
Alteration/Observations:	Diffuse stylolites (compaction) Skarn alteration (epidote)	
Interpretation:	Mixed, reworked bioclastic limestone	


Sample: DCE19-127.4		Locality: El Toqui Mine (Pozo DCE19)	
NX		<div></div>	
Composition:	Mixed calcareous - volcanoclastic		
Classification:	Sandy bioclastic limestone		
Framework:	C Pebble-sized (bioclasts) M-C Sand (crystals) Bivalves (oysters): 30% LVF (rounded porphyric, trachytic, felsitic): 25% Pg >> KFe (euh, poly, zoned): 20%		
Matrix:	Micrite + Microspar		
Structures:	Diffuse lamination (thin)		
Alteration/Observations:	Diffuse stylolites (compaction) Recrystallization of bioclasts		
Interpretation:	Mixed, reworked bioclastic limestone		


Sample: DCE19-128.7		Locality: El Toqui Mine (Pozo DCE19)	
NX		<div></div>	
Composition:	Calcareous		
Classification:	Serpulid-bearing wackestone + fitted packstone		
Framework:	<p>Granule – M Pebble-sized (bioclasts) F-M Sand-sized (terrigenous)</p> <p>Bivalves (thin shell, curved): 10% Serpulids (solitary, nest): 20% Calcareous clasts (rounded): 5 % LVF (<5%, subred, microporphyric)</p>		
Matrix:	Micrite + microspar		
Structures:	<p>Bioerosion in bivalves Geopetal structures within serpulid tubes</p>		
Alteration/Observations:	Pressure seams + horsetail – stylolites		
Interpretation:	Reworked bioclastic limestone + diagenetical compaction		

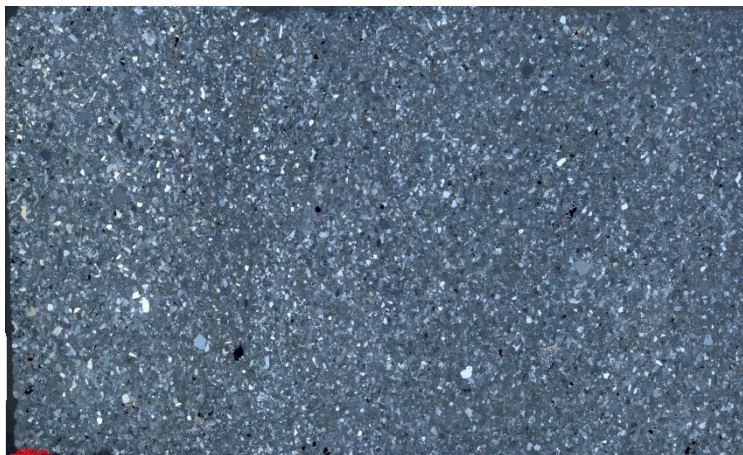
Sample: DCE19-130		Locality: El Toqui Mine (Pozo DCE19)		
NX				
Composition:	Mixed volcanoclastic – calcareous			
Classification:	Bioclastic, tuffaceous muddy sandstone			
Framework:	C sand – F Pebble-sized Very poorly-sorted Calcareous clasts (rounded-tabular, recrystallized): 25% LVF (porphyric): 20 Pg; Qz (scarce): <5%			
Matrix:	Devitrified ash (isotropic)			
Structures:	Pressure seams Aligned tabular clasts (diffuse lamination)			
Alteration/Observations:	Devitrification Recrystallization + silicification of bioclasts Skarn alteration (Garnet + Calcite)			
Interpretation:	Reworked, mixed volcanoclastic – calcareous sediments			


Sample: DCE19-131.7		Locality: El Toqui Mine (Pozo DCE19)	
NX		<div></div>	
Composition:	Volcaniclastic		
Classification:	Volcanic pebbly sandstone to sandy conglomerate		
Framework:	C SS – F Pebble-sized very poorly sorted LVF (trachytic, porphyric, > felsitic): 80% Pg (euh to subhedral; poly, Carlsbad): 10%		
Matrix:	Ash devitrified (isotropic) replaced to chlorite		
Structures:	Aligned/imbrication clasts Some clasts with halo (devitrification, hyaloclastic?)		
Alteration/Observations:	Pressure seams Chl-Ep + Calc alteration (feldspars + matrix)		
Interpretation:	Reworked, subaqueous-settled, volcaniclastic deposits		


Sample: PDT21-088		Locality: El Toqui Mine (Pozo PDT21)		
NX				
Composition:	Tuffaceous			
Classification:	Argillized tuffaceous mudstone			
Framework:	Qz (scarce, subbing-subred): <5% LVF (felsitic, altered, scarce): < 5%			
Matrix:	Clay (secondary)			
Structures:	Diffuse foliation Mottled texture (opaques)			
Alteration/Observations:	Argillization			
Interpretation:	Tuffaceous hemipelagites			


Sample: PDT21-206.9		Locality: El Toqui Mine (Pozo PDT21)
NP		
		
Composition:	Siliciclastic – Volcaniclastic	
Classification:	Foliated mudstone + Arkose (turbidite)	
Framework:	Silt-VF Sand-sized (<5%) F-M Sand-sized Opaques (enlarge, mottled): 10% Pg (eu-subh, altered): 80% Qz (scarce, ang-subred): <5%	
Matrix:	Carbonaceous mud (shale) Clay (turbidite)	
Structures:	Foliation (mudstone) Scour marks (turbidite) - erosive Isolated clast at the top	
Alteration/Observations:	Concentration of opaques in sandstone	
Interpretation:	Contact black shales – volcaniclastic turbidite (Ta)	


Sample: PDT21-250.1		Locality: El Toqui Mine (Pozo PDT21)
NX <div data-bbox="539 277 1054 728">  </div>		
Composition:	Tuffaceous	
Classification:	Argillized tuffaceous mudstone	
Framework:	Silt-VF Sand-sized (<5%) Qz (scarce, sbang-subred):<5% LVF (felsit, altered, scarce): <5% Opagues (similar to mudstone => muddy tuff):<5%	
Matrix:	Clay (secondary) – from devitrified ash	
Structures:	Diffuse foliation/banding Mottled texture (opagues) Bioturbation? (color changes)	
Alteration/Observations:	Argillization	
Interpretation:	Tuffaceous hemipelagites	


Sample: PDT21-298.6		Locality: El Toqui Mine (Pozo PDT21)		
NX				
Composition:	Volcaniclastic			
Classification:	Volcaniclastic feldspathic litharenite			
Framework:	F-M Sand-sized Well-sorted Clast supported Qz (subang-subred, txt deseq, subh):15% Pg (eu-subh, altered): 30% LVF (red-subang, microporphyric, subtrachyctic, felsit): 50% LIF (granite): <5% LMF (or chert?): <5% Opaques: <5%			
Matrix:	Ash devitrified (isotropic)			
Structures:	Diffuse lamination (opaques)			
Alteration/Observations:	N/A			
Interpretation:	Volcaniclastic turbidite (Ta-b)			


Sample: PDT21-302		Locality: El Toqui Mine (Pozo PDT21)
NX <div data-bbox="418 280 1177 739">  </div>		
Composition:	Mixed tuffaceous - calcareous	
Classification:	Alternation: tuffaceous mudstone/sandstone + bioclast-bearing, tuffaceous mudstone	
Framework:	F-M Sand-sized (coarser-part) MF-F sand-sized(finer-part); Pebble-sized (Bioclasts) Qz (ang-subred, > in fine-grained): 5% Pg (eu-subh, poly, zoned, altered): 5% LVF (enlarged-red, felsit) <5% LMV (x1, sutured qz): <1% Bioclasts (bivalves, replaced, reworked): 5% Opaques: <5%	
Matrix:	Ash (isotropic) (matrix-supported)	
Structures:	Diffuse/gradual parallel lamination	
Alteration/Observations:	Replacement of bioclasts Calcification in spots (mottled) Sericitization (partial)	
Interpretation:	Tuffaceous turbidites + reworked bioclastic limestone	

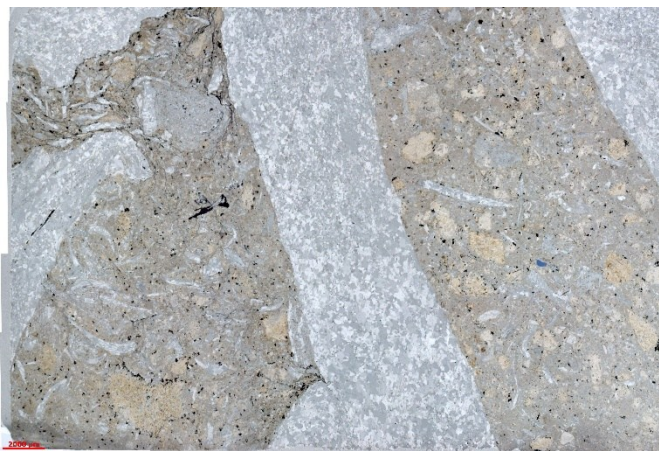
Sample: PDT21-319.7		Locality: El Toqui Mine (Pozo PDT21)		
NX				
Composition:	Tuffaceous			
Classification:	Diffuse laminated tuffaceous mudstone			
Framework:	VF Sand-sized (<5%) Opaques (in cumulus) LVF (scarce, felsit): 1% Qz (scarce, subang-red, ondulose): 1%			
Matrix:	Ash devitrified (clay secondary)			
Structures:	Diffuse foliation (opaques spots-halo, darker areas) Bioturbation?			
Alteration/Observations:	Devitrification (matrix) Spotted, opaque mineralization			
Interpretation:	Tuffaceous hemipelagites, mineralized			


Sample: ASN09-071.6		Locality: El Toqui Mine (Pozo ASN09)		
NX				
Composition:	Siliciclastic + Volcaniclastic			
Classification:	Volcaniclastic feldspathic arenite + tuffaceous-carbonaceous mudstone			
Framework:	M-VC Sand-sized (turbidite) Regular to poorly-sorted M-Sand-sized (in mud) Pg + KFeI (65%, euh-subhedral, altered) Qz (20%, angular) LVF (<10%, felsitic, trachytic, microporphyric)			
Matrix:	Ash (devitrified)			
Structures:	Pressure seams Erosive contact (solemarks) - turbidites Diffuse parallel lamination Normal grading?			
Alteration/Observations:	Low-degree of argillization			
Interpretation:	Contact tuffaceous-carbonaceous mudstone with volcaniclastic turbidite (Ta)			


Sample: ASN09-081		Locality: El Toqui Mine (Pozo ASN09)
NX <div data-bbox="518 280 1066 728">  </div>		
Composition:	Volcaniclastic	
Classification:	Volcanic lithic arkose	
Framework:	M-C Sand-sized Regular to well-sorted Pg (sub-euh, sericit):70% LVF (fine-grained):20% LIF (granite): <1% Qz: 10%	
Matrix:	Ash (devitrified)	
Structures:	Diffuse parallel lamination Zones with > matrix (grading?)	
Alteration/Observations:	Calcification + argillization of feldspars	
Interpretation:	Altered volcaniclastic turbidites (Ta-b)	


Sample: ASN09-111		Locality: El Toqui Mine (Pozo ASN09)	
NX		<div></div>	
Composition:	Volcaniclastic		
Classification:			
Framework:	C Pebble – F Cobble-sized LVF (95%, microporphyric, vitrophyric, subtrachytic, subang-subred) LIF (scarce, granite): <5%		
Matrix:	Clay (secondary, after ash/pumice)		
Structures:	Fiamme texture (diagenetical) Pressure seams (compaction)		
Alteration/Observations:	Argillization of ash Compaction		
Interpretation:	Volcaniclastic sediment-gravity flow		


Sample: ASN09-132.1		Locality: El Toqui Mine (Pozo ASN09)	
NX			
		<div></div>	
Composition:		Volcaniclastic	
Classification:		Sandy, clayey siltstone	
Framework:		Fine-grained sandstone (well-sorted) Qz (ang-round, sub-anhedral, txt dis-equilibrium): 15% Feld (altered, confused with matrix, subh-anhedral): 40 Opaques:< 5%	
Matrix:		Clay (secondary, after ash devitrified)	
Structures:		Diffuse opaque foliation Diffuse pressure seams	
Alteration/Observations:		Argillization of ash Sericitization/Argillization of feldspars	
Interpretation:		Volcaniclastic turbidites Ta-b (distal)	

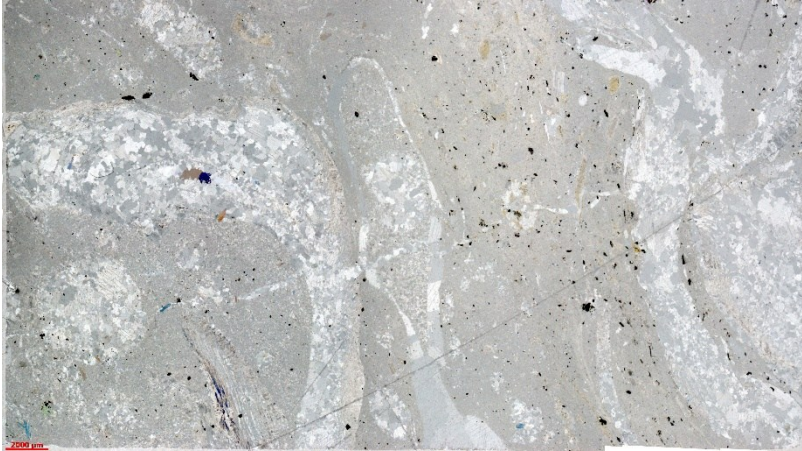
Sample: ASN09-145.5		Locality: El Toqui Mine (Pozo ASN09)	
NX		<div></div>	
Composition:	Mixed calcareous-siliciclastic		
Classification:	Bioclastic floatstone with + volcanic sandy wackestone (matrix)		
Framework:	<p>C-Cobble-sized (Bioclasts) VC sandstone – Pebble-sized (clasts in matrix)</p> <p>Bioclasts (big oysters, several bivalves bioclasts): 50% LVF (ang-round, trachy, poorly-sorted):20 Peloids (intraclasts?):< 5%</p>		
Matrix:	Micrite		
Structures:	Pressure seams + stylolites		
Alteration/Observations:	Recrystallization of bioclasts (blocky spar calcite)		
Interpretation:	Reworked floatstone with packstone matrix		


Sample: ASN09-147.3		Locality: El Toqui Mine (Pozo ASN09)		
NX				
Composition:	Volcaniclastic			
Classification:	Alternation of tuffaceous mudstone (lithic-rich vs ash-rich)			
Framework:	Granule – F Pebble-sized (regular sorting) M-C Sand-sized (regular sorting) LVF (subang-subred, subtrachytic): 30-40% Feld (altered, subhedral): 20% Reworked bioclasts? 5%			
Matrix:	Ash (devitrified, isotropic) Microspar (2°)? (replacement)			
Structures:	Parallel lamination (thin) Normal grading (lithic tuff) Erosive contacts (solemarks)			
Alteration/Observations:	Calcification (feldspar + cement)			
Interpretation:	Volcaniclastic turbidites (Tb)			

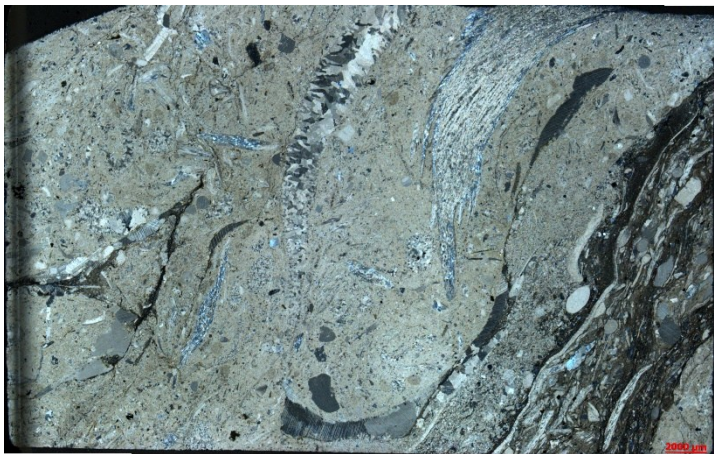
Sample: ASN09-156.2		Locality: El Toqui Mine (Pozo ASN09)
NX <div data-bbox="429 284 1161 728">  </div>		
Composition:	Calcareous + Tuffaceous	
Classification:	Laminated/banded tuffaceous mudstone and bioclastic fitted rudstone	
Framework:	Feld (altered, subh-anhedral): 5% Qz microcrystalline: <5% Bioclasts (oysters, bivalves? concave-up):15% LVF (enlarged, irregular/deform, porphyric, calcified):5% Opaques: <5%	
Matrix:	Ash (tuff, devitrified) Micrite (limestone)	
Structures:	Pressure seams + horsetails + stylolites Foliation of bioclasts (rework.)	
Alteration/Observations:	Erosive contacts (solemarks) Greenish alteration (Cpx, Act) Calcification; devitrification	
Interpretation:	Erosive contact: Limestones and volcanoclastic turbidites (Ta, b)	

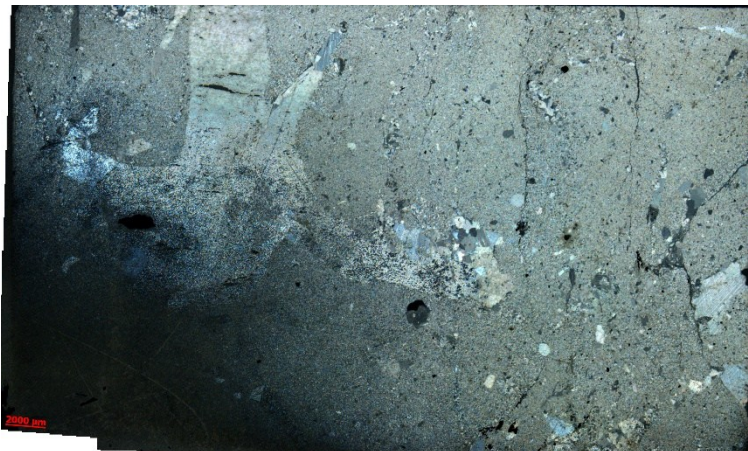
Sample: ASN09-159.8		Locality: El Toqui Mine (Pozo ASN09)
NX		
		
Composition:	Mixed calcareous-siliciclastic	
Classification:	Fitted sandy bioclastic packstone (matrix of large-scale floatstone)	
Framework:	VC sand – Pebble to cobble-sized (bioclasts) Bioclast (recrys, bivalves, echin) + 1 big sized (oyster): 40% LVF (subround, microporphyric, altered): 5% Pg (eu-subhedral, regular-sorted, altered): 5-10% Opaques: <5%	
Matrix:	Micrite - microspar	
Structures:	Pressure seams + stylolites	
Alteration/Observations:	Partial calcification in LVF Recrystallization + silicification of bioclasts	
Interpretation:	Reworked bioclastic limestone	

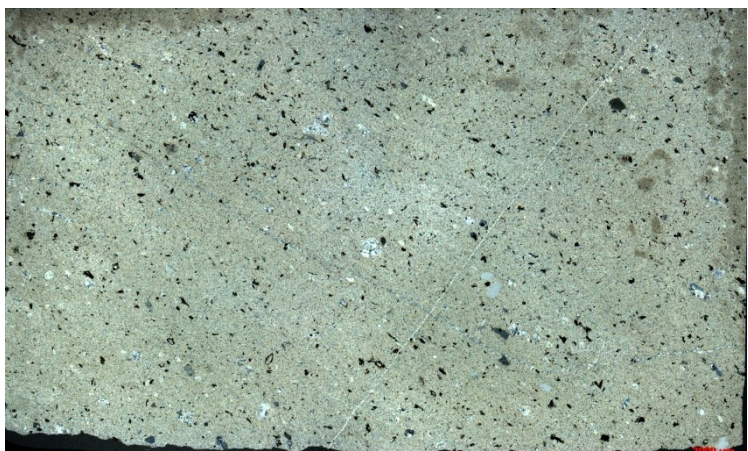
Sample: ASN09-166.6		Locality: El Toqui Mine (Pozo ASN09)		
NX				
Composition:	Calcareous			
Classification:	Bioclastic floatstone with mudstone matrix			
Framework:	Pebble-Cobble-sized (oysters) F-M Sand-sized (sparse bioclasts in matrix) Oysters (reworked): 15% Echinoderms (scarce, plates): <1%			
Matrix:	Microspar			
Structures:	Pressure seams + stylolites + concave-convex contacts			
Alteration/Observations:	Recrystallization of bioclasts Compaction			
Interpretation:	Bioclastic floatstone with mudstone matrix (autoparabiostrome)			

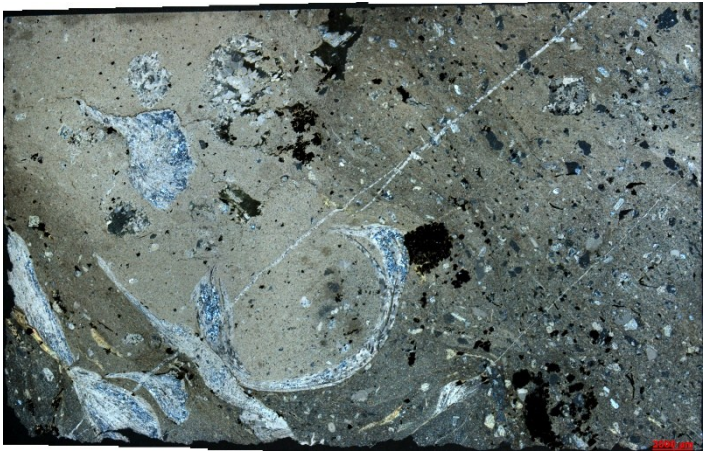
Sample: ASN09-210.5		Locality: El Toqui Mine (Pozo ASN09)
NX		
		
Composition:	Calcareous	
Classification:	Bioclastic floatstone with sandy bioclastic wackestone matrix	
Framework:	Cobble-sized (oysters) M-C Sand-sized (bioclasts in matrix) Oysters (big sized, recrystallized): 40% Other bivalves? 5% Echinoderms (plates, spines): <5% LVF (altered, felsitic): <5% Pg (sub-euhedral, altered total): <1% Opaques: <5%	
Matrix:	Micrite-Microspar	
Structures:	Compaction (concave-convex contacts, diffuse horsetail) Bioerosion in oyster	
Alteration/Observations:	Recrystallization of bioclasts (ghost structures)	
Interpretation:	Reworked, sandy bioclastic limestone (autoparabiostrome)	

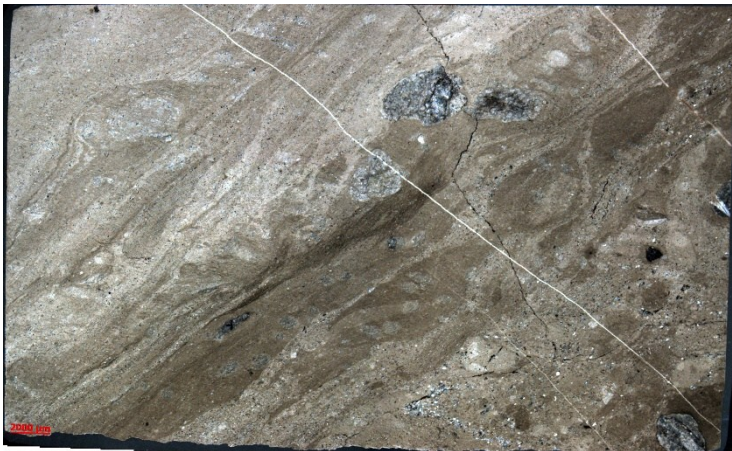
Sample: LCS453-005.6		Locality: El Toqui Mine (Pozo LCS453)		
NX				
Composition:	Calcareous			
Classification:	Oyster-rich floatstone			
Framework:	M-C Pebble-sized (Bioclasts) M-C Sand-sized (terrigenous) Bioclasts (oysters): 30-40% LVF (<5%, rounded, microporphyric) Pg (<5%, euh-subhedral) Opaques: 5%			
Matrix:	Microspar			
Structures:	Massive			
Alteration/Observations:	Recrystallization + silicification of shells			
Interpretation:	Reworked bioclastic limestone			

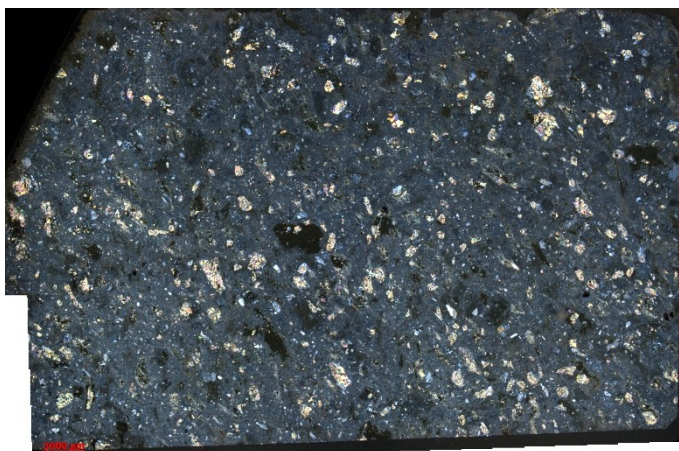
Sample: LCS453-009.4		Locality: El Toqui Mine (Pozo LCS453)	
NX			
		<div></div>	
Composition:		Mixed calcareous-siliciclastic	
Classification:		Bioclastic floatstone – fitted packstone + wackestone/packstone matrix	
Framework:		M-C Pebble-sized (Bioclasts) F-C Sand-sized (Bioclasts), poorly-sorted M Sand-sized (terrigenous) Bivalves (recrystallized, curved, thin): 5% Oysters (silicified, irregular): 25% Echinoderms:1 % Calcareous clasts (reworked): 10% FLV + Pg (< 5 %)	
Matrix:		Micrite	
Structures:		Pressure seams (stylolites) + concave-convex contacts Diffuse imbrication Diffuse parallel lamination	
Alteration/Observations:		Recrystallization + silicification of bioclasts	
Interpretation:		Compacted, reworked bioclastic limestone	

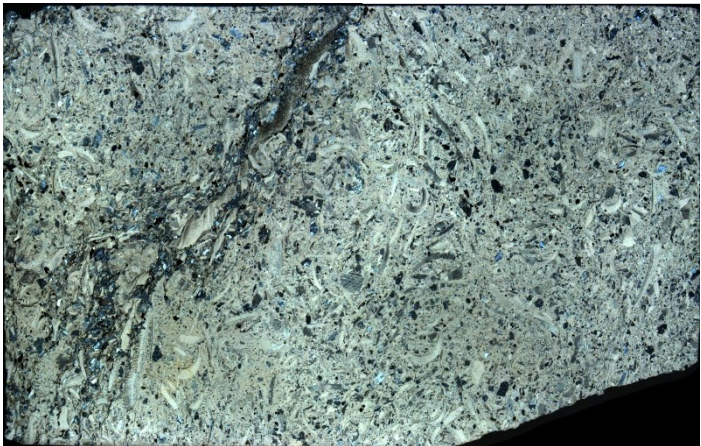
Sample: LCS453-016.3		Locality: El Toqui Mine (Pozo LCS453)		
NX				
Composition:	Calcareous			
Classification:	Bioclastic float-wackestone			
Framework:	F-M-Pebble-sized (Bioclasts) – Oysters? M Sand-sized (Bioclasts) Bioclasts (bivalves, oysters?): 15% Echinoderm:<5%			
Matrix:	Microspar – Micrite			
Structures:	Pressure seams + stylolites			
Alteration/Observations:	Recrystallized bioclasts			
Interpretation:	Reworked bioclastic limestone			

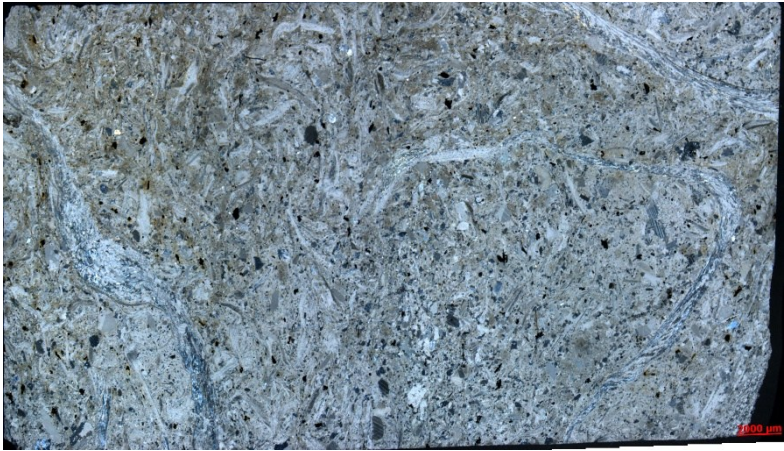
Sample: LCS453-121.4		Locality: El Toqui Mine (Pozo LCS453)	
NX		<div></div>	
Composition:	Mixed calcareous-volcaniclastic		
Classification:	Calcareous, volcanic lithic wacke		
Framework:	F-M sand-sized Regularly to poorly-sorted Bivalves (thin shells): <5% Calcareous clasts (reworked, rounded): <5% Opaques (ovoidal):10% LVF: <10% Pg (< 5%)		
Matrix:	Devitrified ash (secondary clay)		
Structures:	Diffuse banding Aligned opaques		
Alteration/Observations:	Calcification (matrix) Recrystallized bioclasts		
Interpretation:	Bioclasts-bearing, reworked tuffaceous mudstone		

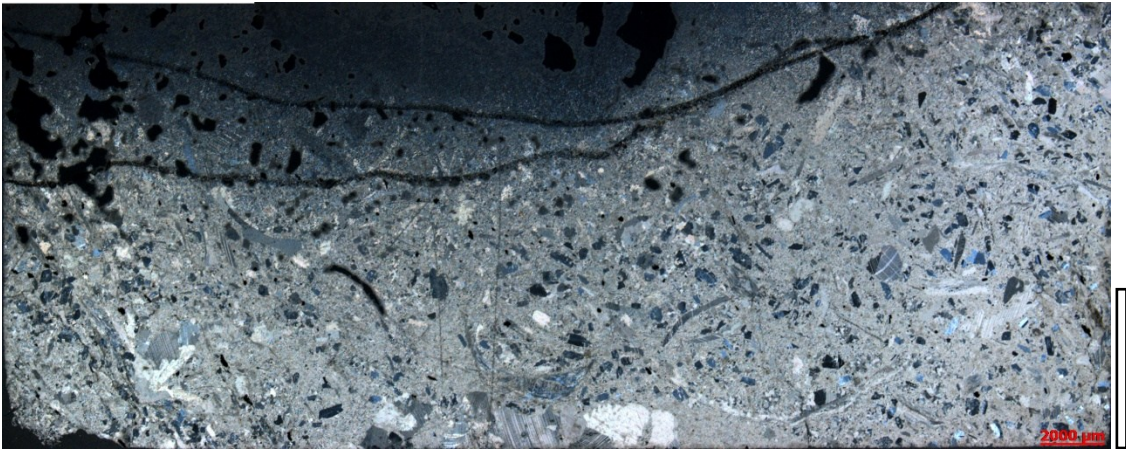
Sample: LCS453-124.3		Locality: El Toqui Mine (Pozo LCS453)
NX		
		
Composition:	Mixed calcareous-siliciclastic	
Classification:	Sandy bioclastic floatstone	
Framework:	F-M Pebble-sized (bioclasts) M-C Sand-sized (terrigenous) Bioclasts (Oysters): 30% Calcareous clasts (reworked): 10% Echinoderms: <5% LVF (rounded-angular, microporphyric) Pg (euh)	
Matrix:	Micrite Microspar	
Structures:	Pressure seams (big area)	
Alteration/Observations:	Recrystallized/silicified bioclasts Opaques mineralization	
Interpretation:	Reworked bioclastic, sandy limestone	


Sample: LCS453-133		Locality: El Toqui Mine (Pozo LCS453)
NX		
		
Composition:	Calcareous	
Classification:	Silty laminated & bioturbated calcimudstone	
Framework:	Granule-sized (clasts): 5% VF-F Sand-sized (crystals): 10% Calcareous clasts (subround): <5%	
Matrix:	Micrite, carbonaceous mudstone	
Structures:	Discontinuous subparallel lamination (thin)? Bioturbation (tubes) & possible neomorphism over plagioclase.	
Alteration/Observations:	Neomorphism in crystals? Plagioclase or dolomite?	
Interpretation:	Bioturbated, laminated mudstone	

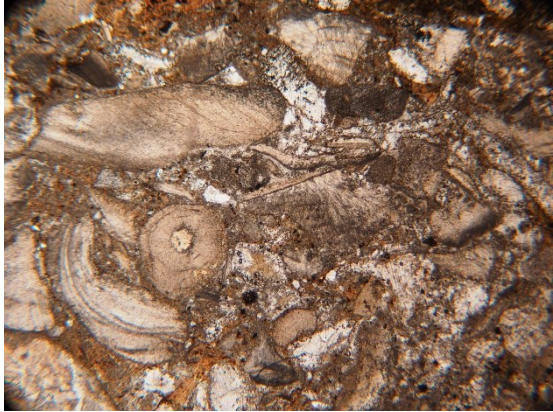
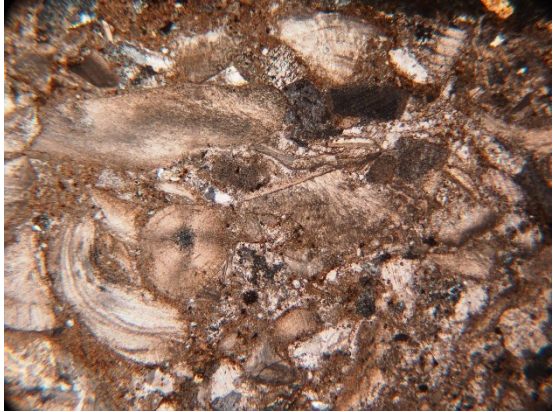
Sample: LCS453-191.3		Locality: El Toqui Mine (Pozo LCS453)		
NX				
Composition:	Volcaniclastic			
Classification:	Tuffaceous sandstone			
Framework:	C SS – Granule-sized Regular sorting Pg (euh-subhedral): 20% LVF (microporphyric, trachytic, opaque): 70%			
Matrix:	Devitrified ash (isotropic)			
Structures:	Matrix supported Diffuse imbrication			
Alteration/Observations:	Epidote in Pg/LVF + Chl-Ep			
Interpretation:	Distal volcanic sediment gravity flow?			

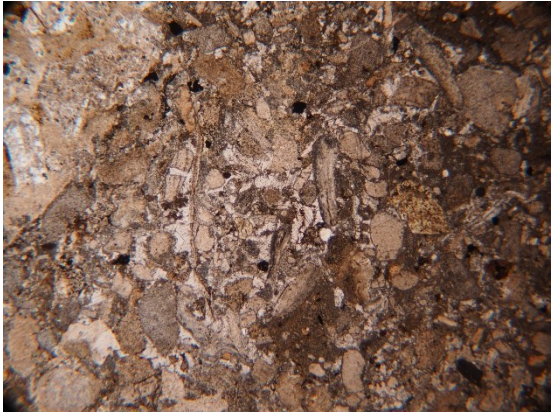
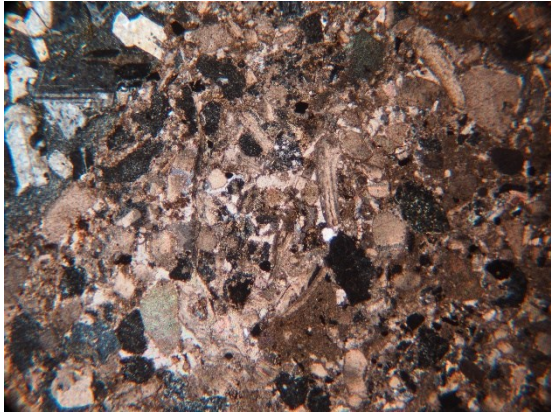
Sample: ESA-006.5		Locality: El Toqui Mine (Estero San Antonio)
NX		
		
Composition:	Calcareous	
Classification:	Sandy bioclastic packstone to fitted packstone	
Framework:	VC Sand – Pebble-sized (reworked) Bivalves (curved, thin, some recrystallized): 50% Serpulids (dark, round, layers): 5% Echinoderms (Syntaxial): <5% LVF (10%, round, microporphyric, vitrophyric, trachytic) Pg (sub-euhedral, polysynthetic): 5%	
Matrix:	Micrite – microspar	
Structures:	Pressure seams (stylolites + horsetail) Fragmented bioclasts	
Alteration/Observations:	Calcareous cementation Recrystallization + silicification of bioclasts (partial) Compaction	
Interpretation:	Oysters autoparabiostrome – parabiostromes (high E reworking)	



Sample: ESA-006.6R		Locality: El Toqui Mine (Estero San Antonio)
NX		
		
Composition:	Calcareous	
Classification:	Bioclastic floatstone with sandy bioclastic packstone matrix	
Framework:	Pebble-Cobble-sized (bioclasts) C Sand-Pebble-sized (clasts in matrix) Bivalves (large, curved, recrystalized): 40-50% Echinoderms: <5% Calcareous clasts (reworked; indet.): 10% Peloids (intraclasts = matrix): <5% LVF (scarce, round, microporphyric): 5-10% Qz (small, angular): <5% Pg (eu-subhedral, altered): <5% Opaques: 5%	
Matrix:	Microspar Blocky cement	
Structures:	Pressure seams + concave-convex contacts – small stylolites Bioerosion in oysters	
Alteration/Observations:	Calcareous cementation Recrystallization + silicification of bioclasts (partial)	
Interpretation:	Reworked bioclastic floatstone (high E environment)	


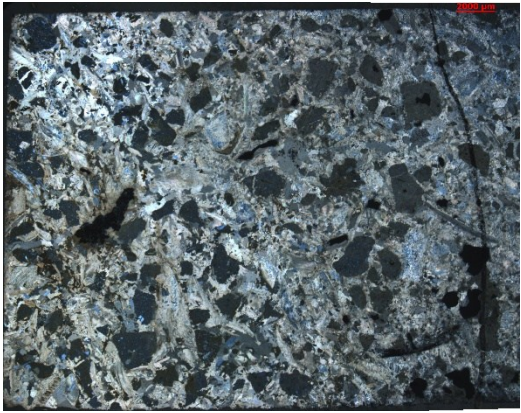
Sample: ESA-009.5		Locality: El Toqui Mine (Estero San Antonio)	
NX			
<div></div>			
Composition:		Mixed calcareous - siliciclastic	
Classification:		Sandy bioclastic wackestone	
Framework:		C Sand – Pebble-sized Bivalves (thin, recrystallized, curved): 15% Echinoderms (1-2%, spines) Calcareous clasts (reworked, indet.): 5% Pg (15%, eu-subhedral, Carlsbad, fractured-angular) LVF (scarce, felsitic, microporphyric): 5% Opaques: <5%	
Matrix:		Microspar	
Structures:		N/A	
Alteration/Observations:		Recrystallization of bioclasts (neomorph.)	
Interpretation:		Reworked bioclastic limestone (autoparabiostrome)	

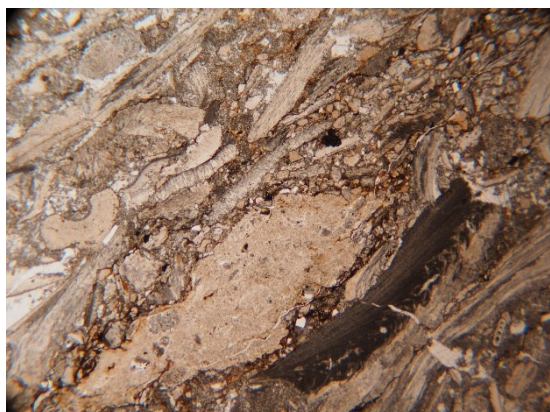
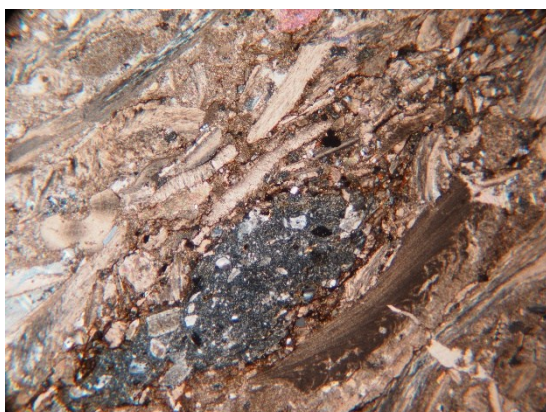
Sample: ESA-010		Locality: El Toqui Mine (Estero San Antonio)
NX <div data-bbox="427 280 1169 723">  </div>		
Composition:	Tuffaceous	
Classification:	Alternation: laminated tuffaceous mudstone + crystal-rich tuff. mudstone	
Framework:	Silt – VF Sand-sized Mostly matrix Pg (scarce, tabular, altered): <5% Opaques: <5%	
Matrix:	Ash (devitrified, isotropic)	
Structures:	Parallel lamination (very thin-thin) Sharp boundaries + diffuse scourmarks Mottled txt (darker halos)	
Alteration/Observations:	Devitrification Sericitization + calcification of plagioclase	
Interpretation:	Subaqueous-settled, fine-grained, sediment-gravity flows	

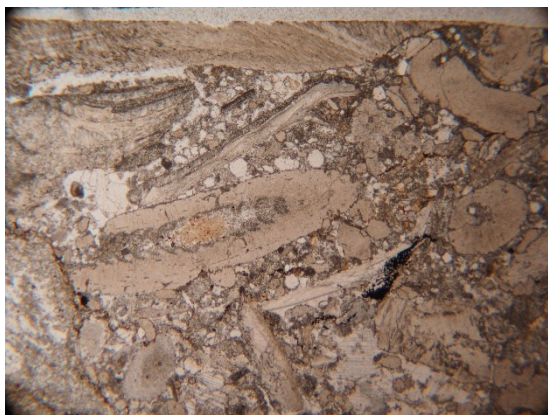

Sample: LRO-2.0		Locality: La Rosita	
NP		NX	
			
Composition:		Calcareous	
Classification:		Sandy bioclastic rudstone (poorly washed)	
Framework:		<p>Framework (50%)</p> <p>Bioclasts</p> <p>1) Oysters (30%): idem previous, size 0.5-6 mm (avrg:2 mm), brown-orange-colored (pale to dark). Round cat. 1-2; regular sorted.</p> <p>2) Other bivalves (1-2%).</p> <p>3) Echinoderms (3%)</p> <p>4) Red algae (5%): <i>Archamphiroa jurassica</i></p> <p>5) Serpulids (1%): tube fragments, circular to ovoidal + inner lamina</p> <p>6) Calcspheres (<1%): isolated, recrystallized, but translucent.</p> <p>Terrigenous:</p> <p>1) LVF (10%): Ang to subred, poorly sorted. Txt vitrophyric, felsitic, intersertal (1), size: 0.3-8 mm (x =0.5-1 mm).</p> <p>2) Pg (1%) euhedral-altered (calcite, partly).</p>	
Matrix:		<p>Matrix: micrite, in zones spotted by FeOx.</p> <p>Cement: syntaxial (echin), intraclastic (2°), blocky & poikilotopic</p>	
Structures:		<p>Massive</p> <p>Slight compaction -> discrete stylolites, small pressure solution seams.</p>	
Alteration/Observations:		<p>Oxidation □ replacement/enrichment with FeOx in matrix. More concentrated around volcanic lithics (already altered).</p> <p>Partial/spotted silicification in some oysters shells.</p>	
Interpretation:		Reworked subtidal, shallow-water carbonates	

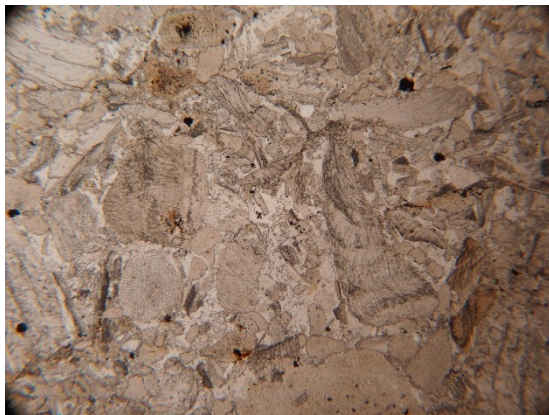
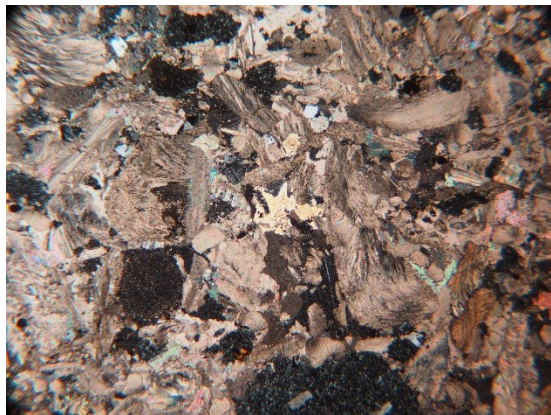
Sample: LRO-3.9		Locality: La Rosita
NP		NX
		
Composition:	Calcareous	
Classification:	Sandy bioclastic grainstone	
Framework:	<p>Framework (70%) Bioclasts (ca. 45%) 1) Bivalves (20%): Oyster and other bivalves. Several shapes: irregular, elongated, wedge-shaped. Poorly sorted. 2) Echinoderms (15%) 3) Red algae (10%)</p> <p>Terrigenous 1) LVF (25%): very poorly sorted, txt vitrophyric, microporphyric, felsitic, subred-subang. 2) Cxls (2%): Isolated, mostly Pg, scarce Qz (volcanic) 3) Glauconite (2 grains): rounded, discrete, slightly compacted.</p>	
Matrix:	<p>Matrix: micrite (scarce), poorly washed.</p> <p>Cement: Granular, Blocky, also dog-tooth to blocky, syntaxial (echin)</p>	
Structures:	<p>Rude parallel bedding, or possible coarse-tail normal grading of volcanic lithics</p> <p>Bierosion in some bivalves, also abraded margins (cortoid-like)</p>	
Alteration/Observations:	Ídem previous (FeOx; Pg, compaction).	
Interpretation:	Reworked subtidal, shallow-water carbonates	

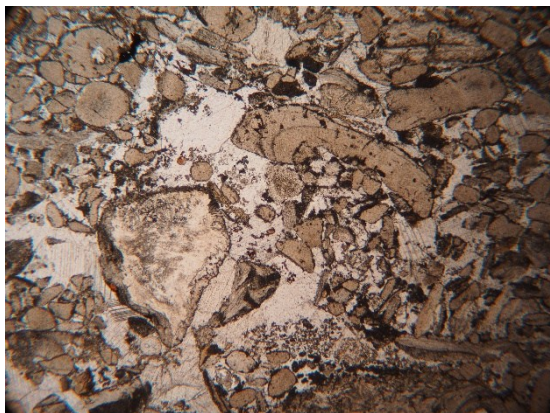
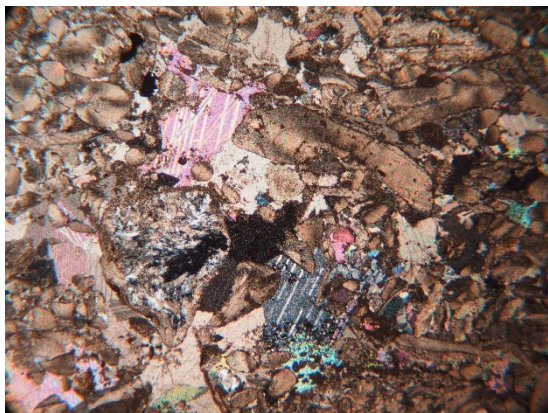
Sample: LRO-8.5		Locality: La Rosita	
NP		NX	
			
Composition:		Mixed volcanoclastic-calcareous	
Classification:		Bioclastic volcanic sandstone	
Framework:		Framework (70%): 1) LVF (50%): subang-subred, regular sorted. Txt felsitic >vitrophyric > trachytic 2) Crystals (2-3%): Pg >> Qz (volcanic) Bioclasts (15%) 1) Oysters (10%) 2) Red algae (5%) 3) Echinoderm (1%)	
Matrix:		Matrix: volcanoclastic (ash-devitrified) Cement (5%): Mosaic, drusy >> dogtooth to drusy	
Structures:		Normal grading: one part volcanic-rich & bigger-sized clast -> to carbonate-rich & smaller clasts. Devitrification of vitreous matrix (similar to clasts) Alteration in Pg (calcite, partly), also marginal replacement of LVF	
Alteration/Observations:		Possible alternation of volcanic-rich & bioclasts-rich layers	
Interpretation:		Coastal, subtidal mixedsediments	

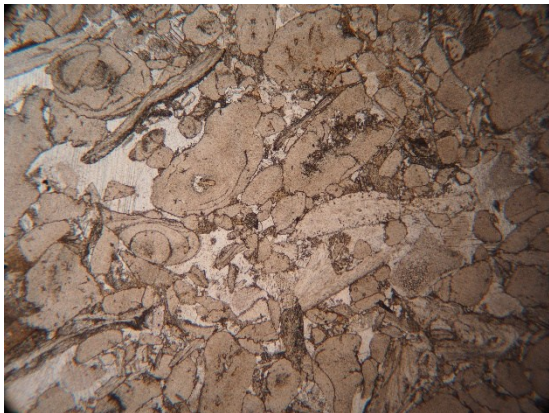
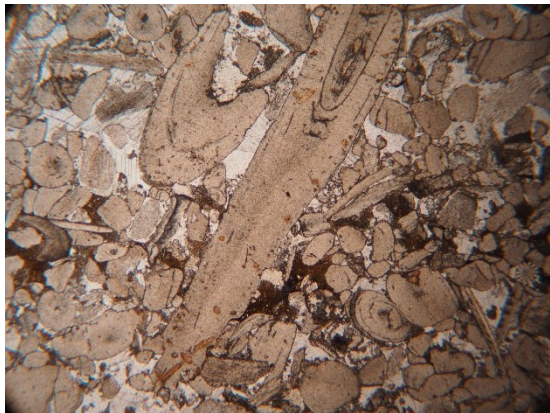
Sample: LRO-13		Locality: La Rosita	
NP		NX	
			
Composition:		Mixed calcareous-volcaniclastic	
Classification:		Sandy bioclastic grainstone (poorly washed)	
Framework:		<p>Framework (55%)</p> <p>Bioclasts</p> <p>1) Bivalves (30%): fragmental, ídem previous, though mixed (oyster 25% + others 5%). Size: 1-2 mm, max 4-5 mm.</p> <p>2) Echinoderm: 3%</p> <p>3) Red algae (5%)</p> <p>Terrigenous</p> <p>1) LVF (20%): regular sorted, txt vitrophyric > felsitic.</p> <p>2) Crystals (1%): Pg > Qz</p>	
Matrix:		<p>Matrix: micrite (10%), FeOx</p> <p>Cement: synt, poikil</p>	
Structures:		*** Similar to LRO-3.9	
Alteration/Observations:		<p>FeOx as 2a matrix/cement (replacement or dissolution + filling?)</p> <p>Calcite in Pg, also within LVF (partly).</p>	
Interpretation:		Reworked subtidal, shallow-water carbonates	

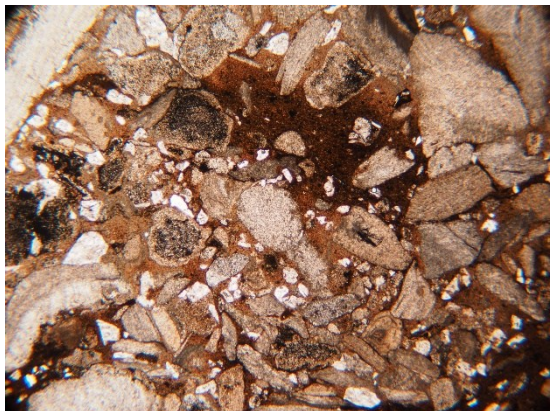
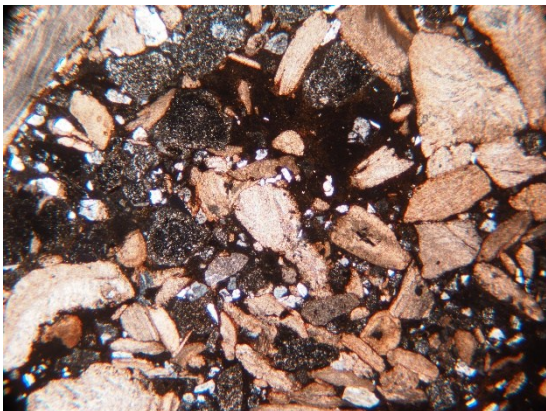
Sample: MCH-0.4		Locality: Muralla China	
NP		NX	
		 <div>2 mm</div>	
Composition:	Calcareous		
Classification:	Sandy bioclastic float-rudstone		
Framework:	<p>Framework (40%)</p> <p>Bioclasts</p> <p>1) Oysters (20%): poorly sorted, elongated, curved, wedge-shaped. Other bivalves (1%)</p> <p>2) Echinoderm (3%)</p> <p>3) Red algae (5%): <i>Archamphiroa jurassica</i>; Type 2 (<1%; very fine laminated, dark-colored, micritized, arch-shaped at margins)</p> <p>4) carbonized wood (<1%), isolated fragments.</p> <p>Terrigenous:</p> <p>1) LVF (5%): microporphy, bad-sorted, subang</p> <p>2) Crystals (1%)</p>		
Matrix:	<p>Matrix (25%): microspar, recrystallized up to silt-sized to VF grained sandstone.</p> <p>Cement (15%): poiki; mosaic/blocky; fine mosaic (recryst?); dogtooth-> block</p>		
Structures:	Aligned bioclasts		
Alteration/Observations:	<p>Recrystallization (matrix)</p> <p>Bioerosion in several bioclasts (Oys; Ech; Alg)</p> <p>Slight oxidation (FeOx) in FLV</p>		
Interpretation:	Wave-reworked, coastal carbonates		

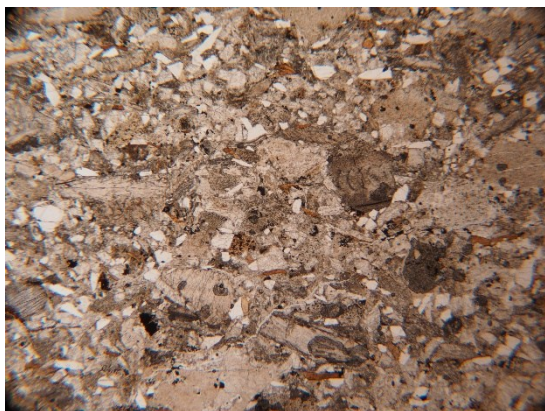
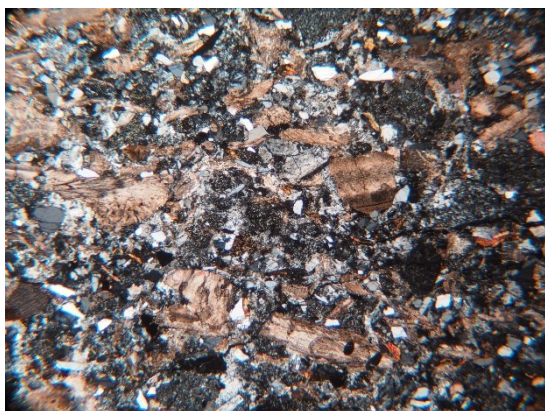
Sample: MCH-3.1		Locality: Muralla China	
NP		NX	
			
Composition:		Calcareous	
Classification:		Sandy bioclastic grainstone	
Framework:		Framework (55%) Bioclasts (50%) 1) Red algae (30%): poorly sorted, rounded, circular-ellipsoidal cross-section 2) Bivalves (15%): Oys>other; elongated & wedge-shaped, foliated, some ribbed. 3) Echinoid (5%) 4) Stromatoporoid (1%): isolated fragments , rounded, brown-colored. No structures in NP, columnar & feather-like extinction in NX. It resembles some altered oyster, though its pattern is bigger & more regular. Terrigenous 1) LVF (3%): rounded, felsitic, microporphyric 2) Crystals (2%): Qz (round-subang, VF-grained); Pg (VF-F grained, partly altered to calcite).	
Matrix:		Matrix: microspar (10%), trapped between allochems Cement (30%): isopach/dogtooth -> blocky, poiki, blocky. Also F-grained mosaic, possibly recrystallized	
Structures:		Aligned elongated bioclasts	
Alteration/Observations:		Discrete stylolites with thin pressure solution areas, enriched in FeOx. Some oysters display silicification in spots. Cemented zones displays connection -> dissolution & 2° fill?	
Interpretation:		Wave-reworked, coastal carbonates	

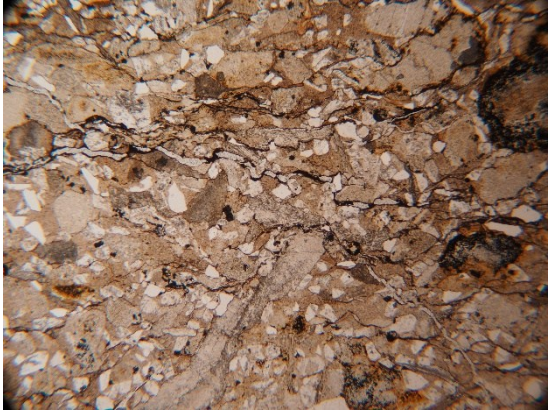

Sample: MCH-12.1		Locality: Muralla China	
NP		NX	
		 <div>2 mm</div>	
Composition:	Calcareous		
Classification:	Sandy bioclastic grainstone		
Framework:	<p>Framework (70%) Bioclasts (55%) 1) Bivalves (20%): oysters, also curved bivalves with a zigzag inner pattern. 2) Red algae (25%): mostly <i>A. jurassica</i>, also red-algae type 2 (<1%), micritized. 3) Echinoid (5%) iv) Stromatoporoid (<1%): isolated fragments v) Forams (<1%): only 2 exemplars observed (!= spp).</p> <p>Terrigenous (15%) 1) LVF (13%): subang-subred, regular-good sorted, txt microporphy. 2) Crystals (2%): Pg (eu-subh, slightly seric); qz (subang-subred). Good sorting</p>		
Matrix:	<p>Matrix: dark brown micrite (<5%), also enriched in FeOx (2°)</p> <p>Cement: (30%): syn ->echin Poiki, iso/dog -> blocky & poik</p>		
Structures:	Massive		
Alteration/Observations:	<p>Micritization in many bioclasts (borders), or abraded margins. Micritization more marked in red algae type-2 (partial loss of internal structure)</p>		
Interpretation:	Wave-reworked, coastal carbonates		

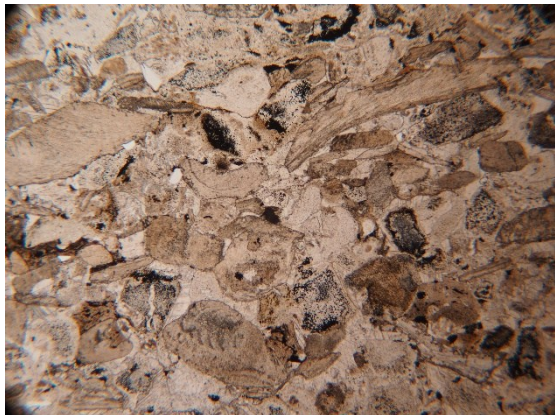
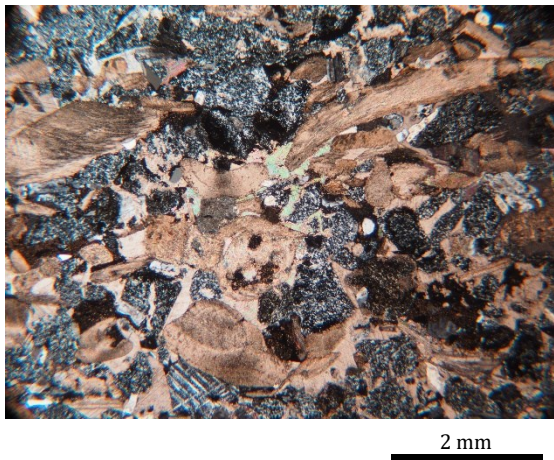
Sample: MCH-27.8		Locality: Muralla China	
NP		NX	
		 <div>2 mm</div>	
Composition:	Calcareous		
Classification:	Red algae-rich grainstone		
Framework:	Framework (55%) Bioclasts 1) Red algae (25%): <i>A. jurassica</i> + algae type-2 (1%) 2) Bivalves (10%): Oysters/other = 1/1 3) Echinoid (5%): mostly spines 4) Carbonized wood (<1%) 5) Corals (<1%): 1 isolated fragment, colonial. Terrigenous 1) LVF (3%) ídem previous 2) Crystals (<1%): Pg; qz		
Matrix:	Matrix: Micrite (ca. 5 %), trapped between allochems Cement (40%): Poiki, blocky, iso/dog -> blocky		
Structures:	Massive		
Alteration/Observations:	N/A		
Interpretation:	Wave-reworked, coastal carbonates		

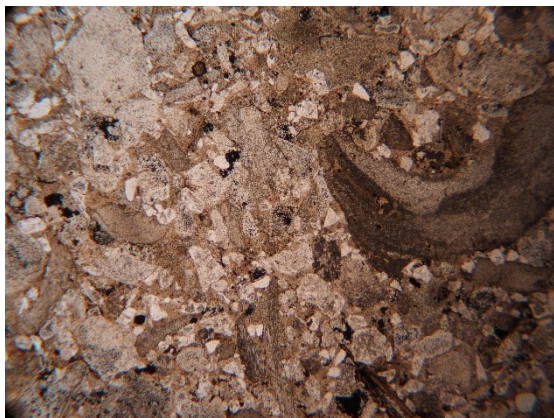

Sample: MCH-29.8		Locality: Muralla China
NP		NX
		 2 mm
Composition:	Calcareous	
Classification:	Red algae-rich, fitted grainstone	
Framework:	Framework (70%): 1) Red algae (60%): <i>A. jurassica</i> , several rounded fragments, very well sorted; some bioeroded. 2) Bivalves (5%): smaller than in previous samples; well-sorted elongated & wedge-shaped, mostly oysters, some bioturbated. 3) Echinoid (5%) 4) Corals (<1%): one fragment, colonial Terrigenous: 1) LVF (3%): felsitic, microporphyr -> altered (yellowish microliths) 2) Crystals (1%): isolated Pg, replaced by calcite (pervasive)	
Matrix:	Matrix: Micrite (5%) Cement (25%): poiki, dog/iso -> blocky, syn -> echin	
Structures:	Massive	
Alteration/Observations:	Alteration of feldspar crystals (yellowish colored).	
Interpretation:	Wave-reworked, coastal carbonates	

Sample: SRP2-1.7		Locality: Salto Río Pólux 2	
NP		NX	
			
Composition:		Mixed calcareous-volcaniclastic	
Classification:		Sandy bioclastic packstone	
Framework:		60% Bioclasts (30%) 1) Bivalves (20%): elongated-curved, wedge-shaped, regular sorted, Oys >> other 2) Red algae (10%): A. jurassica, rounded, well-sorted 3) Stromatoporoid? (<1%): isolated rounded fragments, feather-like extinction Terrigenous: (30%): 1) LVF (20%): F-grained, well-sorted, subang-subred. Txt microporphy > felsitic, concentration of opaques in central part 2) Crystals (10%): Pg: euh-subh, partly altered (ser), twinned, well-sorted, VF-F grained. Qz: suband-subred (ca. 1%); Bt: <1 %	
Matrix:		40% micrite + carbonaceous mudstone; dark reddish brown (FeOx), isotropic	
Structures:		Massive	
Alteration/Observations:		Fitted sample: zones of concentration of fossils (diagenetically compacted – pressure solution, sutured contacts) Bioerosion in Bioclasts	
Interpretation:		Subtidal, mixed deposits (distal tempestites, turbidites?)	

Sample: SRP2-5.85		Locality: Salto Río Pólux 2	
NP		NX	
			
Composition:		Mixed volcanoclastic-calcareous	
Classification:		Bioclastic volcanic sandstone	
Framework:		80% Terrigenous (50%): MF-M grained/ rarely coarse 1) LVF (40%) F-M sized, subred-auband, mpor >> felsi 2) Crystals (10%) mostly Qz, fractutres, anh, subred-ang. Qz 7%, Fel 3% Bioclasts (30%): F-M sized 1) Bivalves (25%): mostly elongated, minor wedge-shaped. Oys (20%) >> other (5%) 2) Red algae (2.5 %): ídem previous 3) Echinoid (2.5%): ídem previous 4) Corals (< 1%): colonial, isolated fragments	
Matrix:		Vitreous (devitrified), isotropic	
Structures:		Parallel lamination (observed in Bt and large bivalve clasts)	
Alteration/Observations:		Devitrification of matrix	
Interpretation:		Subtidal, mixed deposits (distal tempestites, turbidites?)	

Sample: SRP2-6.0		Locality: Salto Río Pólux 2	
NP		NX	
			
Composition:		Mixed siliciclastic-calcareous	
Classification:		Bioclastic volcanic sandstone	
Framework:		60% Terrigenous (55%) 1) LVF: (40%): ídem previous 2) Crystals (15%): F-M grained, Qz = volcanic, ang-subred (10%); Pg = eug-subh, twinned (5%); Bt = 1% (0.1-0.3 mm) Bioclasts (5%): 1) Oys/Biv = ca. 2 % 2) Red algae = ca. 2% 3) Echin = 1%	
Matrix:		vitreous (dev), light brown/isotropic (NX)	
Structures:		Parallel lamination (Bt)	
Alteration/Observations:		Pg -> slight alteration Compaction -> Pressure seams (// to lamination)	
Interpretation:		Subtidal, mixed deposits (distal tempestites, turbidites?)	

Sample: SRP2-7.1		Locality: Salto Río Pólux 2	
NP		NX	
			
Composition:	Mixed siliciclastic-calcareous		
Classification:	Bioclastic volcanic sandstone		
Framework:	90% Terrigenous: 57%; F-M grained 1) LVF (50%): subang-subred, mono/oligo, well sorted, felsitic >> mporphy. Concentration of opaques in central area 2) Crystals (7%): Pg: ídem; Qz: ídem, mono >> poli, very well sorted; Bt: < 1% Bioclasts (33%) 1) Bivalves (20%): Oys >> other 2) Red algae (10%) 3) Echin: 3%		
Matrix:	10% vitreous (dev) Cement: 10%; poiki >> syn (echinoid)		
Structures:	Parallel lamination (arrangement of elongated bioclasts)		
Alteration/Observations:	Pg -> ser (slight) LVF -> opaques (center, spotted) Compaction -> slight, isolated styl. * possibly 2° fill of porosity by poiki cement		
Interpretation:	Subtidal, mixed deposits (distal tempestites, turbidites?)		

Sample: SRP2-7.5		Locality: Salto Río Pólux 2	
NP		NX	
			
Composition:		Bioclastic volcanic sandstone/wacke	
Classification:		Mixed siliciclastic-calcareous	
Framework:		70% Terrigenous (55%) 1) LVF (50%) 2) Crystals (5%) Bioclasts (15%) 1) Bivalves: Oys >> other (10%) 2) red algae (3%) 3) Echinoid (2%)	
Matrix:		30% vitreous (dev)	
Structures:		Massive Bioerosion in shells	
Alteration/Observations:		Pg -> ser (slight) LVF -> opaques (center, spotted) Compaction -> slight, isolated styl. * possibly 2° fill of porosity by poikilotopic cement	
Interpretation:		Subtidal, mixed deposits (distal tempestites, turbidites?)	